Experimental investigation of exhaust valve energy transfer using variable valve motion

Shafie-Pour-Motlagh, M.

Award date:
1988

Awarding institution:
University of Bath

EXPERIMENTAL INVESTIGATION OF EXHAUST VALVE ENERGY TRANSFER USING VARIABLE VALVE MOTION

Submitted by M. Shafie-Pour-Motlagh
for the degree of Ph.D of the
University of Bath
1988

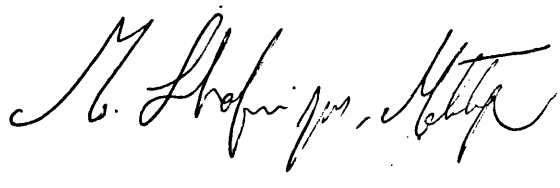

ProQuest LLC
789 East Eisenhower Parkway
P.O. Box 1346
Ann Arbor, MI 48106-1346

Acknowledgement

Foremost, I would like to take this opportunity to express my most sincere gratitude to Dr. S.J. Charlton for his continuous guidance, support, encouragement and supervision during the life of this reseach programme.

I would also like to thank the technical staff, at the university of Bath, for their assistance in manufacturing and assembling the experimental flow rig.

My thanks extend to Ford Motor Company for providing some of the Dover series engine components for the experimental work.

Table Of Contents

CHAPTER 6

Instrumentation and data acquisition

CHAPTER 7

Presentation and discussion of experimental results

CHAPTER 8

Discussion and conclusions

ABSTRACT

This thesis describes an investigation of the energy loss through the exhaust valve of an internal combustion engine. The energy of exhaust gases which is potentially available for expansion through the turbine of a turbocharged engine is affected by the exhaust valve motion and its rate of opening. An approach has been adopted to vary the rate of exhaust valve opening as means of improving energy transfer.

Mechanisms which render valve motion variable have been explored. A mechanism has been proposed which is capable of varying the rate of opening of an exhaust valve whilst the engine is running. Non-linear transient dynamic and rigid-body models of both a conventional valve train and a system incorporating the mechanism have been developed in the feasibility stage of this investigation. The concept has been proved to be feasible.

During the detail design of the mechanism, parametric studies have been performed to arrive at the most suitable dimensions. An experimental flow rig has been designed and constructed to allow investigation of the flow through an exhaust valve as a function of rate of valve opening. The instrumentation and data acquisition system of the flow rig have been described.

The experimental results have been presented and discussed. The exhaust pulse power has been calculated for the conventional and the high-rate systems. It has been shown that using the mechanism at 1000 rev/min has increased the available energy to the turbocharger turbine from 30% to 70% of the theoretical maximum, which corresponds to an increase in the exhaust pulse power of nearly 54%. The thesis ends with a discussion of the project as a whole followed by conclusions and scope for future work.

CHAPTER 1

Introduction

This opening chapter starts with a brief history of the diesel engine and its representation by ideal air-standard cycles which may be used to define the theoretical limits of performance. Supercharging, and in particular turbocharging, is introduced since the main topic of this work is the energy transfer from the cylinder to the turbine of a turbocharged diesel engine.

The chapter concludes by describing the problem area to be investigated, the objectives that were set and an overview of the methods employed.

1.1 Diesel Engines

Although the history of the diesel engine extends back into the closing years of the 19th century when Dr. Rudolf Diesel began his pioneering work on air blast injected stationary engines, and in spite of the dominant position it now holds in many applications, e.g. marine propulsion and land transport, both road and rail, it is today the subject of intensive research and development and remains capable of improvement. The diesel engine is the most efficient liquid fuel burning prime mover in volume production yet derived.

The major distinguishing characteristic of the diesel engine is the compression-ignition principle, i.e. the adoption of a special method of fuel preparation. Instead of relying on the passage of a spark at a predetermined point towards the end of the compression process to ignite a pre-mixed and wholly gaseous fuel-air mixture as in spark-ignition (SI) engines, the compression-ignition (CI) engine operates with a heterogeneous charge of previously compressed air and a finely divided spray of liquid fuel. The latter is injected into the engine cylinder towards the end of compression when, after a suitably intensive mixing process with the air in the cylinder, the self ignition properties of the fuel cause combustion to be initiated from a number of small nuclei. A major subdivision of diesel engines is between two-stroke and four-stroke types, according to the manner in which the gas exchange process is performed. In two-stroke engines combustion occurs in the region of top dead centre of every revolution where as, in four-stroke engines combustion takes place only every other revolution but in principle they both follow the same air-standard cycle.

1.1.1 Air Standard Cycle

The real processes in diesel engine cylinders, particularly those of fuel preparation, combustion and gas exchange are extremely complex and require sophisticated computational techniques which are discussed in a number of recent specialist texts,(1)-(3). Air standard cycles, which are

discussed in most elementry textbooks, provide a useful basis for comparing actual engine performance, especially thermal efficiency, with corresponding values from highly idealised cycles, based on certain drastic simplifying assumptions as follows:

(i) the mass of working fluid remains constant throughout the cycle, i.e. gas exchange and fuel addition are ignored;

(ii) the working fluid throughout the cycle is pure air treated as a perfect gas;

(iii) the combustion and gas exchange processes are replaced by external heat transfer to or from the working fluid under idealized, e.g. constant volume or constant pressure conditions;

(iv) compression and expansion processes are treated as adiabatic and reversible, i.e. friction effects are completely neglected;

(v) at any point of the working cycle, cylinder charge pressure and temperature are completely uniform, i.e. spatial variations in their values as for instance during combustion or scavenging, are completely neglectd.

The most commonly used air-standard cycles are as follows (figure 1.1);

(a) <u>The Constant Pressure or Diesel Cycle</u> (figure 1.1a) Here combustion is simulated by constant pressure heat addition 2-3, and blowdown, followed by scavenge, by

constant volume heat rejection 4-1. Compression 1-2 and expansion 3-4 follow the isentropic state relationships for a perfect gas. This particular cycle has, in the past, been used as a reference cycle for the 'classical' Diesel engine with air blast injection giving a rather long injection and hence heat release period, corresponding to 2-3. It has, however, little relevance to the modern diesel cycle.

(b) The Constant Volume or Otto Cycle (figure 1.1b)
Here combustion is simulated by constant volume heat release 2-3, and the blowdown-gas exchange sequence once again by constant volume heat rejection 4-1. Again compression 1-2 and expansion 3-4 are isentropic.

Traditionally this is the reference cycle for spark-ignition(SI) engines, but it has distinct validity as a reference cycle for diese l engines, particularly under light load conditions when the heat release period is short so that the assumptions of zero heat release duration implied by the constant volume process 2-3 does not introduce excessive errors.

(c) The 'Dual Combustion' or Composite Cycle (figure 1.1c)
This represents a combination of the constant pressure and constant volume cycles and is intended to provide a closer approximation to actual diesel cycles than either of the

above ideal cycles. It is particularly appropriate where comparisons are to be made with actual diesel cycles on the basis of the maximum cylinder pressure obtained during the heat release period.

1.2 Supercharging

Supercharging can be defined as the introduction of air (or air/fuel mixture) into an engine cylinder at a density greater than ambient. This allows a proportional increase in the fuel that can be burned and hence raises the potential power output. The charge is thus compressed both outside and inside the cylinder. The principal objective is to increase power output, not to improve efficiency, although the efficiency may benefit. Since more fuel is burned, for a given swept volume of the cylinders, the power output is increased. Thus the power to weight and volume ratios of the engine increases.

The effect of supercharging on power output can be seen from a cylinder pressure-volume (P-V) diagram. Figure 1.2 (4) shows an ideal naturally aspirated dual combustion cycle. Point 1 denotes the begining of the compression stroke when the piston is at bottom dead centre (BDC). Process 1-2 is the compression stroke. 2-3 is the part of the combustion process occurring (instantaneously) at constant volume (top dead centre, TDC). 3-4 is the remaining part of the combustion process occurring at constant pressure while the

piston is moving along the cylinder. 4-5 is the continuation of the expansion process following the end of combustion. At point 5 the exhaust valve opens, allowing some exhaust gas to leave the cylinder and the pressure to fall back to the ambient level. The intake and exhaust processes are not shown.

Useful work is obtained during process 3-4-5 since the pressure acting on the piston is aiding its outward motion. This is the power stroke. Against this must be set the work required to compress the gas in the cylinder, process 1-2. The work done , W, may be calculated from the integral, (figure 1.2)

$$W = \int P.dV$$

It follows that the net work output (expansion work minus compression work) is given by the area inside the diagram, area 1-2-3-4-5-1. This is the work output per complete cycle. The process described above takes one revolution of the crankshaft. The intake and exhaust processes occupy a second revolution. Useful power is therefore obtained every second revolution of the crankshaft. It follows that the area inside the diagram multiplied by half the engine speed gives the power output of a four-stroke engine.

above ideal cycles. It is particularly appropriate where comparisons are to be made with actual diesel cycles on the basis of the maximum cylinder pressure obtained during the heat release period.

1.2 Supercharging

Supercharging can be defined as the introduction of air (or air/fuel mixture) into an engine cylinder at a density greater than ambient. This allows a proportional increase in the fuel that can be burned and hence raises the potential power output. The charge is thus compressed both outside and inside the cylinder. The principal objective is to increase power output, not to improve efficiency, although the efficiency may benefit. Since more fuel is burned, for a given swept volume of the cylinders, the power output is increased. Thus the power to weight and volume ratios of the engine increases.

The effect of supercharging on power output can be seen from a cylinder pressure-volume (P-V) diagram. Figure 1.2 (4) shows an ideal naturally aspirated dual combustion cycle. Point 1 denotes the begining of the compression stroke when the piston is at bottom dead centre (BDC). Process 1-2 is the compression stroke. 2-3 is the part of the combustion process occurring (instantaneously) at constant volume (top dead centre, TDC). 3-4 is the remaining part of the combustion process occurring at constant pressure while the

piston is moving along the cylinder. 4-5 is the continuation of the expansion process following the end of combustion. At point 5 the exhaust valve opens, allowing some exhaust gas to leave the cylinder and the pressure to fall back to the ambient level. The intake and exhaust processes are not shown.

Useful work is obtained during process 3-4-5 since the pressure acting on the piston is aiding its outward motion. This is the power stroke. Against this must be set the work required to compress the gas in the cylinder, process 1-2. The work done , W, may be calculated from the integral, (figure 1.2)

$$W = \int P.dV$$

It follows that the net work output (expansion work minus compression work) is given by the area inside the diagram, area 1-2-3-4-5-1. This is the work output per complete cycle. The process described above takes one revolution of the crankshaft. The intake and exhaust processes occupy a second revolution. Useful power is therefore obtained every second revolution of the crankshaft. It follows that the area inside the diagram multiplied by half the engine speed gives the power output of a four-stroke engine.

Figure 1.3 shows the ideal dual combustion cycle of a diesel engine in naturally aspirated and supercharged form. The supercharged cycle starts at a higher pressure (and density) point 1′. Extra fuel may be burned between 2′-4′ because more air is available (the same volume but a higher density). Two things are clear: the supercharged engine has a greater power output (see diagram area) and a much higher maximum pressure. Unless the engine is designed to be supercharged, the high maximum pressure may not be acceptable and the engine may not withstand the stresses involved. The compression ratio of the engine must be reduced to prevent an excessive maximum cylinder pressure being reached. By reducing the compression ratio the clearance volume, V_{Cl}, is increased and the maximum pressure will be reduced. If the compression ratio is suitably chosen, the maximum pressure in the supercharged engine can equal that of the naturally aspirated engine, see figure 1.4; the power output of the supercharged engine remains greater than that of the naturally aspirated engine, althoughthe reduced compression ratio may impair fuel consumption and cold starting.

1.2.1 Methods of Supercharging

As discussed earlier the purpose of supercharging is to increase the mass of air trapped in the cylinders of the engine, by raising air density. A compressor is used to achieve the increase in air density. Two methods of

piston is moving along the cylinder. 4-5 is the continuation of the expansion process following the end of combustion. At point 5 the exhaust valve opens, allowing some exhaust gas to leave the cylinder and the pressure to fall back to the ambient level. The intake and exhaust processes are not shown.

Useful work is obtained during process 3-4-5 since the pressure acting on the piston is aiding its outward motion. This is the power stroke. Against this must be set the work required to compress the gas in the cylinder, process 1-2. The work done , W, may be calculated from the integral, (figure 1.2)

$$W = \int P.dV$$

It follows that the net work output (expansion work minus compression work) is given by the area inside the diagram, area 1-2-3-4-5-1. This is the work output per complete cycle. The process described above takes one revolution of the crankshaft. The intake and exhaust processes occupy a second revolution. Useful power is therefore obtained every second revolution of the crankshaft. It follows that the area inside the diagram multiplied by half the engine speed gives the power output of a four-stroke engine.

above ideal cycles. It is particularly appropriate where comparisons are to be made with actual diesel cycles on the basis of the maximum cylinder pressure obtained during the heat release period.

1.2 Supercharging

Supercharging can be defined as the introduction of air (or air/fuel mixture) into an engine cylinder at a density greater than ambient. This allows a proportional increase in the fuel that can be burned and hence raises the potential power output. The charge is thus compressed both outside and inside the cylinder. The principal objective is to increase power output, not to improve efficiency, although the efficiency may benefit. Since more fuel is burned, for a given swept volume of the cylinders, the power output is increased. Thus the power to weight and volume ratios of the engine increases.

The effect of supercharging on power output can be seen from a cylinder pressure-volume (P-V) diagram. Figure 1.2 (4) shows an ideal naturally aspirated dual combustion cycle. Point 1 denotes the begining of the compression stroke when the piston is at bottom dead centre (BDC). Process 1-2 is the compression stroke. 2-3 is the part of the combustion process occurring (instantaneously) at constant volume (top dead centre, TDC). 3-4 is the remaining part of the combustion process occurring at constant pressure while the

piston is moving along the cylinder. 4-5 is the continuation of the expansion process following the end of combustion. At point 5 the exhaust valve opens, allowing some exhaust gas to leave the cylinder and the pressure to fall back to the ambient level. The intake and exhaust processes are not shown.

Useful work is obtained during process 3-4-5 since the pressure acting on the piston is aiding its outward motion. This is the power stroke. Against this must be set the work required to compress the gas in the cylinder, process 1-2. The work done , W, may be calculated from the integral, (figure 1.2)

$$W = \int P.dV$$

It follows that the net work output (expansion work minus compression work) is given by the area inside the diagram, area 1-2-3-4-5-1. This is the work output per complete cycle. The process described above takes one revolution of the crankshaft. The intake and exhaust processes occupy a second revolution. Useful power is therefore obtained every second revolution of the crankshaft. It follows that the area inside the diagram multiplied by half the engine speed gives the power output of a four-stroke engine.

Figure 1.3 shows the ideal dual combustion cycle of a diesel engine in naturally aspirated and supercharged form. The supercharged cycle starts at a higher pressure (and density) point 1'. Extra fuel may be burned between 2'-4' because more air is available (the same volume but a higher density). Two things are clear: the supercharged engine has a greater power output (see diagram area) and a much higher maximum pressure. Unless the engine is designed to be supercharged, the high maximum pressure may not be acceptable and the engine may not withstand the stresses involved. The compression ratio of the engine must be reduced to prevent an excessive maximum cylinder pressure being reached. By reducing the compression ratio the clearance volume, V_{cl}, is increased and the maximum pressure will be reduced. If the compression ratio is suitably chosen, the maximum pressure in the supercharged engine can equal that of the naturally aspirated engine, see figure 1.4; the power output of the supercharged engine remains greater than that of the naturally aspirated engine, althoughthe reduced compression ratio may impair fuel consumption and cold starting.

1.2.1 Methods of Supercharging

As discussed earlier the purpose of supercharging is to increase the mass of air trapped in the cylinders of the engine, by raising air density. A compressor is used to achieve the increase in air density. Two methods of

supercharging can be distinguished by the method used to drive the compressor. If the compressor is driven from the crankshaft of the engine, the system is called 'mechanically driven supercharging' or often just 'supercharching'. If the compressor is driven by a turbine , which itself is driven by the exhaust gas from the cylinders, the system is called 'turbocharging'. The shaft of the turbocharger links the compressor and turbine, but is not connected to the crankshaft of the engine except on some experimental 'Compound' engines (5)-(7). Thus the power developed by the turbine and the volume displaced by the engine determine the compressor operating point.

An advantage of turbocharging, over a mechanically driven supercharger, is that the power required to drive the compressor is extracted from exhaust gas energy rather than the crankshaft. Thus turbocharging is usually more efficient than mechanical supercharging. Figures 1.5 and 1.6 give typical turbocharger compressor and turbine performance maps respectively.

1.3 Turbocharging Systems

Successful design of a turbocharged diesel engine is highly dependent on the choice of system for delivering exhaust gas energy from the exhaust valves or ports to the turbine and its utilization in the turbine.

The ideal thermodynamic cycles of engine operation were presented in section 1.1. Figure 1.7 shows the energy potentially available in the exhaust system, with an ideal cycle. The exhaust valve opens at BDC, point 5, where the cylinder pressure is much greater than the ambient pressure at the end of the exhaust pipe. If the contents of the cylinder at EVO were allowed to expand isentropically down to the ambient pressure (to point 6), then the work that could be done is represented by the cross-hatched area 5-6-1. This work could be recovered by allowing the piston to move further than normal as shown in figure 1.7. However this requires an engine with an exceptionally long stroke and in practice it is found that the additionall piston friction offsets the work gained by an ultra-long expansion stroke.

The work represented by area 5-6-1 is therefore potentially available to a turbocharger turbine placed in the exhaust manifold. It is called the 'blow-down' energy, since it involves the combustion products being 'blow-down' from cylinder pressure point 5 to atmospheric pressure at point 6, when the exhaust valve opens. Figure 1.7 represents a naturally aspirated engine. Consider now an ideal turbocharged four-stroke engine, as shown in figure 1.8. Turbocharging raises the inlet manifold pressure, hence the inlet process 12-1 is at pressure P_1, where P_1, is above ambient pressure P_a. The 'blow-down' energy is represented

by area 5-8-9. The exhaust manifold pressure, P_7, is also above the ambient pressure P_a. The exhaust process from the cylinder is represented by line 5,13,11 where 5,13 is the 'blow-down' period when the exhaust manifold. Process 13,11 represents the remainder of the exhaust process, when the piston moves from BDC to TDC displacing most of the gas from the cylinder to exhaust manifold. This gas is above ambient pressure and therefore also has the potential to expand down to ambient pressure whilst doing useful work. The potential work that could be done is represented by the cross-hatched area 13-9-10-11. This work is done by the piston but could be recovered by a turbine in the exhaust. The maximum possible energy available to drive a turbine will be sum of areas 5-8-9 and 13-9-10-11, but it is impossible to devise a practical system that will harness all this energy. To achieve this, the turbine inlet pressure must instantaneously rise to P_5, when the exhaust valve opens, followed by isentropic expansion of the exhaust gas through P_7 to the ambient pressure ($P_8=P_a$). During the displacement part of the exhaust process, the turbine inlet pressure would have to be held at P_7. Such a series of processes is impractical.

1.3.1 Constant Pressure Turbocharging System

In figure 1.8, consider a simpler process that would occur if a large chamber were fitted between the engine and turbine inlet, such as the arrangement shown in figure 1.9,

in order to damp down the pulsations in exhaust gas flow. The turbine acts as a flow restrictor creating a constant pressure, P_7, in the exhaust manifold chamber. The available energy at turbine is given by area 7-8-10-11 (figure 1.8). This is the ideal 'constant pressure' turbocharging system. With constant pressure turbocharging , the exhaust ports from all cylinders are piped into a common receiver whose volume is sufficiently large to ensure that its pressure is virtually constant. The unsteady exhaust flow processes at the cylinders are damped into a steady flow at the turbine. The major advantages and disadvantages of constant pressure turbocharging system are listed in section 1.3.3.

1.3.2 Pulse Turbocharging System

In figure 1.8, alternatively consider a system, in which a turbine wheel is placed directly downstream of the engine, very close to the exhaust valve, such as the arrangement shown in figure 1.10. The gas would expand directly through the turbine along line 5-6-7-8 (figure 1.8), assuming isentropic expansion and no losses in the exhaust port. If the turbine were sufficiently large, both cylinder and turbine inlet pressure would drop to the ambient pressure before the piston has moved significantly from BDC. Thus piston pumping work would be zero during the ideal exhaust stroke and area 5-8-9 would represent the available energy

at the turbine. This is the ideal 'pulse turbocharging system'.

In practice the systems commonly used and referred to as constant pressure and pulse systems are based on these principles but are far from ideal. In pulse turbocharging the system pressure and velocity fluctuations are generated in individual exhaust pipes of comparatively small diameter, into which flow the exhaust gases of a number of cylinders with suitable timing. The exhaust energy is transported to the turbine mainly in the form of pressure energy, so that there is a back pressure of varying magnitude, which affects the exhaust work done by the piston. The kinetic energy is only a small fraction of the total energy. Like the constant pressure turbocharging system, the advantages and disadvantages of the pulse turbocharging system are listed below.

1.3.3 Advantages & Disadvantages of Constant Pressure And Pulse Systems

(a) Constant Pressure Turbocharging System

(i) Advantages;

- high turbine efficiency, due to steady flow,
- good performance at high load,
- simple exhaust manifold.

(ii) Disadvantages;

- low available energy at turbine,
- poor performance at low speed and load,
- poor turbocharger transient response acceleration.

(iii) Applications;

- large industrial and marine engines operating at steady speed and load, highly rated; two- and four-stroke.

(b) Pulse Turbocharging System

(i) Advantages;

- high available energy at turbine,
- good performance at low speed and load,
- good turbocharger acceleration.

(ii) Disadvantages;

- poor turbine efficiency with both one or two cylinders per turbine entry,
- poor turbine efficiency at very high rating due to highly unsteady flow,
- complex exhaust manifold with large number of cylinders,
- possible pressure wave reflection problems.

(iii) Applications;

- automotive, truck, marine and industrial engines; two- and four-stroke; low and medium rating (e.g. up to 17-18 bar bmep on four-stroke engines).

Also in general terms for a given putput power, the advantages of turbocharging are;

- lower space requirements (few cylinders, shorter engine),
- lower weight, better specific weight,
- better efficiency with exhaust-turbocharging (flatter fuel consumption characteristics),
- lower cost per unit output, in particular for larger engines,
- smaller radiator; less heat is lost than in naturally aspirated engines,
- the exhaust noise is reduced by the exhaust turbine,
- less derating with reduced ambient air density.

The disadvantages of turbocharging are;

- greater mechanical and thermal loads,
- inferior torque characteristics,
- poor acceleration,

the latter two disadvantages relate to exhaust turbocharging with high boost ratios.

1.4 Description of Problem

Turbocharged diesel engines generally suffer from lack of torque at low engine speeds. This is due to the non-linear

characteristic of the turbocharger turbine. If, in a boosted engine, sufficient torque can be made available at lower speeds, the fuelling can be reduced at higher speeds so that improved torque back-up is obtained while the engine still gives adequate rated power.

In order to drive the turbocharger turbine, exhaust gases are transported from the cylinder to the turbine nozzles in a pipe system. It is a well established fact that the available exhaust gas energy is reduced significantly by the time it reaches the turbine. The reasons for this 'loss' of energy are discussed in more detail in the next chapter. When an exhaust valve opens, high pressure gases rush from the cylinder through the port to the exhaust manifold before the valve closes and form a pressure pulse in the exhaust manifold. The rate at which the high pressure gas is released depends upon the rate at which the exhaust valve effective flow area changes which in turn is a function of engine speed and valve gear design. At high engine speeds the exhaust valve opening and closing rates are sufficiently high to allow for more energetic pressure pulses to be formed in the exhaust manifold, whereas at low engine speed this rate is reduced thus resulting in a slower release of the cylinder content and weaker exhaust pulses. It has been stated (9) that utilisation of available turbine energy increases as the rate at which the exhaust valve opens

increases. It is one objective of this investigation to verify this phenomenon!

A device (7) has been proposed and developed that allows the rate of valve opening to be altered independently of engine speed. This mechanism is principally a motion adding device which consists of a hydraulic chamber, input, output and modulating plungers, a rocker, main and secondary cams. A schematic representation of the mechanism is shown in figure 1.14. The main cam displaces the input plunger. At some point the secondary cam actuates the modulating plunger via the rocker which rotates about a pivot point. The motion of the output plunger results from the sum of the motions of the other two plungers. The pivot point on the rocker can freely be adjusted to vary the rocker ratio i.e. to increase or decrease the contribution of the modulating plunger movement to the motion of the output plunger. Detailed description of the mechanism is given in chapter three.

1.5 The Context Of The Current Work

Work on flow through exhaust valves has generally been concerned with improving the coefficient of discharge in order to maximise flow and minimise piston pumping work. Design of exhaust valve gear is traditionally based on the above two mentioned points and obtaining high volumetric efficiency. This is a useful design criterion for naturally

aspirated engines but for an exhaust gas turbocharged engine this may not be a sufficient criterion for an optimum design. This is because the exhaust gas process of a turbocharged engine benefits not only from minimum pumping (largely throttling) losses but also from maximising the energy transport to the turbine (8).

The energy transport of the exhaust gases from the cylinder through the valve to the turbine is a complicated process. During this transfer a large proportion of the available energy of the gas is lost as a consequence of turbulent mixing losses via vortex shedding and throttling (8). Also, a small amount of energy loss results from heat transfer to the port wall and surrondings. If these losses can be reduced, the turbocharger turbine will be capable of producing more useful work. This in turn will improve the performance of the engine. The current work investigates a means to reduce these available energy losses. This is to be achieved by modifying the exhaust poppet valve motion. The problem of energy transfer through exhaust poppet valves is discussed in detail in the literature review in the next chapter.

1.6 Objectives

The basic objective of the project is to investigate the exhaust processes of highly turbocharged high-speed diesel engines. This investigation focuses on the energy transport

from the cylinder through the valve to the turbocharger turbine. The objectives are as follows;

- to quantify the loss of available energy to the turbine,
- to establish means by which the loss of available energy may be reduced,
- to design and develop a specific mechanism / device to alter the rate of valve opening or closing, whilst the engine is running, for general research application,
- to design and construct an experimental flow rig to study in isolation the influence of rate of valve opening on the exhaust gas energy transfer,
- to investigate and correlate the relationship between exhaust valve parameters, in particular the rate of opening, and energy transfer through the turbocharger turbine,
- to use the experimentally obtained results to:
  - (i) Study energy transfer as a functon of rate of valve opening,
  - (ii) Verify the dynamic characteristics of the mechanism,
  - (iii) Validate flow models used in simulation programs.

1.7 An Overview Of The Approach Adopted

In order to study the energy transfer through an exhaust valve a flow rig has been designed which readily allows rate of exhaust valve opening to be varied. Devices which render valve motion variable have been explored. A particular mechanism has been selected for use in the flow rig and a mathematical analysis of this mechanism was necessary as part of the rig design process.

This device is a very versatile mechanism in the sense that it may be modified, by means of alternative secondary cam profiles, to change valve lift, timing or rate at which the valves of an engine open or close. The mechanism has been used primarily to verify the effects of exhaust valve motion on the pulse energy content in the exhaust manifold of a simulated turbocharged diesel engine.

A study of the dynamic behaviour of the mechanism has been carried out using a finite element model. An equivalent model has been used to perform a rigid-body dynamic analysis. The mechanism in isolation has been analysed to facilitate design of the secondary cam profile. Other geometric parameters that may influence the secondary cam profile have also been considered and their corresponding effects studied.

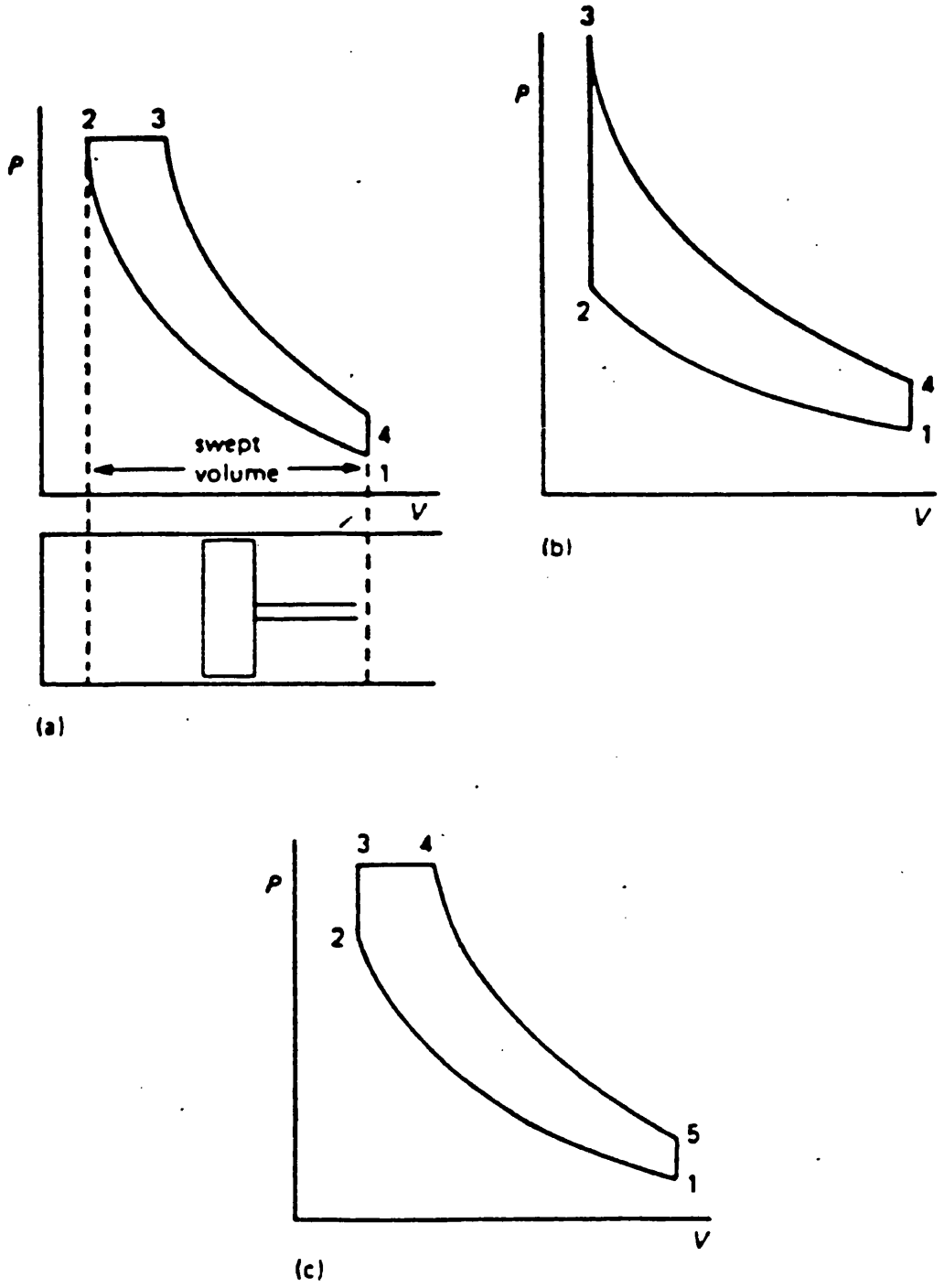

Figure 1.1- Air standard cycles (a) Constant pressure cycle; (b) Constant volume cycle; (c) Dual combustion or composite.

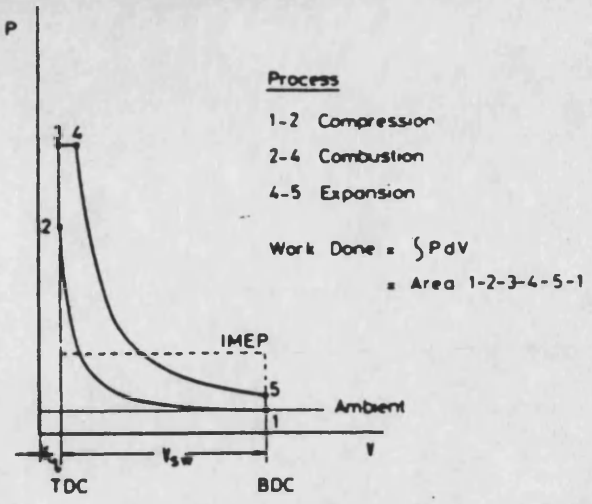

Figure 1.2- Ideal dual-combustion (limited pressure) air standard cycle; Naturally aspirated engine.

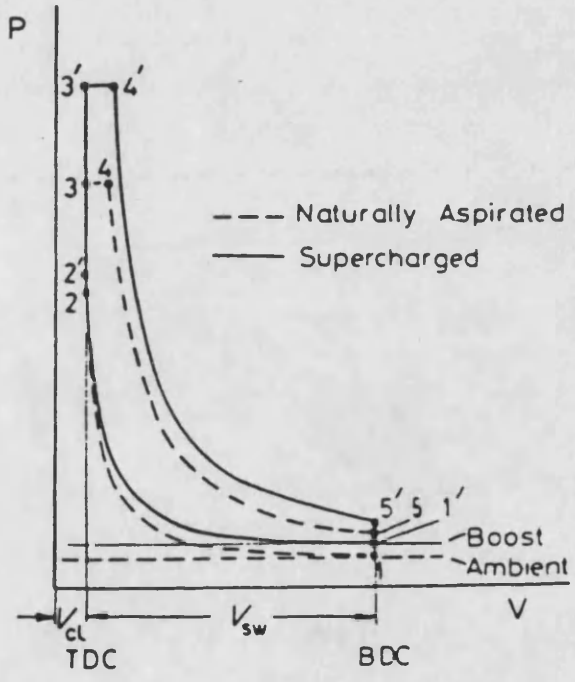

Figure 1.3- Comparison of supercharged and naturally aspirated air standard dual-combustion cycles having the same compression ratio.

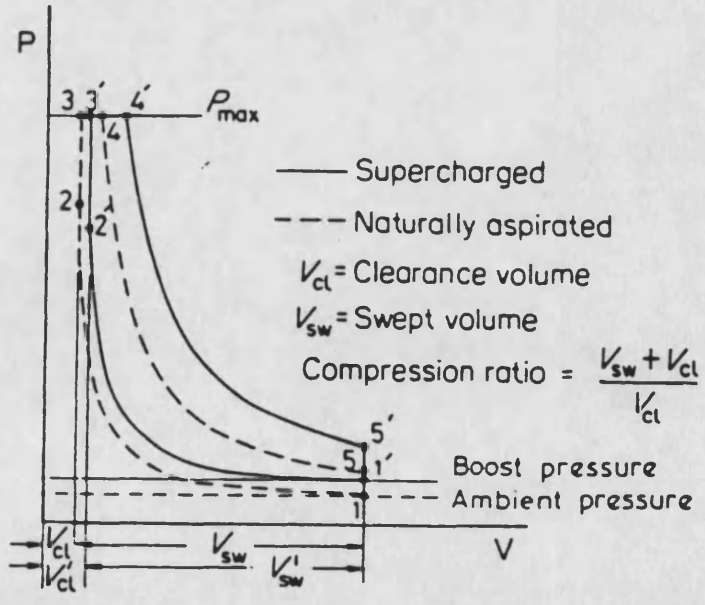

Figure 1.4- Comparison of supercharged and naturally aspirated air standard dual-combustion cycles having the same maximum pressure but different compression ratio.

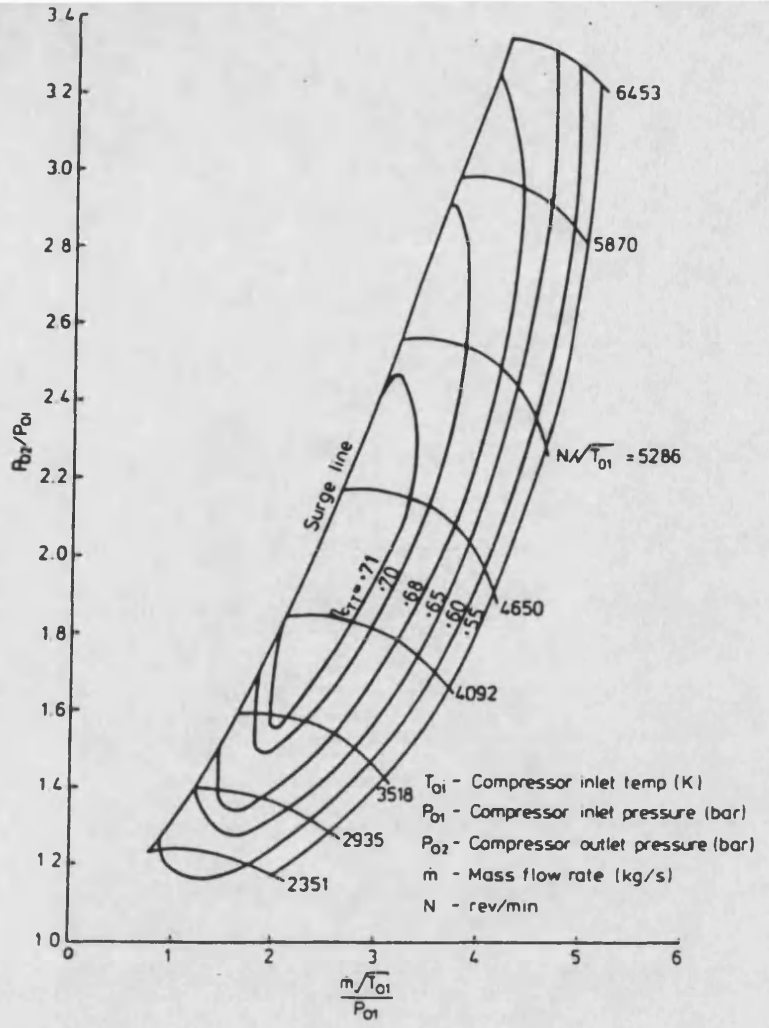

Figure 1.5- A typical compressor performance map.

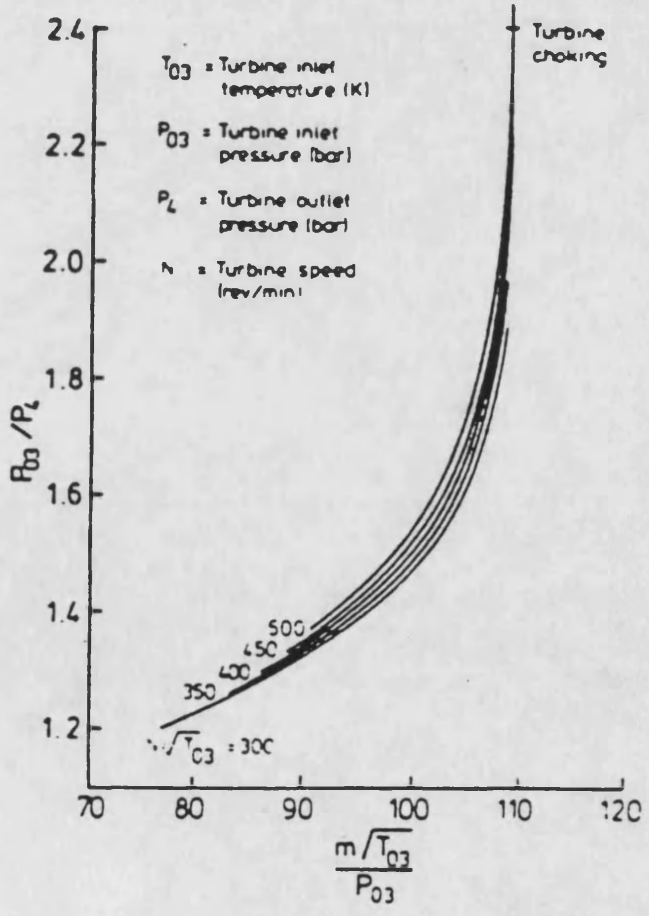

Figure 1.6- A typical axial flow turbine performance map.

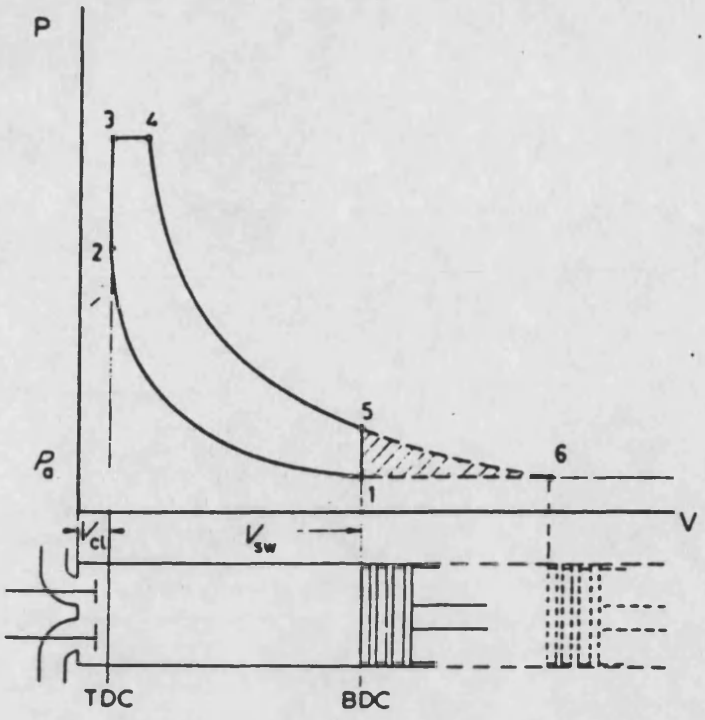

Figure 1.7- Ideal limited pressure cycle- naturally aspirated.

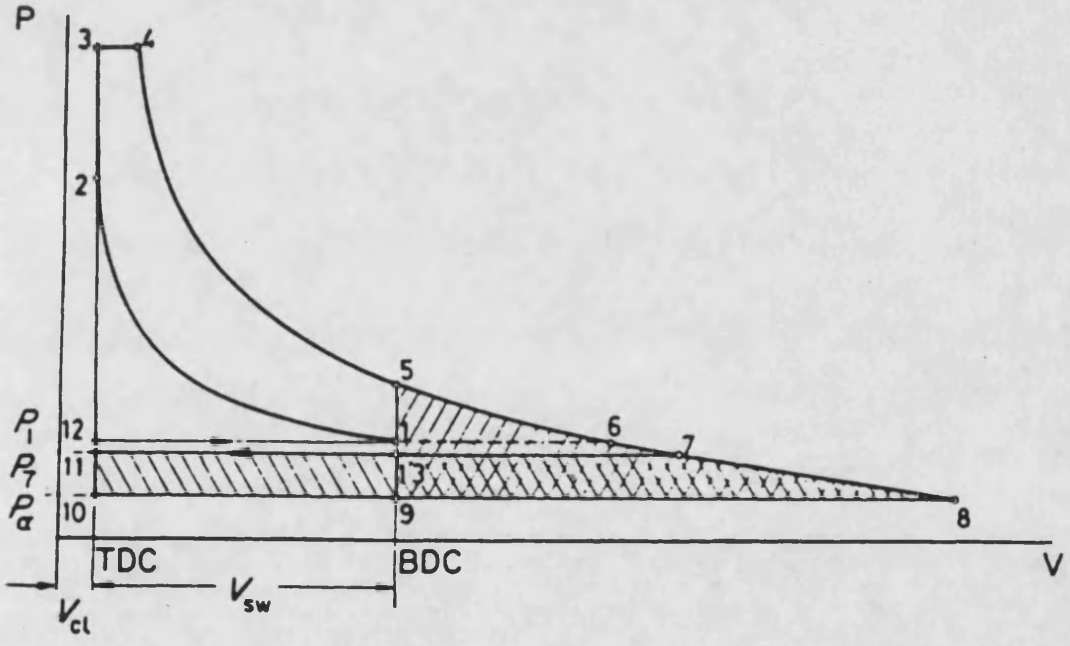

Figure 1.8- Ideal turbocharged limited pressure cycle.

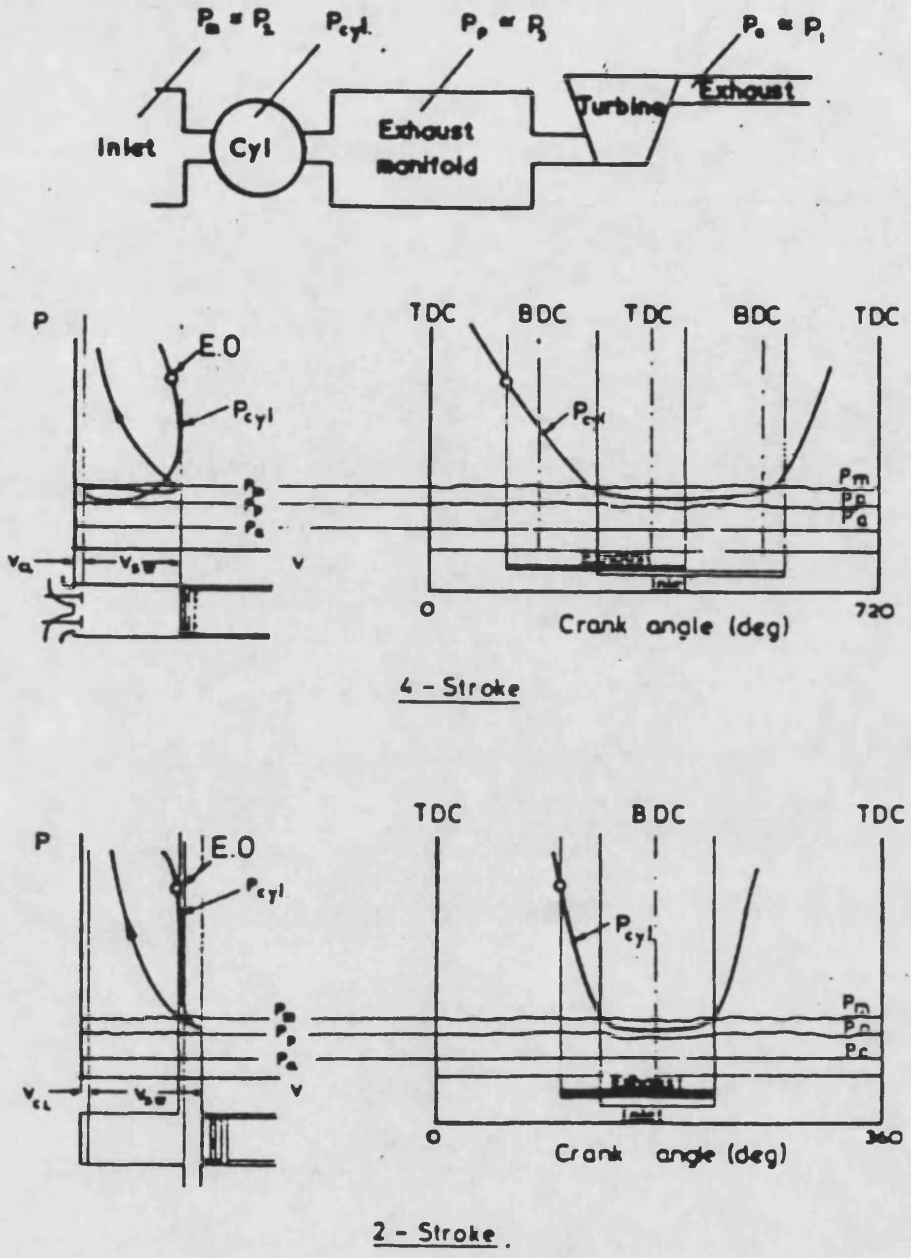

Figure 1.9- Constant pressure turbocharging system.

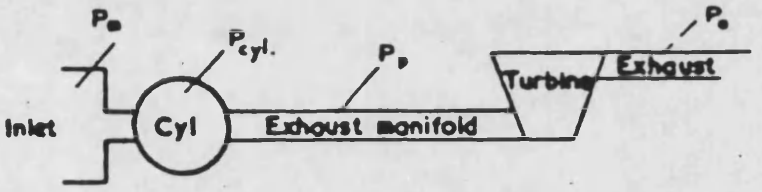

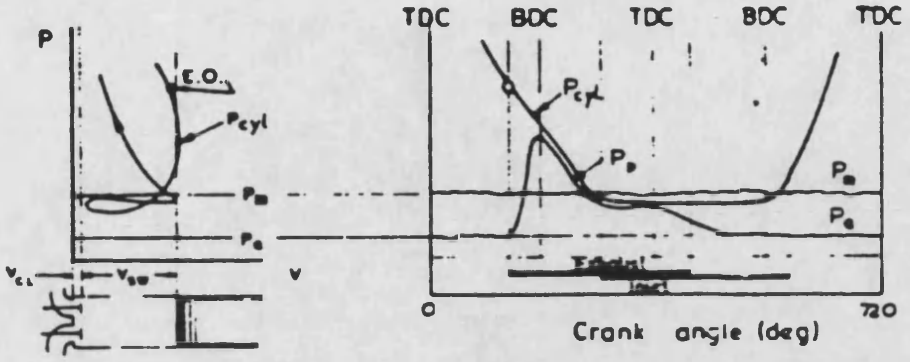

4 - STROKE

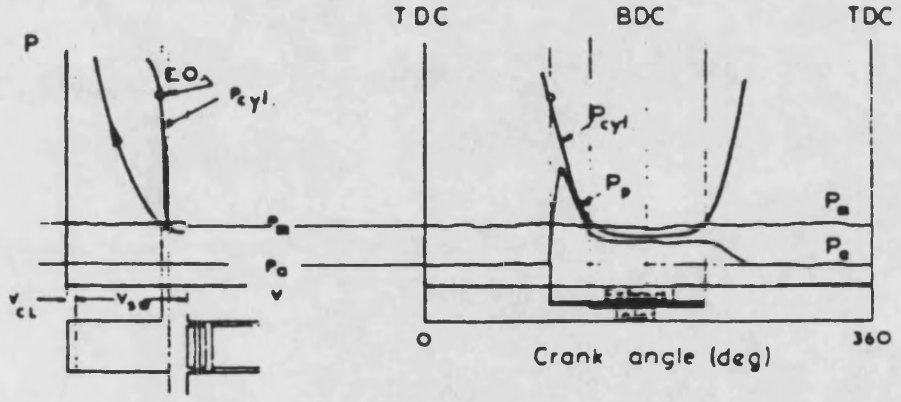

2 - STROKE

Figure 1.10- Pulse turbocharging system.

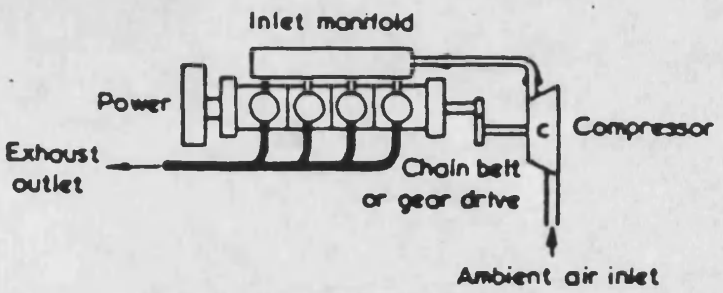

Figure 1.11- Typical arrangement of an engine fitted with a mechanically driven supercharger.

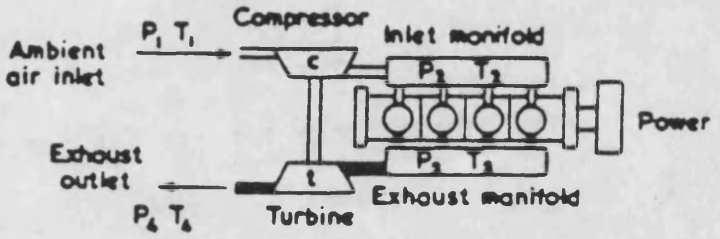

Figure 1.12- Typical arrangement of a turbocharged engine operating with the constant pressure system. The compressor and turbine form a self-contained unit: the turbocharger.

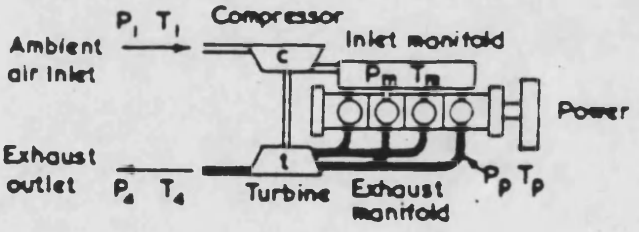

Figure 1.13- Typical arrangement of a turbocharged engine operating with the pulse system. Two-entry turbine inlet casing.

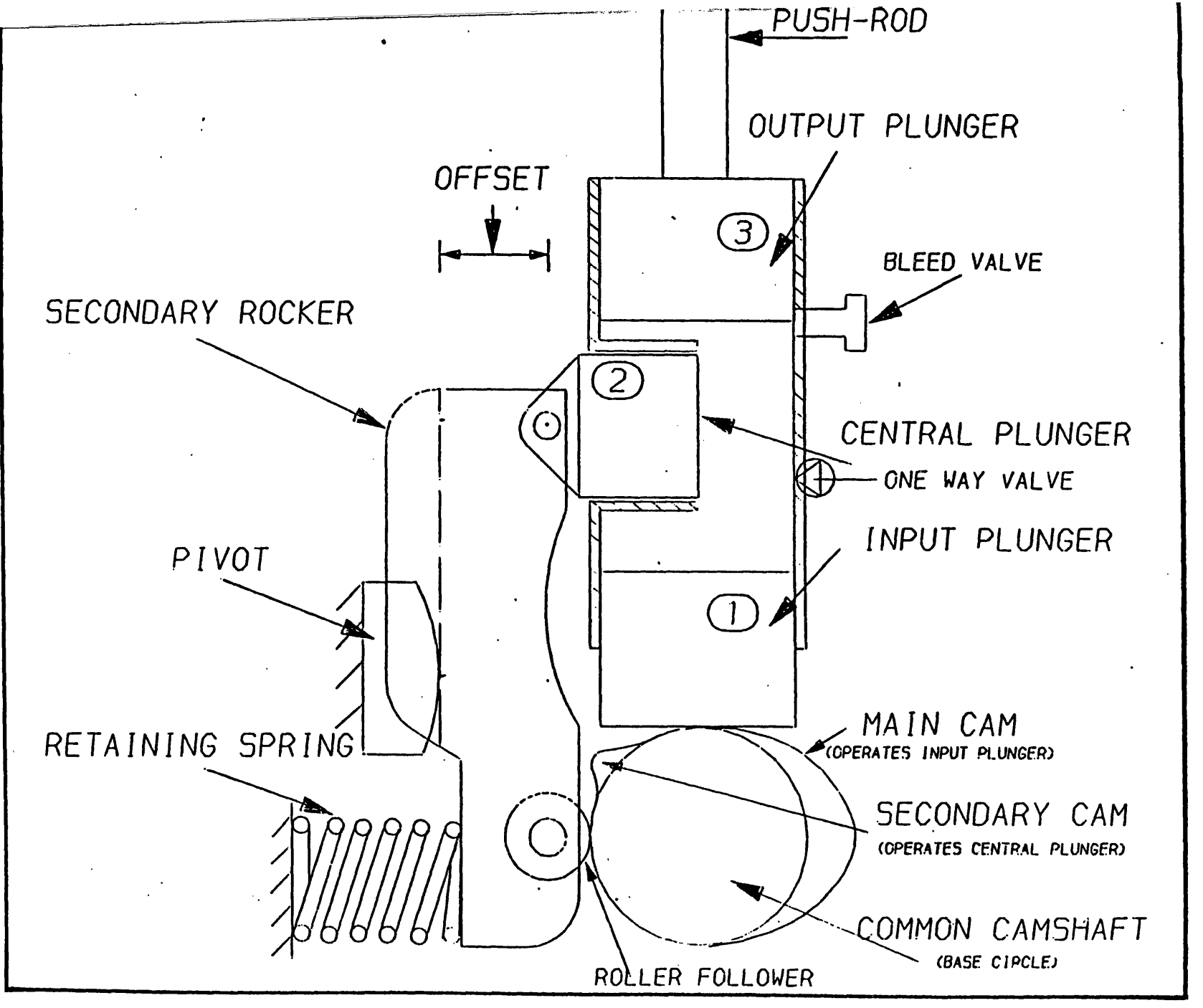

Figure 1.14- Schematic representation of the variable valve rate mechanism.

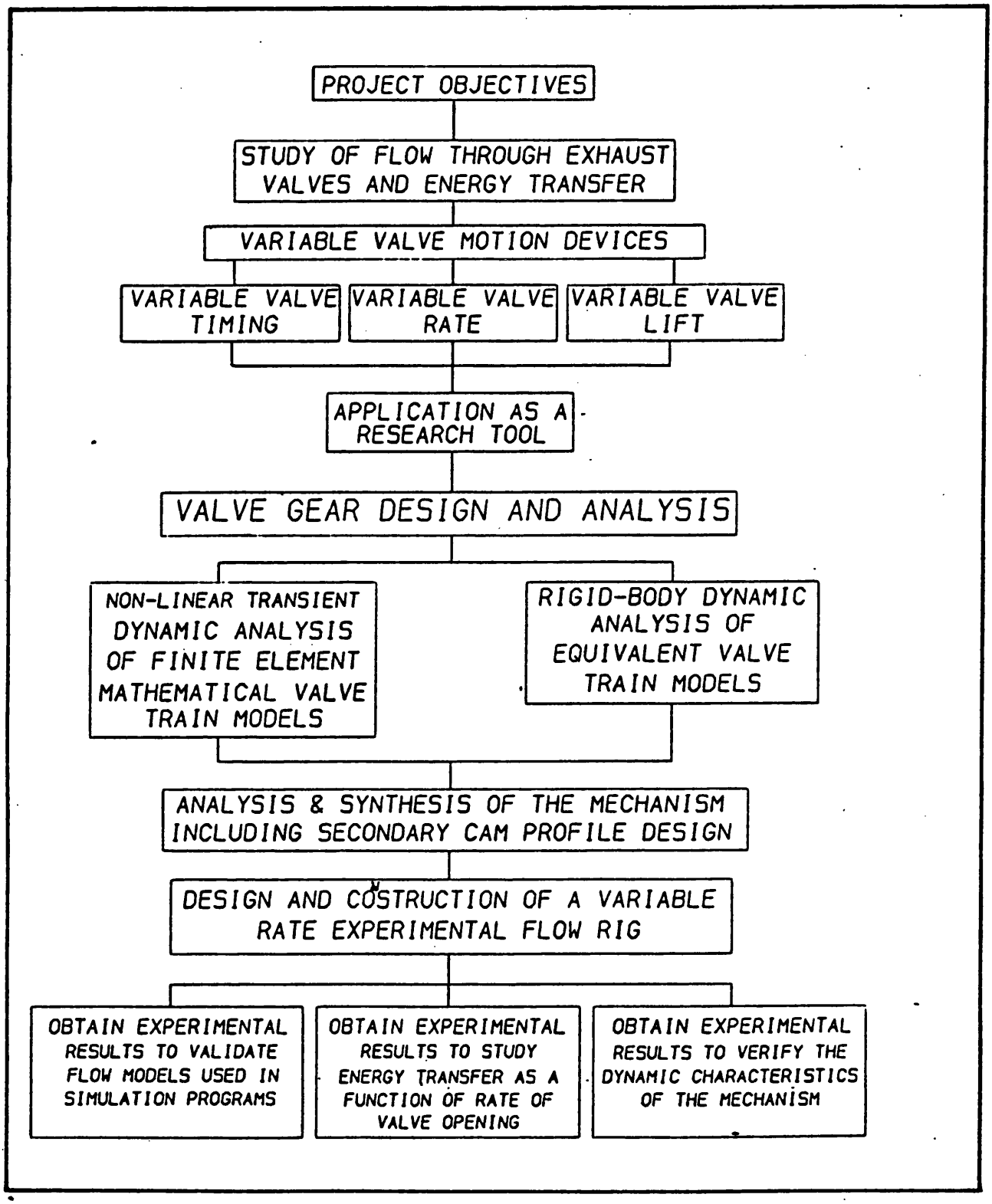

Figure 1.15- Flow diagram of the research plan.

CHAPTER 2

Literature Review

2.0 Introduction

This chapter presents a review of the published literature in the following areas:

1. pulse turbocharging,
2. variable valve motion systems,
3. valve gear design methods,
4. analysis of the unsteady flow in valve-pipe systems.

In general, the references were found by using the computerised on-line search facilities offered by the university library. Also by citation in various engineering journals and technical reports, a large number of relevant references have been discovered.

This chapter discusses the pulse turbocharging system in depth and the problems associated with energy transfer through exhaust valves are described. The energy content of exhaust pulses in the exhaust system of a turbocharged diesel engine has been considered and means by which this energy may be increased have been reviewed using a theoretical model.

The advantages of variable valve motion in general application to internal combustion engines are discussed and mechanisms to alter valve motion have been explored. The greater part of the available literature concenterates on the capability of these mechanisms to change either the timing or the lift of poppet valves used in both spark ignition and compression-ignition engines.

Valve gear design and various mathematical representations of valve trains have been discussed along with their respective analyses. Techniques adopted for a wide range of cam designs are discussed and polynomial cams are described in more detail.

Release of pressure from a cylinder to a pipe (similar to discharge of exhaust gas through the port/valve to exhaust manifold) has been reviewed. Various parameters such as pressure ratio (i.e cylinder to pipe pressure ratio), and exhaust pipe length are amongst those whose influence on the build up of a pressure pulse in the pipe have been reviewed.

2.1 Unsteady Flow In Valve-Exhaust Pipe Systems

Many theoretical and experimental investigations have been carried out (42)-(46) in order to develop methods for calculating the pressure variation in both the cylinder and inlet and exhaust manifolds of an engine. To determine the pressure conditions at entry either to the exhaust or intake

manifolds, boundary equations are required for both inflow and outflow through a poppet valve or a port.

Few suitable models have been developed for the flows in valves and ports but the pioneer theoretical work was performed by Jenny (47). Three possible boundary conditions were proposed by Jenny for flow from a cylinder to a pipe. For flow through a poppet valve he suggested the so-called 'constant pressure' model. 'Pressure drop' and 'sudden enlargement' models were also suggested for flow in port-belt systems and through nozzle into a pipe respectively.

The constant pressure model for valves was later confirmed experimentally by Woods and Khan (42) under cold conditions, and by Benson and Galloway (48) under engine conditions. The most relevant and widely used model is the constant pressure model. Therefore, only this model is considered to be appropriate to be described in the following section.

2.1.1 The Constant Pressure Model

The constant pressure model is valid for both the normal flow direction (through an exhaust valve into a pipe) and reverse flow direction (through an inlet valve into the inlet manifold). The model assumes that the gas leaves the cylinder with stagnation pressure (P_o), refer to figure 2.5, and speed of sound (a_0) and expands isentropically as it passes through the passage between the valve head and the

valve seat. The isentropic expansion is assumed to finish when the gas flow reaches its minimum cross-sectional area when the flow is subsonic in the throat, but with a fall in pressure when it is choked in the throat. With this model the momentum equation is not required and only the energy and continuity conservation equations for steady flow are used. The method of characteristics has been used to solve these equations and for a more detailed calculation and their description reference (46) should be consulted.

2.1.2 Review Of Parameters Affecting Conditions In Cylinder And Exhaust Pipe

Research carried out by Woods and Khan (42) was concerned with the gas exchange processes which occur in an engine. Tests were performed on both steady and unsteady flows within the exhaust pipework and a link between the cylinder and the pipe was established. Their main objectives were to understand the complex wave action processes and to develop methods for predicting the gas exchange processes using a computer program based on a combination of theoretical and empirical techniques.

The general theory of unsteady flow of a perfect gas in pipes is well known. Briefly it comprises of performing calculations by the method of characteristics in each pipe (49) and matching the pipe ends with appropriate boundary conditions. In order to determine the effective areas of

both inlet and exhaust valves, steady flow tests were performed. In these tests flow was from the cylinder with and without a straight pipe fitted. The effective area was determined using a constant pressure model and a static pressure measured in the straight pipe. It was inferred that the effective area was independent of the pipe length (42).

The effect of pressure ratio, that is the ratio of cylinder pressure to pipe pressure, on effective area of the exhaust valve was examined. The steady flow tests revealed that the effective area depended upon the valve lift and the pressure ratio. The effect of pressure ratio is very small. The reasons being that the effective area is independent of pressure ratio at low lifts, and at high valve lifts where it is sensitive to pressure ratio changes there was in fact very little change of pressure ratio in their dynamic tests. It may be seen in figure 2.6 that the effect of pressure ratio on the effective area of the valve may be ignored for all practical calculations.

The effect of exhaust pipe length in relation to the cylinder boundary conditions has been examined by Woods and Khan (43). In order to determine the most appropriate length to use for exhaust pipe, several lengths have been tried on the theoretical model. The corresponding effects of different exhaust pipe lengths on the pressure in the

cylinder and in the pipe adjacent to the nozzle were compared. It was found that the pressures in the cylinder all lie on the same curve corresponding to the choked flow through the exhaust valve. Towards the end of the blow down the calculated pressure in the cylinder exceeds the measured value for the short pipe and underestimates it for the long pipe. these effects are illustrated in figures 2.6, 2.7 and 2.8. The effect of pipe length on the calculation in the pipe near the nozzle reveals that the shorter the pipe length the larger the amplitude of the pressure pulse commencing with an advance in phasing. This is one of their major conclusions and is a very important result.

2.2 Energy Transfer in Pulse Turbocharging

In the introductory chapter methods of turbocharging were outlined. In pulse turbocharging as exhaust gases leave the cylinder for the exhaust manifold through the exhaust valve, pressure and velocity fluctuations are generated in individual exhaust pipes of comparatively small diameter. Exhaust gases normally flow into a common pipe from a number of cylinders with suitable timing intervals. The exhaust energy is transported to the turbine mainly in the form of pressure energy, so that there is a back pressure of varying magnitude, which affects the exhaust work done by the piston. The kinetic energy is only a small portion of the total energy, nevertheless it is important since the pulse system seeks to preserve kinetic energy from the exhaust

valve unlike the constant pressure system. The flow of exhaust gases through poppet valves is very complex and has been the subject of many investigations (8)-(12). The energy potentially available for expansion through the turbocharger turbine is reduced noticeably by irreversibilities in the valve and port regardless of the type of turbocharging system.

Exhaust valve and port testing and optimisation tend to reflect the original concern, based on naturally aspirated engine design, with simply minimising the engine pumping losses. The use of traditional 'bulk' loss measuring techniques are primarily concerned with the fluid dynamics and tend to ignore the thermodynamics of the flow. A number of attempts have been made at energy analyses, but these have tended to concentrate on the cylinder or manifold, in isolation (9),(11)-(15). An energy analysis of the exhaust gas exchange process from the engine cylinder to atmosphere (8) reveals that up to half of the available exhaust gas energy is made unavailable to the turbocharger by the valve, port and pipe. This loss in useful energy is largely a consequence of turbulent mixing via vortex shedding, the loss in availabe energy is shown in figure 2.1. The later part of the exhaust process is subsonic, however, most of the loss occurs in the first 80 degrees of the exhaust period when the flow at the valve throat is sonic or just subsonic (16), a full description of these

processes is given in 2.1.2. One conclusion from this analysis is that the velocity gradients and turbulence intensity of the exhaust gas flow through the valve are reduced at high valve lift. This supports the well-known requirement to open the exhaust valve rapidly for optimum energy transfer to the turbocharger turbine. Oldfield (16) found that energy transfer through the valve was not significantly affected by the geometry of the valve and port within a realistic range.

2.2.1 Problems at Low Engine Speeds

When a turbocharged engine is operated at low engine speed the pressure in the exhaust manifold is small because the mass flow through the engine and turbine is low. Because of the characteristics of the turbine this results in less energy being available to drive the compressor at low engine speeds. Therefore the turbocharger compressor is not capable of developing sufficient boost to meet the needs of the engine. Two requirements for increased low speed boost are as follows:

(i) increased torque back-up to improve driveability,

(ii) utilization of available exhaust gas energy which will improve overall engine efficiency.

The torque curve of a naturally aspirated engine is directly related to the volumetric efficiency and fuelling curves. In the case of a pressure charged engine if sufficient

torque can be made available at the lower speed, the fuelling can be reduced at higher speeds so that improved torque back-up is obtained while the engine still gives adequate rated power (17).

For exhaust energy to be utilized more efficiently, the exhaust valve should open as rapidly as possible (9). The proposed mechanism may improve the low speed boost, to increase torque back-up, by means of increasing rate of exhaust valve opening. This increase in the rate of opening should be controllable to avoid damage to the valve gear at higher engine speeds.

A disadvantage of conventional turbocharging systems is their inability to produce the high boost pressure desired at low engine speeds in order to achieve good low speed engine torque without smoke. Many techniques have been tried to improve the boost provided by the turbocharger at low engine speeds, without overboosting at high speeds. Such techniques include pulse turbocharging, exhaust waste-gates, resonant intake systems (18), variable geometry turbines and compressors (19). Each of these techniques improve low speed torque but either are not effective enough or operate at the expense of performance at higher engine speeds.

Experimental variable geometry turbines have been built and tested, and have recently reached production for small scale

commercial use (20). The benefits have been shown to be significant (20,21) and alternative simple and relatively effecive systems and designs are now being developed that could be cheap, reliable and efficient (22).

2.2.2 Energy Transfer In The Form Of Pulses

It should first be thoroughly understood how exhaust gas energy is transported from the cylinder to the turbocharger turbine in order to obtain a clear insight to the problem of energy utilization in pulse turbocharging. In the pulse turbocharging system due to the small volume of the exhaust manifold, a pressure build-up will occur during the exhaust blow-down period. This results from the flow rate of gases entering the manifold through the valve exceeding that of gas escaping through the turbine. At the moment the exhaust valve starts to open, the pressure in the cylinder will be four to eight times atmospheric pressure, whereas the pressure in the exhaust manifold will be close to atmospheric. At crank position 'a' figure 2.2, a short period after valve opening, the pressure drop across the valve is above the choking (critical) pressure ratio, hence the flow in the valve throat will be sonic, process 01-1 (figure 2.2, position 'a') (4). Further expansion of the gas to the exhaust manifold pressure, P_3, occurs by sudden enlargement of the valve throat, since little or no pressure recovery occurs due to turbulent mixing. The stagnation enthalpy remains constant hence the flow from the valve

throat is shown by line 1-03 accompained by an entropy increase. Finally the gas expands through the turbine to atmospheric pressure (process 03-4), doing useful work, equivalent to Δh_t. The outflowing gas from the cylinder loses a very large part of its available energy ($\Delta h_{cyl}-\Delta h_t$) in throttling and turbulence after passing the minimum section of the exhaust valve. The throttling losses are very large if the ratio of the valve throat area to manifold cross-section area is very small and the pressure drop across the valve is very large, during the initial stages of valve opening.

Following further opening of the exhaust valve the cylinder pressure (P_{01}) falls, but the pressure in the exhaust manifold (P_3) increases. At crank position 'b' the manifold pressure increases to point 3b, reducing the throttling losses across the valve (process 1-03, figure 2.2, position 'b'). The prssure drop across the turbine (P_{03} / P_4) is now much larger than at position 'a', transferring the available energy ($h_{03}-h_{4s}$) to the turbine, which represents a much larger proportion of the available energy in the cylinder(Δh_{cyl}).

At crank position 'c' the flow through the exhaust valve is sub-sonic. The throttling loss is reduced and is equivalent to the kinetic energy $C_2^2/2 = C_1^2/2$ at entry to the exhaust manifold. With pulse operation a much larger portion of the

exhaust energy can be made available to the turbine by considerably reducing throttling losses across the exhaust valve and port. The speed at which the valve opens to its full area (steepness of the valve lift curve), and the size of the exhaust manifold, become important factors so far as energy utilization is concerned. If the exhaust valve can be made to open faster, the throttling losses become smaller during the initial period. Furthermore, the smaller the exhaust manifold, the faster the rise in manifold pressure becomes, contributing to a further reduction in throttling losses in the early stages of the blow-down period. A small exhaust manifold also causes a much more rapid fall of the manifold pressure (P_3) towards the end of the exhaust process improving scavenging and reducing pumping work in a four-stroke engine. Using narrow pipes the area increase following the valve throat is greatly reduced, keeping throttling losses to a minimum (16).

Consider again a single cylinder engine, connected to a turbine by a long narrow pipe as shown in figure 2.3. Since a large quantity of exhaust energy becomes available in the form of a pressure wave, which travels along the pipe to the turbine at sonic velocity, the conditions at the exhaust valve and turbine are not the same at a given time instant. Thus the flow processes at exhaust pipe entry (across the valve) and at the turbine end, have to be presented as shown

in figure 2.3. For simplicity, pressure reflections in the pipe are ignored.

During the first part of the exhaust process, in the period of choked flow through the valve, the gas is accelerated to sonic velocity, C_1, at the valve throat. Since the contents of the pipe are initially at rest at atmospheric pressure, sudden expansion takes place across the valve throat, process 01-1-02. However, some of the kinetic energy $C_1^2/2$ is retained as $C_1^2/2$ dependent on the valve throat area/pipe cross-section area (4). As the valve opens further (see crank position 'a') the pressure at the exhaust pipe entry rises rapidly. This is firstly because a certain time is required for the acceleration of the outgoing gases, and secondly because the gases enter the exhaust pipe from the cylinder at a higher rate (velocity C_2) than they are leaving the exhaust pipe at the turbine end (velocity C_3). The rapid pressure rise at the pipe entry is transmitted along the pipe in the form of a pressure wave travelling at sonic velocity and will arrive at the turbine displaced in time. The displacement is a function of the length of the pipe. At crank position 'b' the pressure drop across the valve is noticeably reduced due to the rapid drop in cylinder pressure (P_{01}) and the rise in pipe pressure (P_2), and also because the valve throat area/pipe area ratio has increased (4). Both effects considerably reduce throttling losses (process 01-1-02-2, figure 2.3, position 'b'). The

velocity (C_3) at the turbine end of the pipe is greater than velocity (C_2) after the valve, due to the arrival of the high pressure wave at the turbine end.

In the sub-critical flow period of blow-down, the pressure in the exhaust pipe falls at the same time as that in the cylinder, position 'c'. The velocity (C_1) at the valve throat is approximately equal to the velocity (C_2) in the pipe, since the valve is fully open. At the turbine the exhaust gas expands from P_{03} to atmospheric pressure, P_a, doing useful work in the turbine (Δh_t) along line 03-3-4.

It has been established that pulse turbocharging results in greater energy availability at the turbine. As the pressure wave travels through the pipe, it carries a large proportion of pressure energy and a small proportion of kinetic energy, which is affected by friction. The gain obtained through the use of a narrow exhaust pipe is achieved partly by reducing throttling losses at the early stages of the blow-down period and partly by preserving kinetic energy ($C_2^2/2$). Thus small-diameter exhaust pipes are essential (and, up to a point, the smaller the better) since this will preserve high gas velocity from the valve to turbine. However, if the pipes are made too narrow, viscous friction at the pipe wall will become excessive. Pipe friction will increase the pressure drop from the valve to turbine, raising the

pressure at the valve throat and hence reducing scavenge air flow and increasing piston pumping work.

In order to increase the proportion of the energy leaving the cylinder that is made available to the turbine, it is desirable to open the exhaust valve as fast as possible so that P_3 increases rapidly, as shown in figure 2.4 (9). However, valve assembly inertia forces will impose a limit to what can be achieved.

2.2.3 Energy Content Of Exhaust Pulses

Earlier in the chapter the practical importance of utilization of the energy available in exhaust gases of turbocharged internal combustion engines was established, (2.1). Attempts have been made to quantify this available energy (11,16) and expressions developed for assessing the energy content of the exhaust gas (11). The energy content of the exhaust pulse at the outlet end of the exhaust pipe is defined as the maximum work that can be performed by the gas in an ideal isentropic gas turbine.

The theoretical analysis carried out by Benson and Woods (11) was first concerned with the development of an expression for assessing the energy content of the exhaust gases and the concept of the Continuous Mean Power (CMP) was derived. The influence of wave action on the continuous

mean power was then examined by utilizing the method of characteristics. The full mathematical analysis of the thermodynamic model is given in reference (11) and in Appendix 9.

It has been concluded (11) that the instantaneous power available in the gas at the nozzle end of the exhaust pipe is a function of the nozzle-area ratio (ratio of the minimum nozzle area to exhaust pipe cross-sectional area) and the upstream pressure. The available power increases with increase in engine speed and release pressure due to the increase in upstream pressure. There is an optimum nozzle-area ratio for maximum instantaneous power and this varies with the incident-pulse pressure in the pipe at the cylinder end. The continuous mean power will vary with nozzle-area ratio, pipe length and diameter. In general, the smaller the nozzle size, pipe length and bore, the greater the available power.. There is, however, an optimum nozzle-area ratio and pipe-area ratio below which there will be a decrease in power.

2.3 Review Of Variable Valve Motion (Timing) Devices

The literature on variable valve timing mechanisms has appeared mainly within the last quarter of a century. In contrast to the large amount of work reported on the application of variable valve timing to spark ignition engines, very little work has been reported on the

application of variable valve timing to diesel engines. The most widely known work is that of R.H Miller (24) in the 1950s. This system allows the point of closure of the intake valve to be advanced or retarded in order to effectively vary compression ratio whilst not affecting expansion ratio.

Miller's variable valve timing device was later the subject of a development by Zappa and Franca (24). Their perhaps ambitious reasons for applying variable valve timing to diesel engines were:

(i) improved starting or the option of a lower compression ratio,
(ii) reduction in diesel knock,
(iii) ability to use lower quality fuels,
(iv) flattening and raising of the torque curve,
(v) improved fuel economy,
(vi) reduced emissions and better control of scavenging in turbocharged engines.

Gains from the application of variable valve timing to diesel engies are likely to be lower than those for spark ignition engines, since the speed range of diesel engines is smaller, although the load range (0-25 bar bmep) is considerably wider.

Many authors (25)-(28) claim increased power output by using variable valve timing, on spark ignition engines, on the grounds that fixed valve timing inevitably represents a compromise, since the dynamic effects that occur in the gas exchange process are a function of the engine speed and load. Thus an engine which is designed to produce maximum torque in the mid-speed range, has its valves open for a shorter period with a smaller valve overlap, than an engine designed to produce maximum torque at high speed. While the large valve overlap (45 degrees) enables full benefit to be obtained from the pulse effect at high speeds, it has a detrimental effect on the mid-speed torque and idle quality. The fuel economy will also suffer at part load since the pressure in the induction manifold is sub-atmospheric whilst the exhaust pressure is greater than atmospheric, consequently the large overlap permits the undesirable mixing of the incoming mixture and exhaust products. The problem is more severe at idling, an important operating condition in urban fuel economy cycles.

It is thus not surprising that in order to show maximum benefits, variable valve timing has most often been applied to engines with a production camshaft designed for maximum torque at a high speed. The results from Torazza (25) are typical, see figure 2.9. In general, variable valve timing enables the torque curve to be improved such that the torque at low and high speeds is increased.

Considerations in selecting a mechanism will include cost, durability and complexity. A taxonomy for variable valve timing mechanisms is shown in figure 2.11 initially prepared by Stone and Kwan (29) which has been updated to include some of the latest mechanisms too, followed by a number of schematic representations of the devices taken from the works by Stone and Kwan (29) and Bell and Howard (30), figures 2.12 to 2.23.

The principal means of providing variable valve timing are best categorized as:

(i) variable geometry cam follower system with fixed camshaft properties,
(ii) variable camshaft properties with fixed geometry cam followers,
(iii) non-cam valve actuation systems.

Titolo of Fiat (31) has developed both a variable valve timing and stroke mechanism which is currently being used on Fiat, Lancia and Ferarri V-8 engines. This mechanism employs cams having profiles which alter continuously in the axial direction to match low and high speed requirements. The controlled movement of the camshaft is rendered by a sliding servo-cylinder / governor system, figures 2.24-2.26. Titolo's continuously variable cam profile mechanism has

been installed in the Lancia 2000 engine and results in higher power, increased mean effective pressure and improved specific fuel consumption (31).

Some mechanisms aim particularly at reducing exhaust emissions and better control of scavenging in engines. Schiele of General Motors Corporation (32) began his investigation with this view in mind. The development of a variable valve timing camshaft was initiated as a potential means of controlling exhaust emissions from a spark ignition piston engine. This approach was based on the fact that valve overlap influences exhaust gas recirculation which in turn affects spark ignition engine emissions and performance.

His approach was to design a multipiece camshaft having the capability of rotating the intake cams relative to the exhaust cams. It became apparent that the camshaft would require fewer parts if it were built for use in an engine which had siamesed inlet and exhaust ports. Camshafts for these engines have the cams arranged in the following sequence: two exhaust, four intake, four exhaust, four intake and two exhaust. This allowed the camshaft to be divided into five segments, with only two intake segments carrying four intake cams each. The general design concept was developed to have the central actuating member translatable along the axis of rotation of the camshaft.

Sliding this central member in and out would have no effect on the exhaust cams, but would rotate the intake cams and shift their angular position relative to the exhaust cams. This concept is shown schematically in figure 2.27 and 2.28.

A prototype system incorporating splines to allow the intake cams to move relative to the exhaust cams, demonstrated that the device improved the engine performanced (32) and it can fit into the space now occupied by a standard camshaft. The General Motors' variable valve timing device is currently being used as a tool for further engine research and development.

The third category of variable valve timing is generally termed 'non-cam systems'. Helenoid actuators (33) are employed to simulate cam operated valves at engine speeds of up to 6000 rev/min. Helenoid actuators are fast acting solenoids with a low armature mass and short magnetic circuits, figure 2.29. The acceleration for a given stroke is constant and independent of the force required. Acting through rocker arms, this particular device produces an initial force of 1600 N increasing to 4000-5000 N. Such high forces are necessary to overcome valve stiction and inertia, valve spring forces, and gas pressure. Travel time which is constant over the engine speed range, is equal to that of a cam operating at an engine speed of 6000 rev/min. An electronic controller, responding to crankshaft angle

signals, permits all valve parameters, namely timing, open period and valve overlap to be readily adjusted whilst the engine is running to obtain optimum engine performance over the entire speed range. The Helenoid application is being used as an aid to engine research and development (figure 2.30) but ultimately once the controller has been optimised, it could be programmed to give the same performance from a production engine.

2.4 A Review Of Valve Gear Design And Analysis

Conventional valve train mechanisms consist of a cam mounted on a shaft, which is driven by the engine. The cam lobe is designed to actuate the valve train so that the valves open and close at certain designated points during the engine cycle. The motion imparted to the follower by the lobe on the cam, as the camshaft rotates, is transferred to the valve through a push rod and a rocker arm. In many cases the rocker arm also serves to magnify the motion. The valve itself is supported by springs, which provide sufficient force to maintain contact between the various valve train members and to return the valve to its seat.

2.4.1 Valve Gear Analysis

In order to study the intrinsic characteristics of a valve train mechanism, both analytically and numerically, attempts have been made to model the system (34)-(38). The mathematical models used extend from simple one mass single-

degree of freedom representations to complex multi-mass multi-degree of freedom representations, as shown in figures 2.31 and 2.32. A valve train consists of several structural members with each component contributing to the overall response. The analytical multi-mass models must, therefore, contain parameters representative of all valve train members. Accordingly, each member is idealized individually as a combination of masses, springs and dashpots at appropriate locations. Many considerations have been included in the analysis of valve train systems such as, jump and bounce as a result of clearances between elastic bodies, internal and external damping effects and correction for gas forces acting on the valve. Valve train representations adopting the multi-mass multi-degree of freedom approach have given more accurate results than single mass one-degree of freedom models (34). There is, of course, a limit to the number of masses used to represent the system beyond which the accuracy is hardly affected.

Simple single mass equivalent systems may also be analysed allowing the system to be studied at either cam or valve end. (A more detailed discription of this approach is given in chapter 3).

2.4.2 Valve Gear Cam Design

In all four-stroke internal combustion engines a cam actuated mechanism is used to achieve the valve motion. It

has been recognised that the motion of the valves of an engine have critical effects on its performance. Therefore, it is necessary to concentrate on the design of a cam whose profile actuates the engine valve motion.

Engine cam design involves the consideration of a great number of interrelated and often conflicting requirements; gas exchange, inertia forces, elemental stresses, contact stresses, acceleration, spring force reserve, wear, noise, vibration and cam manufacture. Details of most are described in the next two chapters.

Cam profile refinement has received a great deal of attention. Therefore, a number of cam design methods have been developed, including three-arc cams, tangential cams, multisine cams, polynomial cams, Fourier cams (39) and Polydyne cams (40). Each cam profile has its own virtues, such as simplicity of manufacture, smoothness of curve, lack of higher harmonics and consideration of the dynamic deflection of the valve train as typically observed in the Polydyne cams.

The elastic behaviour of the valve train under inertia forces thus being established, Dudley (35) introduced in 1947 a method of calculation whereby the desired valve motion was taken as the input. Regarding the valve train as an undamped single-degree of freedom system, figure 2.33,

the cam profile required to produce the prescribed valve motion at a given speed could be calculated. The method, dubbed Polydyne (an acronym derived from Polynomial and dynamic), was expanded by Stoddart and others (40) and aroused great interest.

In essence, the valve motion half event is defined by a polynomial of the form;

$$Y_v = Y_{max} + C_2.(a/a_r)^2 + C_p.(a/a_r)^p + C_q.(a/a_r)^q + C_r.(a/a_r)^r + C_s.(a/a_r)^s$$

where

Y_v is the valve lift,
Y_{max} is the maximum valve lift,
C_2, C_p, C_q, C_r and C_s are coeficients (constants),
a is the instantaneous cam angle,
a_r is the event range,
p, q, r and s are indices.

The procedure acknowledges the critical difference between command and response. Three principal steps mark this design method:

(i) Selection of the desired function to prevail at the end element.

(ii) Determination of those properties of the

follower system that contribute to deviation.

(iii) Development of an actual cam function that effectively counteracts the 'error' of the follower system and produces the desired motion of the end element.

The importance of numerical analysis methods for the design and construction of valve trains has been well known for many years. Suitable computer programs are commonly used to generate cam lift curves (41). The dynamic response of a valve train can be analysed by means of models separating the valve train into one or more lumped masses, ideal springs and damping elements (34).

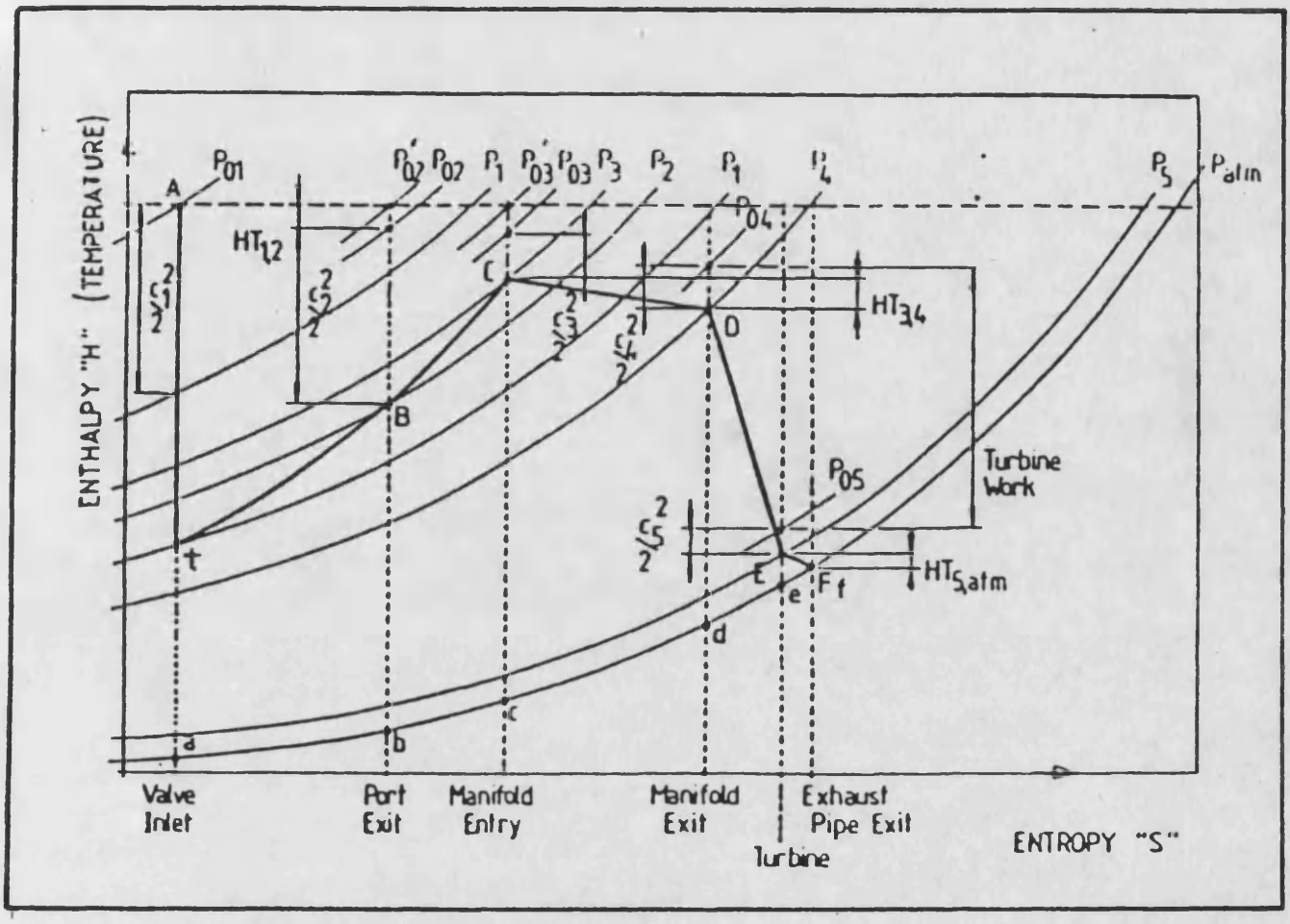

Figure 2.1- Enthalpy-Entropy diagram for an exhaust system indicating the loss in available energy.

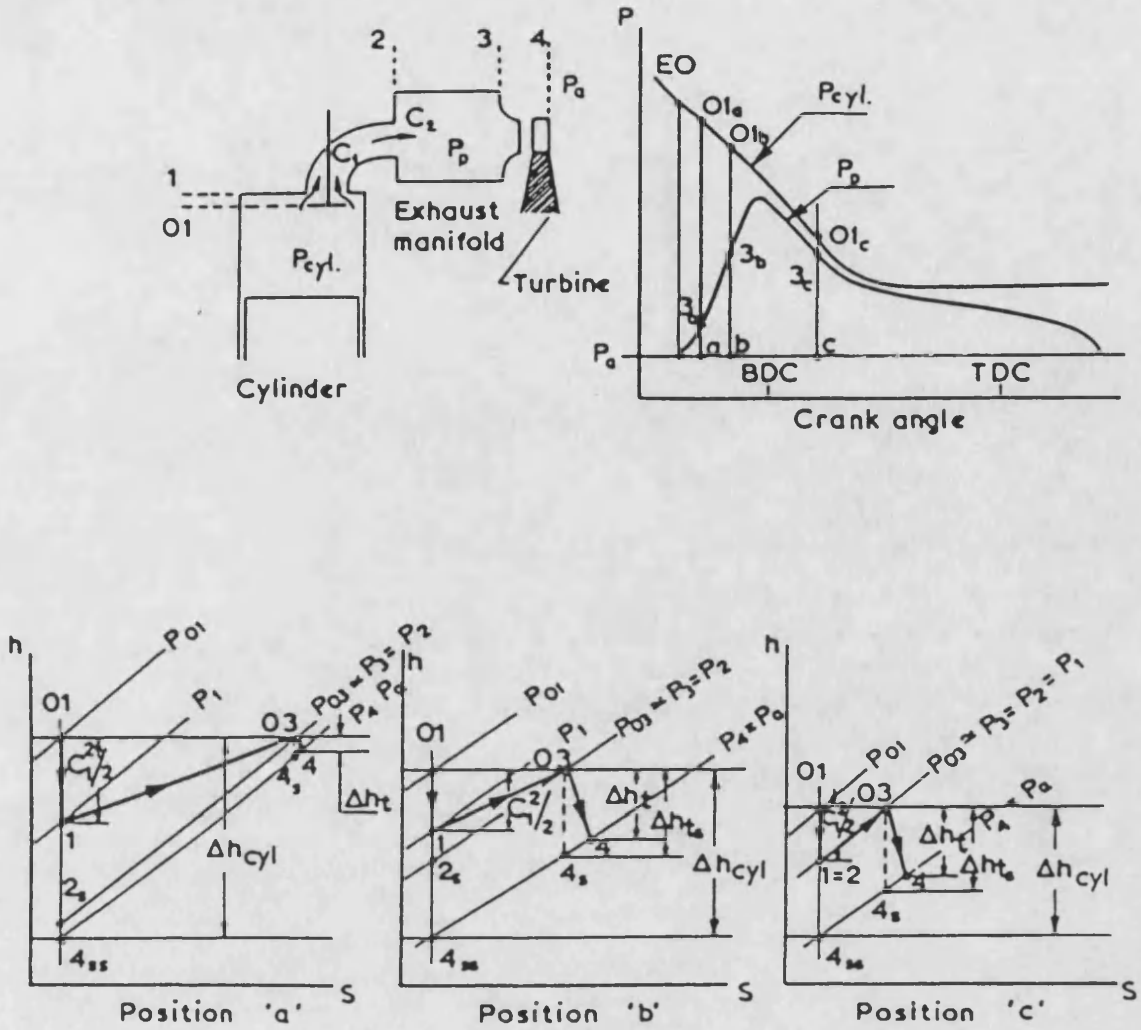

Figure 2.2- Pulse pressure turbocharging:
small exhaust manifold volume.

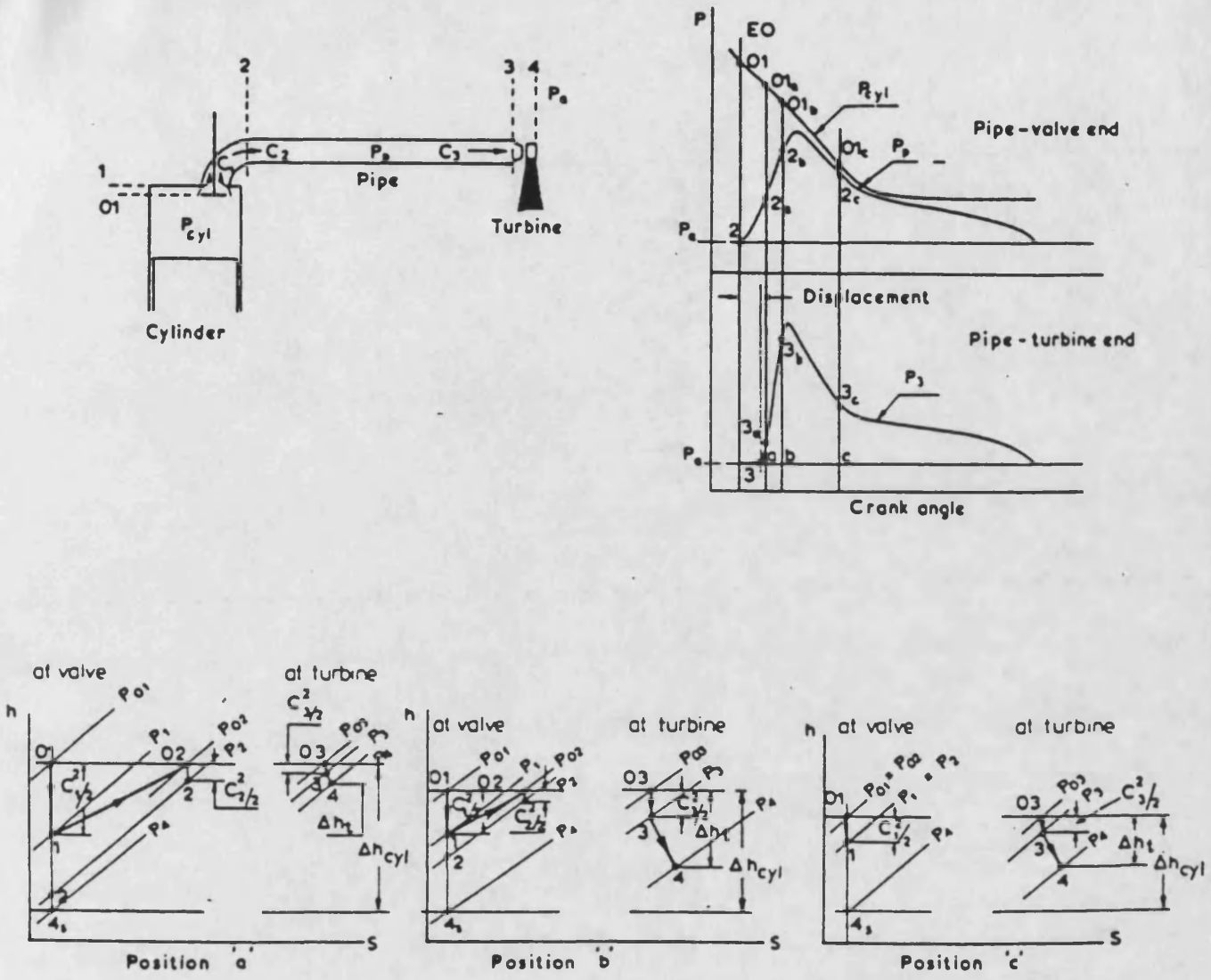

Figure 2.3- Pulse pressure turbocharging: narrow exhaust pipe.

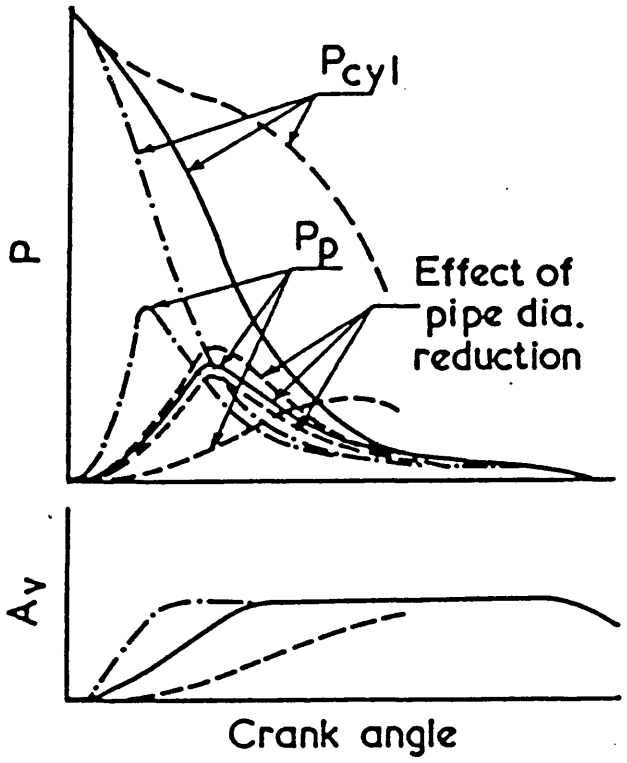

Figure 2.4- Effect of valve area time diagram and pipe diameter,(9).

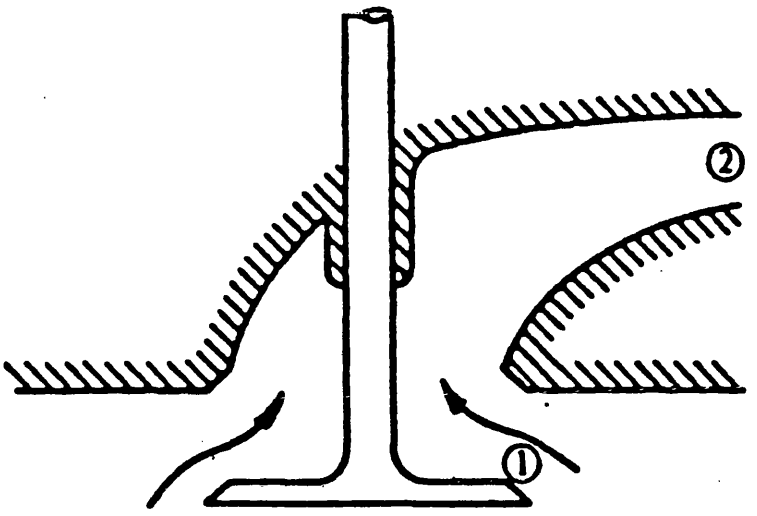

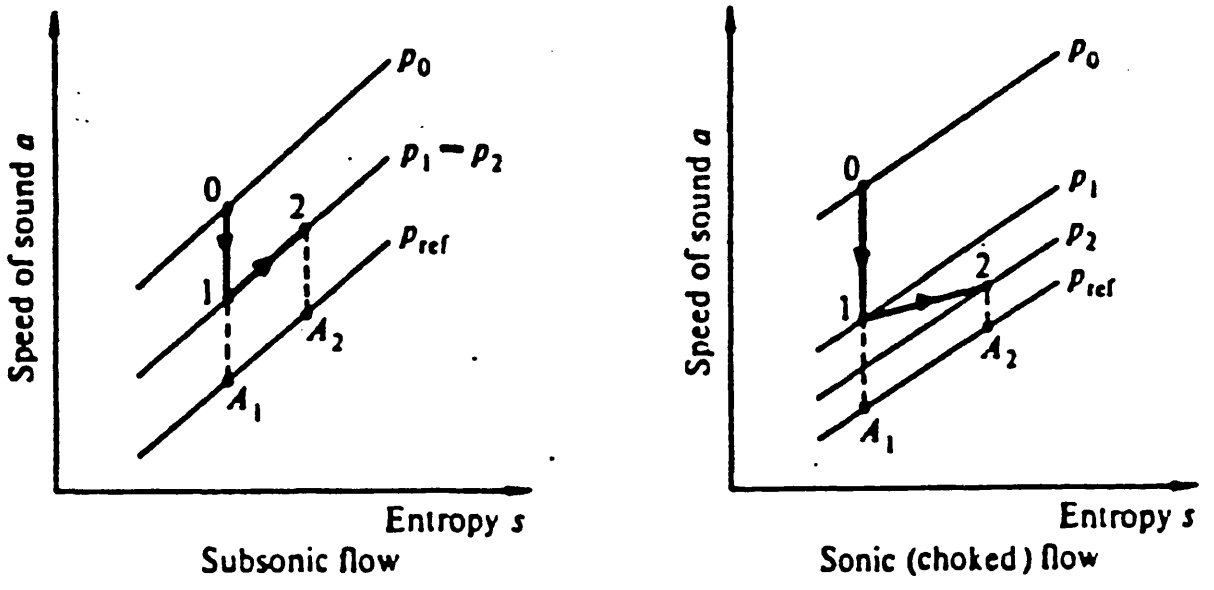

Figure 2.5- Outflow through a poppet valve-constant pressure model.

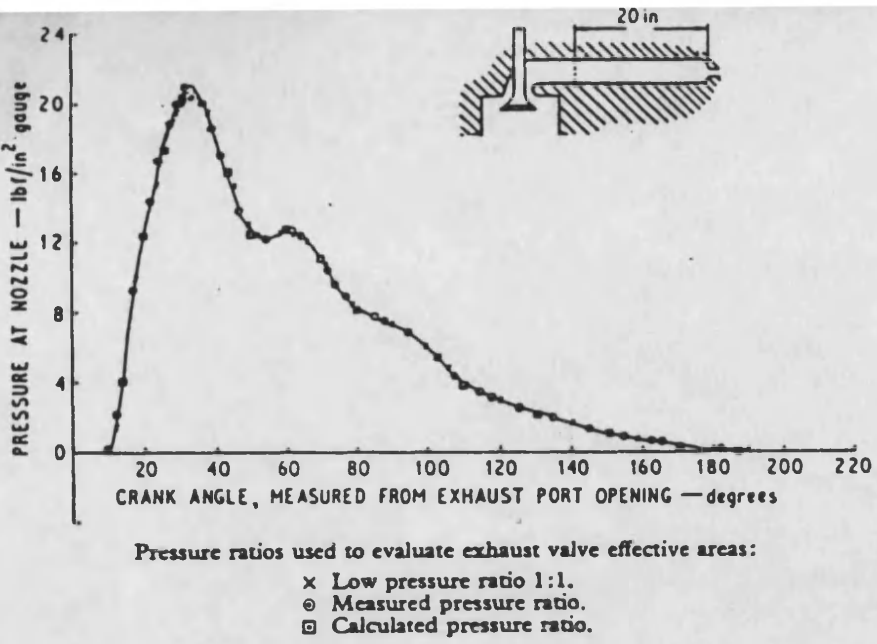

Figure 2.6- Effect of exhaust valve effective area on calculation.

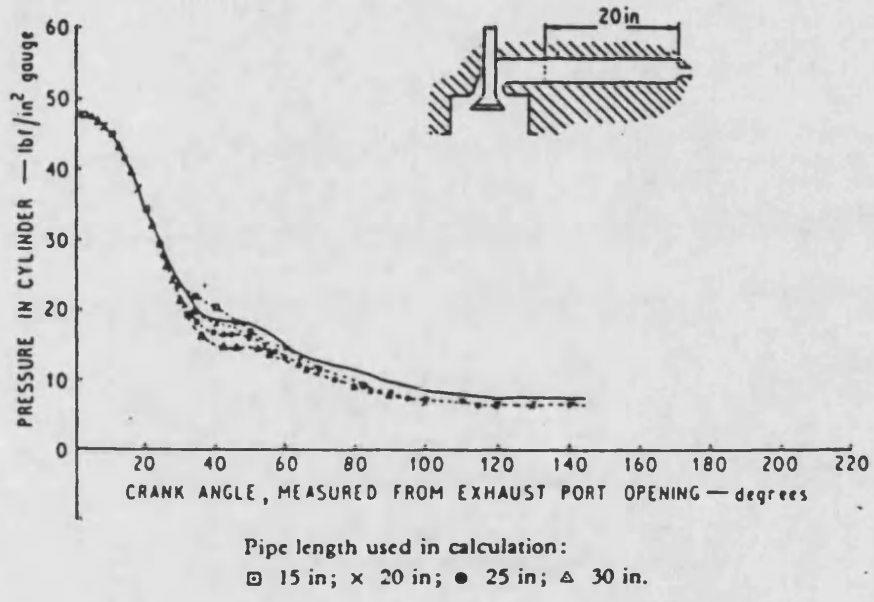

Figure 2.7- Effect of pipe length on calculation in cylinder.

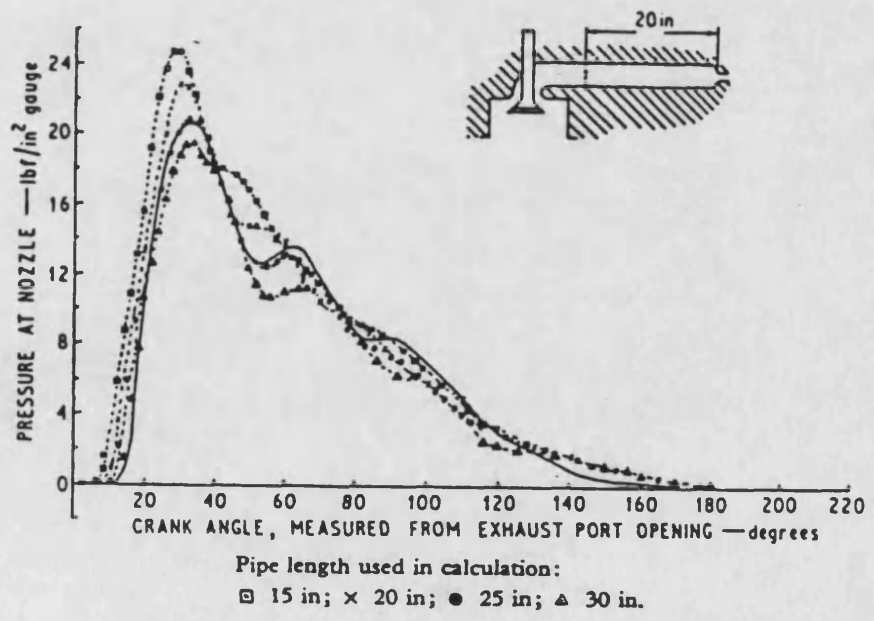

Figure 2.8- Effect of pipe length on calculation in pipe near nozzle.

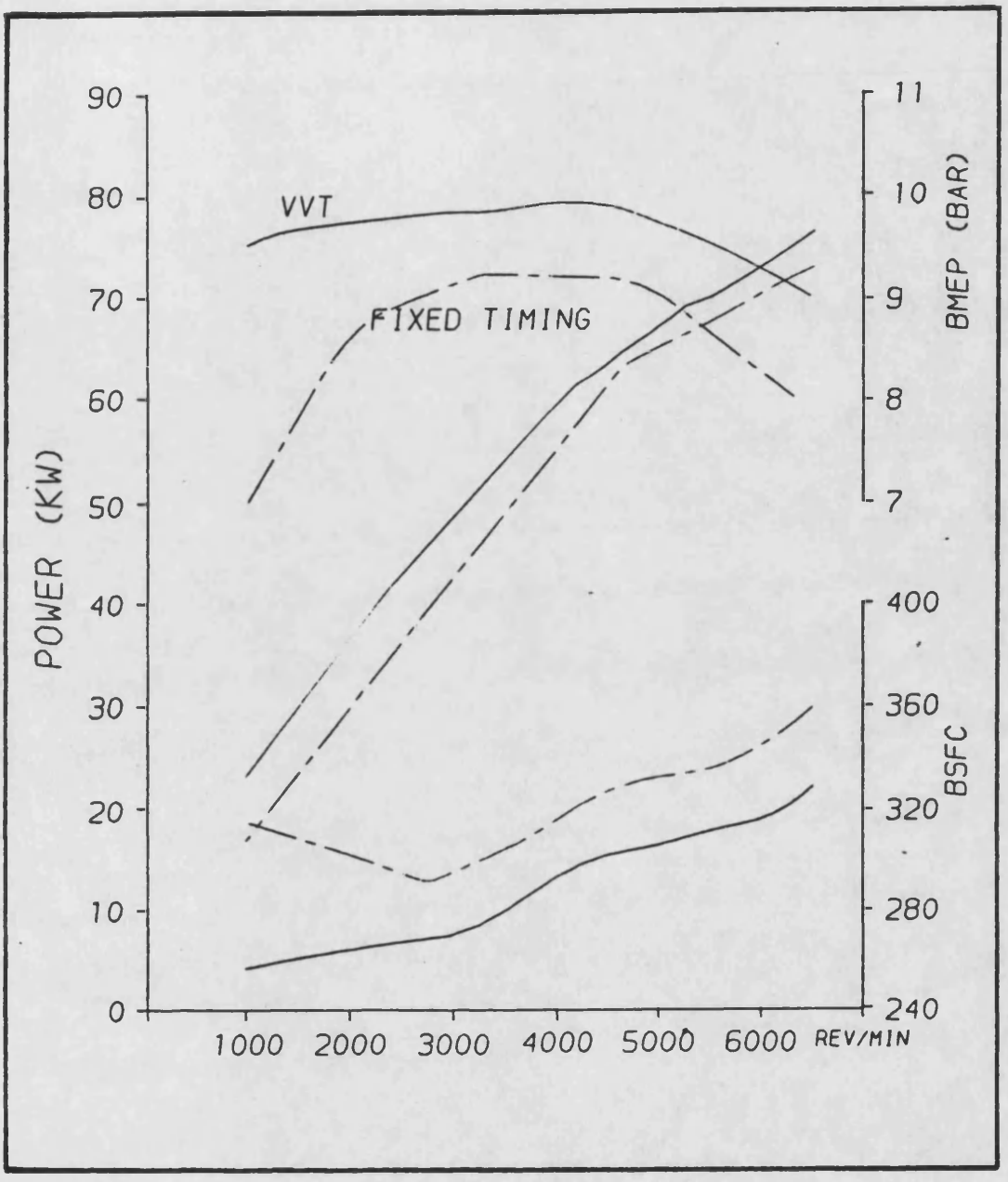

Figure 2.9- Effect of variable valve timing (VVT) on S.I. engine performance, (25).

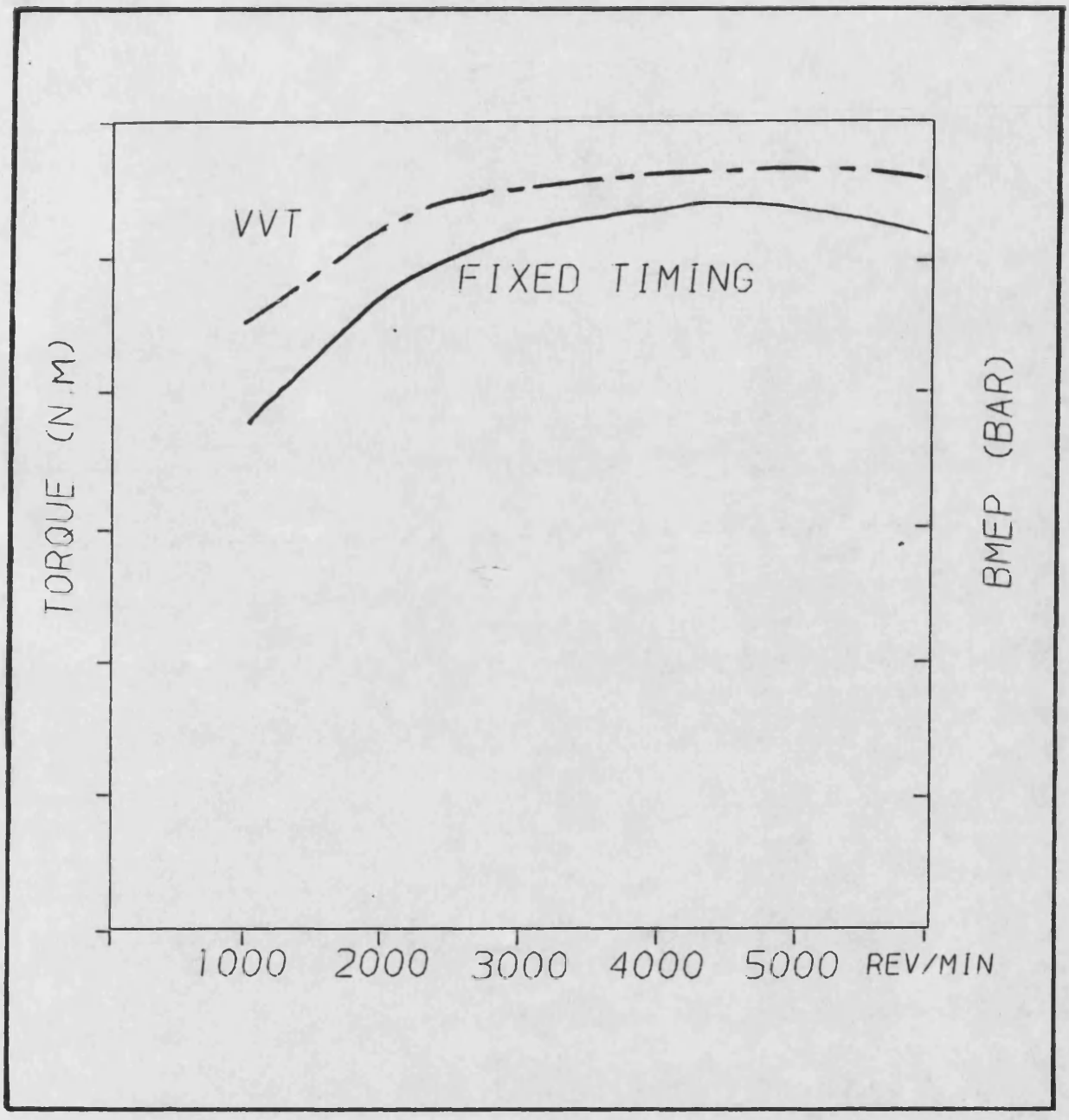

Figure 2.10- Effect of variable valve timing (VVT) on torque curve, (25).

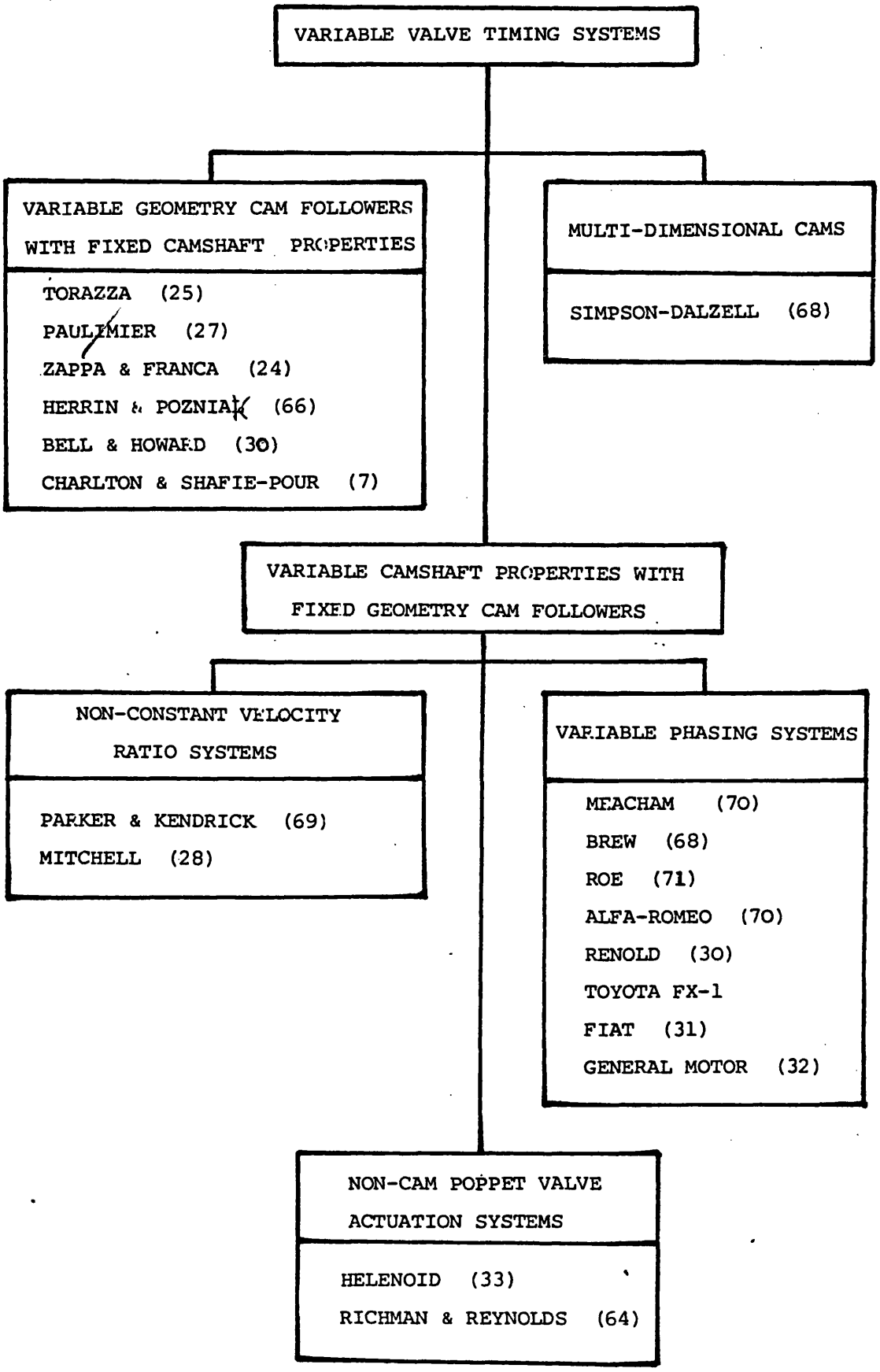

Figure 2.11 - A taxonomy of variable valve timing mechanisms.

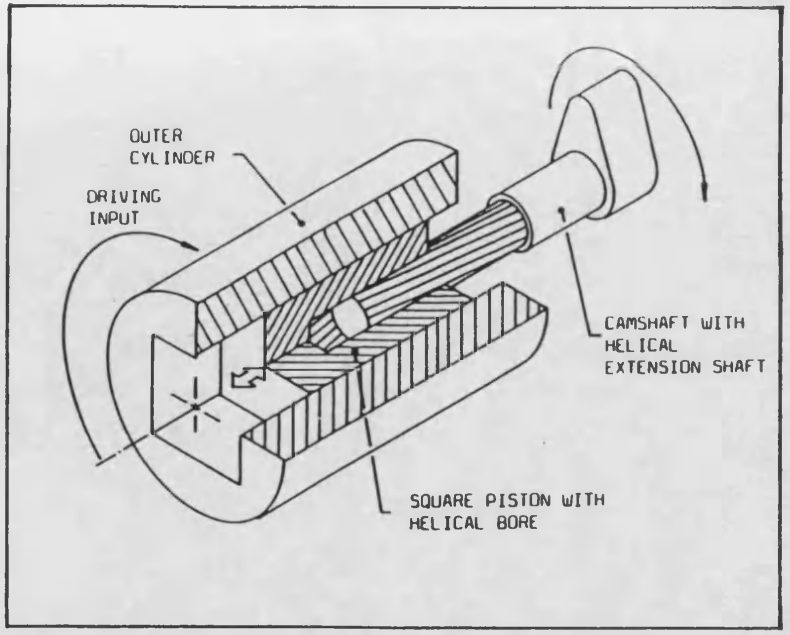

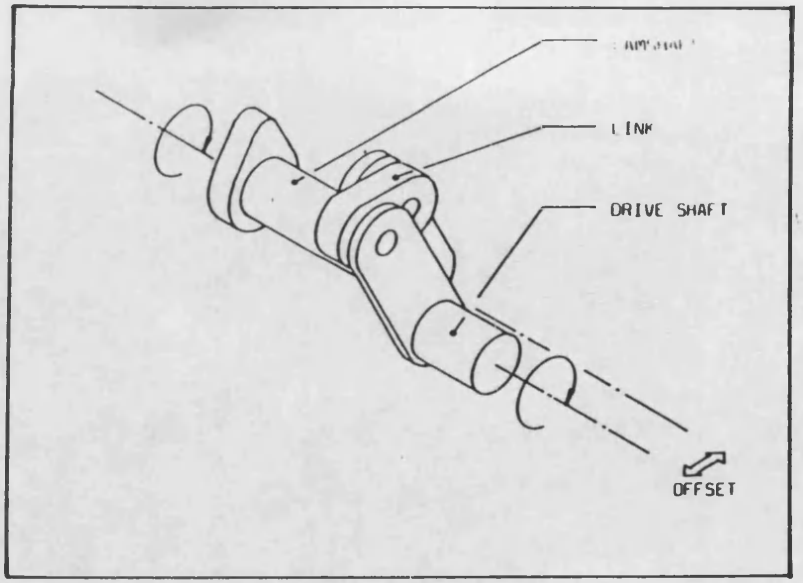

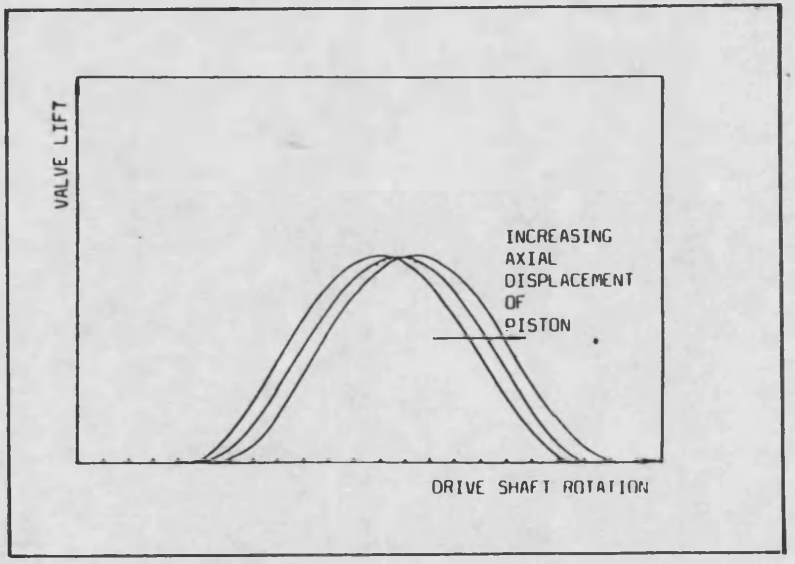

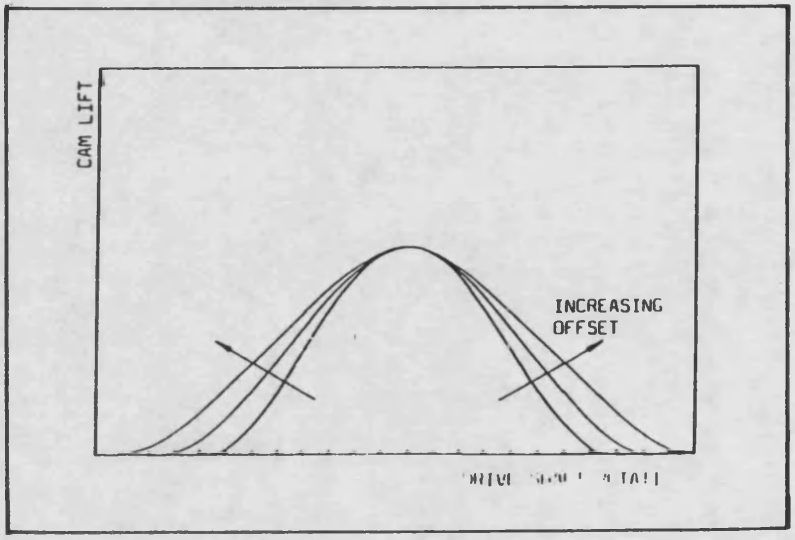

Figure 2.12- Linear to rotary actuator.

Figure 2.13- Meacham variable phasing mechanism.

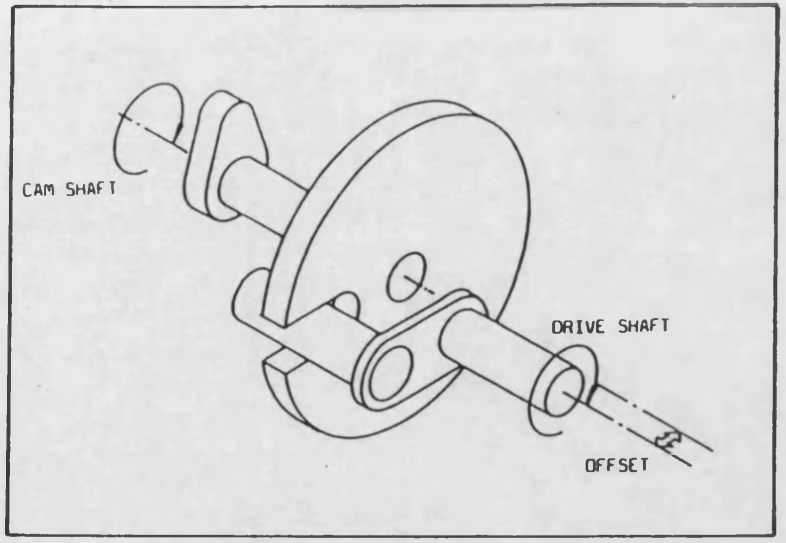

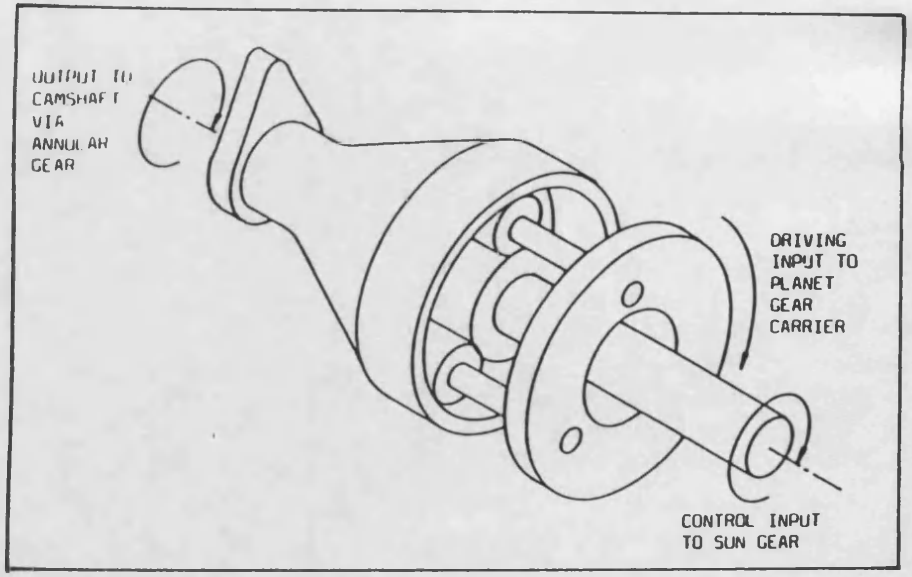

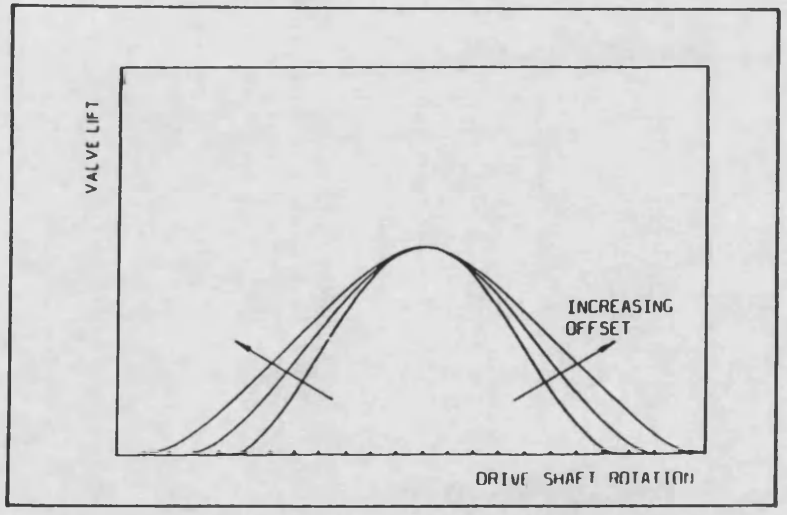

Figure 2.14- Crank-pin and slot mechanism.

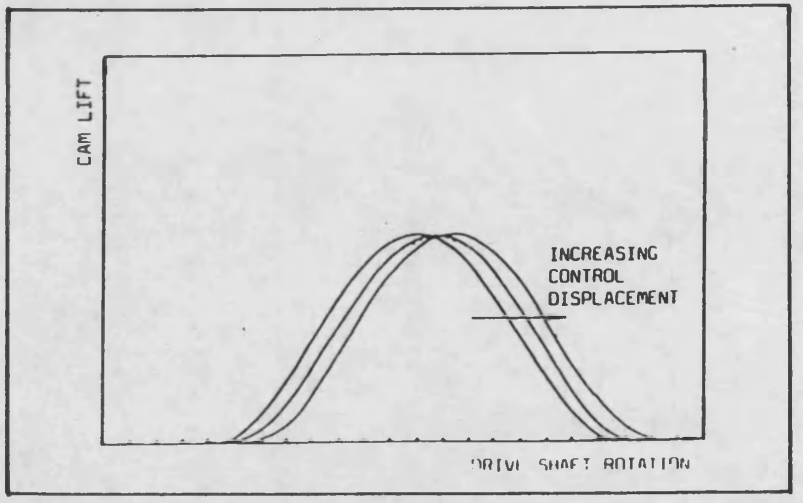

Figure 2.15 Epicyclic mechanism.

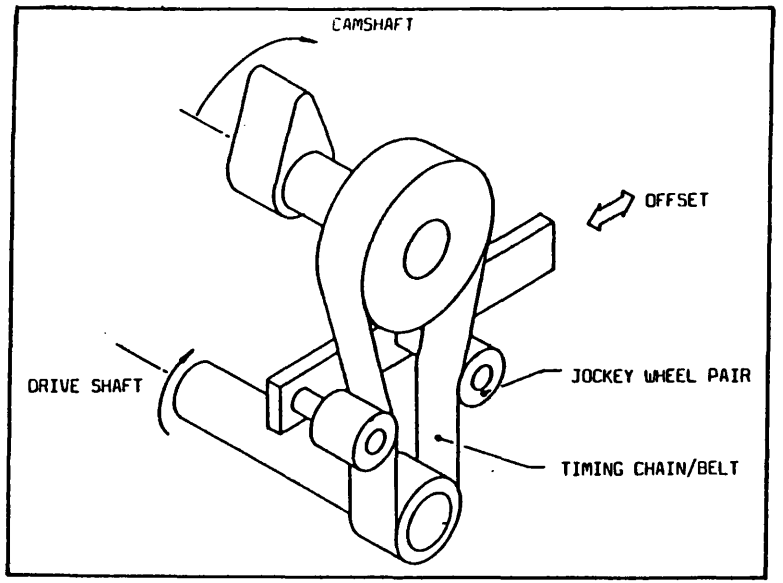

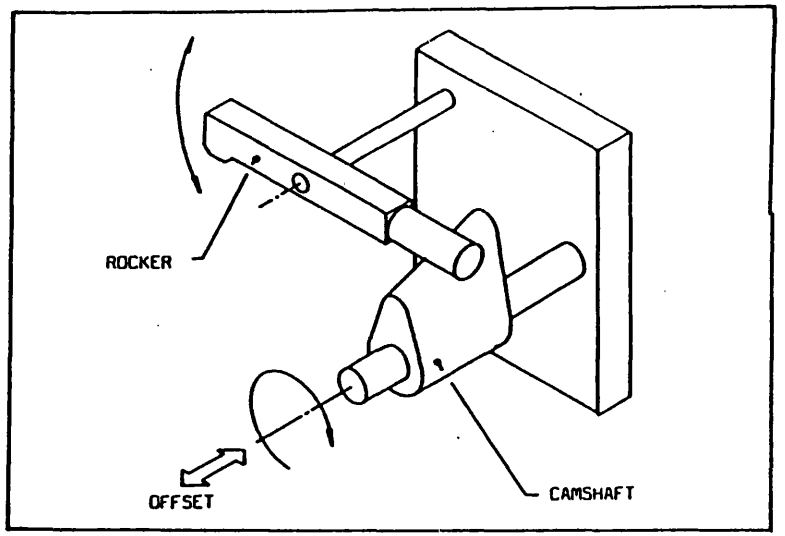

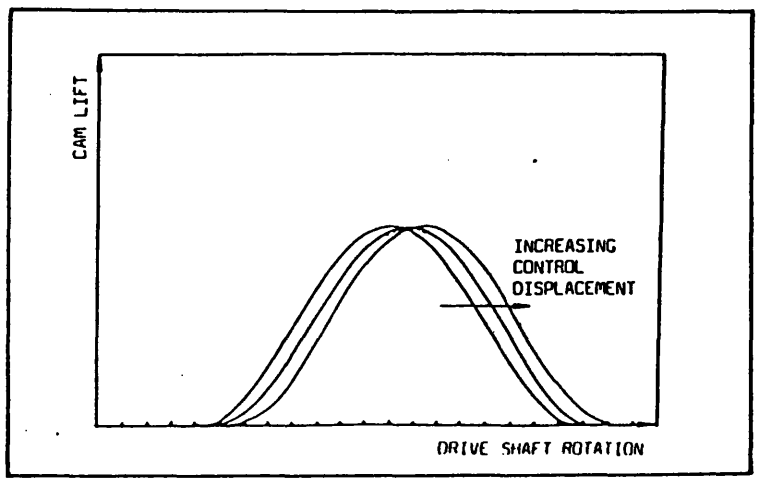

Figure 2.16- Controlled timing chain slack mechanism.

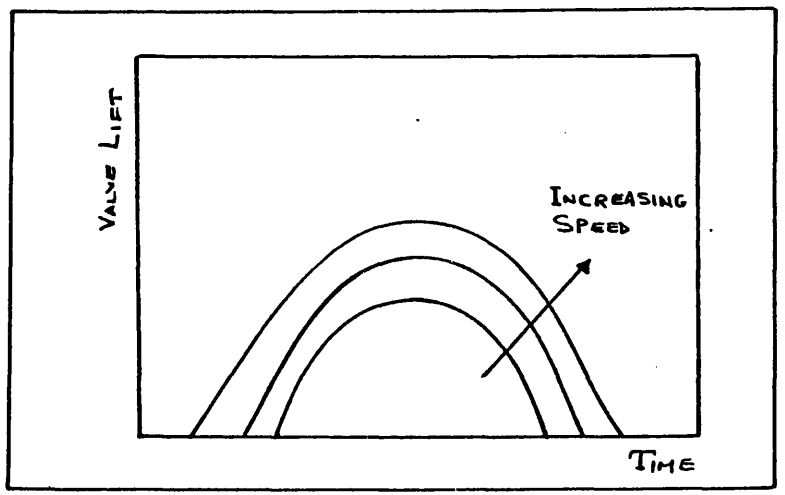

Figure 2.17- Three dimensional cam mechanism.

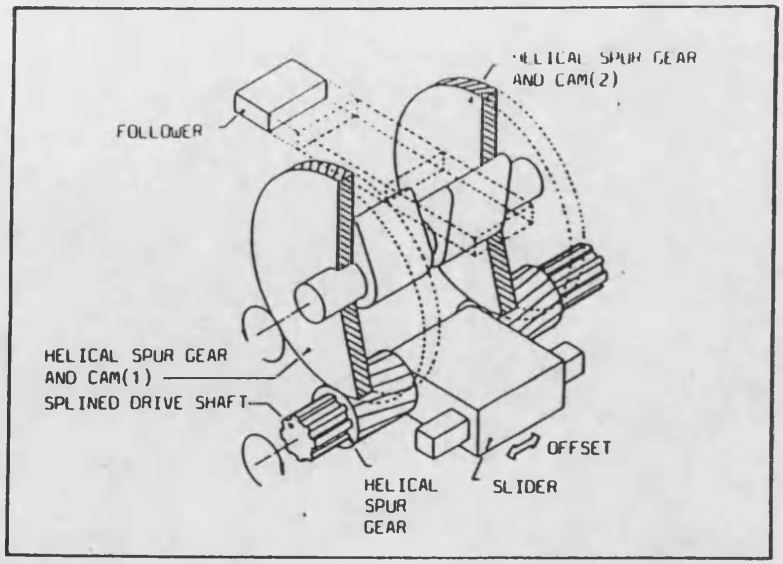

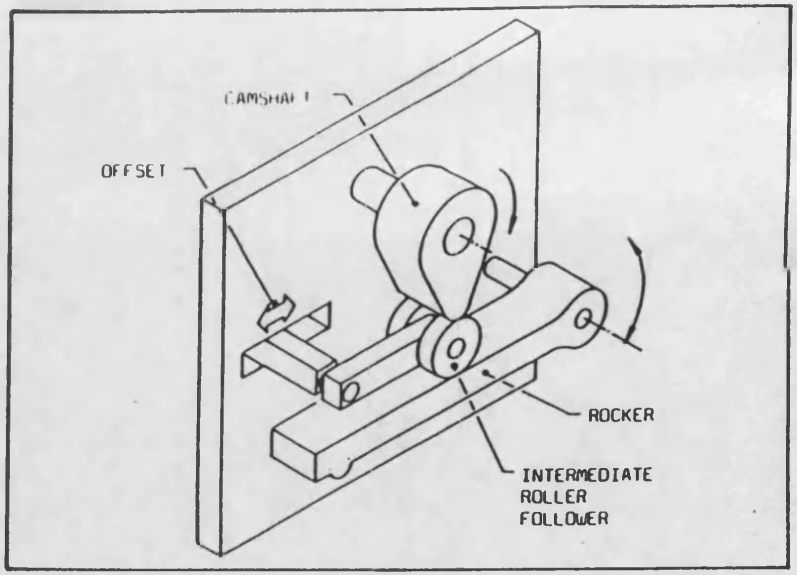

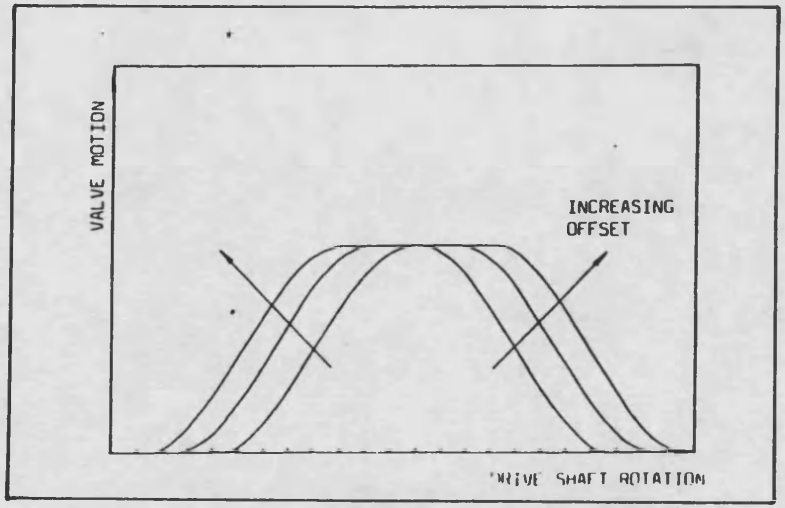

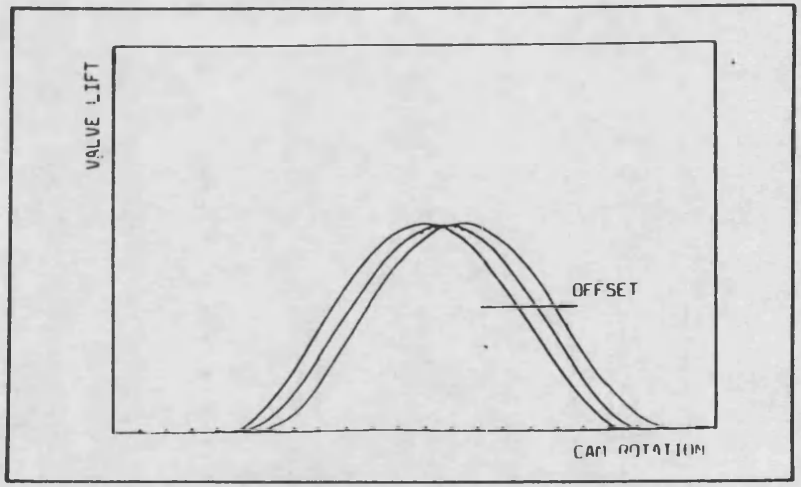

Figure 2.18- Superimposed cams mechanism.

Figure 2.19- Intermediate follower mechanism.

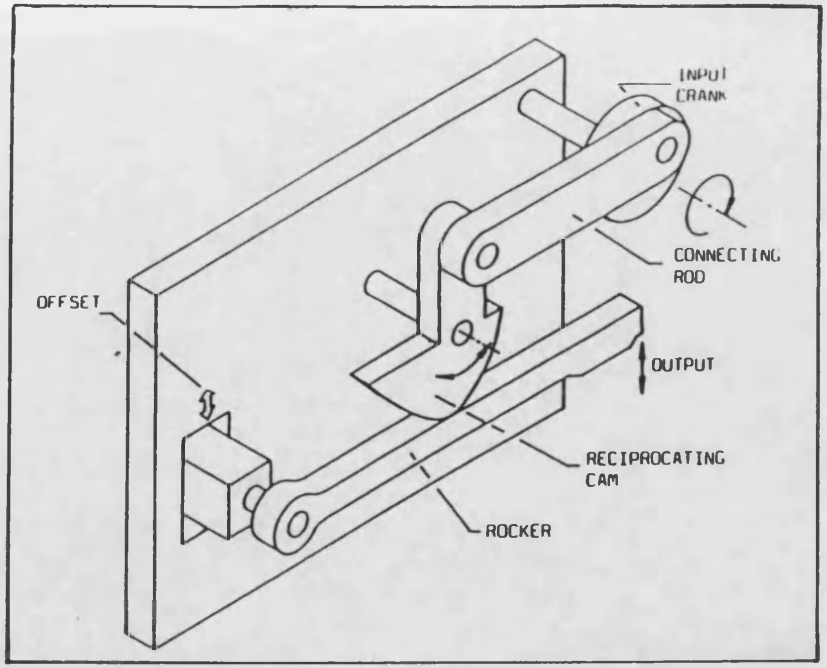

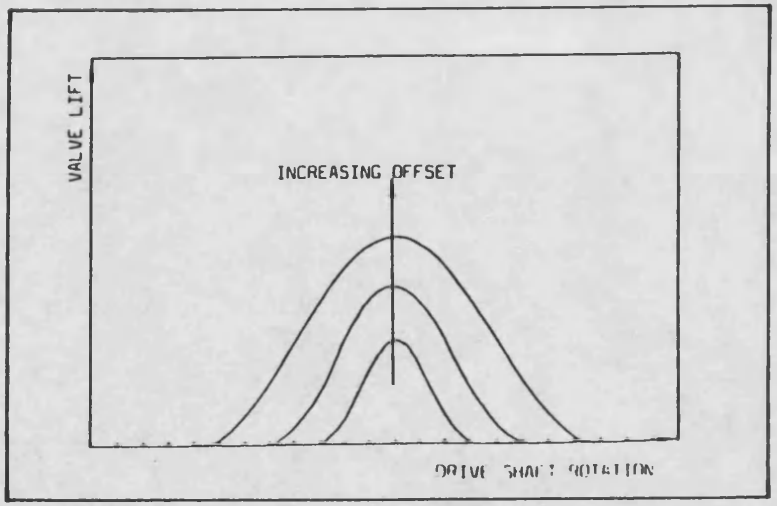

Figure 2.20- Reciprocating cam with adjustable rocker mechanism.

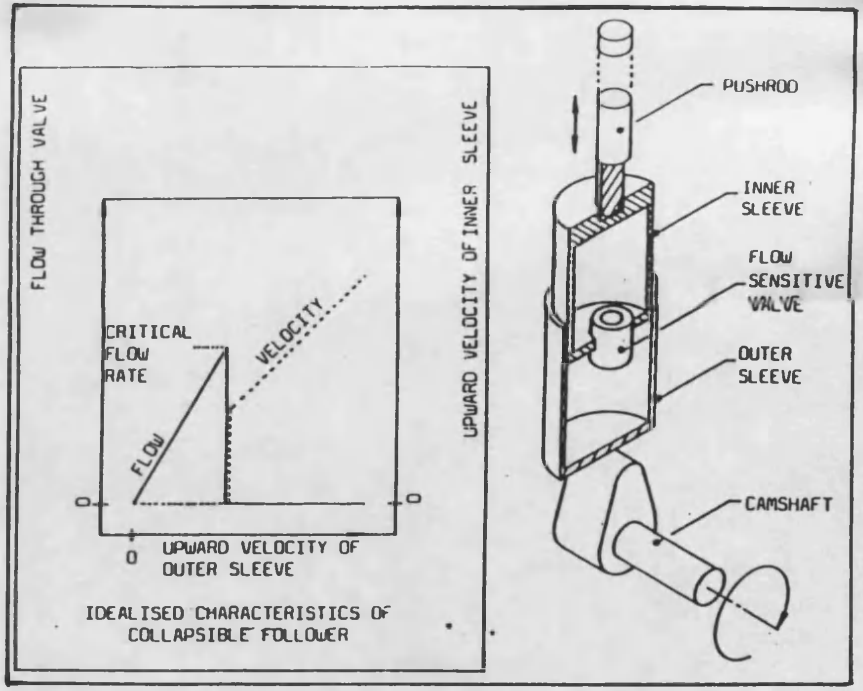

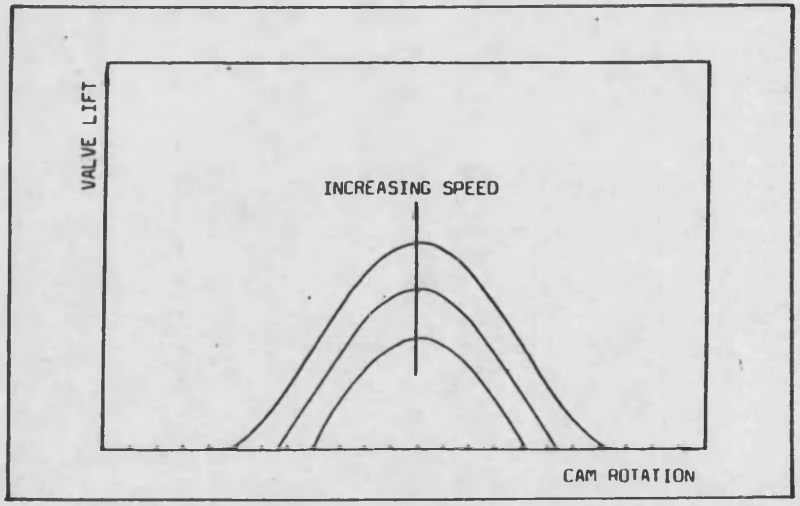

Figure 2.21- Collapsible follower mechanism.

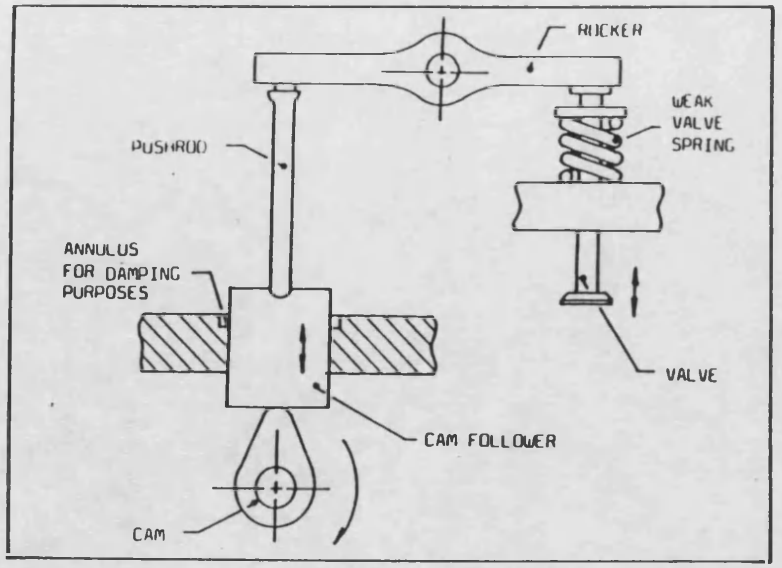

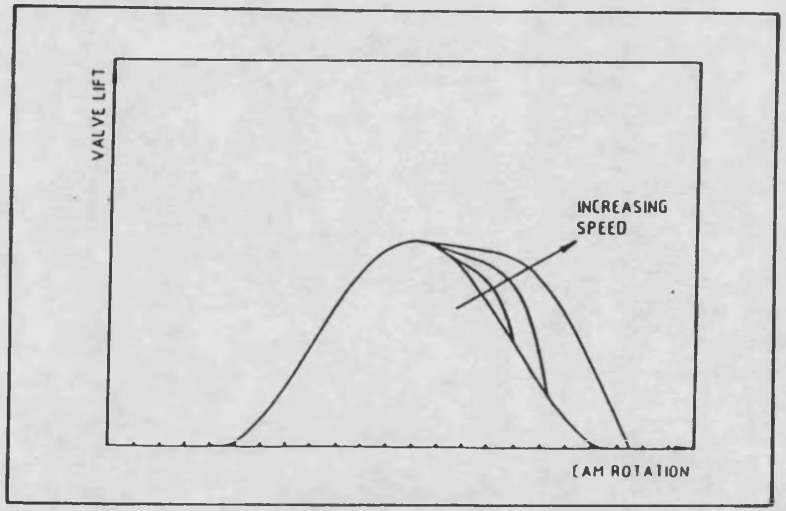

Figure 2.22- Ballistic valve mechanism.

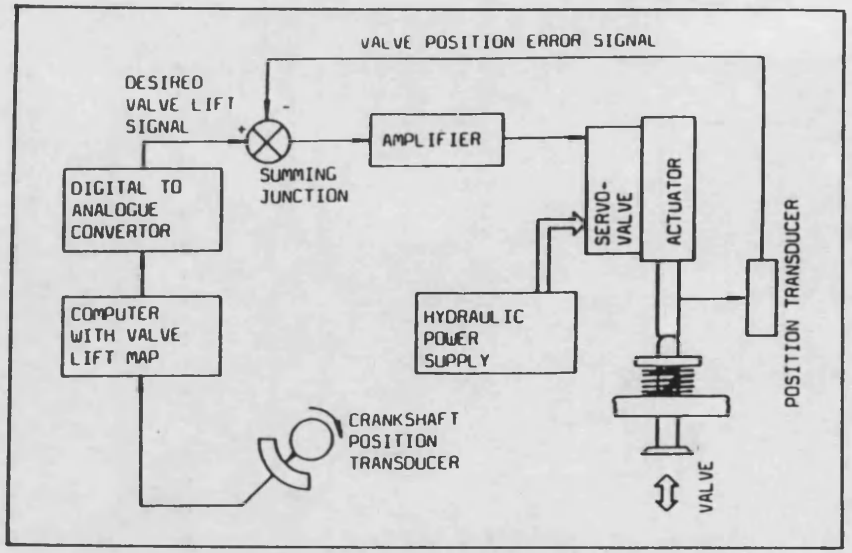

Figure 2.23- Computer controlled hydraulic actuator.

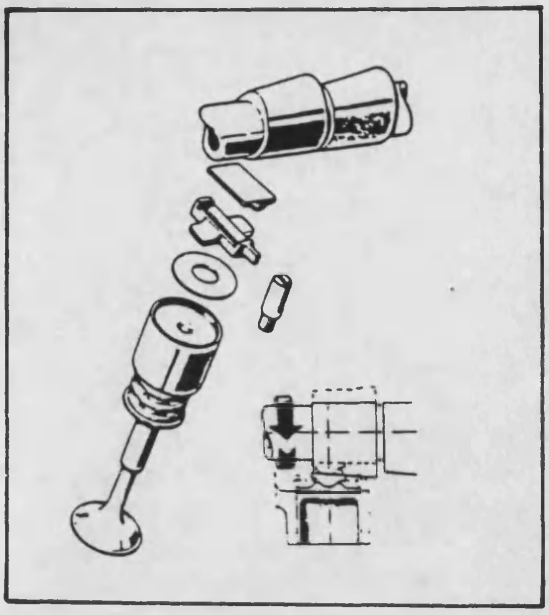

Figure 2.24- Titolo's continuously variable cam profile as used in the Fiat engines. (31).

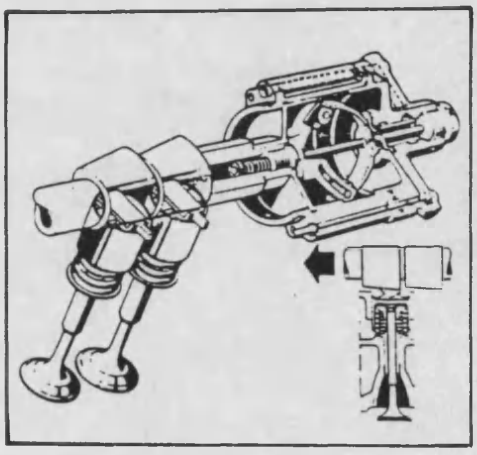

Figure 2.25- Sliding servo-cylinder/governor subgroup at low engine speed.

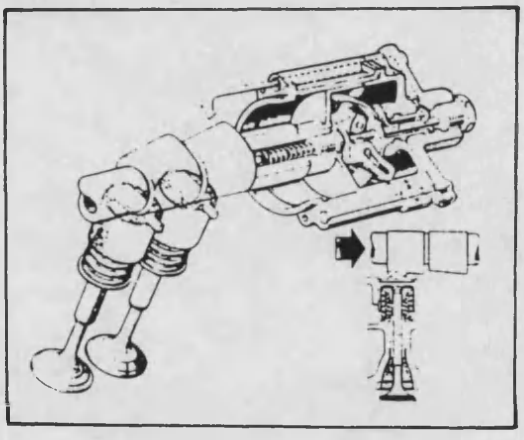

Figure 2.26- Sliding servo-cylinder/governor subgroup at high engine speed.

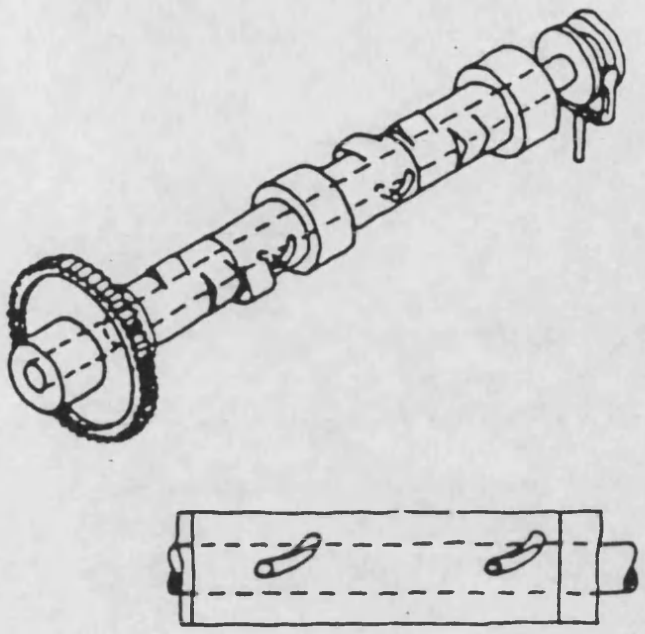

Figure 2.28- Full spline design concept, (32).

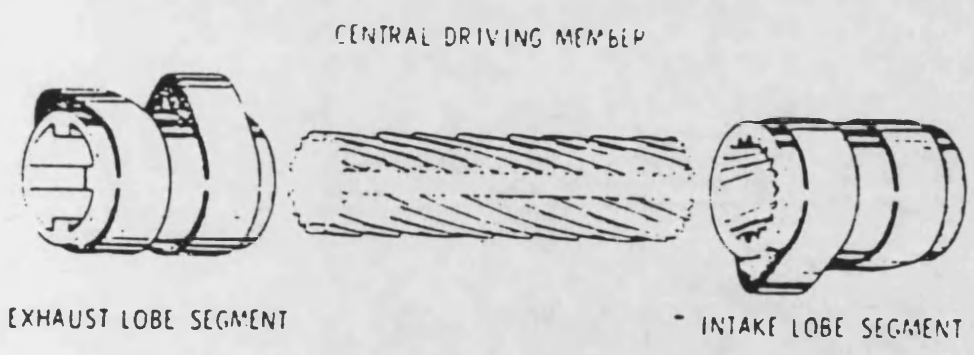

Figure 2.27- General design concept
of GM's mechanism, (32).

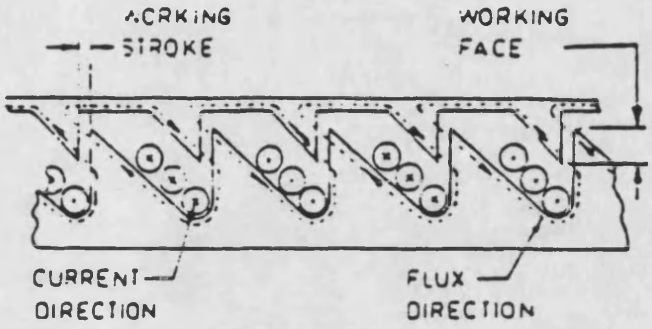

Figure 2.29- Helenoid, (33).

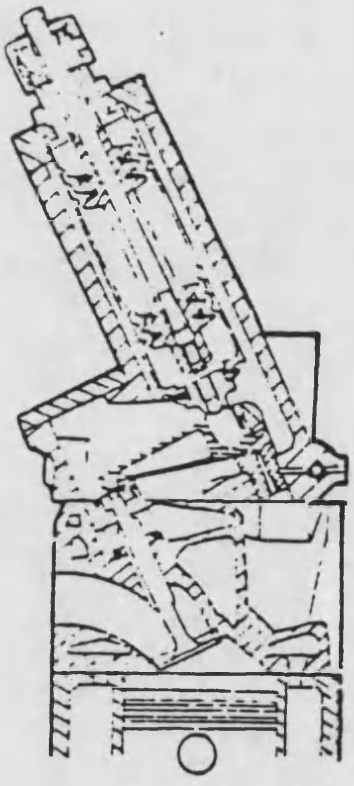

Figure 2.30- Helenoid valve actuator, (33).

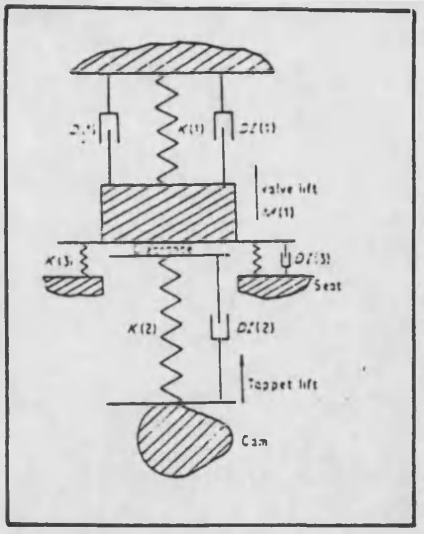

Figure 2.31- One mass simulation.

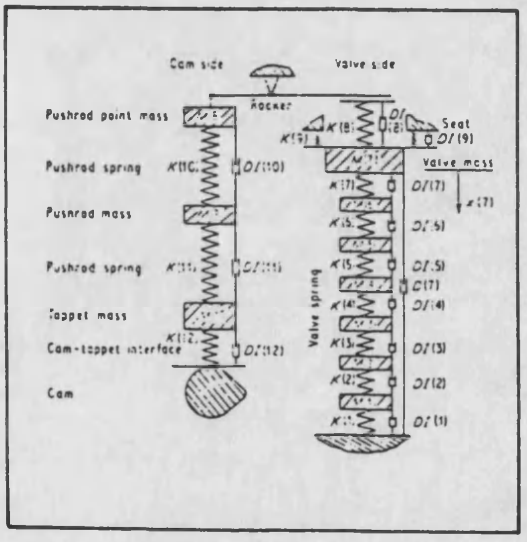

Figure 2.32- Diagram of ten mass system.

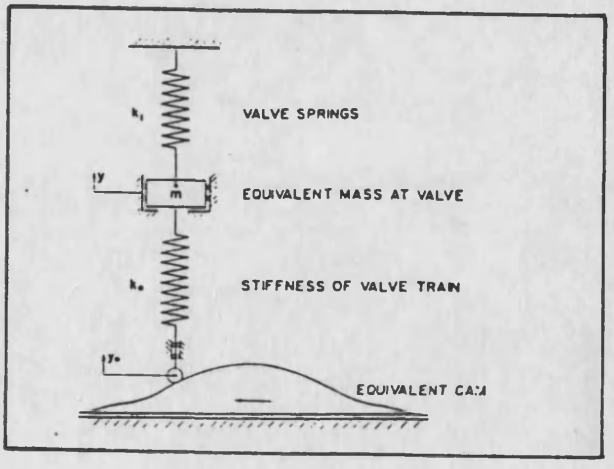

Figure 2.33- Dynamically equivalent system for valve train.

CHAPTER 3

Preliminary Design Of The Variable Valve Rate Mechanism

3.0 Introduction

The preliminary design of a mechanism for controlling the rate of valve opening is presented. Rigid-body models have been developed for both conventional and modified valve trains in order to study the systems feasibility. In these analyses components in the mechanism and the valve trains are treated as inelastic bodies. The conventional valve train system has been reduced to a single-mass one-degree of freedom equivalent system representation. The reduction technique has been stated and the general rules have been given. A three-degree of freedom equivalent system has been developed for the analysis of the continuously variable valve rate mechanism.

A multi degree-of-freedom mathematical representation of the conventional and continuously variable valve trains has been developed in order to examine their dynamic behaviour. These models are non-linear transient dynamic models, solved by the finite element method, thus enabling the inclusion of all the int rinsic non-linearities which exist in the systems, such as linkage separation and damping.

The results from both the rigid-body dynamic analysis and the finite element (non-linear transient dynamic) analysis are discussed followed by a comparison between the two methods. The results show the system to be theoretically feasible.

3.1 Description Of Continuously Variable Poppet Valve Actuator

This mechanism was initially developed to render the motion of engine valves continuously variable so that valve motion could be considered as part of an engine management strategy. The device may be used to control either rate of valve opening or closing, valve timing or valve lift. A line drawing of the mechanism is shown in figure 3.1.

The mechanism employs two cams for each valve to be controlled. The primary cam may be likened to a conventional cam in that it operates on a follower which drives the valve train, in this case through a compact hydraulic chamber. The contribution of the secondary cam may be varied by adjusting the position of the pivot of the rocker arm which operates between the secondary cam and the central piston of the hydraulic chamber. By moving the pivot point so that it is aligned with the central piston, the secondary cam has no modifying effect on the motion. By careful design of the cam profiles the mechanism can be made to vary valve motion over a wide range without over-stressing the linkage. Figure 3.2

shows lift diagrams for the variable rate and variable timing variants.

In the conventional valve train the inertia stresses increase as the square of engine speed, and design is normally based on survival at speeds up to a suitably high overspeed. For a truck diesel engine the minimum duty speed may be 1000 rev/min, the maximum 2200 rev/min and the overspeed limit 3500 rev/min. Thus at the lowest speed the inertia stresses will be less than 1/4 of those at the maximum rated speed and about 1/12th of the design strength.

The proposed mechanism is capable of controlling rate of exhaust valve opening as a function of engine speed such that at low speeds the valve opens with the same acceleration as at the maximum rated speed, thus fully utilizing the design strength.

Maximising the rate of exhaust valve opening has long been recognised as an effective means of improving the energy transfer between the cylinder and turbine of a turbocharged engine (9). The benefit results from the formation of pulses of higher pressure in the exhaust port and manifold which because of the more rapid rise of pressure downstream of the valve also serve to reduce the highly irreversible period of choked flow through the valve. The effect of rate of exhaust valve opening on pulse formation in a simulated truck engine, due to

Charlton and Pappas (50) is shown in figure 3.3. For this particular engine the low speed torque back-up is predicted to increase from 27% to 40% by increasing the rate of exhaust valve opening at low speeds.

3.2 Rigid-Body Dynamic Analysis

In a rigid-body dynamic analysis the members of the mechanism are treated as inelastic bodies. Displacement, velocity and acceleration are readily calculated for each part of the mechanism, from the cam profile, and these may be applied to determine the maximum contact force at the cam, and the required valve spring rate to avoid separation. To ease the calculation procedure a one-degree of freedom equivalent system was derived for the conventional valve train and a one-dimensional three-degree of freedom system for the continuously variable valve actuator. The established procedure for converting valve-side parameters to equivalent cam-side values is as follows:

(i) mass is multiplied by the rocker ratio squared,

(ii) stiffness is multiplied by the rocker ratio squared,

(iii) preload or applied forces are multiplied by the rocker ratio,

(iv) displacement, velocity and acceleration are multiplied by the rocker ratio,

(v) damping coefficients are multiplied by the rocker ratio squared.

The reduction of the conventional valve train to an equivalent one-degree of freedom system is quite straight forward. Mass, stiffness and preload on the valve side are converted to cam side equivalent values. The rocker moment of inertia is converted to an equivalent mass by dividing by the square of the distance between the pivot and the push-rod. These values are then combined with the masses of the push-rod and follower to form an equivalent system mass.

Therefore cam-side equivalent stiffness is determined by the expression:

$$K_{eq} = K.r^2$$

and cam-side equivalent preload by:

$$F_{peq} = F_p.r$$

and finally cam-side equivalent mass by:

$$M_{eq} = M_v.r^2 + M_p + M_f + I_r/a^2$$

for definition of symbols see Appendix 1.

The continuously variable valve actuator system was reduced to a simple system having three degrees of freedom. The valve, rocker, push-rod and upper piston

were combined to form an equivalent mass (M_{eq}). Thus ignoring damping and fluid compressibility the pressure in the hydraulic chamber is given by;

$$P = (M_{eq}.\ddot{X}_3 + K_{eq}.X_3 + F_{peq})/A_3 \qquad \text{-----3.1}$$

and for continuity,

$$A_3.X_3 = A_1.X_1 + A_2.X_2.r_v$$

$$X_3 = (A_1/A_3)\ .X_1 + (A_2/A_3)\ .X_2.r_v \qquad \text{-----3.2}$$

Similarly,

$$\ddot{X}_3 = (A_1/A_3)\ .\ddot{X}_1 + (A_2/A_3)\ .\ddot{X}_2.r_v \qquad \text{-----3.3}$$

Putting equations 3.2 and 3.3 into equation 3.1,

$$P = 1/A_3\ \{M_{eq}\ [(A_1/A_3).\ddot{X}_1 + (A_2/A_3).\ddot{X}_2.r_v]$$

$$+K_{eq}\ [(A_1/A_3).X_1 + (A_2/A_3)\ .X_2.r_v]+F_{peq}\}$$

cam forces are found by adding the forces transmitted to the lower piston, by the hydraulic fluid, to the inertia forces of these pistons and the secondary rocker. Main cam force:

$$F_1 = M_f.\ddot{X}_1 + P.A_1$$

Secondary cam force:

$$F_2 = M_2.\ddot{X}_2 + P.A_2.r_v$$

and

$$M_2 = (I_v/h^2).\ (1 + r_v)^2 + M_f.r_v^2$$

Spring reserve is the margin of spring force to maximum inertia force and is an indicator of the tendency to linkage separation.

Spring Reserve:

$$F_R = F_s - M_{eq}.\ddot{X}_3 - M_2.\ddot{X}_2 - M_1.\ddot{X}_1$$

The equivalent systems for both the conventional and continuously variable valve trains are shown in figure 3.4.

3.3 Multi-Mass Models of The Valve Trains

Valve train modelling may employ multi-mass idealisation in order to model the vibratory response of the linkage. Many multi-mass models have been developed and dealt with over the years (51). It has been found that the accuracy of the models increases with the number of masses, but so does the computing time. This is especially true when the natural frequency is increased, as this is one of the limiting factors on the integration time step size if the model is to be handled using a numerical technique. Therefore, it is in the interest of computer running time to limit the number of masses in the idealisation in accordance with realistic requirements. Increasing the number of masses eventually yields little return in accuracy (34).

3.4 Finite Element Analysis

Finite Element techniques may be employed to determine deflections, stresses, temperature distributions and dynamic/vibration characteristics of structures. The routine applications of the method are: confirmation of new designs once the layout has been optimised; investigation of problems due to deformation, movement or over stressing, and optimisation of sections in components subject to combined thermal and mechanical loads.

Although the finite element method is widely used, its application to engine components demands specialist knowledge and experience if the results are to be valuable. The main phases in any finite element analysis are as follows;

(i) establishing a model of the component or system to be analysed: identification and location of loads; simplification of geometry, 2D, axisymetric, 3D; selection of element type, generation of mesh; consideration of boundary conditions and constraints.

(ii) solution phase,

and finally

(iii) interpretation of results: identification of critical areas; consideration of material strength, for example fatigue prediction and recommendations for modifications.

Determining the idealisation can often be the most critical task. Over-simplification of the model may invalidate the analysis. Past experience will often indicate which factors are likely to be significant and should be modelled.

3.5 Development Of Non-Linear Transient Dynamic Models

It was not thought to be appropriate to spend valuable time writing a new valve train simulation program. The thermal power group obtained the proprietary finite element package ANSYS initially to carry out conventional finite element analyses to predict heat flow and thermal stress in diesel engine components. ANSYS is in fact a more general purpose engineering analysis program which, as well as the more usual finite element solutions, features modal analysis, and non-linear transient dynamic analysis. The non-linear transient dynamic analysis has been used to simulate both the conventional valve train and the proposed continuously variable valve train. Schematic representation of the two systems are given in figures 3.6 and 3.7. Because of restrictions on computing time a lumped parameter model has been chosen rather than a distributed parameter model in which each

component is modelled in detail. In this type of model each component is normally represented by a single concentrated or 'lumped' mass considered to act at a point. Some components, such as the push-rod and the valve spring, have significant mass and elasticity and are usually modelled by more than one mass with equivalent stiffness elements interposed. At present the push-rod is represented by two masses and the valve spring by one mass which is added to the valve assembly, only one third of the valve spring mass is considered to be active.

The program provides elements which can adequately model the main features of valve trains: mass, stiffness, damping, pre-load and gaps for tappet clearance and linkage separation. Displacement and force boundary conditions may be applied at more than one point in the system which for the two-cam model allowed each cam lift curve to operate at different points and for the simulation of gas forces on the valve head. Constraint equations have been used to define the relative motion of different parts of the system, for example, to relate the two ends of the rocker with the pivot, which itself has been mounted on a flexible element modelling the rocker post. A further constraint equation has been used to link the motion of the two input pistons and the output from the hydraulic chamber. Oil compressibility effects have been modelled by a spring element placed between the

output from the constraint equation (node 4) and the mass representing the upper piston (node 5), see figure 3.6.

The presence of a gravitational field could be included in the models and its inclusion appears justified at low engine speeds where peak linkage accelerations are approximately 30 g. Stiffness and damping elements have been built into the models at each metal to metal interface to represent an oil film, however, there seems to be little data in the literature on such effects and almost no guidance on numerical values.

3.5.1 Oil Film Effects

In a conventional valve train a clearance is required to ensure valve closure and to allow for expansion. For that reason it can be assumed that the contact area between the moving valve train components are filled with thin oil films, while the valve train is not actuated. These oil films prevent metallic contact by separating the surfaces and are able to support high loads for short times by means of hydrodynamic effects. The oil film exerts an influence on the dynamic behaviour of the vibratory system by two main effects:

(i) By actuating the valve train, the oil film is, sqeezed out of the contact area. This causes energy losses from the vibratory system and thus damping rates depending on the oil film shapes.

(ii) The compressibility of the oil film has an

influence on the stiffness of the system.

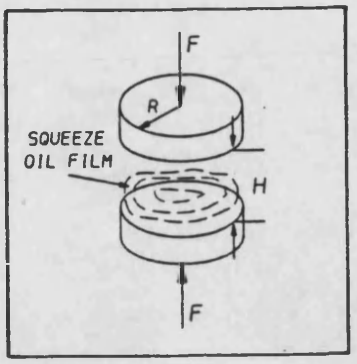

Figure 3.8 - Symbolic representation of a contact area with sqeeze oil film.

Fiqure 3.8 shows a symbolic representation of a contact area with an oil film between components. The formula describing the behviour can be derived from a volume flow balance of the oil film and corresponds to:

$$-dh/dt = (F/K) \cdot H^3$$

K is a constant including the geometry of the contact area as well as the oil viscosity. For instance, an area with a circular surface, figure 3.8, leads to constant K of the form:

$$K = 3/2 \cdot \pi \cdot R^4 \cdot \eta$$

a line contact having a length 'l' and a width 'b' gives:

$$K = l \cdot b^3 \cdot \eta$$

where η is the oil viscosity (41). It is difficult to measure the oil film thickness between cam and follower.

Respective publications (52) show that a capacitance method could give good results. In this method the tappet may be electrically insulated from the test fixture by means of a PTFE guide. The oil film thickness may be computed on the basis of the capacitance values measured between the cam and the tappet. The oil film behaviour is complex and not strictly amenable to representation by unique values of stiffness and damping coefficient. Nevertheless, values of 10 MN/m and 1250 kg/s were used for the oil film stiffnesses and damping coefficients in the models in order to progress the investigation.

3.6 Modal Analysis

Having constructed a working dynamic simulation of a valve train, it was a simple matter to convert this to the form required for a modal analysis. The natural frequencies and modal shapes were computed in only minutes compared with 1-2 hours for a dynamic simulation.

This analysis, one of eight analysis types that ANSYS performs, enables the determination of the natural frequency of the system. This is important when selecting a correct integration time-step size. The speed of operation of a valve train will normally be limited by the fundamental natural frequency of the valve train. Consider a typical valve train mechanism at the commencment of lift. The cam imparts an increasing acceleration force to overcome the valve spring load and accelerate the valve. This results in compression of the

elastic elements of the valve gear and the storage of elastic energy. Since the accelerating force is maintained the system 'rebounds' or vibrates, and this strain energy is converted to kinetic energy at the valve. The acceleration at the valve is momentarily higher than that at the cam. Thus vibration is induced in the system and it is important to stress that the frequency of the vibration is the fundamental natural frequency which is completely independent of engine speed. The amplitude of the vibration depends upon the resonant frequency, the amount of damping present and the applied accelerating forces, causing valve train deflection.

Modal analyses were performed for both lumped parameter models to determine their natural frequencies. Two situations, for each model, were investigated;

(a) valve lash and other system clearances open,

(b) valve lash and other system clearances closed.

The relationship between maximum operating speed and the time for one full cycle of valve train natural frequency should be known since the valve train will be more or less tolerant of the form of the acceleration pattern as long as there is no operating speed at which the width of the pattern approaches the time occupied by one-half cycle (53).

As a logical conclusion from the above, it is extremly desirable that the natural frequency of the valve train be as high as possible. Various parts in a valve train impose to some extent an influence on natural frequency; the mass of the valve has by far the greatest effect, with push-rod stiffness, rocker stiffness, camshaft stiffness, and equivalent mass at the upper end of the push-rod following in that order (53). Stiffness of the valve spring and mass of the tappet have no noticeable effect.

3.7 Results of Rigid-Body Dynamic Analysis

The continuously variable and conventional valve systems were initially studied by a simple rigid-body analysis as shown in figure 3.4. This type of analysis does not take account of vibratory response but does allow meaningful comparisons of the two systems on the basis of ideal acceleration, contact forces and spring reserve. This first stage of the work examines the feasibility of modifying an existing exhaust valve train to be continuously variable. Thus, the profile of the main cam was not considered to be a design parameter.

The secondary cam was defined, as shown in figure 3.9, to produce an acceleration of the push-rod, during the opening phase at an engine speed of 1000 rev/min, exactly equivalent to the acceleration produced by the main cam at 2200 rev/min. These engine speeds correspond to the

operating range of a typical large automotive diesel engine. The gain in the flow area for the design is indicated by the difference between the two high lift curves shown in figure 3.9. The acceleration curves for the main (standard) exhaust cam and the secondary cam are also shown in figure 3.9. Under the action of the variable rocker connecting the secondary cam to the rest of the valve train the contribution of the secondary cam is progressively reduced as engine speed is increased, in order to maintain constant maximum valve acceleration.

The variation of push-rod acceleration with time is shown for a number of engine speeds in figure 3.10. It should be noted that the acceleration during the opening period is identical for each speed. The contribution of the secondary cam is seen to last for exactly half of the period of the main cam. During the dwell period at 1000 rev/min the fall of the secondary cam exactly cancels the rise of the main cam. At 2200 rev/min the secondary cam has no modifying effect on the motion and the acceleration produced is that of the main cam alone. The acceleration curves shown in figure 3.10 appear discontinuous, particularly at the transition with the dwell period. Figure 3.11 shows the jerk (third differential of displacement with respect to time) curve at 1000 rev/min, which is the worst case in this respect. The diagram shows that the discontiniuties are not severe compared to the normal acceleration pulse.

Figure 3.12 shows the variation of cam acceleration, contact force and the required secondary rocker ratio with engine speed calculated by rigid-body analysis. The acceleration curves all correspond to the point of maximum push-rod acceleration, since this is when the maximum contact force will occur. The maximum contact forces are given by the upper curves of figure 3.12. They show that the load on the main cam is increased by the addition of the continuously variable mechanism components by approximately 6 percent at the highest speed. This is entirely due to the additional mass of the system (two followers and secondary rocker).

The maximum contact force on the main cam falls with engine speed and at 1000 rev/min is only 1 percent higher than in the conventional system. Maximum secondary cam forces are 18 percent higher than in the conventional system although in contrast this condition occurs only at the lowest speed so that the net effect on wear may not be severe. Spring reserve is the margin of spring force over system inertia force and indicates the tendency to linkage separation. The spring reserve of the conventional system at 2200 rev/min was 103 N in excess of the inertia force of 564 N. Without modification to the valve spring preload or rate the minimum spring reserve in the continuously variable system is only 25 N over an inertia force of 642 N.

3.8 Results of Non-Linear Transient Dynamic Analysis

Figure 3.13 shows cam forces and hydraulic chamber pressure predicted by dynamic simulation and by the rigid-body analysis. It may be seen that the maximum main and secondary cam forces predicted by the dynamic simulation occur within the early part of the valve opening period. These peaks of approximately 2400 N (main cam) and 2600 N (secondary cam) are reached within the first 25 degrees of cam angle. The rigid-body analysis of the system reveals that the maximum predicted cam force is approximately 1300 N for the main cam and about 1400 N for the secondary cam. These peaks also take place within the first 25 degrees of cam angle, as shown in figure 3.13. The hydraulic chamber pressure peaks of approximately 36 bars and just under 18 bars have been predicted by the dynamic simulation and the rigid-body analysis of the system respectively. The results for the secondary cam force and the hydraulic chamber pressure correspond to the highest secondary rocker ratio and an equivalent engine speed of 1000 rev/min. Generally, the levels of the curves are comparable, small differences arising because the rigid-body analysis did not account for valve lash, damping forces and gas forces.

The system is essentially being disturbed by an impulse since the oscillation is assumed to decay fully between consecutive valve events. Vibrations may persist in the coils of the valve spring, which in high-speed engines can exercise a significant influence over valve motion.

Figures 3.13 and 3.14 show that the acceleration response is highly oscillatory and that the maximum values of cam force and chamber pressure are approximately twice those predicted under the assumption of rigid-body behaviour. The variation of valve acceleration with time is shown in figure 3.14. This shows that the worst conditions are expected to occur at 2200 rev/min for both systems. The maximum acceleration in the valve occurs in response to the positive acceleration pulse in the early part of the valve motion.

3.9 Discussion of The Preliminary Design of The Mechanism

The dynamics of the conventional and the continuously variable valve trains have been investigated. The relationship between modulating plunger and cam angle has been determined by assuming a schedule of rate of exhaust valve opening with engine speed. The schedule is based on maintaing the same rate of exhaust valve opening over the engine speed range 1000 to 2200 rev/min. For the purpose of this study the 'main' cam is that used to operate the exhaust valves of the Ford 'Dover' series of diesel engines. This cam has opening and closing constant velocity ramps intended to take up clearances in the system. The cam profile between the ramps is defined by a polynomial and it is over this range that the modulating plunger motion has been defined, also in the form of a polynomial.

The difference between the conventional and the high-rate valve lift profiles is that in the high-rate case there is a period of dwell at the maximum valve lift. One might immediately conclude that the jerk curve would have a number of severe discontinuities. But the analysis has shown that the discontinuities are not severe compared to the normal acceleration pulse.

The main and the secondary cam contact forces have been found, by the non-linear transient dynamic analysis, to be approximately 2400 N and 2600 N respectively. These maximum forces for the continuously variable system are greater in magnitude by only 1-17 percent than the conventional maximum cam contact force. The rigid-body analysis of the two models gave the maximum cam contact forces of approximately half the values predicted by the non-linear transient dynamic analysis. The maximum pressure inside the hydraulic chamber was found to be 36 bars, taking into account the vibratory response of the system, which is not a particularly high pressure for hydraulic systems.

The rigid-body analysis determined the spring reserve of the conventional system at 2200 rev/min to be 103 N in excess of the inertia force of 564 N but this reserve significantly reduced to only 25 N for the continuously variable system over an inertia force of 642 N. The spring reserve may be found inadequate and the experimental work will be able to verify this. The

preliminary design of the mechanism has proved the system to be feasible and an experimental evaluation is considered to be necessary.

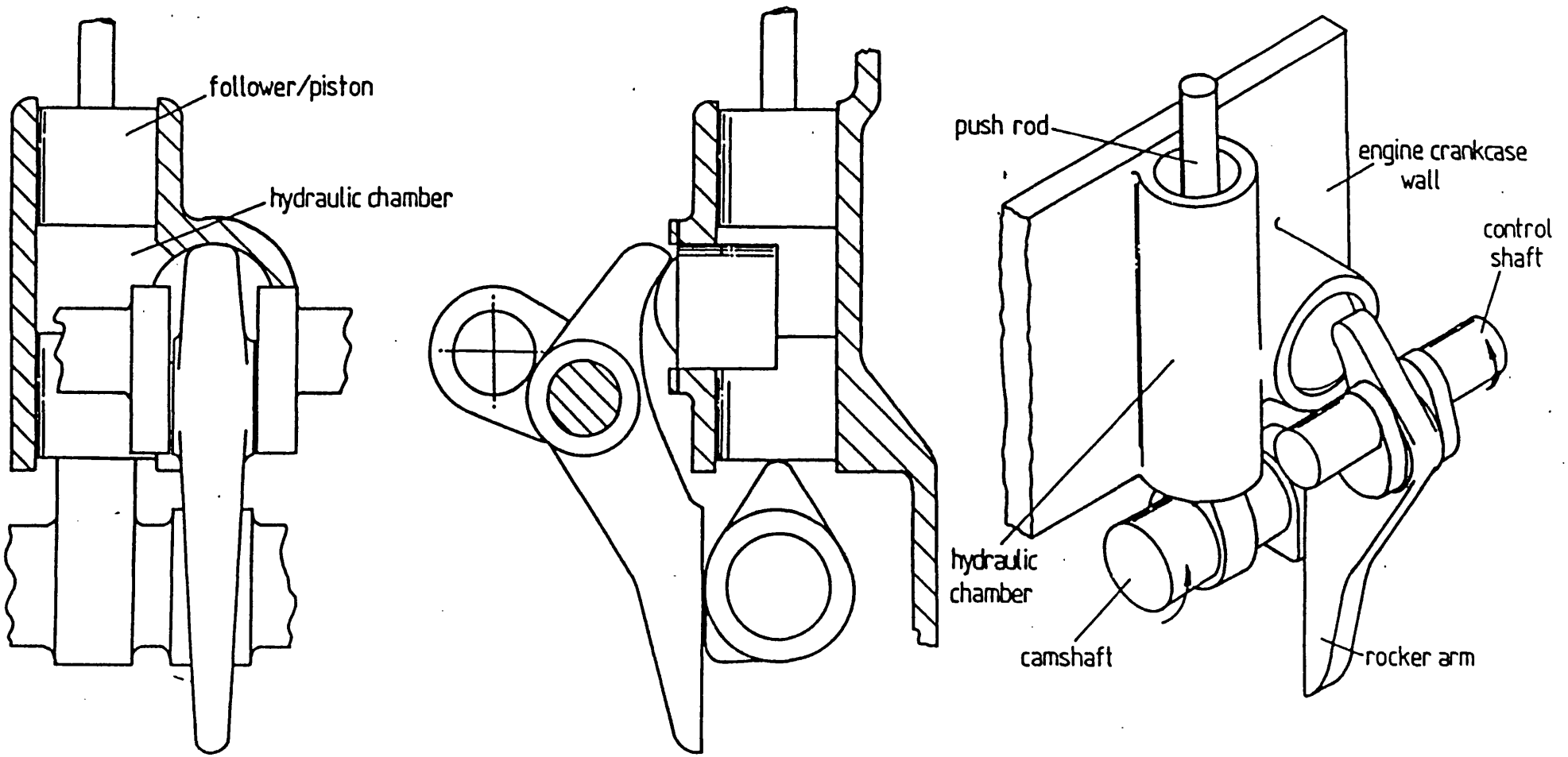

Figure 3.1 Sectional and perspective views of the continuously variable poppet valve actuator, showing the rocker and control shaft. Rotation of the control shaft effects a change of rocker ratio and hence valve motion.

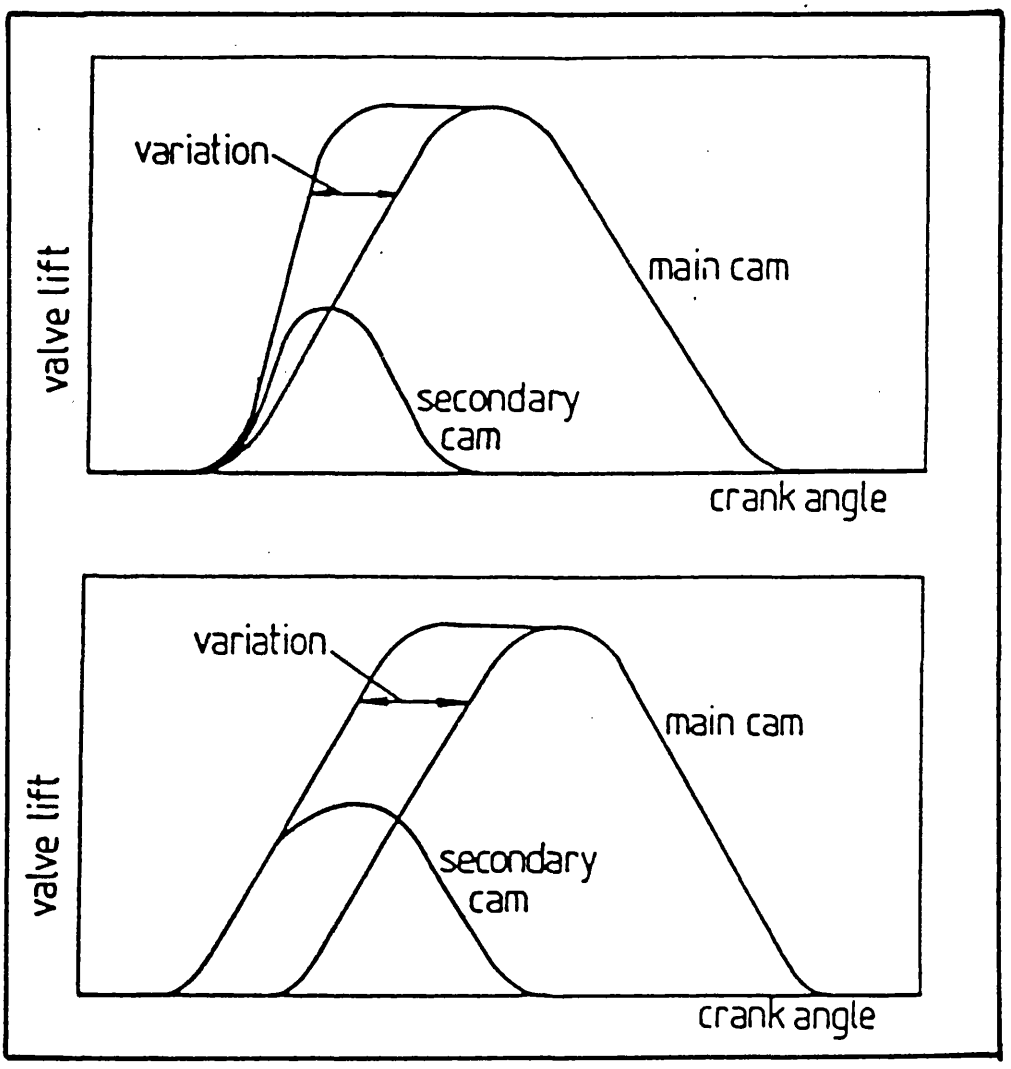

Figure 3.2 - Valve lift diagrams for the continuously variable valve actuator (a) variable rate system (b) variable timing system .

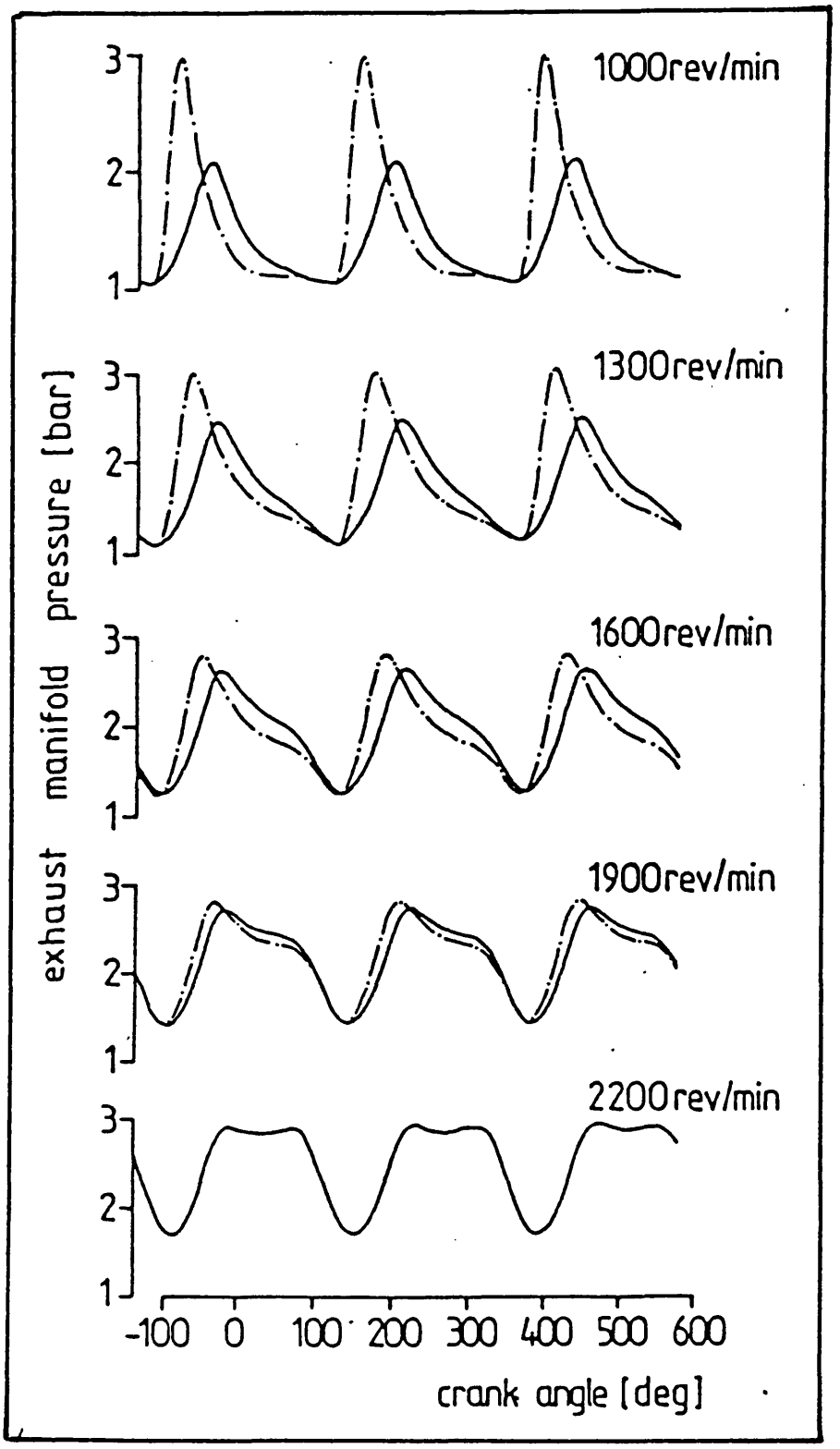

Figure 3.3- The effect of rate of exhaust valve opening on the formation of pulses in the exhaust manifold of a turbocharged diesel engine, (50). Keys:

----- high-rate system,

_____ conventional system.

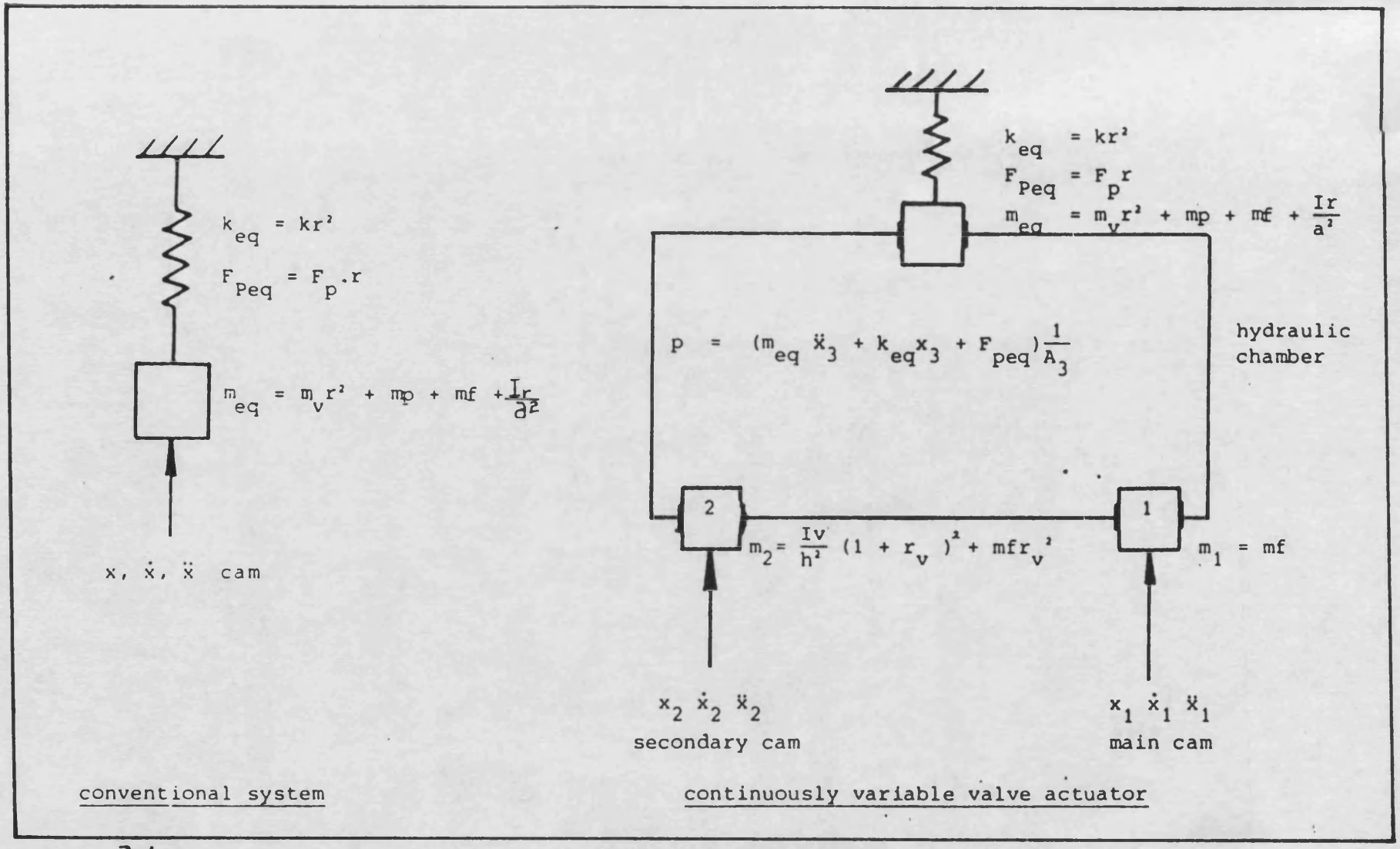

Figure 3.4 Equivalent systems used to calculate cam contact forces, hydraulic chamber pressure and spring reserve assuming rigid-body conditions.

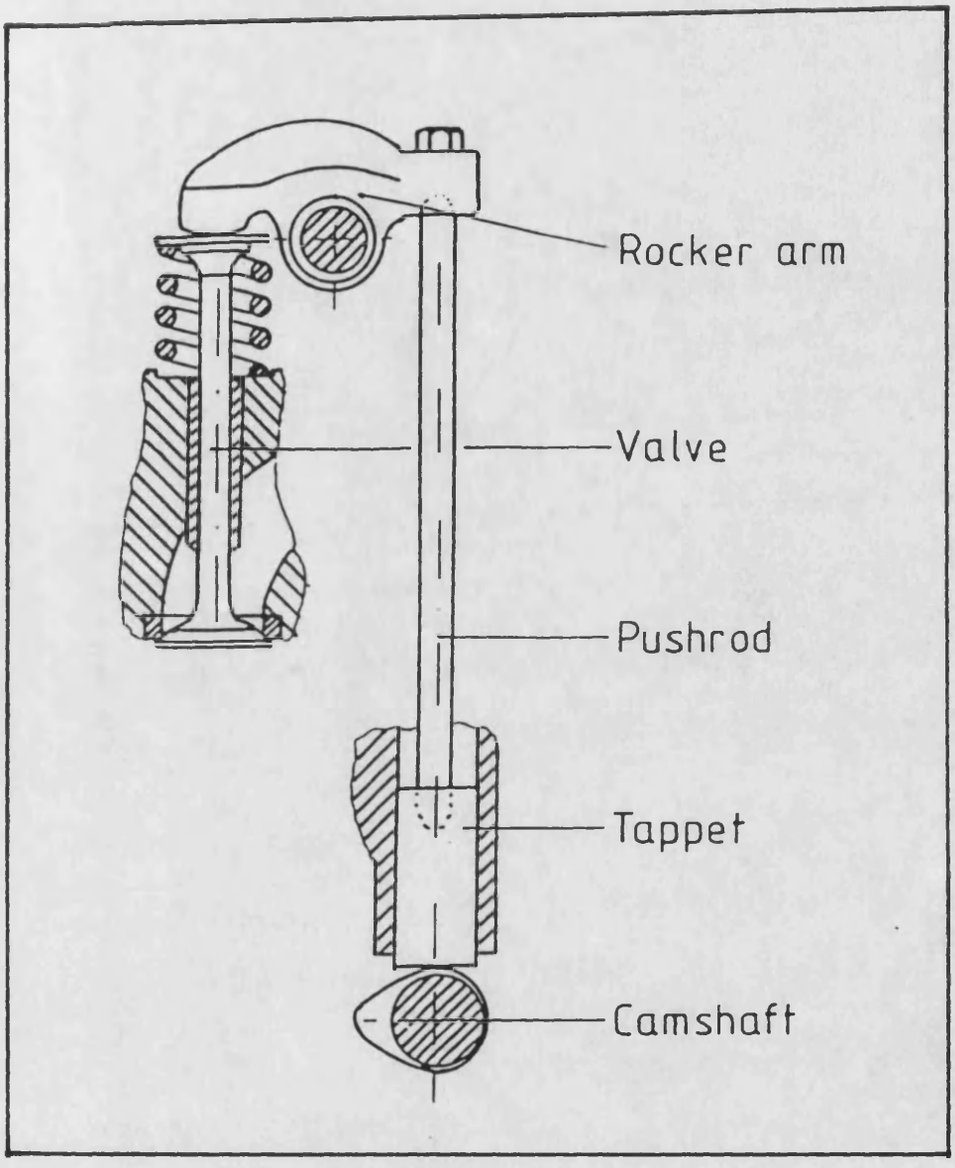

Figure 3.5 - Components of a pushrod actuated valve train.

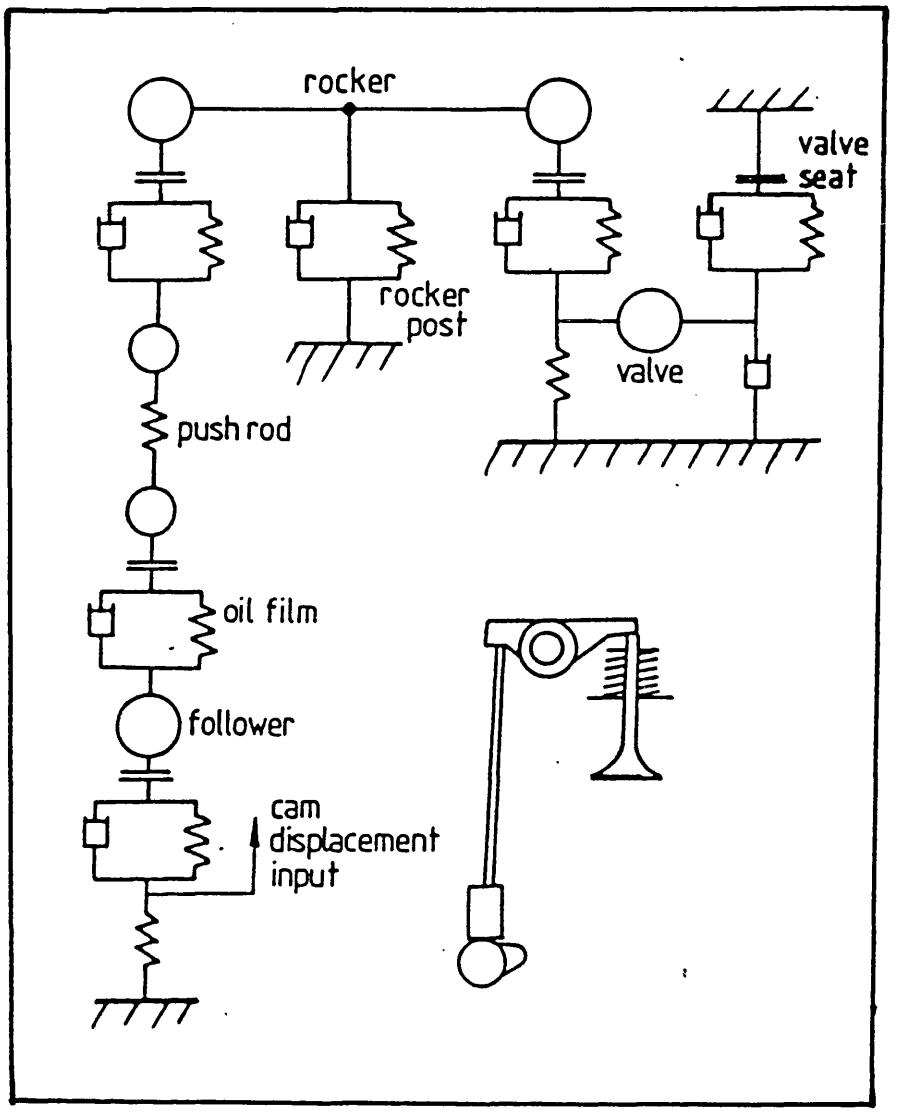

Figure 3.6 - Non-linear transient dynamic model of conventional valve train.

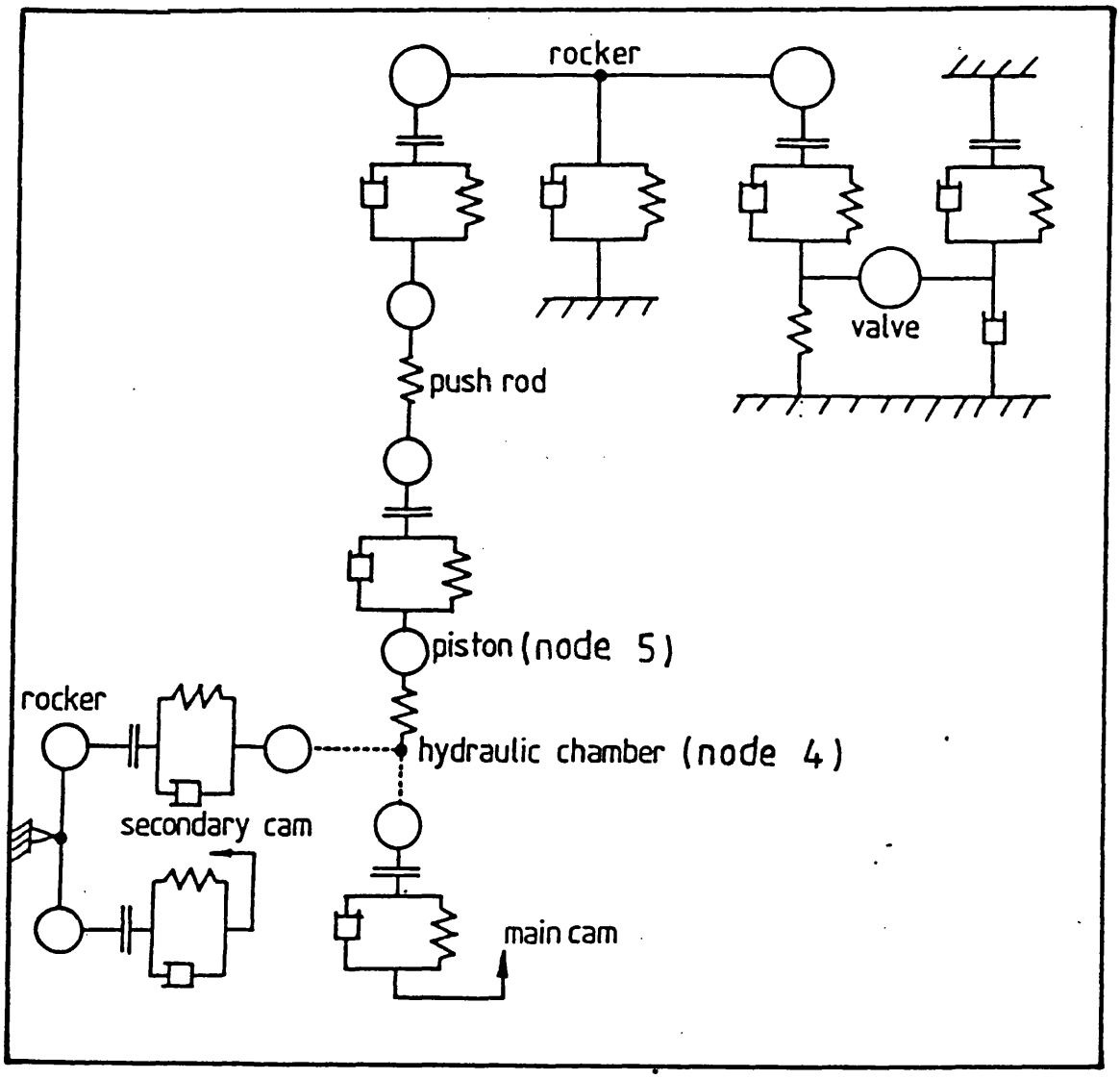

Figure 3.7- Non-linear transient dynamic model of continuously variable valve train.

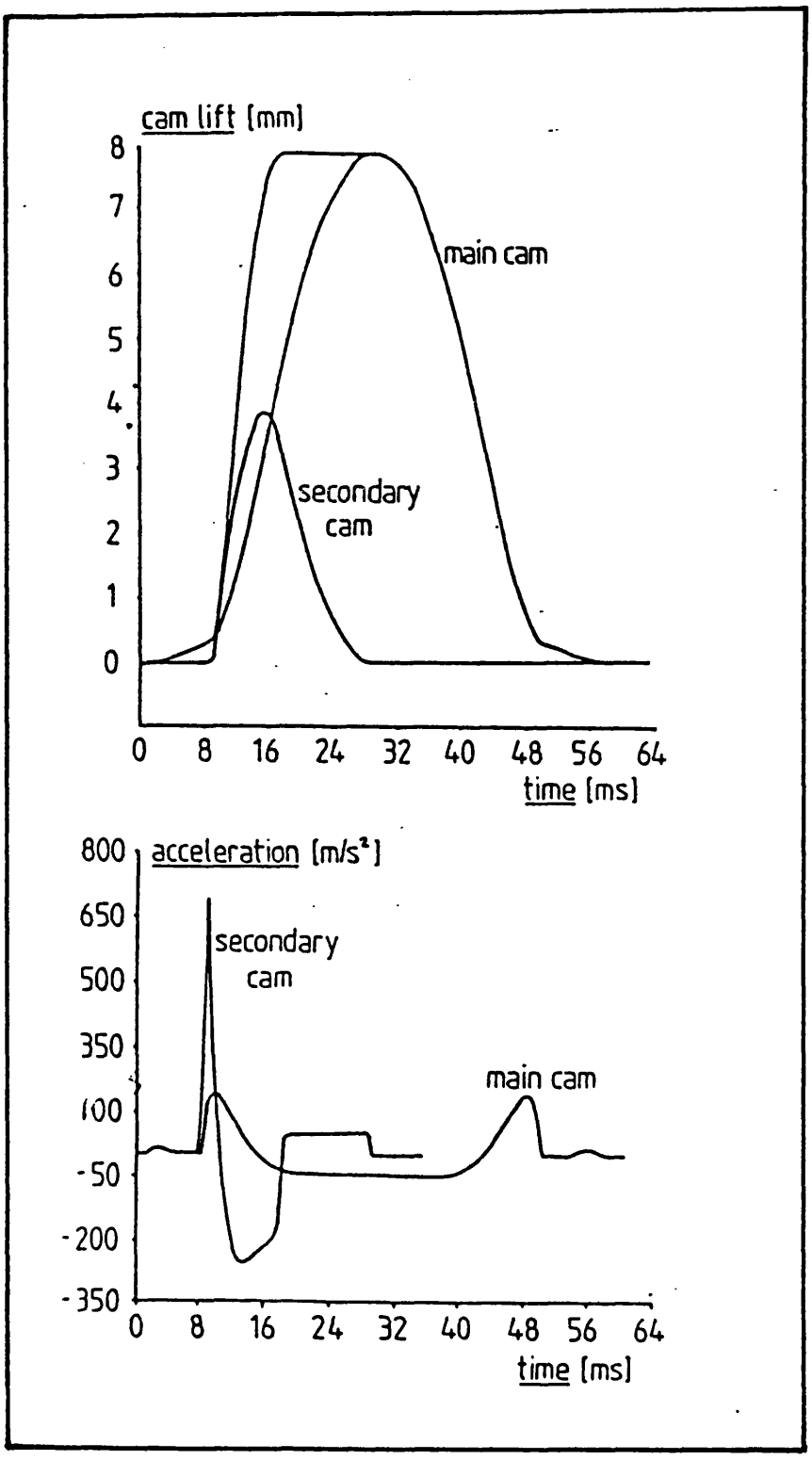

Figure 3.9- The upper curves show the cam lift curves for the continuously variable system at 1000 rev/min. The lower curves show the corresponding cam accelerations.

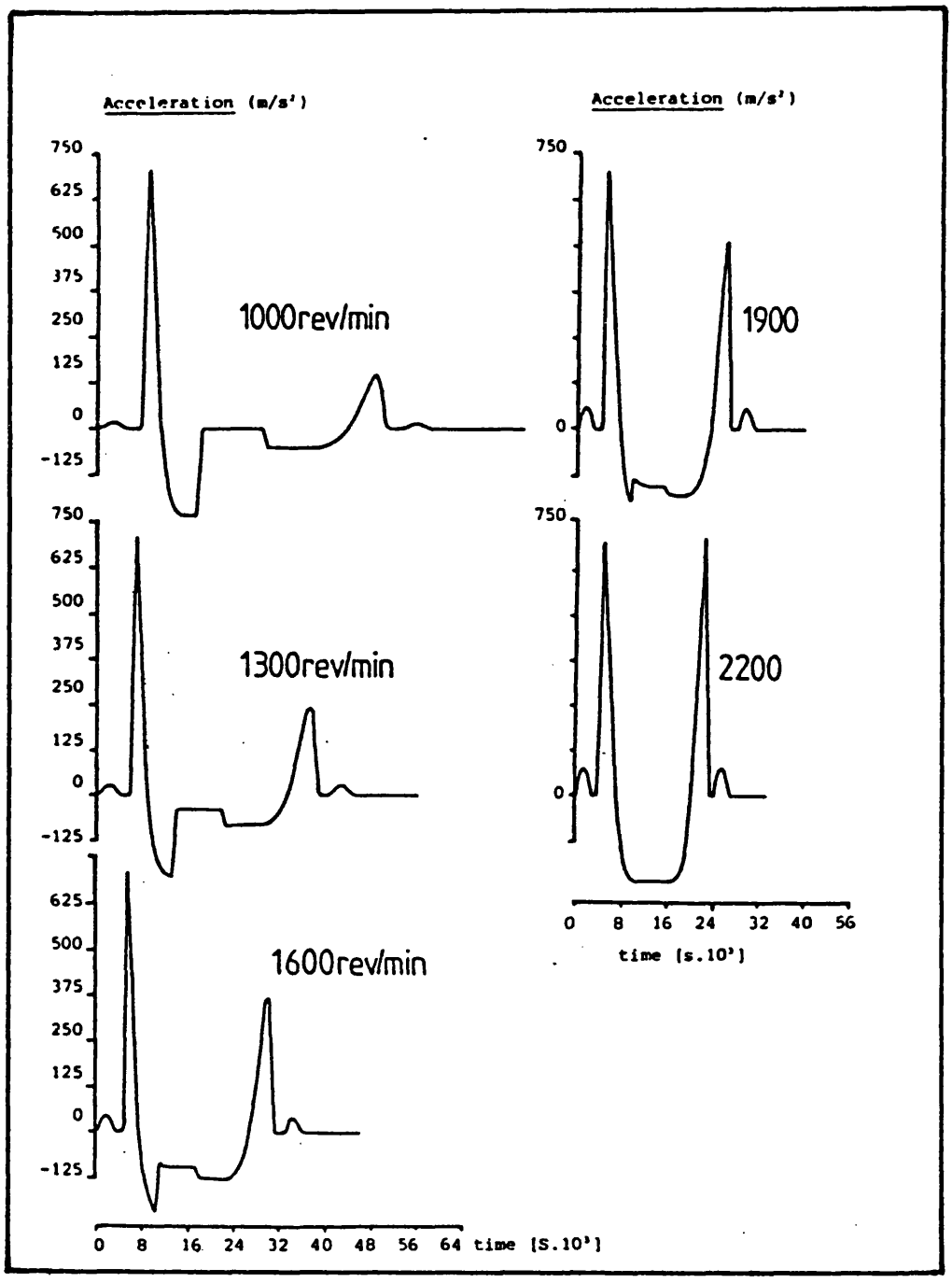

Figure 3.10- Variation of output (push-rod) acceleration versus time for a series of engine speeds and corresponding secondary rocker ratios. Note that maximum acceleration is constant.

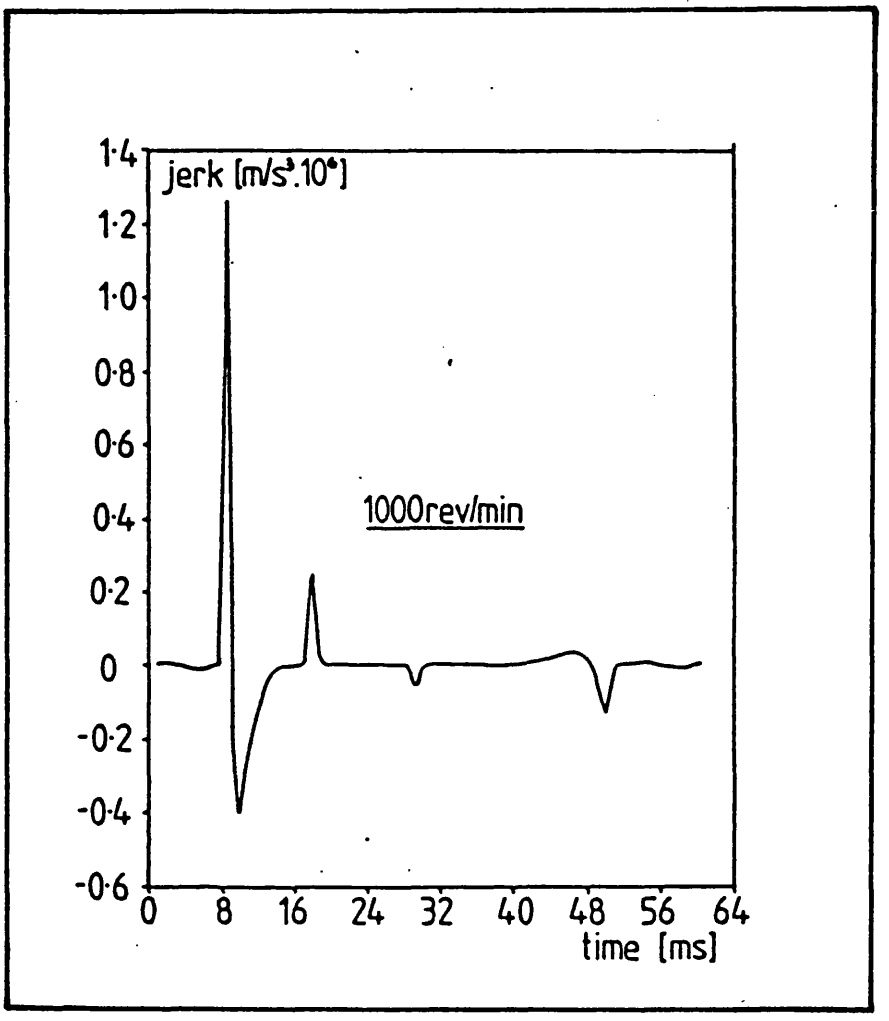

Figure 3.11- Graph of jerk versus time for the push-rod of the continuously variable system at an engine speed of 1000 rev/min.

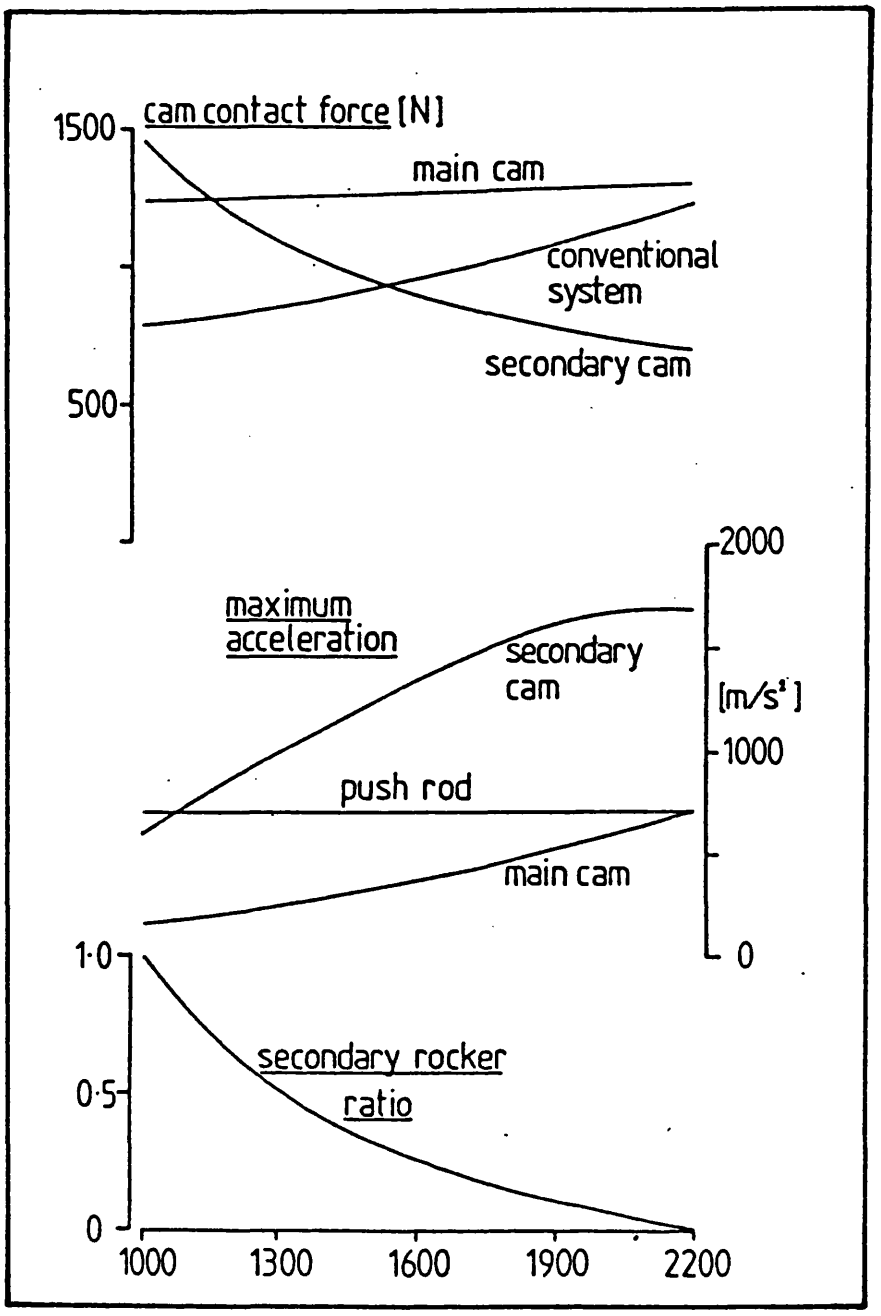

Figure 3.12- Variation of maximum values of contact force and acceleration versus engine speed, showing the secondary rocker ratio required to maintain constant push-rod acceleration.

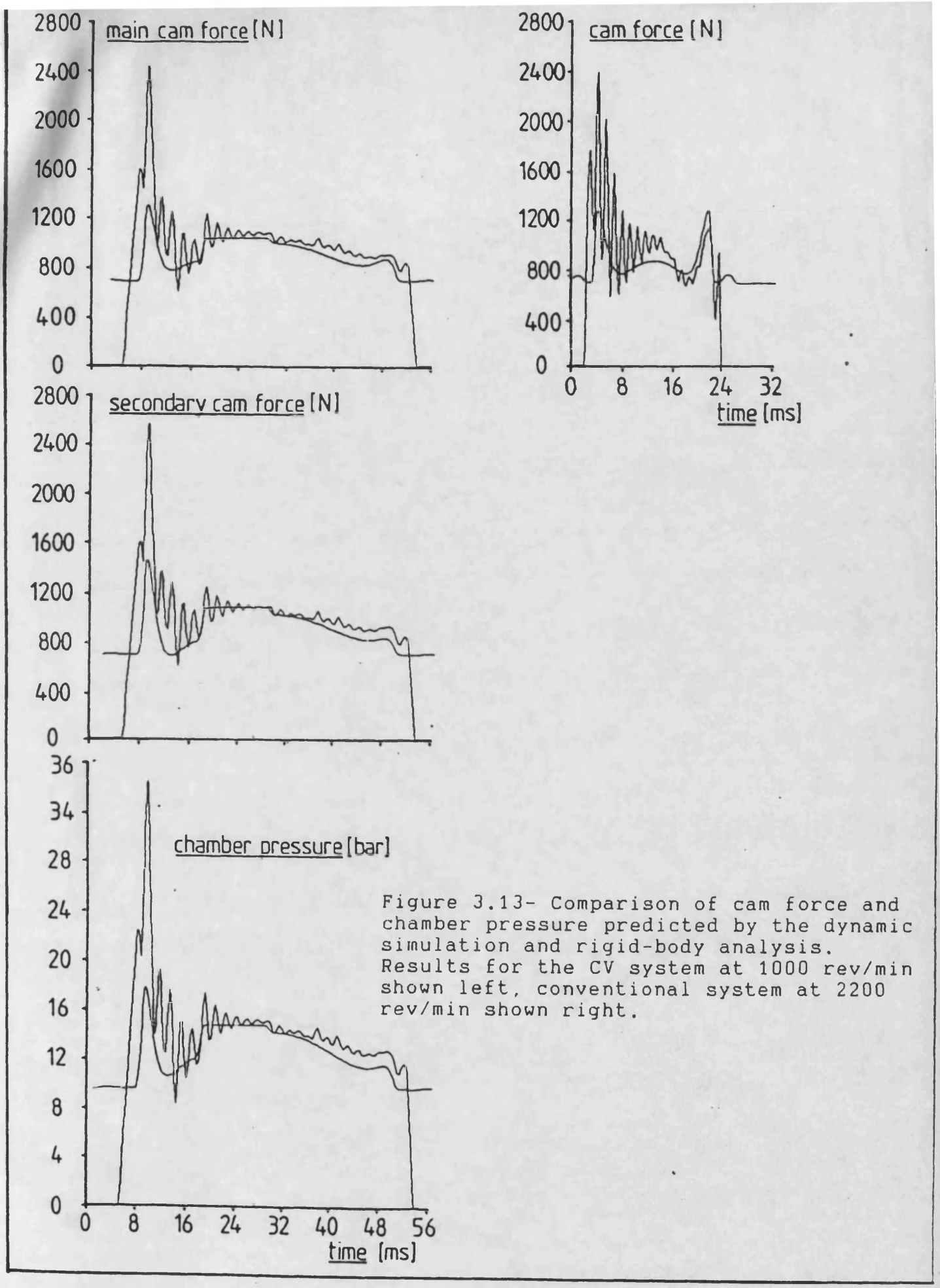

Figure 3.13- Comparison of cam force and chamber pressure predicted by the dynamic simulation and rigid-body analysis. Results for the CV system at 1000 rev/min shown left, conventional system at 2200 rev/min shown right.

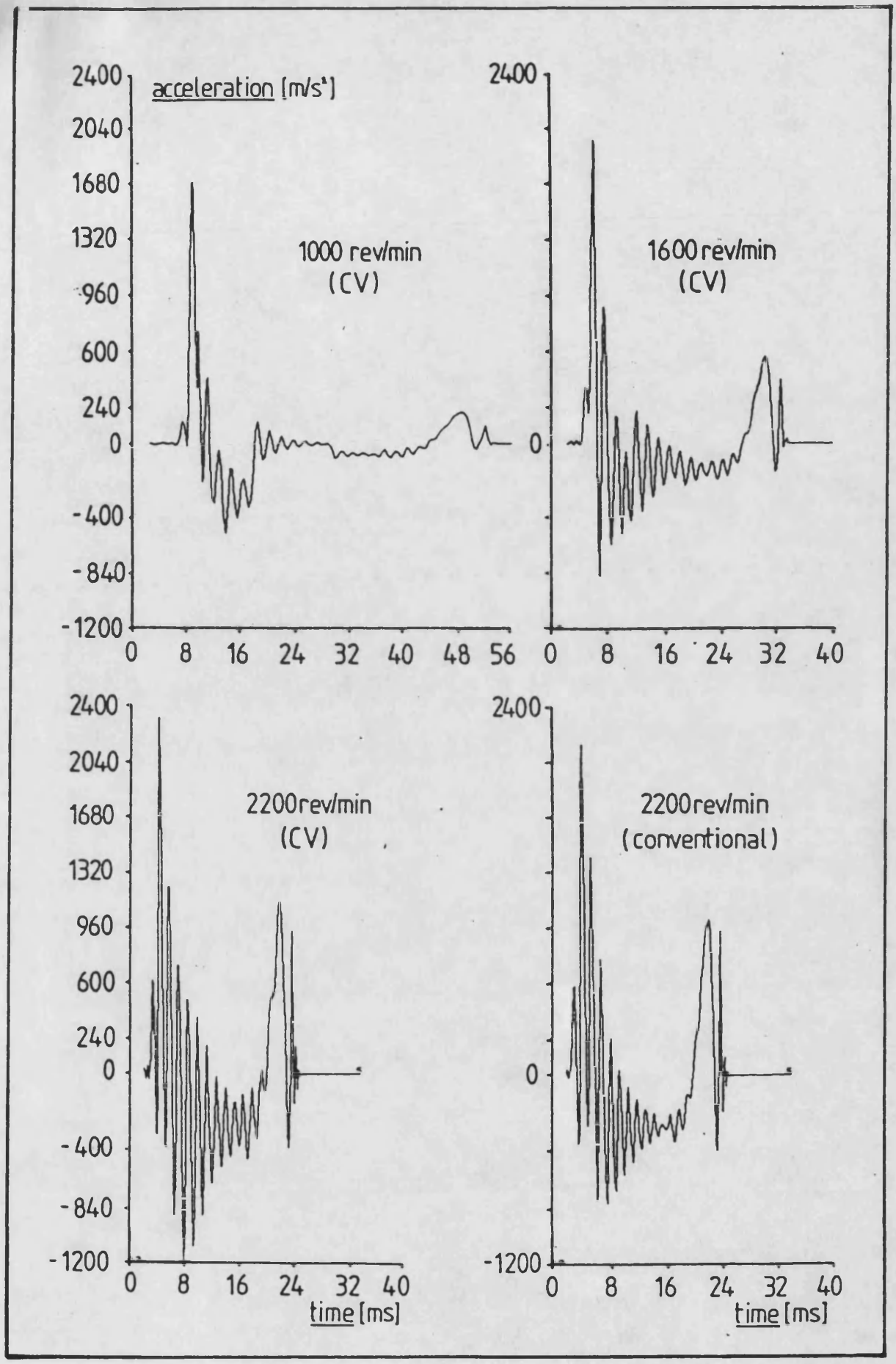

Figure 3.14- Valve acceleration predicted using the dynamic simulation for the continuously variable and conventional valve trains.

CHAPTER 4

Detail Design Of The Variable Valve Rate Mechanism

4.0 Introduction

This chapter describes the overall approach to the detail design of the variable valve rate device. Individual members of the mechanism have been dealt with separately. The following areas have been discussed in details:

1. main cam profile,
2. secondary cam profile,

and 3. Hertzian cam contact stresses.

A major area of difficulty lies in designing the secondary cam profile. It is therefore required to perform a comprehensive parametric study enabling the correct dimensions to be arrived at. Two parametric studies have been carried out for configurations where a roller follower and a flat follower have been used to transfer the displacement imparted by the secondary cam (full details of the studies are given in appendices 4 and 5). Having carried out the parametric studies, the required dimensions of the components of the mechanism have been obtained.

The results of the parametric studies, in particular for the case when a roller follower is employed, have been discussed.

4.1 Cam Profile Design

In any high speed engine, valve gear design is often accompanied by a large number of perplexing problems which have to be solved, e.g. valve linkage separation, jump, bounce, valve spring surge and wear of cam and follower. What makes the design so difficult is that almost all modifications aimed at increased power output may to lead to the above troubles which can often prove fatal to the engine. It is not uncommon for heavy duty truck diesel engines to be driven beyond their rated speed, this in turn makes valve gear design for such vehicles far more critical.

Almost all valve gear mechanisms employ a cam to impart displacement to be transmitted to the valve on the other end of the system, so it can be appreciated that the valve lift profile and its smoothness very much depends upon the cam and its characteristics.

4.1.1 Main Cam Profile

In high speed valve train applications, it is possible to use a polynomial lift curve at the valve and to design the cam profile to correct for the dynamic deflection in the valve train. Such a cam is known as a Polydyne Cam (40).

These cams are readily and quickly designed using computer programs.

Except for the Polydyne approach, the methods described in chapter two for cam design use acceleration diagrams made up of two or more sections each following different laws. A disadvantage of such a method is the sudden change in the rate of change of acceleration (jerk) when the flank period merges into the nose period. This may be avoided by adopting a lift, and acceleration curve, in the form of a polynomial equation:

$$L = C + C_p.x^p + C_q.x^q + C_r.x^r + \ldots$$

By succesive differentiation expressions for velocity, acceleration and jerk may be obtained which, when equated to the end conditions to be observed, permit the values of C, C_p, C_q and C_r to be determined for assumed values of the powers, p, q, r and s. Obviously many different curves may be obtained corresponding to the power laws assumed.

The main cam profile used in developing the two mathematical models representing conventional and continuously variable valve trains has been provided by the Ford Motor Company. The polynomial equation that follows the expression for constant velocity ramp, to take up all clearances in the system, is given below:

$$L = C - C_p.x^p + C_q.x^q - C_r.x^r - C_s.x^s$$

where,

$C = 7.874$	$p = 2.0$
$C_p = 10.79567$	$q = 9.0$
$C_q = 5.693371$	$r = 12.0$
$C_r = 2.351989$	$s = 30.0$
$C_s = 0.08950479$	$0 \leqslant x \leqslant 1.0$

and (x) is defined as the ratio of the instantaneous cam angle over the event range which in this case is 63 degrees. (x) can otherwise be designated as a non dimensional time base.

4.1.2 Secondary Cam Profile Design

Due to the rather complex geometrical structure of the continuously variable mechanism, design of the secondary cam profile demands a careful approach in order to avoid dynamic problems.

In an attempt to deduce the secondary cam profile two displacement characteristics were defined. Firstly the displacement of the main cam and secondly the required motion of the push-rod, that is the sum of the main cam lift and the displacement of the central plunger. Full details of this study are given in Appendix 3. The two polynomial

expressions A.3.4 and A.3.5 constitute the desired motion of the central plunger, attributable to the secondary cam profile. Due to the geometry of the secondary rocker the actual profile of the secondary cam would differ from the motion resulting from expressions A.3.4 and A.3.5.

In order to obtain the exact expressions forming the secondary cam profile a comprehensive analysis of the mechanism has been performed, Appendix 4. Correlations were consequently established between the mechanism's geometric parameters and the resulting secondary cam profile.

Initially a linkage geometry analysis was performed to verify the validity of using a flat follower. The proposed continuously variable valve motion mechanism shown in figure 3.1 employs a flat follower to convey the motion of the secondary cam on to the central plunger via the secondary rocker. For flat followers to be used on cams there is only one condition that needs to be met. The surface of the entire cam profile must be convex. The cam should be convex because if a concavity existed a flat follower would be unable to follow the exact displacement path, as shown in figure 4.2.

In order to demonstrate the possible use of a flat follower with the continuously variable rate valve mechanism a

mathematical concept known as the pedal of a curve was applied.

Following the linkage geometry analysis, adopting a flat follower for the secondary cam, a computer program was written and developed to simulate the proposed mechanism in action. Having obtained the required motion of the central plunger, the exact profile of the secondary cam was obtained.

The linkage geometry analysis which is a complex one yields first and second order differential equations. In order to solve these equations a numerical differentiation approach was considered and compared with an analytical method. The analytical method was not found to be a feasible solution due to the complex nature of the functions involved in the differential equations. The numerical differentiation approach was found reliable and least problematical.

As a result a NAG Library subroutine was selected to perform the numerical differentiations where required in the analysis. D04AAF, which is a semi automatic routine requires the function and a suitable differential step length. It is capable of calculating up to the 14th derivative of the function and also produces an error estimate of the results. The subroutine adopts the Taylor series method. More information about this numerical

routine has been given by Lyness and Moler (54) and Lyness and Sande (55).

By examining the radius of curvature around the cam profile the convexity condition through out did not stand and in fact the cam profile began with a rather steep concave portion, see figure 4.1. Therefore, the possibility of using a flat follower was ruled out and roller followers were, alternatively, considered.

The mechanism was modified to incorporate a roller follower instead of the flat follower for the secondary cam as shown in figure 4.2. Another linkage geometry analysis was performed taking into consideration all the secondary cam profile parameters. Mathematical expressions were derived following the analysis to give the actual secondary cam profile. This was a successful procedure and the actual profile with exact instantaneous radius of curvature values, pressure angle and linkage rotation were obtained, as shown in Appendix 5.

4.2 Hertz Cam Contact Stresses

When contacting members having curved surfaces transmit a load from one member to another, an area of pressure is developed, accompanied by contact (compressive) stresses. This situation occurs commonly in machine designs, for

example mating gear teeth, ball and roller bearings and also cam and roller followers.

The mathematical theory for the surface stresses and deformations produced by contact was first developed by Hertz. A set of formulae relating maximum contact stress to the load, material, and diameter of cylinders in contact parallel to their major axes are given in Appendix 6. The relevant expressions which are given below, were used in the computer programs written by the author to simulate the mechanism in order to determine the instantaneous Hertz contact stresses between the secondary cam and the roller follower and also between the variable geometry (secondary) linkage and the pivot disc. Expressions 4.1 and 4.2 correspond to these contact stresses respectively;

Cam & Roller Follower, $$\sigma_{cmax} = 0.591\sqrt{P.E\left(\frac{D_1+D_2}{D_1.D_2}\right)} \quad \ldots\ldots 4.1$$

Linkage & Pivot Disc, $$\sigma_{cmax} = 0.591\sqrt{\frac{P.E}{D}} \quad \ldots\ldots 4.2$$

[For description of notation see Appendix 6]

The maximum Hertz contact stresses, as can be seen, are dependent upon material and geometric factors. Therefore, maximum allowable Hertz contact stresses were borne in mind

when deciding upon the materials to use in the construction of the proposed mechanism.

4.3 Parametric Study

The final stage in the design of the proposed mechanism is to arrive at the most suitable values of the main design parameters. These parameters are:

1) Radius of the secondary cam base circle (R_B),
2) Radius of the roller follower (R_F),
3) Range of secondary rocker ratio (R_V),
4) Radius of the pivot disc (R_p),
5) Length of the off-set and (λ),
6) Size of the central plunger.

[refer to figure 4.2]

It should be noted that an unduly small mechanism would require excessively fine manufacturing tolerances. For the parametric study each parameter was initially given a datum value and a range of values over which it was to be varied. Each parameter was then varied individually to assess its effect on the performance of the system.

The main objective of this study was to obtain the 'optimum' value of each parameter with a particular view to the fulfilment of all requirments. Figures 4.3 to 4.15

illustrate the change in the characteristics with respect to one of the parameters. Full discussion of these results is given in the next section.

4.4 Discussion Of Results

Basically four important constraints (two major and two minor) have been considered when performing the parametric study in order to obtain the most suitable secondary cam profile. These four constraints are:

1. Maximum allowable pressure angle,
2. Maximum permissible Hertz contact stress at the cam,
3. Minimum radius of curvature of the secondary cam profile,
4. Radius of the cams base-circle.

The maximum pressure angle of any cam should not exceed 30 degrees (56) for durability and manufacturing reasons. The maximum permissible Hertz contact stress at the cam is a material dependent constraint. When using a roller follower of cast iron on a steel cam this maximum value should not exceed 1034 MN/m^2 and if a steel roller follower is incorporated this limit is appreciably increased (56). The base-circle radius (R_B) of the secondary camshaft was chosen to be the same as the base-circle radius of the main camshaft so that both cams could be on a common camshaft and

fit inside the existing camshaft tunnel and bearings. This radius is equal to 20mm. If the cam has a concave portion the minimum radius of curvature of the secondary cam profile is basically determined by the radius of the roller follower. Additionally a small re-entrant radius should be avoided for ease of manufacture. The table below summarizes the values of these constraints

CONSTRAINT	
Pressure angle	<30deg.
Hertz contact stress (material dependant)	$<1034 MN/m^2$
Radius of the cam profile curvature (concave)	$>R_F$
Radius of the common camshaft base-circle	20 mm.

Table 4.1 Summary of the secondary cam profile constraints.

Figure 4.3 shows the instantaneous change of the radius of curvature of a typical secondary cam profile as the cam rotates from start to finish. It may be seen that the cam begins with a concave portion which extends for 32 degrees and over this region the radius of curvature decreases by a very small amount up to 28 degrees then a sharp fall to negative infinity. A singularity can be observed as the

profile switches from concave to convex. At this singularity the surface of the cam is flat with no curvature. The radius of curvature in the convex section decreases very steeply to a minimum before it begins to rise as rapidly as it falls.

The minimum convex radius of curvature is the nose of the cam which is a useful criterion for wear and load considerations. The convex section is followed by another singularity where the cam profile switches back to concave and the radius of curvature rises from negative infinity swiftly before it reaches an almost steady value. The minimum concave radius of curvature is an important criterion when selecting the correct sizes of the mechanism's components such as the radius of the roller follower.

Figure 4.4 illustrates the variation of maximum pressure angle and maximum Hertz contact stress at the secondary cam with respect to change in radius of the roller follower. It can be seen that as the roller follower radius (R_F) increases, the maximum pressure angle decreases. At the same time the maximum Hertz contact stress at the cam decreases exponentially.

Figure 4.5 illustrates the change in both the minimum concave and the minimum convex (nose) radius of curvature

with respect to change in the roller follower radius. It may be seen that the cam nose radius is hardly affected by the size of the roller follower, whereas the minimum concave radius of curvature increases linearly as the radius of the roller follower increases. From figures 4.4 and 4.5 it can be inferred that the higher the roller follower radius, the lower the values of the corresponding maximum pressure angle and Hertz stress at the cam. Also the higher the roller follower radius, the higher the minimum concave radius of curvature of the cam profile. The trend should, therefore, be to select as high a roller follower value as possible with geometric and space constraints considered. Roller follower radii in the range 6 to 10mm are acceptable. A roller follower radius of 8mm has been selected for a smooth cam profile throughout.

The second variable considered in the parametric study was the secondary rocker ratio (R_V). The secondary cam profile was allowed to change whilst the central plunger cross-sectional area remained unchanged. Figures 4.6, 4.7 and 4.8 show the effect of secondary rocker ratio on the maximum pressure angle, Hertz contact stresses, secondary rocker rotation angle and the minimum concave and convex (nose) radius of curvature. The maximum pressure angle decreases as R_V increases. The maximum Hertz contact stress at the cam rises rapidly as R_V increases in value, and so does the maximum Hertz contact stress between the pivot disc and the

secondary rocker. The maximum angle of rotation of the secondary rocker decreases as R_v increases. From figure 4.8 it can be seen that the effects of varying R_v are not very severe on radius of curvature but nevertheless as R_v increases both cam nose and the minimum concave radius of curvature decrease slightly. A compromise is necessary in order to keep the Hertz contact stresses as low as possible for durability without violating the maximum pressure angle constraint. A higher secondary rocker rotation is also desirable because it will be less influenced by manufacturing tolerances. This in turn entails a lower value of R_v. Therefore, the acceptable range of the secondary rocker ratio is between 0.875 and 2.0. For ease of manufacture a secondary rocker ratio of 1.5 has been selected.

The third parameter to be considered was the radius of the pivot disc (R_p). Figures 4.9 and 4.10 show effects of change in values of R_p on the maximum pressure angle, the maximum Hertz contact stresses (both at the cam and at the pivot-rocker interface) and the minimum concave and convex (nose) radii of curvature of the corresponding secondary cam profile. As R_p increases the maximum pressure angle, almost insignificantly, reduces. The maximum Hertz contact stress at the cam increases following approximately an exponential growth and at the pivot-rocker interface Hertz contact stress decreases similarly but following an exponentially

falling curve. As R_p increases, the minimum concave radius of curvature is not influenced and remains at slightly higher than the corresponding roller follower radius. At the same time the minimum convex radius of curvature decreases significantly as R_p increases. An acceptable range was decided upon, bearing all constraints in mind, that is pivot disc radius values of between 25 and 45 mm. A mid range value of R_p = 35 mm was selected.

The fourth parameter to be considered was the offset between the pivot disc-rocker interface point of contact and the vertical line connecting the centre of the roller follower to the central plunger. Figures 4.11 and 4.12 illustrate the variations of the maximum pressure angle, the maximum Hertz contact stress at the cam and the minimum concave and convex radius of curvature of the corresponding secondary cam profile with respect to change in offset values. As the offset increases the maximum pressure angle decreases linearly and the maximum Hertz contact stress increases sharply before it flattens. From figure 4.12 it may be seen that the increase in value of the offset has no significant effect on the minimum concave radius of curvature. However, the increase in offset decreases the minimum convex (nose) radius of curvature relatively fast at first before it falls to a fairly flat region where very much higher values of the offset have almost no effect on it. Since the offset has a second order effect on the secondary cam profile pressure

angle and Hertz contact stresses, any value between zero and 40 mm would be acceptable. Therefore, we have freedom to choose on grounds of lay-out and values greater than 40 mm are unacceptable because of size and geometry of the mechanism. An offset value of 20 mm was accordingly selected to give sufficient strength to the secondary rocker structure to meet the imposed loading.

It is possible to vary the relative areas of the plungers in the system and maintain the desired output by either modifying the secondary rocker ratio or cam lift. A parameter was built into the study designated as an 'area multiplier' (AM) which is simply the ratio of the main follower cross-sectional area over the central plunger cross-sectional area ($AM = Area_{main\ follower} / Area_{central\ plunger}$). It is being assumed that the upper and lower plungers were to the same diameter. The effects of change in AM values on the maximum pressure angle, the maximum Hertz contact stresses, the maximum secondary cam lift, the maximum secondary rocker rotation angle, the corresponding central plunger diameters and the minimum concave and convex radii of curvature of the cam surface are shown in figures 4.13, 4.14 and 4.15. As AM increases the maximum lift of the secondary cam profile and the secondary rocker maximum angle of rotation increase which are both desirable, see figure 4.14. At the same time the diameter of the central plunger decreases parabolically. Similarly, for the other

two major constraints of pressure angle and Hertz contact stresses, as AM increases the maximum pressure angle and the maximum Hertz contact stresses (both at the cam and at the pivot-rocker interface) increase almost linearly, see figure 4.13. The cam nose curvature and the minimum concave radius of curvature of the secondary cam did not change significantly by changes in AM values. In order to satisfy the constraints, an acceptable range of values for AM was developed between 1.6 and 2.0. A mid range value was chosen, that is AM = 1.8. This corresponds to a central plunger diameter of just over 26 mm and a maximum secondary cam lift of close to 3.0 mm. A summary of the selected values of the mechanism's geometry is given below;

Camshaft base-circle radius (R_B)	= 20 mm.
Roller follower radius (R_F)	= 8 mm.
Pivot-disc radius of curvature (R_P)	= 35 mm.
Off-set length (λ)	= 20 mm.
Maximum secondary rocker ratio (R_V)	= 1.5
Central plunger diameter	= 26.7 mm.
Area multiplier (AM)	= 1.8
Maximum secondary cam lift	= 3.01 mm.

The selected values of all these parameters were used to generate the corresponding secondary cam profile which resulted in the following values as stated on the next page;

Maximum pressure angle = 27.84 deg.

Maximum Hertz contact stress at cam = 750 MN/m^2

Maximum Hertz contact stress at pivot-rocker = 619 MN/m^2

Maximum secondary rocker rotation angle = 7.63 deg.

Minimum convex(nose) radius of curvature= 21.25 mm.

Minimum concave radius of curvature = 8.0158 mm.

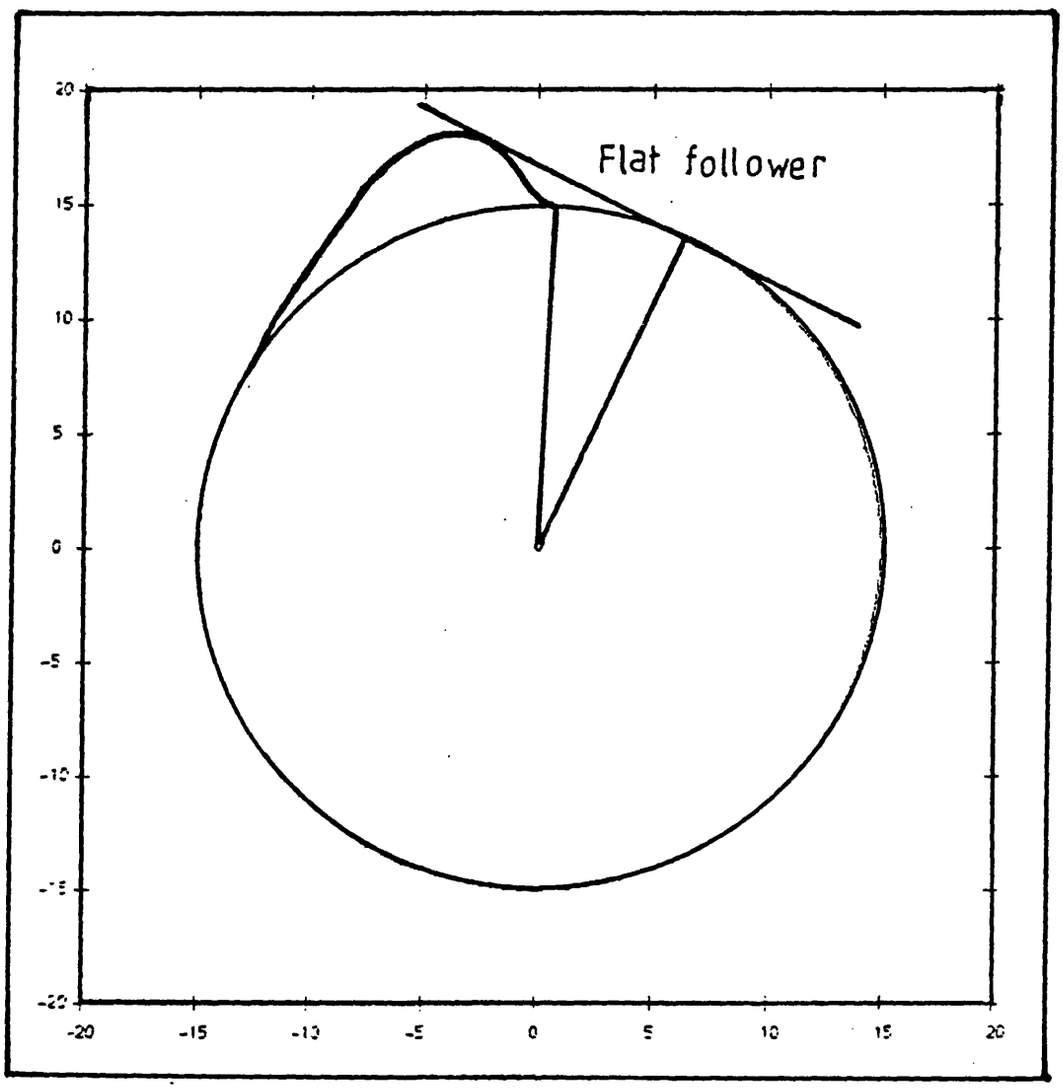

Figure 4.1- Actual secondary cam profile proving the impossibility of using a flat follower.

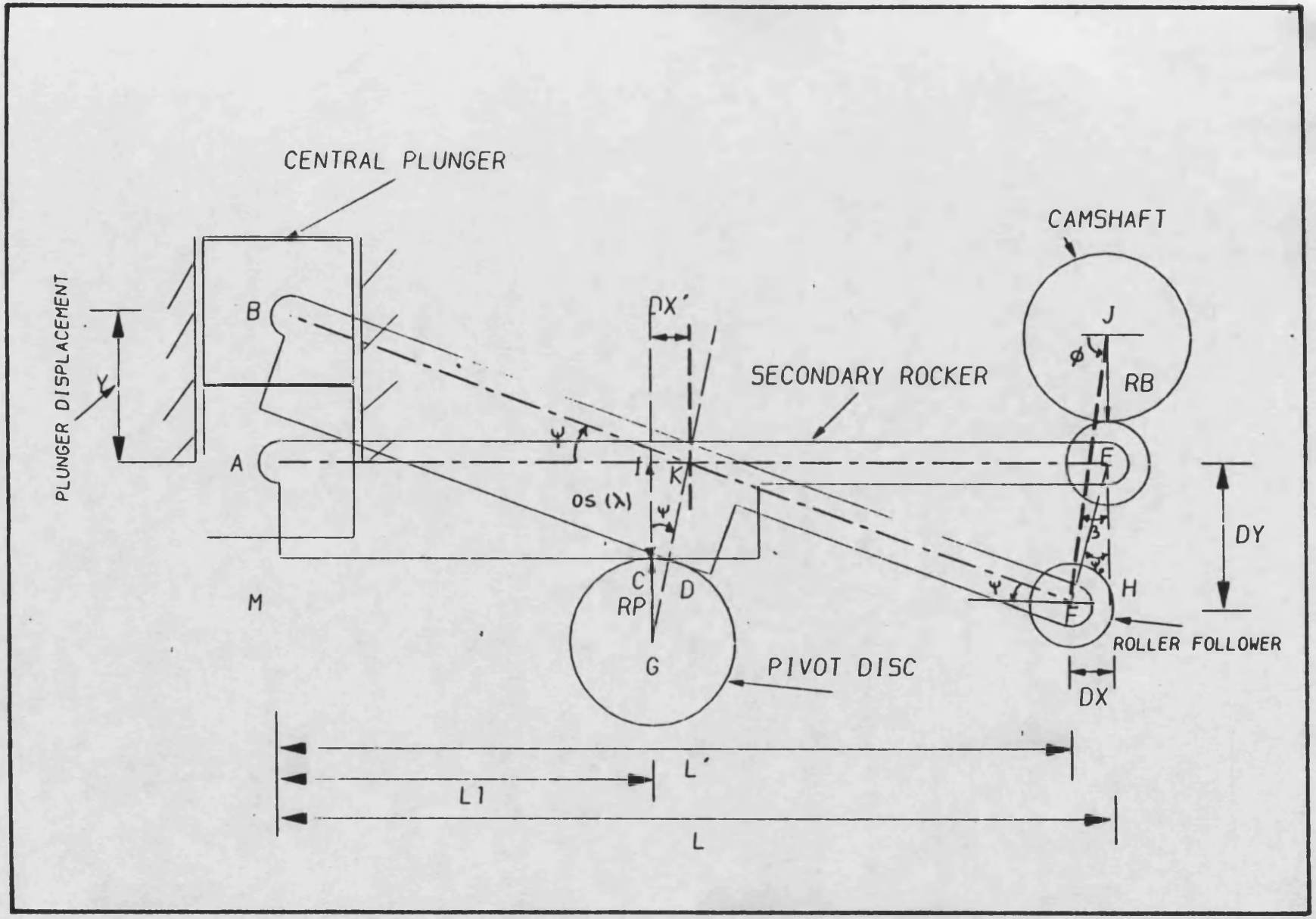

Figure 4.2- The continuously variable mechanism incorporating a roller follower.

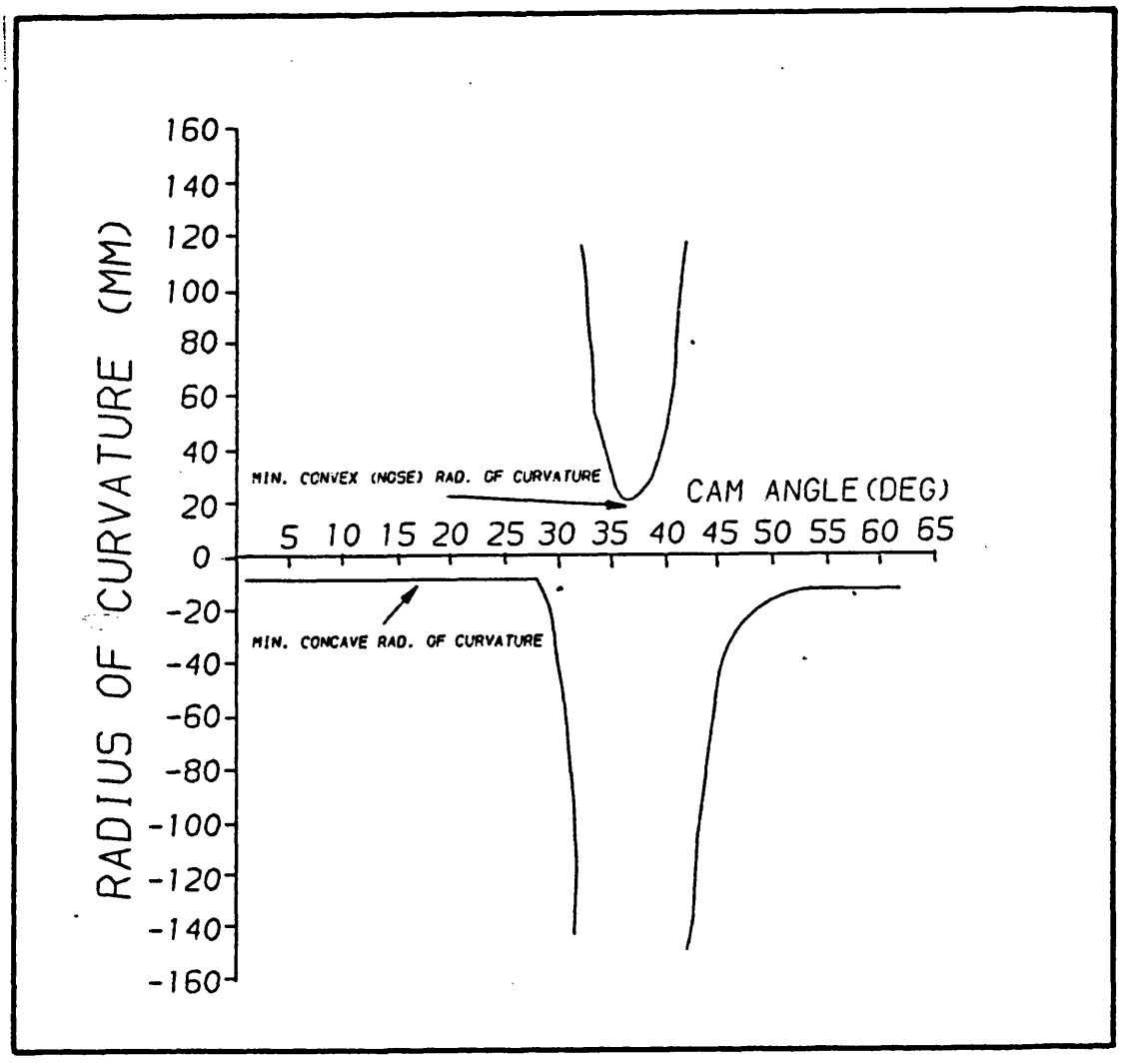

Figure 4.3- Radius of curvature versus cam angle.

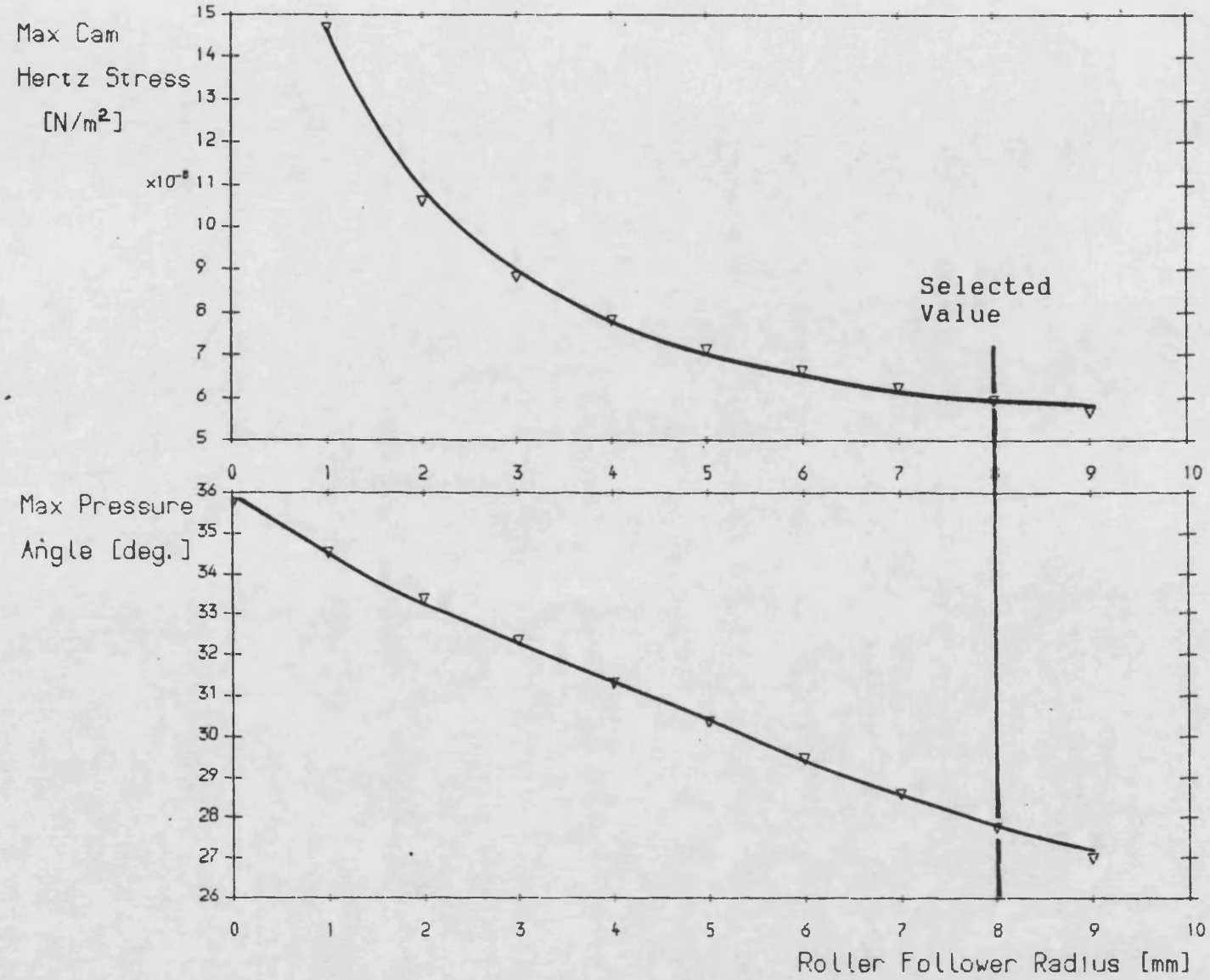

Figure 4.4- Maximum pressure angle and Hertz stress versus roller follower radius.

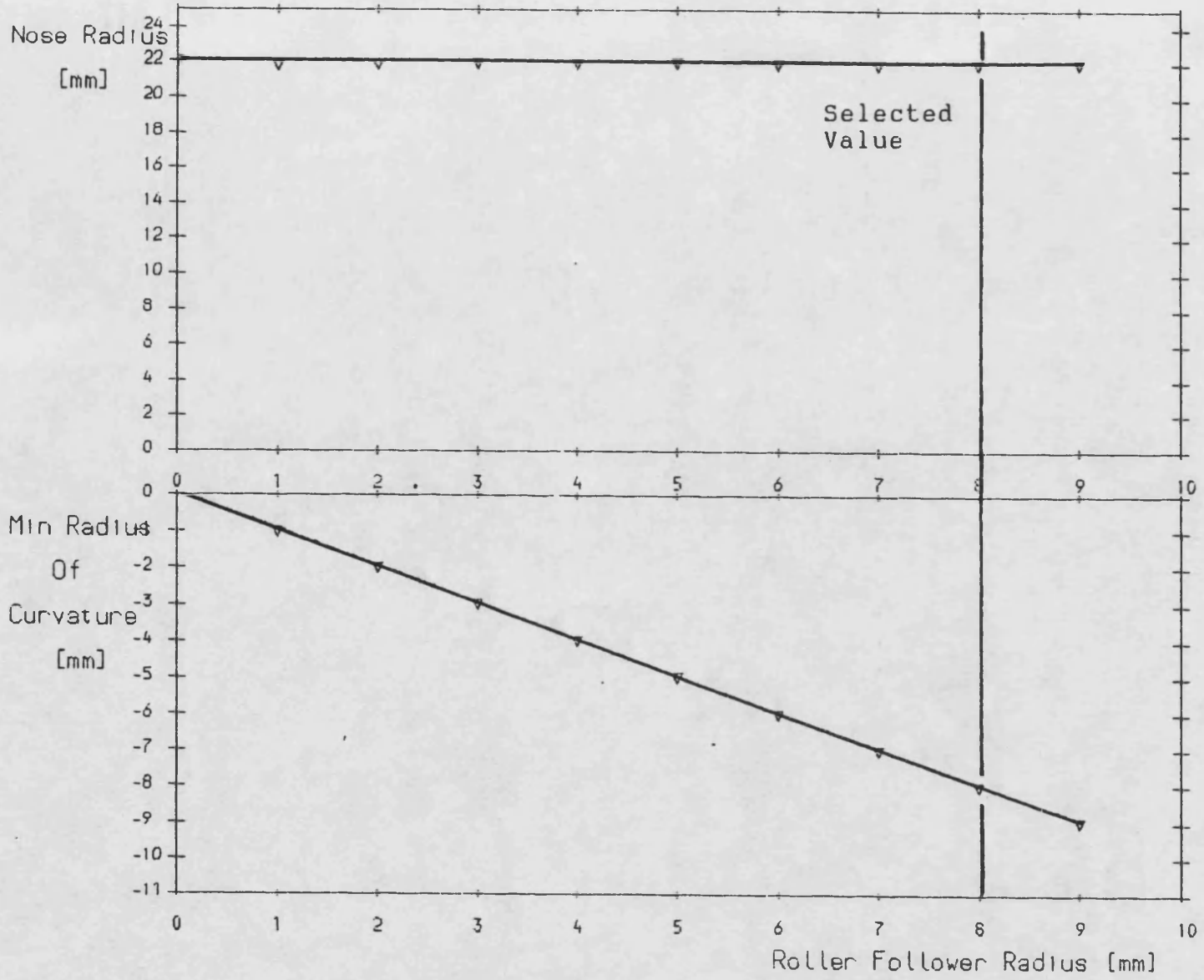

Figure 4.5- Minimum radius of curvature versus roller follower radius.

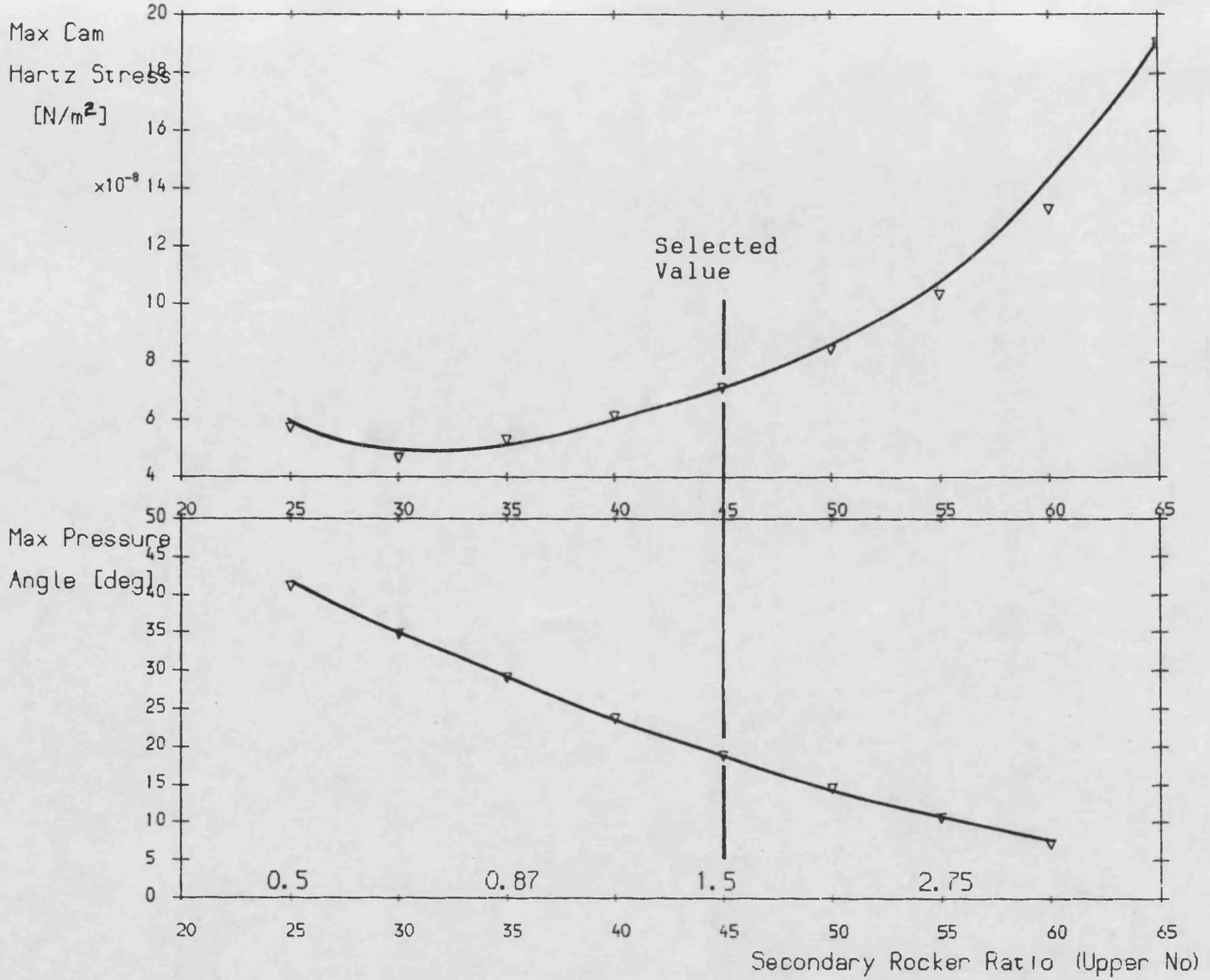

Figure 4.6- Maximum pressure angle and Hertz stress versus secondary rocker ratio.

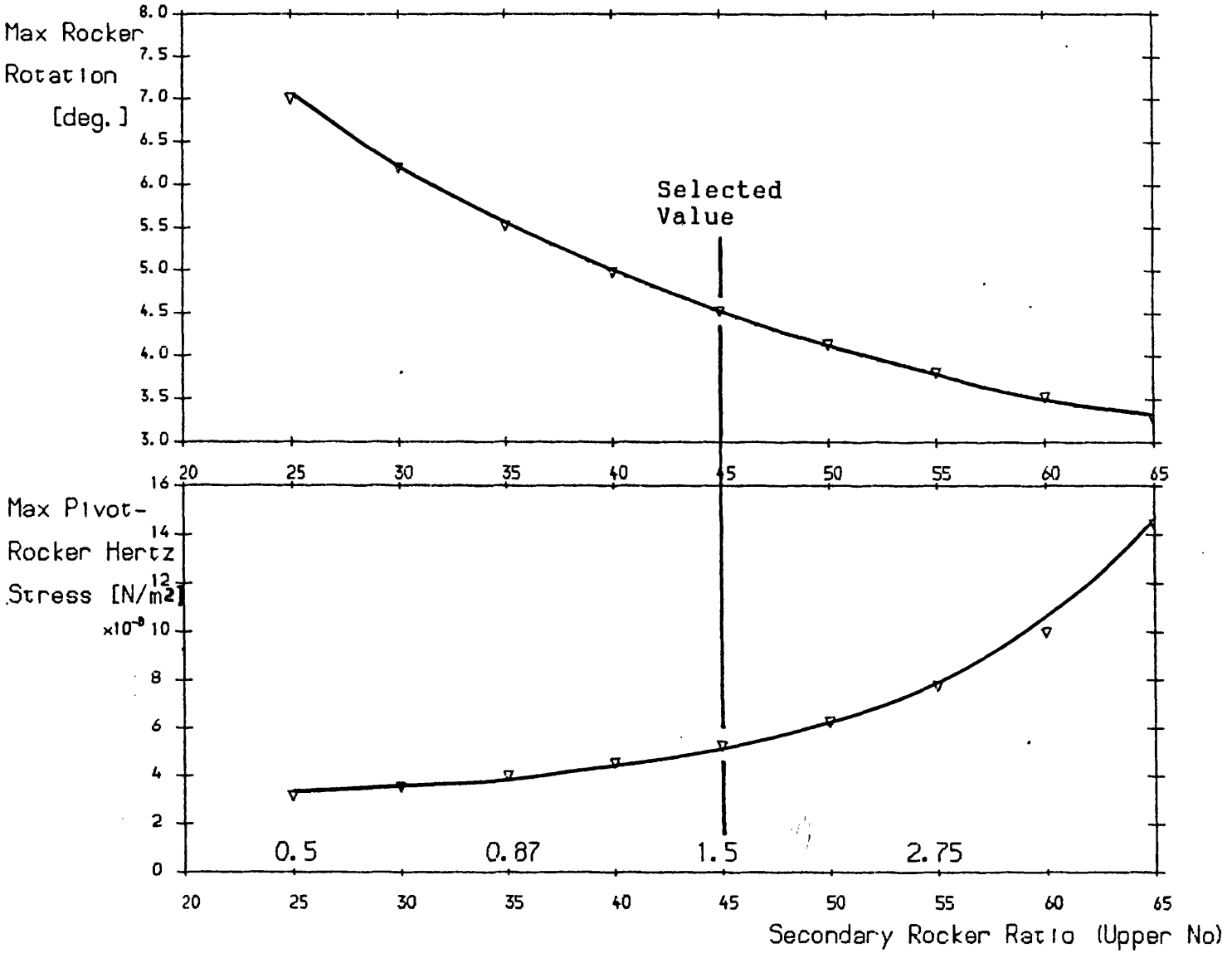

Figure 4.7- Maximum Hertz stress and rocker rotation versus secondary rocker ratio.

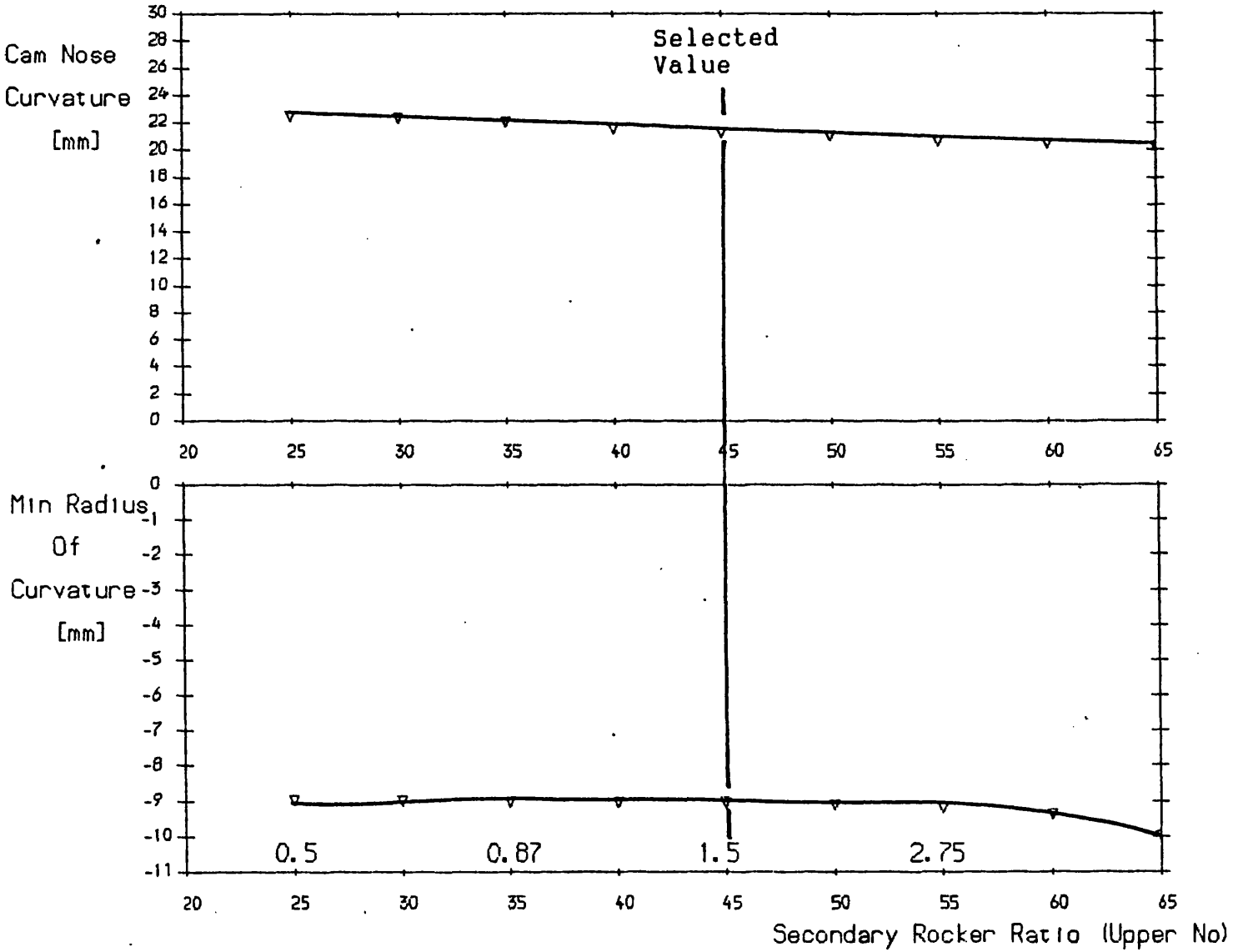

Figure 4.8- Minimum radius of curvature versus secondary rocker ratio.

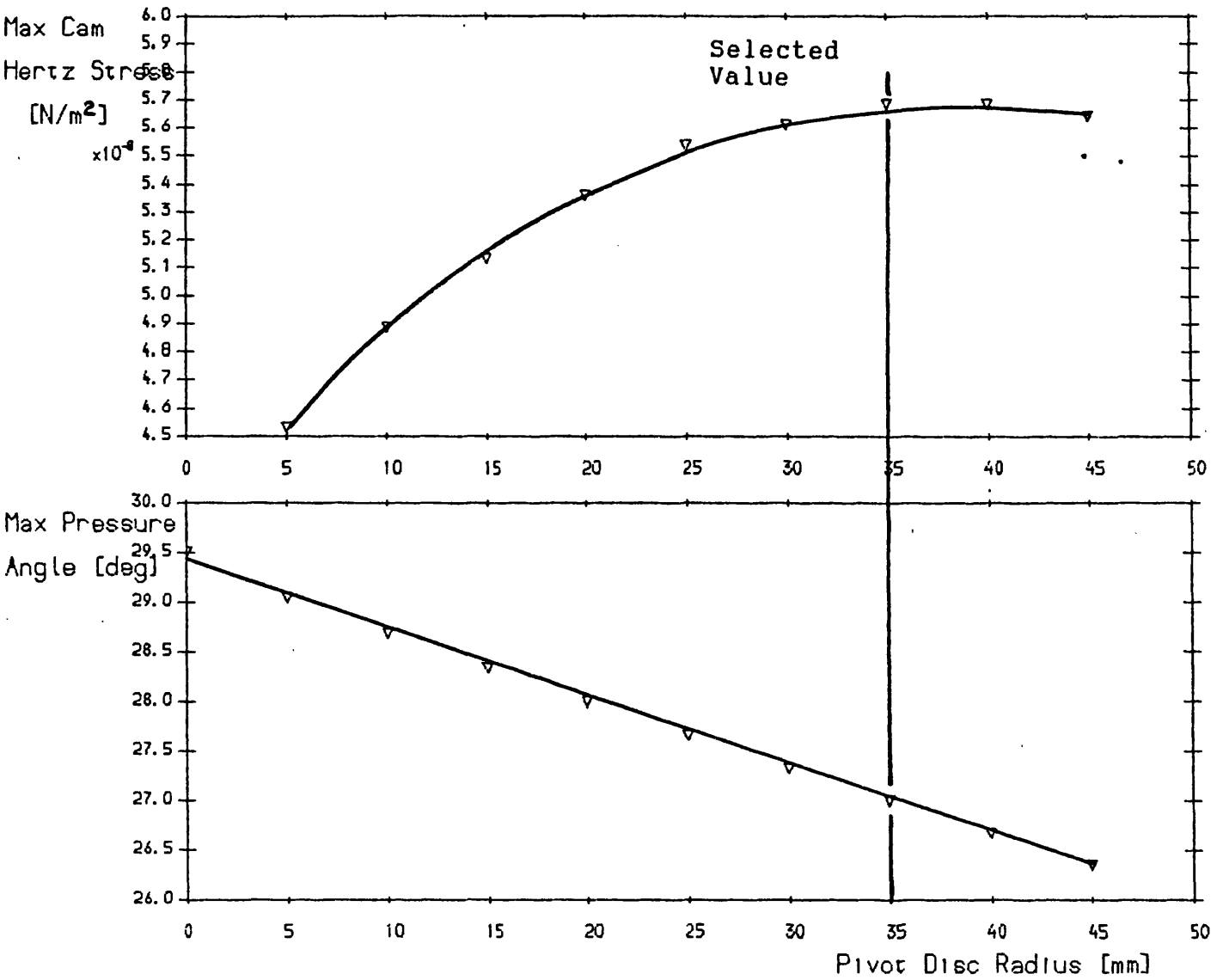

Figure 4.9- Maximum pressure angle and Hertz stress versus pivot disc radius.

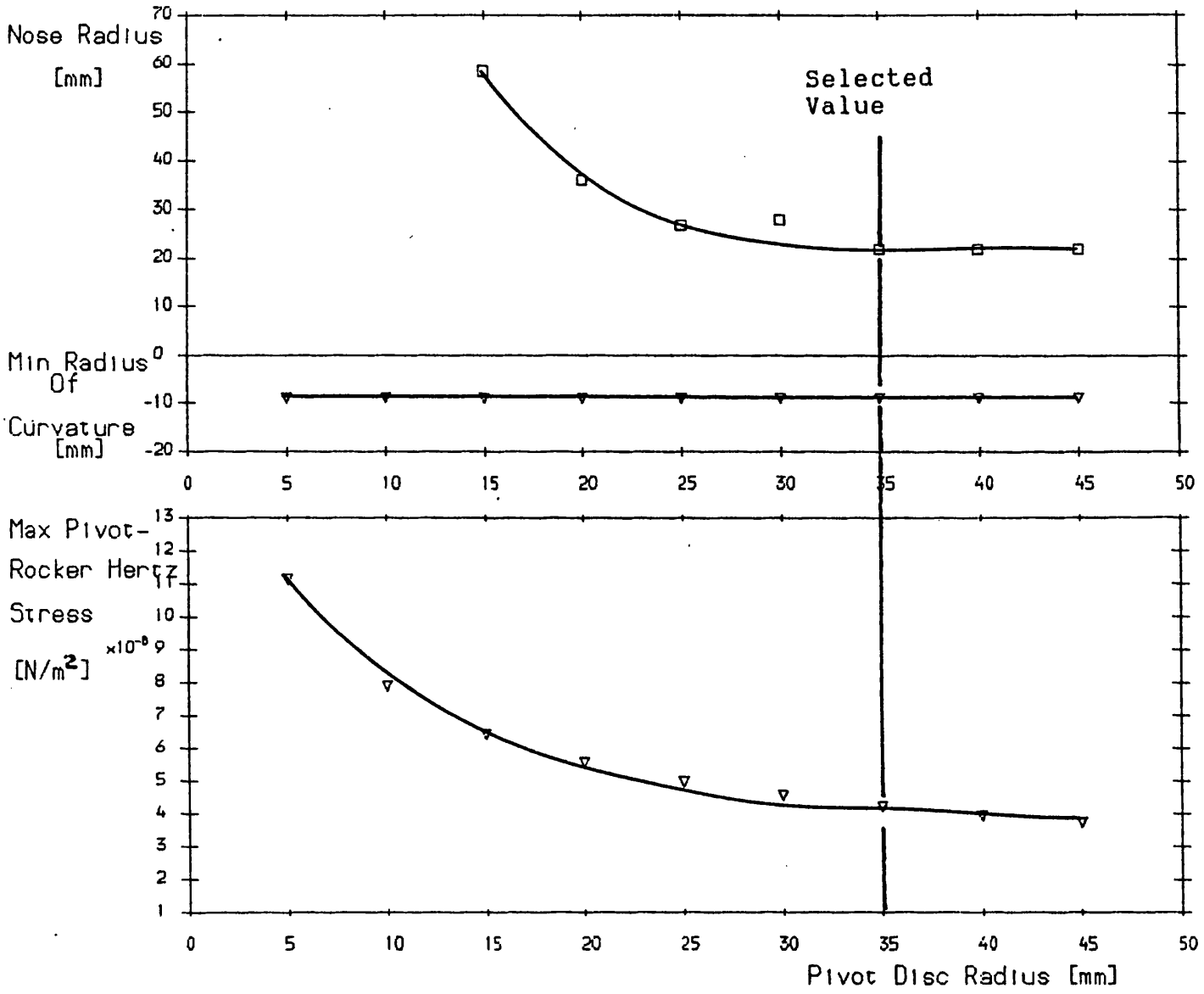

Figure 4.10- Minimum radius of curvature and Hertz stress versus pivot disc radius.

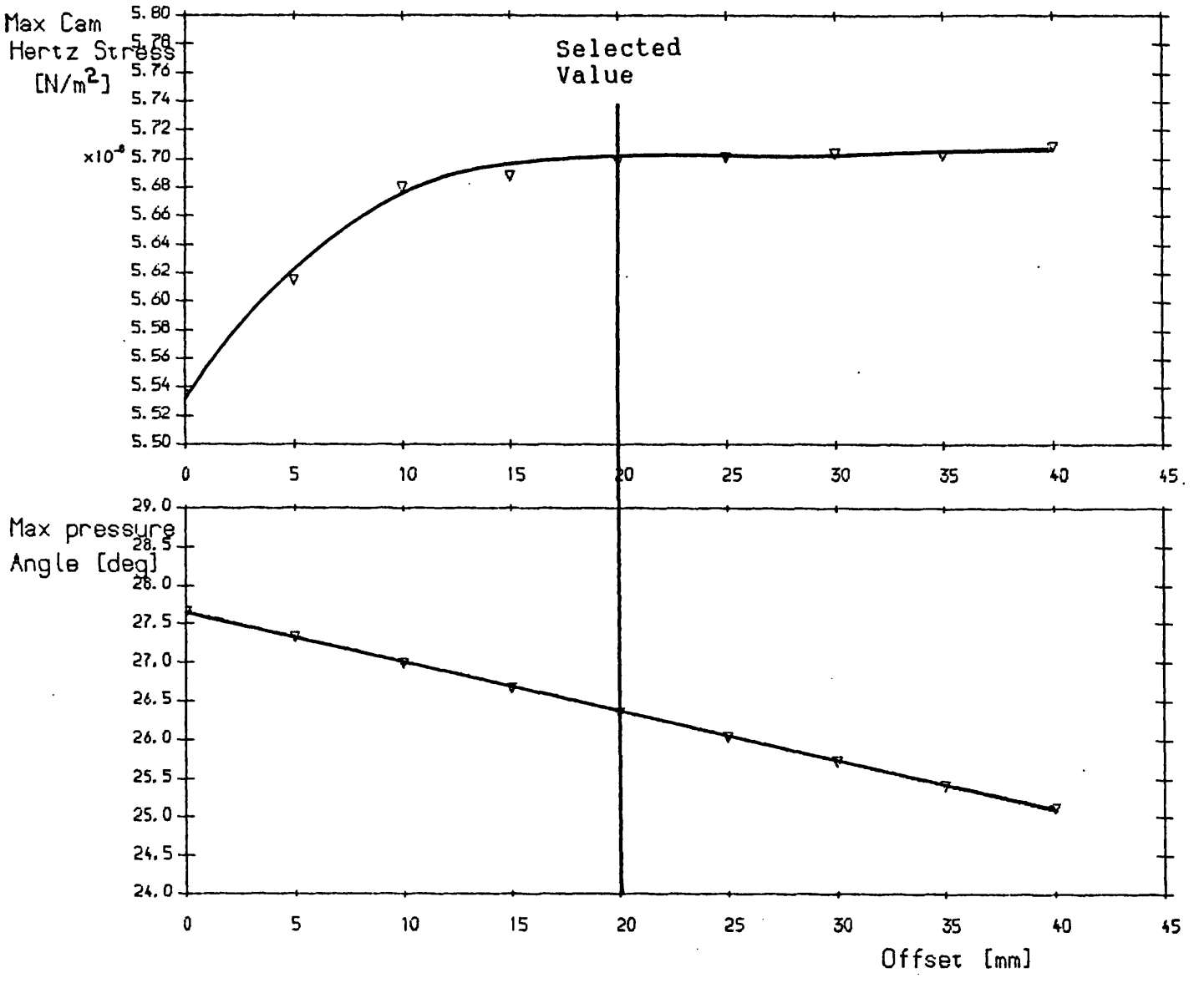

Figure 4.11- Maximum pressure angle and Hertz stress versus offset.

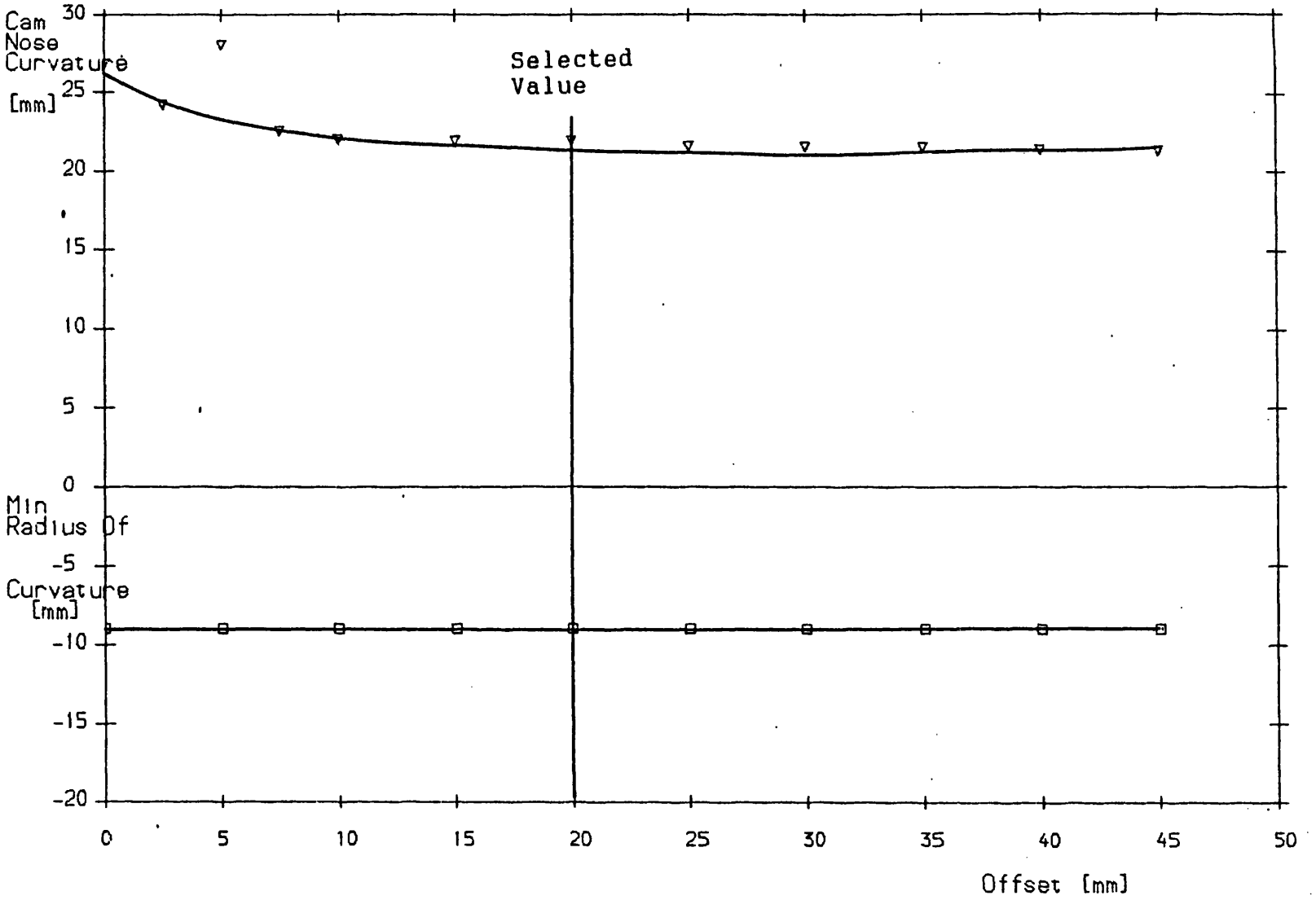

Figure 4.12- Minimum radius of curvature versus offset.

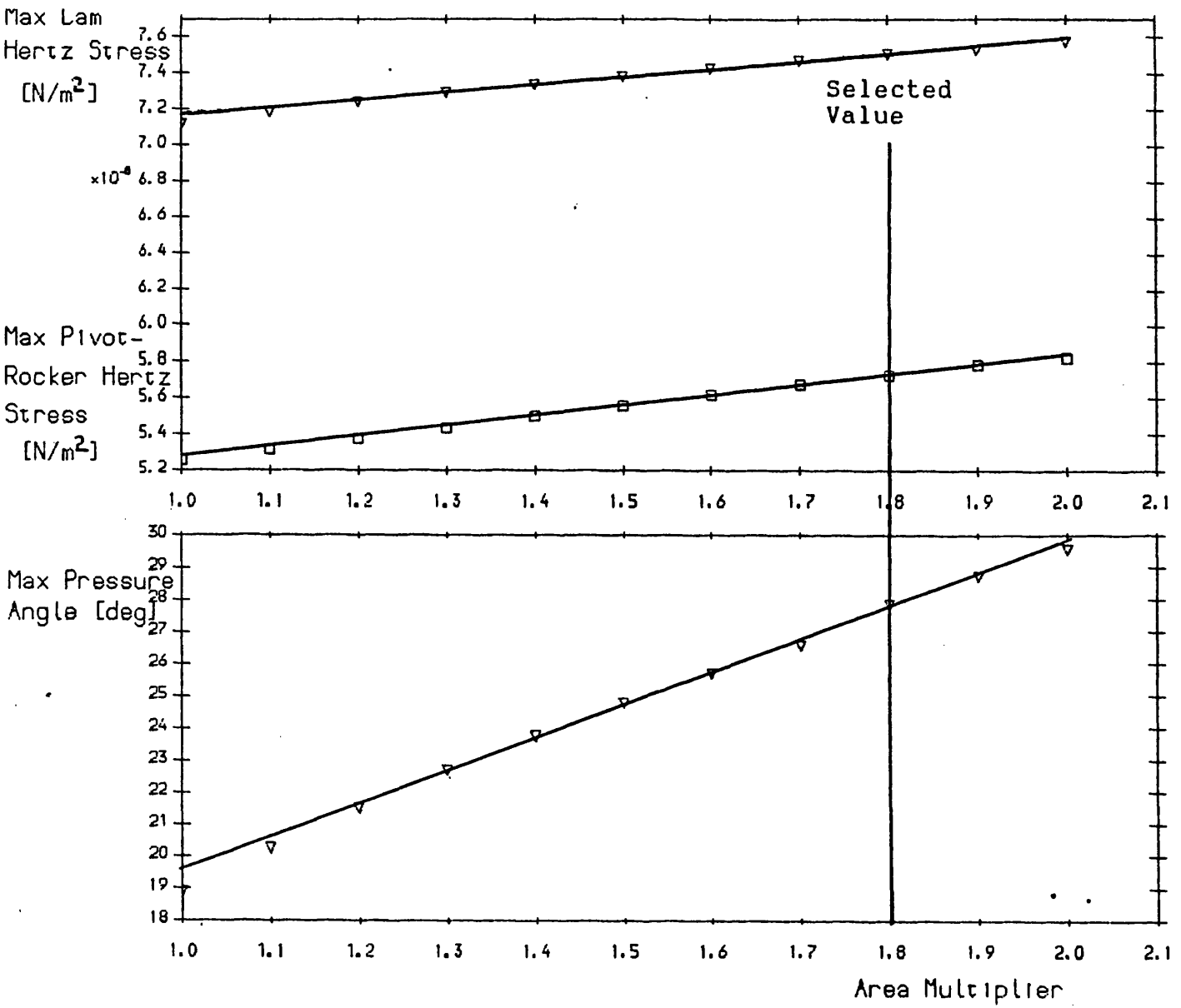

Figure 4.13- Maximum pressure angle and Hertz stresses versus area multiplier.

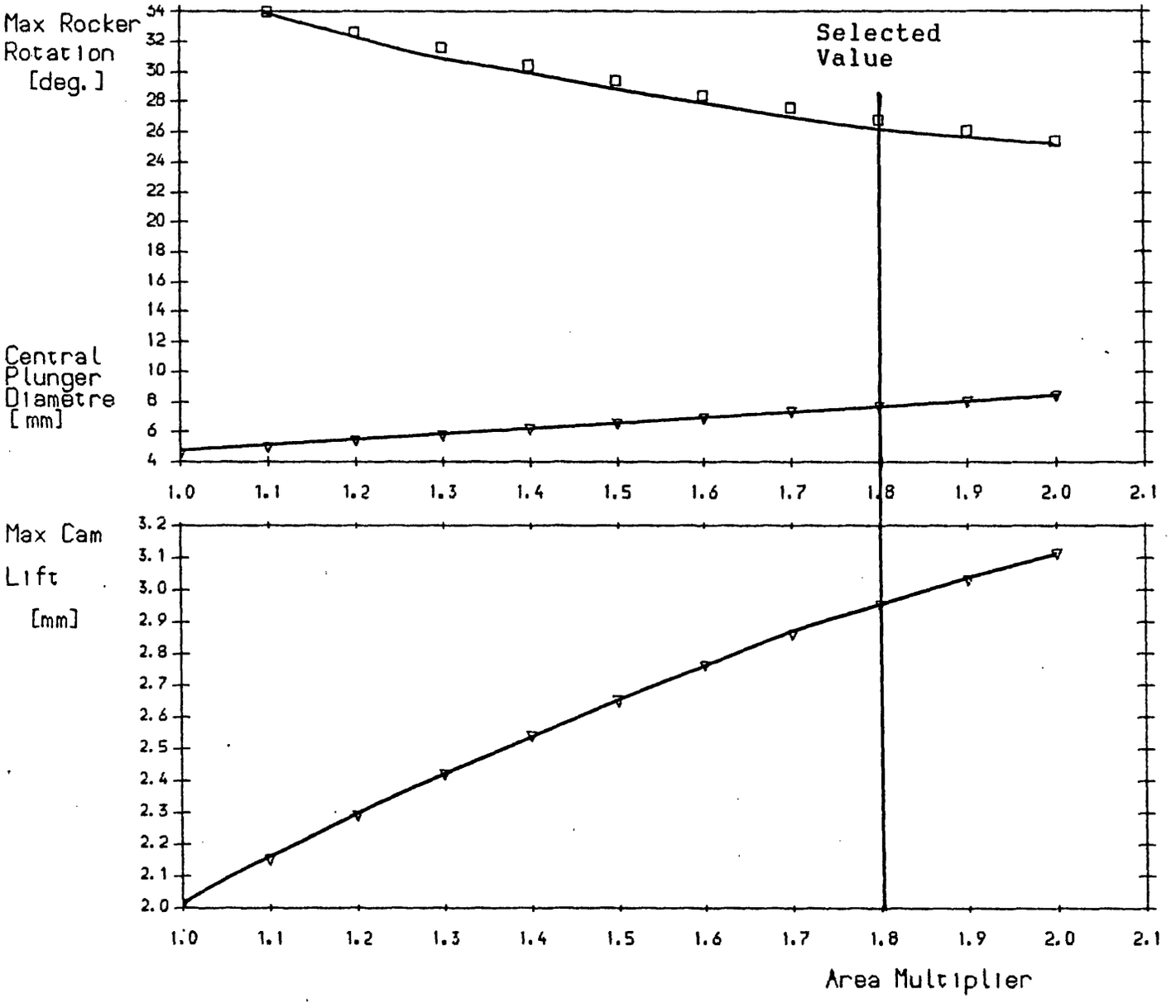

Figure 4.14- Maximum cam lift, rocker rotation and central plunger diameter versus area multiplier.

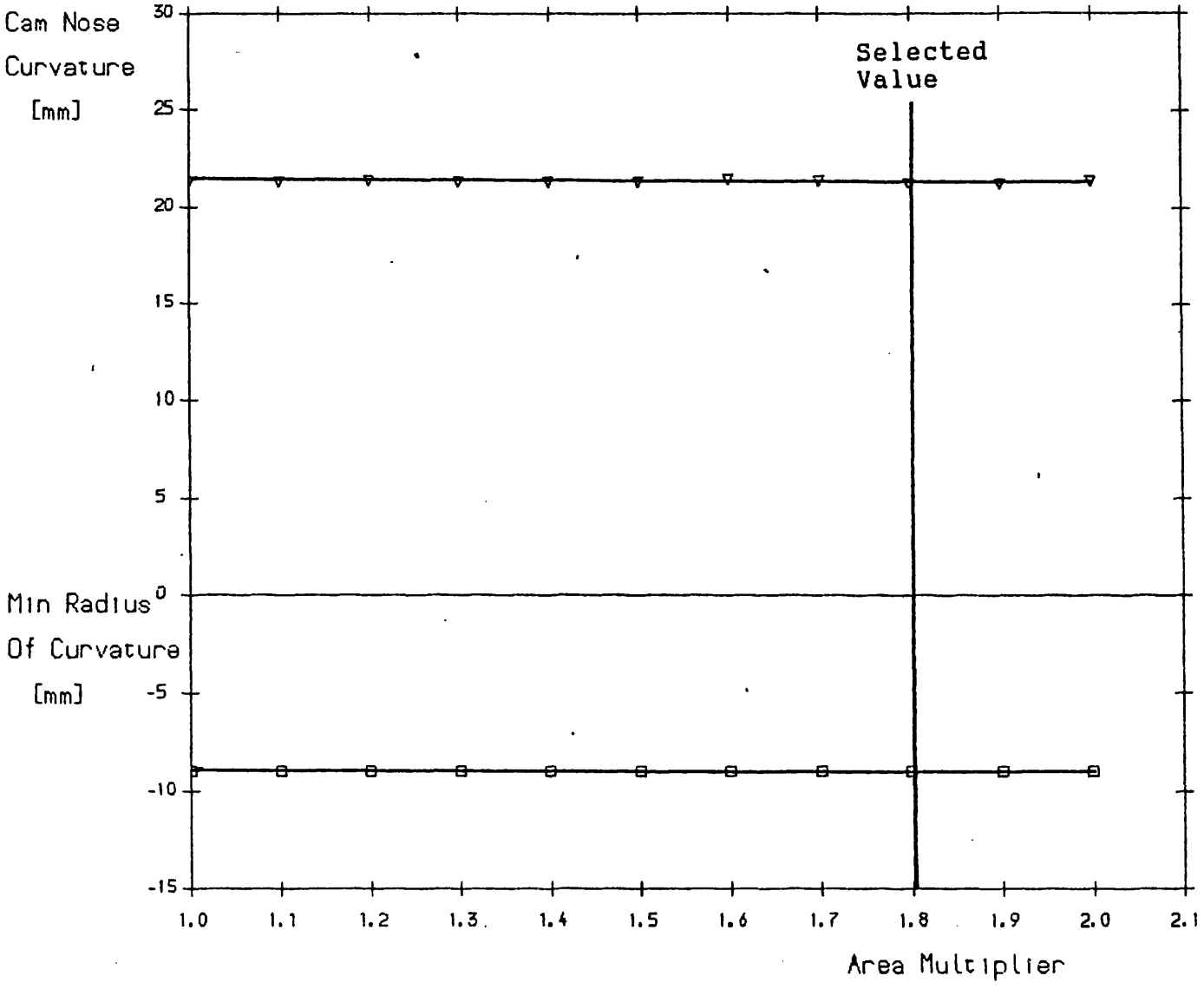

Figure 4.15- Minimum radius of curvature versus area multiplier.

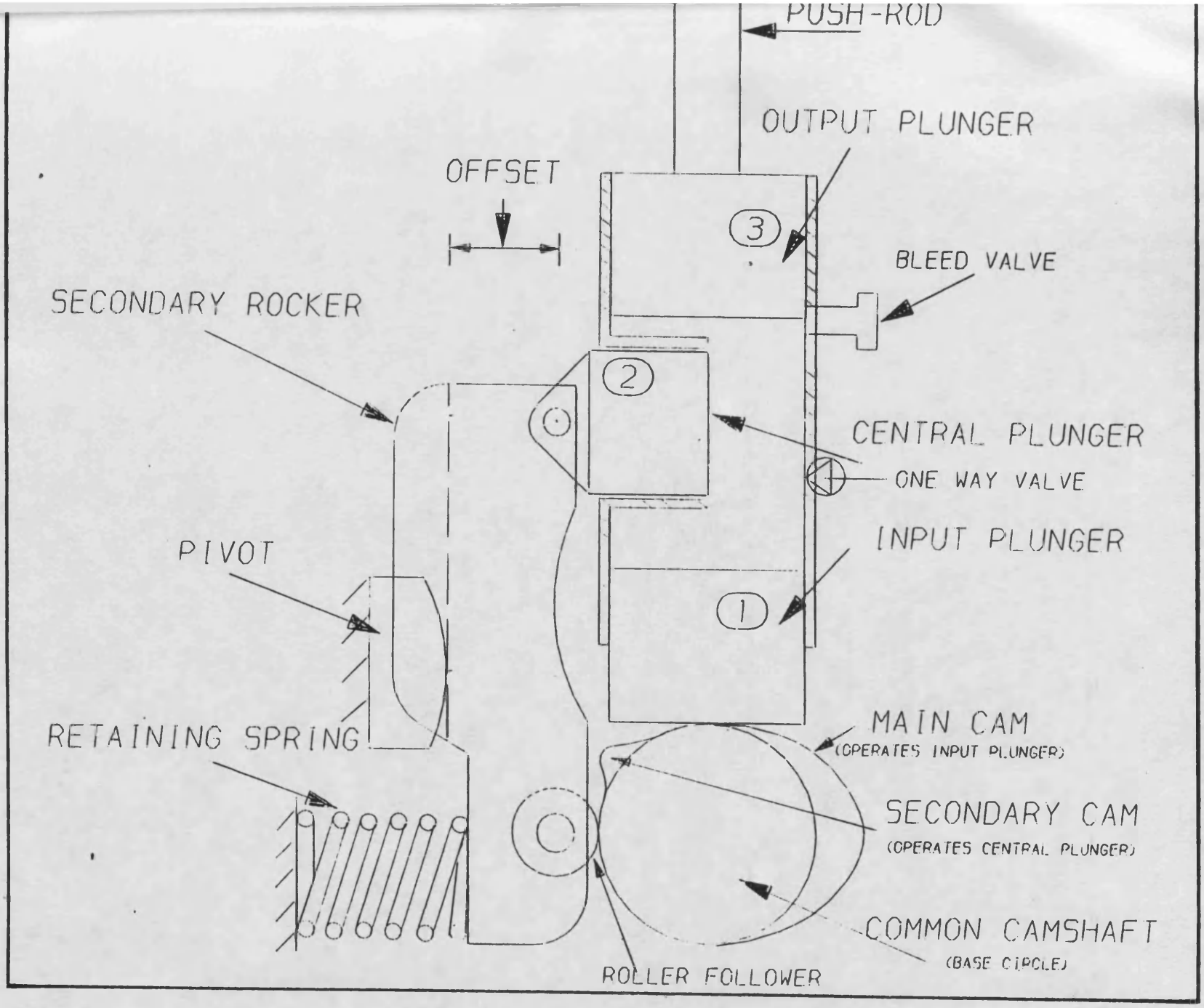

Figure 4.16- Full scale drawing of the mechanism.

CHAPTER 5

Design Of The Experimental Flow Rig.

5.0 Introduction

This chapter describes the experiments to be performed and also discusses the possible methods of obtaining the required experimental results. It establishes that using a real engine for the experimental work is not a practical solution and instead a flow rig is proposed. Consequently the description of the proposed experimental flow rig layout is given.

A simulation of the variable valve rate experimental flow rig is described. This was undertaken in order to arrive at the most suitable dimensions for the exhaust manifold volume and the equivalent turbocharger turbine nozzle diameter. The model of the experimental flow rig has been described. Two simulation techniques, 'filling and emptying' and 'the method of characteristics' have been used to model the experimental rig. The respective models are described and the effects of variations of the exhaust manifold dimensions and the turbine nozzle size on the overall performance of the flow rig are presented.

5.1 Approach to the Experimental Phase

A description of the detailed design of the variable valve rate mechanism was given in chapter 4. The next stage of this investigation is the experimental evaluation of the mechanism. This is to be achieved by means of performing experiments to observe:

(i) the dynamic behaviour of the mechanism, and

(ii) its effects on exhaust pulse formation and energy transfer between the cylinder and the turbocharger turbine.

Two options were initially considered for the way the experiments may be carried out. Using a real high-speed turbocharged diesel engine was one of the two possibilities for the experimental phase of the work. Its suitability for this application was not found to be acceptable for a variety of reasons. First of all, in order to incorporate the variable valve rate mechanism in a real engine a number of major modifications would be necessary to the design of the cylinder block so far as the valve gear side of it is concerned. These modifications are:

a) to re-design the cylinder block to make provision for the inclusion of the hydraulic chamber body, the secondary rocker and the required means of controlling the secondary rocker ratio.

b) to re-design the camshaft housing and possibly the positions of the journal bearings in order to

accommodate the extra cam lobe for each exhaust valve train of the engine.

The above major design modifications were not considered to be a practical solution to the problem. Also, the required experiments would have to be arranged in such a way that the dynamic characteristics of the mechanism may be investigated in isolation. In a real engine there is no possible means of completely eliminating the interactions of the other engine components nor the thermodynamic processes taking place within the engine. The other requirement of the experimental work is to be able to investigate the effects of opening the exhaust valve at a higher rate on the blow-down and the formation of pulses in the exhaust manifold at different cracking pressure levels (cylinder pressure at exhaust valve opening, EVO). In a real engine because of the combustion process, it is impossible to have total control over cracking pressure. As a result the use of a turbocharged diesel engine was ruled out.

The alternative to using a real engine for the experimental work is to a flow rig that allows us to perform all the required experiments. The flow rig should also have all the control features that using a real engine lacks. Using a flow rig offers the facility to eliminate the combustion process and to allow the cracking pressure to be controlled. When there is no air flow to the rig, the mechanism dynamic

performance may be verified without the possible effects of the air flow. Considering all the positive aspects of using an experimental flow rig, this option was chosen.

The basis of the experimental flow rig was to adopt a diesel engine cylinder head and valve gear (for one cylinder only) and modify the camshaft and the exhaust valve train to incorporate the secondary cam and the mechanism. Compressed air may be fed to a constant volume cylinder and later discharged in to the exhaust manifold where pulse formation can be investigated. A detailed description of the flow rig is given below.

5.2 Description of the Experimental Flow Rig

In order to investigate the effects of exhaust valve motion on the energy transport of exhaust gases, and to achieve the objectives of this study, an experimental flow rig has been constructed. In the experimental flow rig compressed air is supplied to the inlet manifold of a Ford 'Dover' diesel engine cylinder head which has only one of the four cylinders present. The cylinder has a constant volume to simulate the volume in the cylinder when the piston is at its bottom dead centre (BDC). The continuously variable valve rate mechanism is installed on the exhaust valve train whilst the inlet valve train is operated conventionally. An exhaust pipe is connected to the exhaust port of the "cylinder", as described above, on the end of which an

orifice plate is mounted to simulate the turbocharger turbine.

The compressed air, which is supplied by a Belliss positive displacement compressor, flows from the inlet manifold to the cylinder as the inlet valve opens. The cylinder may be charged with air at a pressure up to 6 bars corresponding to typical conditions when the exhaust valve of a turbocharged diesel engine is opened. The exhaust valve opens and the air expands from the cylinder pressure to atmospheric pressure in the exhaust pipe. Pressure pulses are generated in the exhaust pipe by the rapid flow through the exhaust valve. The rate at which the exhaust valve opens is controllable using the variable valve rate mechanism.

Since the expansion of air from the cracking pressure to atmospheric conditions is accompanied by a significant drop in the air temperature, provision has to be made to heat the charge in order to ensure that frost is not formed in the exhaust port and pipe. An 18 KW electrical heater is placed before the inlet manifold to increase the temperature of the compressed air. The inlet and exhaust poppet valves are actuated by a camshaft which has three cam lobes. One cam actuates the inlet valve and two actuate the variable valve rate mechanism which actuates the exhaust valve. The three cams are all on one camshaft.

As there is no crankshaft to drive the camshaft an electric motor with a built-in reduction gearbox is used to vary the speed. The electric motor drives the camshaft via a timing belt arrangement giving a 3.5:1 reduction.

A smoothing tank has been used to damp out oscillations in the intake manifold thus supplying a relatively constant pressure flow of air to the cylinder head. The smoothing tank is placed immediately after the electric heater and before the inlet manifold. The smoothing tank has a volume of approximately 57 litres which is sufficiently large to ensure constant pressure air through the experimental flow rig .

A framework has been designed to house the experimental flow rig components, including the cylinder head, variable speed electric motor and the valve gear including the mechanism and the camshaft. A flow diagram of the experimental rig is shown in figure 5.8.

A hydraulic chamber has been designed for the continuously variable valve rate mechanism to house the three input, output and central plungers. Square section piston seals have been used to minimise hydraulic oil leakage. A small amount of hydraulic oil leakage is actually desirable for lubrication between the surfaces in contact. The parametric study, which was discussed earlier (results of which have

been discussed in the preceding chapter), enabled the design of the central plunger, the secondary rocker with the roller follower and the pivot disc radius of curvature. The respective dimensions of the mechanism's components are exactly those proved to be the most suitable by the parametric study. Following the design of the three plungers, the secondary rocker was designed to transmit the motion of the secondary cam to the central plunger. The three plungers and the secondary rocker have all been made of steel and later hardened to a high degree. The pivot point is required to move vertically along the back of the secondary rocker to vary the mechanism's rocker ratio. For this purpose a pivot was designed which can be moved along a tee-guide using a lead thread. In order to ensure contact between the roller follower and the secondary cam, especially when the pivot is in the upper position, a helical spring with a preload is placed between the lower section of the secondary rocker and a bracket which holds the pivot disc, the tee-guide and the lead thread mechanism. This arrangement is shown in figure 5.9. The bracket has been designed in such a way that it rests against, and clamps on to, a post which is part of the supporting framework. The post is securely connected to the rest of the framework so that flexing is prevented.

The choice of materials is a very important consideration, especially so that the surfaces having relative motion are

compatible from a wear point of view. Originally the material chosen for the hydraulic chamber block was mild steel. The three plungers were made of high grade steel and then hardened. This arrangement later proved to be quite problematic during early experimental work. The use of non-compatible materials resulted in excessive hydraulic chamber wear and occasional local seizure. Figure 5.10 illustrates the variable valve rate mechanism with the mild steel hydraulic chamber block. Note that the camshaft and the pivot arrangement have not been shown. The pushrod used on the exhaust valve train is the standard pushrod used on the Dover engine, shortened to the required length.

The modified design of the hydraulic chamber has been more successful. The wear capability of a high-grade cast-iron (the trade name for which is 'meehanite') has been found to be quite acceptable for the hydraulic chamber block material. Apart from the change in material, the block has been redesigned to include two extra features. These are the inclusion of the inlet valve follower, which was previously supported seperately and an increase of the block's overall height. The height of the block was increased from the top and the bottom to give more support to the input and output plungers, thus reducing the inevitable tipping of the plungers. Figure 5.11 shows the variable valve rate mechanism with the cast-iron hydraulic chamber block. The inlet valve follower and the pushrod are

also shown. The camshaft and the pivot arrangement have not been included in the figure.

In order to fill the hydraulic chamber with hydraulic oil a hand pump is used to draw oil from a sump. Air inside the hydraulic chamber is purged out through a bleed valve situated on the side of the block. When the exhaust valve mechanism is in operation a small loss of hydraulic oil is inevitable through leakage. To compensate for this an oil reservoir has been placed between the delivery side of the hand pump and a check-valve mounted on the back of the hydraulic chamber block. The oil reservoir is kept pressurized to allow a free flow of hydraulic oil to the chamber. Oil from the hand pump is passed through a very fine filter (2 microns) before reaching the oil reservoir. The check-valve is of the spring loaded poppet valve type. A pressure differential of approximately 6600 N/m^2 (1.0 lbf/in^2) opens the check-valve to allow flow of oil to the chamber.

A small plenum has been designed for the exhaust side of the experimental flow rig to obtain non-fluctuating pressure downstream of the turbine nozzle. A silencer is connected downstream of the plenum to reduce the noise before the air is discharged to the surroundings. Figure 5.12 shows an overall side view of the complete experimental flow rig.

5.3 Description of the Experimental Flow Rig Models

A study has been undertaken in order to arrive at the most suitable dimensions for the exhaust manifold volume and the equivalent turbocharger "turbine" nozzle diameter. The model of the experimental flow rig for this study is a very simple representation of the actual experimental rig whose detail description is given in the preceding section. For the purpose of computer simulation, the model of the experimental flow rig has been simplified to include only those parts which influence the flow of air through the system. The model comprises of intake and exhaust manifolds, a constant volume to represent the engine cylinder at exhaust valve opening (EVO), an inlet and exhaust valve, a nozzle mounted on the end of the exhaust manifold to simulate the turbocharger turbine, and a crankshaft to provide a time base for the valves.

The motion of the inlet valve is fixed and does not vary with engine speed but the exhaust valve motion changes as the engine speed changes in order to simulate the inclusion of the variable valve rate mechanism. The high pressure air enters the intake manifold, from a compressor which supplies high density air to a heater placed before the intake manifold (the compressor and the heater are not modelled), before entering the cylinder. The inlet valve opens and the air may enter the constant volume until the inlet valve closes (AVC). The conditions inside the constant volume

cylinder simulate the conditions in a turbocharged diesel engine cylinder at the point of exhaust valve opening (EVO). The cracking (cylinder) pressure and temperature are approximately the same as those of the air supplied to the constant volume. As the exhaust valve opens the air expands from the cracking pressure to atmospheric pressure in the exhaust manifold. The exhaust valve motion is made to change with speed in such a way that it opens more rapidly at the lower engine speeds, thus allowing the exhaust gases to be discharged to the exhaust manifold more rapidly. Exhaust pressure pulses are formed in the exhaust manifold and are eventually discharged to the surroundings through the nozzle which simulates the turbocharger turbine.

5.3.1 Rig Simulation Using The Filling and Emptying Technique

'Filling and emptying' methods of analysis range from being slightly more complex than quasi-steady models (not described here but may be found in reference 46) to being almost as involved as wave action techniques, which are described later. The basic characteristics of all filling and emptying models is that the manifolds between the engine and turbocharger components are represented by finite volumes. This means that the manifolds are capable of accumulating gas, the components can not be connected by a common air mass flow rate as in quasi-steady models.

The result is a set of first-order non-linear ordinary differential equations which define the conditions in the manifold, cylinder and, for transient performance, the engine and turbocharger dynamics. The filling and emptying method is used extensively throughout industry both for the design of engines and manifolds, and turbocharger matching. These models are more realistic than quasi-steady ones and require less empirical data; however, the computer time needed for their solution is an order of magnitude greater.

Since these models characterise the manifold conditions by one pressure and one temperature it is not possible to evaluate manifold tuning or mixture maldistribution using such an approach; detailed manifold design requires use of a wave action technique.

The 'filling and emptying' program used to model the experimental flow rig is known as 'SPICE' written by S.J. Charlton (61).

One area of vital importance to the simulation of any engine, and in particular for the purpose of the experimental flow rig simulation, is the inlet and exhaust valves effective flows areas. There are two ways of determining these areas, either to measure experimentally or to calculate theoretically using valve lift, valve head and port size relationships coupled with assumed discharge

coefficients. For this study the valve effective areas were calculated rather than measured. A full description of the valve effective area measurement method which is based on relationships between cylinder size, valve lift, valve head diameter, valve seat angle port shape, pressure drop and steady-state flow rate is given in appendix 8.

As the inlet valve opens, the pressurised air enters the cylinder from the inlet manifold and fills the cylinder. The pressure inside the cylinder is intended to be at the same level as it would be in an engine at the time of exhaust valve opening (EVO). Then the exhaust valve opens and the air is released to the exhaust manifold before discharging to atmosphere. A schematic representation of the model is shown in figure 5.1.

The exhaust valve effective flow areas have been determined by applying the ideal motion and the variation range is shown in figure 5.2. The shape of the effective flow are versus crank angle curve changes as the engine speed (shaft speed in the model) increases from 1000-2200 rev/min to simulate the effect of varying the secondary rocker ratio.

5.3.2 Experimental Flow Rig Simulation Using Wave Action Theory

Simulating a turbocharged diesel engine adopting the 'filling and emptying' method has one important disadvantage

with respect to the pulse turbocharging system. In such simulations the exhaust manifolds are treated as simple thermodynamic 'control volumes', where the variation of gas state, for example pressure and temperature, spatially along the manifold is ignored. Yet the pulse turbocharging system relies on energy transfer in the form of a pressure wave, hence the instantaneous pressure at each end of the manifold, at any instant, could be different. Neglecting these spatial variations introduces an error and its consequences will depend upon how long it takes for the pressure wave to travel the length of the manifold. If this time interval, expressed in terms of crankshaft angular displacement, is very small, the error will be small. This will usually be the case with small pulse turbocharged engines. However, for large engines the time interval may be long and a significant error will be introduced if pressure wave effects are ignored, particularly if the engine also runs at high speeds. One of the important effects is the modelling of the scavenge period of the cylinder from which the pulse was issued viz-a-viz the time of return of the reflected wave.

Riemann (57) made a significant contribution by proposing the 'method of characteristics' technique which takes account of waves travelling in both directions; De Halter (58) applied this technique to the exhaust system of an engine and Jenny (59) extended it to include area changes,

friction, heat transfer and flow through turbochargers. Wallace (60) and Benson (49) also extensively applied the characteristics methods to engines.

The method of characteristics is a mathematical technique for solving hyperbolic partial differential equations such as those obtained for waves in a compressible flow. Engine simulation programs based on the wave action theory (46), which adopts the method of characteristics, apply the technique to model pressure wave action principally in the exhaust manifolds. There is no reason why treatment of the remainder of the engine system (cylinders, valves, compressor, turbine and possibly intake manifold) should be any different from that adopted in filling and emptying programs.

Although the equations that represent the flow in the pipes may be solved by the method of characteristics, the flow itself is governed by what happens at the boundaries, at each end of the pipes. Thus the analysis must be coupled with the solution of boundary conditions representing the exhaust valves, the turbine or the nozzle that may simulate it and junctions of various pipes.

The variable valve rate experimental flow rig was simulated in order to determine the most appropriate dimensions, such as exhaust manifold length and diameter and equivalent

turbine nozzle diameter. The flow rig has been simulated using two different simulation programs. The two programs are different in the way they process the input data using different methods as described below.

For this study, the particular area of interest is the pressure pulse formation in the exhaust pipe of the simulated engine. A simple FORTRAN program for a single-cylinder engine and single exhaust pipe configuration, written by R.S. Benson (46), has been adopted to model the flow rig. This program models a single-cylinder engine with a constant pressure inlet manifold and a single exhaust pipe. It uses a number of subroutines, for example to handle the cylinder and exhaust pipe boundary conditions.

In the cylinder subroutine the time step is set in degrees crank angle and logical decisions are made to test the length of the calculation at any point and adjust the angle when it exceeds 360 or 720 degrees, depending on the engine type. The testing of the valve opening and closing time is incorporated in the valve area-crank angle diagram, as shown in figure 5.2. The flow areas of the effective intake and exhaust valves used were the same as those used for the filling and emptying study described earlier.

The single-cylinder engine model is a very simple one, and schematicaly is represented by a constant volume for the

engine cylinder which is connected to a pipe designated the exhaust pipe on the end of which a nozzle is mounted to simulate the turbocharger turbine. The cylinder is charged with air to a pressure and temperature corresponding to those prevailing at exhaust valve opening (EVO) in a turbocharged engine. As the exhaust valve opens the air discharges to the exhaust pipe, which is initially at atmospheric pressure, through the exhaust valve and port. This process allows the formation of a pressure wave which travels along the pipe towards the nozzle. The profile, and the energy content, of the pressure pulse varies from the cylinder end to the nozzle end of the exhaust pipe. The program offers the capacity to observe these variations by selecting different positions along the exhaust pipe. Of significant interest here is the exhaust pressure history at the nozzle end of the pipe.

5.4 Discussion of the Rig Simulations Results

(a) Discussion of the 'Filling and Emptying' Results

The objective of simulating the experimental flow rig was to give a clear insight of the likely events occuring within the rig, in order to arrive at the most suitable exhaust manifold dimensions and equivalent 'turbine' nozzle diameter. Two main studies were to be performed. The first study examines the effect of nozzle diameter on exhaust pulse form. The aim of this study was to achieve complete expansion of the exhaust pulses within 40-60 degrees of EVC

in order to simulate the blow down process in a typical turbocharged diesel engine. This has been achieved by varying the nozzle diameter. Figure 5.3 illustrates the effect of this variation on the exhaust pressure pulse.

With an exhaust manifold volume of 10 litres at an engine speed of 1000 rev/min, the nozzle diameter was varied over the range 15 to 25mm as shown in figure 5.3. At the lowest nozzle diameter value of 15mm, the exhaust pulse rises rapidly but does not decay to atmospheric pressure until almost a complete engine cycle. As the nozzle diameter is increased a fall in the peak pressure is observed and a more rapid expansion towards atmospheric pressure follows. With the largest nozzle diameter of 25mm a satisfactory exhaust pressure pulse has been formed which fulfills the first of the two requirements mentioned earlier.

The second study examines the effect of exhaust pipe dimensions (volume) on the pulse form. This study aims to achieve a pressure pulse comparable in shape to the pulse observed in the exhaust system of a turbocharged engine. A nozzle diameter of 25mm was used for this study and the exhaust manifold volume was varied between 1.5 and 6 litres. It can be seen from figure 5.4 that as the exhaust manifold volume decreases, the exhaust pulses have a higher maximum value. It is also observed that the pulse expands to

atmospheric pressure earlier as the exhaust manifold volume is reduced.

(b) Wave Action Results

A wave action model, based on the method of characteristics, has been used to study events in the exhaust pipe of the experimental rig as an aid to design. In this study the constant volume cylinder is filled with air at a pressure of 6 bars, a realistic cracking pressure in a turbocharged diesel engine. An exhaust pipe length of 1.2 metres and internal diameter of 40mm were chosen and the nozzle diameter was varied over the range 17-25 mm. Figure 5.5 shows behaviour similar to that predicted by the filling and emptying model. As the nozzle diameter is increased the exhaust pulse peak pressure falls and expands to atmospheric conditions earlier. As the nozzle diameter is increased from 17 to 25 mm the peak pressure falls from approximately 2.6 to 2.15 bars.

A nozzle diameter value of 25mm was, therefore, chosen to observe the effects of changes in exhaust pipe length (volume in the previous study) on the exhaust pressure pulse. Four different exhaust manifold volumes have been used corresponding to exhaust pipe lengths of 1.2-4.8 metres as shown in figure 5.6. It can be seen that as the exhaust manifold length and volume increase, the peak value of the exhaust pressure pulse decreases quite significantly. An

increase of exhaust manifold volume from 1.5 to 6.0 litres has the effect of reducing the pulse peak value from approximately 2.15 to 1.4 bar. This confirms the well known requirement for exhaust manifolds to be as compact as possible.

Figure 5.7 compares the exhaust pulses predicted by both the filling and emptying and the method of characteristics techniques. As described earlier in section 5.2.3 the method of characteristics is capable of showing the spatial variation of the exhaust pressure pulse in the exhaust manifold. Three locations along the exhaust pipe have been selected to monitor the exhuast pulse formations. These locations are: immediately after the exhaust valve in the port, the mid-point along the pipe length and immediately before the turbine nozzle. The variation in the pulse form along the pipe is quite apparent. The exhaust pulse profile and its peak pressure value changes from the valve end to the nozzle end of the pipe. There is also a delay in the start of the exhaust pulse formation further away from the exhaust valve indicating the time taken for the pulse to travel along the pipe.

The exhaust pulse predicted by the filling and emptying model of the experimental flow rig seems to be very close to the exhaust pulse obtained at the mid-point of the pipe using the method of characteristics. The peak pressure

value of the pulse predicted by the filling and emptying technique is approximately 1.95 bars and the mid-point pulse prediction by the method of characteristics has got a peak value of approximately 1.90 bars.

Thus, a comparison between the results obtained from the filling and emptying rig simulation and those of the method of characteristics shows that they are in very good agreement. Comparing identical situations, that is using the same size exhaust pipe and equivalent turbine nozzle, reveals that the exhaust pulse peak pressures of approximately 1.95 and 2.15 bars may be observed, as seen in figures 5.4 and 5.6, confirming the good agreement between the two simulation techniques for small exhaust manifolds.

5.5 Final Design of The Exhaust Side of The Experimental Flow Rig

The results obtained from the simulations of the experimental flow rig have enabled the preliminary design of the exhaust side of the rig to be settled. The exhaust manifold consists of a pipe of 40mm internal diameter with a length of 1.2m including the exhaust port bend. These dimensions correspond to an exhaust manifold volume of approximately 1.5 litres which is 1.5 times the engine swept volume. The exhaust pipe and turbine nozzle dimensions have thus been estimated to reproduce pulses on the flow rig

comparable to those observed on an equivalent size turbocharged engine.

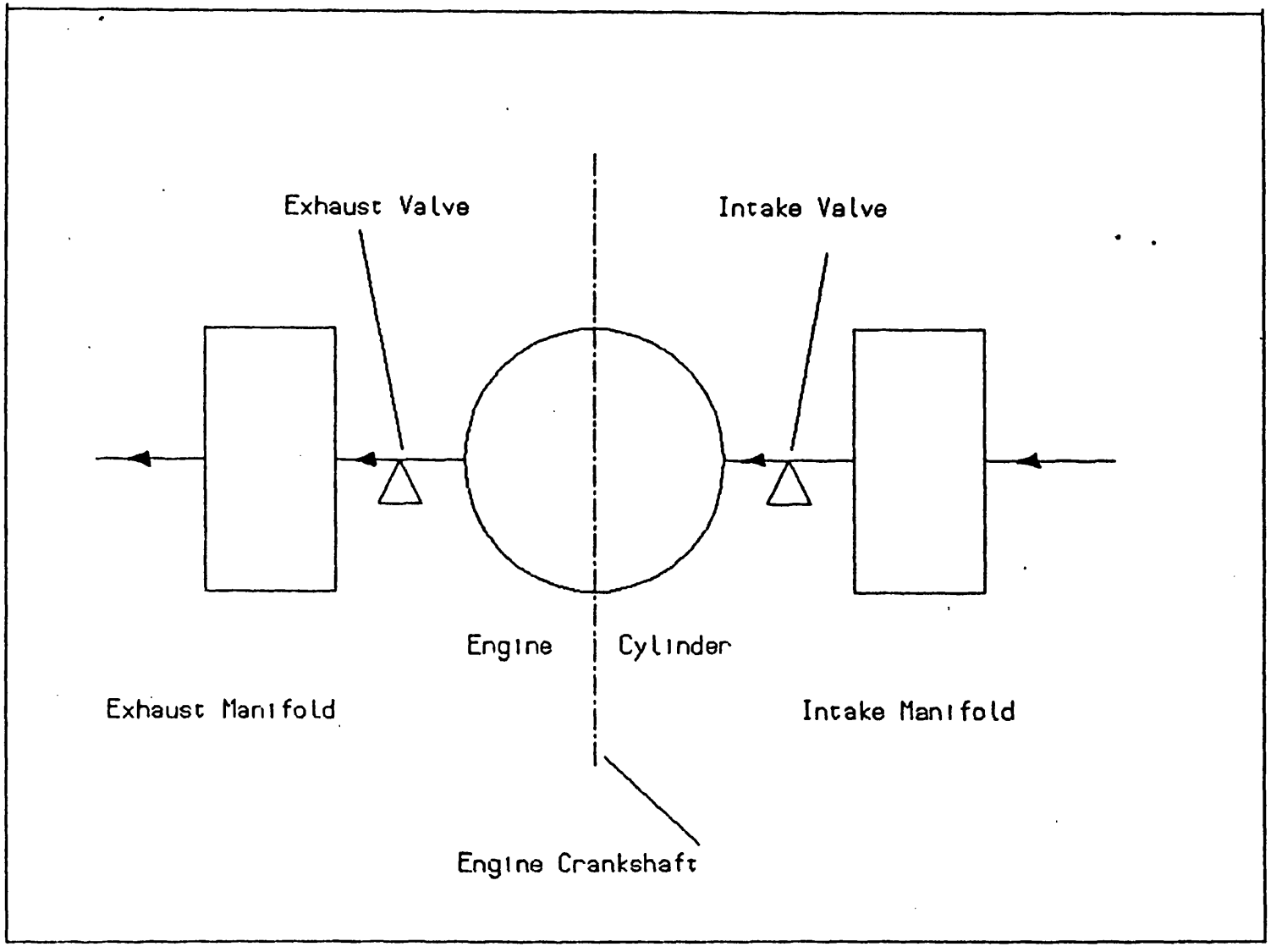

Figure 5.1- Schematic representation of the Experimental Flow Rig Model in 'SPICE'.

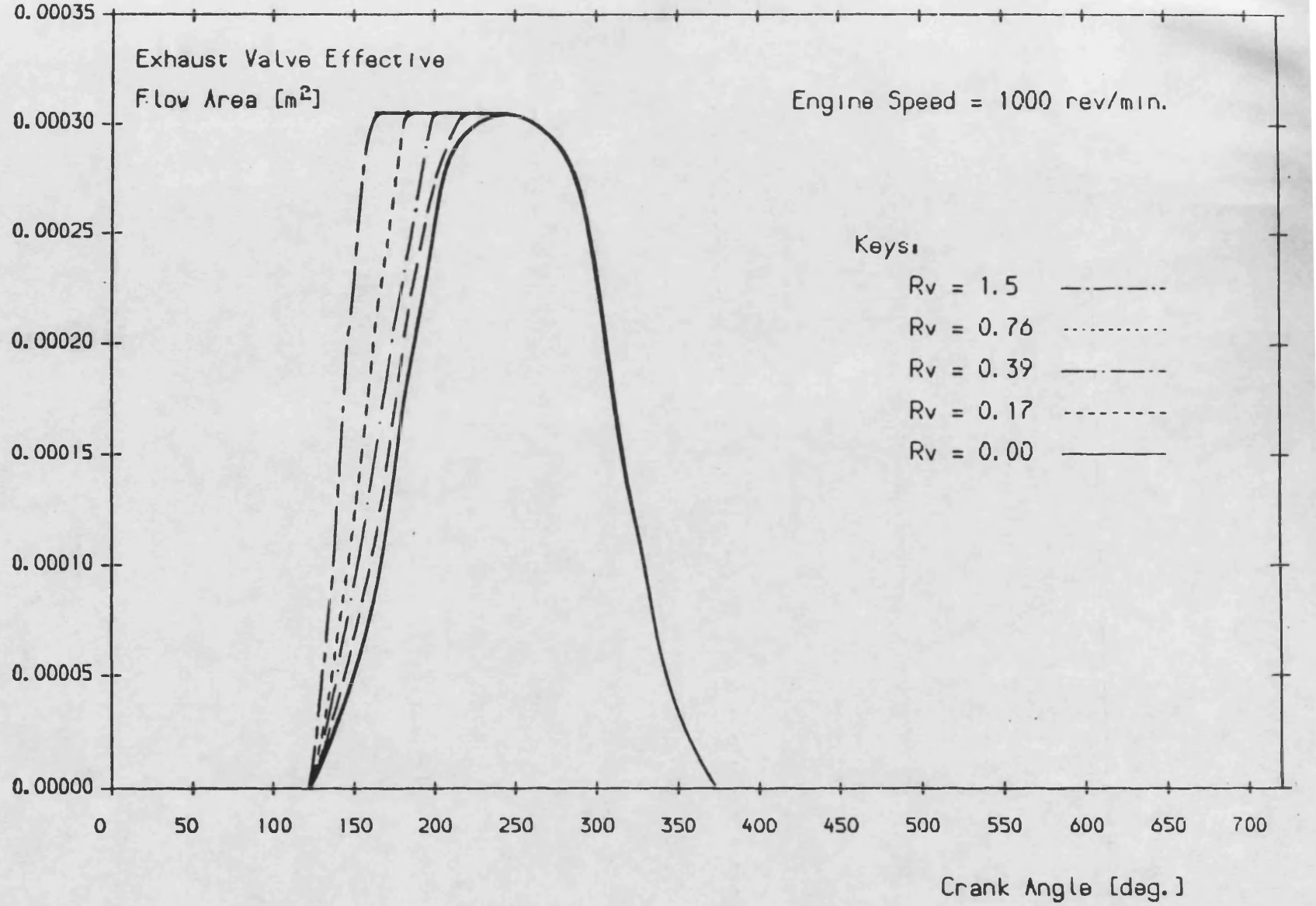

Figure 5.2- Variation of exhaust valve effective flow area with changes in secondary rocker ratio.

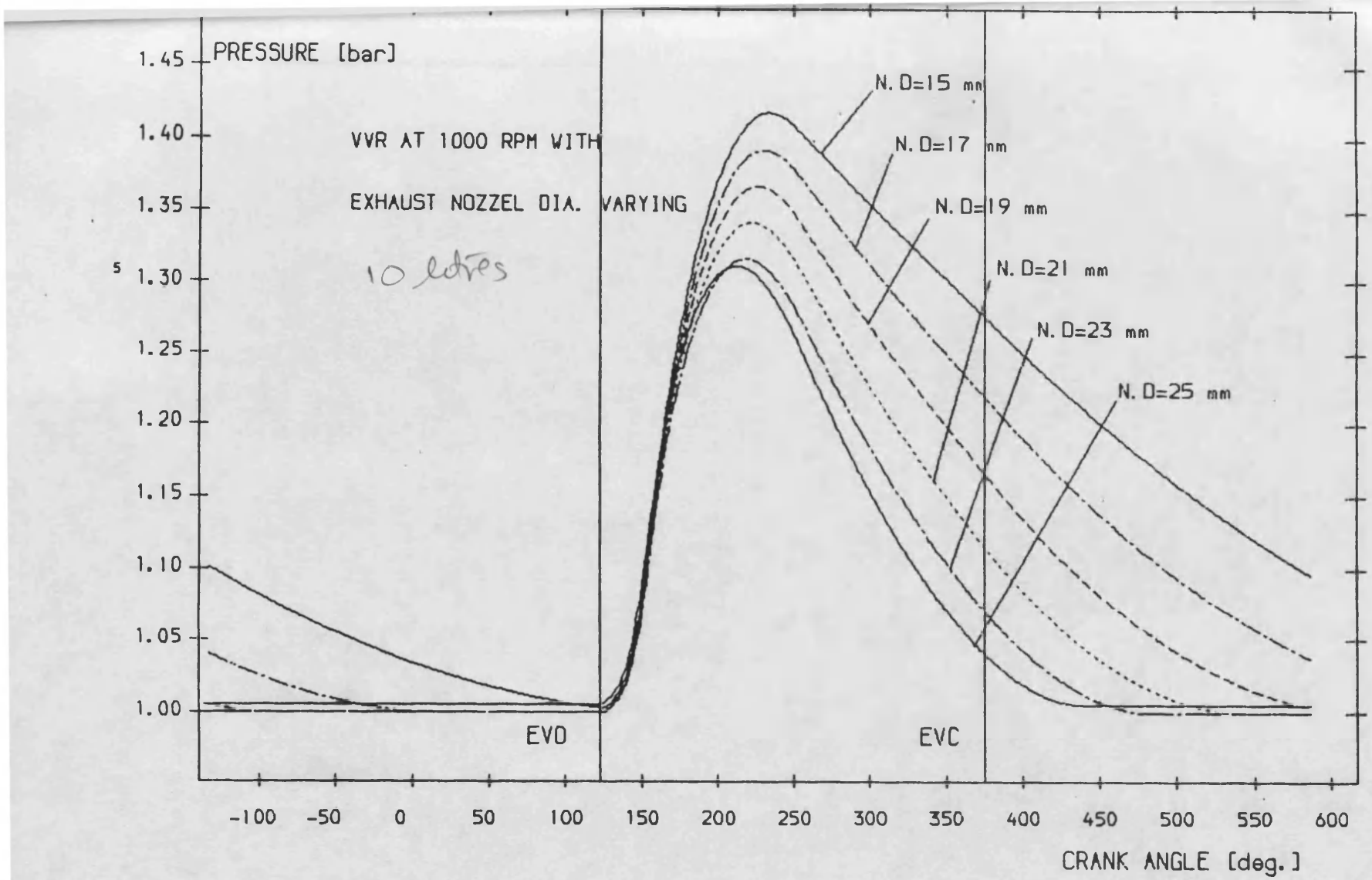

Figure 5.3- Effects of varying 'turbine' nozzle diameter on the exhaust pulse in 'SPICE'.

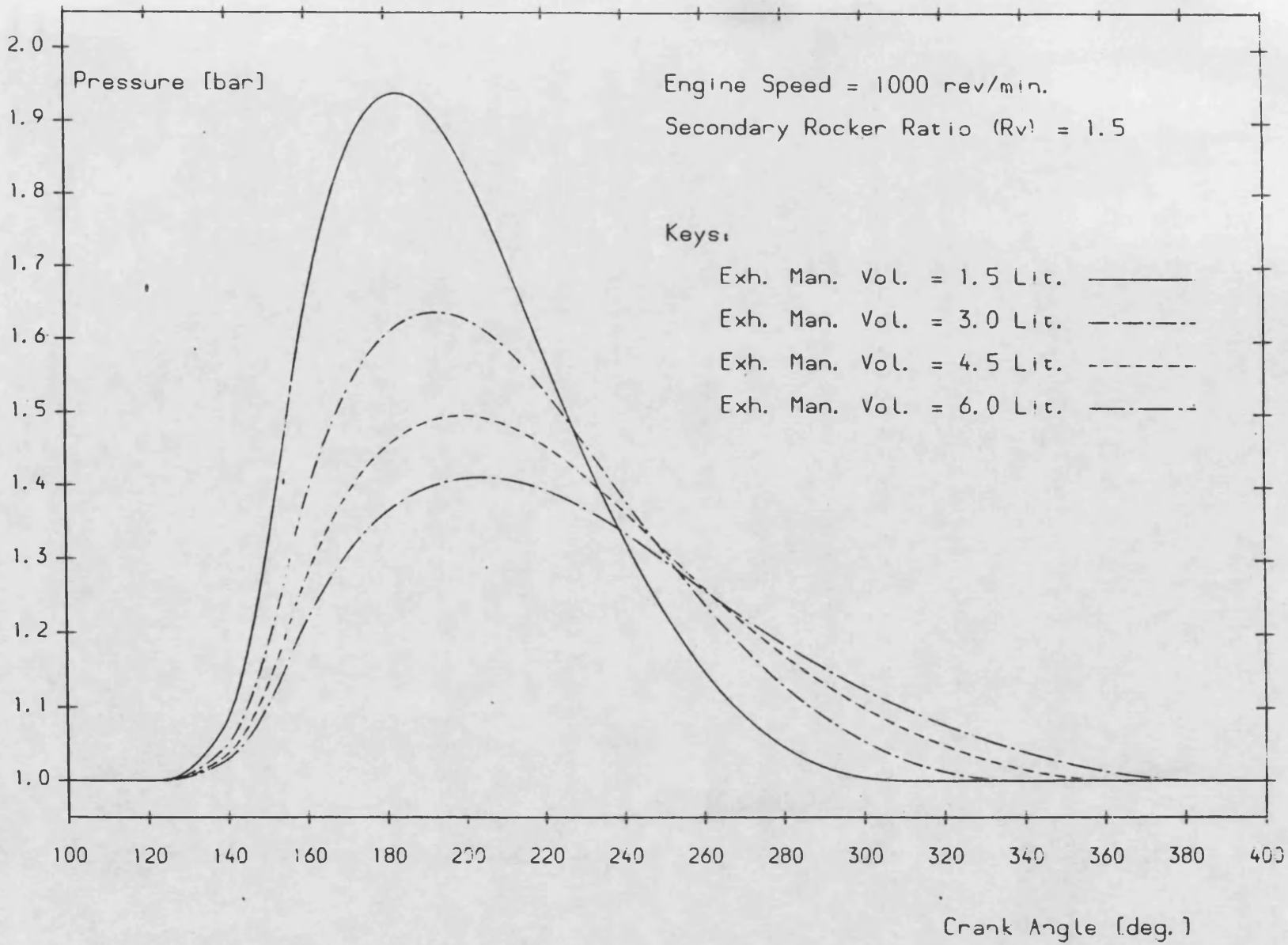

Figure 5.4- Effects of varying exhaust manifold volume on the exhaust pulse in 'SPICE'.

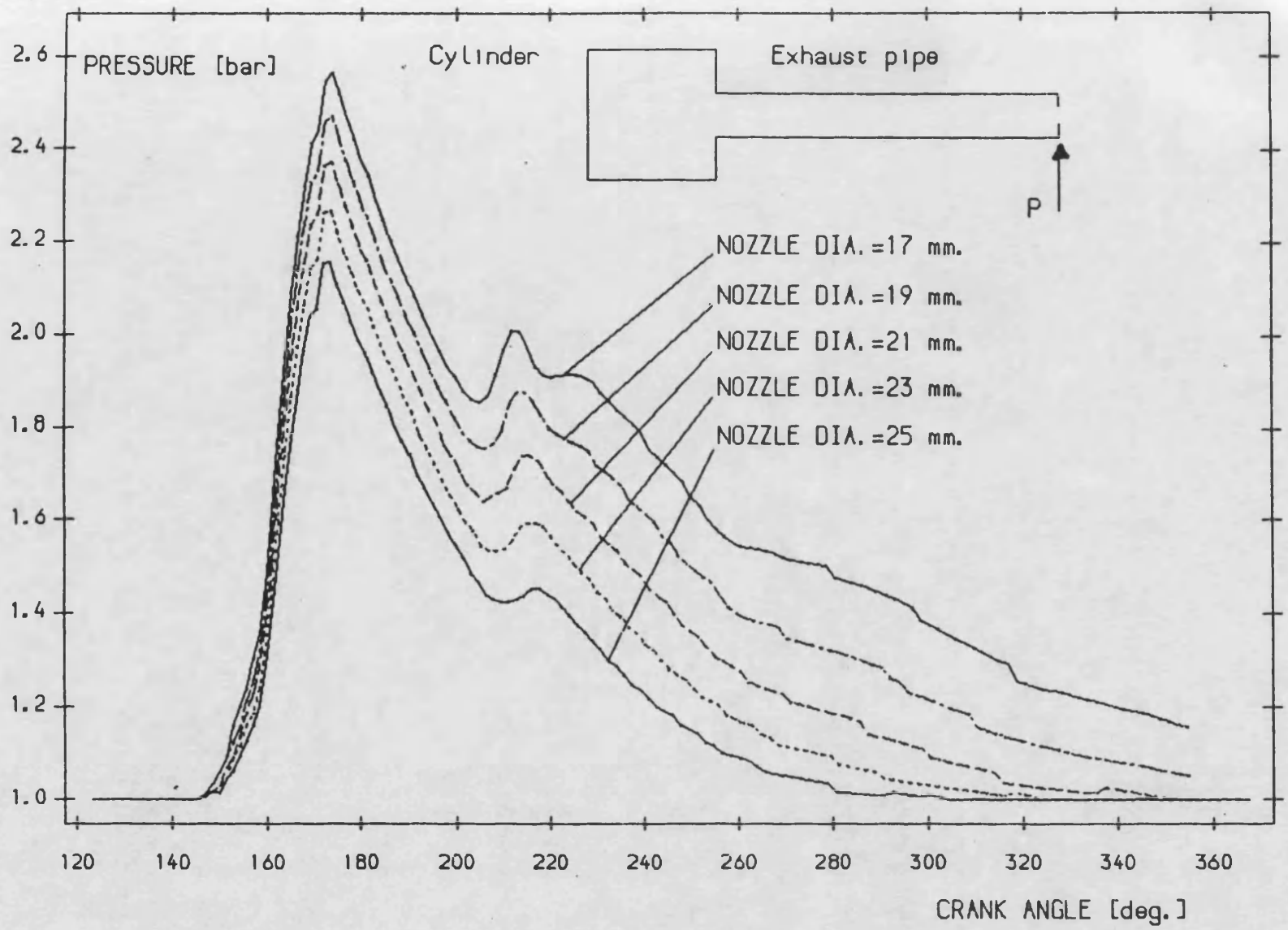

Figure 5.5- Effects of varying 'turbine' nozzle diameter on the exhaust pulse in the Wave Action model of the rig.

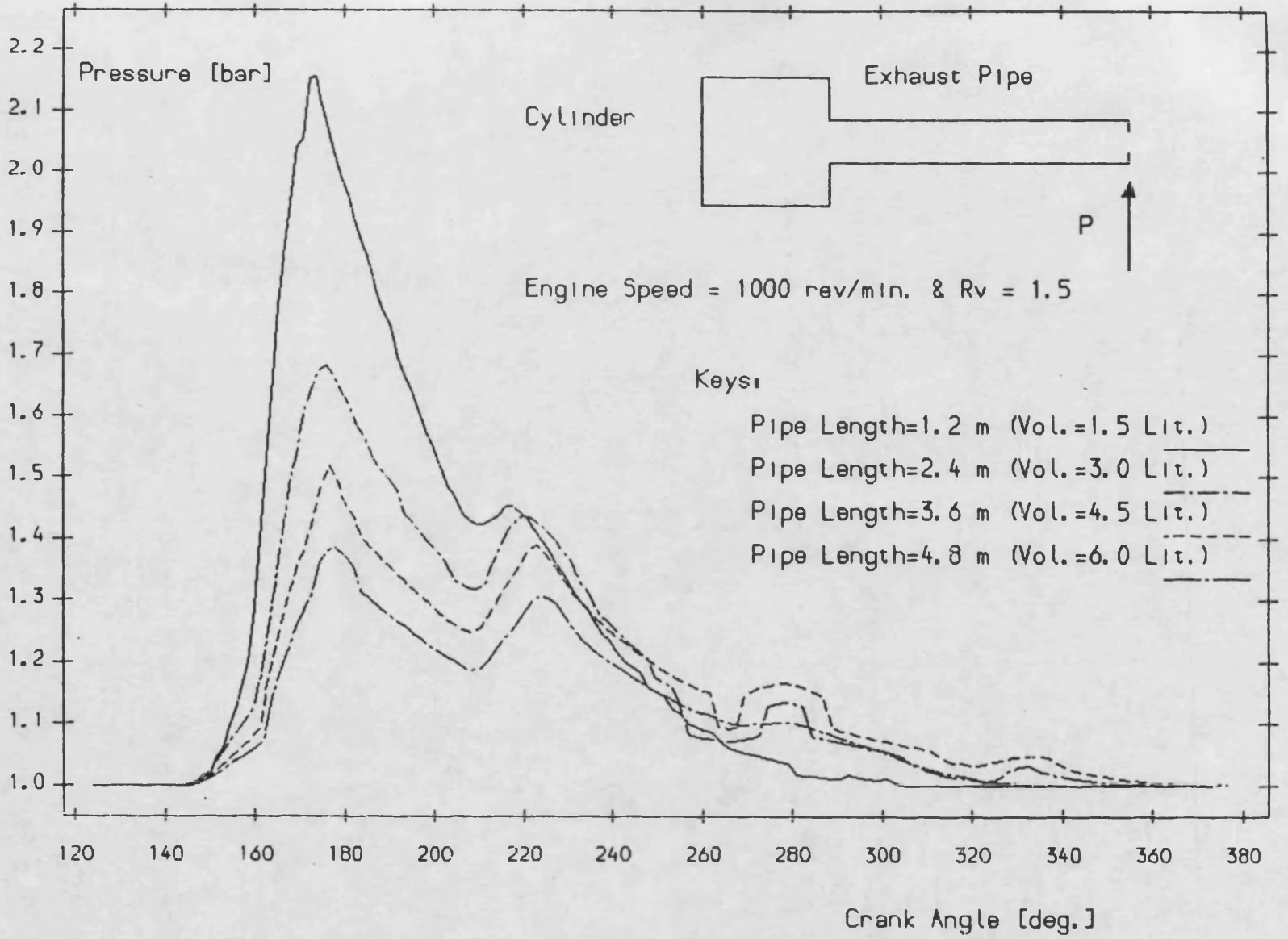

Figure 5.6- Effects of varying exhaust pipe length on the exhaust pulse in the Wave Action model of the rig.

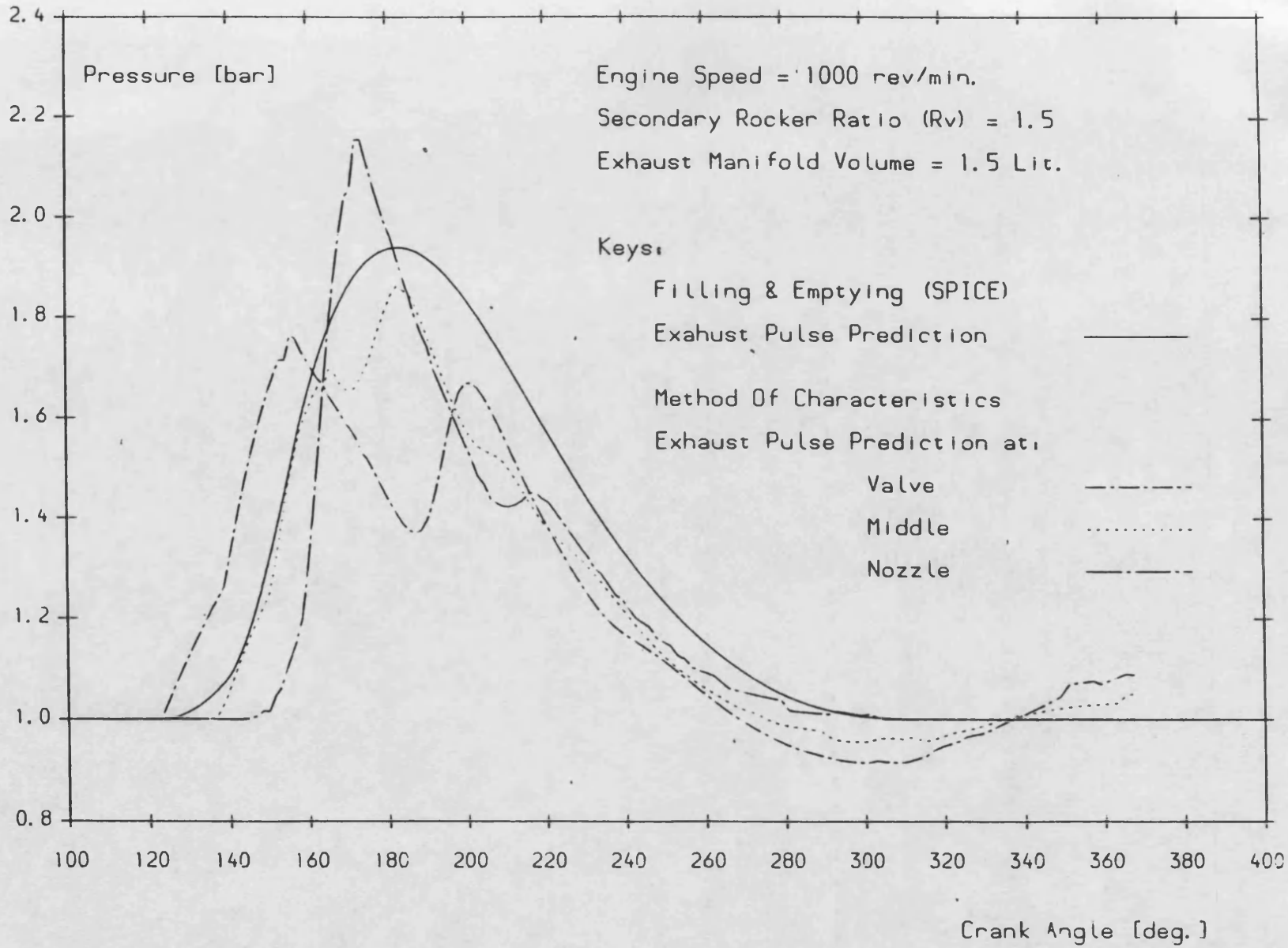

Figure 5.7- Comparison between exhaust pulses obtained using SPICE and the Wave Action models of the flow rig.

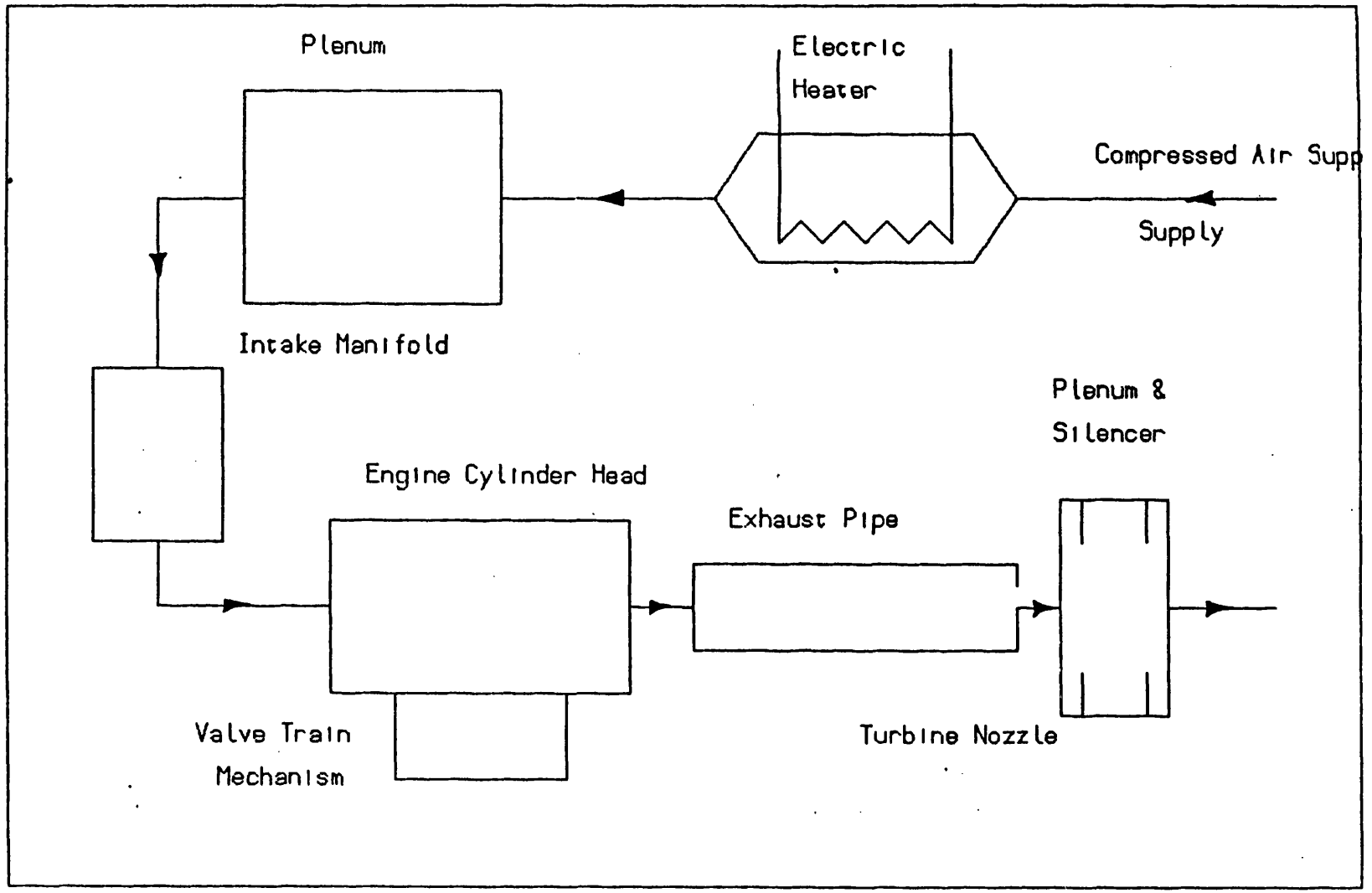

Figure 5.8- Flow diagram of the experimental flow rig.

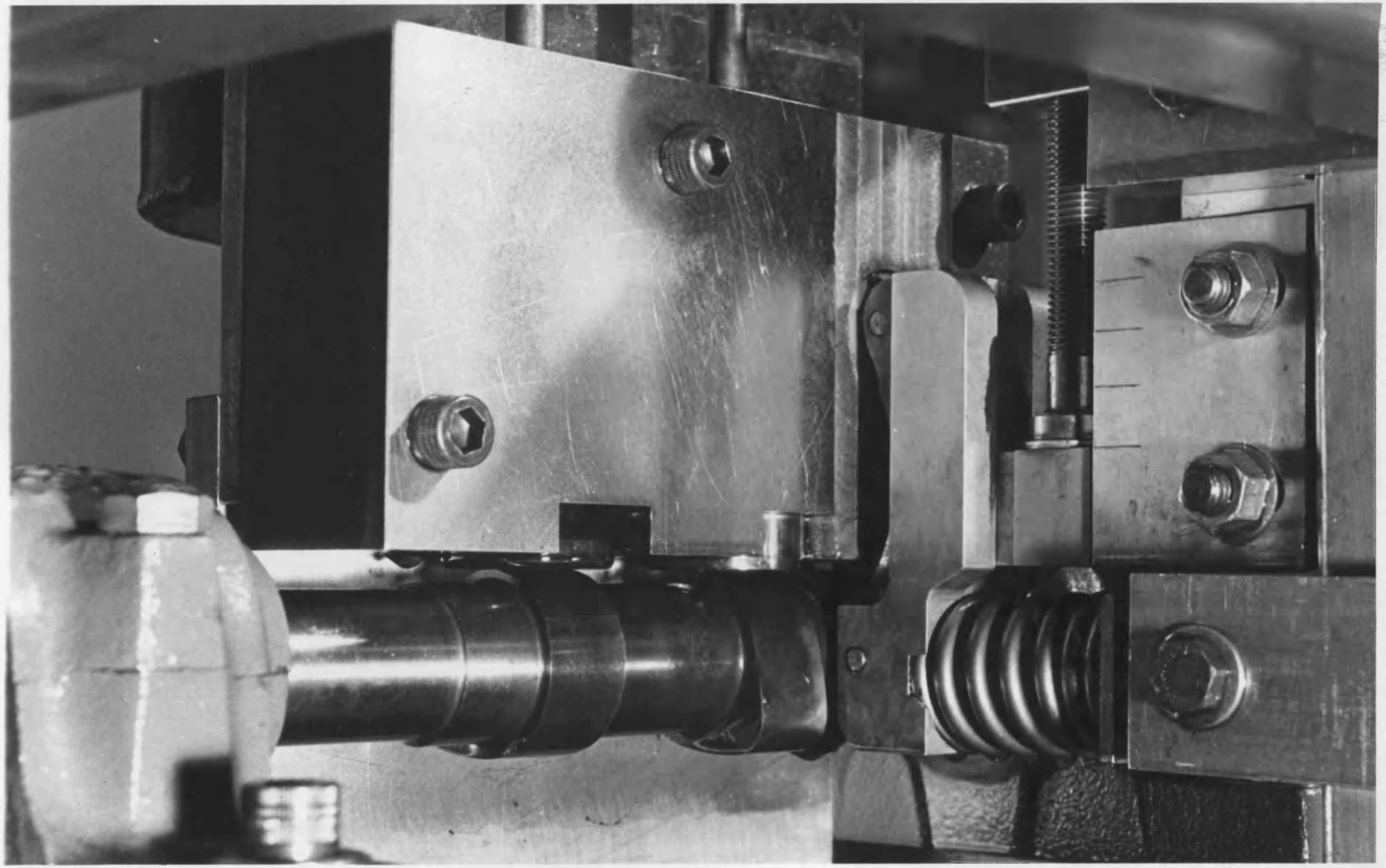

Figure 5.9 - The retaining spring which is placed between the lower section of the secondary rocker and the bracket holding the pivot disc, the tee-guide and the lead thread.

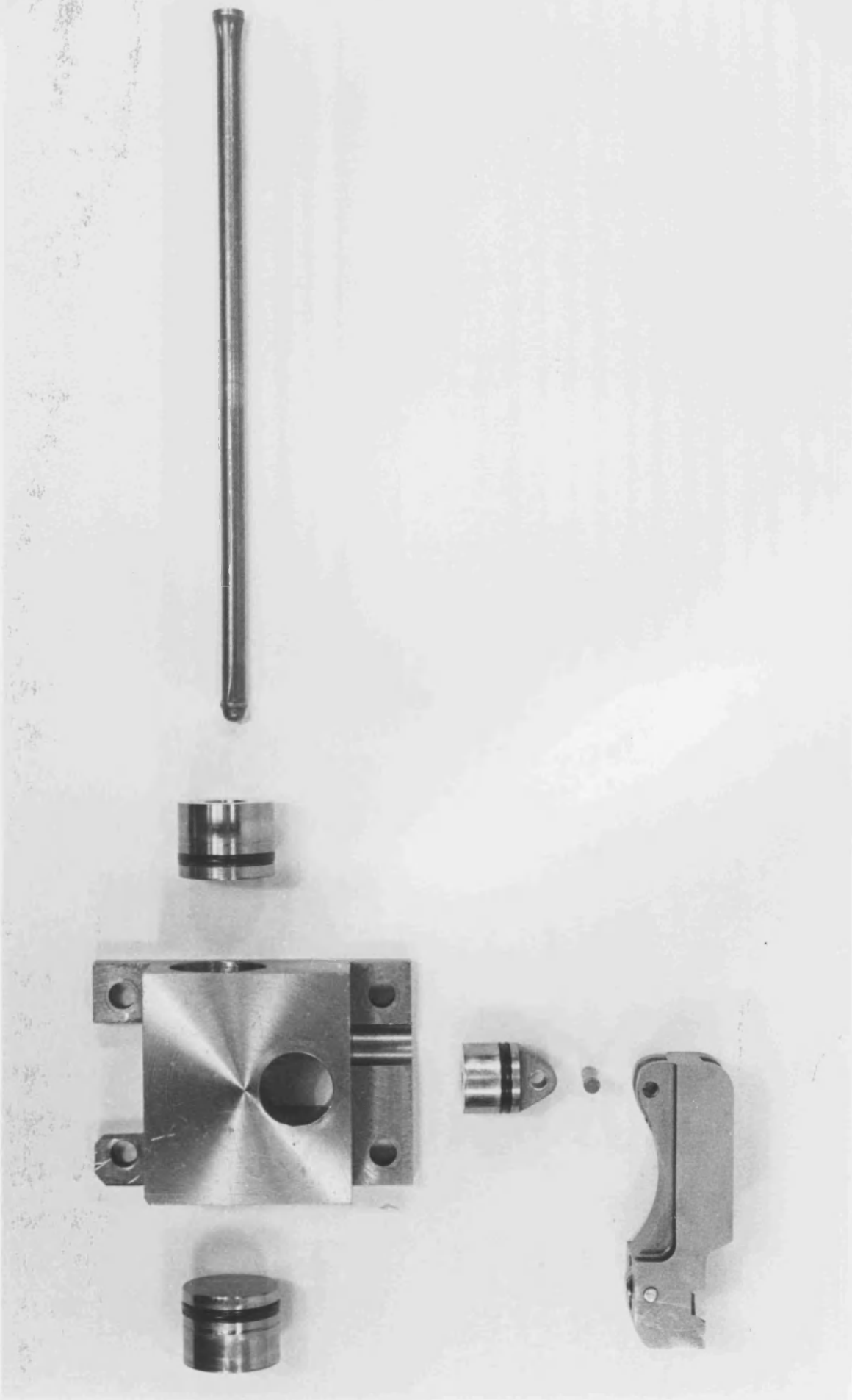

Figure 5.10 - Exploded view of the mechanism with a mild steel hydraulic chamber.

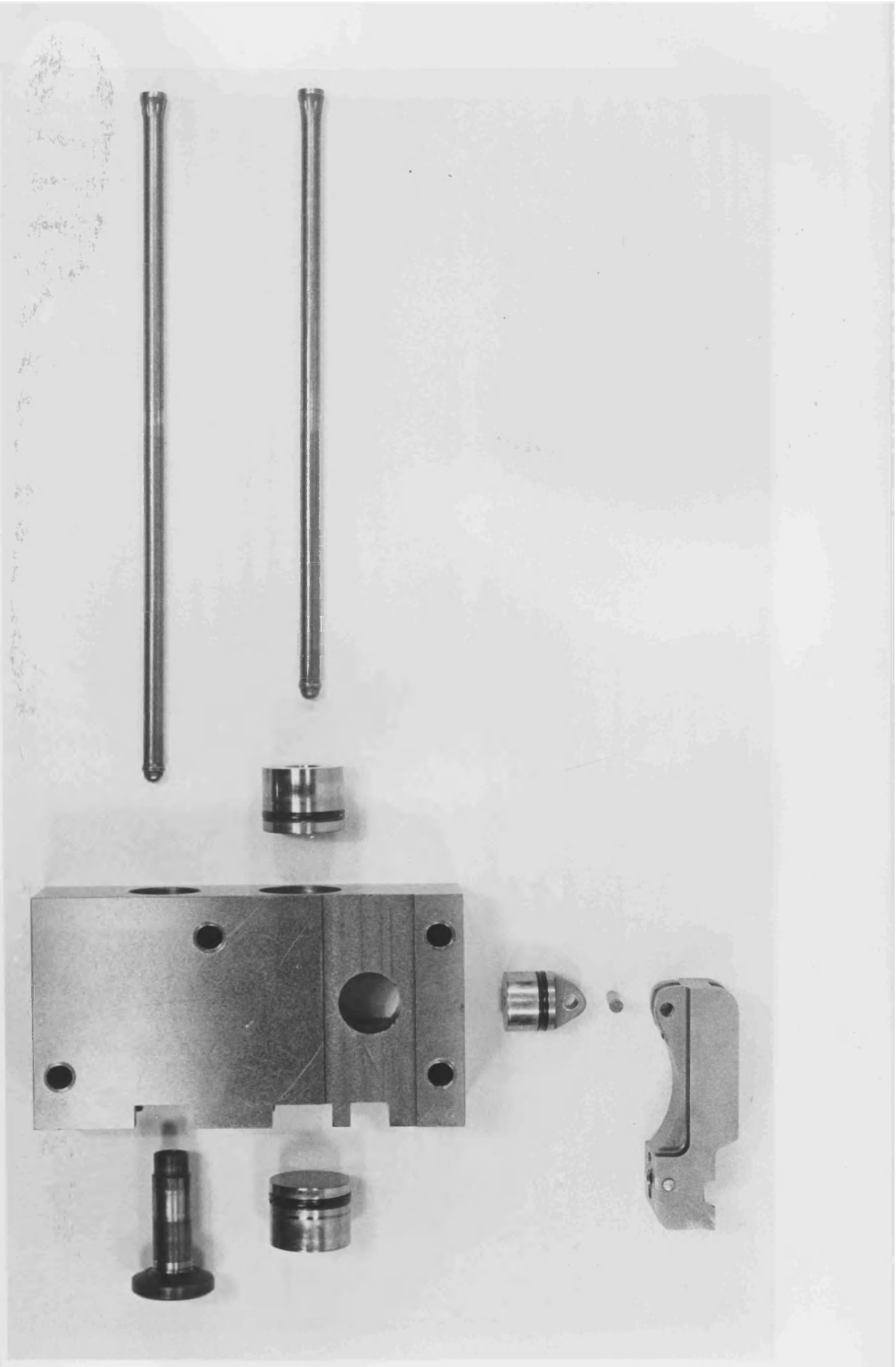

Figure 5.11 - Exploded view of the mechanism with cast iron hydraulic chamber.

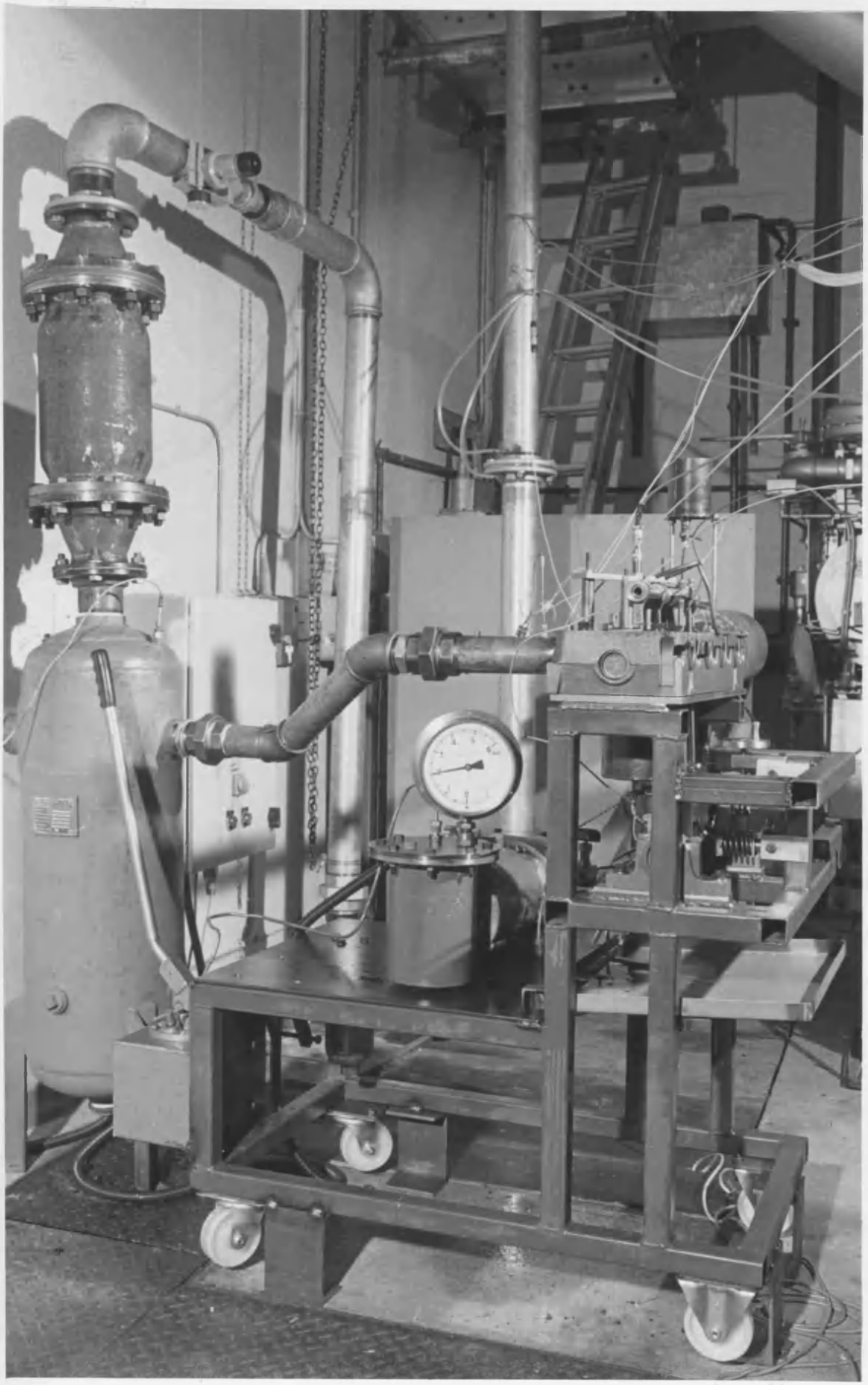

Figure 5.12 - An overall side view of the experimental flow rig.

CHAPTER 6

Instrumentation And Data Acquisition

6.0 Introduction

This chapter describes the instrumentation and data acquisition system used on the experimental flow rig for gathering experimental data. The instrumentation of the experimental rig is described and the measurements to be taken are briefly discussed. Five measurements are discussed in detail, these are:

i) rate of air flow,
ii) air temperature,
iii) pressure,
iv) exhaust valve displacement, and
v) the camshaft rotational speed and position measurements.

Control systems for pressure and temperature are described. The chapter ends with a description of the optical shaft encoder which has been used to trigger the external clock of the acquisition system by sending 1800 pulses per camshaft revolution.

6.1 Instrumentation

The flow rig is used to investigate the effects of exhaust valve opening rate on the energy transfer from a cylinder to

a turbocharger turbine. Thus, the experimental rig has to be equipped with measuring instruments which enable the verification of the events taking place within the valve mechanism and its effects on the overall behaviour of the simulated turbocharged diesel engine. The instrumentation measures the rate of air flow through the rig, the exhaust valve lift, the pressures and the temperatures in various locations within the experimental rig.

A butterfly shut-off valve has been placed immediately upstream of the flow rig. When the shut-off valve is closed the mechanism may be investigated without air flow in order to observe its dynamic characteristics. An orifice plate has been placed after the shut-off valve to measure the air flow rate. At this point a thermocouple senses the upstream temperature. A diaphragm type pressure regulating valve is located after the orifice plate in order to control the downstream air pressure, as shown in figure 6.1. This enables the constant volume cylinder to be charged with compressed air at a pressure level corresponding to that in the cylinder of a turbocharged diesel engine at the point of exhaust valve opening (cracking pressure). The compressed air delivered to the flow rig from the compressor is at ambient temperature and the expansion from the cylinder cracking pressure of approximately 6 bars absolute to atmospheric pressure in the exhaust pipe produces a significant drop in the air temperature. If the compressed

air is at ambient temperature inside the constant volume cylinder, the formation of frost in the exhaust port and pipe will be inevitable. To avoid freezing, the air entering the cylinder is heated by an electric heater which is placed downstream of the pressure regulator. A temperature controller is used to control temperature downstream of the heater. The temperature of the air is measured in the inlet manifold immediately before entering the cylinder. A pressure transducer has been inserted into the cylinder through the fuel injector hole in the cylinder head. This allows the pressure in the cylinder to be measured and recorded, enabling the cracking pressure to be determined.

A pressure transducer is mounted on the back of the hydraulic chamber block to measure the variations of oil pressure inside the block, and a thermocouple is inserted into the hydraulic chamber to register the temperature. An inductive displacement transducer is used to measure the exhaust valve lift.

Pressure and temperature measurements are taken in the exhaust pipe. Two identical pressure transducers have been positioned in the exhaust pipe. One is located immediately after the exhaust valve in the port, the other is mounted immediately before the "turbine" nozzle. The mean exhaust gas temperature is measured using a thermocouple inserted

into the exhaust pipe. The exhaust gas temperature varies with the pressure changes in the pipe and the frequency response of the thermocouple is very low hence the measured temperature is a time-averaged value.

All of the pressure transducers, the valve lift transducer and the thermocouple in the hydraulic chamber are linked to a high-speed data acquisition system. The system consists of proprietory A/D hardware and software controlled from an IBM 'AT' personal computer. An optical shaft encoder is mounted on the camshaft in order to send pulses to trigger and drive the external clock of the acquisition system. The shaft encoder transmits 1800 pulses per camshaft revolution. Therefore, the time interval between each reading corresponds to 1/5th of a degree of rotation. The camshaft rotational speed is inferred from the shaft encoder pulses using a computing counter which also displays the speed on a digital display readout unit. A selector switch and digital display unit have been used to show the thermocouple readings at various locations around the experimental rig.

The rate at which the exhaust valve opens is controlled by varying the the secondary rocker ratio of the mechanism. This is achieved using the lead screw on which the pivot-disc is mounted, so that different positions of the pivot-disc offer a different value of the secondary rocker ratio.

A schematic representation of the experimental flow rig is shown in figure 6.1. Figure 6.2 shows an overall view of the experimental flow rig. Figure 6.3 shows the mechanism with the pivot-disc at its lowest point of contact with the secondary rocker, resulting in the maximum rocker ratio of 1.5.

6.1.1 Air Flow Measurement

A very popular and simple technique for measuring the steady flow of fluids in pipes is to use an orifice plate. To measure the air flow rate passing through the experimental flow rig an orifice plate has been placed downstream of the shut-off valve between two flanges with manometer pressure tappings on the upstream and downstream sides. It has been designed according to British Standard 1042, which also specifies the relative positions of the pressure tappings. Similarly, the minimum required length of straight pipe both upstream and downstream of the orifice have been used in accordance with the British Standard, to allow a uniform and fully developed turbulent flow profile. A water filled U-tube manometer has been used to show the pressure differential across the orifice plate. It is required to obtain a pressure level difference at the manometer large enough for accurate readings to be taken at the minimum and the maximum flow rates. The maximum air flow through the simulated engine may be determined using the following expression;

$$\dot{M}_{MAX} = V_S \cdot N_{MAX} / 2 \cdot (\rho_{evo} - \rho_{atm}) \qquad \text{6.1}$$

where,

$\dot{M}_{MAX}$ = maximum air flow rate [kg/s],

V_S = piston swept volume [m^3],

N_{MAX} = maximum engine speed [rev/s],

ρ_{evo} = air density at EVO [kg/m^3],

ρ_{atm} = atmospheric air density [kg/m^3].

The Dover diesel engine has a cylinder swept volume of approximately 1 litre and a maximum engine running speed of 2200 rev/min. If the cylinder cracking pressure of 6 bars absolute and cylinder temperature of 500 K are assumed, the maximum air flow rate through the simulated engine will be equal to 0.0766 Kg/s using expression 6.1. The orifice flow meter has been designed to give 400 mm of water pressure drop when the maximum air flow rate is passing through. The required orifice flow diameter has been determined using the expression for orifice flow measurement;

$$\dot{M}_{MAX} = C \cdot \sqrt{\Delta H_{MAX} \cdot \rho_{air}} \qquad \text{6.2}$$

where,

$$C = C_D \cdot A_O \cdot \sqrt{2 \cdot g \cdot \rho_{water}}$$

therefore,

$$D^2 = 4 \cdot \dot{M}_{MAX} / \pi \cdot C_D \cdot \sqrt{2 \cdot g \cdot \Delta H_{MAX} \cdot \rho_{air} \cdot \rho_{water}} \qquad \text{6.3}$$

where,

ΔH_{MAX} = maximum head difference [m],

A_O = orifice flow area [m^2],

D_O = orifice flow diameter [m],

C_D = coefficient of orifice discharge [60%],

ρ_{air} = density of air [kg/m^3],

ρ_{water}= density of water at 20°C[998kg/m^3],

g = acceleration due to gravity [9.81m/s^2],

π = constant [3.14].

Substituting the above values in expression 6.3 gives the orifice flow diameter of;

D_O = 41 mm.

Therefore the actual compressed air flow rates may be measured at different simulated engine speeds by measuring the water level difference of the manometer.

6.1.2 Pressure Control System

The compressed air entering the experimental flow rig is at a pressure level up to 5.7 bars (85 lb/in^2) gauge. In order to be able to change the in-cylinder pressure, to verify the effect of cracking pressure on the performance of the mechanism and pulse energy, the upstream pressure to the constant volume cylinder is required to be controllable. A pressure regulator is employed upstream of the electric heater to regulate the air pressure. The pressure regulator is of the spring- diaphragm type, series R15 manufactured by Norgren Martonair limited. There is an adjustment which puts load on the spring until the required downstream pressure is obtained.

The R15 pressure regulator is capable of coping with compressed air flow rates of up to 200 dm^3/s (400 scfm).

6.1.3 Temperature Controller

In order to control the output temperature from the electric heater to suit the running requirement a temperature controller has been used. A 'Eurotherm 818' temperature controller has been selected because it is flexible and combines simplicity of operation with powerful control capability. It is equipped with two $4^1/_2$ digit displays which show the demanded and actual temperatures.

For tuning, the controller offers two separate PID loop tuning algorithms (self-tuning and adaptive-tuning) which automate the tedious part of the commissioning routine, and help to maintain good control despite changing conditions. The controller has a low level I/P analogue to digital convertor which is continuously corrected for drift. Operating at a speed of 8 updates per second this gives very high stability and rapid response to changes.

A platinum resistance thermometer (PRT) has been placed in the plenum immediately after the electric heater and before the short intake manifold. The output temperature from the heater is sensed in the plenum by the PRT which is used as a feed back to the controller. Two thyristor units are used

to control the current to the electrical resistance heater. A thyristor is a semiconductor device which acts as a switch. That is, it can be switched on to rectify an alternating current which is supplied to it. It will be switched off when the current is reduced below the thyristor 'latching' current, and will remain off until the gate is re-triggered. The device, once switched on, can not be switched off until the current reaches zero. Since it does not conduct until its gate is triggered and then only in one direction, two thyristors are normally used, connected in inverse parallel to control the alternating current to a load from zero to maximum.

When the demanded temperature is achieved, the controller cuts off the current passing through the thyristors over a certain number of cycles thereby modulating the power supplied to the electric heater.

6.1.4 Temperature Measurement

Four temperature measurements are required on the experimental flow rig. Thermocouples have been used to measure the temperature at each of four locations. The first temperature that is required is the compressed air temperature upstream of the flow-metering orifice plate. The second is the compressed air temperature entering the constant volume cylinder; and for this purpose another thermocouple has been placed in the inlet manifold.

Similarly, it is required to measure the temperature of the air leaving the cylinder in the exhaust pipe. Due to the formation of the pressure pulses in the exhaust manifold and their fluctuating nature, the air temperature changes with pressure over the entire length of the exhaust pipe. A thermocouple has been placed in the exhaust pipe measuring the mean air temperature in the pipe. The fourth temperature to be measured is in the hydraulic chamber. A thermocouple has been inserted into the chamber block to measure the temperature of the hydraulic oil. Figure 6.4 shows the position of the thermocouple inserted through the side of the hydraulic chamber.

The thermocouples are nickel chromium/nickel aluminium (type K) supplied by BICC Pyrotenax Limited. The overall diameter of the sensing probes is 1.5 $\pm$ 0.02 mm. The maximum temperature at which the sheath material (stainless steel, AISI 321) can operate is 800^{o}C. These thermocouples offer excellent resistance to corrosion and retain good repeatability.

6.1.5 Pressure Measurement

The locations where the pressure variation is measured are as follows:

(a) The hydraulic chamber in the mechanism.

(b) The constant volume cylinder.

(c) The exhaust pipe.

Two locations along the exhaust pipe have been chosen in order to monitor the exhaust pressure pulses, one as near as possible to the exhaust valve in the port and the other immediately before the "turbine" nozzle. Different types of pressure transducers have been used as described individually below.

(a) **Hydraulic oil pressure transducer** - the pressure transducer used is the model PDCR 10/T manufactured by Druck Limited. The transducer can be compensated over different temperature ranges up to a maximum of 125°C, and the PTFE cable is generally resistant to the fluids used in aerospace and automobile applications. The operating pressure range is 70 mbar to 135 bar gauge. Its linearity is ± 0.1% B.S.L for ranges to 60 bars and ±0.2% B.S.L for pressures up to 135 bars. Thermal stability is ± 2.5% total error band -25° to +125°C. The rated pressure can be exceeded by a factor of four. An operating temperature range of -25°C to 125°C is standard but may be extended. The transduction principle is that of an integrated silicon strain gauge bridge. The hydraulic chamber pressure transducer is shown in figure 6.5. The piezoresistive strain-gauge element is a solid-state, silicon resistor which changes electrical resistance in proportion to applied mechanical strain. Since it is a single crystal it is not only strong but virtually free of mechanical hysteresis with inherently good linearity. The significant characteristic of this element is that its

change of resistance is large relative to its change in length. It has a gauge factor many times greater than the typical wire strain gauge. Piezoresistive element gauge factors range typically from 50 to 200.

Gauge Factor K = $(\Delta R/R) / (\Delta L/L)$

Where:

ΔR = change in resistance,

R = initial resistance,

ΔL = change in length of element,

L = initial length of element.

Piezoresistive strain gauges are usually wired into a Wheatstone bridge with an external power source, giving zero unbalance signal at zero pressure. Increasing pressure gives increasing strain which gives an increasing unbalance signal. Typical connections within a piezoresistive pressure transducer are shown below.

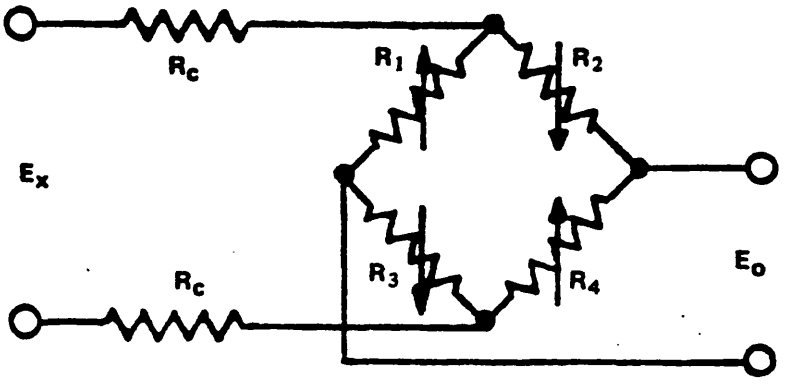

- Typical Connections within a Piezoresistive Transducer.

This pressure transducer has been used to measure the in-cylinder pressure and monitor the expansion of the compressed air from the cracking pressure to the atmospheric conditions in the exhaust pipe.

(c) **Exhaust pipe pressure transducers-** two identical pressure transducers have been used to measure the exhaust pulse pressure at two points in the exhaust pipe. The locations where the pressure transducers have been placed are immediately after the exhaust valve and just before the "turbine" nozzle. The type of transducers used are most often used in 'Scanivalve' applications. The model PDCR 22 by Druck limited was used. The PDCR 22 is a special-purpose transducer for pressure scanning applications. It features excellent linearity and negligible hysteresis. The end caps are generally interchangeable and variations are available for flush mounting applications. The operating pressure range of this transducer may be between 70 mbar and 35 bars gauge or differential but the pressure range selected for this application is 70 mbar to 7 bars gauge. The rated pressure can be exceeded by a multiple of four causing negligible calibration change. The transduction principle is that of an integrated silicon strain gauge bridge. The operating temperature range is between -40^{o} to $+80^{o}C$ standard but may be extended.

6.1.6 Valve Displacement Measurement

An AVL type 425 valve lift transducer has been used to measure the exhaust valve displacement. The transducer housing is mounted in a support bracket by means of an adjustment plate as shown in figure 6.5. The lift movement of the exhaust valve is transmitted by means of a magnetic core with extension rod. This is attached to the exhaust valve spring retainer by means of a threaded portion with fixing nut. The AVL valve lift transducer is of the inductive type based on the half-bridge circuit principle.

The supply to the AVL valve lift transducer is provided by a 3075-A02 Carrier Amplifier which is intended for use for measurement of rapid events in the frequency range of 0 to 20 kHz. A carrier frequency of 100 kHz, used to excite the transducer, is generated by a built-in oscillator. The oscillator provides a voltage of approximately 14V peak to peak at a minimum resistance of 50 ohms. The measuring signal produced by the transducer is conditioned, that is demodulated, filtered and amplifed in the instrument.

The temperature of the AVL valve lift transducer, at the connector, should not exceed 80^{o}C. The linearity error is $\pm$ 1% and the transducer's sensitivity is approximately 3.2 volts per 0.1mm lift at maximum gain. In figure 6.5 the AVL valve lift transducer is shown as installed on the exhaust valve spring retainer. The inlet manifold thermocouple and

the hydraulic chamber pressure transducer are shown in the same figure.

6.2 High-Speed Data Acquisition System

The unsteady measurements taken by the transducers on the experimental rig are collected for processing by a data acquisition system. The system comprises an IBM 'AT' personal computer and a high-speed data acquisition card installed in the computer. The IBM 'AT' has a processor clock speed of 10 MHz and is equipped with 640 kbytes of random access memory (RAM) and a hard disc with a storage capacity of 20 Mbytes.

The data acquisition card is the Computerscope ISC-67 marketed in the UK by Advanced Instruments and Measurement Systems limited, (AIMS). The Computerscope ISC-67 is a fully integrated hardware and software package designed to permit IBM PC or PC/XT/AT personal computers to perform as sophisticated data acquisition and analysis laboratory instruments. The ISC-67 Data Acquisition package consists of a 16-channel multiplexed A/D board, an external instrument interface and software. The package is capable of recieving up to 16 channels of data input at an aggregate sampling rate of up to 1 MHz. Digital conversion is achieved with 12 bit accuracy over an input range of -10 to +10 volts.

The software offered in the basic ISC-67 package is designed to effectively emulate a digital storage oscilloscope. Fully automated keystroke commands give fast and effective control over all of the features of the system, including channel selection, waveform manipulation and display, trigger control (external or any input channel, +/- level or slope), memory buffer size (1 to 64K), pretrigger viewing and cursor measurement.

The sample period indicates the period of time elapsed between samples of incoming data. The system may be triggered internally by using the internal clock or externally by a device which sends TTL pulses, such as an optical shaft encoder. For this application the external trigger mode has been selected in conjunction with the shaft encoder described in the following section.

The data collected is transferred from the IBM 'AT' personal computer to the school's VAX11/750 super mini computer for further processing of the results as presented in chapter 7.

6.2.1 Shaft Encoder

An optical shaft encoder, model I58T manufactured by Mclennan Limited, has been used to trigger the data acquisition system externally as described earlier. The shaft encoder employed is capable of sending 1800 pulses per

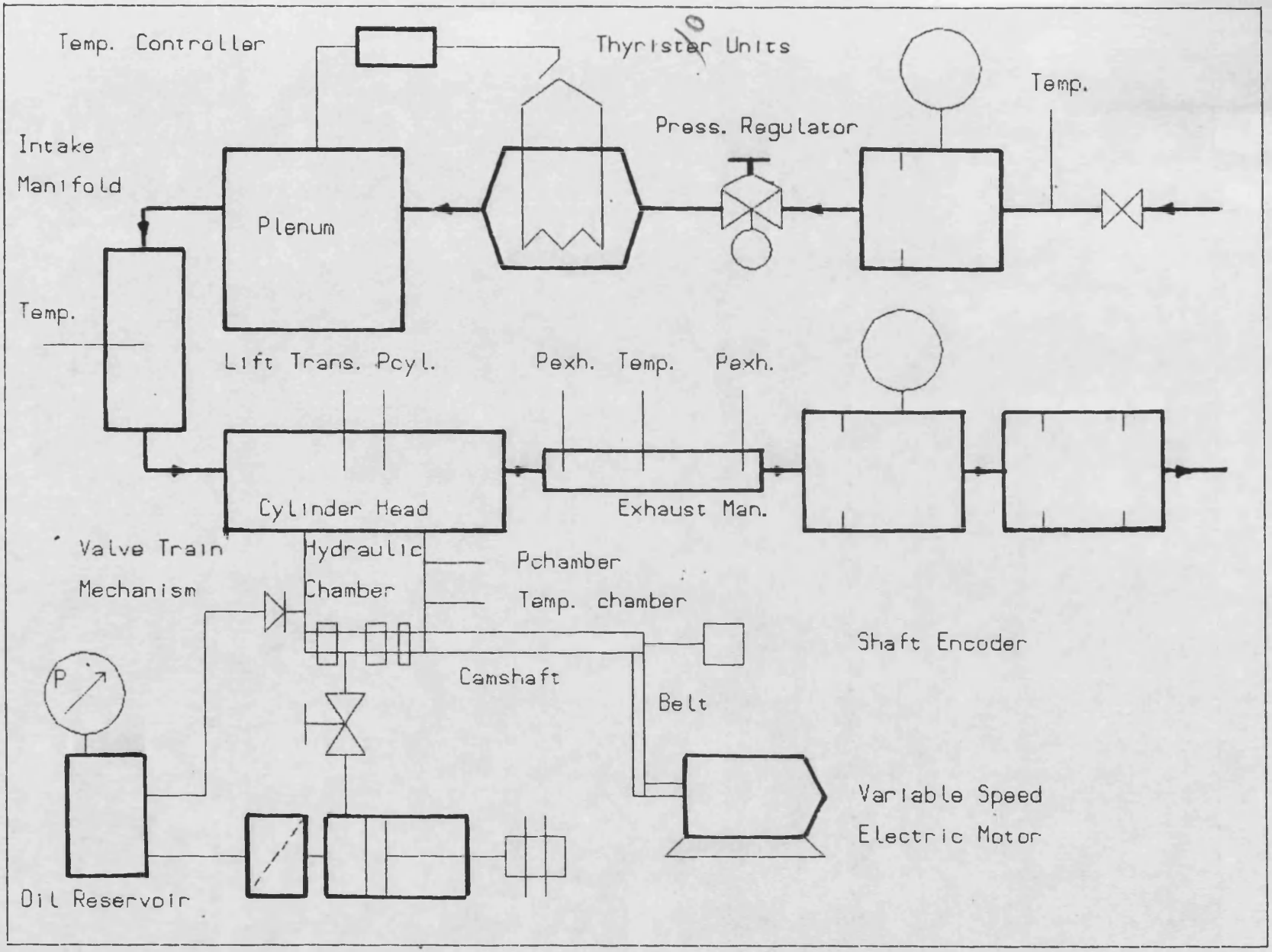

Figure 6.1- Schematic representation of the experimental flow rig.

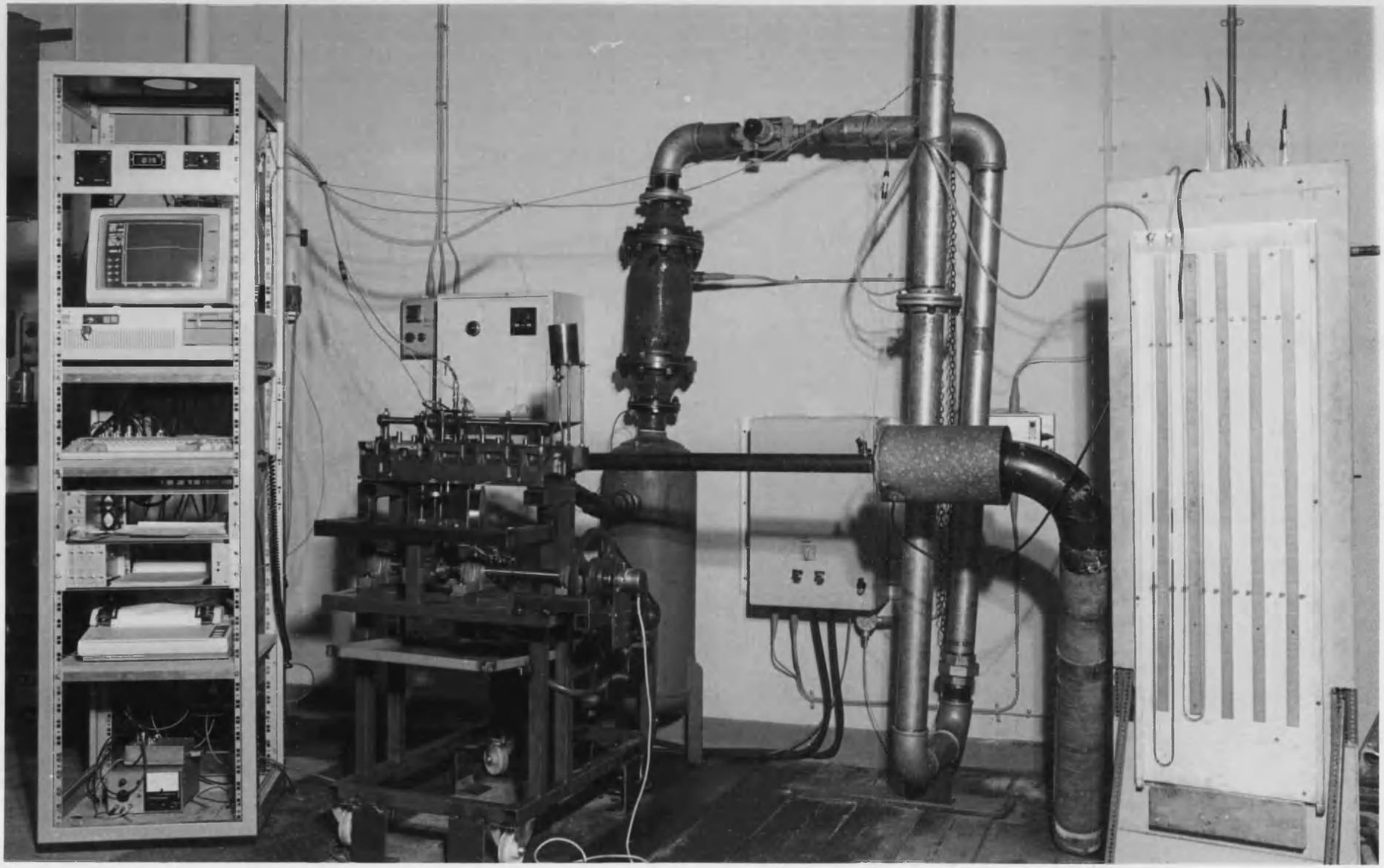

Figure 6.2 - An overall view of the experimental flow rig.

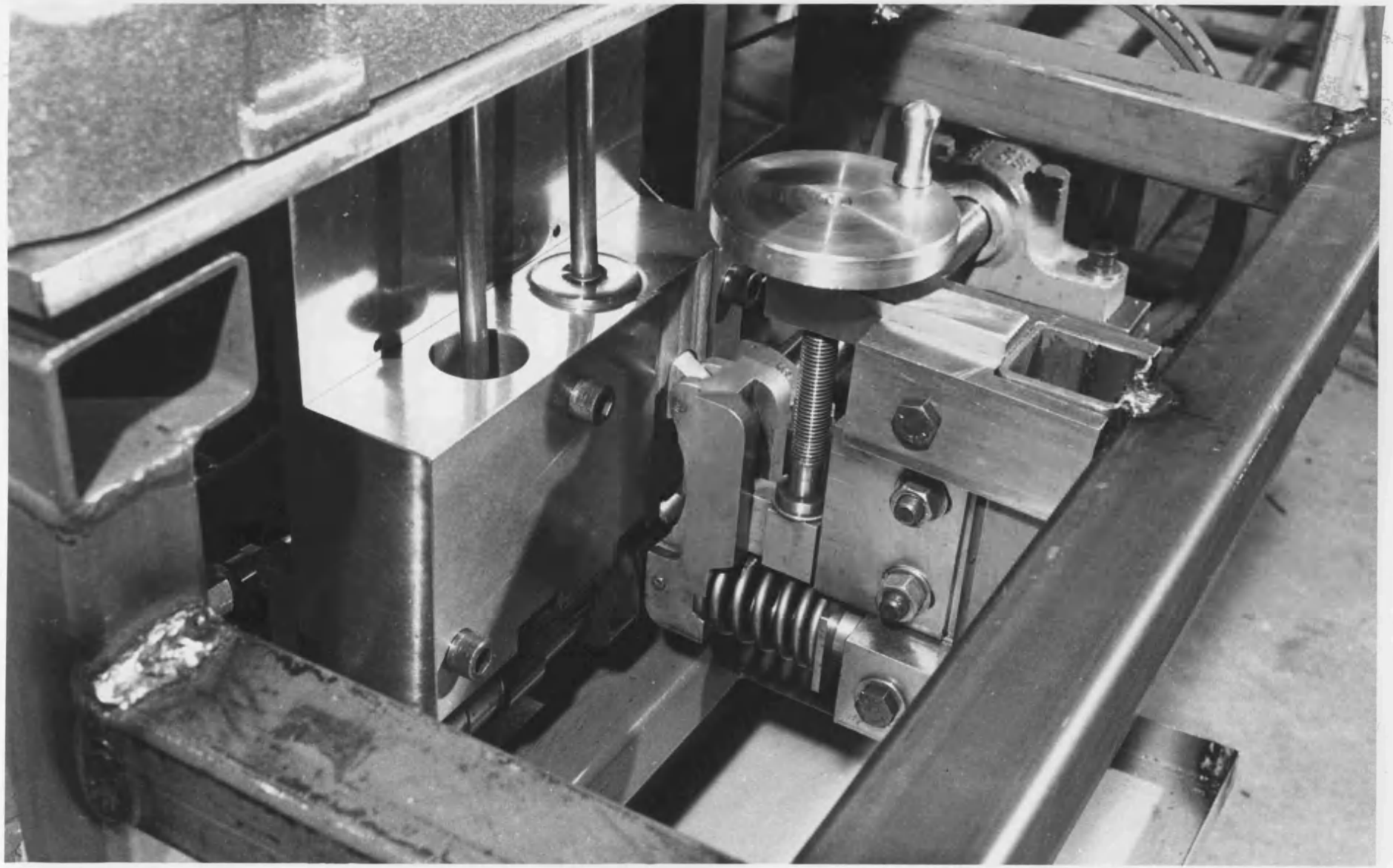

Figure 6.3 - Mechanism with the lowest pivot point resulting in the highest rocker ratio of R_v=1.5

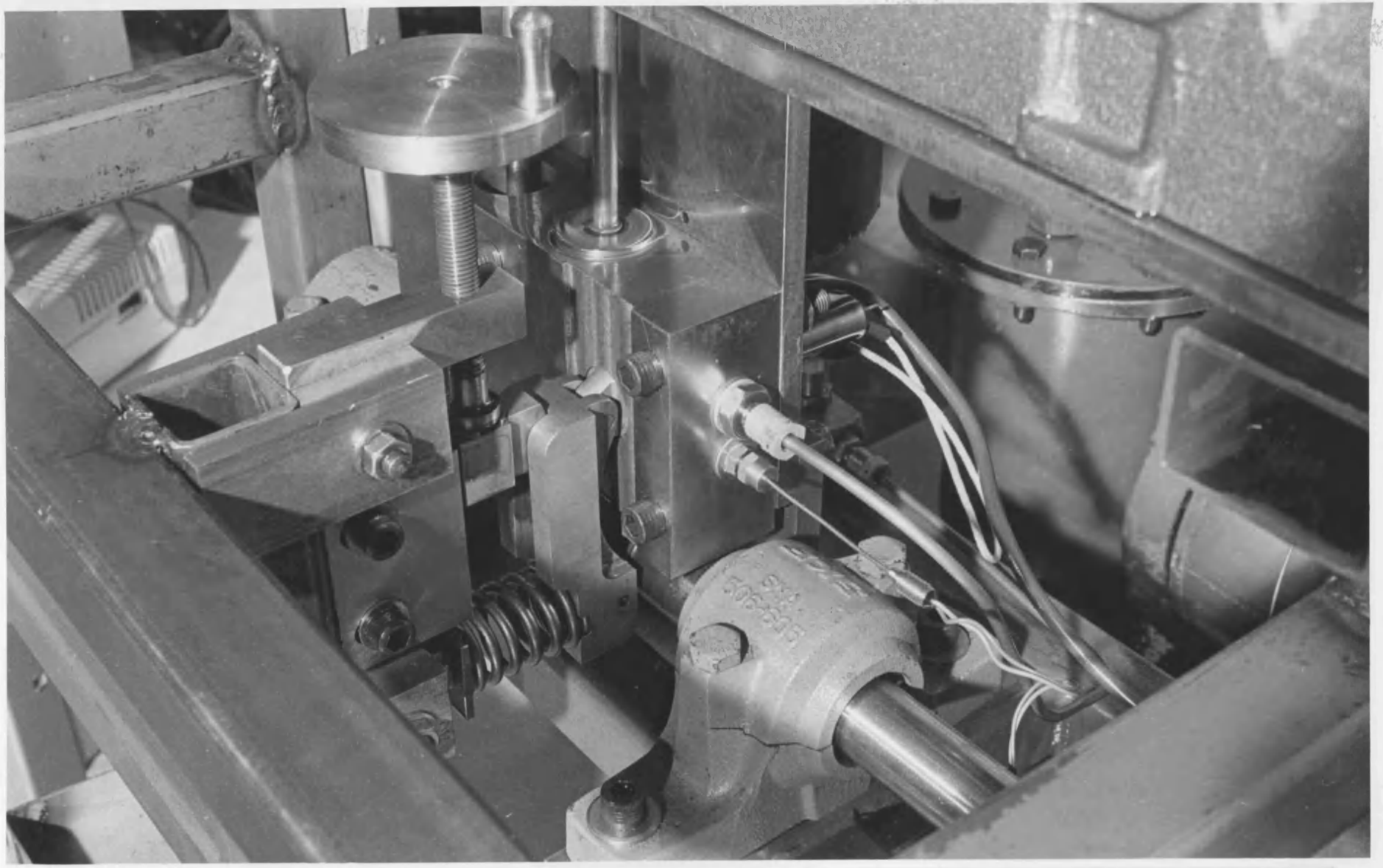

Figure 6.4 - Mechanism with the highest pivot point resulting in the lowest rocker ratio of R_v=0.0, the pressure transducer and the thermocouple in the hydraulic chamber are also shown.

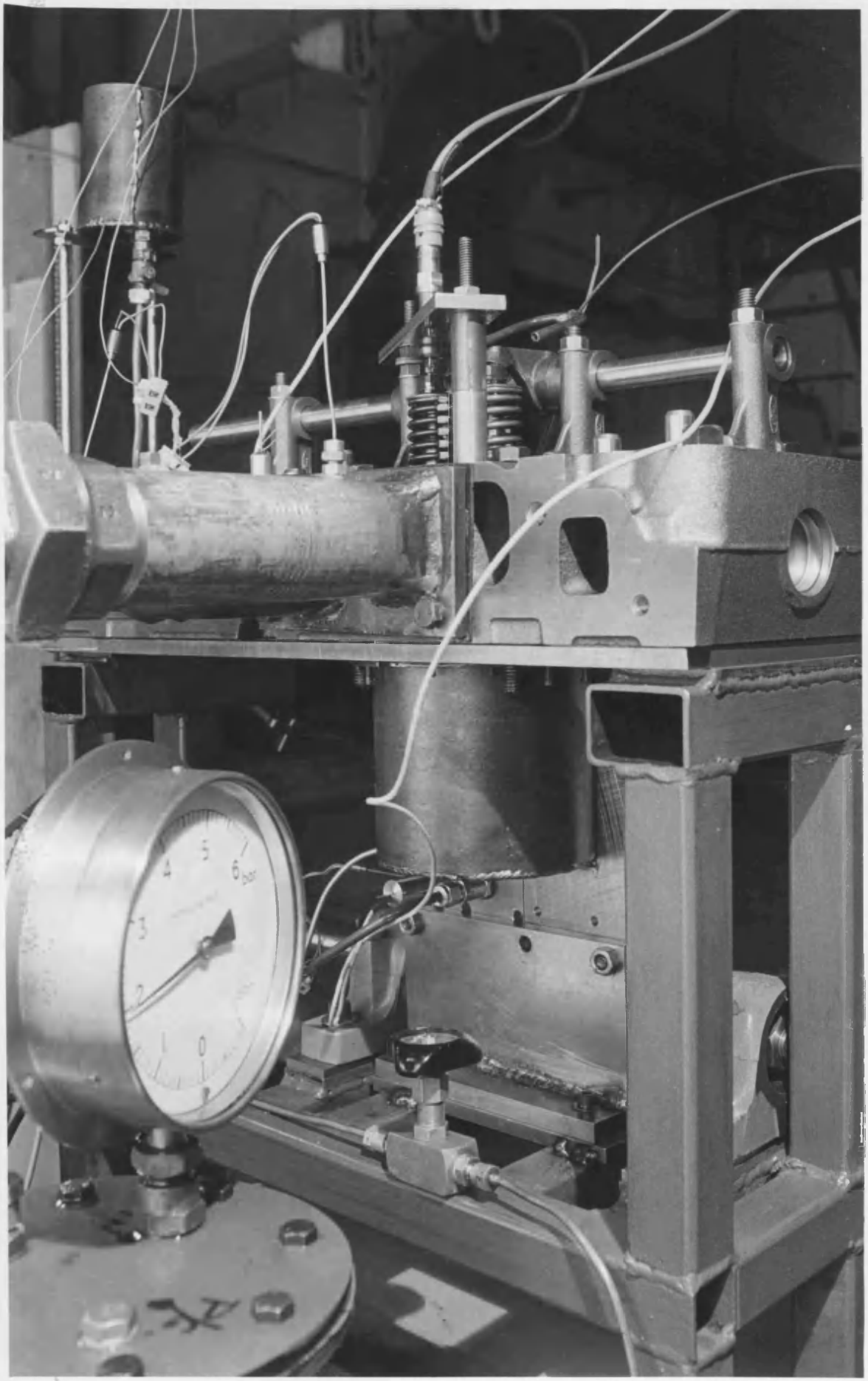

Figur 6.5 - AVL valve displacement transducer and the top-up oil resorvior are shown.

CHAPTER 7

Presentation And Discussion Of Experimental Results

7.0 Introduction

Results from the variable valve rate experimental rig are presented and discussed in this chapter. The presented experimental results refer to:

i) behaviour of the mechanism, and

ii) gas flow and pulse energy.

The energy content of the exhaust pulses at various engine speeds is calculated and the change in pressure ratio across the 'turbine' nozzle, velocity of the exhaust gas in the pipe and through the nozzle, the exhaust mass flow rate and the pulse power follow the energy calculations. The gains in pulse power are discussed showing significant improvement in the exhaust gas energy transport to the turbocharger turbine when a high rate of exhaust valve opening is adopted.

7.1 Discussion of Experimental Results

It was established in chapter two that in order to utilize more of the exhaust pulse energy, the exhaust valve should open rapidly. The design criterion for the rig was based on achieving the same rate of exhaust valve opening at both the

lower and the upper limits of the engine operating speed range. Hence, maintaining the exhaust valve opening rate constant from 1000 to 2200 rev/min. Table 7.1 shown below, illustrates the parametric variations that have been studied:

Engine Speed (RPM)	Secondary Rocker Ratio (R_V)	Cracking Pressure (Bar Abs.)
1000	0.0 to 1.5	2 to 6
1300	0.0 & 0.76	2 to 6
1600	0.0 & 0.39	2 to 6
1900	0.0 & 0.17	2 to 6
2200	0.0	2 to 6

Table 7.1 - Parametric Variations Studied.

7.1.1 Exhaust Valve Lift

The measured exhaust valve lifts are illustrated in figure 7.1 corresponding to an equivalent engine speed of 1000 rev/min for secondary rocker ratios, R_V, of 0.0 to 1.5. The motion of the valve train when $R_V = 0.0$ is due solely to the main cam profile. For $R_V > 0.0$ the motion of the valve train is due to a combination of the inputs from the main and the secondary cam profiles. The first and the last 25

degrees of the main cam profile displacement are occupied by two constant velocity ramps that in a conventional valve train are used to take up clearances on the opening phase and to ensure complete valve closure on the closing phase. When the mechanism is employed and pressure exists in the hydraulic chamber, there is no longer any clearance in the valve train, thus the opening ramp may be either removed or modified to be used to compensate for the hydraulic oil compressibility. As for the constant velocity ramp on the closing phase it may be eliminated from the main cam profile. As the pivot point is lowered, R_V increases gradually from 0.0 to a maximum of 1.5 thus increasing the contribution of the central plunger which consequently increases the rate at which the exhaust valve opens. At lower values of R_V the lift curves are very smooth and behave in a very desirable manner. But at the highest value, $R_V = 1.5$, the exhaust valve train becomes dynamically unstable and oscillations occur. The oscillations are not evident until approximately 70% of the full valve lift has been achieved. The oscillation lasts for 4 to 5 cycles before being damped out completely at the begining of the closing phase. At the start of the closing phase at approximately 80% lift the family of curves collapse to follow the primary cam profile under the action of the valve spring. The oscillation was not observed at equivalent engine speeds of below 950 rev/min, at the highest secondary rocker ratio of 1.5. To date the exact cause of these

oscillations is not known with certainty; however, it is considered to be due either to hydraulic compressibility or to separation between the secondary rocker and the pivot-disc. Lack of exhaust valve spring reserve was also considered to be another possibility and in fact in a later experimental study when a stiffer valve spring was used in conjunction with a lighter output plunger, the valve lift curve was improved significantly. Ultimately a stiffer valve spring should smooth out the lift curve completely, at the highest secondary rocker ratio but at the expense of higher contact forces.

7.1.2 Hydraulic Chamber Pressure

Figures 7.2 to 7.11 show the pressure variation of the hydraulic oil in the hydraulic chamber over a secondary rocker ratio (R_V) range of 0.0 to 1.5. In figure 7.2 the hydraulic fluid pressure at an equivalent engine speed of 1000 rev/min is shown for both the baseline case (R_V = 0.0) and a higher rate case (R_V = 0.17). It can be seen that the pressure of the hydraulic fluid for the high-rate case is always greater than the baseline. The peak pressures for both systems occur at the maximum valve lift. The maximum pressure of 12.7 bars for the baseline is increased to 13.2 bars for the high-rate case. The theoretical maximum static pressure at full lift to hold the valve open is 10.17 bars. Figure 7.3 compares the hydraulic fluid pressure for the baseline and high-rate cases with a secondary rocker ratio

of 0.39. As can be seen, the peak pressure increased to 13.5 bars. This peak also occurs at the point of maximum valve lift. It should be noted that the crank angle degrees on the horizontal axis bear no relationship to the actual timing of the valve opening and closing (57^{o} BBDC-15^{o} ATDC). The range of 250-970 degrees of crank angle just covers one complete simulated engine cycle. The secondary rocker ratio has been increased to 0.76 in figure 7.4 and this time the peak pressure is further increased to 14.8 bars, corresponding to the maximum valve lift crank angle. When the maximum secondary rocker ratio of 1.5 is used, figure 7.5, the oscillations appear and the peak pressure no longer takes place at maximum lift. The maximum pressure is now 16 bars and the oscillations have a frequency of approximately 180 Hz. Figure 7.6 indicates that the exhaust valve lift oscillations coincide with the violent fluctuations of the hydraulic fluid pressure. It should be noted that in all of these situations the pressure starts and returns to 4 bars and is at all times above atmospheric pressure, therefore cavitation would not be expected.

Figures 7.7 to 7.9 show the hydraulic pressure for the baseline and the highest rate settings for engine speeds of 1300, 1600 and 1900 rev/min. The cracking pressure has been kept constant at 5 bars. The relative rise in pressure at each speed is quite evident. It is basically due to the contribution made by the central plunger motion. At 1300

rev/min, figure 7.7, the pressure starts at 14 bars and peaks at 20 bars for the baseline and approximately 25.5 bars absolute for the highest-rate case. Towards the end of the exhaust valve opening period, an undesirable high-frequency pressure fluctuation occurs before rapidly being damped out. The reason for this fluctuation is considered to be due to flexing in the camshaft. This flexing is thought to be caused by the reaction of the inertia forces needed to open the intake valve. The pressure fluctuations coincide with the intake valve opening. At 1600 rev/min, figure 7.8, the hydraulic fluid peak pressure for the baseline has increased to 22 bars, but the peak pressure for the highest rate remains steady at 25.5 bars similar to that of the 1300 rev/min case. For the baseline case, the pressure in the hydraulic chamber increases as the operating engine speed increases as would be expected. At 1900 rev/min, figure 7.9, this peak has increased further to 24 bars whereas the peak pressure of the highest-rate case is again approximately 25.5 bars absolute. The constant value of 25.5 bars is an indication that constant acceleration has been achieved over the entire operating speed range of 1000-2200 rev/min.

Figure 7.10 compares the hydraulic fluid pressure at the lower and the upper limits of the speed range (1000 rev/min when R_V = 1.5 and 2200 rev/min when R_V = 0.0). It can be seen that at an equivalent engine speed of 1000 rev/min and

secondary rocker ratio of 1.5 the initial peak pressure is 25 bars. When the engine speed is increased to 2200 rev/min. and the secondary rocker ratio decreased to 0.0, the peak hydraulic fluid pressure is just under 25 bars, thus, indicating that the design criterion of maintaining the same exhaust valve opening rate over the speed range of 1000-2200 rev/min has probably been achieved.

7.1.3 Effect Of Cylinder Pressure On Hydraulic Chamber Pressure

Figure 7.11 illustrates the effect of cylinder pressure at the point of exhaust valve opening, EVO, on the pressure in the hydraulic chamber. These curves have been produced at the highest operating engine speed of 2200 rev/min when the exhaust valve motion is due to the main cam only. Since there is no clearance in the exhaust valve train, the cylinder pressure imposes forces acting upon the exhaust valve head which is transmitted to the hydraulic chamber at the start of valve opening. Therefore, the early part of the valve opening phase is most significantly affected by the cracking pressure. The first peak in the pressure curve reaches 11.9, 14.4 and 17.5 bars for cracking pressures of 2,4 and 6 bars respectively. The violent high frequency pressure oscillations, due to the camshaft flexing, are also apparent towards the end of the valve opening period.

7.1.4 Cylinder Pressure Expansion

The cylinder pressure expansion is shown in figure 7.12, for the baseline and highest-rate cases at an engine speed of 1000 rev/min. It can be seen that for the highest-rate case, shown by the dotted line, the expansion from the cracking pressure to the exhaust pipe pressure takes place more rapidly than the baseline case, shown by the solid line. The rapid expansion of the exhaust gas would be expected to reduce the choked flow duration through the valve significantly. Some pressure oscillations are evident during the exhaust valve opening period before the inlet valve opens and a rapid rise in cylinder pressure follows as the cylinder is filled with fresh charge. Towards the end of the pressure rise, due to the inlet valve opening, a low frequency fluctuation occurs before being damped out promptly. This is thought to be due to pressure wave reflections in the intake pipe and plenum.

Figure 7.12 illustrates the difference in the rate at which the cylinder pressure expands between the two lowest and highest secondary rocker ratio settings of 0.0 and 1.5 at an engine speed of 1000 rev/min. In the highest-rate case the cylinder pressure expands to the same level as that of the baseline case approximately 23 crank angle degrees earlier, resulting in significant reduction in choked flow duration through the valve, which may be expected to improve energy

transfer through the valve because of reduced turbulent mixing in the port downstream of the valve.

As the equivalent engine speed is progressively increased, the secondary rocker ratio is decreased, to maintain constant inertia forces, and the rate of decay of cylinder pressure reduces accordingly. This phenomenon has been shown in figure 7.13 at 1300 rev/min, figure 7.14 at 1600 rev/min and figure 7.15 at an equivalent engine speed of 1900 rev/min.

7.1.5 Exhaust Pressure Pulses

Cracking pressure has been varied over the range 2 to 6 bars absolute and its influence on the formation of the exhaust pulse has been studied. Figures 7.16-7.19 correspond to a cracking pressure of 2 bars at an engine speed of 1000 rev/min. The secondary rocker ratio is progressively increased from 0.0 to 1.5. The exhaust pressure pulse profile follows a rapid rise path before decaying to atmospheric conditions. When the secondary rocker ratio has no effect on the exhaust valve motion (R_V = 0.0) the peak pulse pressure is approximately 1.32 bars, see figure 7.16. When R_V is increased to 0.17 this peak rises to 1.36 bars. R_V is further increased to 0.39 in figure 7.17 and the rapid rise in the pulse pressure continues to a peak of 1.37 bars. This peak increases slightly more to 1.39 when secondary rocker ratio is increased to 0.76 in figure 7.18.

When R_V has its highest value of 1.5 the rise in pulse pressure is much more rapid than for the baseline case. This is shown in figure 7.19 exhibiting a peak pressure of 1.47 bars when R_V = 1.5.

Figures 7.20-7.23 correspond to an engine speed of 1000 rev/min covering the secondary rocker ratio of 0.0 to 1.5 when the cracking pressure is increased to 3 bars. For the baseline case the peak pressure achieved in the pulse is almost 1.69 bars, whereas this peak increases to approximately 1.73 bars at a higher-rate (R_V = 0.17), as shown in figure 7.20. The exhaust pulse profile has a very rapid rise from the exhaust pipe conditions followed by a gradual decay to the pipe conditions. As expected the peak pulse pressure for the high-rate system increases as the secondary rocker ratio is progressively increased. The exhaust pulse peak pressure is significant because, in general, the higher the peak the greater the expansion ratio will be across the turbocharger turbine nozzle, thus providing more useful work for the turbocharger turbine. A pulse peak pressure of 1.75 bars is observed in figure 7.21 when R_V is increased to 0.39. In figure 7.22 the peak pressure of 1.79 bars is reached when R_V has changed to 0.76. The highest pulse peak is achieved when R_V = 1.5, shown in figure 7.23. This peak is 1.91 bars which is 0.22 bars higher than the peak of the baseline case.

Figure 7.25A has been produced t show the effect of changing the secondary rocker ratio from R_V = 0.0 to its highest value of R_V = 1.5 at an engine speed of 1000 rev/min when the cracking pressure is set at 3 bars. It is clearly seen that as the secondary rocker ratio progressively is increased, the amplitude of the exhaust pulse increases accordingly.

When the cracking pressure is increased to 4 bars at an engine speed of 1000 rev/min, evidence of pressure wave reflections within the exhaust pipe appear. Thus, the pulse profile is no longer a continuous rise and fall pattern. In fact it takes approximately 9.6 ms for a complete return journey of a pressure wave from the exhaust valve to the "turbine" nozzle and back. The frequency of this oscillation is about 104 Hz and the first peak for the baseline case does not exceed 1.98 bars. A peak pressure of 2.02 bars is achieved when R_V is set at 0.17, as shown in figure 7.24. At first one might assume that the wave travels at sonic velocity which may be obtained using expression 7.1 given below:

$$a = \sqrt{\gamma.R.T} \qquad \text{7.1}$$

where,

a = speed of sound in air [m/s],

γ = specific heats ratio [1.4 for air],

R = specific gas constant [287.1 kJ/kgK],

T = exhaust pulse temperature [K].

For an exhaust temperature of 300K, the sonic velocity (a) of 347.25 m/s will be obtained. But in fact the process is much more complicated than it may appear. A number of variables interact simultaneously which affect the wave travel, such as the operating engine speed, the flow characteristics through the "turbine" nozzle, pulse pressure and temperature change. From the 'method of characteristics', the propagation velocity of a single wave train may be derived from first principles (46). The propagation velocity can, thus, be determined using the following expression:

$$C = a \left[6 \left(P/P_O\right)^{\frac{\gamma - 1}{2\gamma}} - 5 \right] \quad \text{7.2}$$

where,

C = pressure wave propagation velocity [m/s],

a = sonic velocity of pressure wave [m/s],

P = pulse peak pressure [bars],

P_O= reference pressure [1 bar atmospheric].

The variation of the calculated propagation velocity for each operating engine speed for the two cases of the baseline and the high-rate are discussed in depth in the next chapter. The same type of oscillations occur when R_V is increased to 0.39, but this time the first peak increases fractionally to 2.04 bars as shown in figure 7.25. When R_V is changed to 0.76 the first peak increases further to a pressure level of 2.06 bars as shown in figure 7.26. The

first peak pressure in the exhaust pulse increases to a significantly higher level of 2.38 bars when R_V takes its highest value of 1.5, and much earlier than when R_V = 0.0, as shown in figure 7.27.

Figures 7.28-7.31 illustrate the exhaust pressure pulse at the nozzle end of the exhaust pipe at an engine speed of 1000 rev/min, over the entire secondary rocker ratio range of 0.0-1.5 when the cracking pressure is 5 bars. From these figures, evidence of pressure wave reflections is quite apparent, and the time taken for the pressure wave to travel from the exhaust valve to the nozzle and back is found to be approximately 9.6 ms. There are three wave reflections before the pulse decays to atmospheric conditions in the pipe. For the baseline case (R_V = 0.0) the first peak reached is approximately 2.35 bars and increases to 2.39 bars when the secondary rocker ratio is changed to 0.17, as shown in figure 7.28. The first peak for the higher-rate case increases to 2.40 bars when R_V = 0.39 and quickly reaches 2.36 bars when R_V = 0.76 as shown in figures 7.29 and 7.30 respectively. When the secondary rocker ratio is adjusted to offer the maximum ratio of 1.5, the first peak very quickly rises to approximately 2.70 bars before successive peaks are formed due to wave reflections, as can be seen in figure 7.31.

The maximum cracking pressure used in the tests was 6 bars. Figures 7.32-7.35 correspond to this case at an equivalent engine speed of 1000 rev/min for secondary rocker ratios of 0.0-1.5 respectively. When the exhaust valve motion is due to the main cam only (R_V = 0.0) the first peak of the exhaust pulse as measured immediately before the "turbine" nozzle does not reach beyond 2.48 bars, shown in figure 7.32. In the same figure another curve is shown relating to the case when R_V = 0.17 indicating a first peak of 2.58 bars. Pressure wave reflections are also evident with a wave travel time of 9.6 ms. Figure 7.33 shows that the first peak increases to 2.60 bars when R_V = 0.39. This first peak reaches the same pressure level of 2.60 bars when R_V is further increased to 0.76, but the pressure reaches this level more rapidly as shown in figure 7.34. When the maximum secondary rocker ratio of 1.5 is applied, figure 7.35, the first peak rises swiftly to 2.90 bars before reflections occur.

Figure 7.35A summarizes the effect of varying the cracking pressure on the exhaust pulse profile and amplitude. This figure correspond to the pulses obtained for the baseline case at an engine speed of 1000 rev/min. It is seen that the higher the cracking pressure the larger the pulse amplitude. It should also be noted that at higher cracking pressure levels the pulse profile becomes more fluctuating.

Figure 7.36 compares the measured exhaust pulses in the exhaust pipe immediately before the "turbine" nozzle, between the baseline and the high-rate cases, at an equivalent engine speed of 1300 rev/min. The cracking pressure for this comparison is 5 bars. As can be seen, the wave reflections are quite apparent and the return travel time is approximately 11.3 ms. The peak pressure attained for the high-rate case is 2.40 bars which is 0.10 bars greater than the baseline case.

The same type of comparison has been shown in figure 7.37 corresponding to an equivalent engine speed of 1600 rev/min. The pressure wave reflection period has been found to be approximately 6 ms. The peak of 2.38 bars for the baseline case increases to 2.48 bars for the high-rate case. Figure 7.38 compares the experimentally measured pulses of the two systems at an equivalent engine speed of 1900 rev/min. There is only one reflection taking place at a travel period of 5.37 ms. The peak pressure level of 2.50 bars for the baseline case increases to approximately 2.60 bars for the high-rate system.

Figure 7.39 shows a comparison of the measured exhaust pulses at the "turbine" nozzle between engine speeds of 1000 rev/min (R_V = 1.5) and 2200 rev/min (R_V = 0.0) when the cracking pressure is 5 bars. As may be seen the two pulses rise rapidly, along the same path, to almost the same peak

pressure level of 2.70 bars. This means that the aim of maintaining the exhaust valve opening rate constant is achieved. The pressure wave periodic time at an engine speed of 2200 rev/min has been measured to be 3.78 ms. It is shown in expression 7.2 that the wave propagation velocity is independent of the time taken for a complete journey of a single wave, because there are so many factors interacting together that influence the pressure wave travel, as mentioned earlier. The pulse peak pressure and the wave sonic velocity determine the wave propagation velocity.

7.1.6 Exhaust Pulse Power Calculation

The exhaust pulse power calculation used was that described by Benson and Woods (11), details of which are given in appendix 9. The power calculation is based on the power developed by a hypothetical isentropic turbine at the exhaust nozzle. The rate of change of the pressure ratio across the "turbine" nozzle ($P_{atm.}$ / P_{pipe}) is illustrated in figure 7.42 for both the baseline (R_V = 0.0) and the highest-rate cases (R_V = 1.5). The equivalent engine speed and the cracking pressure for figures 7.40-7.46 are 1000 rev/min and 6 bars respectively. It should be noted that the variables plotted in these figures cover the blow-down (exhaust valve opening to intake valve opening) period only. It is clearly seen that when the exhaust valve opens at the highest-rate the critical pressure ratio for the start of

the choked flow at the nozzle throat is reached earlier than for the baseline case. In fact, the start of choked flow for the baseline case is approximately 8.12 ms (48.75 crank angle degrees) later than the highest-rate case. Figure 7.41 shows the velocity of exhaust gas in the pipe upstream of the nozzle for the two cases. It may be seen that the pipe velocity for the highest-rate case (R_V = 1.5) rises more rapidly than that of the baseline case (R_V = 0.0). The start of the choked flow at the nozzle for both cases occurs when the pipe velocity reaches approximately 53 m/s.

The velocity of the exhaust gas at the "turbine" nozzle is shown in figure 7.42. A comparison between the two cases may be made. The choked flow starts 48.75 crank angle degrees earlier in the highest-rate case than the baseline case corresponding to a nozzle velocity of 350 m/s. The nozzle and the pipe velocities for both the baseline and the highest-rate cases are shown in figures 7.43 and 7.44 respectively. The rise in pipe and nozzle velocity for the highest-rate case is more rapid than those for the baseline case, as expected.

The rapid opening of the exhaust valve in the highest-rate case, allows the gas to flow from the cylinder to the exhaust manifold more rapidly than in the baseline case. This is illustrated in figure 7.45, thus, it may be seen that a much larger proportion of the exhaust gas has been

released through the exhaust valve in the highest-rate than in the baseline case. In the highest-rate case, choked flow through the "turbine" nozzle starts 48.75 degrees of crank angle earlier than in the baseline case. For the higher rate of opening the peak instantaneous mass flow rate is attained within this period. This peak is approximately 0.17 kg/s which is about 0.02 kg/s greater than the maximum flow rate in the baseline case.

It can be seen in figure 7.46 that as a result of the increase in the rate of exhaust valve opening, the pulses in the manifold transport a greater proportion of the available exhaust energy to the "turbine" nozzle. Like the exhaust mass flow rate the peak power in the high-rate system is achieved in the first 48.75 CA degrees (8.12 ms) period. The instantaneous peak exhaust pulse power values of 18 kW and 14 kW are obtained at the highest-rate and for the baseline case respectively.

Figure 7.47 shows the percentage gain in the exhaust pulse power compared with the baseline case, at an equivalent engine speed of 1000 rev/min and the highest secondary rocker ratio of 1.5, as the cracking pressure changes from 2 to 6 bars. It may be seen that the gain in pulse power increases with increase in the cracking pressure. This gain ranges between 22.51% and 57.73%. Using the same calculation, the power of the exhaust pulses for both the

highest-rate and the baseline cases were determined for the entire speed range, as shown in figure 7.48. At 1000 rev/min the mean exhaust pulse power of 2.403 kW in the baseline case increses to 3.689 kW in the highest-rate case which is 70% of the maximum theoretically available power. This increase corresponds to a 54% gain in pulse power. As the equivalent engine speed increases, the gain in pulse power decreases. This would be expected since the design only allows an increase of valve opening at low speeds. The exhaust pulse power gain at 1300 rev/min is 45.22%, at 1600 rev/min is 23.63%, at 1900 rev/min is 12.22% and there is no gain in pulse power at 2200 rev/min.

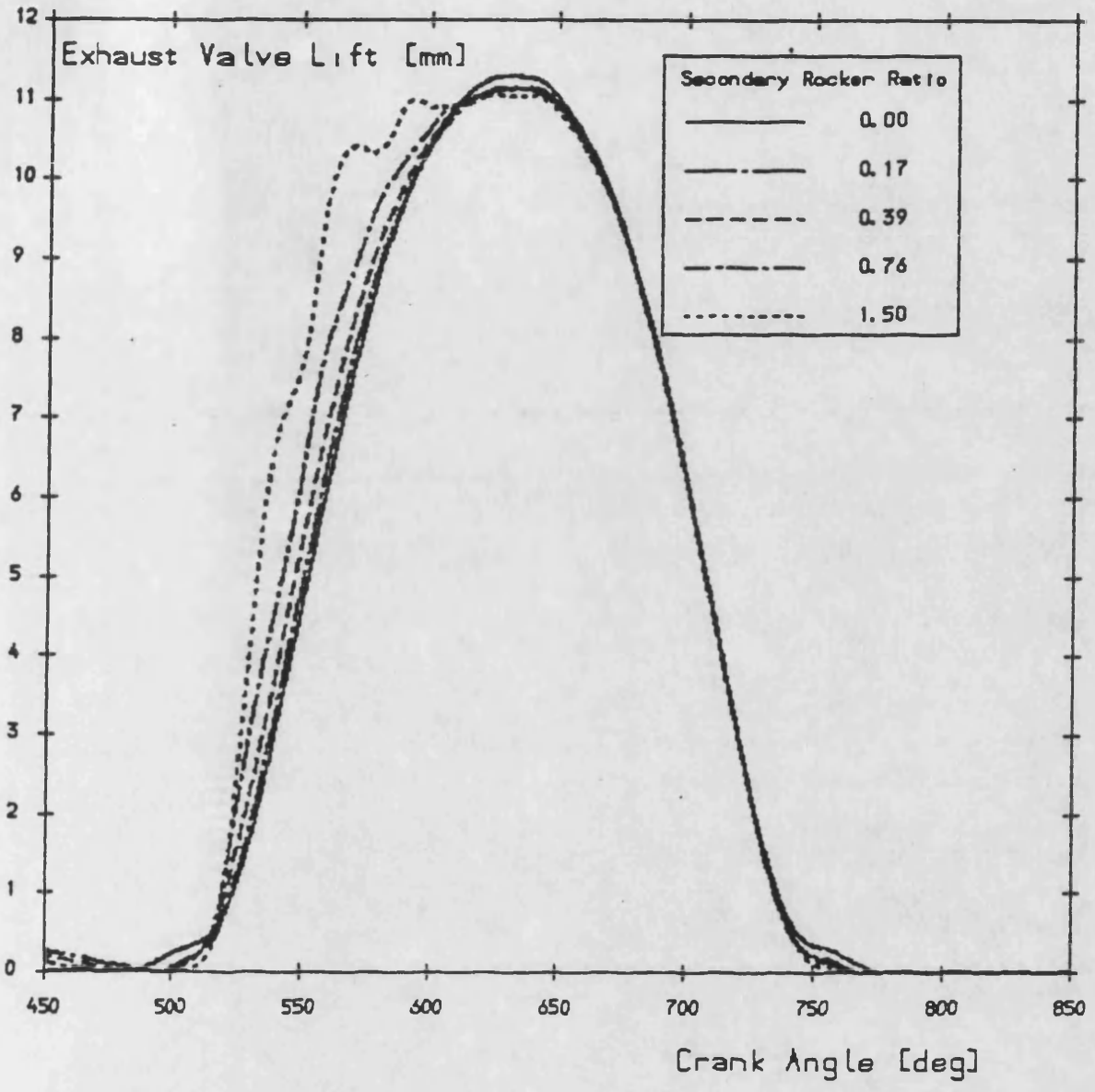

Figure 7.1- Measured valve lift curves at 1000 rev/min showing instability at the highest rate of opening.

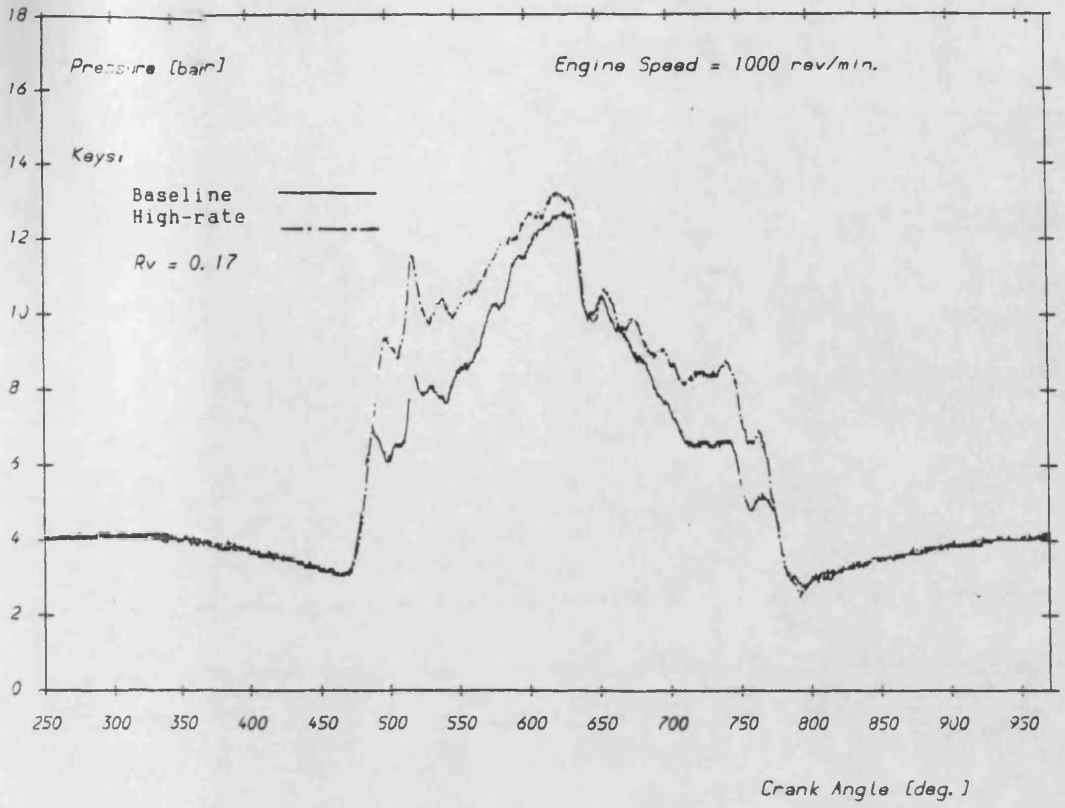

Figure 7.2- Variation of hydraulic chamber pressure at 1000 rev/min.
Cracking pressure = Atmospheric.

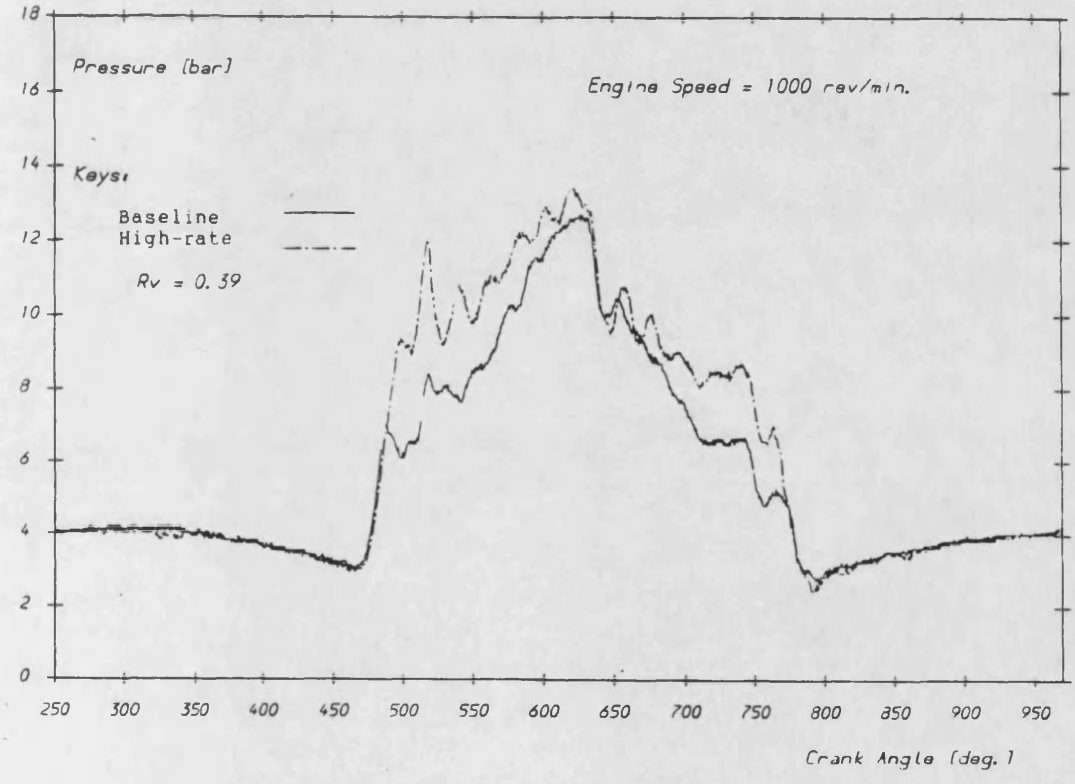

Figure 7.3- Variation of hydraulic chamber pressure at 1000 rev/min.
Cracking pressure = Atmospheric.

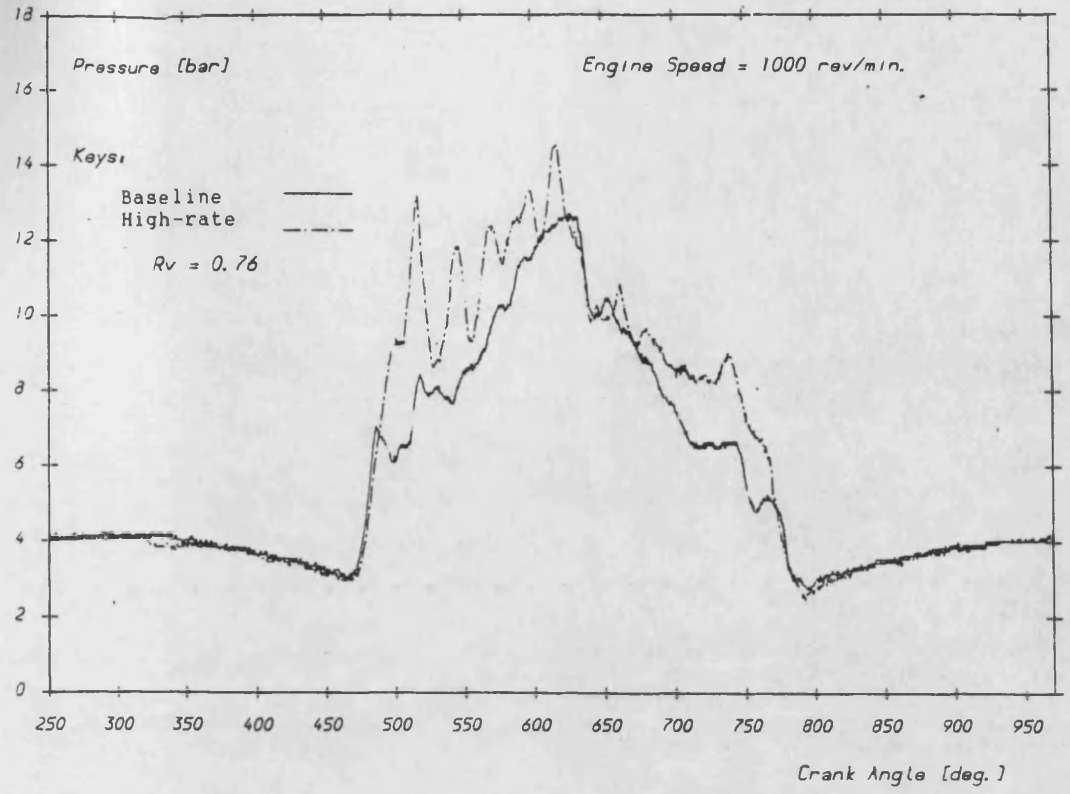

Figure 7.4- Variation of hydraulic chamber pressure at 1000 rev/min.
Cracking pressure = Atmospheric.

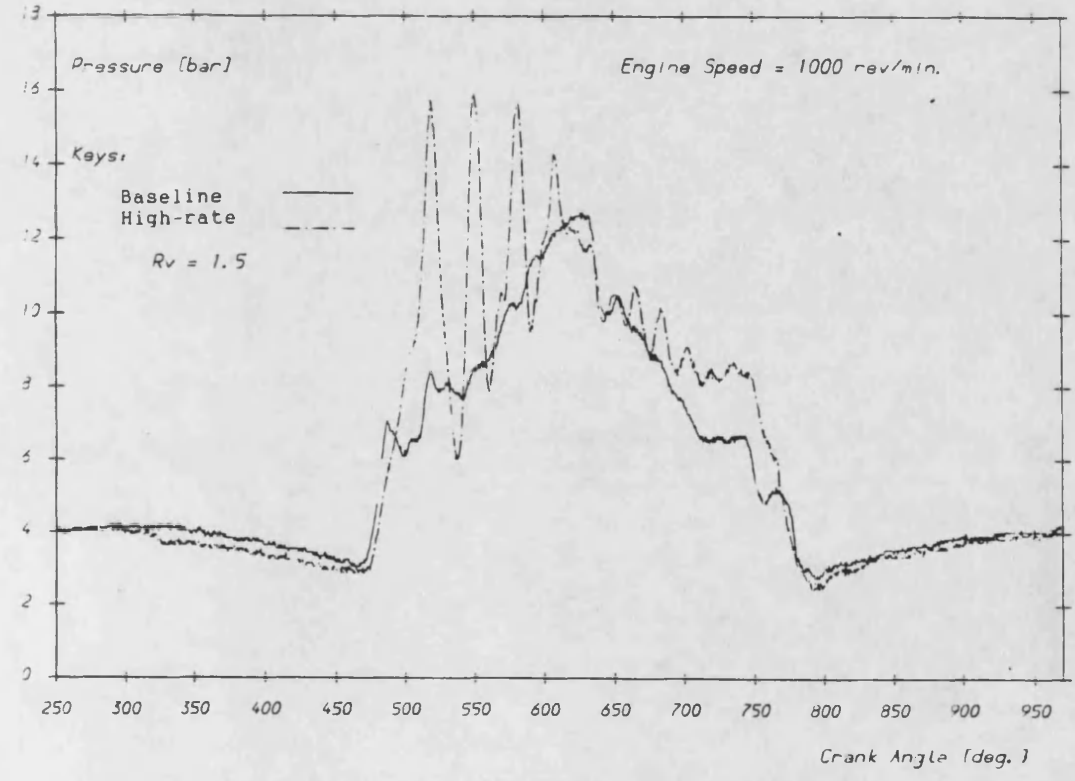

Figure 7.5- Variation of hydraulic chamber pressure at 1000 rev/min.
Cracking pressure = Atmospheric.

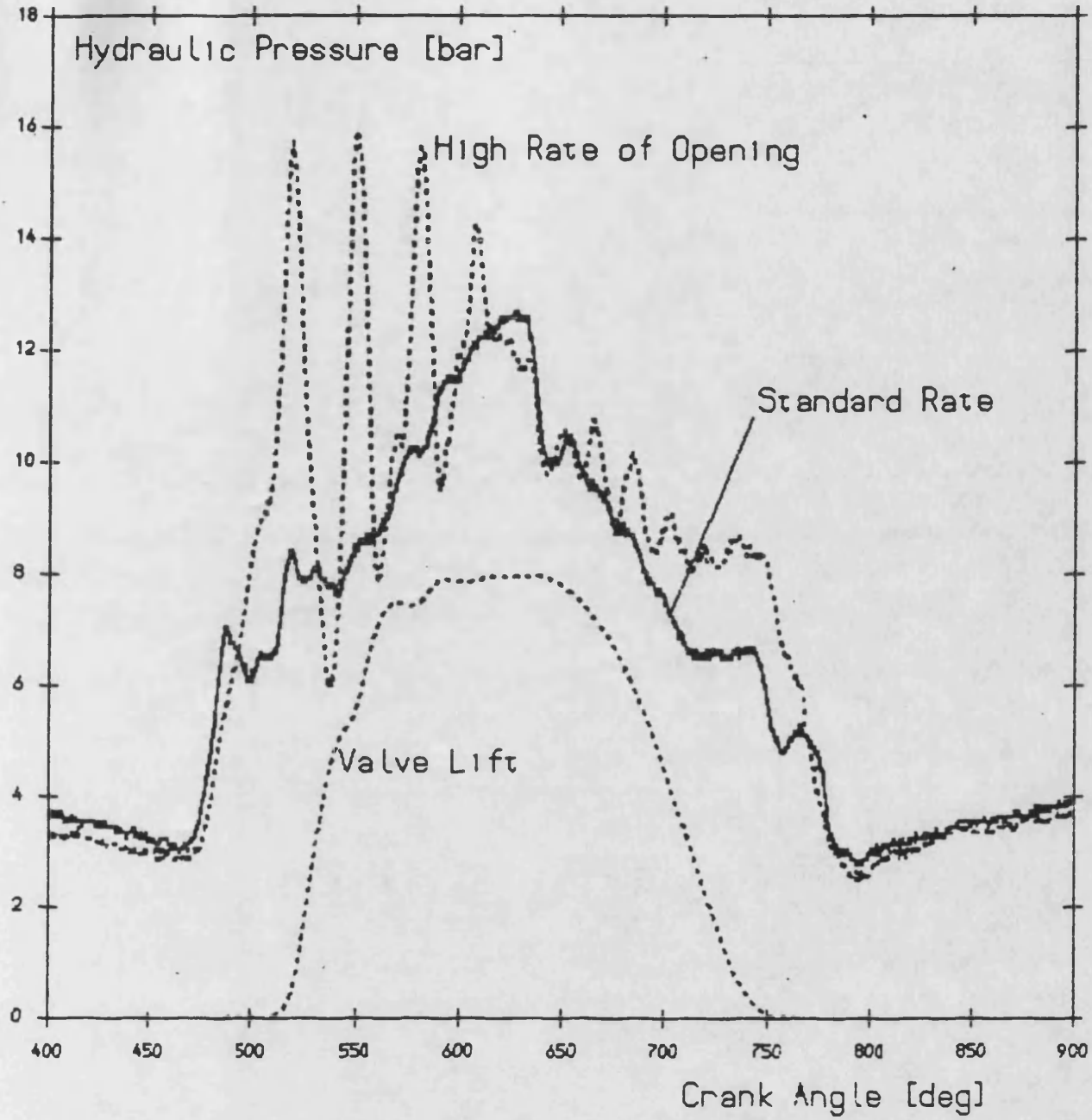

Figure 7.6- Upper curves show variation of hydraulic chamber pressure for the highest rate and standard rate at 1000 rev/min. Valve lift shown for the highest case.

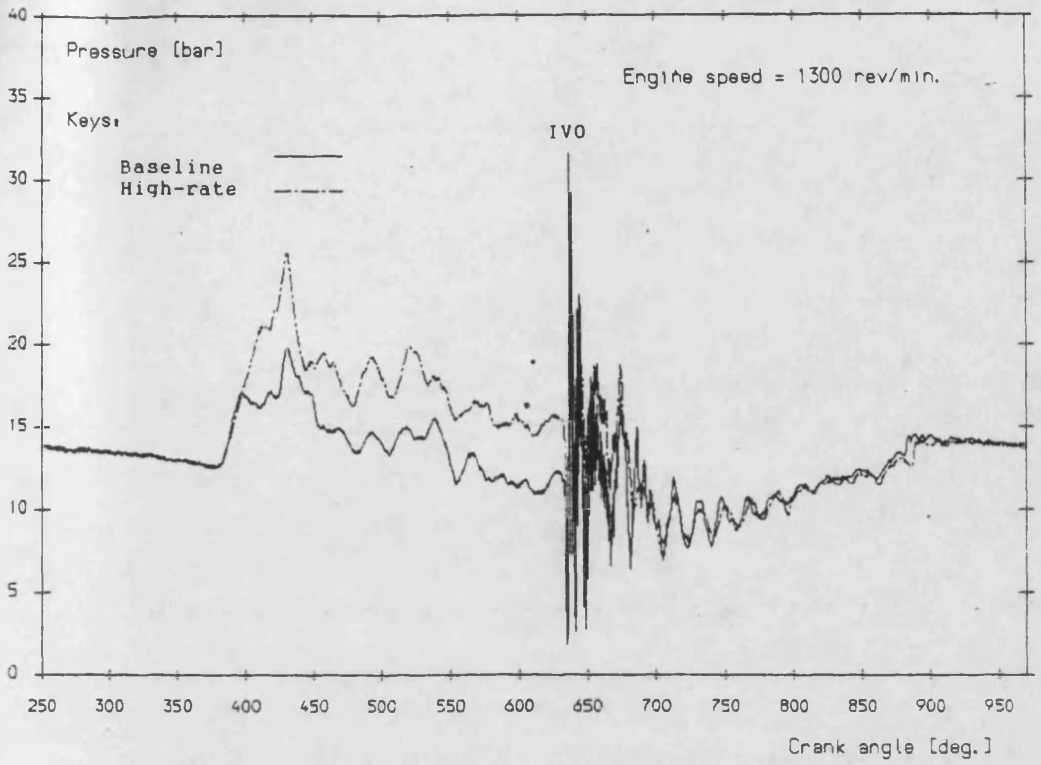

Figure 7.7- Variation of hydraulic chamber pressure at 1300 rev/min.
Cracking pressure = 5 bars.

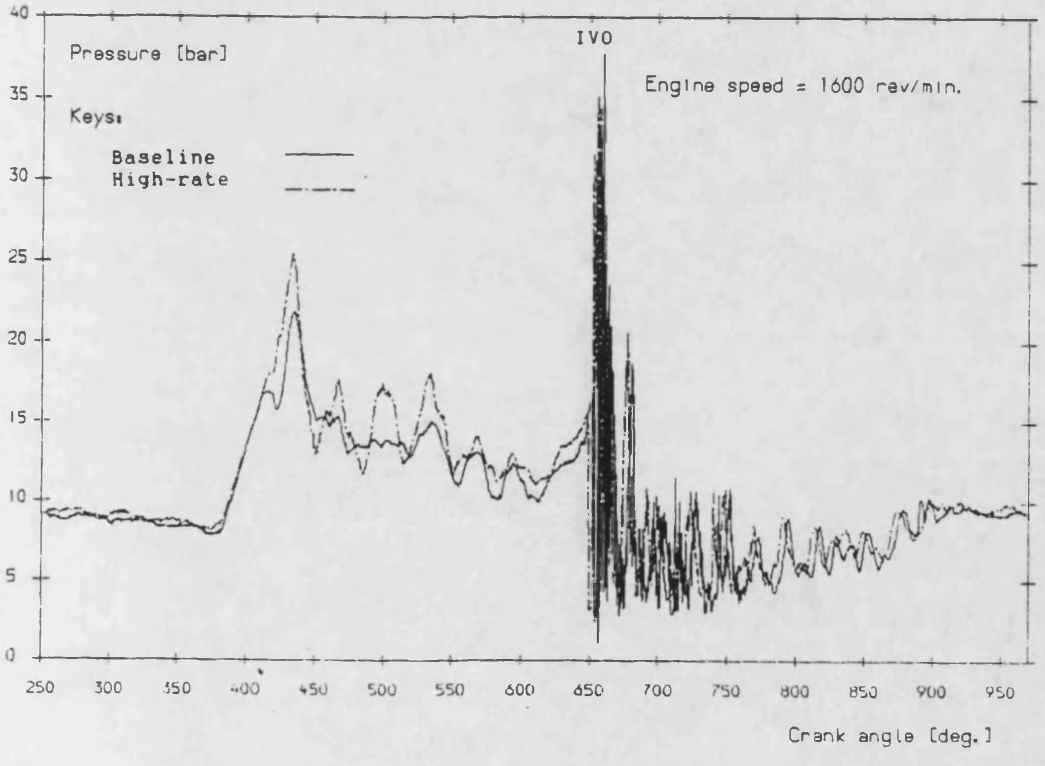

Figure 7.8- Variation of hydraulic chamber pressure at 1600 rev/min.
Cracking pressure = 5 bars.

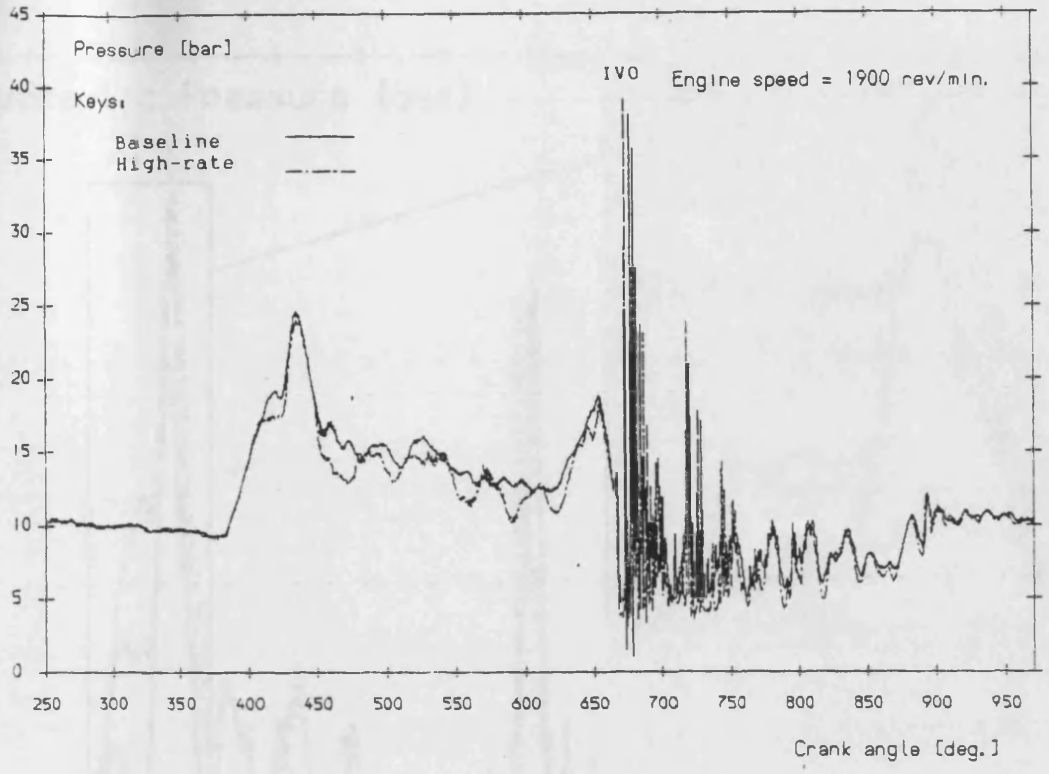

Figure 7.9- Variation of hydraulic chamber pressure at 1900 rev/min. Cracking pressure = 5 bars.

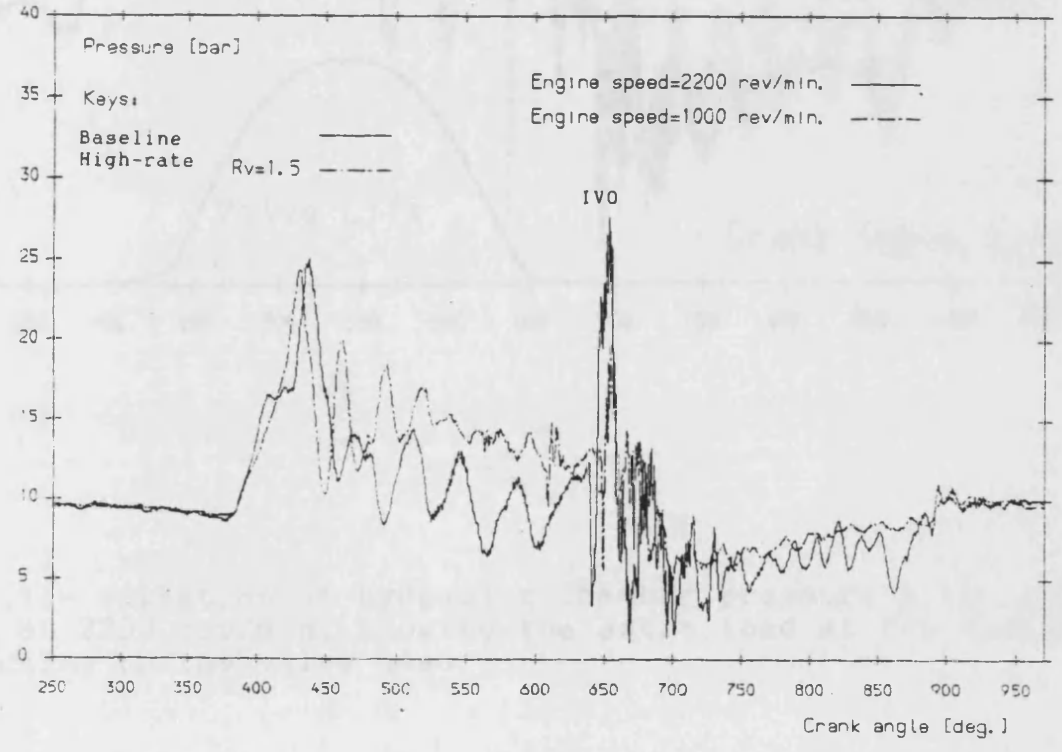

Figure 7.10- Comparison of hydraulic chamber pressure at 1000 (highest rate) and 2200 rev/min. Cracking pressure = 5 bars.

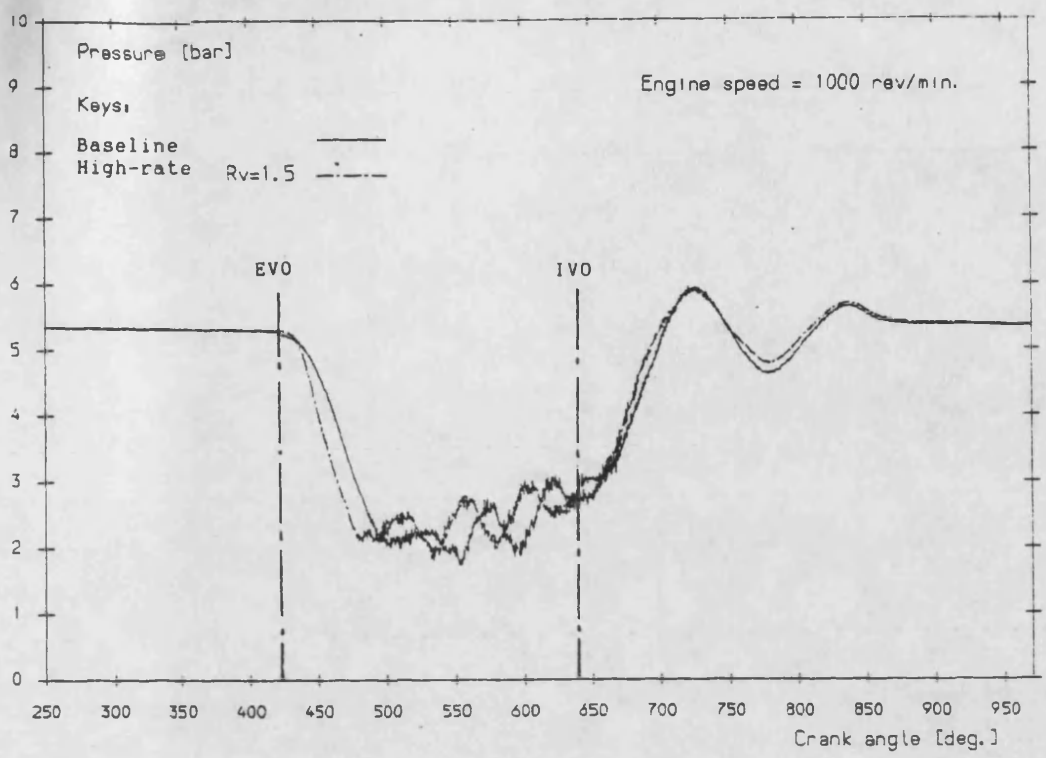

Figure 7.12- Cylinder pressure expansion at 1000 rev/min.

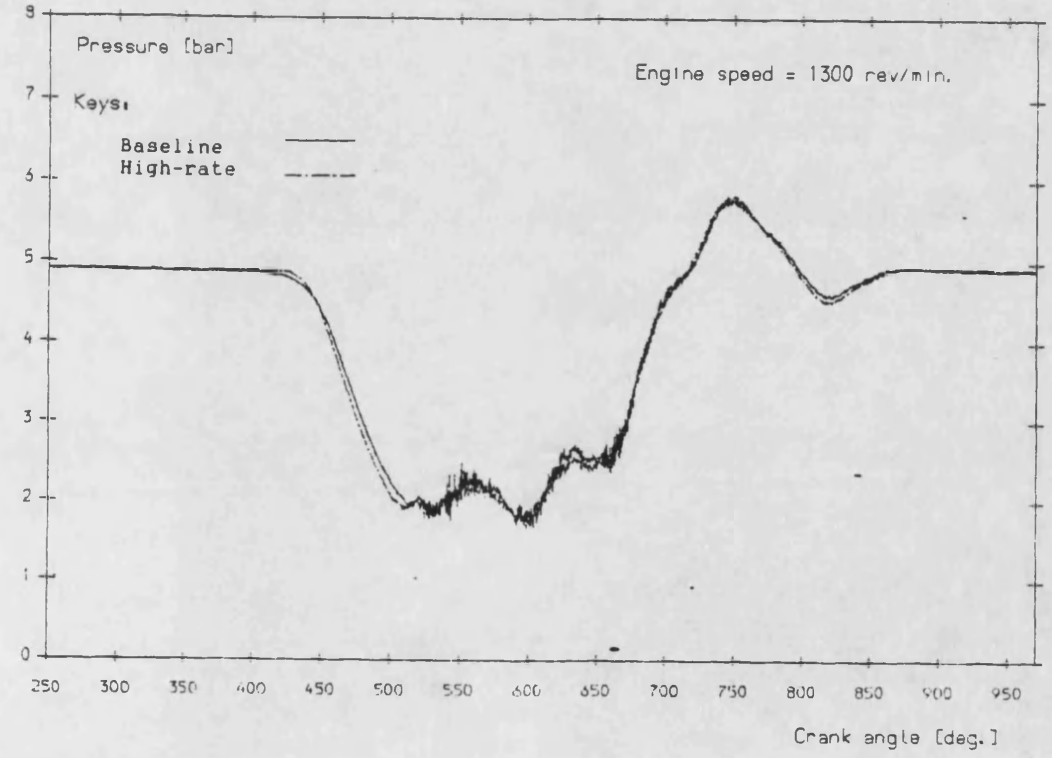

Figure 7.13- Cylinder pressure expansion at 1300 rev/min.

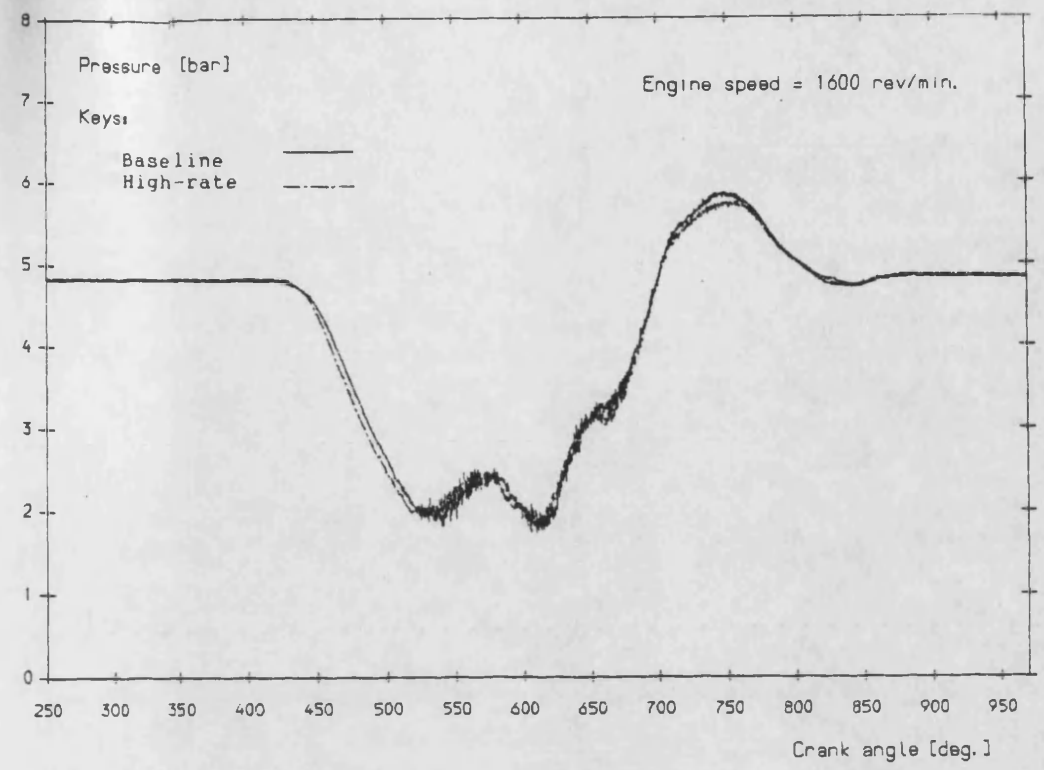

Figure 7.14- Cylinder pressure expansion at 1600 rev/min.

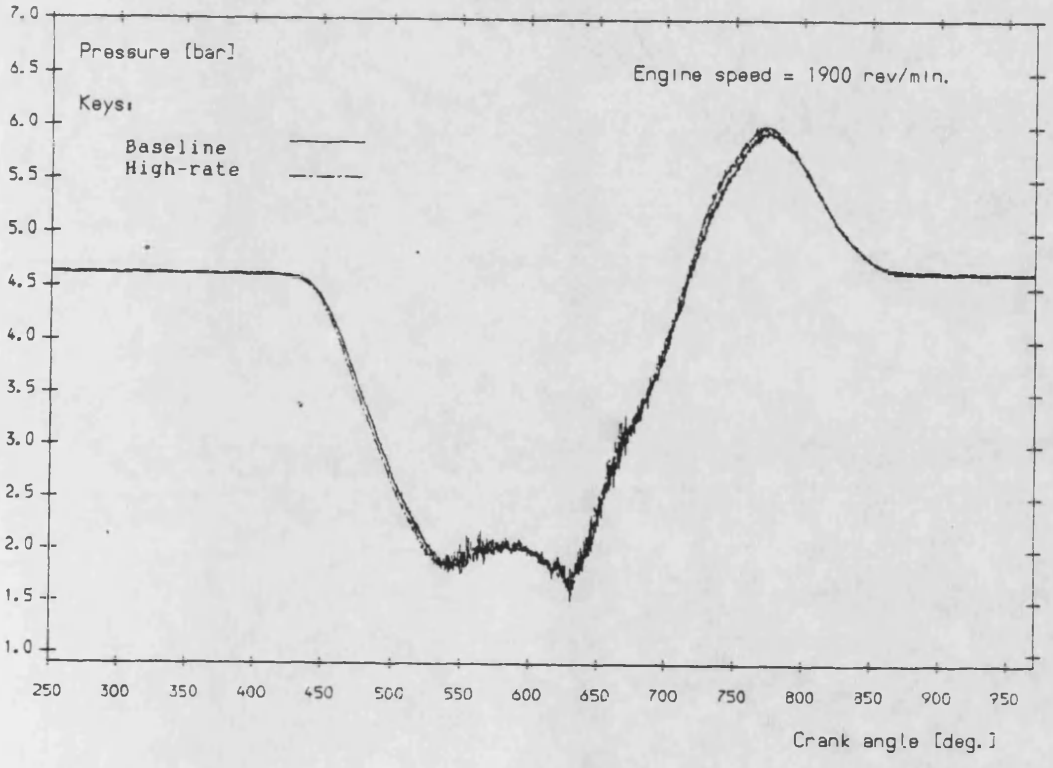

Figure 7.15- Cylinder pressure expansion at 1900 rev/min.

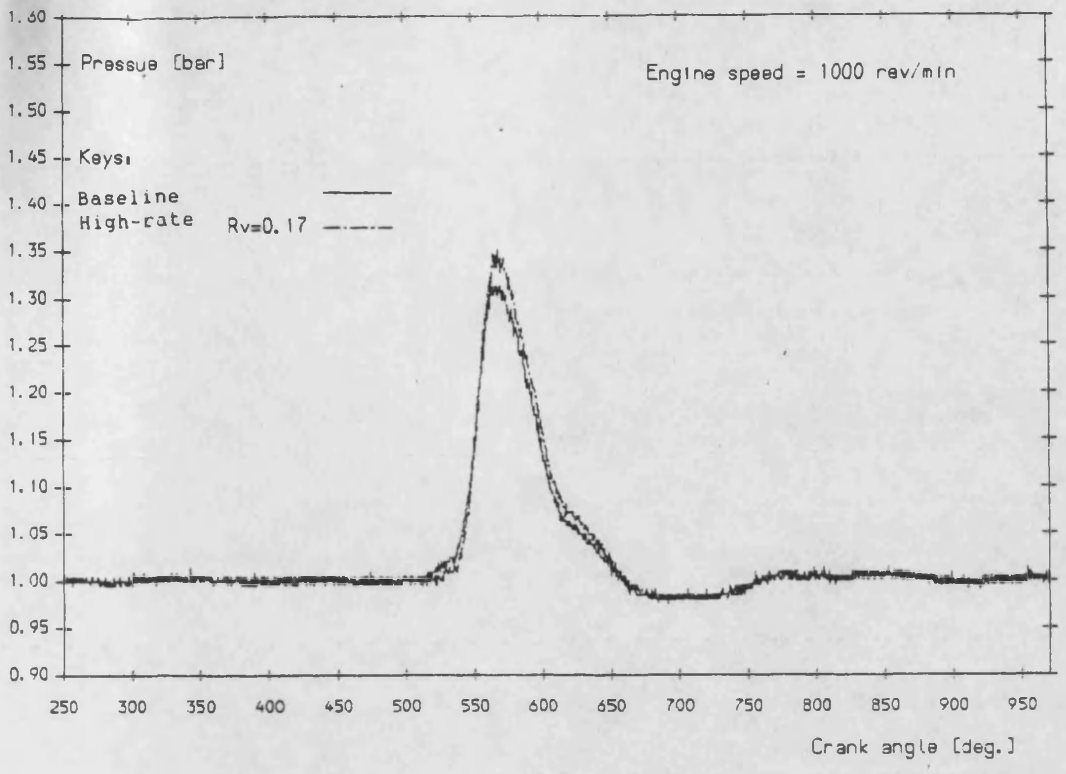

Figure 7.16- Comparison of exhaust pulses at 1000 rev/min.
Cracking pressure = 2 bars.

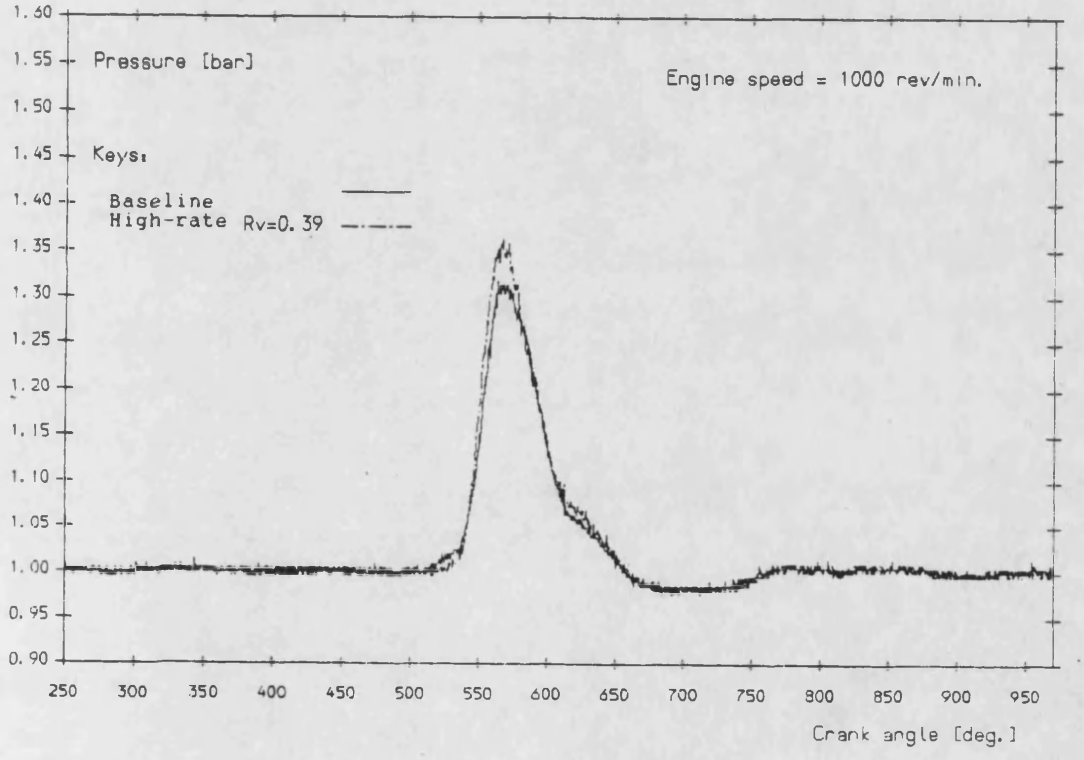

Figure 7.17- Comparison of exhaust pulses at 1000 rev/min.
Cracking pressure = 2 bars.

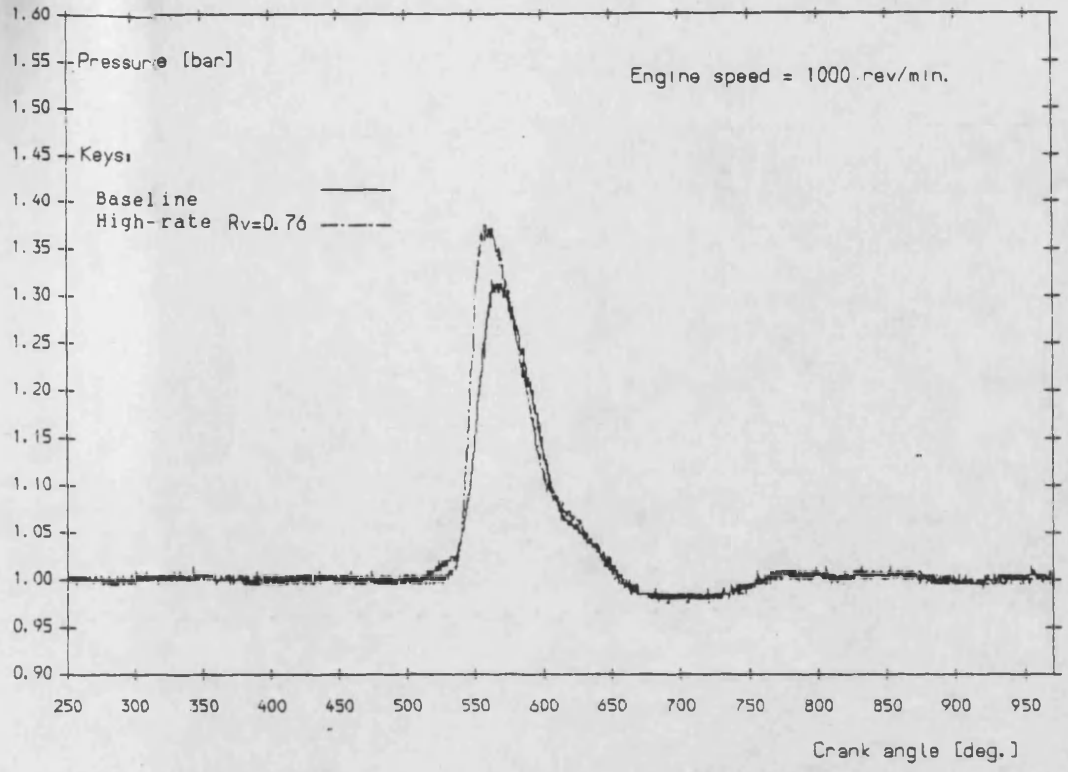

Figure 7.18- Comparison of exhaust pulses at 1000 rev/min.
Cracking pressure = 2 bars.

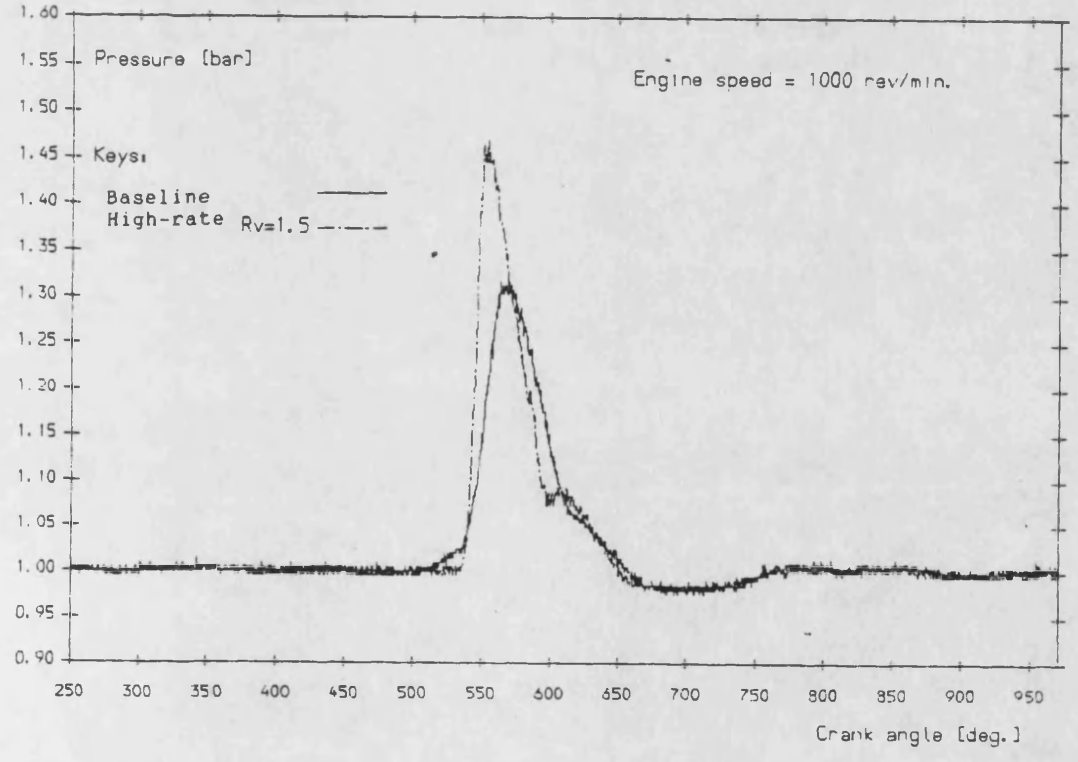

Figure 7.19- Comparison of exhaust pulses at 1000 rev/min.
Cracking pressure = 2 bars.

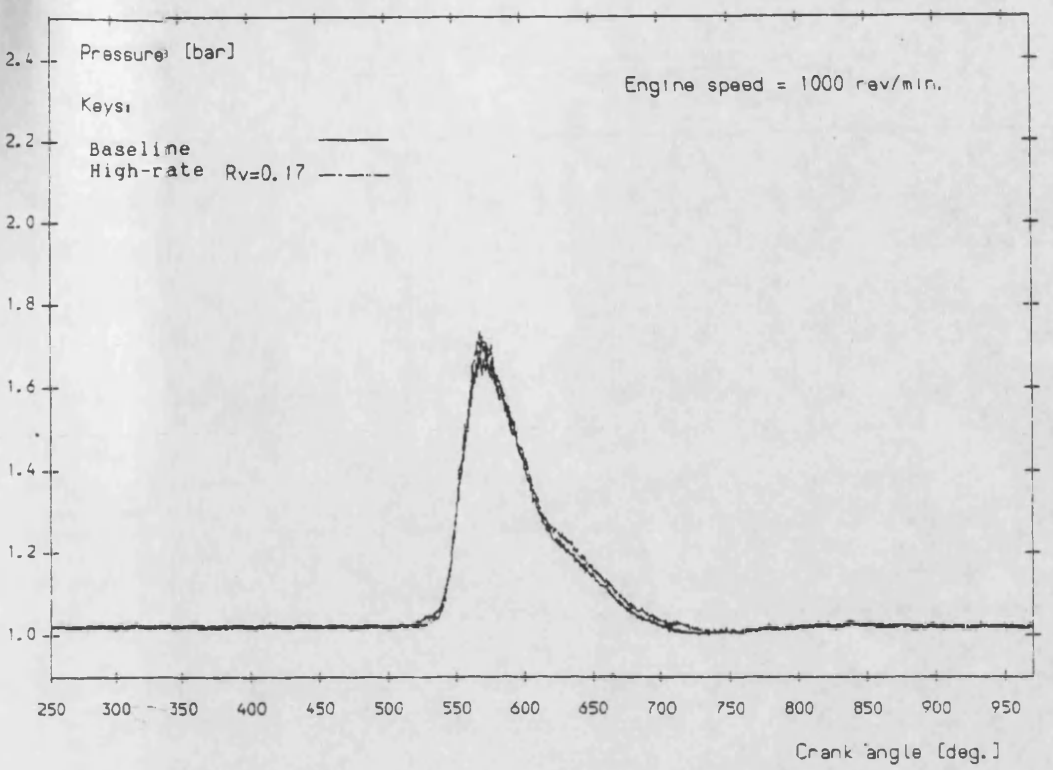

Figure 7.20- Comparison of exhaust pulses at 1000 rev/min.
Cracking pressure = 3 bars.

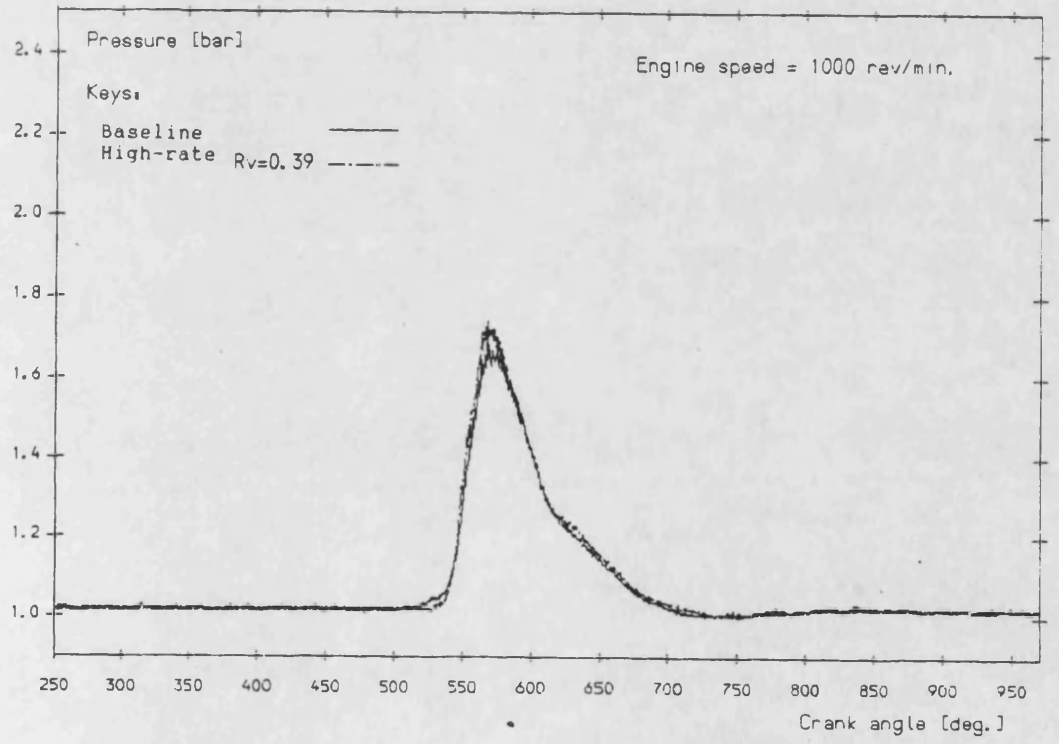

Figure 7.21- Comparison of exhaust pulses at 1000 rev/min.
Cracking pressure = 3 bars.

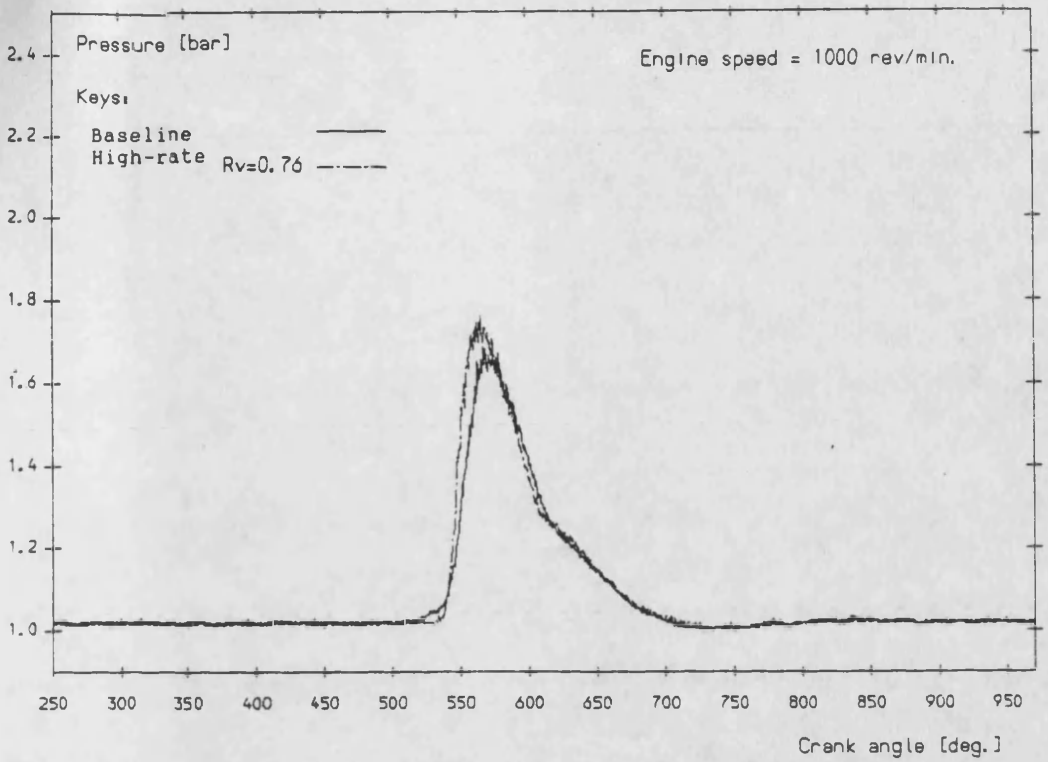

Figure 7.22- Comparison of exhaust pulses at 1000 rev/min.
Cracking pressure = 3 bars.

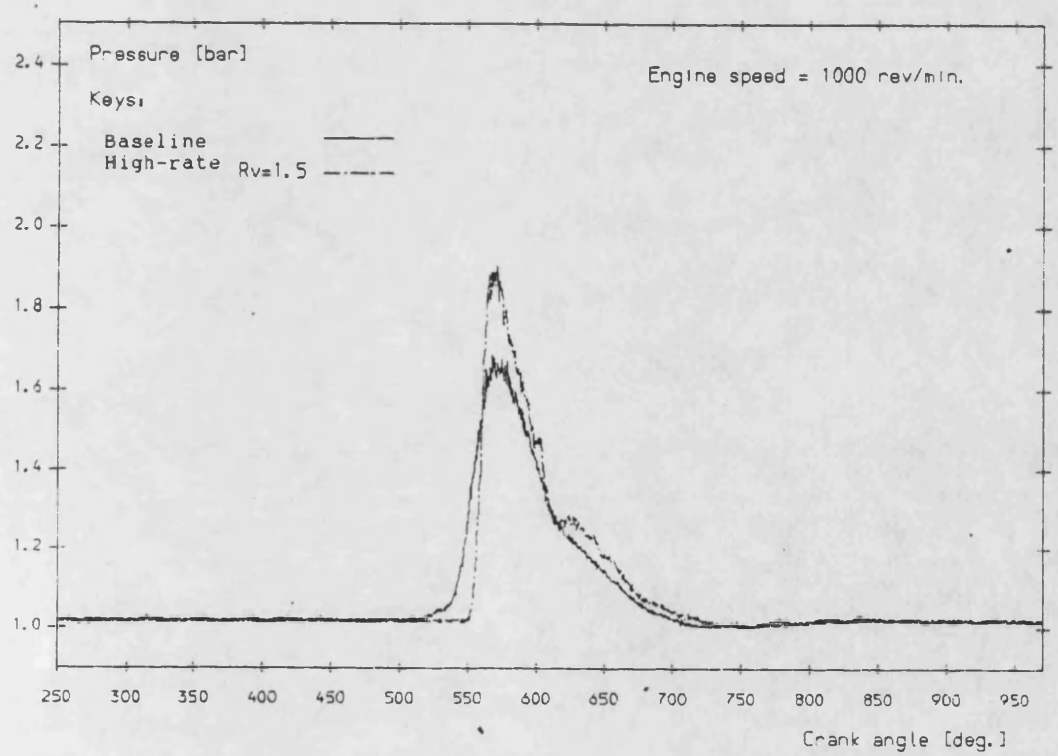

Figure 7.23- Comparison of exhaust pulses at 1000 rev/min.
Cracking pressure = 3 bars.

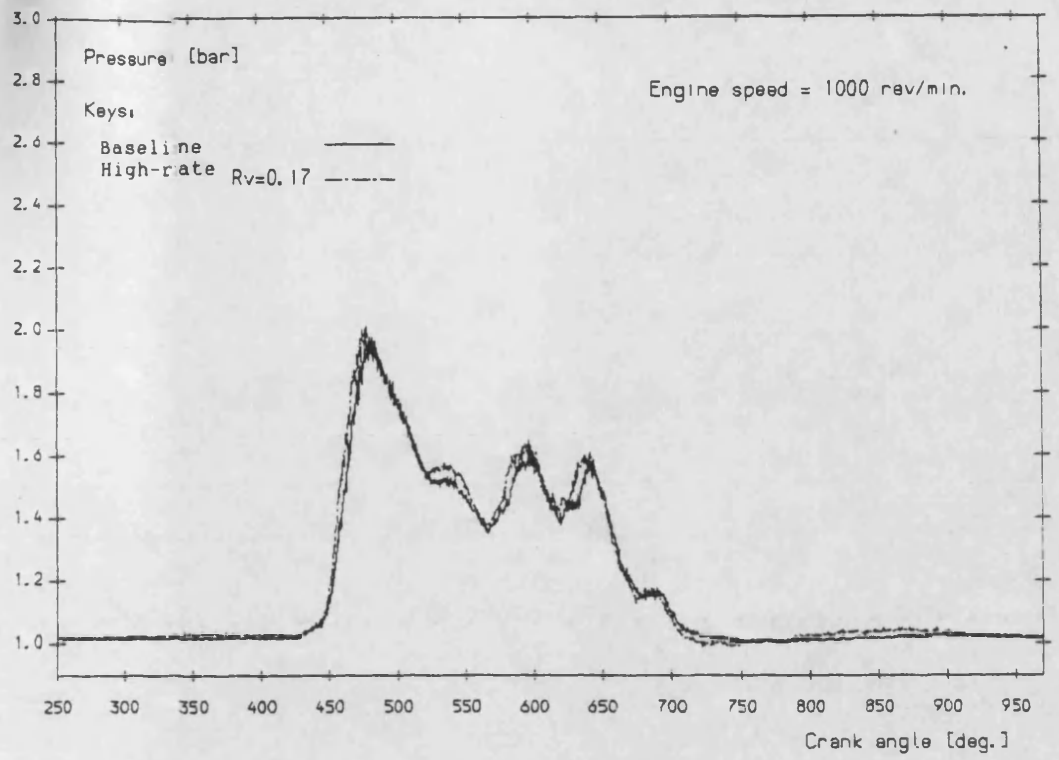

Figure 7.24- Comparison of exhaust pulses at 1000 rev/min.
Cracking pressure = 4 bars.

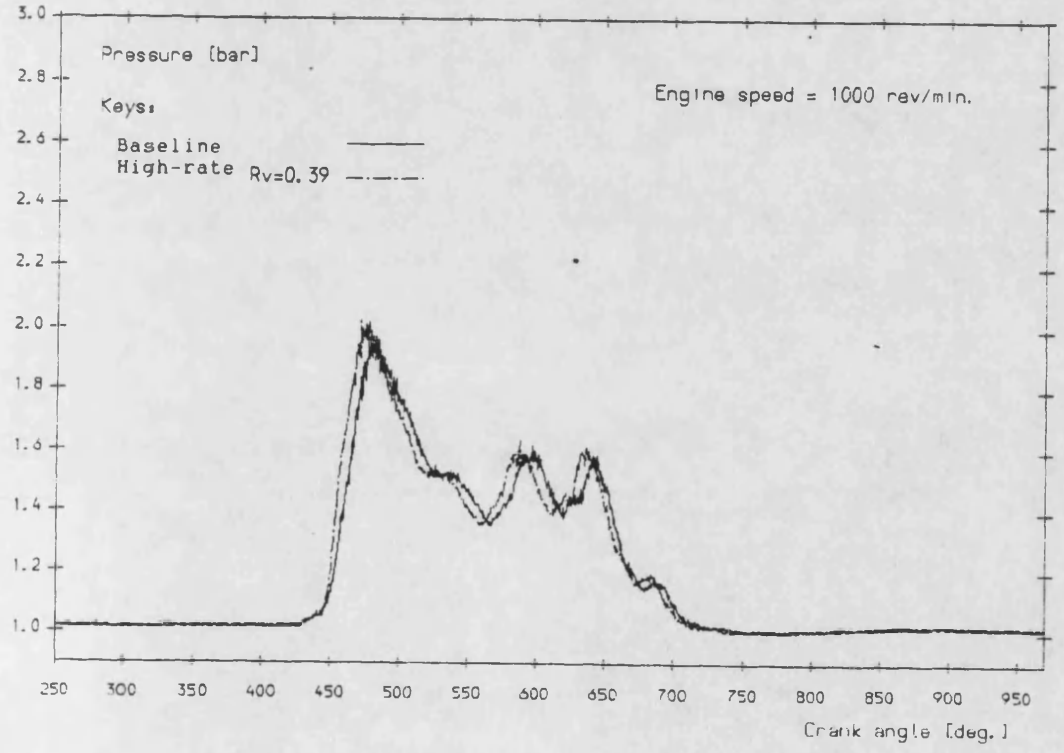

Figure 7.25- Comparison of exhaust pulses at 1000 rev/min.
Cracking pressure = 4 bars.

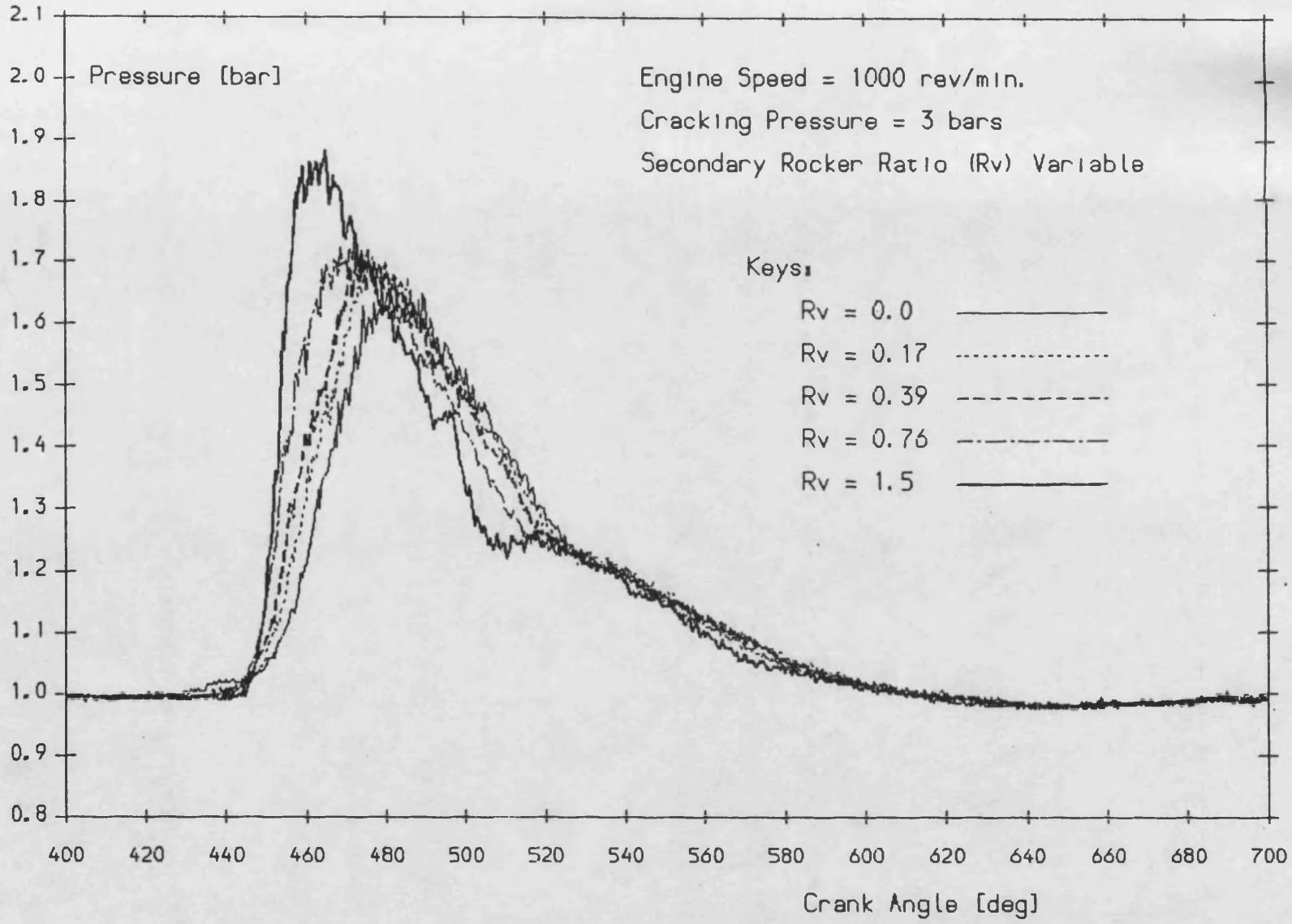
Pressure [bar]
Engine Speed = 1000 rev/min.
Cracking Pressure = 3 bars
Secondary Rocker Ratio (Rv) Variable
Keys:
Rv = 0.0
Rv = 0.17
Rv = 0.39
Rv = 0.76
Rv = 1.5
2.1
2.0
1.9
1.8
1.7
1.6
1.5
1.4
1.3
1.2
1.1
1.0
0.9
0.8
400
420
440
460
480
500
520
540
560
580
600
620
640
660
680
700
Crank Angle [deg]

Figure 7.25A

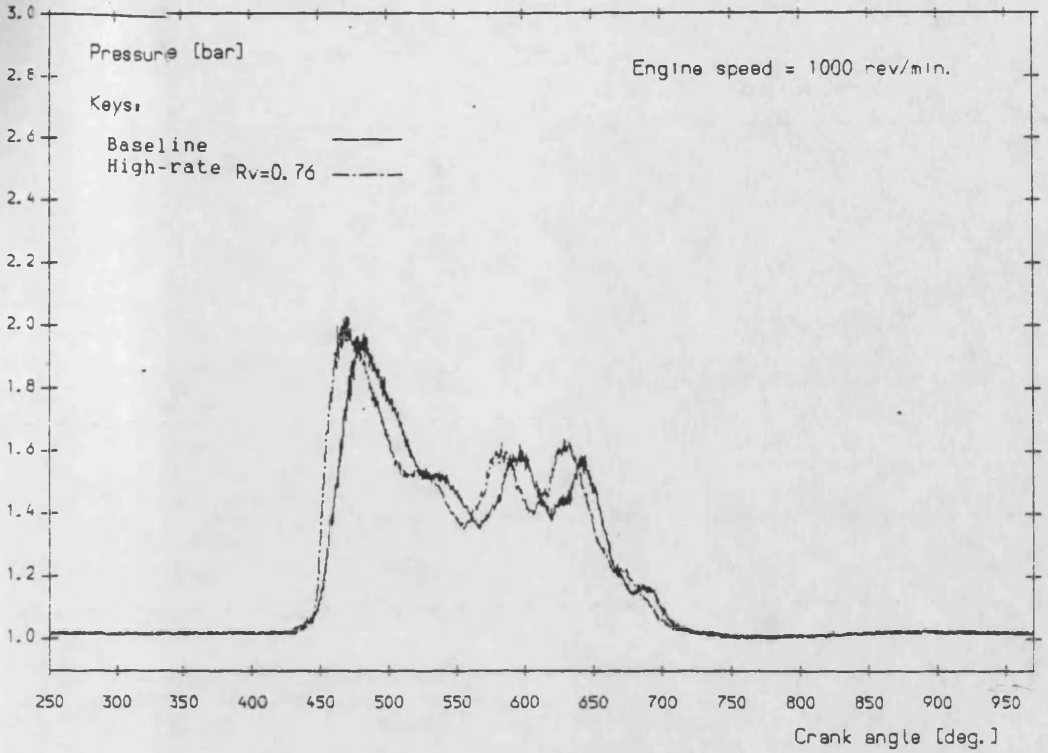

Figure 7.26- Comparison of exhaust pulses at 1000 rev/min.
Cracking pressure = 4 bars.

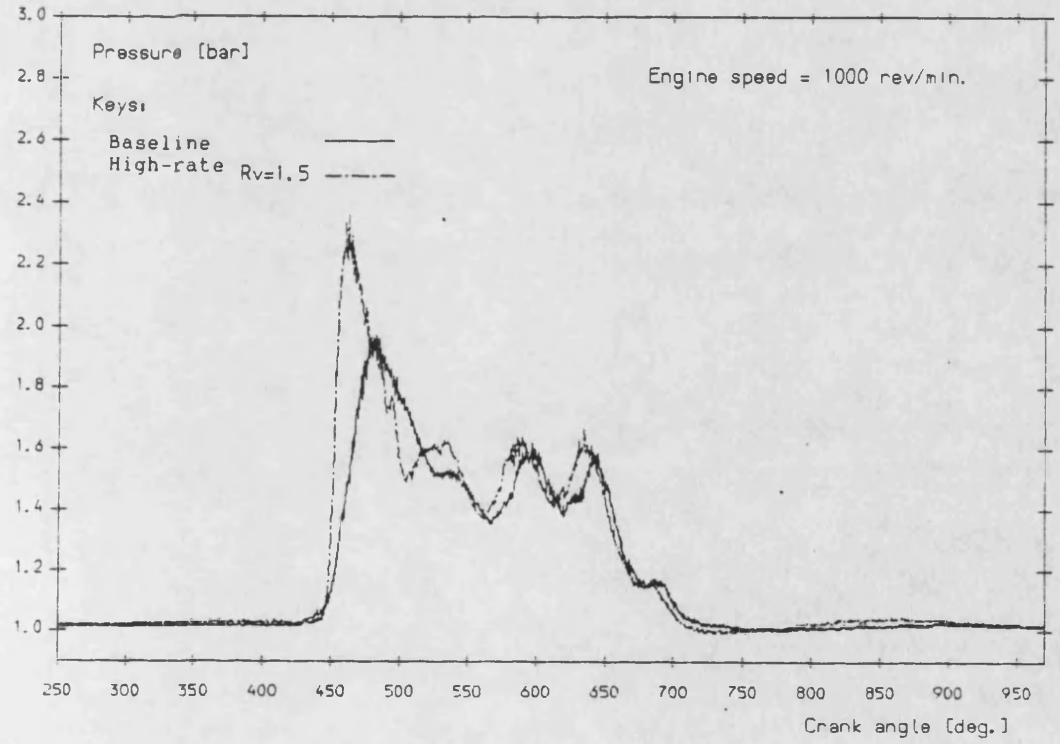

Figure 7.27- Comparison of exhaust pulses at 1000 rev/min.
Cracking pressure = 4 bars.

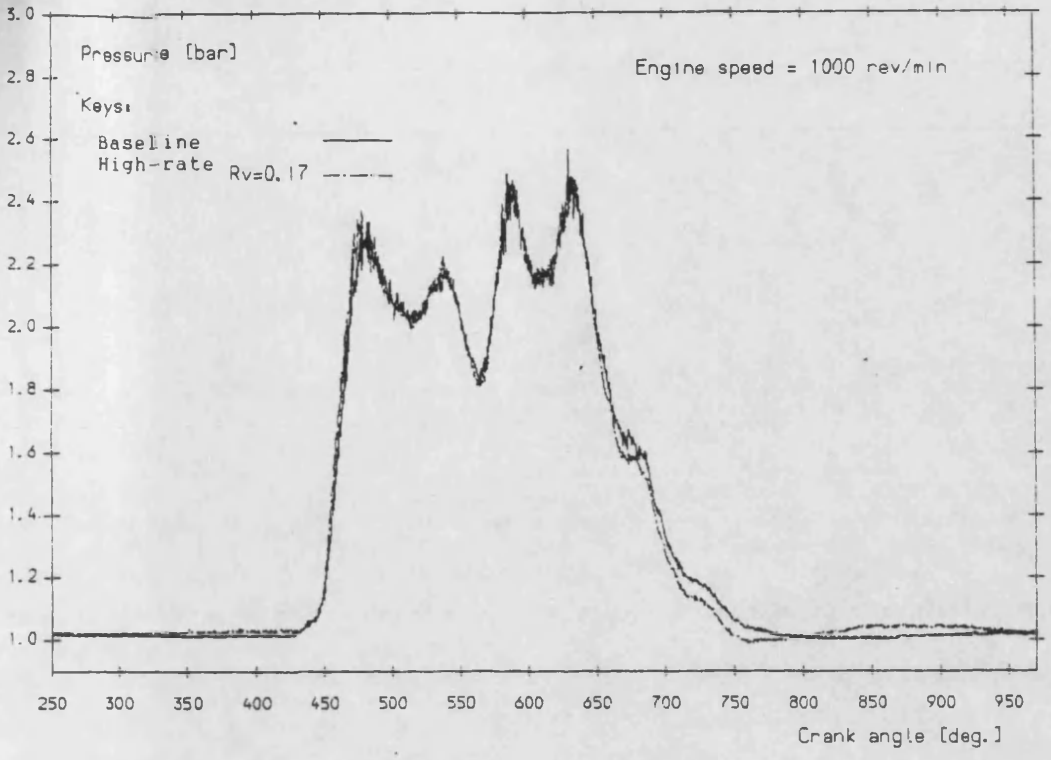

Figure 7.28- Comparison of exhaust pulses at 1000 rev/min.
Cracking pressure = 5 bars.

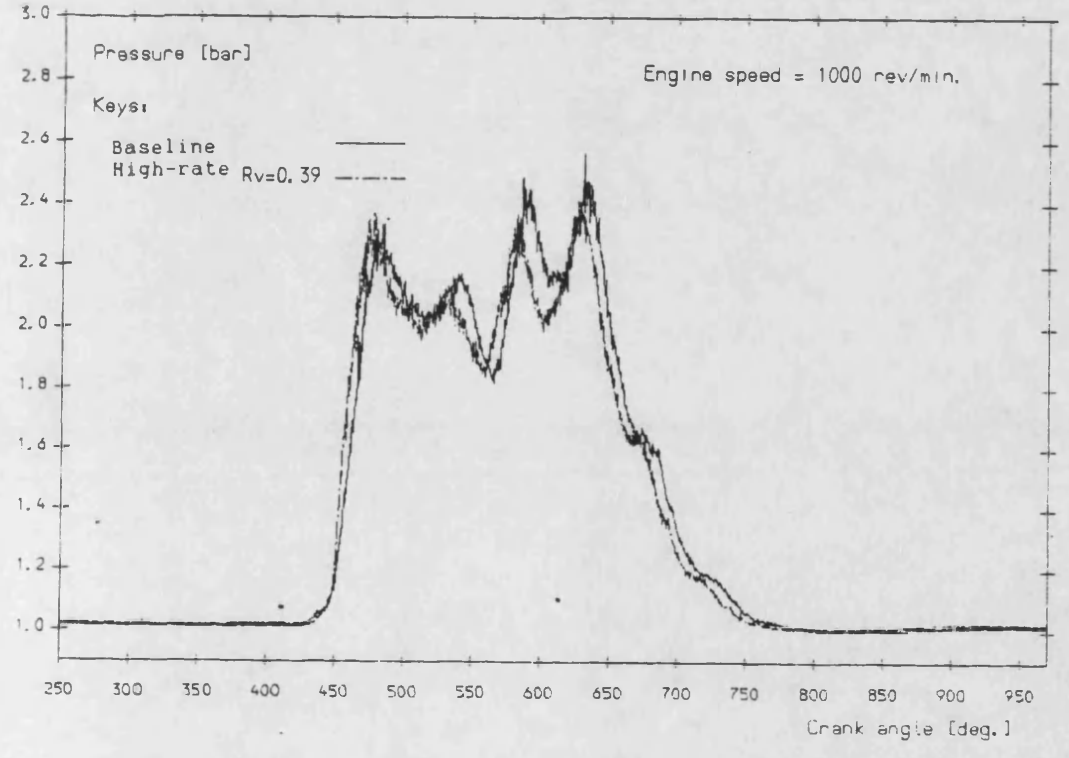

Figure 7.29- Comparison of exhaust pulses at 1000 rev/min.
Cracking pressure = 5 bars.

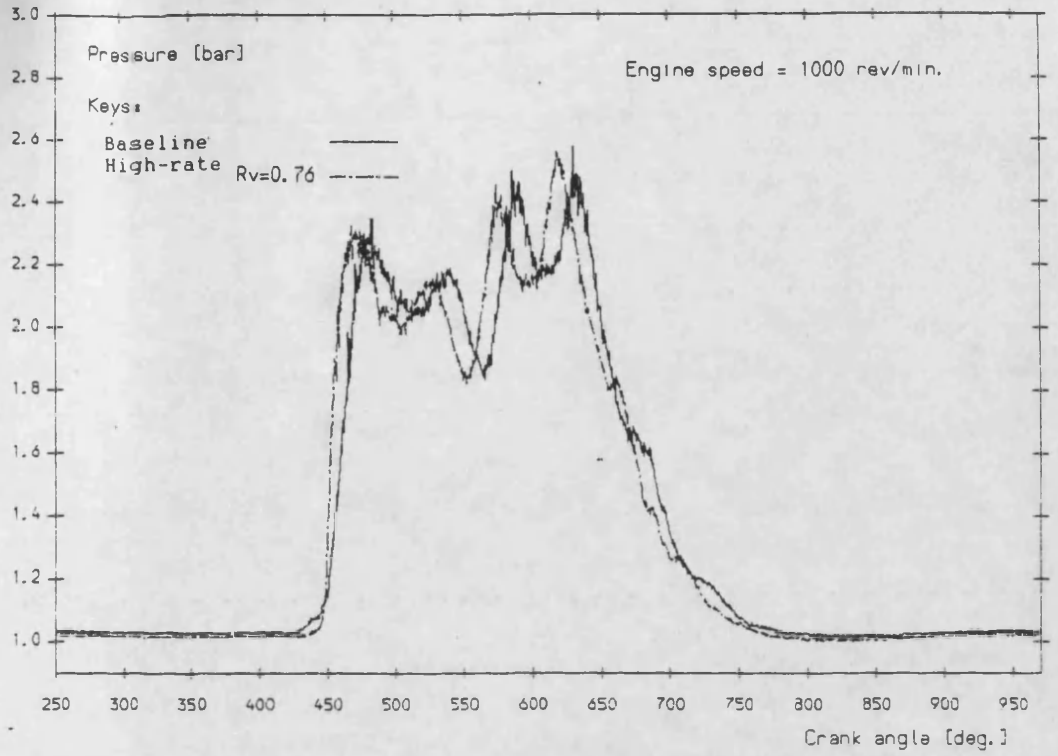

Figure 7.30- Comparison of exhaust pulses at 1000 rev/min.
Cracking pressure = 5 bars.

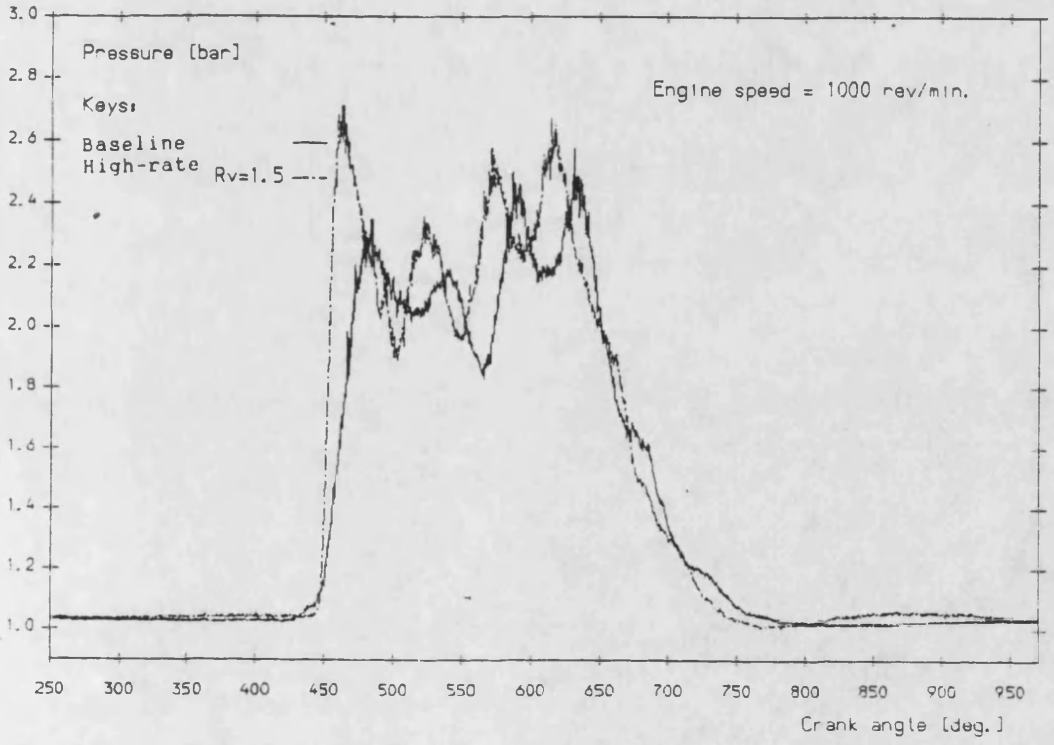

Figure 7.31- Comparison of exhaust pulses at 1000 rev/min.
Cracking pressure = 5 bars.

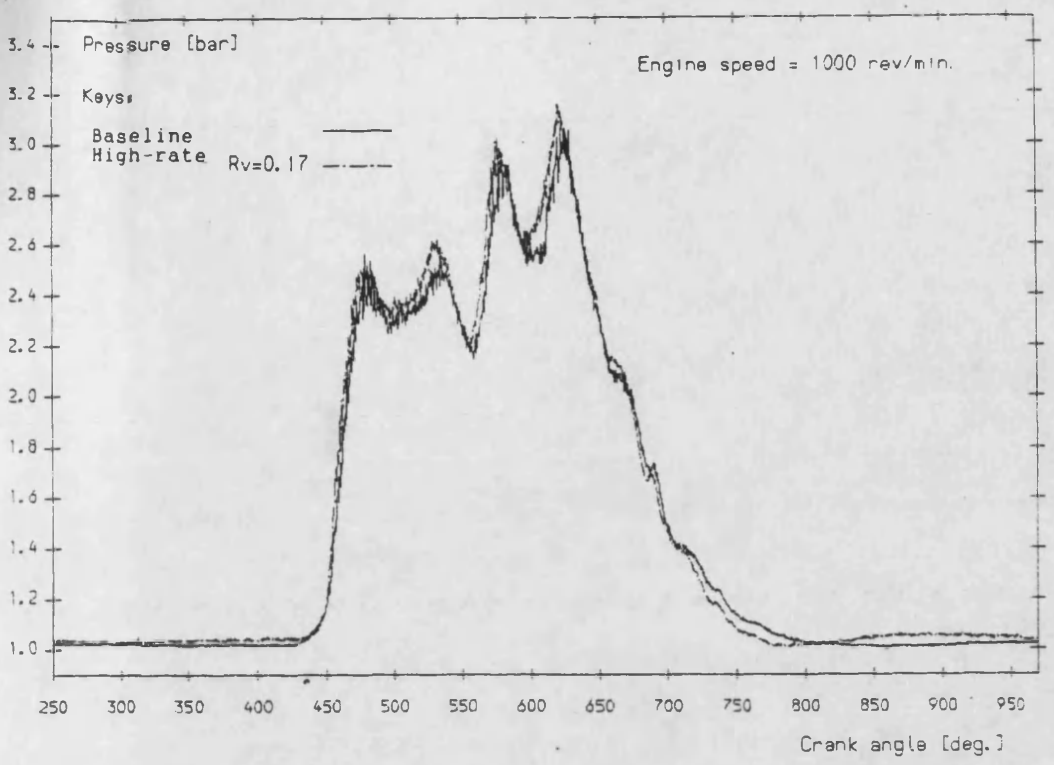

Figure 7.32- Comparison of exhaust pulses at 1000 rev/min.
Cracking pressure = 6 bars.

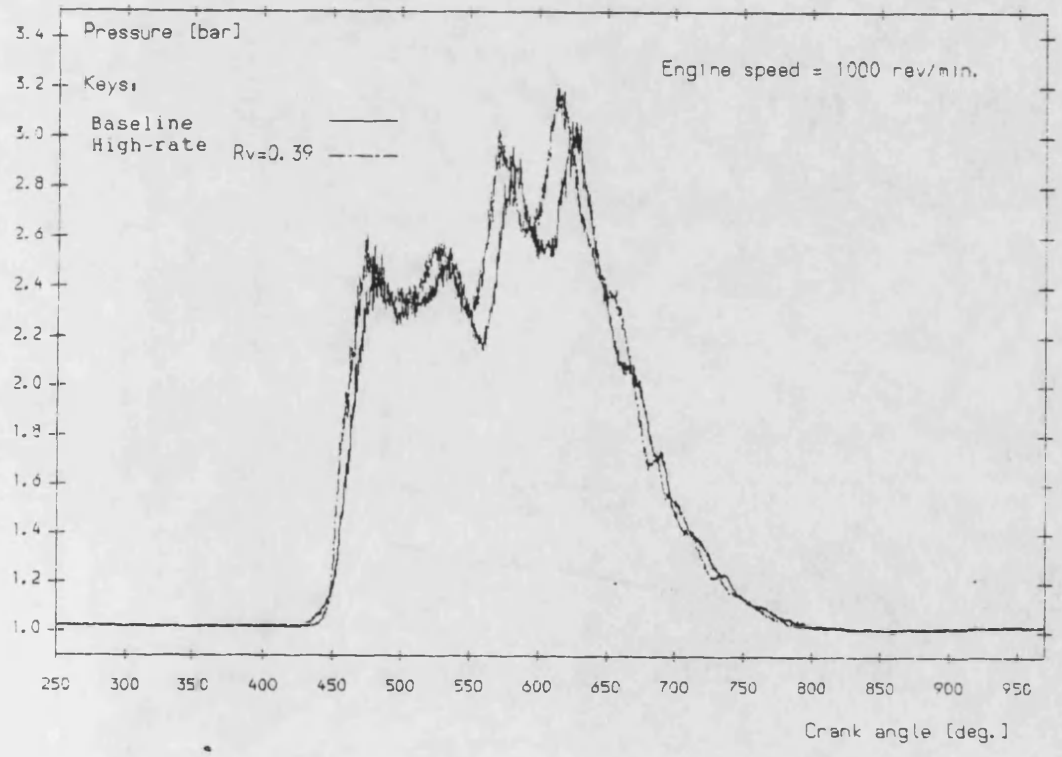

Figure 7.33- Comparison of exhaust pulses at 1000 rev/min.
Cracking pressure = 6 bars.

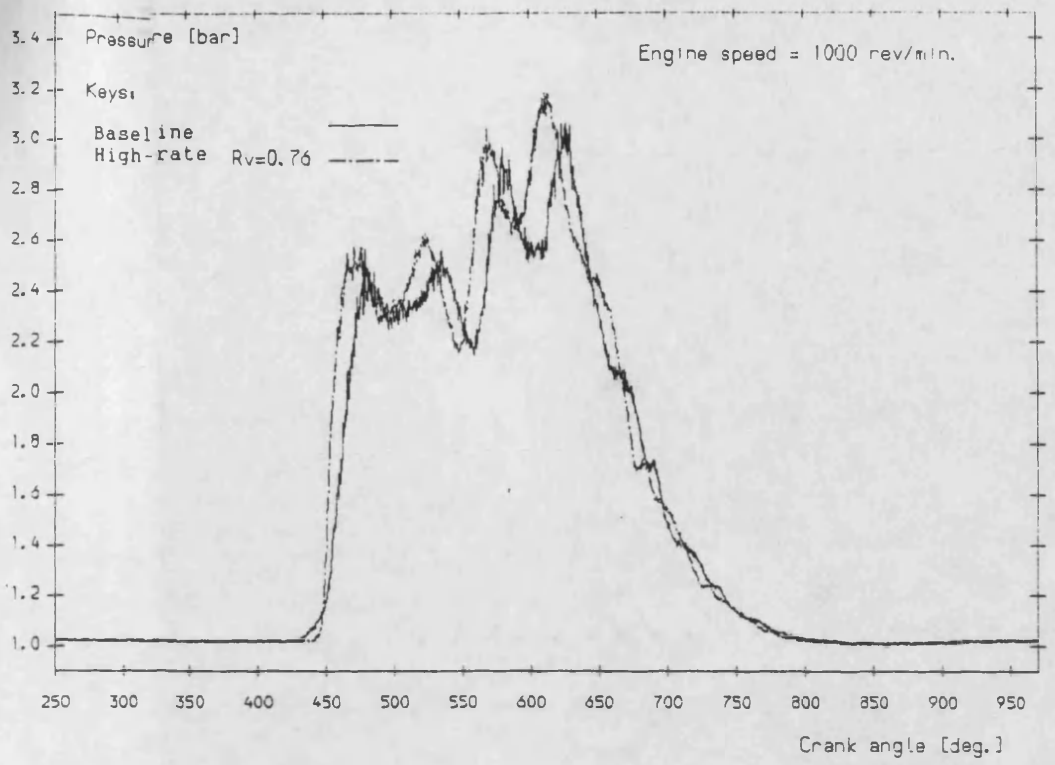

Figure 7.34- Comparison of exhaust pulses at 1000 rev/min.
Cracking pressure = 6 bars.

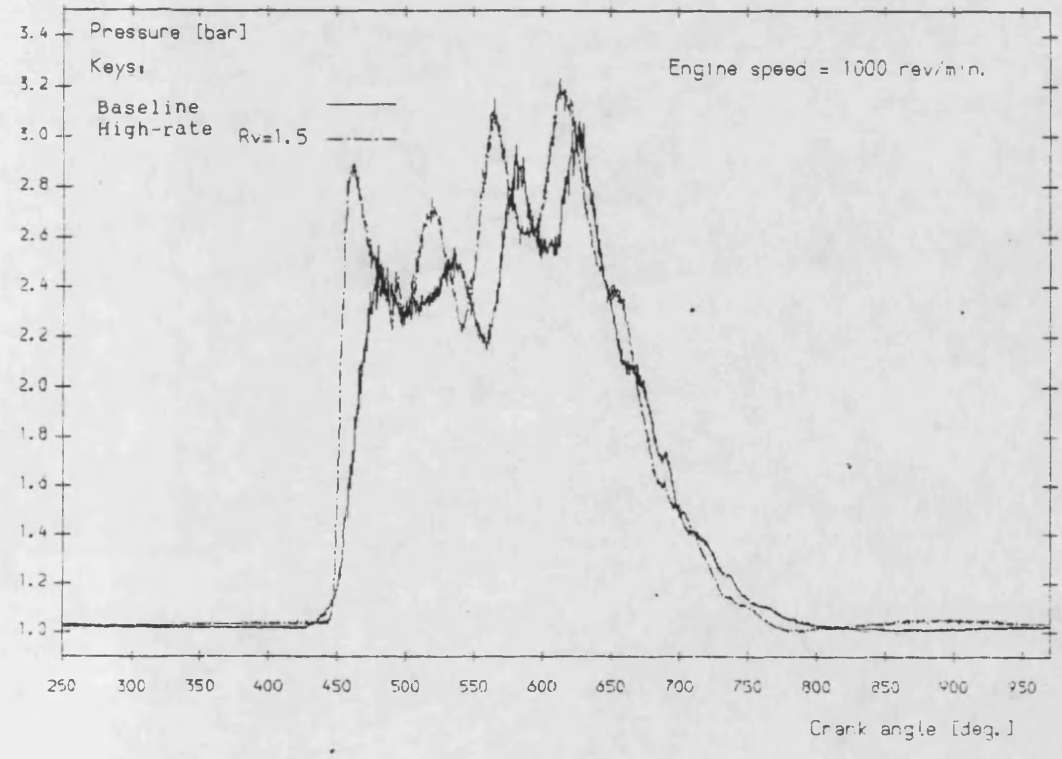

Figure 7.35- Comparison of exhaust pulses at 1000 rev/min.
Cracking pressure = 6 bars.

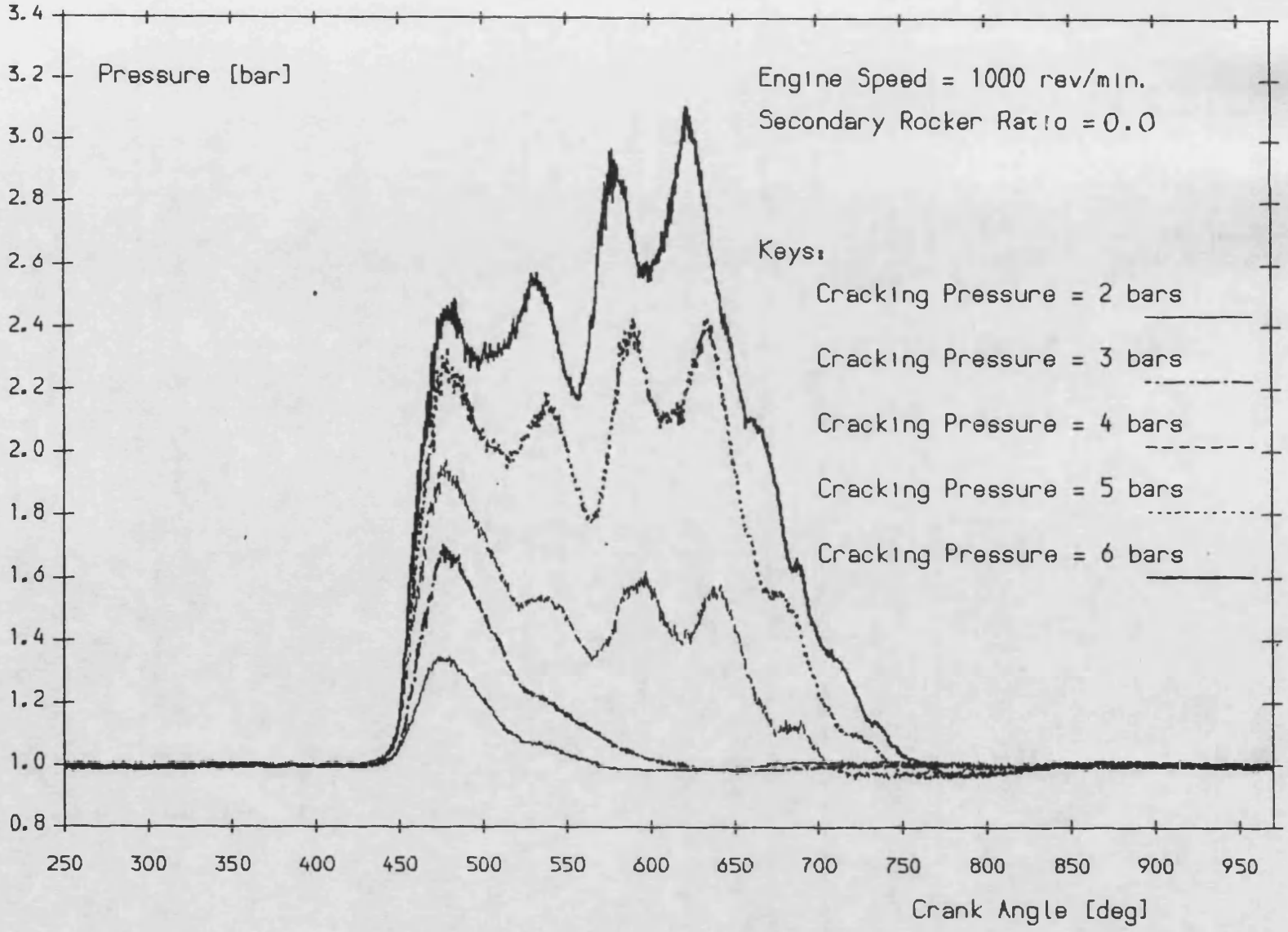
Pressure [bar]
Engine Speed = 1000 rev/min.
Secondary Rocker Ratio = 0.0
Keys:
Cracking Pressure = 2 bars
Cracking Pressure = 3 bars
Cracking Pressure = 4 bars
Cracking Pressure = 5 bars
Cracking Pressure = 6 bars
3.4
3.2
3.0
2.8
2.6
2.4
2.2
2.0
1.8
1.6
1.4
1.2
1.0
0.8
250
300
350
400
450
500
550
600
650
700
750
800
850
900
950
Crank Angle [deg]

Figure 7.35A

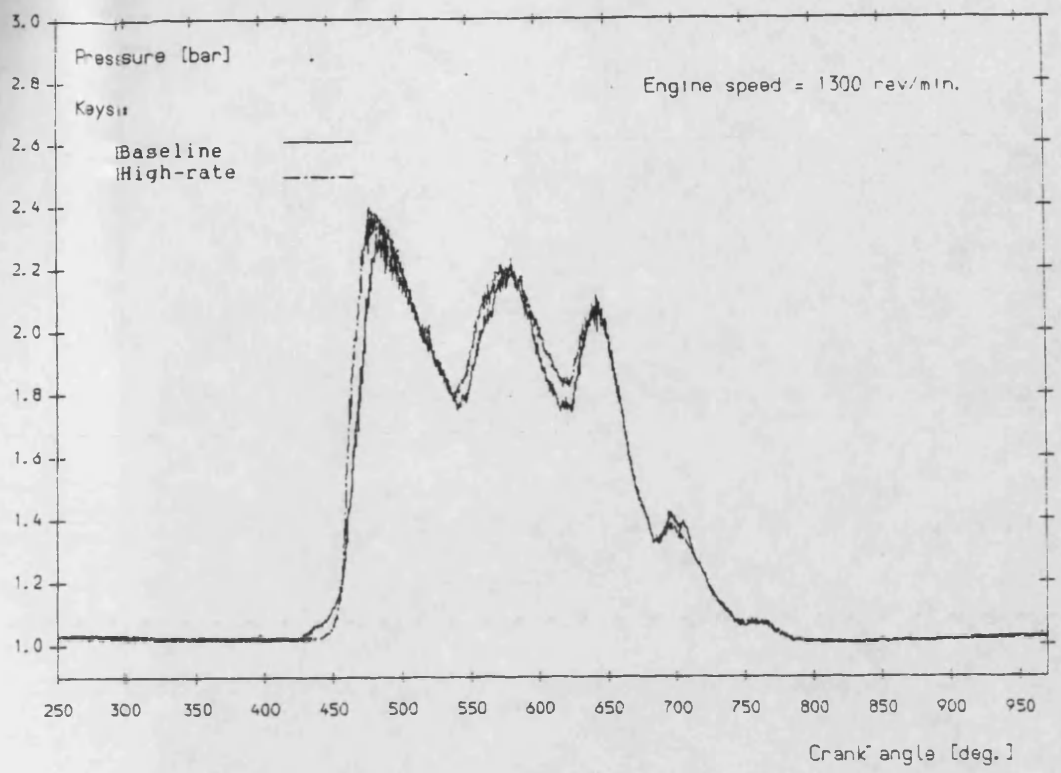

Figure 7.36- Comparison of exhaust pulses at 1300 rev/min.
Cracking pressure = 5 bars.

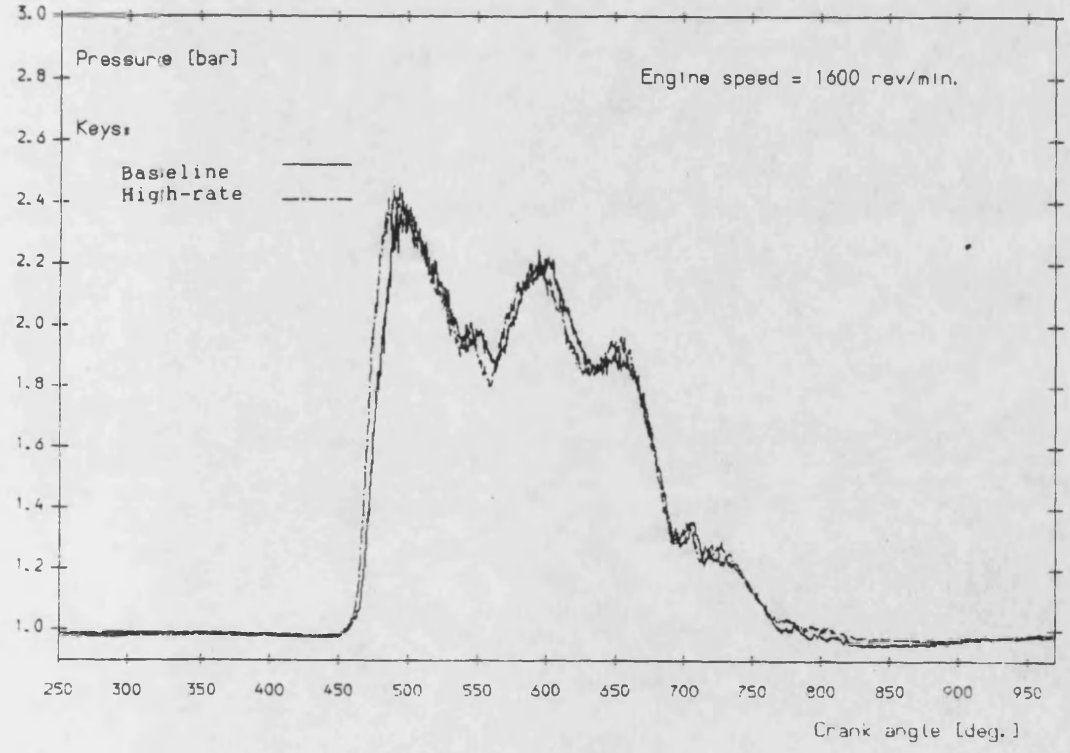

Figure 7.37- Comparison of exhaust pulses at 1600 rev/min.
Cracking pressure = 5 bars.

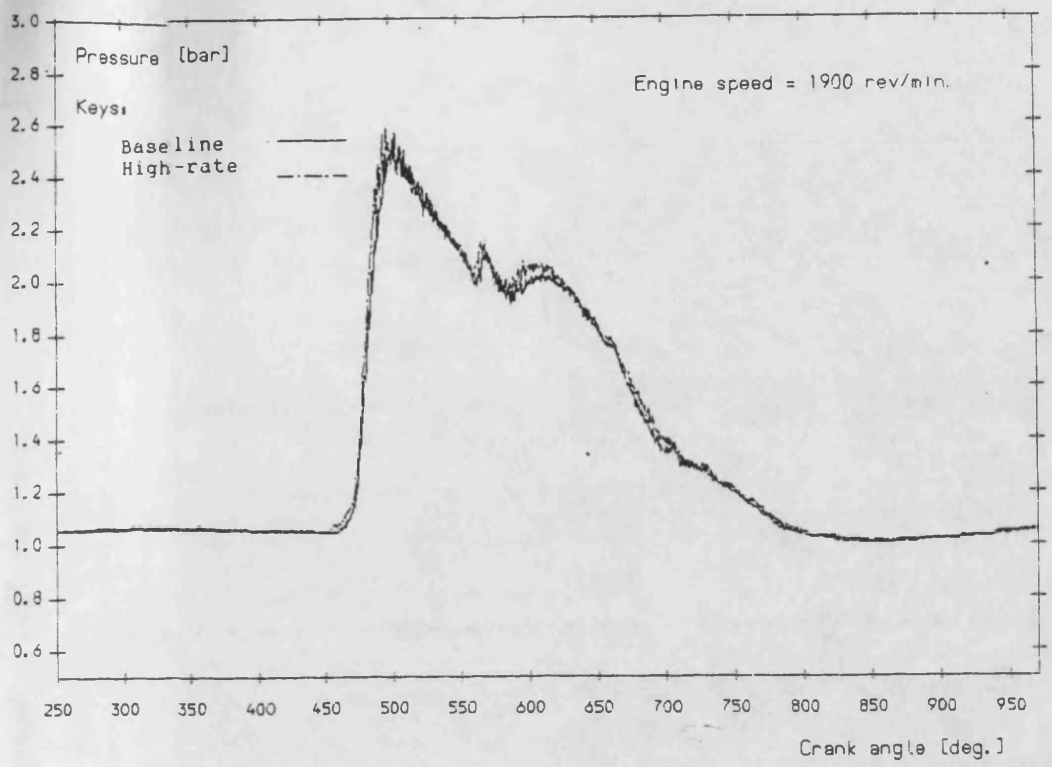

Figure 7.38- Comparison of exhaust pulses at 1900 rev/min.
Cracking pressure = 5 bars.

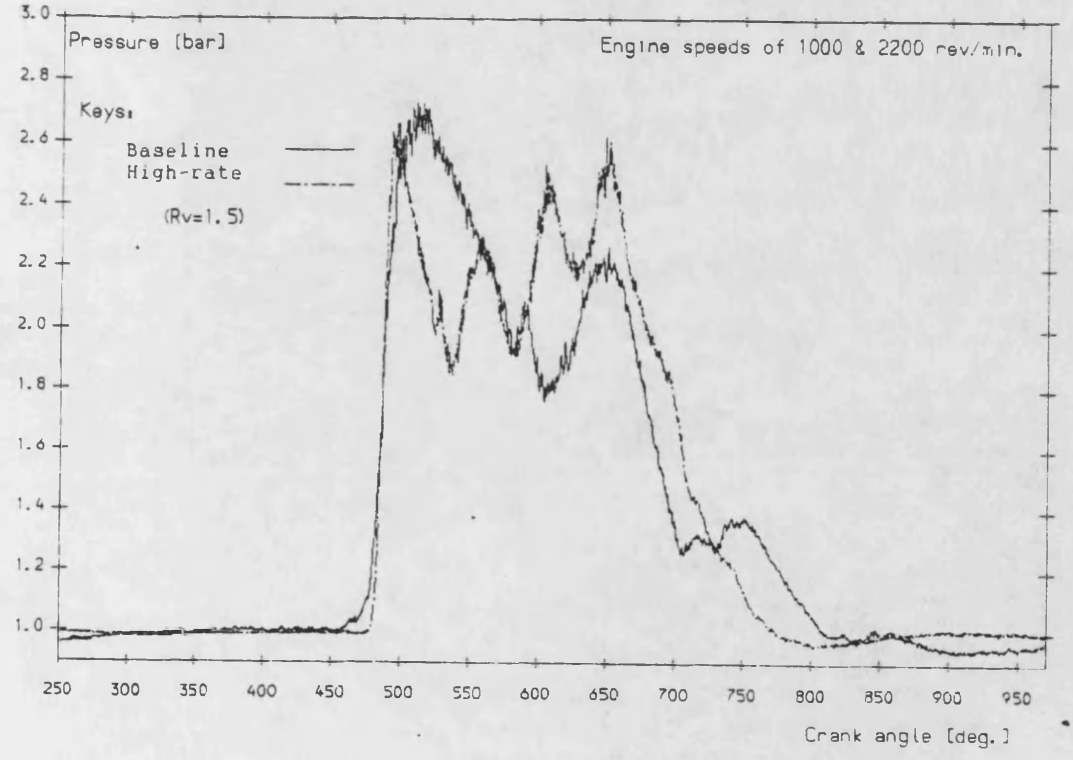

Figure 7.39- Comparison of exhaust pulses at 1000 (highest rate)
and 2200 rev/min. Cracking pressure = 5 bars.

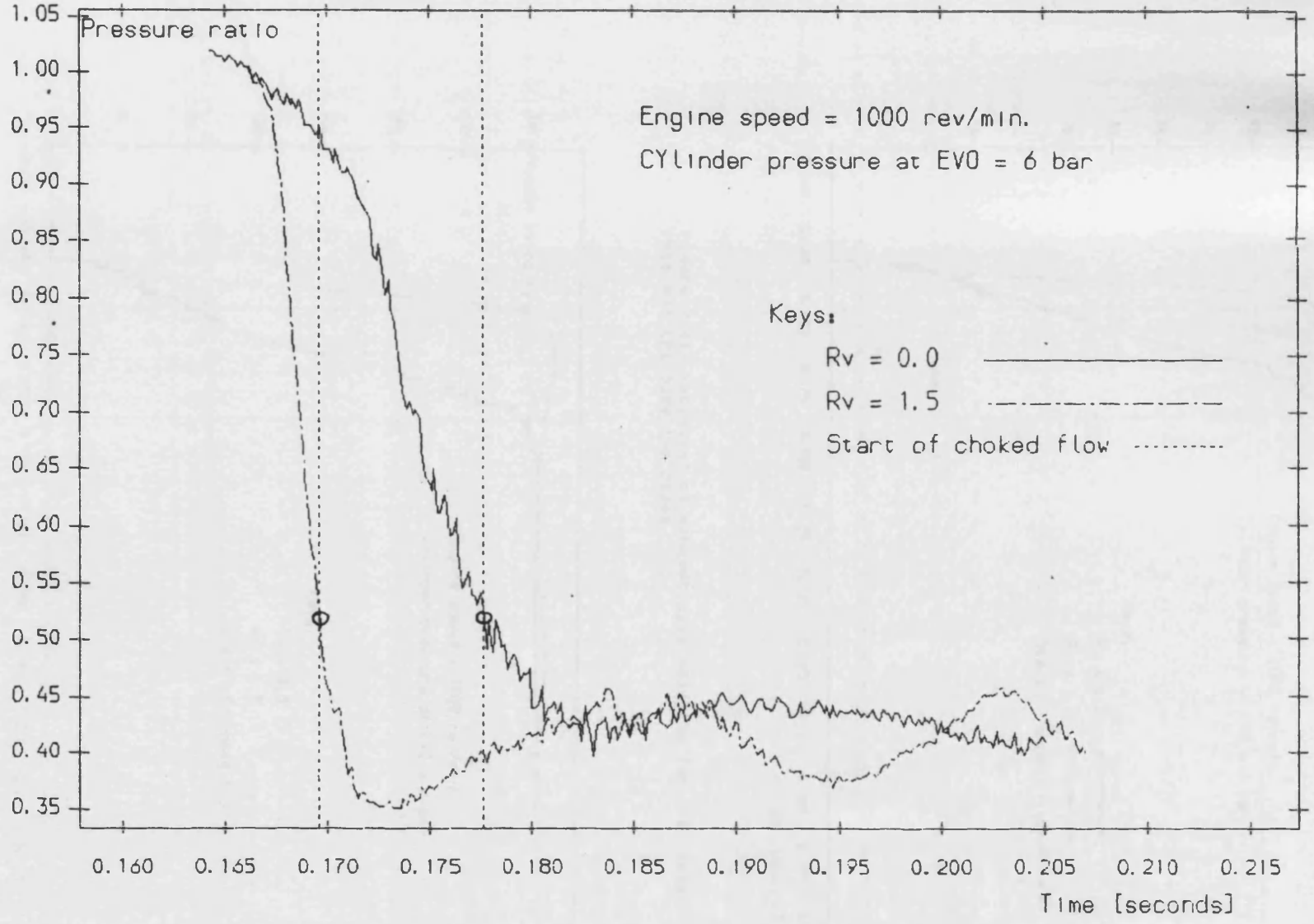

Figure 7.40- Variation of pressure ratio across the 'turbine' nozzle for the highest rate and the baseline cases.

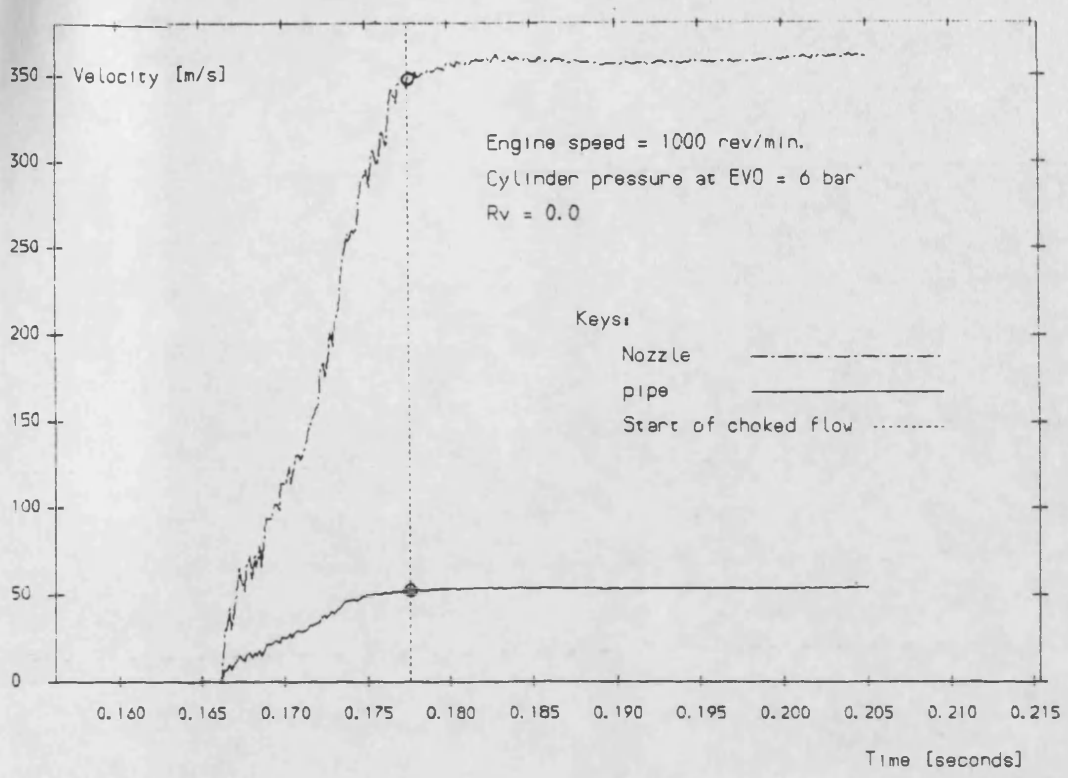

Figure 7.43- Comparison between the pipe and nozzle velocities for the baseline case.

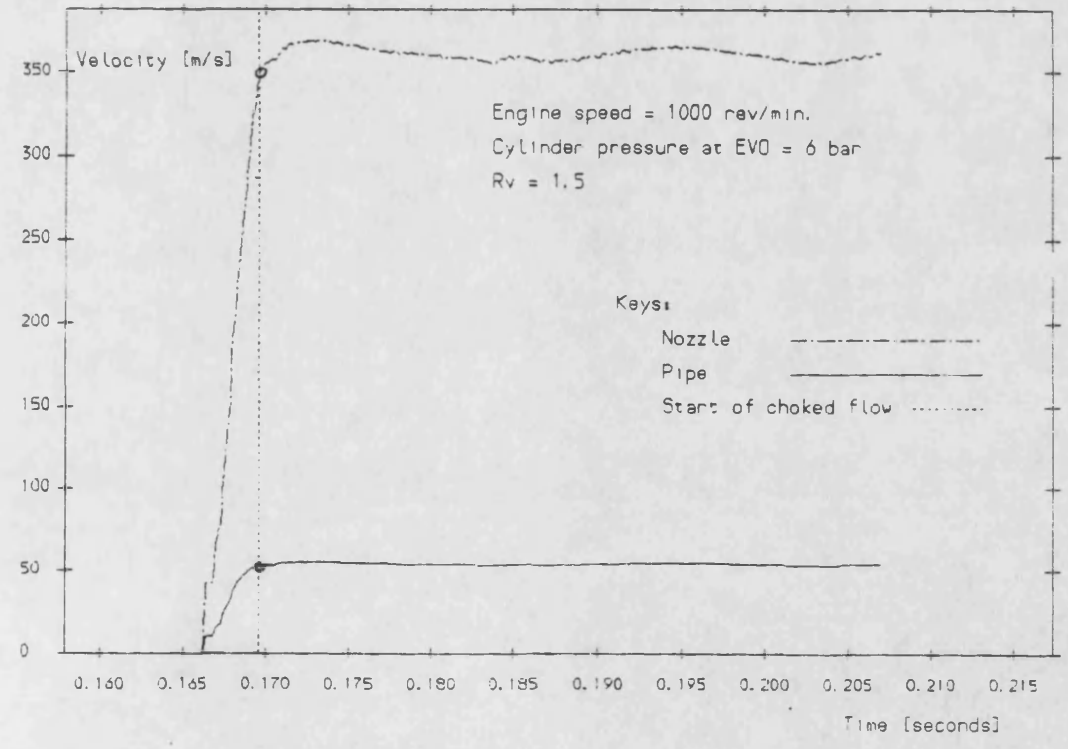

Figure 7.44- Comparison between the pipe and nozzle velocities for the highest rate case.

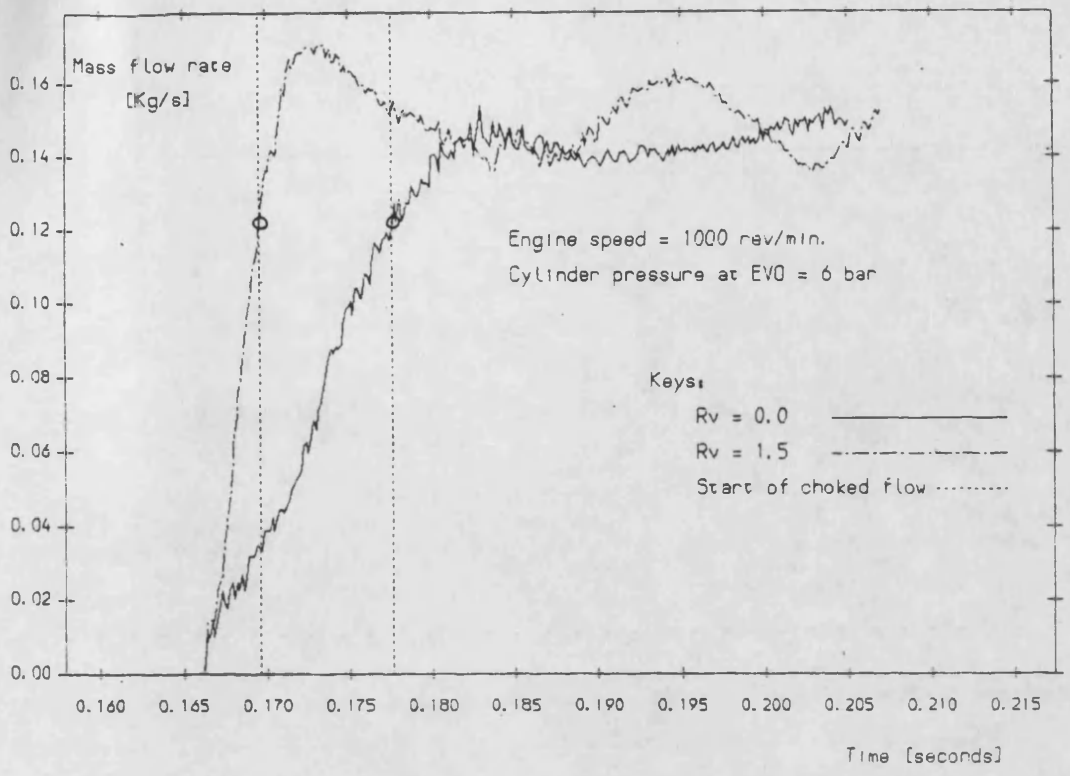

Figure 7.45- Variation of exhaust mass flow rate through the nozzle for the highest rate and the baseline cases.

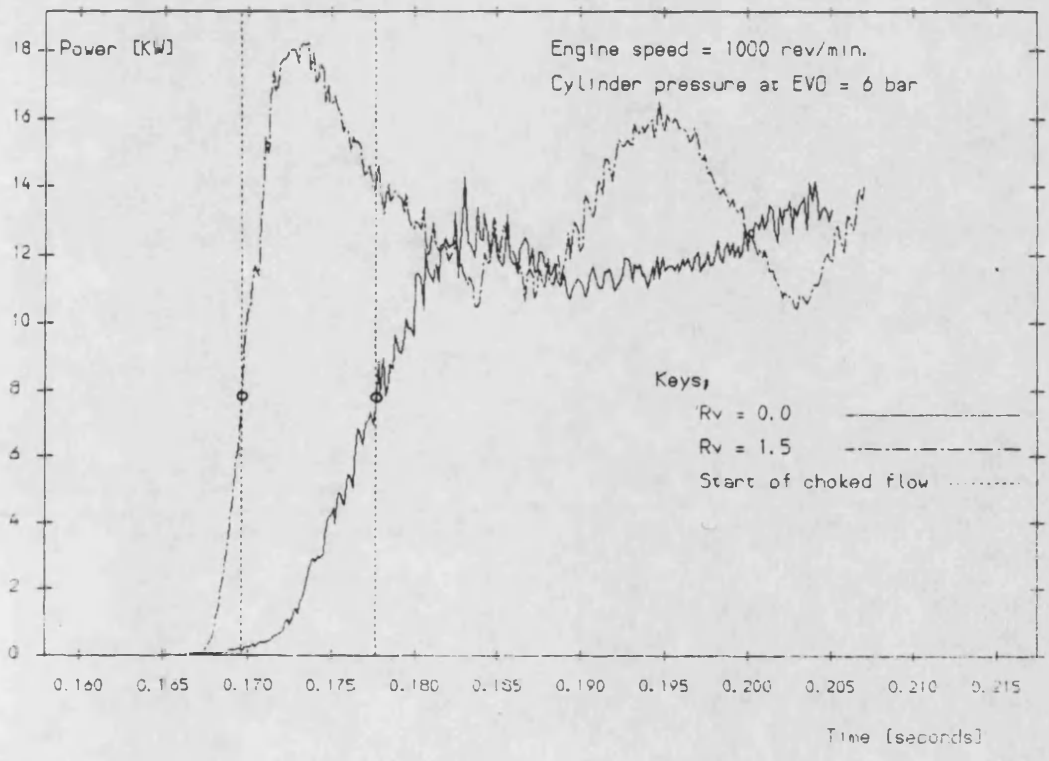

Figure 7.46- Variation of exhaust pulse power content for the highest rate and the baseline cases.

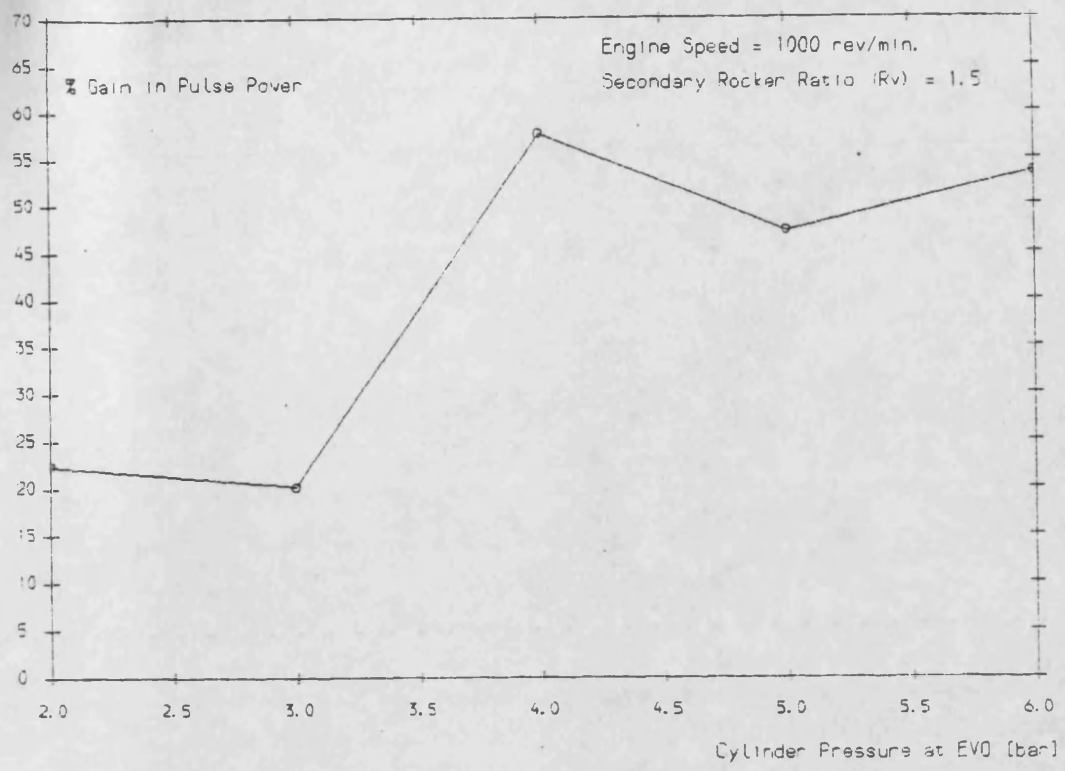

Figure 7.47- Gain in exhaust pulse power versus cracking pressure at 1000 rev/min for the highest rate case.

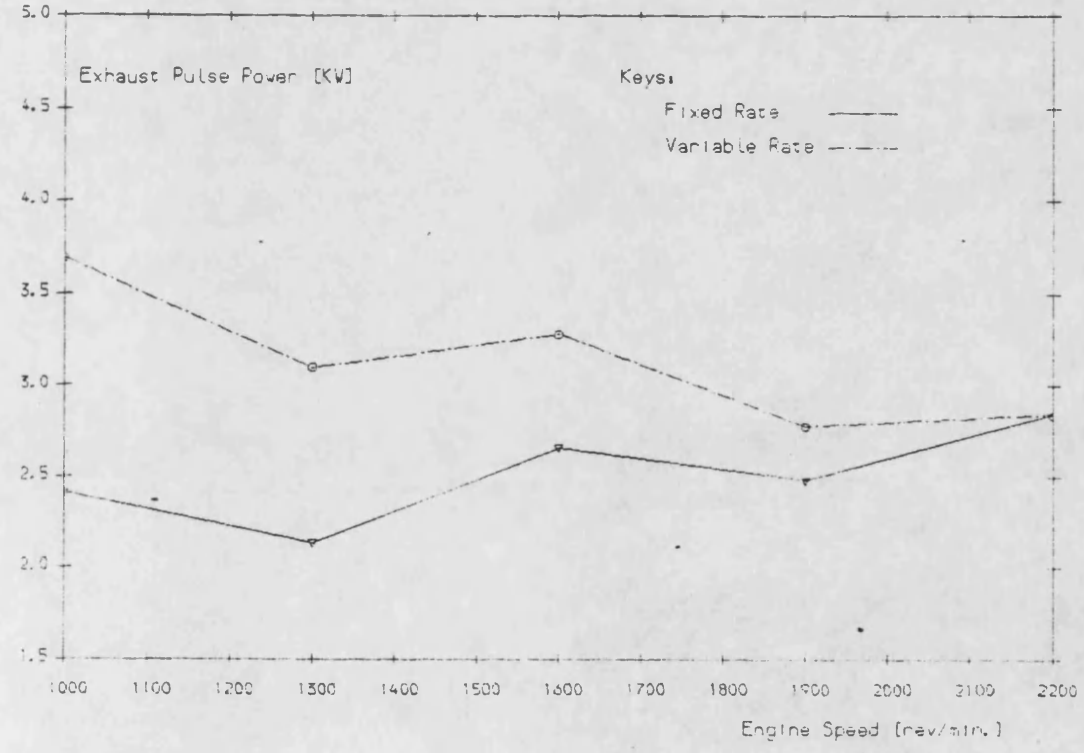

Figure 7.48- Improvement in exhaust pulse power due to a higher rate of exhaust valve opening over the operating speed range.

CHAPTER 8

Discussion And Conclusions

8.0 Introduction

This chapter discusses the project as a whole, in particular the experimental stage of the research programme. Comparisons between the predicted results obtained from both the rigid-body analysis and the non-linear transient dynamic model of the mechanism (using ANSYS) and the experimentally measured results have been made. The exhaust pulses obtained from simulations of the flow rig have been compared with the exhaust pulse measured at the "turbine" nozzle of the experimental rig.

Following the discussion, conclusions for the three stages of the project are given. These stages are:

i) feasibility study,

ii) design phase, and

iii) experimental evaluation.

Finally the scope for future work is outlined and the major areas of concentration for further investigation are suggested.

8.1 Discussion

Investigating the exhaust gas energy transfer from the cylinder to the turbocharger turbine has been one of the main objectives of this research programme. This was to be achieved by increasing the rate at which the exhaust valve of an engine opens where this is possible within the constraints of inertia forces. The rate of exhaust valve opening is required to remain constant over the entire operating speed range of a high-speed turbocharged diesel engine in order to fully exploit the design strength of the valve gear.

A mechanism has been designed which is capable of rendering the rate of exhaust valve opening variable. A full description of the mechanism has been given in chapters 3 and 4. Since the mechanism employs a hydraulic chamber to transmit the forces, the maximum pressure inside the chamber is of some importance to the practicability of the system. When the mechanism was modelled using the finite element program ANSYS, the maximum hydraulic oil pressure, for the worst case of the highest secondary rocker ratio, was found to be 36 bars. This maximum pressure is low enough to ensure good easy sealing with very little compressibility.

8.1.1 Hydraulic Chamber Pressure

Figure 8.1 illustrates the variation of the maximum hydraulic chamber pressure versus the secondary rocker ratio

obtained both experimentally using the flow rig and the rigid-body analysis of the system. The equivalent engine speed used to produce this graph was 1000 rev/min and the effect of exhaust gas forces on the hydraulic chamber pressure was eliminated by making the cracking pressure atmospheric. It can clearly be seen that as the secondary rocker ratio (R_V) increases, the hydraulic chamber maximum pressure increases. In fact over the secondary rocker ratio of 0.0-1.5 the maximum measured chamber pressure increases from 12.7 bars to 16 bars. The rigid-body analysis does not take account of any vibratory response of the valve train. Over the same secondary rocker ratio range, the predicted maximum hydraulic chamber pressure increases from 11.3 bars (R_V = 0.0) to 17.2 bars (R_V = 1.5). However, the rigid-body analysis under-estimates the chamber pressure at the lowest secondary rocker ratio (R_V = 0.0) by 12% and over-estimates at the highest secondary rocker ratio (R_V = 1.5) by 7.5%. Nevertheless, the predicted values are very compatible with experimental values. Figure 8.2 shows a comparison between the non-linear transient dynamic (ANSYS) prediction of the hydraulic chamber pressure and the results obtained experimentally. The conditions for this comparison correspond to an engine speed of 1000 rev/min and secondary rocker ratio of 1.5. As can be seen the predicted maximum chamber pressure is at all times greater than the measured values. The predicted maximum hydraulic chamber pressure of 36 bars is 2.25 times greater than the maximum pressure

neasured experimentally. In ANSYS model of the high-rate system, a spring element was used to represent the hydraulic oil. Thus, from figure 8.2, it appears that the selected spring stiffness in the model has not been sufficiently low to represent the true effect of the hydraulic oil. Using a much weaker spring element in the model should significantly improve the accuracy of the prediction.

Figure 8.3 summarises the peak hydraulic chamber pressure for the two cases of the baseline and the high-rate over the engine speed of 1000-2200 rev/min. The corresponding cracking pressure for this figure is 5 bars. For the baseline case (R_V = 0.0), as the engine speed increases the peak hydraulic chamber pressure increases, as would be expected. For the high-rate case (R_V > 0.0), the idea is to maintain constant exhaust valve opening acceleration over the entire engine speed range. The peak chamber pressure for the high-rate case remains fairly constant with only a small variation between just under 25 bars to 25.5 bars. The reason for this small variation could be due to the presence of air bubbles in the hydraulic chamber. A further investigation (73) in to the situation has revealed that indeed some 3% of the total hydraulic oil volume may be filled by air. A complete purge of air out of the hydraulic chamber may require additional bleeding outlets. When the cracking pressure is set at 5 bars the measured peak chamber

pressure of 25.5 bars is 30% lower than the maximum predicted chamber pressure.

The violent effect of camshaft flexing on the hydraulic chamber pressure, observed in chapter 7, would not be expected when installed in an engine. The journal bearings of a conventional camshaft are positioned close enough together in a way that flexing of the camshaft will usually be quite small.

The power consumption of the mechanism is likely to be very low. Since the hydraulic oil is effectively only being compressed, in order to transmit the forces, with only a small amount of flow, the fluid friction losses are likely to be small compared with the potential gains in engine performance. The linkage and two extra plungers will also absorb some power. During tests on the experimental rig the temperature rise of the trapped oil was approximately 10oC in 10-15 minutes, with very little make-up flow.

8.1.2 Exhaust Manifold Pressure Pulses

Figure 8.4 illustrates the three exhaust pulses obtained using the experimental flow rig and the rig simulations using the method of characteristics and 'filling and emptying' technique adopted in SPICE. The general conditions for all these three cases are as follows: engine speed of 1000 rev/min, cracking pressure of 4 bars and the

highest secondary rocker ratio of 1.5. The exhaust 'pipe' does not have length in the SPICE model, and therefore a constant volume was used to represent the exhaust pipe. Thus, the exhaust pressure pulse appears to be predicted at the exhaust valve in the 'filling and emptying' model of the rig, whereas in the other two cases the pulse is referred to the "turbine" nozzle end of the pipe. It can be seen that the start of the pulse formation at the nozzle is 23 degress of crank angle after the exhaust valve opens. The exhaust pulse predicted by the model of the rig within SPICE has a very continuous rise and decay profile and it peaks at approximately 1.94 bars. The predicted exhaust pulse at the 'turbine' nozzle using the method of characteristics has a more rapid rise to a pressure of 2.18 bars before the start of the decay phase towards atmospheric conditions. Unlike the method of characteristics, the 'filling and emptying' technique is incapable of taking account of the spatial variation. Evidence of wave reflection is only apparent in the exhaust pulse profile predicted by the method of charateristics. The measured exhaust pulse at the 'turbine' nozzle of the experimental flow rig reveals that approximately for the first 75 degrees of crank angle the pulse profile resembles the pulse predicted by the method of characteristics. The experimentally measured pulse peaks at 2.38 bars. The wave reflections are more evident in the measured pulse and in fact three successive reflections may be observed before atmospheric conditions are reached. The

two predicted exhaust pulses return to atmospheric pressure at the same time, whereas the measured pulse endures for 109 degrees of crank angle longer.

Increasing the cracking pressure has a direct effect on the exhaust pulse peak pressure. Similarly, the higher the rate at which the exhaust valve opens the peakier the pulses become. This is shown in figure 8.5. It may be seen that the gain in pulse peak pressure is greater at higher secondary rocker ratios. Comparison between the baseline case (R_V = 0.0) and the highest rate case (R_V = 1.5), over the cracking pressure range of 2-6 bars, reveals that the peak pulse pressure for the baseline only increases by 11.36% as opposed to 17% for the highest rate case.

8.1.3 Wave Propagation Velocity

The pressure wave propagation velocities for the baseline and the high-rate cases have been determined, using expression 7.2, for the engine speed range of 1000-2200 rev/min with the cracking pressure set at 5 bars. The propagation velocity is directly proportional to sonic velocity and the amplitude of the pulse (pulse peak pressure). It has been shown in figure 8.5 that opening the exhaust valve more rapidly results in a greater exhaust pulse peak pressure. Cosequently the pressure wave propagation velocity for the high-rate case would be expected to be higher than the baseline case. This is shown

to be true in figure 8.6 which compares the calculated propagation velocities between the baseline and the high-rate cases. Nevertheless, it is only at the highest rate (R_V = 1.5) that the wave propagation velocity is significantly higher. An increased pressure wave propagation velocity implies that the pulse arrives at the turbocharger turbine earlier which does not give any particular advantage. Figure 7.33 (chapter 7) shows that the pressure pulse profile has not become more pulsating as a result of increasing the rate of exhaust valve opening. Thus, increased wave propagation velocity will not be seen as a problem and what ultimately matters is the energy available at the turbine which has ,indeed, been increased by approximately 54% as a result of opening the exhaust valve more rapid ly.

8.2 Conclusions

A concept has been described which allows the motion of engine poppet valves to be controlled in various ways by employing a continuously variable poppet valve mechanism. To date, there is no evidence of the existence of any other mechanism to vary the rate of poppet valve opening independently of the maximum lift and valve timing, or closing whilst the engine is running. Therefore, emphasis has been put on the development of a mechanism which makes the rate of exhaust valve opening of a turbocharged

diesel engine continuously variable in order to improve energy transport to the turbine.

During the first phase of this research programme, that is the feasibility study, the following observations were made:

(1) Mathematical models of both conventional and continuously variable valve trains were developed which enabled the study of valve train dynamics including displacement, velocity, acceleration, inertia forces and stresses as functions of time.

(2) A proprietary finite element program, ANSYS, was used to model the valve trains by adopting a non-Linear Transient Dynamic analysis approach. This analysis allowed many features to be accounted for, such as component elasticity which helps to simulate the vibratory response of the systems.

(3) Rigid-body analyses were performed for both systems. The results obtained from the rigid-body analyses were in close agreement with those of the dynamic models. The peak values of the dynamic models had approximately a 2:1 ratio over the rigid-body results due to the dynamic effects of the systems.

(4) The analyses of the system proved the concept to be feasible theoretically.

From the design phase of the study the following conclusions may be drawn:

(5) Linkage geometry analyses were necessary in order to obtain the secondary cam profile which generates the required motion of the central plunger.

(6) The possibility of using a flat follower for the secondary cam was examined. As the surface of the corresponding secondary cam happened to contain concave segments, because of its high lift within its short duration, the use of a flat follower was ruled-out. Consequently, a roller follower was found to be necessary to transfer the motion of the secondary cam to the rest of the mechanism.

(7) A parametric study was carried out in order to finalise the design of the key components and to arrive at the proportions of the mechanism.

The theoretical study was followed by experimental evaluation in the third and final phase of the project. The following conclusions have been drawn:

(8) The exhaust valve exhibited dynamic oscillation at the highest secondary rocker ratio. The dynamic instability of the system was thought to be due to lack of valve spring reserve and the presence of air in the hydraulic chamber. The presence of air in the hydraulic chamber, which could be of the order of 3% of total volume, added to the valve oscillation. Using a stiffer valve spring diminished the amplitude of the oscillation and improved the valve lift significantly. Reduction of the hydraulic chamber volume may also augment the valve motion as a direct result of reduction in compressibility. The presence of air is a problem and every step should be taken to completely remove it.

(9) Constant velocity ramps used on conventional camshafts to take up valve train clearances may be removed since when the mechanism is used there is no longer any clearance in the valve train.

(10) The amount of hydraulic oil leakage from the mechanism was found to be quite negligible. The hydraulic chamber could easily be topped up through a non-return valve with supply pressure of approximately 2 bars which is encouraging

for conventional engine applications without the need for an auxiliary oil pump.

(11) The maximum hydraulic chamber pressure was found experimentally to be 25.5 bars and remains almost constant over the entire speed range for the high-rate case. This pressure is over 10 bars less than the maximum predicted pressure using the dynamic model of the system.

(12) Opening the exhaust valve at a higher rate has significantly improved the exhaust gas energy transport from the cylinder to the turbocharger turbine. In fact at an engine speed of 1000 rev/min and the highest secondary rocker ratio of 1.5, the power content of the exhaust pulse has been increased by almost 54% in comparison with the base line case. That is, the pulse energy utilisation due to a higher rate of exhaust valve opening has increased from just over 30% to 70% at an engine speed of 1000 rev/min.

(13) The significant increase of the exhaust gas energy utilisation on a real engine enables the turbocharger turbine to develop more power which in turn allows the turbocharger compressor to do more useful work to produce

more boost, especially at low engine speed, thus increasing the low speed torque back-up. Opening the exhaust valve more rapidly to its full lift during the early part of the valve opening period, permits the exhaust gases to be released to the exhaust more rapidly quicker resulting in a reduction of the piston pumping work. Increasing the unsteadiness of the flow through the turbocharger turbine may reduce its efficiency.

8.3 Scope For Future Work

The undesirable presence of dynamic effects in the form of oscillation of the valve and the hydraulic pressure will have to be eliminated. Further development of the mechanism will investigate the benefits of reducing the volume of the hydraulic fluid, reducing the mass of the three plungers, increasing the valve spring reserve and finding effective ways of removing air from the hydraulic chamber. This is expected to improve the dynamic behaviour and smooth out the motion of the valve.

It may be possible to replace the secondary cam and the variable rocker by an electromechanical actuator such as a solenoid or magnetostrictive device. Such a system, in which the greater part of the valve motion is provided by an engine driven cam with only the modulation provided

electrically, could be extremely attractive for production engines. A useful range of variation could be provided by an electromechanical actuator either acting directly, or through a linkage to magnify the motion. In the system described here the stroke of the modulating plunger was only 4.5 mm and could readily have been reduced by increasing the plunger area. It is hoped that the successful implementaion of such a system will allow a wide range of valve motions controlled from software in response to engine operating condition.

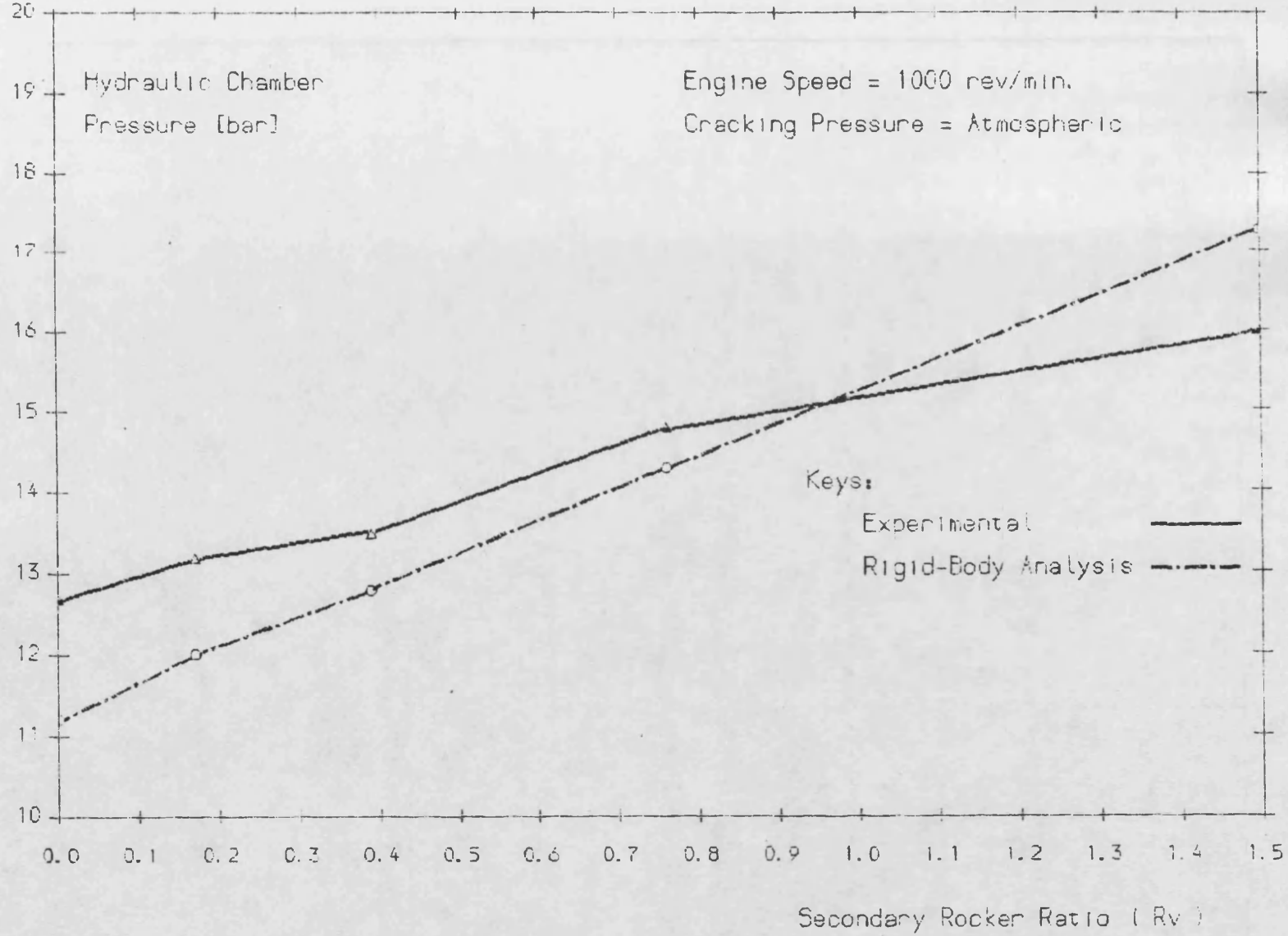

Figure 8.1- Variation of hydraulic chamber pressure versus the secondary rocker ratio for the experimental and rigid-body analysis results.

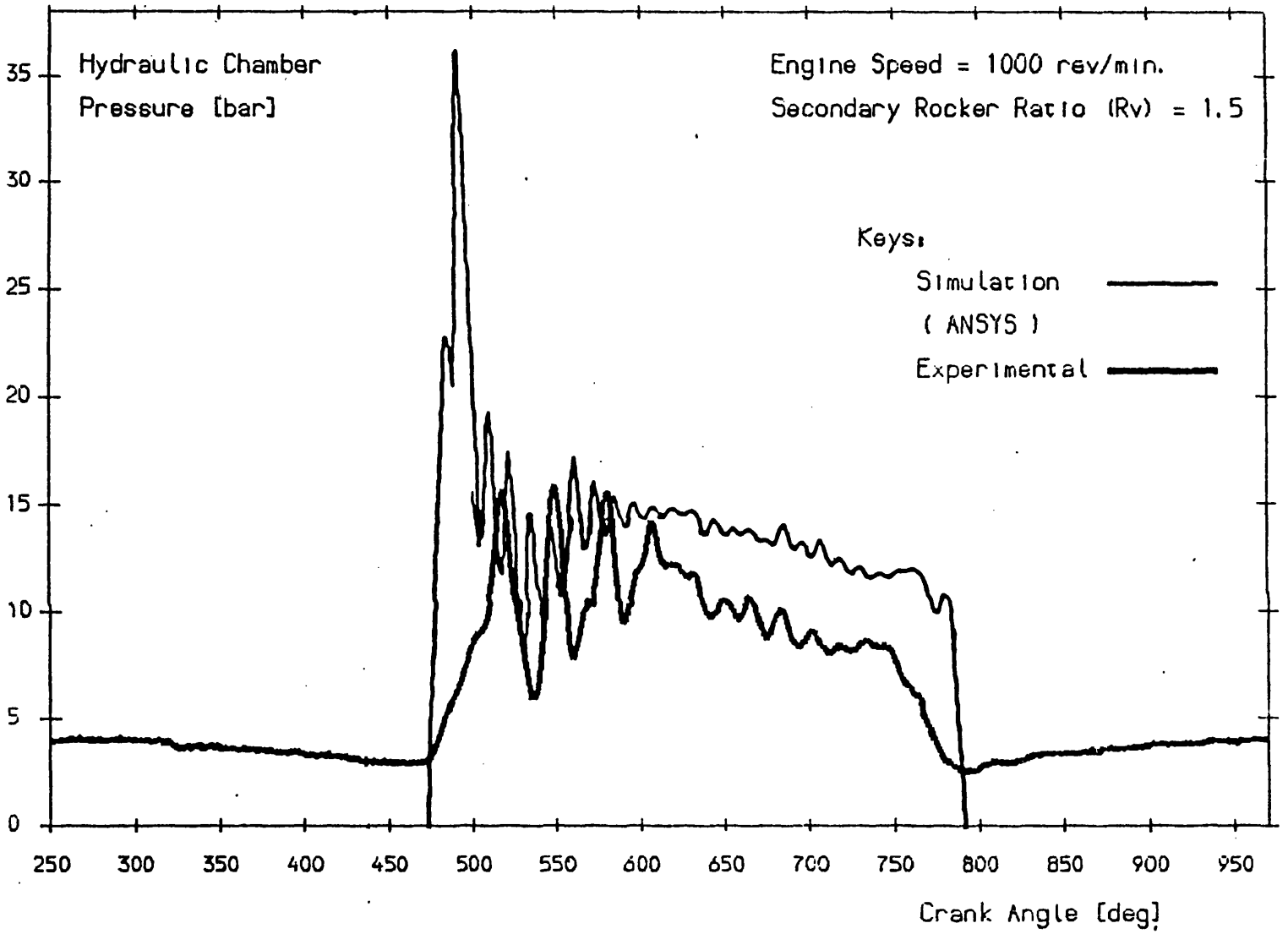

Figure 8.2- Comparison of the hydraulic chamber pressure results between the results obtained using 'ANSYS' and the experimental flow rig.

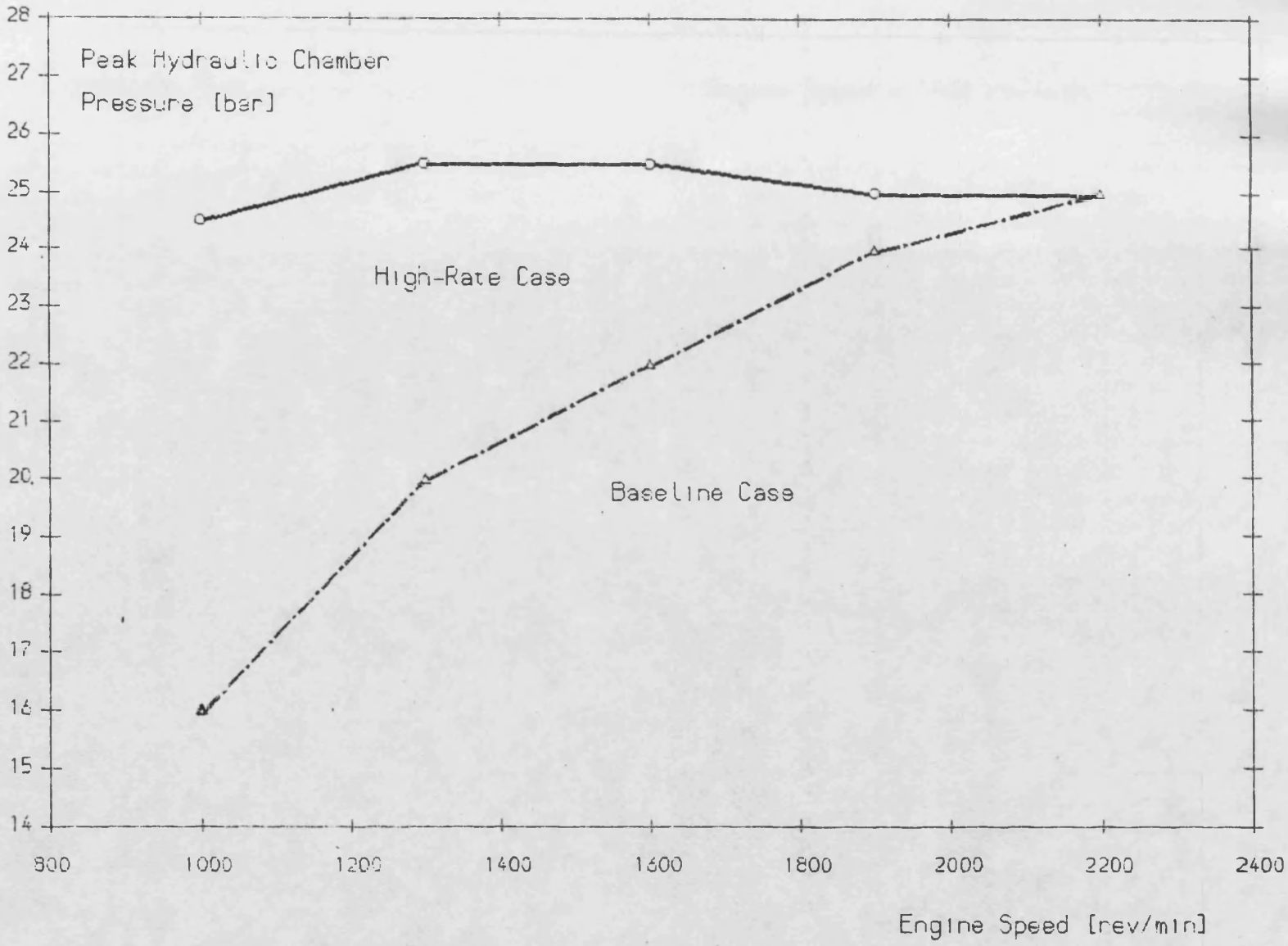

Figure 8.3- Peak hydraulic chamber pressure versus engine speed for the high-rate and the baseline cases.

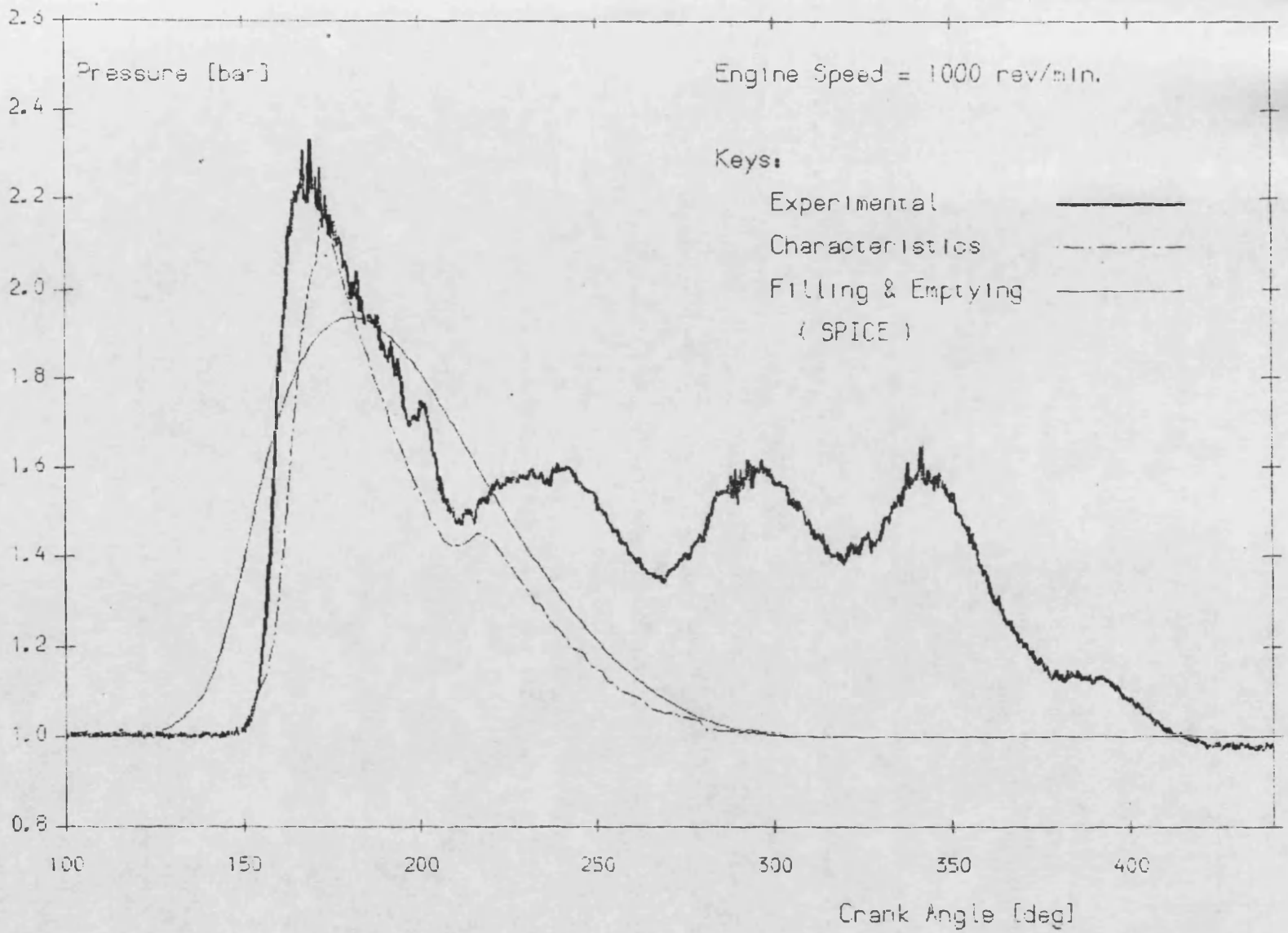

Figure 8.4- Comparison between the experimental and the rig simulation exhaust pulses.

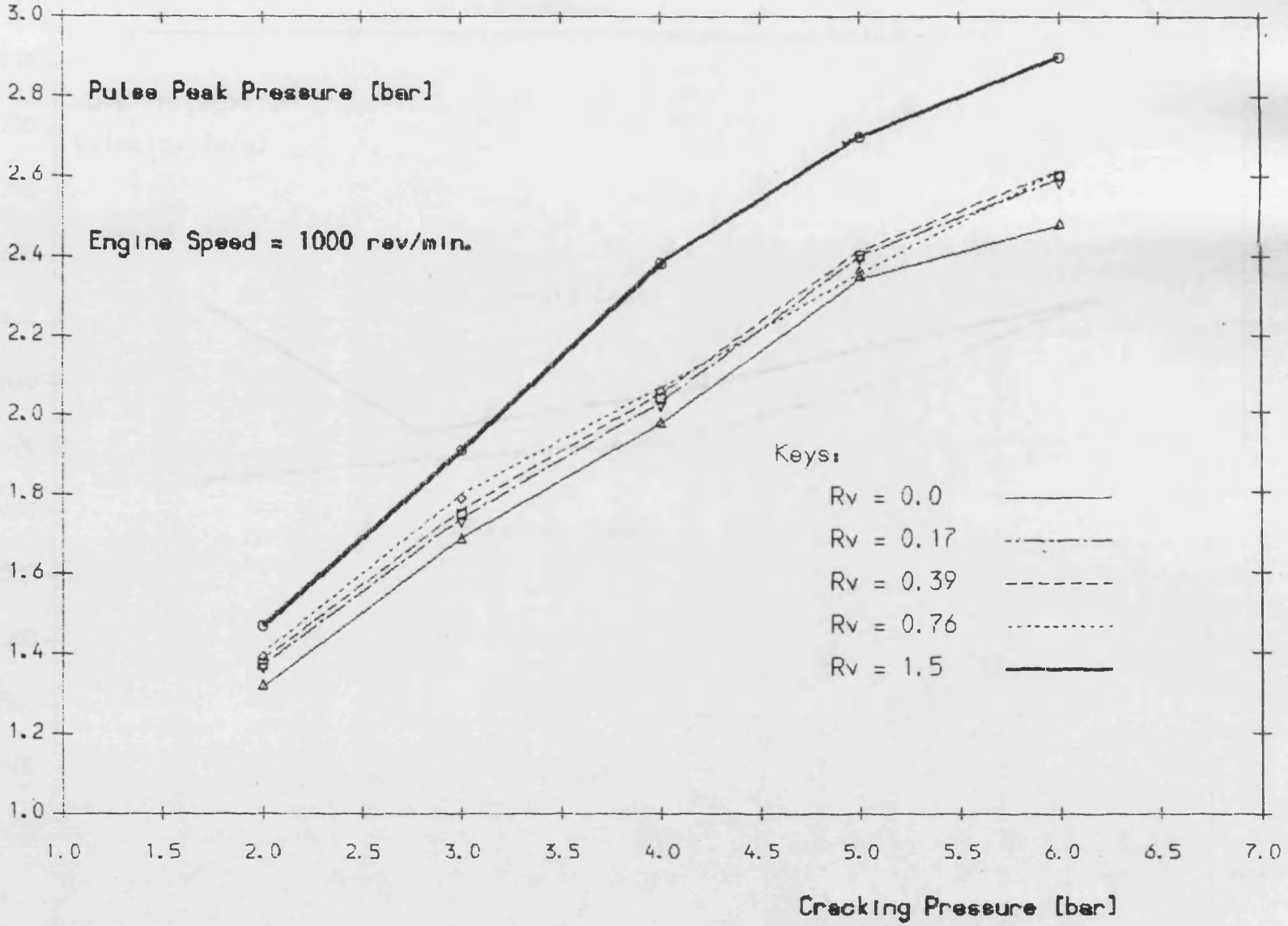

Figure 8.5- Variation of pulse peak pressure versus cracking pressure over the entire secondary rocker ratio of 0.0-1.5.

REFERENCES

1) BENSON, R.S. and WHITEHOUSE, N.D.
'Internal Combustion Engines',
Vols. 1 & 2, Pergamon Press, Oxford 1979.

2) RICARDO, H.R. and HEMPSON, J.G.G.
'The High Speed Internal Combustion Engines',
(5th ed), Blakie, Oxford 1968.

3) 'Symposium on Diesel Engine Combustion',
Proc. I.Mech.E., London 1970.

4) WATSON, N. and JANOTA, M.S.
'Turbocharging The Internal Combustion Engines',
The Macmillan Press, 1982.

5) WALLACE, F.J.
'The Differential Compound Engine',
SAE, Detroit, Paper 670110, Jan 1967.

6) WALLACE, F.J.
'The Differential Compound Engine',
Proc. I.Mech.E., 187, 48/73, p.548, 1973.

7) CHARLTON, S.J. and SHAFIE-POUR, M.
'A Continuously Variable Poppet Valve Actuator For Internal Combustion Engines',
Proc. I.Mech.E., Vol.200, No A3, July 1986.

8) WATSON, N. and OLDFIELD, S.G.
'The Influence of Exhaust Valve and Port Design on Energy Transfer to The Turbocharger Turbine',
ASME, 84-DGP-7, 1983.

9) JENNY, E.
'Utilization of Exhaust Gas Energy in The Supercharging of The Four-Stroke Diesel Engine',
Brown Boveri Review, 37 (1), 1950.

10) WOODS, W.A. and KHAN, S.R.
'Discharge From a Cylinder Through a Poppet Valve to an Exhaust Pipe',
Proc. I.Mech.E., Vol. 182 Pt. 3H, 1967-68.

11) BENSON, R.S. and WOODS, W.A.
'The Energy Content of Exhaust Pulses in The Exhaust System of a Supercharged Two-Stroke Engine Model',
Int. J. Sci., Vol.2 , pp 231-250, 1961.

12) HORLOCK ,J.H. and BENSON ,R.S.
'The Matching of Two-Stroke Engines and Turbochargers',

CIMAC 1962.

13) HORLOCK ,J.H. and WOODS ,W.A.
'The Thermodynamics of Charging and Discharging Processes',
Proc. I.Mech.E., Vol.180, Pt.3J, 1965-66.

14) PATTERSON, D.J. and VAN WYLEN, G.J.
'A Digital Computer Simulation For Spark Ignited Engine Cycles',
SAE Progress in Technology Series, No.7, 1964.

15) BENSON, R.S. and WHITEHOUSE, N.D.
'Internal Combustion Engines',
Pergamon Press, 1979.

16) OLDFIELD, S.G.
'Mass and Energy Transfer Through a Poppet Exhaust Valve of a Turbocharged Internal Combustion Engine',
Ph.D thesis, University of London, 1982 .

17) MONAGHAN, M.L.
'Boosting for a Purpose',
Paper C55/78, Turbocharging and Turbochargers Conference,
I.Mech.E., London, April 1978.

18) CSER, G.
'Some Results of Combined Charging Applications',

Paper C64/78, Turbocharging and Turbochargers Conference, I.Mech.E., London, April 1978.

19) **FRANKLIN, P.C. and WALSHAM, B.E.**
'Variable Geometry Turbochargers in The Field',
Paper C121/86, Turbocharging and Turbochargers Conference, I.Mech.E., London, May 1986.

20) **OKAZAKI, Y.**
'A Case of Variable Geometry Turbocharger Development',
Paper C111/86, Turbocharging and Turbochargers Conference, I.Mech.E., London, May 1986.

21) **BERENYI, S.G. and RAFFA, C.J.**
'Variable Area Turbocharger for High Output Diesel Engines',
Turbochargers and Turbocharged engines.
SAE 790064, SP 442, 1979.

22) **WALLACE, F.J., BAGHERY, A. and WAY, R.J.**
'Variable Geometry Turbocharging, The Realistic Way Forward',
SAE 810336, 1981.

23) **WATSON, N.**
'Turbochargers for The 1980's- Current Trends and Future Prospects',
SAE, Paper 790063, 1980.

24) ZAPPA, G. and FRANCA, T.
'A 4-Stroke High Speed Diesel Engine With Two-Stage Supercharging and Variable Compression Ratio',
Session B3 paper D19, 13th CIMAC Congress, Vienna, 1979.

25) TORAZZA, G.
'A Variable Lift and Event Control Device for Piston Engine Valve Operation',
Paper 2/10 pp 59-67, 14th FISITA Congress 1972.

26) PARKER, D.A. and KENDRICK, M.
'A Camshaft With Variable Lift-Rotation Characteristics; Theoretical Properties and Application to The Valve Gear of a Multi-Cylinder Piston Engine',
Paper B-1-11 pp 224-232, 15th FISITA Congress 1974.

27) PAULMIER, C.
'Variable Valve Timing for Poppet Valve of Internal Combustion Engines',
Ingens de L'Auto, p442, June/July 1974.

28) KERR, J.
'Variable Valve Timing to Boost any Engine',
The Engineer, pp28-29, 54:3 July 1980.

29) **STONE, C.R. and KWAN, E.K.M.**
'Variable Valve Timing for I.C. Engines',
Automotive Engineers, pp.54-58, Aug/Sep. 1985.

30) **BELL and HOWARD**
'Variable Valve Motion Devices',
Bath University, Final Year Design Report, 1985-86.

31) **TITOLO, A.**
'Variable Valve Control From Fiat',
MTZ, pp185-188, Journal 1986.

32) **SCHIELE, C.A. and et al.**
'Design and Development of a Variable Valve Timing (VVT) Camshaft',
SAE, 740102, March 1974.

33) **SASTRY, B.S.**
'Note on Modern Trends in Heavy Vehicle Electrical/ Electronic Systems',
Def. Sci. J., Vol. 32, No 2, pp 105-111, April 1982.

34) **WAGSTAFF, P.R.**
'Analysis of Valve Gear Dynamics With a Digital Computer'
Paper 14 of Symposium in Manchester, I.Mech.E. pp141-148, April 1968.

35) DUDLEY, W.M.
'New Methods in Valve Cam Design',
SAE, Vol. 2, No.1, Jan. 1948.

36) KISHIRO, A. and et al.
'A Comprehensive Simulation of High Speed Driven Valve Trains',
SAE, 810865, 1981.

37) WINFREY, R.C., ANDERSON, R.V. and GNILKA, C.W.
'Analysis of Elastic Machinery With Clearances',
Journal of Engineering for Industry, pp695-703, Aug 1973.

38) SUBRAMANIAM, A.K.
'Evaluation of Internal Combustion Engines Valve Trains by an Emperically Tuned Simulation Model',
ASME, 78-DGP-9.

39) HARDIMAN, J.L. and SPECKHART, F.H.
'Fourier Cam Design Techniques',
SAE, paper 710544, 1971.

40) STODDART, D.A.
'Polydyne Cam Design',
Machine Design, Vol. 25, p121, Jan. 1953, p146, Feb. 1953, p149, March 1953.

41) PISCHINGER, F. and KREUTER, P.
'Valve Train Calculation Model With Regard to Oil Film Effects',
SAE, paper 850399, 1985.

42) WOODS, W.A. and KHAN, S.R.
'An Experimental Study of Flow Through Poppet Valves',
Proc. I.Mech.E., Vol. 180, Pt 3N, 1965-66.

43) WOODS, W.A. and KHAN, S.R.
'Discharge From a Cylinder Through a Poppet Valve to an Exhaust Pipe',
Proc. I.Mech.E., Vol. 182, Pt 3H, 1967-68.

44) BENSON, R.S., CRAG, R.D., and WOODS, W.A.
'Unsteady Flow in Pipes With Gradual or Sudden Area Changes',
Proc. I.Mech.E., Vol. 178, Pt 3I, 1963-64.

45) LUCK, C.E.
'The Pressure Drop Through Poppet Valves',
ASME, Trans. 1906, 27,232.

46) BENSON, R.S.
'The Thermodynamics and Gas Dynamics of Internal Combustion Engines',
Vol. 1, Clarendon Press, Oxford 1982.

47) JENNY, E.
'Berechnungen und Modellversuche uber Druckenwellen grosser Amplitude in Auspuff-Leitungen',
ETHZ thesis, 1949.

48) BENSON, R.S. and GALLOWAY, K.
'An Experimental and Analytical Investigation of The Gas Exchange Process in a Multi-Cylinder Pressure Charged Two-Stroke Engine',
Proc. I.Mech.E., Vol. 183, I, 1968-69.

49) BENSON, R.S. GRAG, R.D., and WOOLLATT, D.
'A Numerical Solution of Unsteady Flow Problems',
Int. F. Mech. Sci. 6, 117, 1964.

50) CHARLTON, S.J. and PAPPAS, P.
'A Parametric Study Of The Exhaust Valve Requirements of High Output Truck Engines',
SAE Congress, Detroit, 850243, Feb. 1985.

51) SARSTEN, A. and et al.
'Computer Assistance in Valve Design',
Engineering Tech. Conf. ASME, 1974.

52) DYSON, A., NAYLOR, H. and WILSON, A.R.
'The Measurment of Oil Film Thickness in Elastohydrodynamic Contact',
Proc. I.Mech.E., Vol. 180, Pt.3B, 1956-66.

53) ROGGENBUCK, R.A.
'Designing The Cam Profile for Low Vibration at High Speeds',
SAE, Detroit, 1953.

54) LYNESS, J.N. and MOLER, C.B.
'Numerical Differentiation of Analytic Functions',
SIAM J. Numer. Anal., Vol. 4, No.2, pp202-210, 1967.

55) LYNESS, J.N. and SANDE, G.
'Algorithm 413, ENTCAF and ENTCRE: Evaluation of Normalised Taylor Coeffiecients of an Analytic Function',
Comm. ACM, Vol. 14, No. 10, pp669-675, Oct. 1971.

56) KEMP'S ENGINEERING YEAR BOOK
F6/38 - F6/45, 1983.

57) RIEMANN, B.
'Uber die fortpflanzung ebener luftwellen von endlicher schwingungsweife',
Bott, Abh. 8, (Math), 1885.

58) DE HALLER, R.
'The Application of a Graphic Method to Some Dynamic Problems in Gases',
Sulzer Technical Review1, 6, 1945.

59) JENNY, E.
'Unidimensional Transient Flow With Consideration of Friction, Heat Transfer and Change of Section',
Brown Boveri Review, 37, 11, 447, 1950.

60) WALLACE, F.J. and BOXER, G.
'Wave Action in Diffusers for Exhaust Pipe Systems With Special Reference to The Scavenging of Two-Stroke Engines',
Proc. I.Mech.E., Vol. 170, 1956.

61) CHARLTON, S.J.
'Simulation Program for Internal Combustion Engines',
SPICE User Manual, University of Bath, April 1986.

62) GUYAN, R.J.
'Reduction of Stiffness and Mass Matrices',
AIAA, Vol. 3, p380, 1965.

63) STOJEK, D. and STWIOROK, A.
'Valve Timing and Variable Overlap Control',
FISITA, paper 840026, 1984.

64) RICHMAN, R.M. and REYNOLDS, N.C.
'A Computer Controlled Poppet Valve Actuator for Application on Research Engines',
SAE, paper 840340, 1984.

65) BATHE, K.J. and WILSON, E.L.
'Numerical Methods in Finite Element Analysis',
Hemel Hempstead (Prentice-Hall), 1976.

66) HERRIN, R.J. and POZNIAK, D.J.
'A Lost Motion Variable Valve Timing System for Automotive Piston Engines',
SAE, paper 840335, 1984.

67) KANESAKA, H., AKIBA, K. and SAKAI, H.
'A New Method of Cam Design-HYSDYNE-Cam',
SAE, paper 770777, 1977.

68) SMITH, P.H.
'Valve Mechanisms for High Speed Engines',
pp.108-9, Foulis, 1967.

69) PARKER, D.A. and KENDRICK, M.A.
'A Camshaft With Variable Lift-Rotation Characteristics, Theoretical Properties and Application to Valve Gear of a Multi-cylinder Piston Engine',
Paper B-1-11, pp. 224-232, 15th FISITA Congress, 1974.

70) MEACHAM, G.B.K.
'Variable Cam Timing as an Emission Control Tool',
SAE paper 730673, 1973.

71) ROE, G.E.
'Variable Valve Timing Unit Suitable for Internal Combustion Engines',
Proc. I.Mech.E., Vol.186, 23/72, 1972.

72) MOLIAN, S.
'The Design of Cam Mechanism and Linkages',
First published 1968 (text).

73) WHITE, B and WHITEMAN, R.
'Investigation of The Dynamic Performance of a Hydraulic Poppet Valve Control System',
Final Year Design Project, University Of Bath, 1988.

74) LILLY, L.C.R.
'Diesel Engine Reference Book',
Butterworth Publishers, 1984.

75) ZINNER, K.
'Supercharging of Internal Combustion Engines',
Springer-Verlag, Berlin Heidelberg New York 1978.

76) CHARLTON, S.J. and SHAFIE-POUR, M.
'A Hydraulic Valve Control System and its Application to Turbocharged Diesel Engines',
SAE Congress, Detroit, 880603, Feb/March 1988.

Appendix 1

Notation

Chapter 2

a cam angle

a_r event range

C_2, C_p, C_q, C_r, C_s polynomial constants

p, q, r, s polynomial indices

Y_{max} maximum valve lift

Y_v valve lift

Chapter 3

A_1, A_2, A_3 cross-sectional area of plungers

a distance from pushrod to rocker post

F_1 main cam force

F_2 secondary cam force

F_p preload

F_{peq} equivalent preload

F_R spring reserve force

F_s spring force

h distance from central plunger axis to cam centre line

I_r, I_v moments of inertia of rocker and secondary rocker

K, K_{eq} stiffness, equivalent stiffness

M, M_f, M_{eq} mass, follower mass, equivalent mass

P hydraulic chamber pressure

r, R_v rocker ratio, secondary rocker ratio

X displacement

$\dot{X}$ velocity

$\ddot{X}$ acceleration

C, C_p, C_q, C_r polynomial constants

D, D_1 pivot disc and roller follower diameters

D_2 secondary cam instantaneous diameter

E modulus of elasticity

P load per unit length

p, q, r polynomial indicies

X non-dimensional cam angle

σ_c Hertz contact stress

Appendix 2

$[C]$ damping matrix

$\{F\}$ force vector

$[K]$ stiffness matrix

$[m]$ mass matrix

$\{U\}$ nodal displacement vector

$\{\dot{U}\}$ nodal velocity vector

$\{\ddot{U}\}$ nodal acceleration vector

$\Delta t, t$ integration time step, time

Appendix 3

b ratio of minimum to maximum operating speeds

C, C_p, C_q, C_r, C_s polynomial constants

L_1 input plunger motion

L_2 output plunger motion

L_3 central plunger motion

p,q,r,s polynomial indicies

X_1, X_2 non-dimensional cam angles

θ cam angle

$\Delta\theta_1$ main cam event range

$\Delta\theta_2$ output plunger event range

Appendix 4

A vertical distance between pivot disc and central plunger

L length of the upper arm of the secondary rocker

R polar radius of pedal of the cam profile

R_B base circle radius.

Rp pivot disc radius

u,v cartesian co-ordinates of the cam profile

y central plunger displacement

Y secondary cam lift

α polar angle of the cam profile

β refer to configuration

θ cam angle

ϕ polar angle of pedal of the cam profile

Ψ_o initial secondary rocker angle

Ψ_1 maximum secondary rocker angular rotation

ρ polar radius of the cam profile

$1/\sigma$ radius of cam profile curvature

Appendix 5

L entire secondary rocker length

L_1 length of the upper arm of secondary rocker

OS offset

R distance from centre of base circle to centre of roller follower

R_B base circle radius

R_F roller follower radius

Rp pivot disc radius

u,v cartesian co-ordinates of the cam profile

$\Delta x', \Delta x, \Delta y$ refer to figure A.5.1

α polar angle of the cam profile

ρ polar radius of the cam profile

θ cam angle

β, ϕ refer to figure A.5.1

γ pressure angle

Ψ secondary rocker angular rotation

y central plunger displacement

Appendix 6

b	width of rectangular contact area
D	diameter (mm)
E	modulus of elasticity
F_{peq}	equivalent preload
I_v	moments of inertia of secondary rocker
K_{eq}	equivalent stiffness
L	cylinder length (mm)
M_{eq}	equivalent mass of secondary rocker
M_f	follower mass
P	load (force) per unit length of cam width (N/mm)
R_v	secondary rocker ratio
Y_1, Y_2	lifts
$\ddot{Y}_1, \ddot{Y}_2$	accelerations
δc	unit compressive contact stress
γ	poission's ratio

Appendix 7

F_{max}	maximum applied force
I_v	moments of inertia of secondary rocker
K	valve spring stiffness
L	entire length of secondary rocker
M	total system mass
M_{eq}	equivalent mass
M_f	roller follower mass

M_S valve spring mass

R_V secondary rocker ratio

$\ddot{X}_{max}$ maximum acceleration

Δ preload

Appendix 2

Dynamic Simulation

The non-linear transient dynamic analysis within ANSYS is essentially a numerical integration of the general equation of motion for a structural system, which in matrix form is:

$$[m]\{\ddot{U}\} + [C]\{\dot{U}\} + [K]\{U\} = \{F\} \quad \text{___ (1)}$$

Starting from a given initial state of the system (t=0) equation (1) is solved at successive time steps taking account of the opening and closing of gaps, damping and other non-linearities. Displacements are assumed to vary cubically during an iteration. Thus the velocity varies quadratically and acceleration varies linearly during the iteration.

The velocity and acceleration vectors may be re-written in terms of the unknown displacement for the current iteration and the displacements for the previous three iterations:

$$\{\dot{U}_n\} = 1/6\Delta t\,[11\{U_n\} - 18\{U_{n-1}\} + 9\{U_{n-2}\} - 2\{U_{n-3}\}] \quad \text{___ (2)}$$

$$\{\ddot{U}_n\} = 1/\Delta t^2\,[2\{U_n\} - 5\{U_{n-1}\} + 4\{U_{n-2}\} - \{U_{n-3}\}] \quad \text{___ (3)}$$

Equations (2) and (3) are substituted into equation (1). Then the only unknown is the displacement vector $\{U_n\}$ which is calculated at each point in the dynamic transient analysis. This method is known as the Houbolt time integration scheme (65).

Three different starting procedures are available, all of these commence with a static analysis to establish the initial displacements. The three starting assumptions available are:

(a) initial velocity defined by first two iterations,

(b) initial velocity equal to zero,

(c) initial velocity and acceleration equal to zero.

Appendix 3

Derivation Of An Expression For The Output Plunger Motion

In an attempt to develop a secondary cam profile for the mechanism to be capable of varying the rate of exhaust valve opening two lift curves have to be defined. One is the main cam profile, L1, which has been provided by the Ford Motor Company. The main cam profile begins with a constant velocity ramp for the first 24 degrees before it follows a polynomial expression. The profile is symetrical and the polynomial is followed by another constant velocity ramp completes the main cam lift curve.

Another one of the two lift curves is the desired motion of the output plunger, L_2, see figure A.3.1. L_2 is the sum of the main and the secondary cam lifts. The secondary cam profile, L_3, is determined simply by subtracting L_1 from L_2 as shown in figure A.3.2.

In the following attempt is made to deduce these functions resulting in the required lift. The first and last 16 degrees of both L_1 and L_2 are defined separately. From 17 to 24 degrees a constant velocity ramp is used to take up the clearances in the system. This lift during the ramp is given by:

$$L_1,\ L_2 = 0.1702 + 0.02\ .(\theta - 17) \qquad \text{___ (1)}$$

The polynomial expression giving L_1 is of the form stated below:

$$X_1 = \theta/\Delta\theta_1 \ ,$$

$$L_1 = C - C_p.X_1^{p} + C_q.X_1^{q} - C_r.X_1^{r} - C_s.X_1^{s} \qquad \text{___ (2)}$$

where,

θ is the instantaneous cam angle,

$\Delta\theta 1$ is half the duration of the cam event excluding the constant velocity ramps,

C	=	7.874	$0 \leq X1 \leq 1.0$
C_p	=	10.79568	$p = 2$
C_q	=	5.693371	$q = 9$
C_r	=	2.351989	$r = 12$
C_s	=	0.08950479	$s = 30$

and X_1 is defined as the non-dimensional cam angle which is the ratio of cam angle over the event range, $\Delta\theta_1$, which in this case is 63 degrees, being equal to half of the cam motion. Another event range is defined, $\Delta\theta_2$, forthe output plunger motion, L_2. Typical minimum and the maximum diesel engine operating speeds are 1000 rev/min and 2200 rev/min respectively. Therefore, it is intendedto use the mechanism

to open the exhaust valve at an engine speed of 1000 rev/min at the same rate (with respect to time) as when operating at 2200 rev/min. This in turn is the criterion used when defining an event range for cam2. Therefore,

$$1000/2200 = 0.4545 = b$$

$$\Delta\theta_2 = \Delta\theta_1 \cdot b$$

$$X_2 = \theta - \Delta\theta 1\ (1 + b)/\Delta\theta_2$$

It can be seen that from 25 to 53 degrees L_2 is given by:

$$L_2 = C - C_p.X_2^p + C_q.X_2^q - C_r.X_2^r - C_s.X_2^s \quad \text{___ (3)}$$

where C, C_p, C_q, C_r, C_s, p, q, r, and s retain their respective values. L_2 dwells from 53 to 88 degrees. For the next 63 degrees both L_1 and L_2 follow expression (2). A closing constant velocity ramp is also used of the form:

$$L_1,\ L_2 = 0.3302 + 0.02\ .(\theta - 151) \quad \text{___ (4)}$$

Therefore, the motion of the secondary cam as seen by the central (modifying) plunger, L_3, is determined by:

$$L_3 = L_2 - L_1$$

when θ = 1 to 24 , $L_3 = 0.0$,

when θ = 25 to 53 ,

$$L_3 = C_p .(X_1 - X_2)^p + C_q .(X_2 - X_1)^q +$$

$$C_r .(X_1 - X_2)_r + C_s .(X_1 - X_2)^s \quad \text{___ (5)}$$

and when O = 54 to 88,

$$L_3 = C_p .X_1^p - C_q .X_1^q + C_r .X_1^r + C_s .X_1^s \quad \text{___ (6)}$$

The two polynomial expressions (5) and (6) constitute the desired motion of the central plunger. But due to thegeometry of the secondary rocker the actual secondary cam profile would differ from that of the central plunger.

A computer program was accordingly written to generate the motion resulted by expressions (5) and (6). In order to establish corrolations between the secondary rocker geometry, central plunger motion and the actual secondary cam profile, analyses have been performed that are described in Appendices (4) and (5).

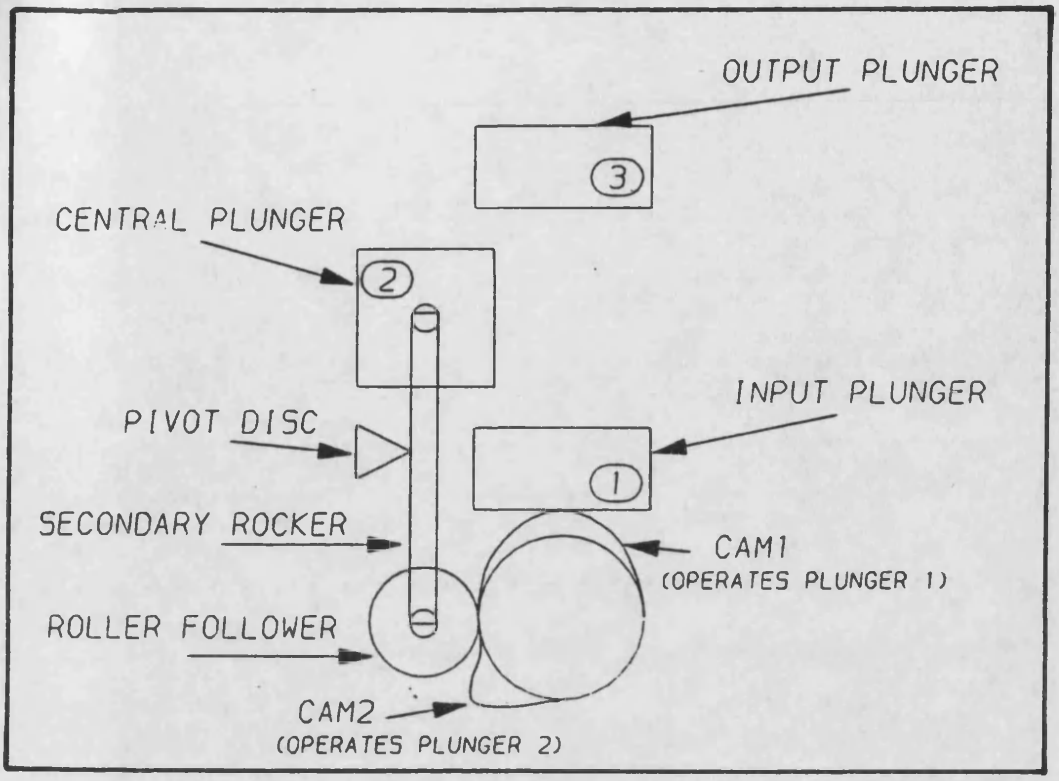

FIGURE A.3.1

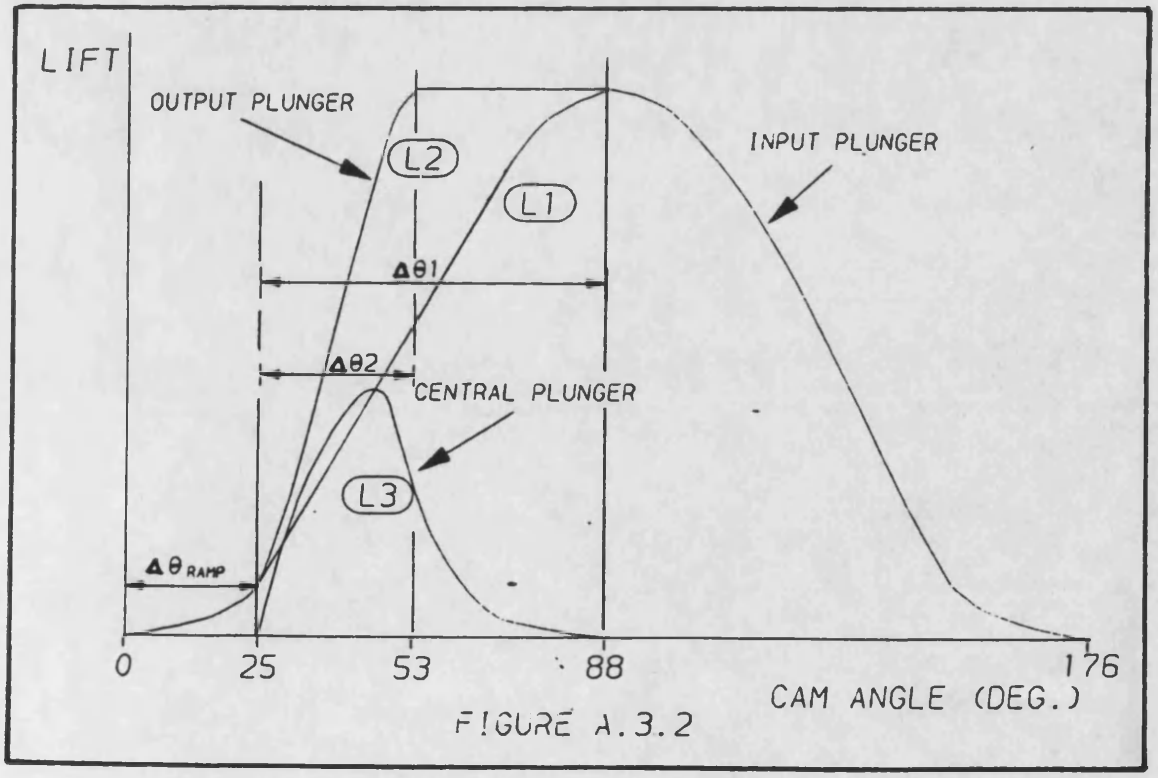

FIGURE A.3.2

Appendix 4

Continuously Variable Linkage Geometry Analysis

Case 1: Flat follower.

The analysis is very easy to follow and mathematically self-descriptive. First the central plunger motion is closely examined as follows,

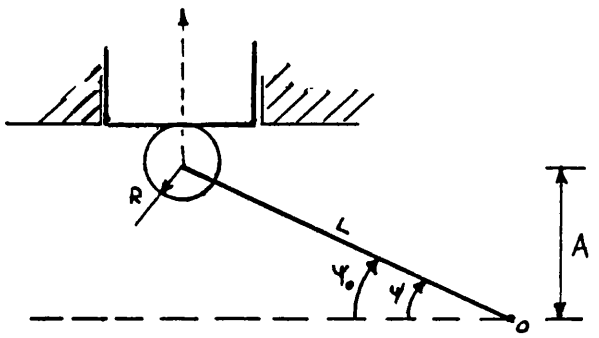

Initial condition:

$$\psi = \psi_0 \quad , \; y = yo = 0.0$$

where y is the central plunger displacement,

and O is the secondary rocker angular displacement,

$$\text{Sin}\,\psi o = A / L$$

$$A = L \cdot \text{Sin}\,\psi o \quad \text{or}$$

$$\psi o = \text{Sin}^{-1}(A / L) \qquad \text{(1)}$$

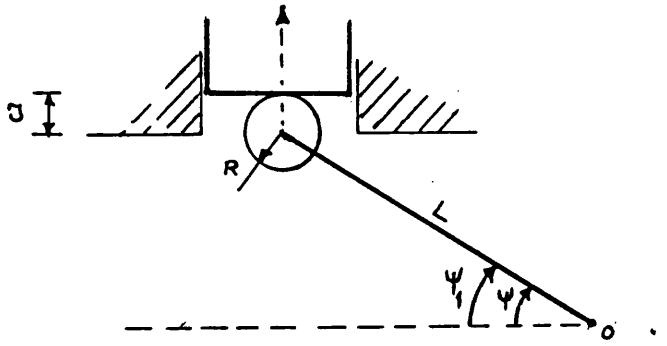

Maximum lift condition:

$$\psi = \psi_1 \quad , \; y = ymax$$

. Y is the secondary cam lift,

$$Y = L \cdot \sin\psi_1 + R$$

$$y = L \cdot \sin\psi_1 + R - L \cdot \sin\psi o - R$$

i.e. $\sin\psi_1 = y / L + \sin\psi o$

substitution for o in expression (1) gives;

$$\psi_1 = \sin^{-1}[\ (A + y) / L\ ]$$

in general for any ψ we shall have;

$$\psi = \psi_1 - \psi_0$$

or

$$\psi = \sin^{-1}[(A + y) / L] - \sin^{-1}(A / L) \quad \text{___} \quad (2)$$

Now we analyse the secondary cam side motion.

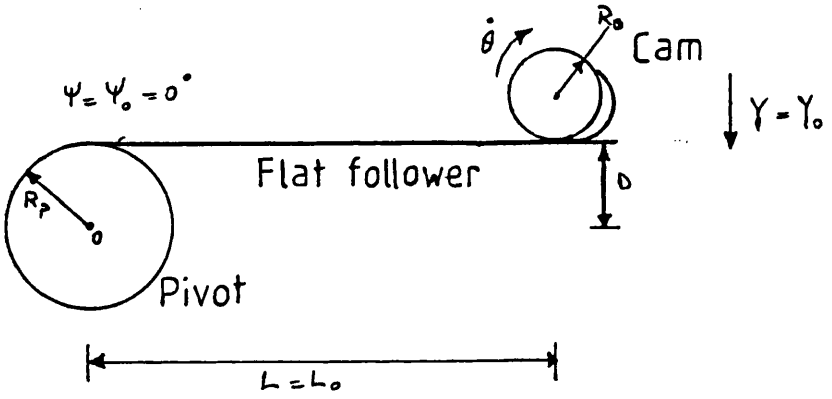

The above configuration corresponds to the initial condition, that is when the flat follower is in contact with the camshaft base circle. The angular rotation is the same as when we analyse the secondary cam side motion. The angular rotation ψ is the same as the angular rotation ψ which was previously derived using expression (2).

The maximum lift condition occurs when the lift profile reaches its maximum,

i.e. $Y = Y_{max}$

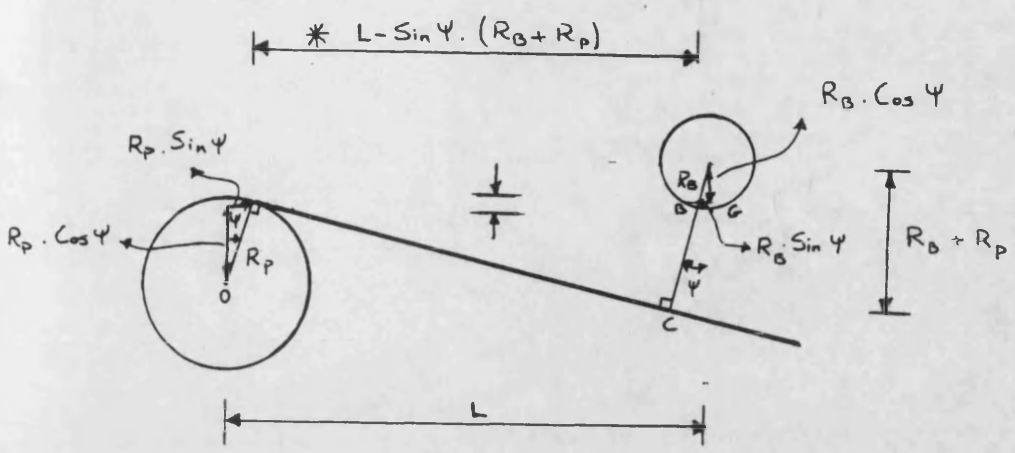

*

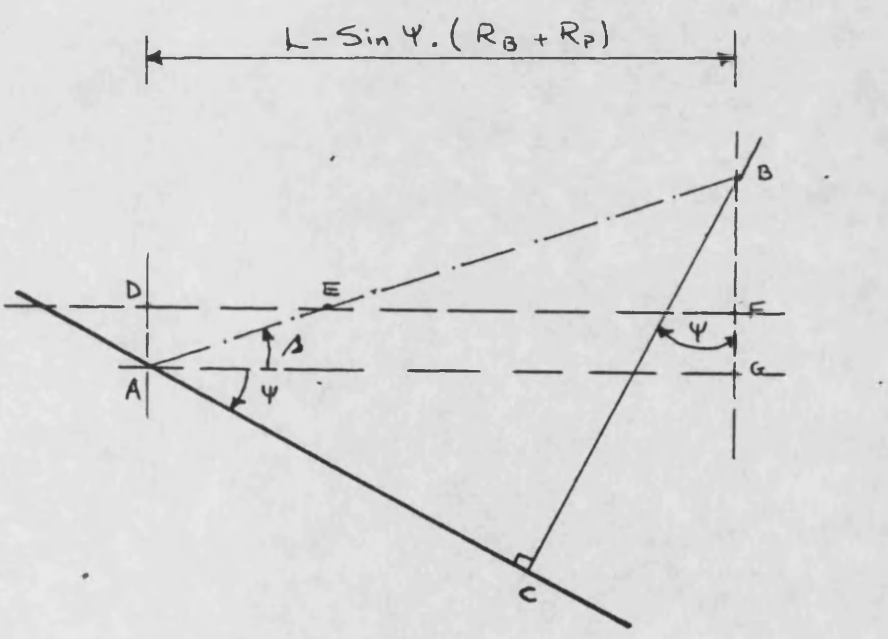

we have from the previous page;

$$BG = BF + FG$$

where

$$BF = R_B + R_B \cdot \cos\Psi = R_B \cdot (1 - \cos\Psi)$$

and

$$FG = Rp - Rp \cdot \cos\Psi = Rp \cdot (1 - \cos\Psi)$$

therefore,

$$BG = (R_B + Rp) \cdot (1 - \cos\psi) \qquad \text{___ (3)}$$

$\triangle$ ABG : $\quad AB^2 = AG^2 + BG^2$

$$= (L - (R_B + R_r).\sin\psi)^2 + (R_B + R_r)^2.(1 - \cos\psi)^2$$

___ (4)

$\triangle$ ABG : $\quad \beta = \text{Tan}^{-1}(BG / AG)$

$$\beta = \tan^{-1}\left\{\frac{(R_B + R_r).(1 - \cos\psi)}{L - (R_B + R_r).\sin\psi}\right\} \qquad \text{___ (5)}$$

$\triangle$ ABC : $\quad BC = AB \cdot \text{Sin}.(\psi + \beta)$

substituting for AB and using expressions (4) and (5) results in;

$$BC = \{[1 - (R_B + Rp).\text{Sin}\psi]^2 + (R_B + Rp)^2.(1 - \text{Cos}\psi)^2\}^{1/2}.$$

$$\text{Sin}\{\psi + \text{Tan}^{-1}[\frac{(R_B + Rp) \cdot (1 - \text{Cos}\psi)}{(L - (R_B + Rp) \cdot \text{Sin}\psi)}]\} \qquad \text{___ (6)}$$

A point of vital importance should be borne in mind that use of flat followers is only possible when the surface of the cam nose consists of convex portions only. For this part of the analysis a mathematical concept should be fully understood prior to setting off to design the secondary cam profile. This mathematical concept is known as the PEDAL OF A CURVE.

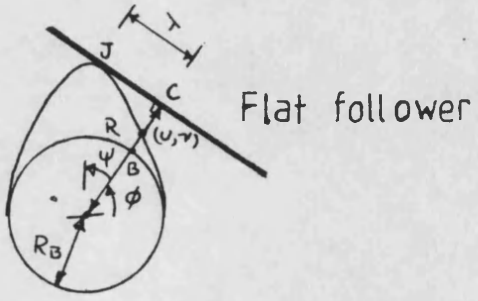

If a perpendicular is dropped from a fixed point on to the tangent to a curve, intersecting the tangent at a point 'C', the locus of 'C' is known as the pedal of the curve with respect to the fixed point; the latter is known as the pole.

The curve itself is called the inverse pedal of the locus of 'C'. The theory of pedal of curves is given in treatises on calculus. Using this theory in our treatment of cams using flat followers; expressions can be derived for the cam profile (72).

The cam profile is the inverse pedal of the locus of 'C' defined by the polar co-ordinates (ρ, α) is given by;

and
$$\rho = \sqrt{R^2 + \left(\frac{180}{\pi}\right)^2 \cdot \left(\frac{dR}{d\phi}\right)^2} \qquad \text{___ (6)}$$

$$\alpha = \phi + \tan^{-1}\left\{\frac{\left(\frac{180}{\pi}\right)}{R} \cdot \frac{dR}{d\phi}\right\} \qquad \text{___ (7)}$$

Since R and ϕ appear in terms of θ, we put these equations in the form;

and
$$\rho = \sqrt{R^2 + 3280\left(\frac{dR}{d\theta}\right)^2 \cdot \left(\frac{d\theta}{d\phi}\right)} \qquad \text{___ (8)}$$

$$\alpha = \phi + \tan^{-1}\left(\frac{57.3}{R} \cdot \frac{dR}{d\theta} \cdot \frac{d\theta}{d\phi}\right) \qquad \text{___ (9)}$$

where,
$$\lambda = 57.3 \frac{dR}{d\theta} \cdot \frac{d\theta}{d\phi}$$

The cam profile is however, usually easier to treat this type of cam in rectangular co-ordinates, in which the equations of the profile are;

$$u = R\cos\psi - 57.3 \frac{dR}{d\theta} \cdot \frac{d\theta}{d\psi} \sin\psi \qquad \text{___ (10)}$$

and

$$v = R\sin\psi + 57.3\frac{dR}{d\theta}.\frac{d\theta}{d\psi}.\cos\psi \qquad \text{___ (11)}$$

In the rectangular co-ordinates (u,v) the cam profile curvature is given by;

$$\frac{1}{\sigma} = \frac{\left\{\left(\frac{du}{d\theta}\right)^2 + \left(\frac{dv}{d\theta}\right)^2\right\}^{3/2}}{\frac{du}{d\theta}.\frac{d^2v}{d\theta^2} - \frac{dv}{d\theta}.\frac{d^2u}{d\theta^2}} \qquad \text{___ (12)}$$

The condition for convexity, and hence the possibility of using a flat folower, is given by;

$$\left(\frac{du}{d\theta}.\frac{d^2v}{d\theta^2} - \frac{dv}{d\theta}.\frac{d^2u}{d\theta^2}\right) > 0.0 \qquad \text{___ (13)}$$

The polar radius R is given by;

$$R = R_B + BC \qquad \text{___ (14)}$$

BC, which is the instantaneous perpendicular distance between the follower and the surface of the base circle, was previously derived and is given by expression (5). BC is expressed in terms of angle of rotation ψ and having obtained expression (2) for ψ a straight forward substitution will result in an expression all in terms of y i.e. the central plunger motion.

$$\psi = \mathrm{Sin}^{-1}[(y + A) / L] - \mathrm{Sin}^{-1}(A / L) \qquad \text{___ (2)}$$

In order to satisfy the convexity condition, equation (13), (10) and (11) need be differentiated with respect to θ. It is already known that there are a series of implicit functions needed to be differentiated for (13) to be valid. A numerical differentiation subroutine was selected from NAG.LIB. to perform the differentiation.

Appendix 5

Continuously Variable Linkage Geometry Analysis

Case 2: Roller follower.

A possible arrangement of the secondary cam, the continuously variable rocker and the central plunger is sketched in figure A.5.1. This configuration takes account of all governing factors that may impose influence on the required secondary cam profile.

A geometrical analysis was carried out to establish important and meaningful expressions required to enable the deduction of the secondary cam profile.

The analysis explained in the next few pages is mathematically self-descriptive and easy to follow. It should be noted that expressions (9), (10) and (11) are extracted from reference (72).

$\triangle$ ABK : $\mathrm{Tan}\Psi = (y / L_1 + \Delta x')$

$$\Psi = \mathrm{Tan}^{-1}(y / L_1 + \Delta x') \qquad \text{___ (1)}$$

$\triangle$ GIK : $\mathrm{Tan}\Psi = (\Delta x' / \lambda + Rp)$

$$\Psi = \mathrm{Tan}^{-1}(\Delta x' / \lambda + Rp) \qquad \text{___ (2)}$$

Equating (1) to (2) gives;

$$\left(\frac{y}{L_1} + \Delta x'\right) = \left(\frac{\Delta x'}{\lambda} + R_F\right)$$

Cross multiplying and re-arranging results in;

$$\Delta x' = \frac{-L_1 + \sqrt{L_1^2 + 4y(\lambda + R_F)}}{2} \qquad \text{___ (3)}$$

△ MBF : $\text{Cos}\,\psi = L' / L$

$L' = L \,.\, \text{Cos}\,\psi$ and

$\Delta x = L - L' = L \,.\, (1 - \text{Cos}\psi)$

△ FBM : $\Delta y = L \,.\, \text{Sin}\psi - y$

EFH : $\text{Tan}\,\psi_o = \Delta x / \Delta y$ therefore $\Delta y = \Delta x / \text{Tan}\,\psi$

Substitution for $\text{Tan}\,\psi$ from (1) gives;

$\Delta y = \Delta x / \text{Tan}\psi = L \,.\, (1 - \text{Cos}\psi) / \text{Tan}\,\psi$

therefore

$\Delta y = L \,.\, (1 - \text{Cos}\psi) / \text{Tan}\psi$ ___ (4)

△ JFH : $\text{Tan}\beta = (\Delta x / \Delta y + R_B + R_F)$

$\therefore \beta = \text{Tan}^{-1}(\Delta x / \Delta y + R_B + R_F)$ ___ (5)

also

$$\text{Sin}\beta = \Delta x \,/\, R \qquad \text{or} \qquad R = \Delta x \,/\, \text{Sin}\beta \quad \text{___ (6)}$$

substitution of (5) in (6) gives;

$$R = \frac{\Delta x}{\text{Sin}[\ \text{Tan}^{-1}(\Delta x / \Delta y + R_B + R_F\ )]} \quad \text{___ (7)}$$

Assuming the cam profile starts at 0 degree;

$$\phi = \theta + \beta \quad \text{___ (8)}$$

Pressure angle is determined by (72);

$$\gamma = \text{Tan}^{-1}[(\ dR / d\phi\ ) / R\ ] \quad \text{___ (9)}$$

therefore, the actual cam profile in polar co-ordinates is expressed by equations below;

$$\rho = \sqrt{R^2 + R_F^2 - 2R.R_F.\cos\gamma} \quad \text{___ (10)}$$

and

$$\alpha = \phi + \cos^{-1}\left(\frac{R^2 + \rho^2 - R_F^2}{2R\rho}\right) \quad \text{___ (11)}$$

The secondary cam profile in cartesian co-ordinates is, therefore, given by;

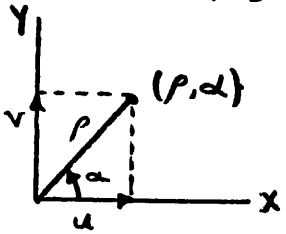

$$u = \rho\ .\ \text{Cos}\alpha$$

$$v = \rho\ .\ \text{Sin}\alpha \quad \text{___ (12)}$$

A computer program was written to accomodate all these expressions in order to generate the actual required secondary cam profile.

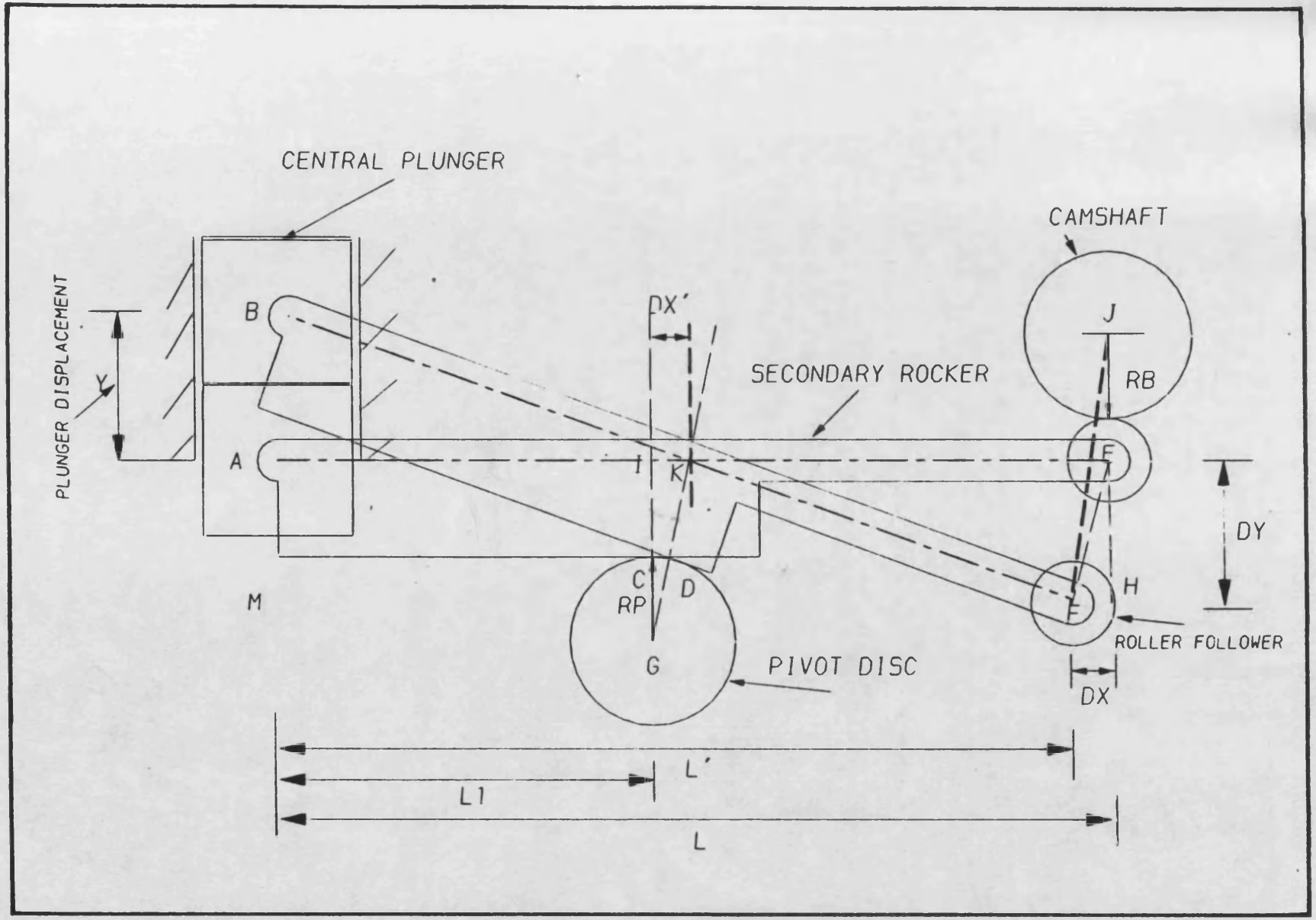

Figure A.5.1 - The continuously variable mechanism incorporating a roller follower.

Appendix 6

Hertz Contact Stresses

When contact members having curved surfaces transmit load, P, from one member to another, an area of pressure is developed, accompanied by contact (compressive) stresses. This situation occurs commonly in machine design such as, mating gear teeth, ball and roller bearings, and cam and roller followers.

The mathematical theory for the surface stresses and deformations produced by pressure between curved bodies was first developed by Hertz. A set of formula relating maximum contact stress to the load, material, and diameter of cylinders in contact parallel to their major axes is given below. For description of notations see Appendix 1.

Cylinder On Cylinder (axes parallel)

$$b = 1.6\sqrt{P.\frac{D_1 D_2}{D_1 + D_2}\left\{\frac{1-\nu_1^2}{E_1} + \frac{1-\nu_2^2}{E_2}\right\}}$$

$$\sigma_{cmax} = 0.798\sqrt{\frac{P.\frac{D_1 D_2}{D_1 + D_2}}{\frac{1-\nu_1^2}{E_1} + \frac{1-\nu_2^2}{E_2}}}$$

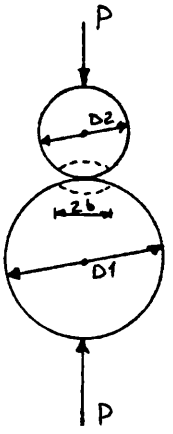

For like materials;

$$E_1 = E_2 = E = 200\ GN/m^2$$

$$\nu_1 = \nu_2 = \nu = 0.3$$

Therefore ,

$$b = 2.15\sqrt{\frac{P}{E}\cdot\frac{\frac{D_1}{D_2}}{D_1 + D_2}}$$

and

$$\sigma_{cmax} = 0.591\sqrt{P.E.\left(\frac{D_1 + D_2}{D_1.D_2}\right)} \qquad \text{(1)}$$

Elastic Cylinder And Plane Surface

Similarly for like materials we have;

$$E_1 = E_2 = E = 200\ GN/m^2$$

$$b = 2.15\sqrt{\frac{PD}{E}}$$

$$\sigma_{cmax} = 0.591\sqrt{\frac{PE}{D}} \qquad \text{(2)}$$

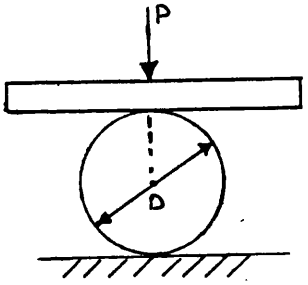

Expression (1) enables one to determine the Hertz contact stresses between the secondary cam and the roller follower. Expression (2) is to be used to determine the Hertz contact stress between the pivot disc and the secondary rocker.

For the latter to be performed a simple beam arrangement, illustrated below, can be used to obtain the reaction force at the pivot disc point of contact.

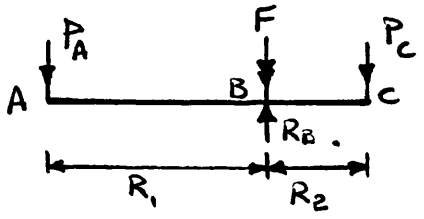

Resolving forces vertically;

$$P_A + P_C + F = R \qquad \text{(i)}$$

Taking moments about pivot point B;

$$P_A \times R1 = Pc \times R2$$

$$Pc = P_A \cdot R1/R2 \qquad \text{___ (ii)}$$

R1/R2 is the secondary rocker ratio. Assuming for a particular arrangement R1/R2 = 2.0, therefore,

$$Pc = 2 \cdot P_A$$

substitution for Pc in expression (i) gives;

$$R_B = P_A + 2.P_A + F$$

therefore $$R_B = 3.P_A + F$$

where P is the compressive force between the secondary cam and the roller follower, and F is the force due to inertia of the secondary rocker assuming to be acting at the pivot point of contact, that is,

$$F = M_{eq} \cdot g$$

where

$$M_{eq} \text{ of rocker} = I_V \, (1 + R_V)^2 / L$$

Secondary Cam Instantaneous Contact Force

When the rigid-body dynamic analysis was performed, expressions were derived giving the contact forces for the

main and the secondary cams. The expressions related to the secondary cam are;

$$R_v = L_1 / (L - L_1) \qquad \text{___ (3)}$$

$$\text{Pres.} = [\, M_{eq} ((A_1/A_3).\ddot{Y}_1 + (A_2/A_3).\ddot{Y}_2.R_v) + K_{eq} ((A_1/A_3).Y_1 + (A_2/A_3).Y_2.R_v) + F_{peq} \,] / A_3$$

$$M_2 = I_v \cdot (1 + R_v)^2 / L + m_f \cdot R_v^2$$

or

$$M_2 = I_v /(L - L_1)^2 + m_f \cdot R_v^2 \qquad \text{___ (4)}$$

$$F_2 \text{ (or P)} = M_2.\ddot{Y}_2 + \text{Pres}.A_2.R_v$$

where

$A_1 = A_2 = A_3 = A = \pi D^2/ 4$

$M_{eq} = 0.7943$ kg

$K_{eq} = 46907$ N/m

$F_{peq} = 666.1$ N

$I_v = 0.000068$ kg.m^2

$m_f = 0.10$ kg

$E = 200$ GN/m^2

Y_1 and Y_2 are the main cam and the central plunger motion lifts respectively. Similarly, $\ddot{Y}_1$ and $\ddot{Y}_2$ are their respective accelerations.

As the instantaneous values of Y_1, Y_2, $\ddot{Y}_1$ and $\ddot{Y}_2$ vary with time, it results in changes in values of the compressive force P.

In order to determine the instantaneous secondary cam compressive force, using the rigid-body analysis expressions, $\ddot{Y}_1$ and $\ddot{Y}_2$ expressions were derived analytically as given below;

<u>Main cam</u>:

θ = 0 to 24 degrees,

$$\ddot{Y}_1 = 0.0$$

θ = 25 to 88 degrees,

$$Y_1 = (C - C_p.X_1^p + C_q.X_1^q - C_r.X_1^r - C_s.X_1^s)/1000$$

and

$$\ddot{Y}_1 = (-2.C_p + 72.C_q.X_1^7 - 132.C_r.X_1^{10} - 870.C_s.X_1^{28})/$$

$$3969 \times 1000 \quad m/deg.^2$$

Central plunger motion:

θ = 0 to 24 degrees,

$$\ddot{Y}_2 = 0.0$$

θ = 25 to 53 degrees,

$$Y_2 = C_p.(X_1^p - X_2^p) + C_q.(X_2^q - X_1^q)$$

$$+ C_r.(X_1^r - X_2^r) + C_s.(X_1^s - X_2^s) /1000$$

and

$$\ddot{Y}_2 = (2.C_p + 72.C_q.(X_2^7 - X_1^7) + 132.C_r.$$

$$(X_1^{10} - X_2^{10}) + 870.C_s.(X_1^{28} - X_2^{28}))/ 3969 \times 1000$$

θ = 54 to 88 degrees,

$$Y_2 = (C_p.X_1^p - C_q.X_1^q + C_r.X_1^r + C_s.X_1^s) /1000$$

and

$$\ddot{Y}_2 = (2.C_p - 72.C_q.X_1^7 + 132.C_r.X_1^{10} +$$

$$870.C_s.X_1^{28}) / 3969 \times 1000$$

where,

$$X_1 = \theta / \Delta\theta_1$$

and

$$X_2 = \theta - \Delta\theta_1 \ (1 + b) \ / \ \Delta\theta_2$$

Conversion from mm/deg^2 to m/s^2:

$$(mm/deg^2) \times 0.001 \times (6/2 \ . \omega_{\in})^2 = m/s^2$$

Appendix 7

Retaining Spring Force

In order to keep the roller follower in contact with the secondary cam, so that the secondary rocker will not bein seperation and avoid undesirable impact, a retaining spring is required to be incompression to offer secure contact between the secondary cam and the roller follower.

The amount of compression (preload) is dependent on the stiffness of the spring as well as the magnitude of theopposing forces that it has to overcome. Assuming a spring identical to the Dover Ford engine valve spring, which has stiffness value of K = 23932 N/m, is used the following calculation determines the required amount of preload to ensure complete contact over the entire operating speed;

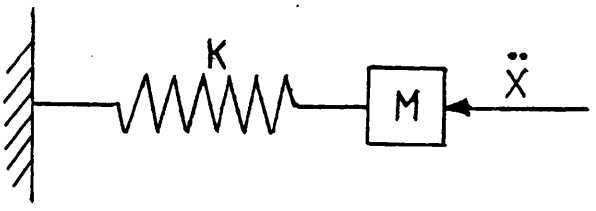

where,

$M = M_f + M_{eq.}$ of rocker + 1/3 M spring

$M_{eq} = I_v \cdot (1 + R_v)^2 / L$

Data: $R_v = 1.5$

$L = 75$ mm

$I_v = 0.000068$ kg.m^2

$M_{spring} = 0.0925$ kg

$M_f = 0.10$ kg

$\ddot{X}_{max} = 710$ m/s

$K = 23932$ N/m

therefore,

$M = 0.1874$ kg

$F_{max} = M \cdot \ddot{X}_{max}$

i.e. $F_{max} = 133.07$ N

$F_{max} = K \cdot \Delta_{max}$ therefore,

$\Delta_{max} = 0.00556$ m

that is <u>Preload of $\leq$ 5.6 mm</u>

Appendix 8

Determination Of Effective Valve Flow Areas

Figure A.8.1 shows a poppet valve lifted from its seat. At low lifts, shown on the right, the flow area normal to the seat faces is that of the surface for part of a frustrum of a cone. The diameters for the cone are d_1 and d_2. Then XY is the slant height,

$$XY = L.\ Cos\alpha = S \text{ (say)} \qquad \text{A.8.1}$$

where

L = Valve lift; and

α = Angle of valve seat.

Now
$$d_L = d_1 + 2XZ = d_1 + 2XY\ .\ Sin\alpha$$
$$= d_1 + 2L\ .\ Cos\alpha\ .\ Sin\alpha \qquad \text{A.8.2}$$

The surface area of a right circular cone is;

$$A = \pi/2\ .\ S\ (d_1 + d_L) \qquad \text{A.8.3}$$

his gives the valve opening area per valve,

$$A_V = \pi .\ L.\ Cos\alpha\ (d_1 + L.\ Cos\alpha Sin\alpha) \qquad \text{A.8.4}$$

$$= \pi d_1^2\ .\ L/d_1.\ Cos\alpha\ (1 + L/d_1.\ Cos\alpha Sin\alpha)$$

$$= \pi d_1^2.\ Cos\alpha\ (1 + L/d_1.\ Cos\alpha Sin\alpha).\ L/d_1$$

$$\text{A.8.4a}$$

This last equation has been derived since it is useful when comparing flows on an L/d_1 basis, as a non-dimensional lift, which is convinent when comparing flow characteristics for differing valves and ports (74).

For valves having a 45^o seat angle, the expression A.8.4a becomes:

$$A_v = \pi d_1^2 \ (0.7071 + 0.35354 \ L/d_1) \ L/d_1 \qquad \text{A.8.4b}$$

Figure A.8.2 shows a typical curve for flow coefficient against L/D ratio for an exhaust valve and port, where L is the valve lift and D is the valve head diameter. The valve effective flow area is the product of conical frustrum flow area as derived in exprression A.8.4 and the flow coefficient determined from the curve in figure A.8.2 based on the annular area. Therefore:

$$A_{eff} = A_v \cdot C_D \qquad \text{A.8.5}$$

The valve effective flow areas in the experimental flow rig simulations have been determined using expression A.8.5.

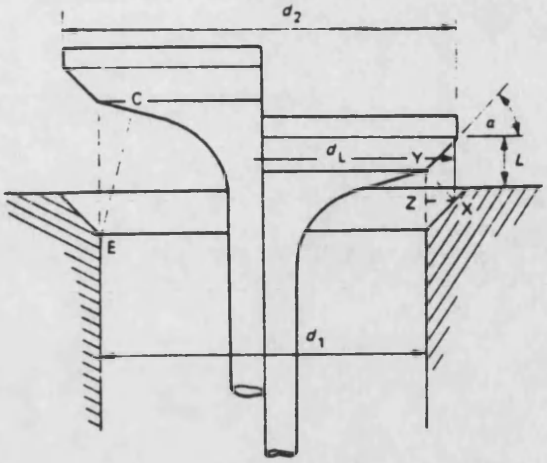

Figure A.8.1 - Valve area with conical seats.

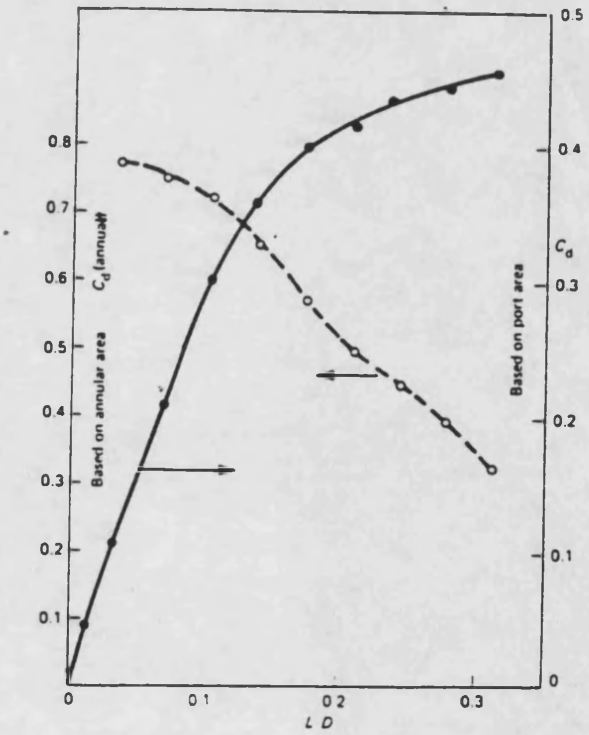

Figure A.8.2 - Flow coefficient vs L/D ratio for a non-swiring inlet valve and port.

Appendix 9

Energy Content Of Exhaust Pulses (11)

The energy content of the exhaust pulse at the outlet end of the exhaust pipe is defined as the work that may be performed by the gas by expansion through an ideal isentropic gas turbine. The thermodynamic model for the system is shown in figure A.9.1; the ideal isentropic gas turbine is placed immediately downstream of the exhaust pipe and quasi-steady flow is assumed.

Applying the first law of thermodynamics to the control volume enveloping the inlet and outlet ducts of the turbine we have;

$$\cancel{\dot{Q}}_{0} - \dot{W} = \dot{m}\,(h_3 - h_1) + \dot{m}\,([U_3^2/2 - U_1^2/2]) + \dot{E}_{CV} \quad (1\text{-}3)$$

A.9.1

For the nozzle the corresponding equation is;

$$\cancel{\dot{Q}}_{0} - \cancel{\dot{W}}_{0} = \dot{m}\,(h_2 - h_1) + \dot{m}\,([U_2^2/2 - U_1^2/2]) + \dot{E}_{CV} \quad (1\text{-}2)$$

A.9.2

where suffixes 1,2 and 3 refer to the positions given in figure A.9.1, also

$\dot{Q}$ = rate of heat added or extracted from the system,

$\dot{W}$ = rate of work done by or on the system,

$\dot{m}$ = rate of gas mass flow,

h = specific enthalpy,

U = specific velocity,

$\dot{E}$ = rate of internal energy of the control volume.

It the length of the gas path in the turbine is small compared with the exhaust pipe length, it may be assumed that at any instant of time the gas mass flow rate from position 1 to 3 is constant, therefore:

$$\dot{E}_{cv\ (1-3)} = \dot{E}_{cv\ (1-2)} = 0$$

The model shown in figure A.9.1 is an ideal isentropic, purely impulse gas turbine; when the flow is unchoked the entire pressure drop takes place in the fixed nozzle and the kinetic energy produced in the gas stream is then transferred to the rotor. For maximum work from the turbine $U_3 = 0$, hence, subtracting expression A.9.1 from A.9.2 and noting that $h_2 = h_3$ we shall have;

$$\dot{W} = \dot{m} \cdot U_2^2/2 \qquad \text{A.9.3}$$

This is the kinetic energy of the gas stream leaving the nozzle. When choked the pressure is only partially dropped in the nozzle and further expansion occures in the 'blades' hence,

$$\dot{W} = \dot{m}\ (h_{01} - h_{03}) \qquad \text{A.9.4}$$

where,

$$h_{01} = h_1 - U_1^2/2$$

and

$$h_{03} = h_3 - \cancel{U_3^2/2}^{\,0}$$

therefore expression A.9.4 may be rewritten on the form;

$$\dot{W} = \dot{m}\,(h_1 + U_1^2/2 - h_3) \qquad \text{A.9.5}$$

Note that from the choking condition 'm' will be determined at the nozzle throat. Applying the steady flow energy equation for the nozzle results in expression A.9.2 which may be given as;

$$\cancel{\dot{Q}}^{\,0} - \cancel{\dot{W}}^{\,0} = h_2 - h_1 + U_2^2/2 - U_1^2/2$$

therefore,

$$U_2^2/2 = h_1 - h_2 + U_1^2/2$$

$$= C_p\,(T_1 - T_2) + U_1^2/2$$

$$= C_p \cdot T_1\,[1 - (P_2 / P_1)^{\frac{\gamma-1}{\gamma}}] + U_1^2/2$$

$$\text{A.9.10}$$

also $U_2 = a_2$ = velocity of sound in gas which may be determined using:

$$U_2^2 = a_2^2 = \gamma RT_2 = \gamma RT_1\left(\frac{P_2}{P_1}\right)^{\frac{\gamma-1}{\gamma}} \qquad \text{A.9.11}$$

Let $\frac{\gamma-1}{\gamma} = K$ and $P_2/P_1 = R_p$ and equating A.9.10 and A.9.11 gives;

$$(C_p + \cancel{8}.R/2).\ T_1\ .\ R_p^K = C_p.T_1 + U_1^2/2 \qquad \text{A.9.12}$$

From continuity we have;

$$\dot{m}_1 = \rho_1 \cdot A_1 \cdot U_1 = (P_1/R.T_1) \cdot A_1 \cdot U_1$$

and

$$\dot{m}_2 = \rho_2 \cdot A_2 \cdot U_2 = (P_2/R.T_2) \cdot A_2 \cdot \sqrt{\gamma.R.T_2}$$

where

A = cross-sectional area [m^2],

P = pressure [N/m^2],

R = specific gas constant [kJ/kgK],

T = temperature [K],

ρ = density [kg/m^3].

From adiabatic expansion of 1-2 we have;

$T_2 = T_1 \cdot R_p^K$ therefore,

$$\dot{m}_2 = P_2 \cdot A_2 \, (\gamma/R.T_2)^{1/2}$$

$$= P_2 \cdot A_2 \, (\gamma/R)^{1/2} \cdot 1/T_1^{1/2} \cdot (P_1/P_2)^{\gamma-1/2\gamma}$$

hence,

$$\dot{m}_2 = P_2 \cdot A_2 \, (\gamma/R.T_1)^{1/2} \cdot (P_1/P_2)^{\gamma-1/2\gamma}$$

but $\dot{m}_1 = \dot{m}_2$ thus giving;

$$(P_1/R.T_1) \cdot A_1 \cdot U_1 = P_2 \cdot A_2 \, (\gamma/R.T_1)^{1/2} \cdot (P_1/P_2)^{\gamma-1/2\gamma}$$

therefore,

$$U_1 = (P_2/P_1) \cdot \phi \cdot (\gamma.R.T_1)^{1/2} \cdot (P_2/P_1)^{1-\gamma/2\gamma}$$

$$U_1 = \phi \cdot a_1 \cdot (P_1/P_2)^{-(\gamma+1)/2\gamma} \qquad \text{A.9.13}$$

Substituting A.9.13 for U_1 in A.9.12 results in;

$$\phi^2 = \frac{(2C_p + \gamma R).R_p^{\kappa} - 2C_p}{\gamma R.R_p^{\frac{\gamma+1}{\gamma}}} \qquad \text{A.9.14}$$

where,

$$\phi = A_2/A_1.$$

The critical pressure ratio (static to ambient) is in fact dependent up on the area ratio since the upstream conditions are NOT stagnation conditions. If C_p = 1005 [KJ/KgK], γ = 1.4 and R = 287 [J/KgK] expression A.9.14 becomes;

$$\phi^2 = \frac{2411.8R_p^{0.2857} - 2010}{401.8R_p^{1.714}}$$

A.9.15

The nozzle diameter and the exhaust pipe diameter of the experimental flow rig are 25mm and 40mm respectively, thus the critical pressure ratio is approximately 1.867 if the ratio of specific heats is taken as 1.4.

In the exhaust system of an internal combustion engine the pressure pulses occur in a cyclic sequence, the maximum energy available per cycle is therefore (11);

$$W = \oint (dW/dt) \; . \; dt$$

Determining the gas temperature in the exhaust pipe, T_1, is very complex because the flow is unsteady and the temperature changes with any change in the pulse pressure. A reasonable assumption may be made that considers a 'quasi-steady' flow and thermal conditions from the cylinder to the turbine end of the exhaust pipe. This means that the

exhaust valve remains open long enough for the conditions in the exhaust pipe to reach quasi-steady. This is probably the best assumption which may be made that assumes the instantaneous flow through the valve and through the nozzle are the same. Figure A.9.2 illustrates the expansion of gases from the cylinder to the "turbine" nozzle on a T-S diagram.

The gas expands from the cracking pressure level in the cylinder to the pressure level at the throat of the exhaust valve before recovering to a pressure level corresponding to that of the exhaust pipe. The fall in temperature of the gas is due to the loss in the kinetic energy of the gas in the pipe, $U_{Pipe}^2/2C_p$. Then the gas adiabatically expands further through the "turbine" nozzle to atmospheric conditions. From the T-S giagram in figure A.9.2 it may be seen that;

$$T_{Pipe} = T_{cyl} - U_{Pipe}^2/2C_p \qquad \text{A.9.16}$$

and

$$T_{cyl} = T_o \cdot (P_{cyl} / P_o)^K \qquad \text{A.9.17}$$

Therefore, substituting for T_{cyl} in A.9.16:

$$T_{Pipe} = T_o \cdot (P_{cyl} / P_o)^K - U_{Pipe}^2/2C_p \qquad \text{A.9.18}$$

where,

T_o = initial cylinder temperature [K],

P_o = initial cylinder pressure [N/m^2],

C_p = specific heat at constant pressure [J/kgK].

Maximum Theoretical Available Turbine Power

A hypothetical situation may be considered where the turbocharger turbine is placed immediately downstream of the exhaust valve so that the entire energy of the gases leaving the cylinder is utilized by the turbine. This means that the expansion of exhaust gas, from the time of the exhaust valve opening, to atmospheric conditions takes place in the turbocharger turbine. This process is shown in figure A.9.4 (75). The adiabatic turbine work may be determined using;

$$W = \int_2^1 V.dp \qquad \text{A.9.19}$$

and

$$P.\ V^{\gamma} = P_1\ .\ V_1^{\gamma} \text{ therefore, } V = V_1\ (P_1/P)^{1/\gamma}$$

hence,

$$W = \int_2^1 V_1\ (P_1/P)^{1/\gamma}\ .\ dp = V_1 \int_2^1 P_1^{1/\gamma}\ .\ P^{-1/\gamma}\ .\ dp$$

Finally after integrating with respect to P, the adiabatic turbine work becomes;

$$W = P_1\ .\ V_1\ .\ K\ [1 - R_p^K]$$

$$= m\ .\ R\ .\ T_1\ .\ K\ [1 - R_p^K]$$

$$W = m\ .\ C_p\ .\ T_1\ [1 - R_p^K] \qquad \text{A.9.20}$$

where,

V_s = piston swept volume [m^3],

V_c = combustion chamber volume [m^3],

W = adiabatic turbine work [W],

$K = \frac{\gamma - 1}{\gamma}$,

$R_p = P_2 / P_1$.

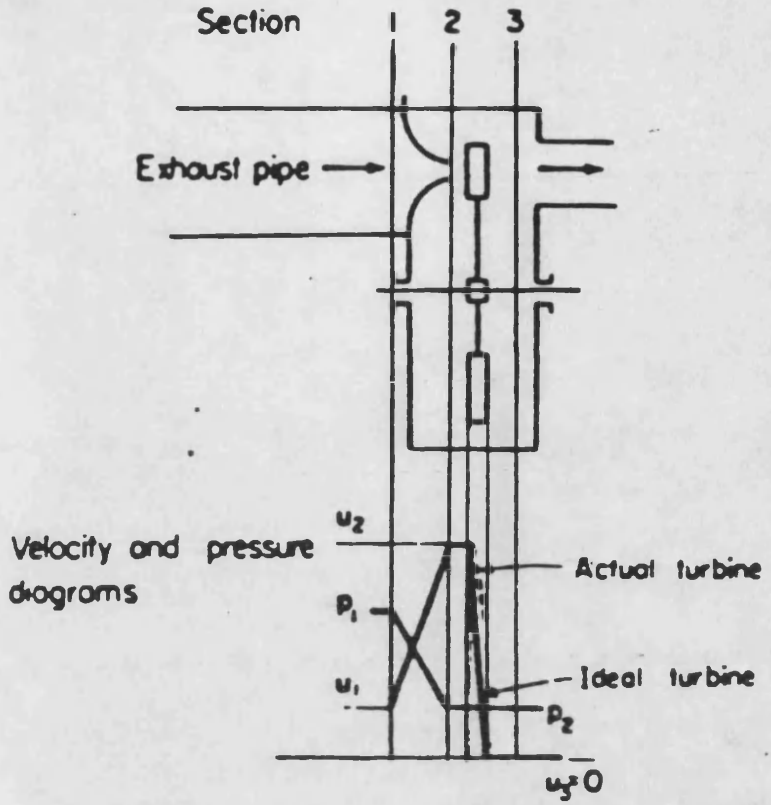

Figure A.9.1 - The thermodynamic model of an ideal isentropic gas turbine.

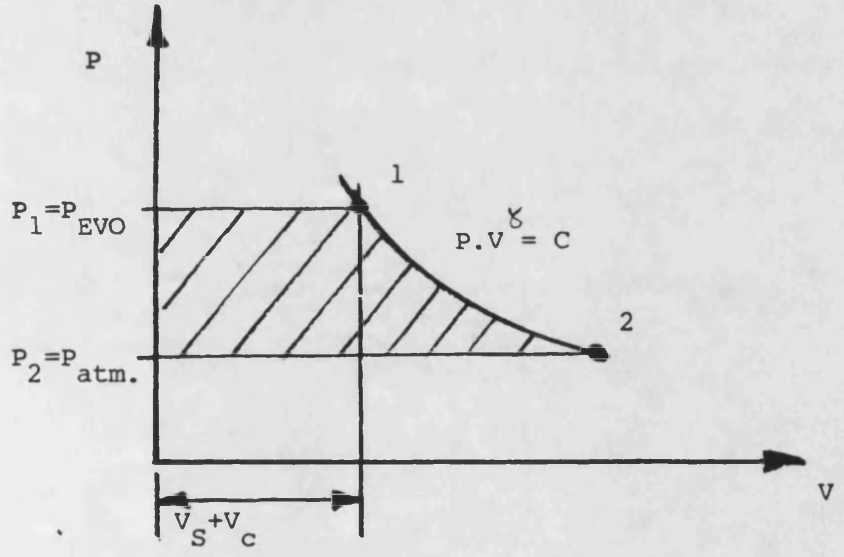

Figure A.9.4 - P-V diagram of the exhaust turbine.

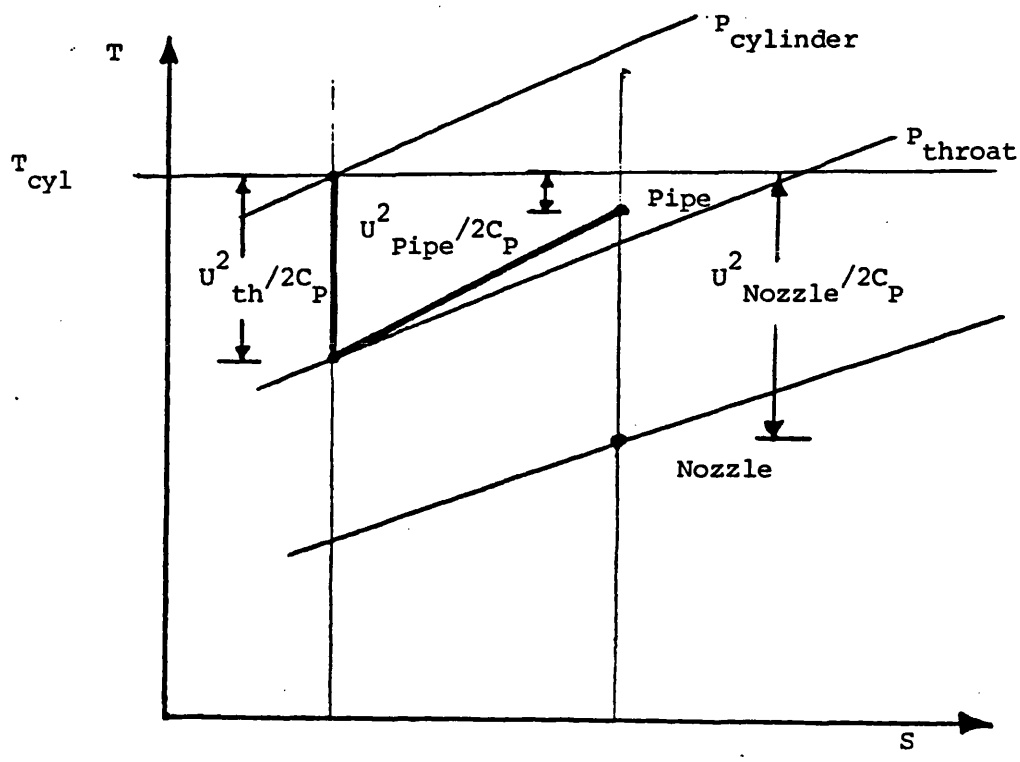

Figure A.9.2 - T-S diagram of gas expansion from the cylinder to the turbine nozzle.

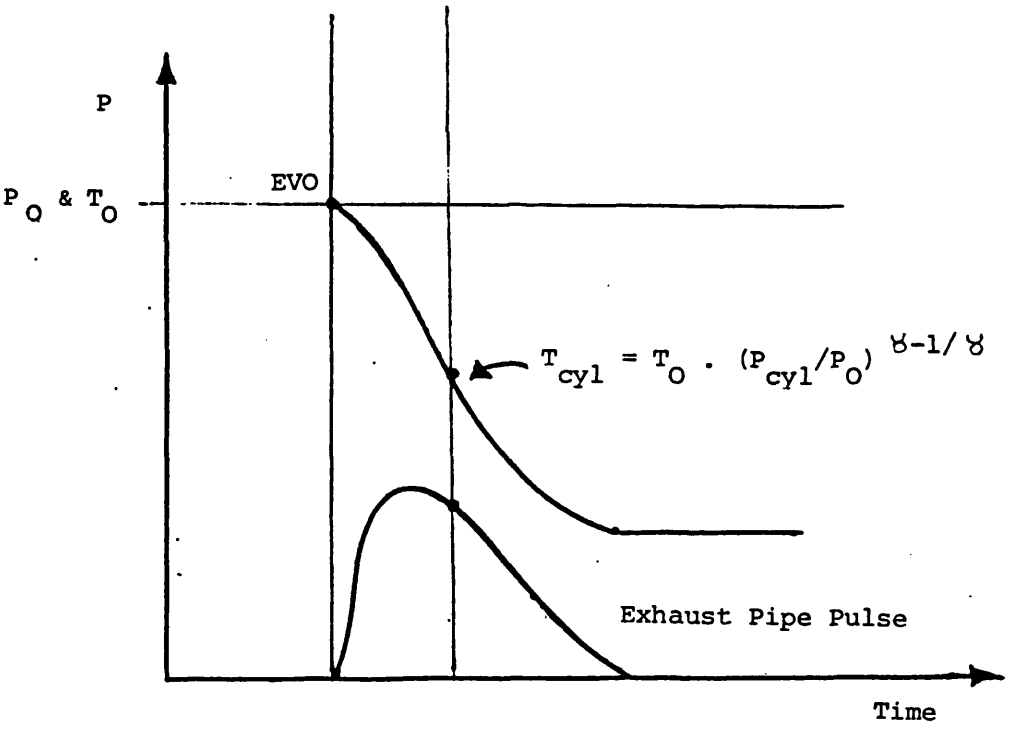

Figure A.9.3 - P-t diagram of gas expansion at EVO and formation of the exhaust pulse.

APPENDIX 10

Published papers.

A continuously variable poppet valve actuator for internal combustion engines

S J Charlton, BSc, PhD, CEng, MIMechE and **M Shafie-Pour**, BSc
School of Engineering, University of Bath

The paper describes a continuously variable poppet valve actuation system which may be applied to internal combustion engines to render the valve motion controllable while the engine is running.

The first phase of a programme to develop the device is described. The results of a rigid-body dynamic analysis are presented followed by a dynamic simulation of the mechanism using a proprietary finite element program. These give an insight into its operation and clarify some of the problems to be solved if the device is to be successfully applied.

1 INTRODUCTION

In recent years much effort has gone into the development of electronic engine management systems, both for petrol and diesel engines. In general, such devices receive a continuous flow of information from a number of sensors distributed around the engine and after processing the data, send out signals to actuators which operate on controllable engine elements in order to modify performance in line with a control strategy. The sensors may be monitoring crankshaft speed, crankshaft torque, air flow, fuel flow, exhaust emissions or even the absence or presence of 'knocking' combustion. The control strategy may be to minimize fuel consumption, maximize power, to provide low-speed torque or to minimize exhaust pollutants. The successful application of such techniques will require the availability of engine and transmission elements which are controllable. In this category are variable injection timing, variable geometry turbocharger compressors and turbines, mixture strength control and continuously variable transmissions.

Additionally, the mechanism may be used in research and development as a means of varying valve motion or timing on a running engine, as a means of determining optimum cam profiles for an otherwise conventional engine.

This mechanism was developed specifically to render the motion of engine poppet valves continuously variable so that valve motion may be considered as part of an engine management strategy. The device may be used to control either rate of valve opening or closing, valve timing or valve lift. A line drawing of the mechanism is shown in Fig. 1. The mechanism employs two cams for each valve to be controlled. The primary cam may be likened to a conventional cam in that it operates on a follower which drives the valve train, in this case through a compact hydraulic chamber. The contribution of the secondary cam may be varied by adjusting the position of the pivot of the rocker arm which oper-

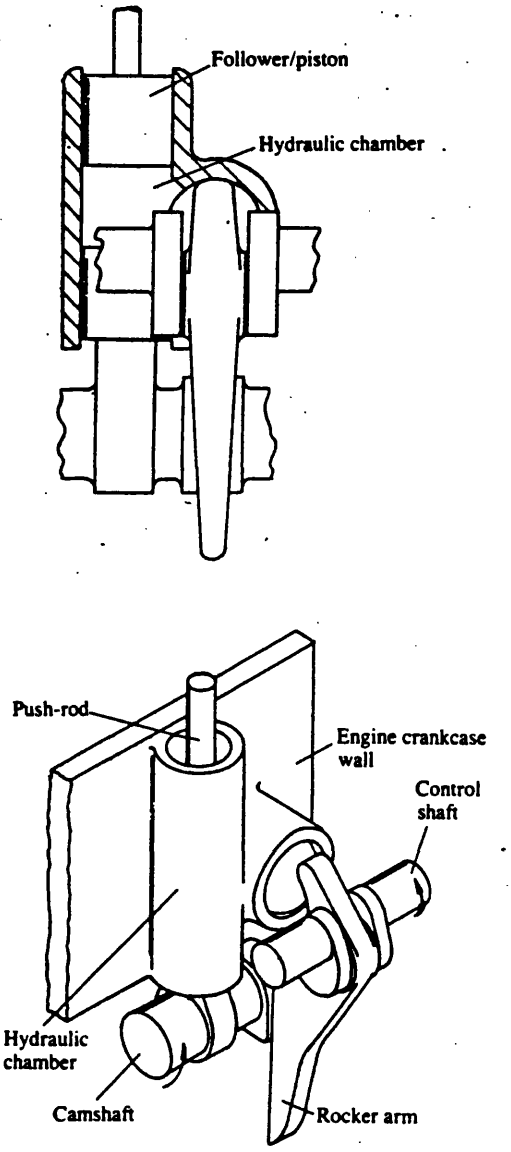

Fig. 1 Sectional and perspective views of the continuously variable poppet valve actuator, showing the rocker and control shaft. Rotation of the control shaft effects a change of rocker ratio and hence valve motion

This paper was presented at a conference on 'Mechanisms and machinery' held at Cranfield Institute of Technology on 17–18 September 1985. The MS was received on 30 September 1985 and was accepted for publication on 3 January 1986.

0263-7138/86 $2.00 + .05

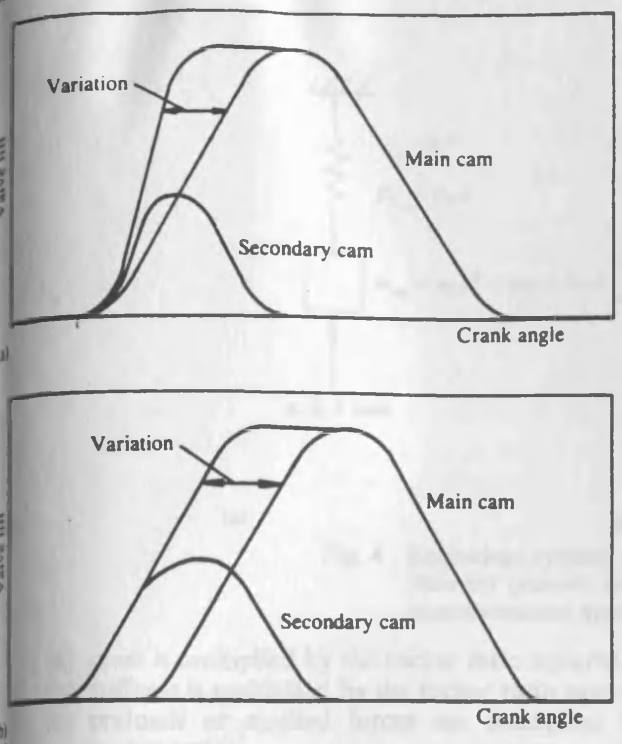

Fig. 2 Valve lift diagrams for the continuously variable valve actuator (a) variable rate system (b) variable timing system

es between the secondary cam and the central piston f the hydraulic chamber. By moving the pivot point so hat it is aligned with the central piston, the secondary am has no modifying effect on the motion. By careful esign of the cam profiles the mechanism can be made o vary valve motion over a wide range without over-tressing the linkage. Figure 2 shows lift diagrams for he variable rate and variable timing variants.

The rigid-body analysis and dynamic simulation pre-ented relate to a variable rate of opening system pplied to the exhaust valve of a six-litre turbocharged ruck engine. In this application the actuator is used to ncrease the low-speed torque of the engine and hence mprove driveability.

In the conventional valve train the inertia stresses ncrease as the square of engine speed and design is ormally based on survival at speeds up to a suitably igh overspeed. For a truck diesel engine the minimum uty speed may be 1000 r/min, the maximum 2200 min and the overspeed limit 3500 r/min. Thus at the owest speed the inertia stresses will be less than one-uarter of those at the maximum rated speed and about ne-twelfth of the design strength.

The mechanism proposed is capable of controlling he rate of exhaust valve opening as a function of engine peed such that at low speeds the valve opens at the ame rate as at the maximum rated speed, thus fully tilizing the design strength.

Increasing the rate of exhaust valve opening has long een recognized as an effective means of improving the nergy transfer between cylinder and turbine of a turbo-harged engine (1). The benefit results from the forma-ion of more energetic pulses in the exhaust port and anifold which, because of the more rapid rise of press-re downstream of the valve, also serve to reduce the ighly irreversible period of choked flow through the

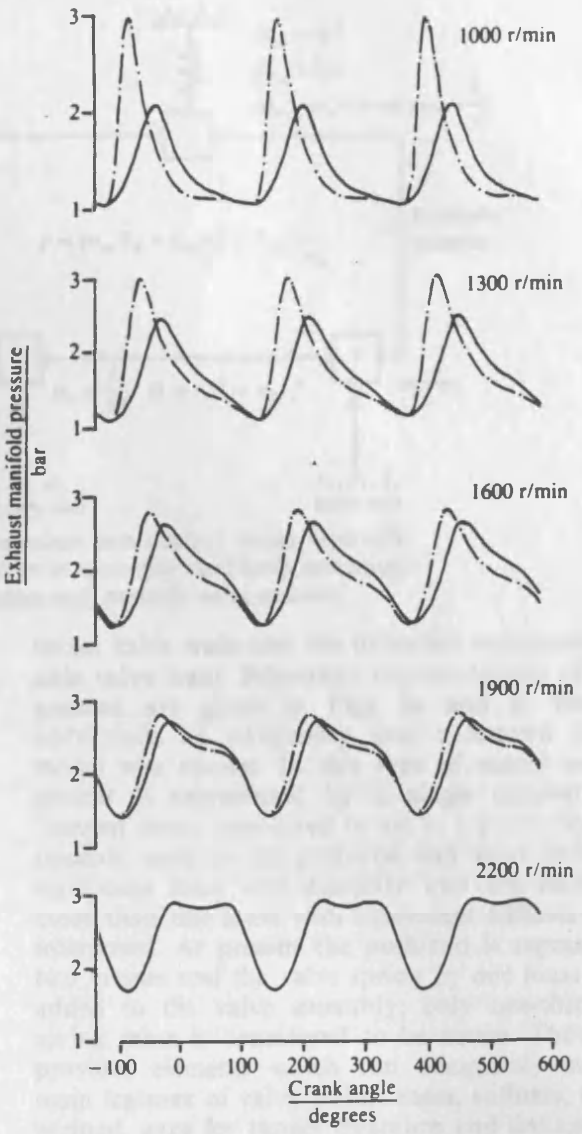

Fig. 3 The effect of rate of exhaust valve opening on the formation of pulses in the exhaust manifold of a turbocharged diesel engine (2) ---- continuously variable system ——— conventional system

valve. The effect of rate of exhaust valve opening on pulse formation, due to Charlton (2), is shown in Fig. 3.

For this particular engine the low-speed torque back-up is predicted to increase from 27 to 40 per cent (2) by adopting the continuously variable valve actuator.

2 RIGID-BODY DYNAMIC ANALYSIS

In a rigid-body dynamic analysis the members of the mechanism are treated as rigid-bodies. Displacement, velocity and acceleration are readily calculated for each part of the mechanism and these may be applied to determine the maximum contact force at the cam and the required valve spring rate. To ease the calculation procedure a one degree of freedom equivalent system was derived for the conventional valve train and a one-dimensional, three degree of freedom system for the continuously variable actuator. The established procedure for converting valve-side parameters to equivalent cam-side values is as follows:

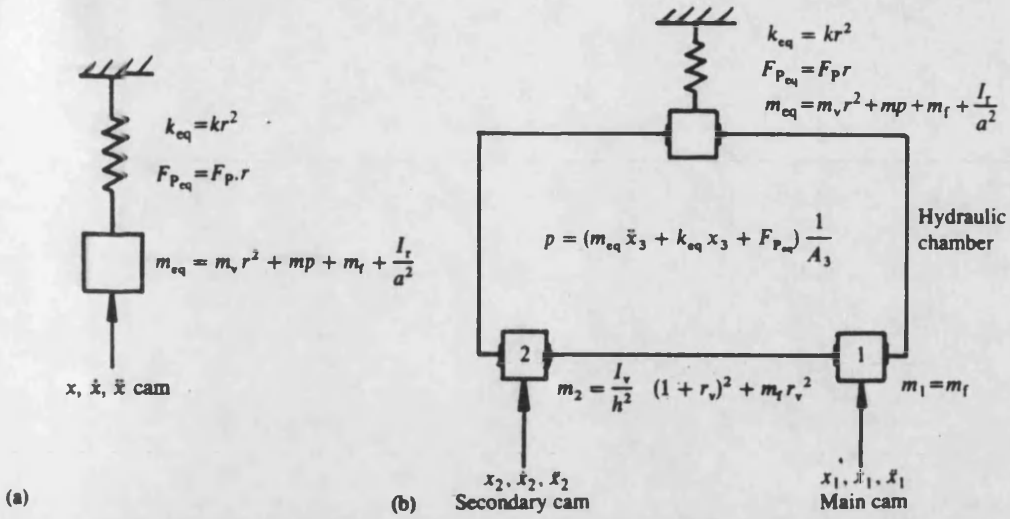

Fig. 4 Equivalent systems used to calculate cam contact forces, hydraulic chamber pressure and spring reserve assuming rigid-body conditions (a) conventional system (b) continuously variable valve actuator

(a) mass is multiplied by the rocker ratio squared;
(b) stiffness is multiplied by the rocker ratio squared;
(c) preloads or applied forces are multiplied by the rocker ratio;
(d) displacement, velocity and acceleration by the rocker ratio;
(e) damping coefficient is multiplied by the square of rocker ratio.

The equivalent systems for both the conventional and continuously variable valve trains are shown in Fig. 4.

3 DEVELOPMENT OF NON-LINEAR TRANSIENT DYNAMIC MODEL

In early attempts to model valve train dynamics the system was reduced to an equivalent system having one degree of freedom. Usually the mass of the valve assembly is converted to an equivalent mass on the cam-side which may then be 'lumped' together with the push-rod and tappet masses. Linkage, valve spring and valve seat stiffnesses were usually incorporated along with associated internal damping coefficients. Such models provide surprisingly good results, when compared with experimental data, considering the simplicity of the model. They are perhaps most useful for predicting contact forces at the cam during design.

The widespread availability of digital computers has alleviated the problems of solving multi-mass systems. However, the solution of high-order models with a suitably small integration time step can require a great deal of computer processing time and expense.

The objectives of this study are primarily to develop more versatile and effective means of opening the valves of internal combustion engines. Thus the authors did not feel it appropriate to spend valuable time writing a new valve train simulation program. The thermal power group obtained the proprietary finite element (FE) package ANSYS initially to carry out conventional finite element analyses to predict heat flow and thermal stress in diesel engine components. ANSYS is in fact a more general purpose engineering analysis program which, as well as the more usual FE solutions, provides modal and non-linear dynamic analyses. The non-linear dynamic analysis was used to simulate both the conventional valve train and the proposed continuously variable valve train. Schematic representations of the two systems are given in Figs 5a and b. Because of restrictions on computing time a lumped parameter model was chosen. In this type of model each component is represented by a single concentrated or 'lumped' mass considered to act at a point. Some components, such as the push-rod and valve spring, have significant mass and elasticity and are modelled by more than one mass with equivalent stiffness elements interposed. At present the push-rod is represented by two masses and the valve spring by one mass which is added to the valve assembly; only one-third of the spring mass is considered to be active. The program provides elements which can adequately model the main features of valve trains: mass, stiffness, damping, preload, gaps for tappet clearance and linkage separation. Displacement and force boundary conditions may

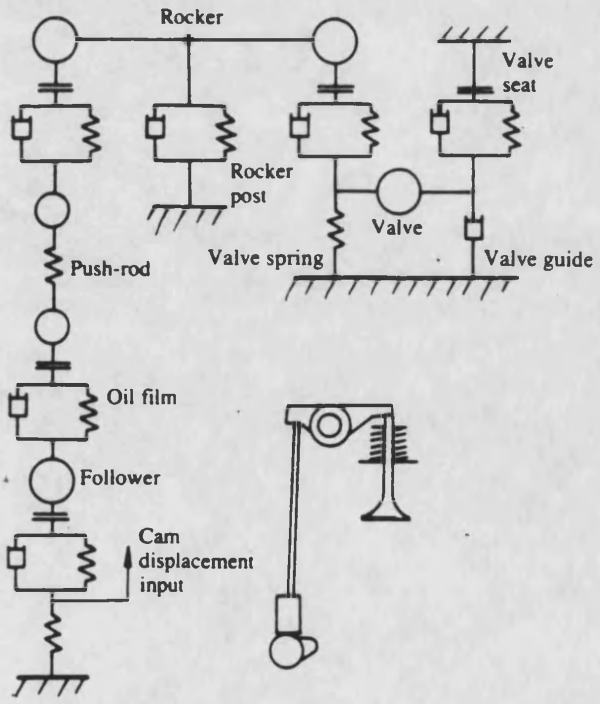

Fig. 5a Non-linear transient dynamic model of conventional valve train

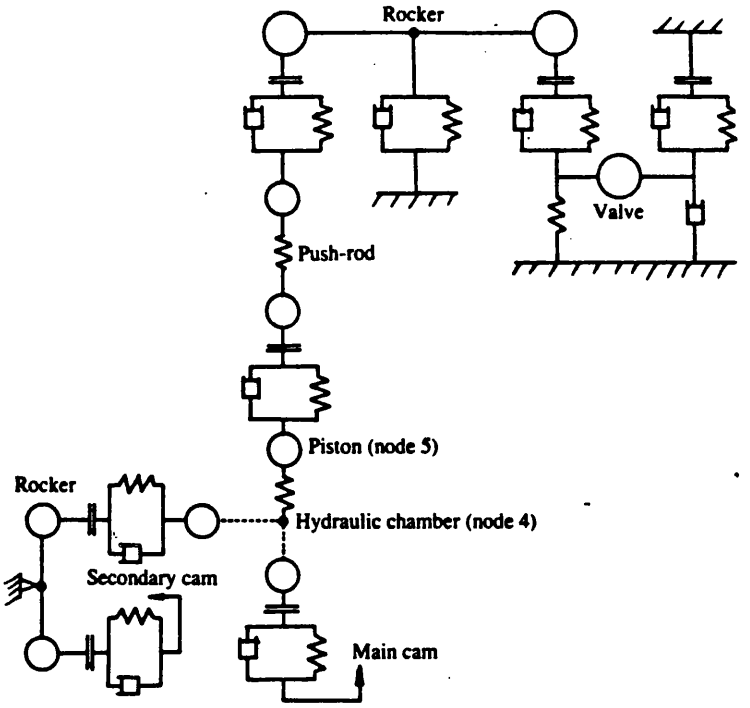

Fig. 5b Dynamic model of continuously variable valve system

be applied at more than one point in the system which for the two-cam model allows each cam lift curve to operate at different points and for the simulation of gas forces on the valve head. Constraint equations were used to define the relative motion of different parts of the system, for example, to relate the two ends of the rocker with the pivot, which itself was mounted on a flexible element modelling the rocker post. A further constraint equation was used to link the motion of the two input pistons and the output from the hydraulic chamber. Oil compressibility effects were modelled by a spring element placed between the output from the constraint equation (node 4) and the mass representing the upper piston (node 5) (see Fig. 5). The presence of a gravitational field could be included in the model and its inclusion may be justified at low engine speeds where peak linkage accelerations are approximately 30g. Stiffness and damping elements were built into the model at each metal-to-metal interface to represent oil film behaviour, however, there seems to be little data in the literature on such effects and almost no guidance on numerical values. The authors believe that the oil film behaviour is complex and not strictly amenable to representation by unique values of stiffness and damping coefficient.

Having constructed a working dynamic simulation of a valve train, it was a simple matter to convert this to the form required for a modal analysis. The natural frequencies and modal shapes were computed in only minutes compared with one to two hours for a dynamic simulation.

4 DISCUSSION OF RESULTS

The continuously variable (CV) and conventional valve systems were initially studied by a simple rigid-body analysis as shown in Fig. 4. This type of analysis does not take account of vibratory response but does allow meaningful comparisons of the two systems on the basis of ideal acceleration, contact forces and spring reserve. This first phase of the work examines the feasibility of modifying an existing exhaust valve train to be continuously variable. Thus, the profile of the main cam was not considered to be a design parameter.

The secondary cam was defined, as shown in Fig. 6, to produce an acceleration of the push-rod, during the opening phase at an engine speed of 1000 r/min, exactly equivalent to the acceleration produced by the main cam at 2200 r/min. These engine speeds correspond to the operating range of a typical large automotive diesel engine. The gain in flow area for this design is represented by the difference between the two high-lift curves shown in Fig. 6a. The acceleration curves for the main (standard) exhaust cam and the secondary (CV) cam are shown in Fig. 6b. Under the action of the variable rocker connecting the secondary cam to the rest of the valve train the contribution of the secondary cam is progressively reduced as the engine speed is increased, in order to maintain constant maximum valve acceleration.

The variation of push-rod acceleration with time is shown for a number of engine speeds in Fig. 7. It should be noted that the acceleration during the opening period is identical for each speed. The contribution of the secondary cam is seen to last for exactly half of the period of the main cam. During the dwell period at 1000 r/min the fall of the secondary cam exactly cancels the rise of the main cam. At 2200 r/min the secondary cam has no modifying effect on the motion and the acceleration produced is that of the main cam alone. The acceleration curves shown in Fig. 7 appear discontinuous, particularly at the transition with the dwell period. Figure 8 shows the jerk (third differential of displacement with respect to time) curve at 1000 r/min, which is the worst case in this respect. The diagram shows that the discontinuities are not severe compared to the normal acceleration pulse.

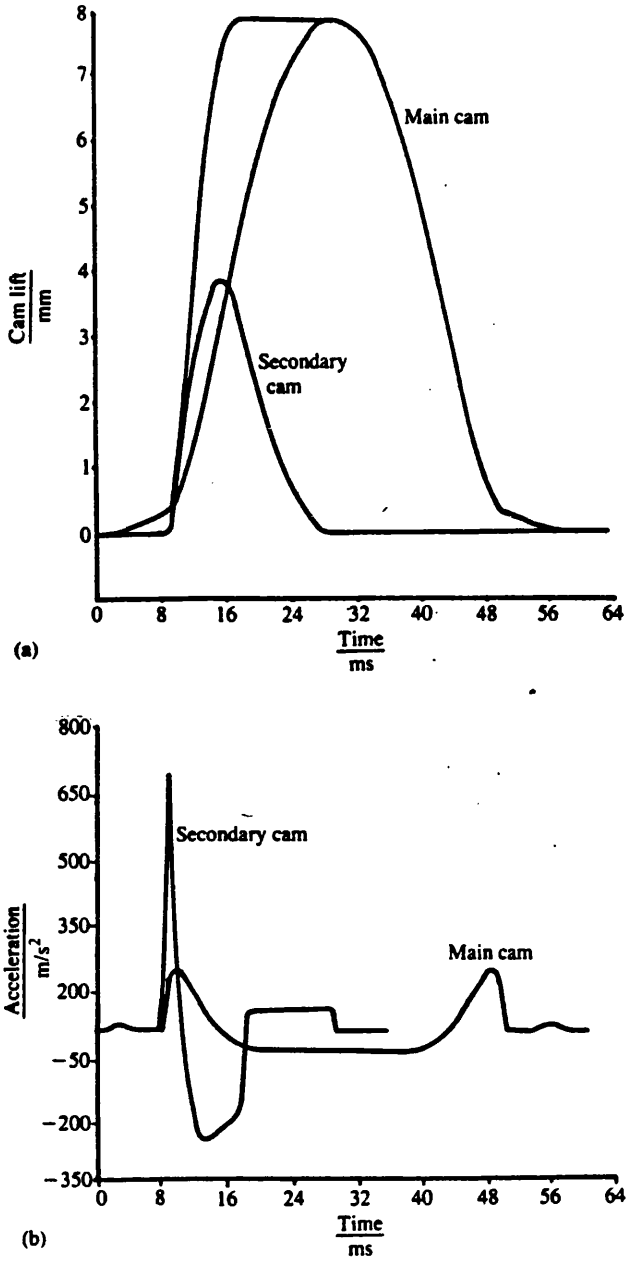

Fig. 6 Continuously variable system: at 1000 r/min (a) cam lift curves (b) cam accelerations

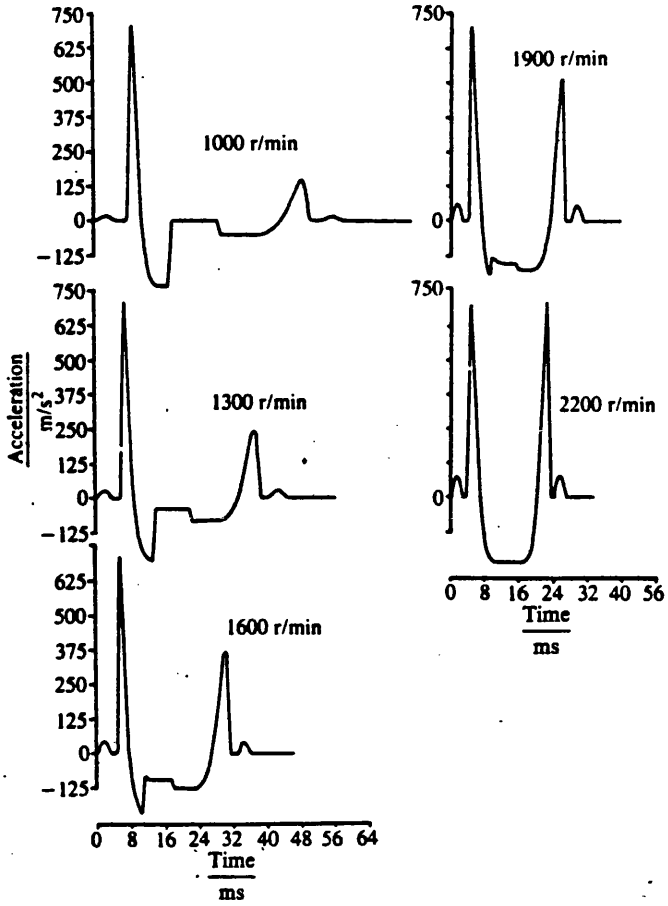

Fig. 7 Variation of output (push-rod) acceleration versus time for a series of engine speeds and corresponding secondary rocker ratios (note that maximum opening acceleration is constant)

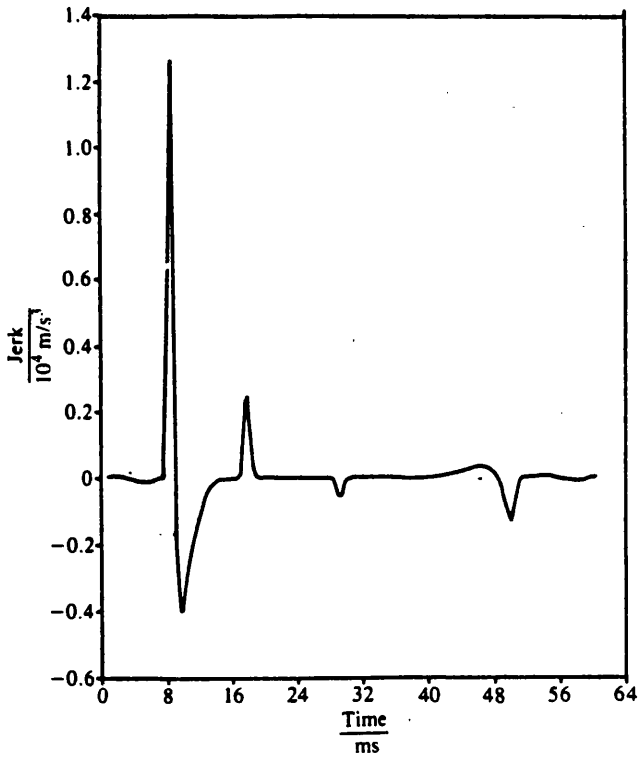

Fig. 8 Graph of jerk versus time for the push-rod of the continuously variable system at an engine speed of 1000 r/min

Figure 9 shows the variation of cam acceleration, contact force and the required secondary rocker ratio with engine speed calculated by rigid-body analysis. The acceleration curves all correspond to the point of maximum push-rod acceleration, since this is when the maximum contact forces will occur. The maximum contact forces are given by the upper curves of Fig. 9. They show that the load on the main cam is increased by the addition of the CV components by approximately 6 per cent at the highest speed. This is entirely due to the additional mass of the system (two followers and secondary rocker). The maximum contact force on the main cam falls with engine speed and at 1000 r/min is only 1 per cent higher than in the conventional system. Maximum secondary cam forces are 18 per cent higher than in the conventional system although in contrast this condition occurs only at the lowest speed so that the net effect on wear may not be severe. Spring

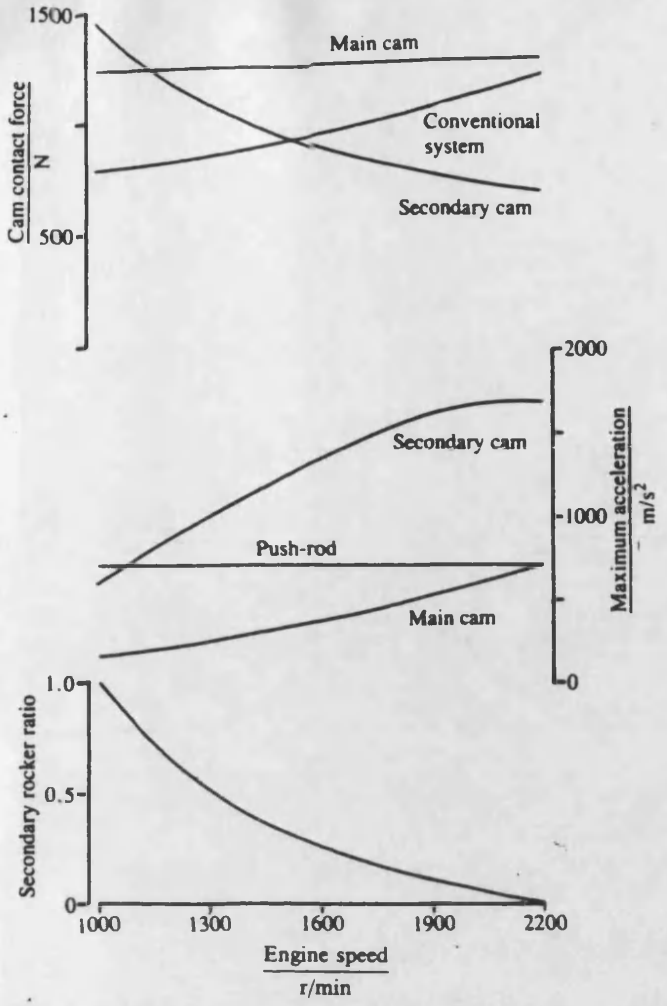

Fig. 9 Variation of maximum values of contact force and acceleration versus engine speed, showing the secondary rocker ratio required to maintain constant push-rod acceleration

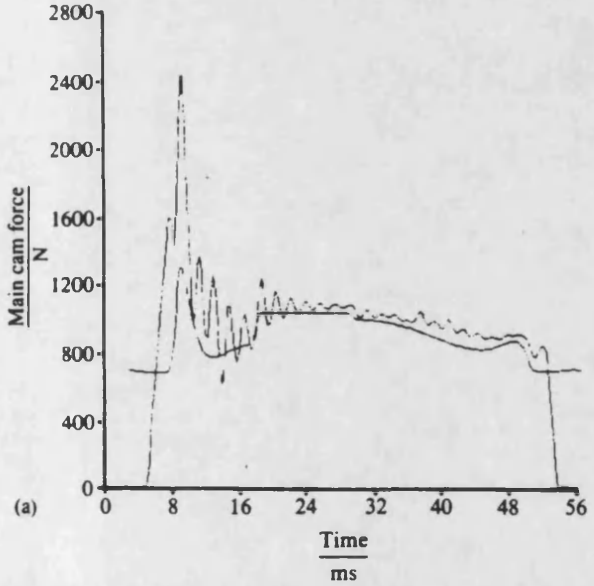

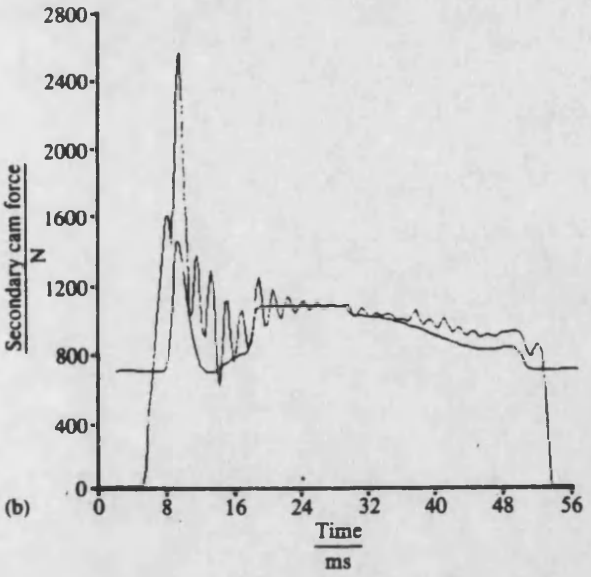

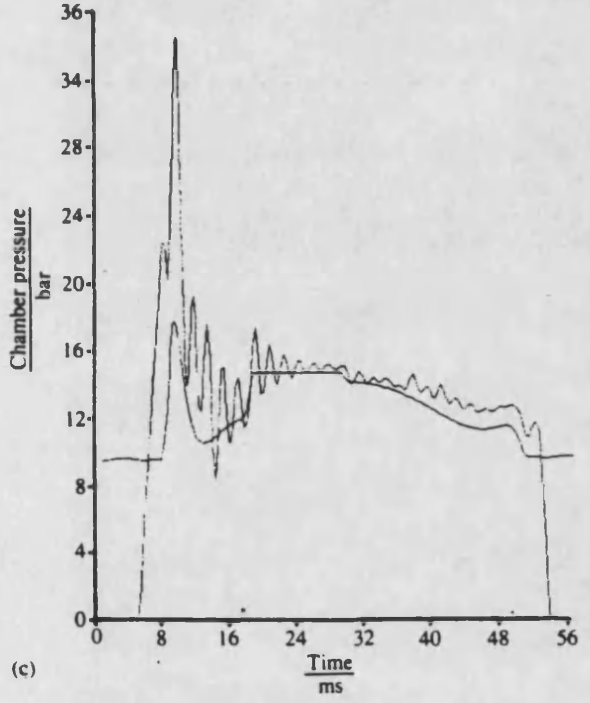

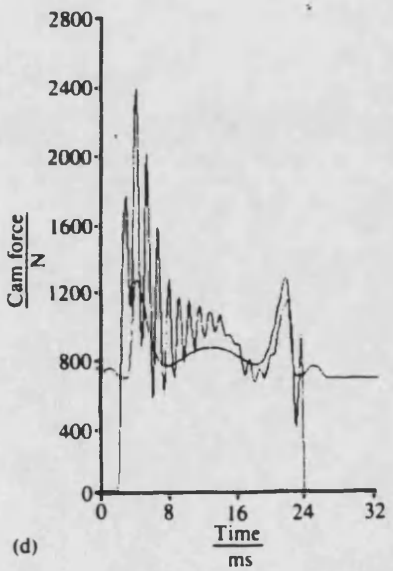

Fig. 10 Comparison of cam force and chamber pressure predicted by the dynamic and rigid-body analyses. The cam force curves (a) and (d) illustrate the design concept of the CV system which is to exploit the design strength of the valve train at all speeds, thus the maximum cam forces under these conditions are broadly comparable
(a), (b) and (c) continuously variable system at 1000 r/min (d) conventional system at 2200 r/min

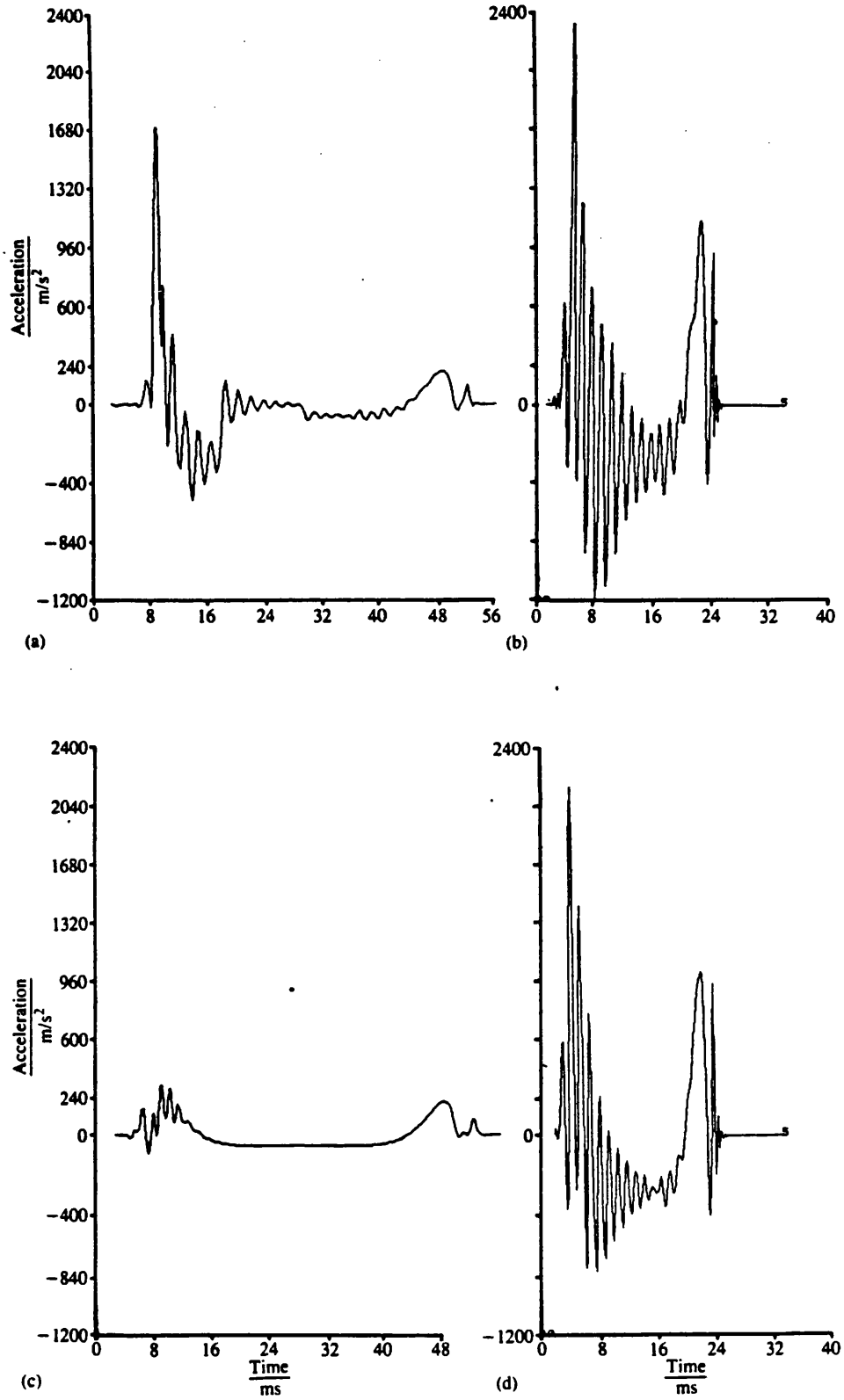

Fig. 11 Valve acceleration predicted using the dynamic simulation
(a) continuously variable system at 1000 r/min
(b) continuously variable system at 2200 r/min
(c) conventional system at 1000 r/min
(d) conventional system at 2200 r/min

reserve is the margin of spring force over system inertia force and indicates the tendency to linkage separation. The spring reserve of the conventional system at 2200 r/min was 103 N in excess of the inertia force of 564 N. Without modification to the valve spring preload or rate the minimum spring reserve in the CV system was only 25 N over an inertia force of 642 N.

Figure 10 compares cam forces and hydraulic chamber pressure predicted by dynamic simulation and rigid-body analysis. Generally, the levels of the curves are comparable, small differences arising because the rigid-body analysis did not account for valve lash, damping forces and gas forces.

The system is essentially being disturbed by an impulse since the oscillations are assumed to decay fully between consecutive valve events. Vibrations may persist in the coils of the valve spring, which in high-speed engines can be a significant influence on valve motion. Figures 10 and 11 show that the vibratory acceleration response is highly oscillatory and that the maximum values of cam force and chamber pressure are approximately twice those predicted under the assumption of rigid body behaviour. The variation of valve acceleration with time is shown in Fig. 11. This shows that the worst conditions are expected to occur at 2200 r/min for both systems. The maximum acceleration in the valve occurs in response to the positive acceleration pulse in the early part of the valve motion.

5 DISCUSSION AND CONCLUSIONS

A concept has been described which theoretically allows the motion of engine poppet valves to be controlled in various ways. The theoretical study will be followed by experimental evaluation; however, before this stage is reached several technically difficult problem areas will have to be addressed. These include detail design of the secondary cam, CV rocker and hydraulic chamber. This represents an interesting optimization problem as different combinations of plunger area, rocker ratio and secondary cam lift may produce the same push-rod motion but with differing implications for layout, size, cam force, rubbing velocity, wear and dynamic behaviour.

REFERENCES

1 **Jenny, E.** Utilisation of exhaust gas energy in the supercharging of the four-stroke diesel engine. *Brown Boveri Review*, 1950, 37(1).
2 **Charlton, S. J.** and **Pappas, P.** A parametric study of the exhaust valve requirements of high output truck engines. SAE Congress, Detroit, Feb. 1985.
3 **Stojek, D.** and **Stwiorok, A.** Valve timing and variable overlap control. FISITA paper 840026, 1984.
4 **Richman, R. M.** and **Reynolds, N. C.** A computer controlled poppet valve actuator for application on research engines. SAE paper 840340, 1984.
5 **Charlton, S. J.** An adjustable means of operating the valves of an engine. UK Patent Application 8504888, 26 Feb. 1985.
6 **Bathe, K. J.** and **Wilson, E. L.** *Numerical methods in finite element analysis*, 1976, (Prentice Hall, Hemel Hempstead).

APPENDIX

Notation

a	distance from push rod to rocker pivot
$[C]$	damping matrix
$\{F\}$	force vector
F, F_s, F_R, F_P	force, spring force, spring reserve, preload
h	distance from secondary piston axis to cam centre-line
I_R, I_v	moment of inertia of rocker and secondary rocker
$[k]$	stiffness matrix
k, k_{eq}	stiffness, equivalent stiffness
$[m]$	mass matrix
m, m_f, m_{eq}	mass, mass of follower, equivalent mass
p	hydraulic chamber pressure
r, r_v	rocker ratio, secondary rocker ratio
Δt, t	integration time step, time
$\{U\}$	nodal displacement vector
$\{\dot{U}\}$	nodal velocity vector
$\{\ddot{U}\}$	nodal acceleration vector
x	displacement
$\dot{x}$	velocity
$\ddot{x}$	acceleration

Rigid-body dynamic analysis (reference to Fig. 4)

The reduction of the conventional valve train to an equivalent one degree of freedom system is quite straightforward. Mass, stiffness and preload on the valve-side are converted to cam-side equivalent values. The rocker moment of inertia is converted to an equivalent mass by dividing by the square of the distance between the pivot and the push-rod. These values are then combined with the masses of the push-rod and follower to form an equivalent system mass.

The continuously variable valve actuator was reduced to a simple system having three degrees of freedom. The valve, rocker, push-rod and upper piston were combined to form an equivalent mass m_{eq}. Spring rate and preload were also converted to cam-side equivalent values. Thus ignoring damping and fluid compressibility the pressure in the chamber is given by

$$p = (m_{eq}\ddot{x}_3 + k_{eq}x_3 + F_{P_{eq}})\frac{1}{A_3} \qquad (1)$$

and for continuity

$$A_3 x_3 = A_1 x_1 + A_2 x_2 r_v$$

$$x_3 = \frac{A_1}{A_3}x_1 + \frac{A_2}{A_3}x_2 r_v \qquad (2)$$

similarly

$$\ddot{x}_3 = \frac{A_1}{A_3}\ddot{x}_1 + \frac{A_2}{A_3}\ddot{x}_2 r_v \qquad (3)$$

putting equations (2) and (3) into equation (1)

$$p = \frac{1}{A_3}\left[m_{eq}\left(\frac{A_1}{A_3}\ddot{x}_1 + \frac{A_2}{A_3}\ddot{x}_2 r_v\right) + k_{eq}\left(\frac{A_1}{A_3}x_1 + \frac{A_2}{A_3}x_2 r_v\right) + F_{P_{eq}}\right]$$

Cam forces are found by adding the forces transmitted to the lower pistons, by the hydraulic fluid, to the inertia forces of these pistons and the secondary rocker

main cam force $\quad F_1 = m_f\ddot{x}_1 + p \cdot A_1$

secondary cam force $\quad F_2 = m_2\ddot{x}_2 + p \cdot A_2 \cdot r_v$

and

$$m_2 = \frac{I_v}{h^2}(1 + r_v)^2 + m_f r_v^2$$

Spring reserve is the margin of spring force to system inertia force and is an indicator of the tendency to linkage separation

spring reserve $F_R = F_s - m_{eq}\ddot{x}_3 - m_2\ddot{x}_2 - m_1\ddot{x}_1$

Dynamic simulation

The non-linear transient dynamic analysis within ANSYS is essentially a numerical integration of the general equation of motion for a structural system, which in matrix form is

$$[\mathbf{m}]\{\ddot{U}\} + [\mathbf{C}]\{\dot{U}\} + [\mathbf{k}]\{U\} = \{F\} \quad (1)$$

Starting from a given initial state of the system ($t = 0$) equation (1) is solved at successive time steps taking account of the opening and closing of gaps, damping and other non-linearities. Displacements are assumed to vary cubically during an iteration. Thus the velocity varies quadratically and acceleration varies linearly during the iteration.

The velocity and acceleration vectors may be rewritten in terms of the unknown displacement for the current iteration and the displacements for the previous three iterations:

$$\{\dot{U}_n\} = \frac{1}{6\Delta t}[11\{U_n\} - 18\{U_{n-1}\} + 9\{U_{n-2}\} - 2\{U_{n-3}\}] \quad (2)$$

$$\{\ddot{U}_n\} = \frac{1}{\Delta t^2}[2\{U_n\} - 5\{U_{n-1}\} + 4\{U_{n-2}\} - \{U_{n-3}\}] \quad (3)$$

Equations (2) and (3) are substituted into equation (1). Then the only unknown is the displacement vector $\{U_n\}$ which is calculated at each point in the dynamic transient analysis in the same way as a conventional finite element static analysis. This method is known as the Houbolt time integration scheme (6).

Three different starting procedures are available; all of these commence with a static analysis to establish the initial displacement. The three starting assumptions available are:

(a) initial velocity defined by first two iterations;
(b) initial velocity equal to zero;
(c) initial velocity and acceleration equal to zero.

The Engineering Society
For Advancing Mobility
Land Sea Air and Space®

400 COMMONWEALTH DRIVE WARRENDALE, PA 15096

SAE Technical Paper Series

880603

A Hydraulic Valve Control System and its Application to Turbocharged Diesel Engines

S.J. Charlton and M. Shafie-Pour
School of Mechanical Engineering
University of Bath

International Congress and Exposition
Detroit, Michigan
February 29-March 4, 1988

880603

A Hydraulic Valve Control System and its Application to Turbocharged Diesel Engines

S.J. Charlton and M. Shafie-Pour
School of Mechanical Engineering
University of Bath

ABSTRACT

The paper describes the development of a hydraulic variable valve motion system which has been used successfully to study the relationship between rate of exhaust valve opening and exhaust pulse energy with reference to exhaust turbocharging. The device may be configured to provide variation of timing, rate of opening or closing, or lift. Each of these variations could be achieved independently, for example, the start of valve opening could be varied without altering either the rate of opening or the full lift. The device is described in detail and preliminary experimental results are given. An alternative configuration in which the variation of motion may be achieved digitally is described.

THE READY AVAILABILITY of sophisticated engine management systems has led to a resurgence of interest in "variable" engine systems for such controllers to act on. Examples include variable geometry turbocharging, continuously variable transmissions, variable swirl ports and variable intake systems. Variable valving systems have been proposed as a means of improving engine performance over a wide load and speed range from the earliest days of engine development and the patent literature is comprehensive on the subject (1)-(5)*. Systems are beginning to appear on commercial engines, in small quantity production, for example, the Alfa Romeo engine (6) in which the phasing of one of a pair of overhead camshafts is varied as a means of controlling valve overlap in response to engine speed and load. Fiat (7) also have a variable valve motion system in which a three dimensional cam acts on an articulated follower. In this system variation of valve motion is achieved by moving the camshaft axially to allow different cam profiles to act on the follower.

Whilst the great majority of known systems are mechanical or hydromechanical in concept and permit only a limited range of variation of valve motion the most desirable system is one in which all, or at least part of the motion may be defined digitally and be generated by computer control. Such a system was developed by Richman and Reynolds (8) in which the complete valve motion could be defined by software, within the frequency response of the actuator. Their valve actuator used a high pressure hydraulic supply to a spool valve controlled power piston. The spool valve was controlled by a voice coil driven by an analogue control signal. This system gave excellent valve control, but only at engine speeds below 3000 rev/min, and it was far too complex to be applied to commercial engines.

The research work presented in this paper relates to the application of a novel hydromechanical device which was first described in reference (9). Its effects on the performance of a turbocharged diesel engine were presented in reference (10). The subject of this paper is the performance of the device on an experimental flow rig (11). The rig was constructed to enable investigation of the relationship between rate of exhaust valve opening and exhaust pulse energy.

DESCRIPTION OF THE MECHANISM

The concept consists of a conventional engine driven cam which acts on a follower. The follower also acts as a piston which operates on a small hydraulic volume to transmit the opening force to another piston which drives the push rod and valve gear. Thus in the line of action from the cam to the valve is a small quantity of hydraulic fluid.

* References are listed at the end of the paper

0148-7191/88/0229-0603$02.50

Variations of valve motion are achieved by modulating this hydraulic volume using a third piston, during the valve period, as shown in figure 1. The hydraulic volume, being essentially incompressible, acts as an "adding" device, allowing the contributions of the two input pistons to be combined at the output piston. Many methods exist to modulate the third piston. For this work, which is purely a research application, a direct acting cam driven system was chosen, as shown in figure 2. The motion of the third piston is generated by a specially tailored secondary cam, mounted on the camshaft next to the conventional cam. The motion is transferred from the secondary cam to the piston by a secondary rocker which has an adjustable pivot point. The degree of modulation is varied by moving the pivot point between positions A and B as shown in figure 2. When the pivot is in position B the secondary cam is unable to move the modulating piston and the motion of the valve is dictated solely by the motion of the primary cam. When the pivot is in position A, approximately half way between the camshaft and the modulating piston, the motion of the secondary cam is transferred directly to the modulating piston, thus varying the valve motion. Secondary rocker ratio is defined here as the ratio of the displacement of the modulating piston to the displacement of the secondary cam. In this design the ratio could be continuously varied from 0.0 to 1.5. By careful design of the profile of the secondary cam, a useful range of variable valve motions is possible. Figure 3 shows examples of variable valve timing, rate and lift that could be achieved by different secondary cams applied to this mechanism. In all cases, the valve motion is given by the upper curve and is achieved by the addition of the motions of the primary and secondary cams. The device which forms the subject of this paper, produces the motion shown in figure 3c.

EXPERIMENTAL RIG AND INSTRUMENTATION

The experimental rig for the study of energy transfer through exhaust valves is shown in figure 4. The rig consists of a cylinder head and constant volume 'cylinder'. The valves in the cylinder head are operated by a motor driven camshaft. The inlet valve gear is conventional whilst the exhaust valve is equipped with the mechanism described above. The variation of exhaust valve motion is achieved by moving the pivot using a lead screw which is operated manually.

Compressed air is fed to the rig at absolute pressures of up to 6 bars, in order to represent conditions in the cylinder at the point of exhaust valve opening in a turbocharged engine (cracking pressure). The 'cylinder' volume was chosen to represent the engine cylinder volume at bottom dead centre since the object of the study was to examine the exhaust blowdown process and its relationship to rate of exhaust valve opening. The air flow rate is measured by an orifice plate located upstream of a smoothing tank. An 18kW electrical heater is also placed in the flow in order to prevent icing of the exhaust duct and to allow the inlet temperature to be controlled. The exhaust pipe test section is 1.2m in length, having an inside diameter of 40mm. At the downstream end of the exhaust pipe is an orifice plate behind which is located a plenum and an exhaust silencer. The orifice plate diameter was chosen to represent the properties of a turbocharger turbine of the size that would be used on this size of engine. Basic data is given in Appendix A.

The instrumentation consisted of two pressure transducers in the exhaust manifold, immediately after the port and before the orifice, a pressure transducer in the cylinder and a variable reluctance valve lift transducer on the exhaust valve. These measurements were used to study the development of exhaust pulses during blowdown. The performance of the variable valve motion mechanism was studied using the valve lift data and the hydraulic pressure measurement taken from a pressure transducer located in the hydraulic volume.

The measurements were taken by a high-speed data acquisition system controlled by an IBM AT microcomputer. Triggering was controlled by an optical shaft encoder at intervals equivalent to 0.2 degrees of camshaft rotation.

EXPERIMENTAL RESULTS

The inertia forces and contact stresses in valve-gear vary as the square of camshaft speed. Thus conventional valve-gear is designed to operate at a suitable margin of 'overspeed'. Under part speed operation the valve gear is, therefore, extremely lightly loaded and scope exists to open the valves more rapidly. Bearing in mind the difficulties of providing turbocharged engines with boost at low speeds, a device that can keep the rate of valve opening constant across the speed range, thereby fully exploiting the design strength, should be of benefit since it has been known for many years (12) that exhaust valves should be opened rapidly to maximise exhaust pulse energy.

The schedule of variation of the device was based on maintaining the rate of valve opening constant from the minimum engine speed of 1000 rev/min up to the maximum engine speed of 2200 rev/min.

Figure 5 shows the valve lift measured at an equivalent engine speed of 1000 rev/min, for secondary rocker ratios of 0.0 to 1.5. The figure shows that as the rocker ratio is progressively increased the rate of valve opening increases as expected. For the lowest ratios presented, 0.17 and 0.39, the valve motion departs very little from the motion

achieved with no input from the secondary cam, shown as a solid curve. At the highest rocker ratio of 1.5 the initial rate of valve opening is very rapid until 70% of the full lift when evidence of valve oscillation appears. The oscillation lasts for 4 or 5 cycles before being damped out at the start of the closing phase. Soon after the start of the closing evidence at 80% lift the family of curves oscillapses to follow the primary cam profile under the action of the valve spring. At present, the precise cause of the oscillation at the highest rocker ratio is not known with certainty; however, it is thought to be due either to hydraulic compressibility or to separation between the secondary rocker and the pivot.

Figure 6 shows the pressure in the hydraulic fluid at an equivalent engine speed of 1000 rev/min, for rocker ratios of 0.0 and 1.5. When the primary cam alone operates the valve the pressure builds up rapidly from 6 to 11 bars before peaking at 13 bars, the curve exhibiting very little oscillation. When the rocker ratio is 1.5 and both cams operate the valve the pressure in the hydraulic fluid rises rapidly from 3.5 to 17 bars before oscillating violently at a frequency of about 180Hz. Not surprisingly the oscillations of the valve displacement have the same frequency as the pressure oscillations.

The effects of the higher rate of valve opening on the form of the exhaust pulse are shown in figure 7(a). The pressure is shown to rise very rapidly for the higher rate of valve opening, from the atmospheric pressure of 1 bar to a peak of 1.45 bars after 18 deg of crank angle. With the standard rate of valve opening the pulse rises at a lower rate, reaching a peak of 1.30 bars after 37 degs. This result corresponds closely with the effects predicted by the senior author using a computer simulation of a turbocharged diesel engine having variable rate of exhaust valve opening (10).

Figure 7(b) shows the marked improvement in exhaust turbine energy across the engine speed range achieved by using a higher rate of valve opening at lower speeds. At 1000 rev/min the turbine power is increased from 2.4 to 3.7 kW which would be expected to lead to an increase of turbocharger speed and boost. As engine speed is increased the secondary rocker ratio is progressively reduced to maintain acceptable inertia stresses in the system, and at 2200 rev/min only the standard rate of opening is permissible. Figure 7(b) was based on a constant cracking pressure of 6 bars and single cylinder operation. The energy calculation used was that described by Woods and Benson (13) based on the power developed by a hypothetical isentropic turbine at the exhaust nozzle.

The effect of cylinder pressure at the point of exhaust valve opening on the pressure in the hydraulic space is shown in figure 8. These curves were produced at the highest engine speed of 2200 rev/min when the motion was due to the primary cam only. As may be expected, the early part of the opening phase is most significantly affected by the cracking pressure. The first peak in the pressure curve reaches 11.9, 14.4 and 17.5 bars for cracking pressures of 2,4 and 6 bars respectively. At 2200 rev/min the hydraulic pressure curves shown in figure 8 show violent high frequency oscillations particularly towards the end of the valve open period. It should be noted that the pressure is at all times greater than atmospheric pressure, hence cavitation would not be expected.

DISCUSSION

Preliminary results from a novel variable valve motion mechanism have been presented. Whilst these show the presence of undesirable dynamic effects in the form of oscillation of the valve and hydraulic pressure, the feasibility of the concept has largely been demonstrated. Further development of the device will investigate the benefits of reducing the volume of hydraulic fluid and reducing the mass of the three pistons. This is expected to improve the dynamic behaviour and smooth out the motion of the valve.

Estimates of the power consumption of the device are extremely encouraging. Since the oil is effectively only being compressed, in order to transmit the forces, with only a small amount of flow, the fluid friction losses are likely to be insignificant compared with the potential gains in engine performance. During tests on the experimental rig the temperature rise of the trapped oil was approximately 10°C in 10-15 minutes, with very little make-up flow.

In the near future it is proposed to replace the secondary cam and variable rocker by an electromechanical actuator such as a solenoid or magnetostrictive device, as shown in figure 9. Such a system, in which the greater part of the valve motion is provided by an engine driven cam with only the modulation provided electrically, could be extremely attractive for production engines. A useful range of variation could be provided by an electromechanical actuator either acting directly, or through a linkage to magnify the motion. In the system described here the stroke of the modulating piston was only 4.5 mm and this could readily have been reduced by increasing the piston area. It is hoped that the successful implementation of such a system will allow a wide range of valve motions controlled from software in response to engine operating condition.

ACKNOWLEDGEMENTS

The authors wish to acknowledge the support of the Ford Motor Company Limited for providing the cylinder head, associated valvegear and design data.

APPENDIX A - Basic Data

Cylinder volume	1.0ℓ
Cylinder diameter	105.0mm
Exhaust valve diameter	35mm
Primary cam lift	7.874mm
Secondary cam lift	3.010mm
Primary rocker ratio	1.4
Secondary rocker ratio	0-1.5:1
Volume of hydraulic fluid	80 cm^3
Oil supply pressure	2.5-3.0 bar

REFERENCES

1) KERR, J. 'Variable Valve Timing to Boost any Engine', The Engineer, pp28-29, 54:3,July 1980.
2) PARKER, D.A. and KENDRICK, M.A. 'A Camshaft with Variable Lift-Rotation Characteristics, Theoretical Properties and Application to the Valve Gear of a Multi-Cylinder Piston Engine', Paper B-1-11, pp224-232, 15th FISITA Congress 1974.
3) TORAZZA, G., 'A Variable Lift and Event Control Device for Piston Engine Valve Operation', Paper 2/10, pp 59-67, 14th FISITA Congress 1972.
4) ZAPPA, G. and FRANCA, T., 'A Four-Stroke, High-Speed Diesel Engine with Two-Stage Supercharging and Variable Compression Ratio', Session B3,Paper D-19, 13th CIMAC Congress, Vienna, 1979.
5) HERRIN, R.J. and POZNIAK, D.J. 'A Lost Motion Variable Valve Timing System for Automotive Piston Engines', SAE Paper 840335, 1984.
6) MEACHAM, G.B.K., 'Variable Cam Timing as an Emission Control Tool', SAE Paper 730673, 1973.
7) TITOLO, A., 'Variable Valve Control from FIAT', MTZ Journal pp 185-188, 1986.
8) RICHMAN, R.M. and REYNOLDS, N.C., 'A Computer Controlled Poppet Valve Actuator for Application on Research Engines', SAE Paper 840340, 1984.
9) CHARLTON, S.J. and SHAFIE-POUR, M., 'A Continuously Variable Poppet Valve Actuator for IC Engines', Proc.IMechE, Vol 200, No.A3, 1986.
10) CHARLTON, S.J. and PAPPAS, P., 'A Parametric Study of the Exhaust Valve Requirements of High Output Truck Engines', SAE Paper 850243, Feb.1985.
11) SHAFIE-POUR, M., 'Experimental Investigation of Exhaust Valve Energy Transfer using Variable Valve Motion', Ph.D Thesis, University of Bath, 1988.
12) JENNY, E., 'Utilization of Exhaust Gas Energy in the Supercharging of the Four-Stroke Diesel Engine'Brown Boveri Review, 37(1) 1950.
13) BENSON, R.S. and WOODS, W.A. 'The Energy Content of Exhaust Pulses in the Exhaust System of a Supercharged Two-stroke-engine Model', Int.J.Mech.Sci., Vol 2,pp231-250, Mar.1960.

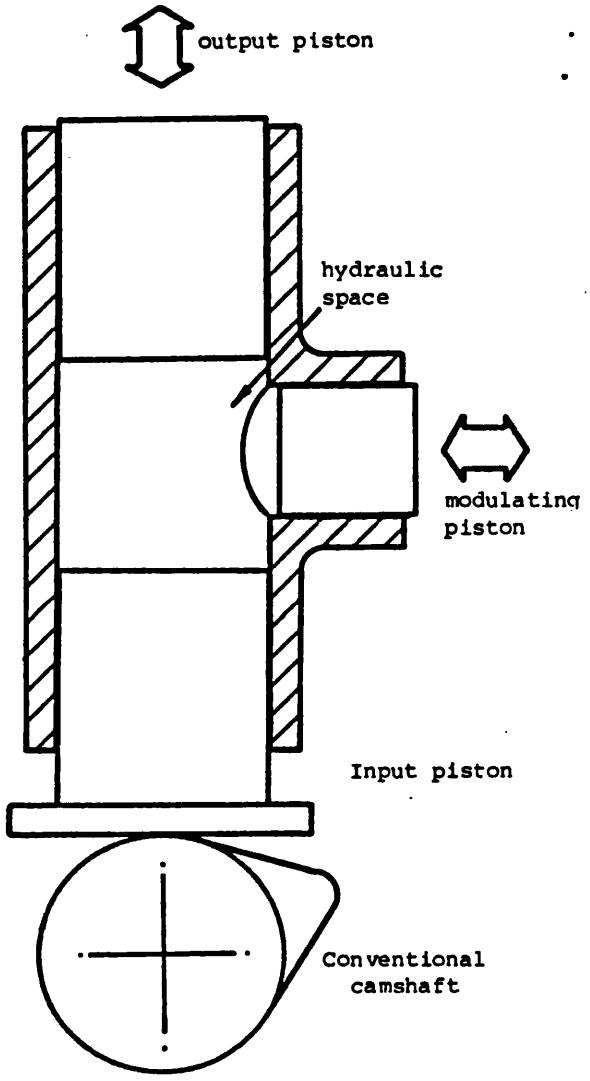

Figure 1, Schematic diagram of the hydraulic variable valve motion concept.

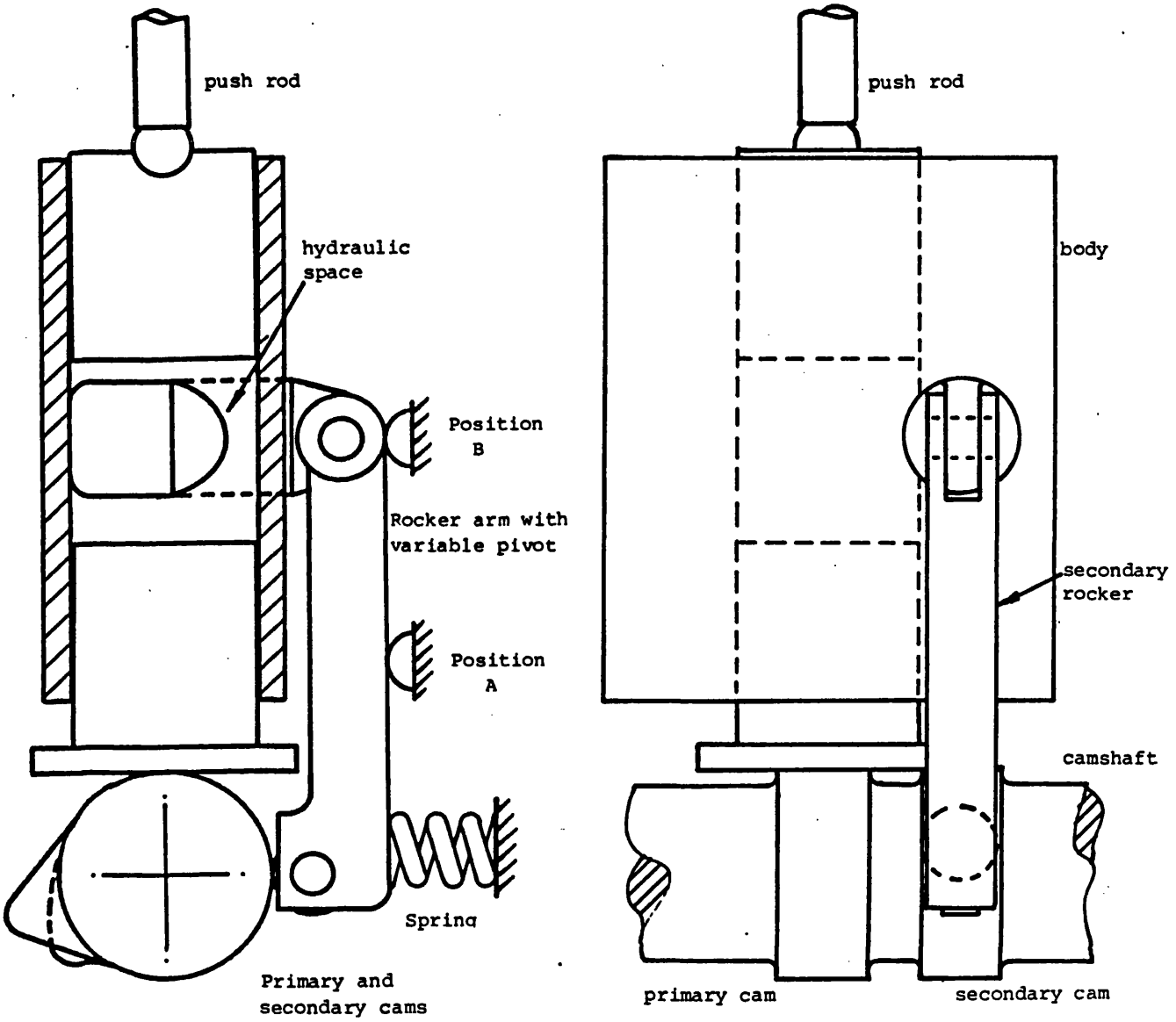

Figure 2, Sectional view of the variable rate mechanism used for the study of exhaust pulse energy.

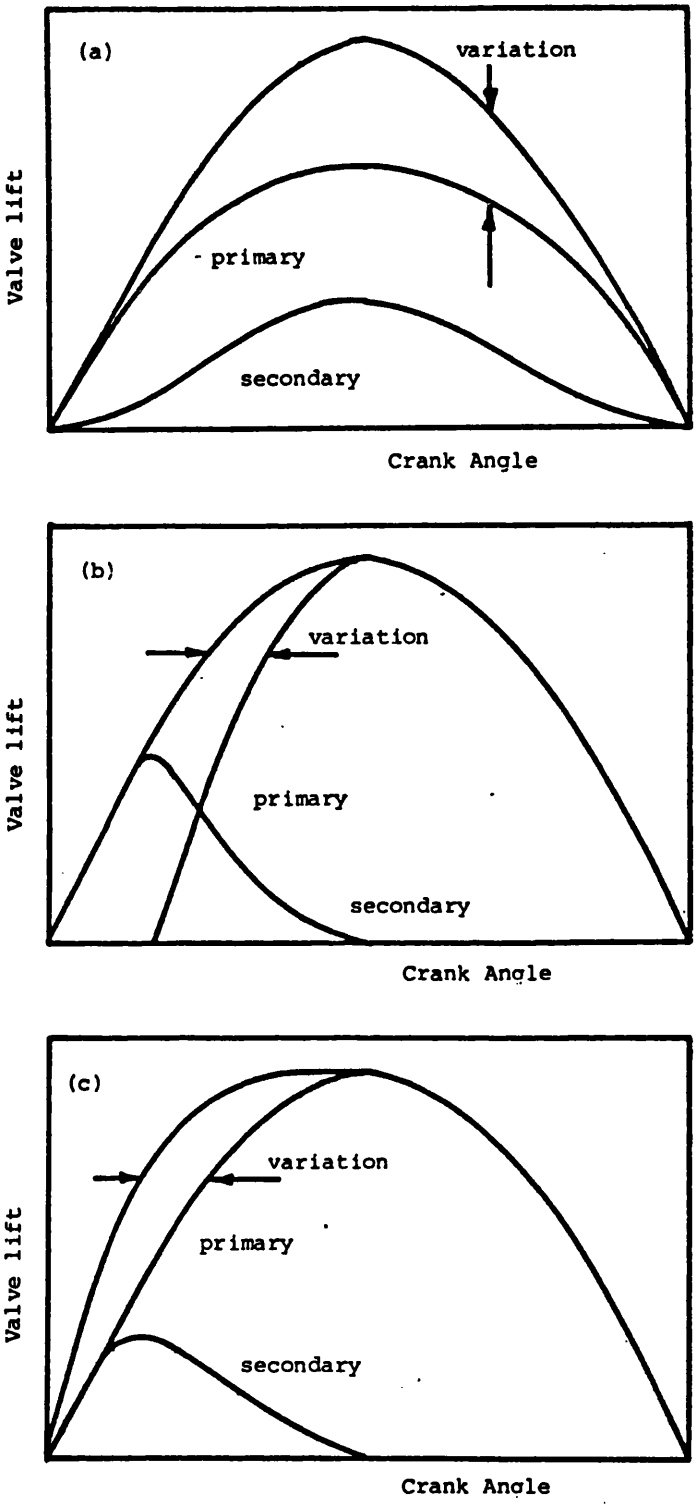

Figure 3, Valve lift curves that may be generated by the device (a) Variable lift (b) Variable timing and (c) Variable rate of opening.

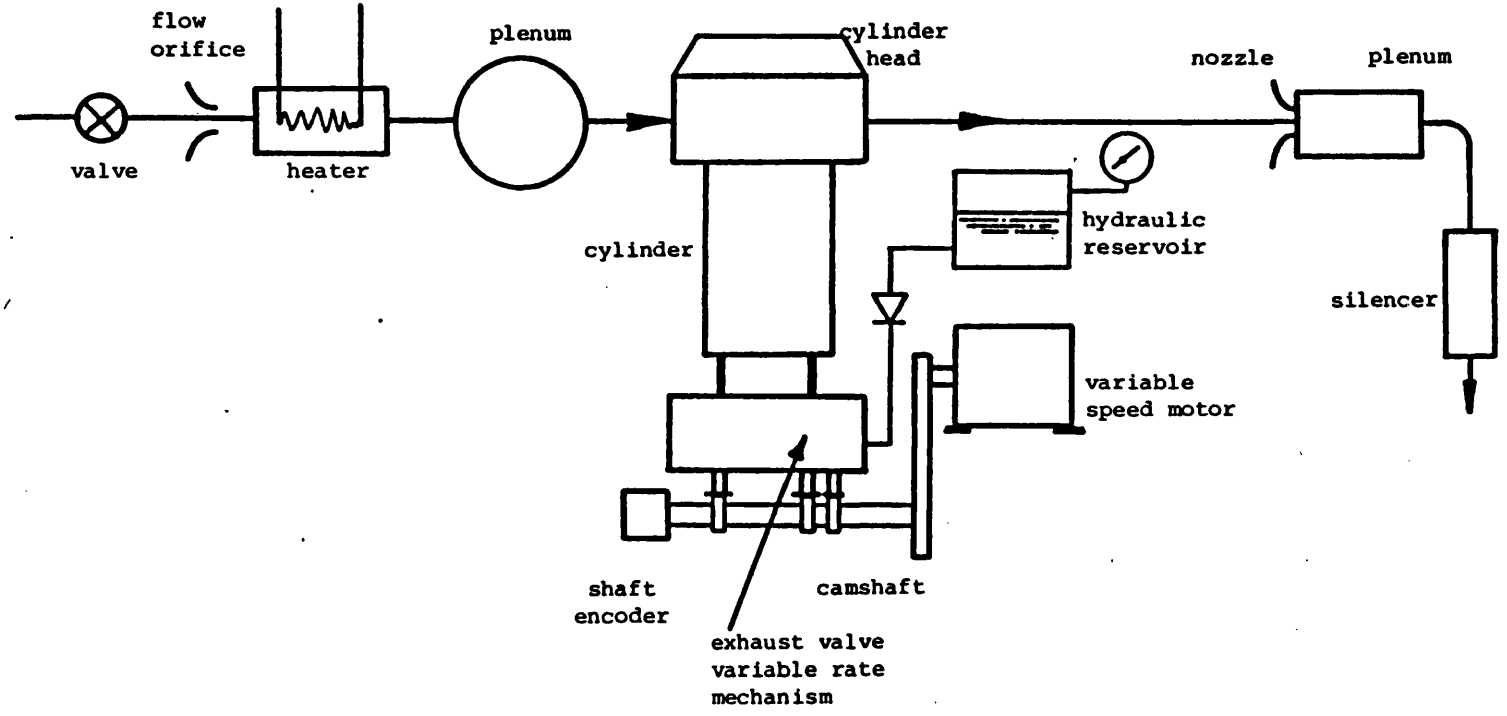

Figure 4, Schematic view of the experimental rig used to study the relationship between rate of exhaust valve opening and pulse energy.

880603

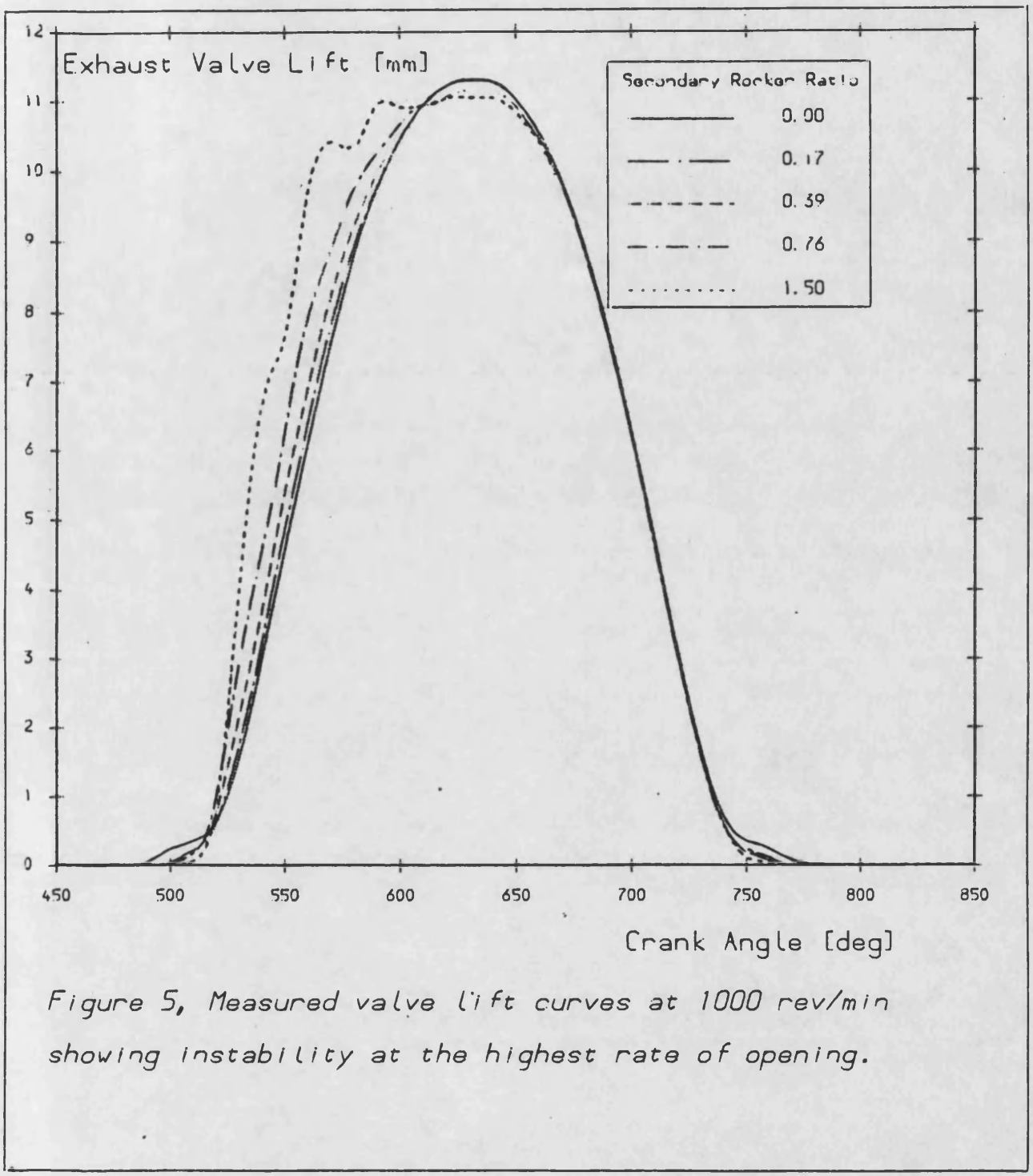

Figure 5, Measured valve lift curves at 1000 rev/min showing instability at the highest rate of opening.

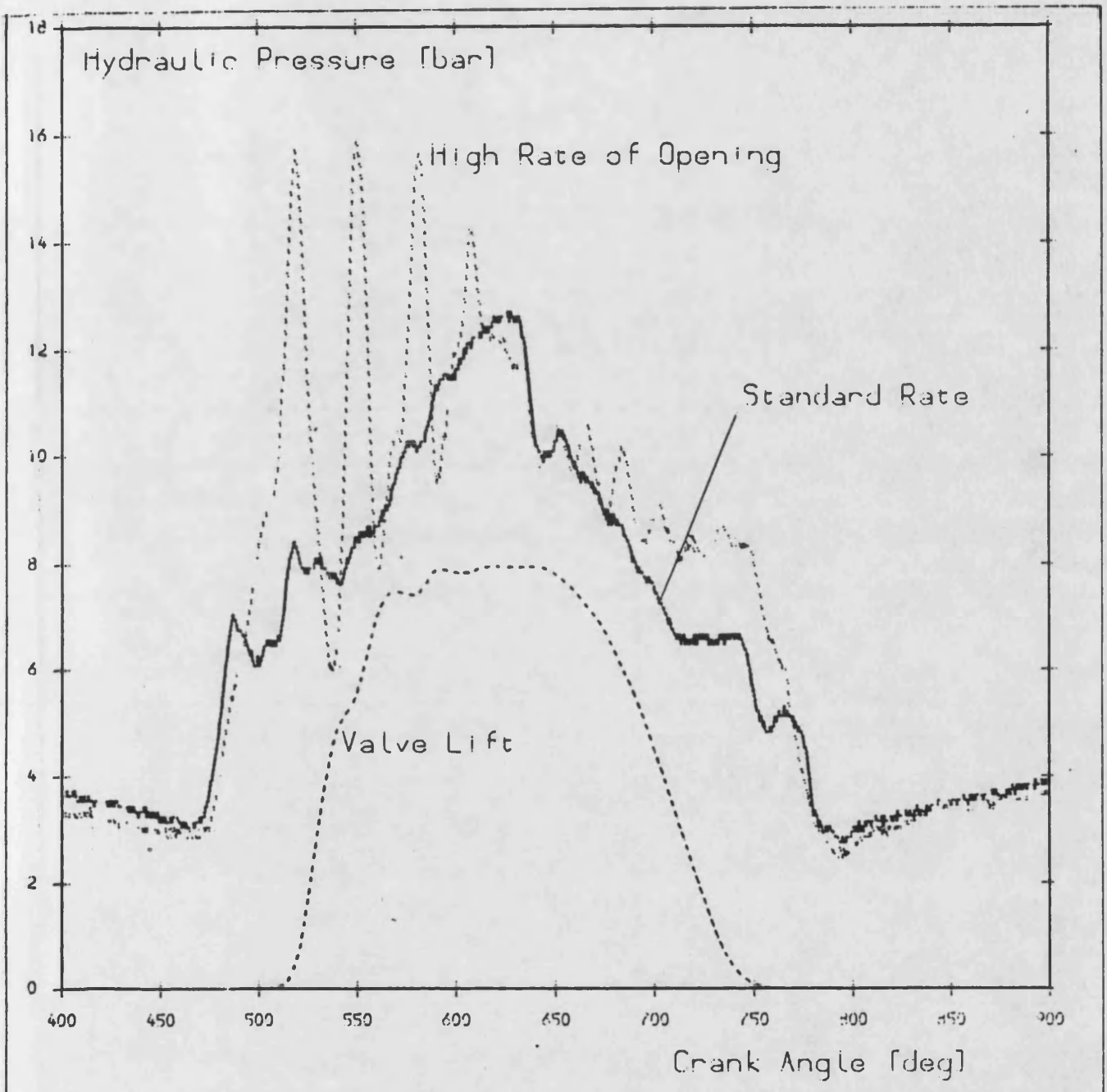

Figure 6, Upper curves show variation of hydraulic pressure for the highest rate and standard rate at 1000 rev/min. Valve lift shown for high rate case

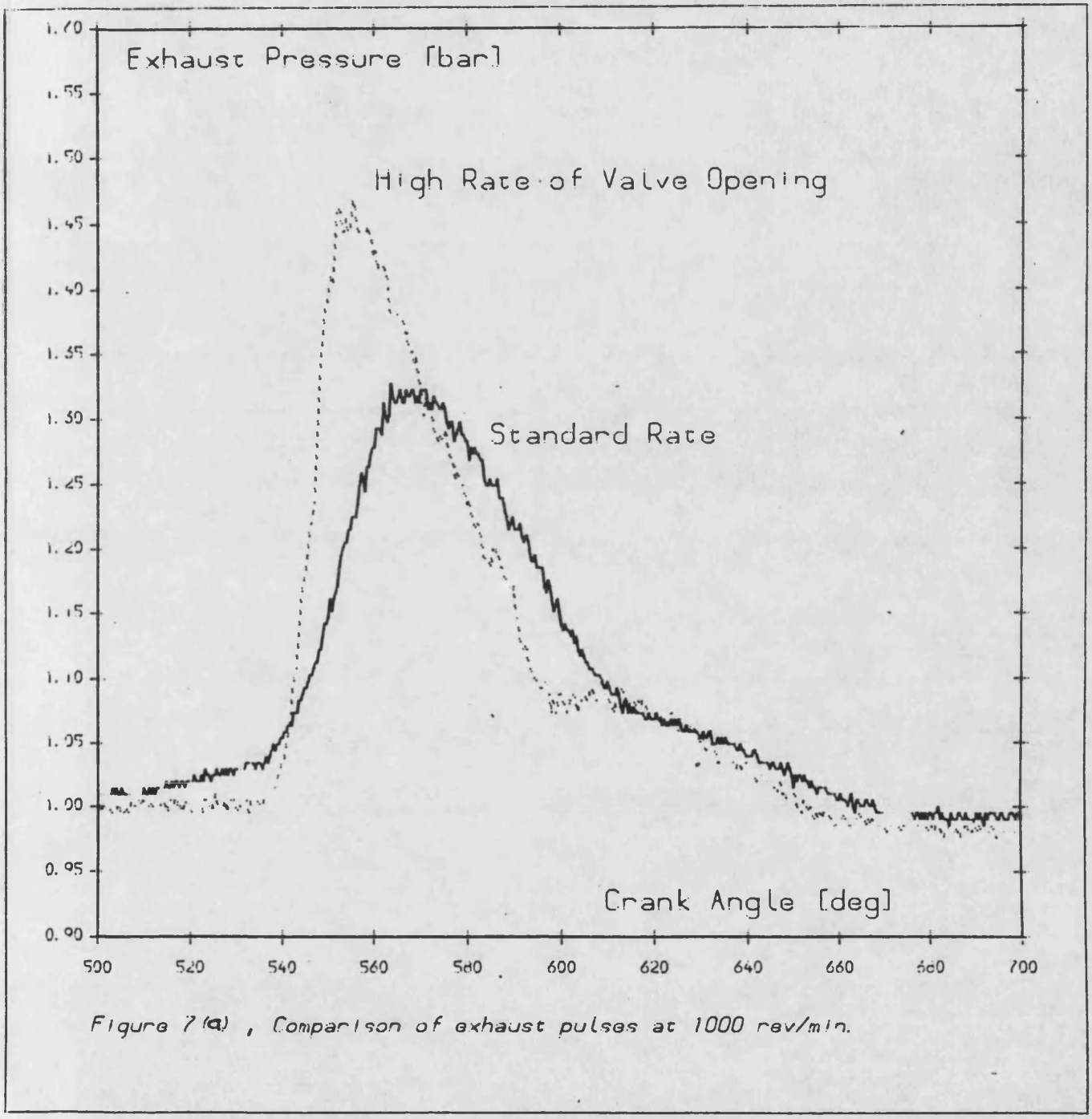

Figure 7(a) , Comparison of exhaust pulses at 1000 rev/min.

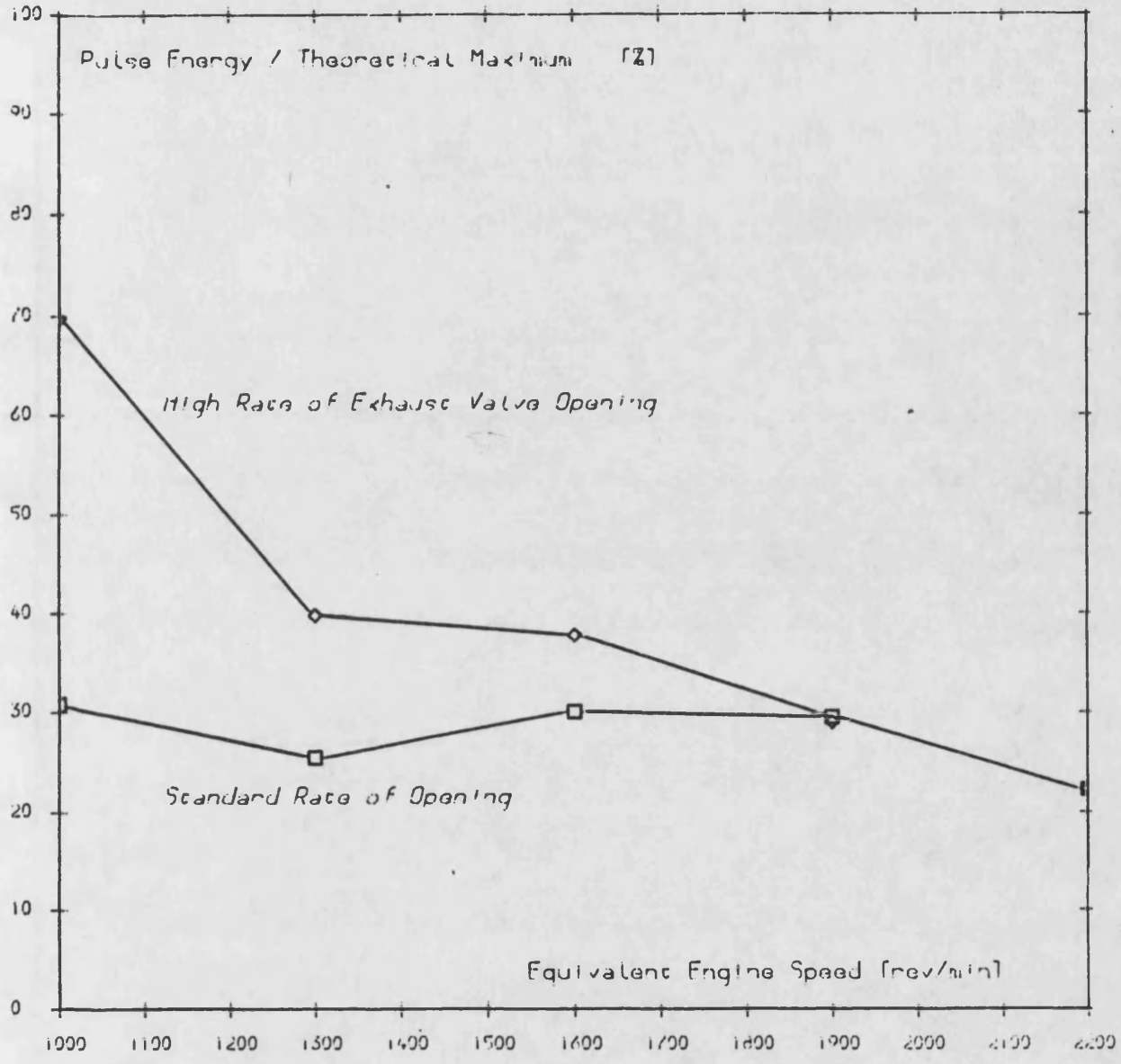

Figure 7(b)

Improvement in pulse energy utilisation due to a higher higher rate of exhaust valve opening at low engine speeds.

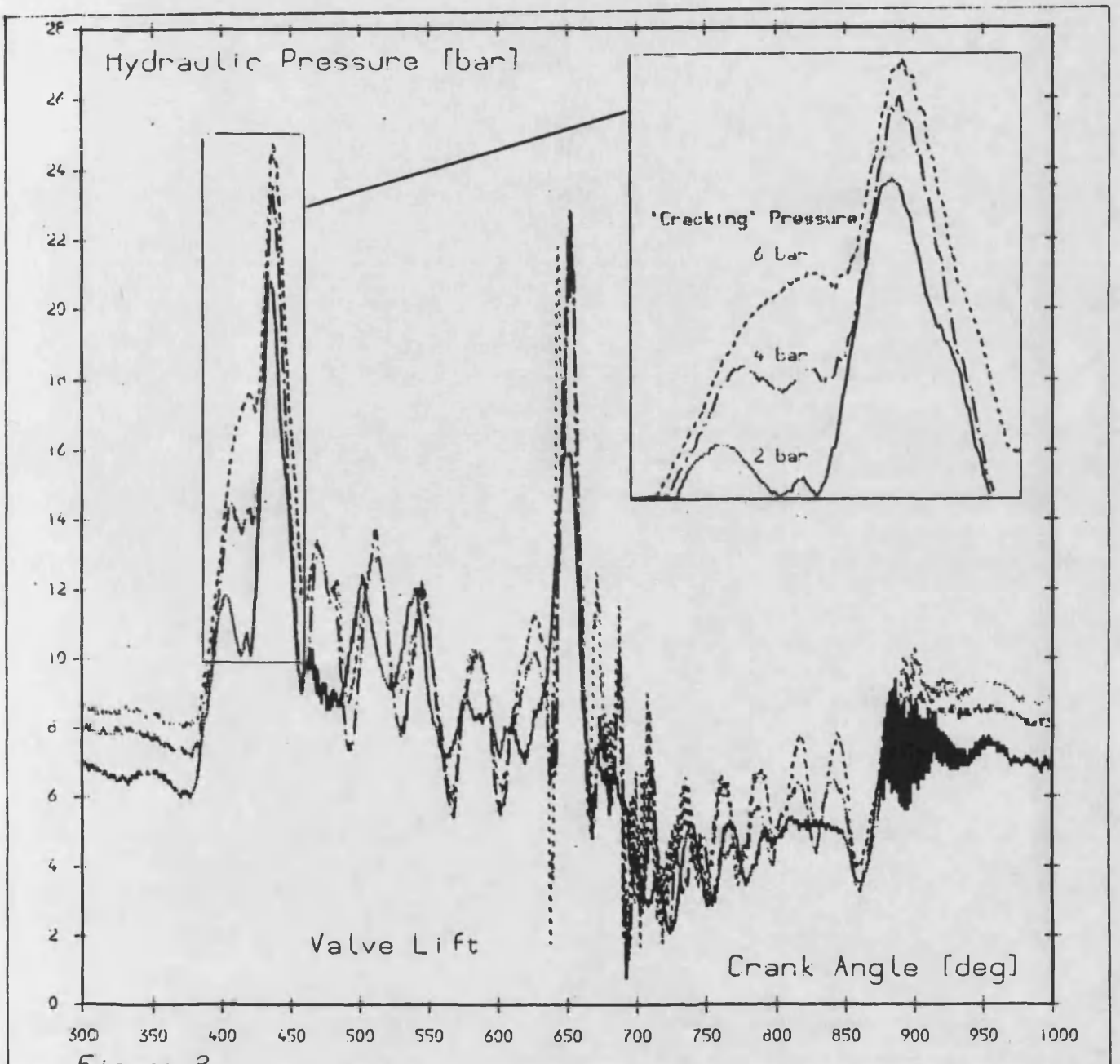

Figure 8,
Variation of hydraulic pressure with 'cracking' pressure at 2200 rev/min, showing the extra load at evo due to gas forces on the valve head.

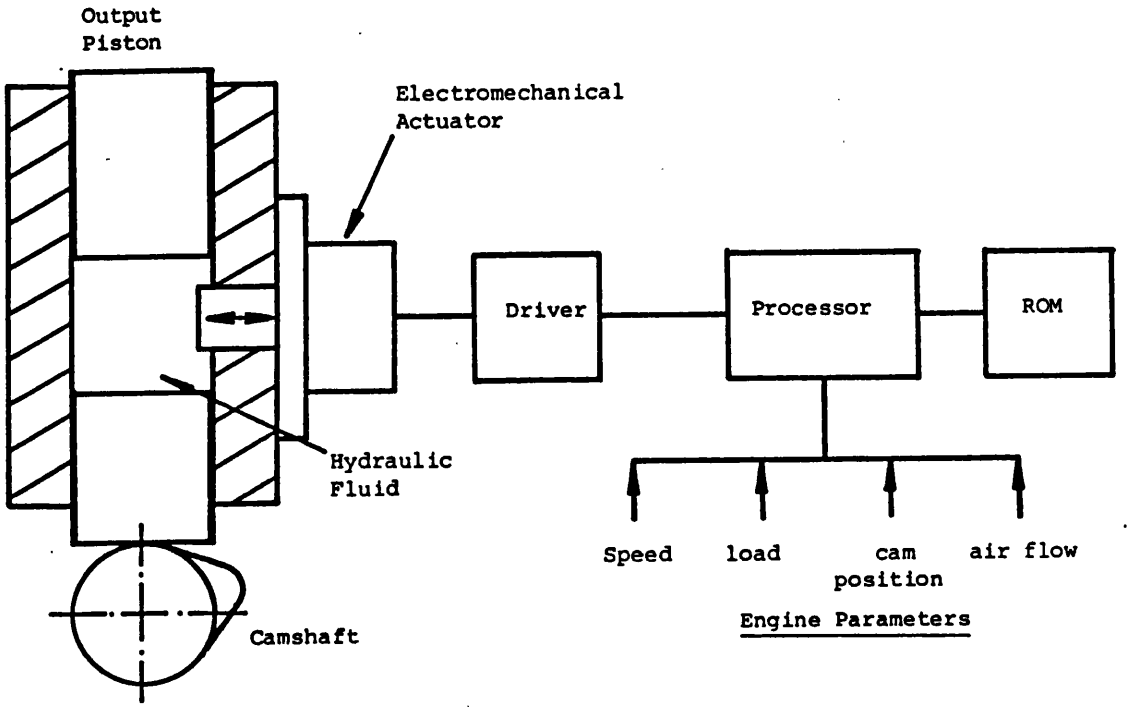

Figure 9, Proposed hybrid cam-electromechanical system.

APPENDIX 11

Computer programs.

```
CEEE
```

```
C*************************************************************************
C***** MAJ3.FOR **** A PROGRAM TO CONVERT A POLYNOMIAL CAM PROFILE ***********
C*************** INTO A SET OF LOAD STEPS FOR INPUT TO 'ANSYS' ***************
C************** INCORPORATING EXHAUST GAS FORCES FOLLOWING AN ****************
C************************ EXPONENTIAL DECAY FUNCTION *************************
C***** 14TH,JUNE 1985 ***************************************************
C************************ CONSTANTS ***************************************
      REAL L1,L2,L3
      A=2.
      B=9.
      C=12.
      D=30.
C*************************"VARYING ENGINE SPEED" ***************************
C******************** CONVENTIONAL VALVE TRAIN [C.V.T]************************
C***************************** 1000 RPM C.V.T *******************************
      WRITE(6,*)' WHAT ENGINE SPEED?'
      READ(5,*)N
C******* N:ENGINE SPEED ******
      IF(N.EQ.100) THEN
                   M=57
                   FIOGAS=932.0
                   RK=-0.17093
      END IF
C***************************** 1300 RPM C.V.T *******************************
      IF(N.EQ.130) THEN
                   M=57
                   FIOGAS=911.06
                   RK=-0.17036
      END IF
C***************************** 1600 RPM C.V.T *******************************
      IF(N.EQ.160) THEN
                   M=57
                   FIOGAS=921.53
                   RK=-0.17065
      END IF
C***************************** 1900 RPM C.V.T *******************************
      IF(N.EQ.190) THEN
                   M=57
                   FIOGAS=905.82
                   RK=-0.17022
      END IF
C***************************** 2200 RPM C.V.T *******************************
      IF(N.EQ.220) THEN
                   M=57
                   FIOGAS=863.93
                   RK=-0.16903
      END IF
C*************************************************************************
C*********** CONTINUOSLY VARIABLE VALVE TRAIN [C.V.V.T] ********************
C***************************** 1000 RPM C.V.V.T *****************************
      IF(N.EQ.1000) THEN
                    M=37
                    FIOGAS=1093.20
                    RK=-0.34984
      END IF
C***************************** 1300 RPM C.V.V.T *****************************
      IF(N.EQ.1300) THEN
                    M=47
                    FIOGAS=1043.00
                    RK=-0.23166
      END IF
C***************************** 1600 RPM C.V.V.T *****************************
      IF(N.EQ.1600) THEN
                    M=57
                    FIOGAS=1011.60
                    RK=-0.17298
      END IF
C***************************** 1900 RPM C.V.V.T *****************************
      IF(N.EQ.1900) THEN
                    M=67
                    FIOGAS=967.60
                    RK=-0.13749
      END IF
C***************************** 2200 RPM C.V.V.T *****************************
      IF(N.EQ.2200) THEN
                    M=77
                    FIOGAS=917.30
                    RK=-0.11369
      END IF
C*************************************************************************
C*************************************************************************
C*************EXPONENTIAL DECAY OF EXHAUST GASES*****************************
      DO 190 I=1,16,1
  190 WRITE(10,105)FLOAT(I),L1/1000.

      DO 200 I=17,M,1
      FORCE=FIOGAS*EXP(RK*(FLOAT(I)  7))
      IF(I.GT.M) FORCE=FORCE-1.0
  200 WRITE(10,101)FLOAT(I),L1/1000.0,L3/1000.0,FORCE

C*************************************************************************
C***** CONSTANT VELOCITY RAMP ********************************************
```

```
        L1=.1702+.02*(FLOAT(I)-17)
        L3=0.
  110   WRITE(10,101)FLOAT(I),L1/1000.,L3/1000.0,FORCE
C*************************************************************************
C*********************QUARTER DEGREE CAM ANGLE (63/252)*********************
        DO 100 I=252,213,-1
        X1=FLOAT(I)/252.
        X2=(FLOAT(I)-137.454545)/114.545454
        IF(I.EQ.252) THEN
           X1=1.
           X2=1.
        END IF

        L1=7.874-10.79568*(X1)**A+5.693371*(X1)**B-2.351986*(X1)**C
     1       -0.08950479*(X1)**D

        IF(X2.LE.1.00.AND.X2.GT.0) THEN
        L2=7.874-10.79568*(X2)**A+5.693371*(X2)**B-2.351986*(X2)**C
     1       -0.08950479*(X2)**D
        END IF

C***** FULLY OPEN **********
        IF(X2.LE.0) L2=7.874
C***** L1 REQUIRED FROM SECONDARY CAM *******
        L3=L2-L1

        WRITE(10,101)25+ABS((FLOAT(I)-252)/4.),L1/1000.,L3/1000.,FORCE
  101   FORMAT(' ITER,2,1 $TIME,S.',F6.2,' $D,2,UY,',F12.10,
     1         ' $D,18,UX,',F12.10,/,' F,14,FY,',F7.2,' $LWRITE')
  105   FORMAT(' ITER,2,1 $TIME,S.',F5.1,' $D,2,UY,',F12.10,' $LWRITE')
        WRITE(6,*)I,X,L1
  100   CONTINUE
        DO 120 I=53,0,-1
        X1=FLOAT(I)/63.
        X2=(FLOAT(I)-34.363636)/28.636363
        IF(I.EQ.63) THEN
           X1=1.
           X2=1.
        END IF

        L1=7.874-10.79568*(X1)**A+5.693371*(X1)**B-2.351986*(X1)**C
     1       -0.08950479*(X1)**D

        IF(X2.LE.1.00.AND.X2.GT.0) THEN
        L2=7.874-10.79568*(X2)**A+5.693371*(X2)**B-2.351986*(X2)**C
     1       -0.08950479*(X2)**D
        END IF

C***** FULLY OPEN **********
        IF(X2.LE.0) L2=7.874
C***** L1 REQUIRED FROM SECONDARY CAM *******
        L3=L2-L1

        WRITE(10,101)25+ABS(FLOAT(I)-63),L1/1000.,L3/1000.,FORCE
  120   CONTINUE

C*************************************************************************
        DO 104 I=1,63
        X=FLOAT(I)/63.
        L1=7.874-10.79568*(X)**A+5.693371*(X)**B-2.351986*(X)**C
     1       -0.08950479*(X)**D
        WRITE(6,*)I,X,L1
  104   CONTINUE

C*************************************************************************
C***** CONSTANT VELOCITY RAMP ********************************************
        DO 130 I=152,159
        L1=.3302-.02*(FLOAT(I)-151)
  130   WRITE(10,105)FLOAT(I),L1/1000.
C*************************************************************************
        DO 300 I=160,175,1
  300   WRITE(10,105)FLOAT(I),L1/1000.0
C*************************************************************************
        DO 400 I=176,221,5
  400   WRITE(10,105)FLOAT(I),L1/1000.
C*************************************************************************

        STOP
        END
```

```
C*************************
C******* MAND.FOR ***** A FORTRAN PROGRAMME TO GENERATE LOAD STEPS*************
C********************** AS INPUTS TO "ANSYS"FOR VARIABLE TIMING ***************
C********************** VALVE ACTUATION CONFIGUERATION ************************
C****** 25TH,JUNE,1985 ***********************************************************
C*******************************************************************************
      DIMENSION RL(63),RL1(138),RL2(138),RL3(138)
      REAL L1
C*******************************************************************************
C******* INDECIS OF THE POLYNOMIAL*********************************************
C*******************************************************************************
      A=2.
      B=9.
      C=12.
      D=30.
C*******************************************************************************
C******* FIRST 16 VALUES OF RL1 & RL2 CAM LIFTS ********************************
C*******************************************************************************
C*******************************************************************************
      RL2(1)=0.0000270
      RL2(2)=0.0003300
      RL2(3)=0.0012580
      RL2(4)=0.0031390
      RL2(5)=0.0062660
      RL2(6)=0.0108660
      RL2(7)=0.0171950
      RL2(8)=0.0253250
      RL2(9)=0.0353440
      RL2(10)=0.0472510
      RL2(11)=0.0609780
      RL2(12)=0.0763890
      RL2(13)=0.0932900
      RL2(14)=0.1114310
      RL2(15)=0.1305190
      RL2(16)=0.1502250
      RL1(51)=RL2(1)
      RL1(52)=RL2(2)
      RL1(53)=RL2(3)
      RL1(54)=RL2(4)
      RL1(55)=RL2(5)
      RL1(56)=RL2(6)
      RL1(57)=RL2(7)
      RL1(58)=RL2(8)
      RL1(59)=RL2(9)
      RL1(60)=RL2(10)
      RL1(61)=RL2(11)
      RL1(62)=RL2(12)
      RL1(63)=RL2(13)
      RL1(64)=RL2(14)
      RL1(65)=RL2(15)
      RL1(66)=RL2(16)
C*******************************************************************************
C******* CONSTANT VELOCITY RAMP RL2 OPENING ************************************
C*******************************************************************************
      DO 90 I=17,24
      RL2(I)=.1702+.02*(FLOAT(I)-17)
      RL1(I)=0.
   90 CONTINUE
C*******************************************************************************
C******* POLYNOMIAL SECTION OF RL  OPENING *************************************
C*******************************************************************************
      DO 95 J=63,0,-1
      X2=(FLOAT(J)/63.)
      IF(J.EQ.63) THEN
         X2=1.
      END IF
      IF(X2.LE.1.0.AND.X2.GT.0.) THEN
      RL(J)=7.874-10.79568*(X2)**A+5.693071*(X2)**B-2.351986*(X2)**C
     1      -0.08950479*(X2)**D
      END IF

   95 CONTINUE
C*******************************************************************************
C******* POLYNOMIAL SECTION OF RL2 OPENING *************************************
C*******************************************************************************
      J=64
      DO 100 I=25,87
      J=J-1
      RL2(I)=RL(J)
  100 CONTINUE
C******* CONSTANT VELOCITY RAMP OF RL1 OPENING ********************************
C*******************************************************************************
      DO 120 I=67,74
      RL1(I)=.1702+.02*(FLOAT(I)-67)
  120 CONTINUE
C*******************************************************************************
C******* POLYNOMIAL SECTION OF RL1 OPENING *************************************
C*******************************************************************************
      J=64
      DO 130 I=75,138
      J=J-1
      RL1(I)=RL(J)
```

```
C******* RL2 DURATION OF DWELL
C*****************************************************************************
      DO 140 I=88,138
      RL2(I)=7.874
  140 CONTINUE
C*****************************************************************************
C******* RL3 i.e VG CAM PROFILE DETERMINED FORM RL2 & RL1 ********************
C*****************************************************************************
      DO 145 I=1,138
  145 RL3(I)=RL2(I)-RL1(I)
C*****************************************************************************
      DO 150 I=1,138
  150 WRITE(10,101)FLOAT(I),RL1(I)/1000.,RL3(I)/1000.
C*****************************************************************************
C******* POLYNOMIAL SECTION OF RL1 & RL2 CLOSING *****************************
C*****************************************************************************
      DO 104 I=1,63
      X=FLOAT(I)/63.
      L1=7.874-10.79568*(X)**A+5.693371*(X)**B-2.351986*(X)**C
     1         -0.08950479*(X)**D
      WRITE(10,105) 75+FLOAT(I)+63.,L1/1000.
      WRITE(6,*)I,X,L1
  104 CONTINUE
C*****************************************************************************
C******* CONSTANT VELOCITY RAMP CLOSING **************************************
C*****************************************************************************
      DO 160 I=202,209
      L1=0.3302-0.02*(FLOAT(I)-201)
  160 WRITE(10,105)FLOAT(I),L1/1000.
C*****************************************************************************
C******* FORMATS *************************************************************
C*****************************************************************************
  101 FORMAT(' ITER,2,1 $TIME,S.',F6.1,' $D,2,UY,',F12.10,
     1       ' $D,18,UX,',F12.10,' $LWRITE')
  105 FORMAT(' ITER,2,1 $TIME,S.',F6.1,' $D,2,UY,',F12.10,' $LWRITE')
      WRITE(6,*)I,X,L1
C*****************************************************************************
      DO 165 I=210,225
  165 WRITE(10,105)FLOAT(I),L1/1000.
C*****************************************************************************
      DO 170 I=226,251,5
  170 WRITE(10,105)FLOAT(I),L1/1000.
C*****************************************************************************
      STOP
      END
```

[EOB]

```
C*************************************************************************
C******* MAND.FOR ***** A FORTRAN PROGRAMME TO GENERATE LOAD STEPS*********
C********************** AS INPUTS TO "ANSYS"FOR VARIABLE TIMING **********
C********************** VALVE ACTUATION CONFIGUERATION **********************
C****** 25TH,JUNE,1985 ***************************************************
C*************************************************************************
      DIMENSION RL(63),RL1(  ),RL2(138),RL3(138),FORCE(17:77)
      REAL L1
C*************************************************************************
C******* INDECIS OF THE POLYNOMIAL*****************************************
C*************************************************************************
      A=2.
      B=9.
      C=12.
      D=30.
C*************************************************************************
C*********************"VARYING ENGINE SPEED"*******************************
C***************** CONTINUOSLY VARIABLE VALVE TRAIN [C.V.V.T] ***************
C*************************************************************************
      WRITE(6,*)' WHAT ENGINE SPEED?'
      READ(5,*)N
C******** N:ENGINE SPEED ***************************************************
C************************** 1000 RPM C.V.V.T ********************************
      IF(N.EQ.1000) THEN
                    M=37
                    FIOGAS=1093.20
                    RK=-0.34984
      END IF
C************************** 1300 RPM C.V.V.T ********************************
      IF(N.EQ.1300) THEN
                    M=47
                    FIOGAS=1043.00
                    RK=-0.23166
      END IF
C************************** 1600 RPM C.V.V.T ********************************
      IF(N.EQ.1600) THEN
                    M=57
                    FIOGAS=1011.60
                    RK=-0.17298
      END IF
C************************** 1900 RPM C.V.V.T ********************************
      IF(N.EQ.1900) THEN
                    M=67
                    FIOGAS=967.60
                    RK=-0.13749
      END IF
C************************** 2200 RPM C.V.V.T ********************************
      IF(N.EQ.2200) THEN
                    M=77
                    FIOGAS=917.30
                    RK=-0.11369
      END IF
C*************************************************************************
C************** EXPONENTIAL DECAY OF EXHAUST GASES ***************************
C*************************************************************************
      DO 80 I=17,M,1
      FORCE(I)=FIOGAS*EXP(RK*(FLOAT(I)-17))
   80 WRITE(10,101)FLOAT(I),RL1(I)/1000.,RL3(I)/1000.,FORCE(I)
C*************************************************************************
C******* FIRST 16 VALUES OF RL1 & RL2 CAM LIFTS ****************************
C*************************************************************************
      RL2(1)=0.0000270
      RL2(2)=0.0003300
      RL2(3)=0.0012580
      RL2(4)=0.0031390
      RL2(5)=0.0062660
      RL2(6)=0.0108660
      RL2(7)=0.0171950
      RL2(8)=0.0253250
      RL2(9)=0.0353440
      RL2(10)=0.0472510
      RL2(11)=0.0609780
      RL2(12)=0.0763890
      RL2(13)=0.0932900
      RL2(14)=0.1114310
      RL2(15)=0.1305190
      RL2(16)=0.1502250
      RL1(51)=RL2(1)
      RL1(52)=RL2(2)
      RL1(53)=RL2(3)
      RL1(54)=RL2(4)
      RL1(55)=RL2(5)
      RL1(56)=RL2(6)
      RL1(57)=RL2(7)
      RL1(58)=RL2(8)
      RL1(59)=RL2(9)
      RL1(60)=RL2(10)
      RL1(61)=RL2(11)
      RL1(62)=RL2(12)
      RL1(63)=RL2(13)
      RL1(64)=RL2(14)
```

```
        RL1(66)=RL2(16)
C*************************************************************************
C******* CONSTANT VELOCITY RAMP RL2 OPENING ******************************
C*************************************************************************
        DO 90 I=17,24
        RL2(I)=.1702+.02*(FLOAT(I)-17)
        RL1(I)=0.
   90   CONTINUE
C*************************************************************************
C******* POLYNOMIAL SECTION OF RL  OPENING ********************************
C*************************************************************************
        DO 95 J=63,0,-1
        X2=(FLOAT(J)/63.)
        IF(J.EQ.63) THEN
           X2=1.
        END IF
        IF(X2.LE.1.0.AND.X2.GT.0.) THEN
        RL(J)=7.874-10.79568*(X2)**A+5.693371*(X2)**B-2.351986*(X2)**C
     1        -0.08950479*(X2)**D
        END IF

   95   CONTINUE
C*************************************************************************
C******* POLYNOMIAL SECTION OF RL2 OPENING ********************************
C*************************************************************************
        J=64
        DO 100 I=25,87
        J=J-1
        RL2(I)=RL(J)
  100   CONTINUE
C******* CONSTANT VELOCITY RAMP OF RL1 OPENING ***************************
C*************************************************************************
        DO 120 I=67,74
        RL1(I)=.1702+.02*(FLOAT(I)-67)
  120   CONTINUE
C*************************************************************************
C******* POLYNOMIAL SECTION OF RL1 OPENING ********************************
C*************************************************************************
        J=64
        DO 130 I=75,138
        J=J-1
        RL1(I)=RL(J)
  130   CONTINUE
C*************************************************************************
C******* RL2 DURATION OF DWELL ********************************************
C*************************************************************************
        DO 140 I=88,138
        RL2(I)=7.874
  140   CONTINUE
C*************************************************************************
C******* RL3 i.e VG CAM PROFILE DETERMINED FORM RL2 & RL1 *****************
C*************************************************************************
        DO 145 I=1,138
  145   RL3(I)=RL2(I)-RL1(I)
C*************************************************************************
        DO 150 I=1,138
  150   WRITE(10,101)FLOAT(I),RL1(I)/1000.,RL3(I)/1000.,FORCE(I)
C*************************************************************************
C******* POLYNOMIAL SECTION OF RL1 & RL2 CLOSING **************************
C*************************************************************************
        DO 104 I=1,63
        X=FLOAT(I)/63.
        L1=7.874-10.79568*(X)**A+5.693371*(X)**B-2.351986*(X)**C
     1          -0.08950479*(X)**D
        WRITE(10,105) 75+FLOAT(I)+63.,L1/1000.
        WRITE(6,*)I,X,L1
  104   CONTINUE
C*************************************************************************
C******* CONSTANT VELOCITY RAMP CLOSING ***********************************
C*************************************************************************
        DO 160 I=202,209
      . L1=0.3302-0.02*(FLOAT(I)-201)
  160   WRITE(10,105)FLOAT(I),L1/1000.
C*************************************************************************
C******* FORMATS **********************************************************
C*************************************************************************
  101   FORMAT(' ITER,2,1 $TIME,S.',F6.1,' $D,2,UY,',F12.10,
     1         ' $D,18,UX,',F12.10,/,' F,14,FY,',F7.2,' $LWRITE')
  105   FORMAT(' ITER,2,1 $TIME,S.',F6.1,' $D,2,UY,',F12.10,' $LWRITE')
        WRITE(6,*)I,X,L1
C*************************************************************************
        DO 165 I=210,225
  165   WRITE(10,105)FLOAT(I),L1/1000.
C*************************************************************************
C*************************************************************************
        DO 165 I=210,225
  165   WRITE(10,105)FLOAT(I),L1/1000.
C*************************************************************************
        DO 170 I=226,251,5
  170   WRITE(10,105)FLOAT(I),L1/1000.
C*************************************************************************
        STOP
        END
```

```
C*************************************************************************
C***** RED.FOR *** A PROGRAMME TO GENERATE CAM PROFILE D-R-D ***************
C********** WITH A STRATEGIC VIEW TO REDUCTION OF CRITICAL FORCES **********
C***** 15TH,JULY,1985 ****************************************************
C***** CONSTANTS **********************************************************
      REAL L
      C1=0.6166274
      C2=0.1891375
      H=7.5438E-3
      P=2.0
      Q=4.0
      R=0.15
C*********************"VARYING ENGINE SPEED"*********************************
C***************** CONVENTIONAL VALVE TRAIN [C.V.T] ************************
C***** 1000 RPM [C.V.T] ***************************************************
C      WRITE(6,*)' WHAT ENGINE SPEED?'
C      READ(5,*)N
C***** N:ENGINE SPEED ****************************************************
      IF(N.EQ.1000) THEN
                    M=57
                    FIOGAS=932.0
                    RK=-0.17093
      END IF
C***** 1300 RPM [C.V.T] ***************************************************
      IF(N.EQ.1300) THEN
                    M=57
                    FIOGAS=911.06
                    RK=-0.17036
      END IF
C***** 1600 RPM [C.V.T] ***************************************************
      IF(N.EQ.1600) THEN
                    M=57
                    FIOGAS=921.53
                    RK=-0.17065
      END IF
C***** 1900 RPM [C.V.T] ***************************************************
      IF(N.EQ.1900) THEN
                    M=57
                    FIOGAS=905.82
                    RK=-0.17022
      END IF
C***** 2200 RPM [C.V.T] ***************************************************
      IF(N.EQ.2200) THEN
                    M=57
                    FIOGAS=863.93
                    RK=-0.16903
      END IF
C*************************************************************************
C***** FIRST 16 DEGREES OF D-R-D CAM ***************************************
C***** ALSO EXPONENTIAL DECAY OF EXHAUST GASES *****************************
C*************************************************************************
      DO 100 I=1,16
      X1=FLOAT(I)/44.0
      L=C1*H*(X1**P-C2*(X1**Q))*(X1**R)
      FORCE=0.0
  100 WRITE(10,101) FLOAT(I),L,FORCE
C*************************************************************************
      DO 103 I=17,43
      X1=FLOAT(I)/44.0
      L=C1*H*(X1**P-C2*(X1**Q))*(X1**R)
      FORCE=FIOGAS*EXP(RK*(FLOAT(I)-17))
  103 WRITE(10,101) FLOAT(I),L,FORCE
C*************************************************************************
C***** FROM 44TH-57TH DEGREE  OF D-R-D CAM *********************************
C*************************************************************************
      DO 110 I=44,57
      X2=((88.0-FLOAT(I))/44.)
      L=H-(C1*H*(X2**P-C2*(X2**Q))*(X2**R))
      FORCE=FIOGAS*EXP(RK*(FLOAT(I)-17))
      WRITE(10,101) FLOAT(I),L,FORCE
  110 CONTINUE
C*************************************************************************
C***** FROM 58TH-87TH DEGREE OF D-R-D CAM **********************************
C*************************************************************************
      DO 115 I=58,87
      X2=((88.0-FLOAT(I))/44.)
      L=H-(C1*H*(X2**P-C2*(X2**Q))*(X2**R))
      WRITE(10,105) FLOAT(I),L
  115 CONTINUE
C*************************************************************************
C***** FROM 88TH-132TH DEGREE  OF D-R-D CAM ********************************
C*************************************************************************
      DO 120 I=88,44,-1
      X2=((88.0-FLOAT(I))/44.)
      L=H-(C1*H*(X2**P-C2*(X2**Q))*(X2**R))
      WRITE(10,105) 88+ABS(88-FLOAT(I)),L
  120 CONTINUE
C*************************************************************************
C***** FROM 133TH-176TH DEGREE OF D-R-D CAM ********************************
C*************************************************************************
      DO 130 I=43,0,-1
      X1=FLOAT(I)/44
```

```
  130  WRITE(10,105) 88*ABS(88-FLOAT(I)),L
C*************************************************************************
C***** FROM 177TH-202TH DEGREE OF D-R-D CAM ****************************
C*************************************************************************
      DO 140 I=177,202,5
      L=0.0
  140 WRITE(10,105) FLOAT(I),L
C*************************************************************************
C***** FORMATS *********************************************************
C*************************************************************************
  101 FORMAT(' ITER,2,1 $TIME,S.',F6.2,' $D,2,UY,',F12.10,
     1       ' $F,13,FY,',F7.2,' $LWRITE')
  105 FORMAT(' ITER,2,1 $TIME,S.',F6.2,' $D,2,UY,',F12.10,' $LWRITE')
      WRITE(6,*) I,X,L
C*************************************************************************
      STOP
      END
```

```
C*************************************************************************
C***** DRIL.FOR ***** A program to convert a polynomial cam profile into ******
C****************** into a set of load steps for input to ANSYS **************
C***** 17TH,JULY, 1985 ***************************************************
C***** CONSTANTS *********************************************************

        REAL L
        A=2.
        B=9.
        C=12.
        D=30.

C*************************************************************************
C***** A POLYNOMIAL WHOSE EVENT RANGE IS 88 DEGREES **********************
C*************************************************************************
        DO 100 I=88,0,-1
        X=FLOAT(I)/88.
        IF(I.EQ.88) THEN
           X=1.
        END IF

        L=7.874-10.79568*(X)**A+5.693371*(X)**B-2.351986*(X)**C
     1       -0.08950479*(X)**D-0.3302
        WRITE(10,101)ABS(FLOAT(I)-88),L/1000.
C***** FORMATS **********************************************************
  101   FORMAT(' ITER,2,1 $TIME,S.',F5.1,' $D,2,UY,',F12.10,
     1         ' $LWRITE')
  105   FORMAT(' ITER,2,1 $TIME,S.',F5.1,' $D,2,UY,',F12.10,' $LWRITE')
        WRITE(6,*)I,X,L
  100   CONTINUE
C*************************************************************************
C***** CLOSING SECTION OF THE POLYNOMIAL CAM ******************************
C*************************************************************************
        DO 104 I=1,88
        X=FLOAT(I)/88.
        L=7.874-10.79568*(X)**A+5.693371*(X)**B-2.351986*(X)**C
     1       -0.08950479*(X)**D-0.3302
        WRITE(10,105) FLOAT(I)+88.,L/1000.
        WRITE(6,*)I,X,L
  104   CONTINUE

C*************************************************************************
        DO 120 I=177,202,5
        L=0.0
  120   WRITE(10,101) FLOAT(I),L
C*************************************************************************
        STOP
        END
```

[EOB]

```
C*******************************************************************************
C***** MAJ4.FOR **** A PROGRAM TO CONVERT A POLYNOMIAL CAM PROFILE ************
C*************** INTO A SET OF LOAD STEPS FOR INPUT TO 'ANSYS' *****************
C*************** INCORPORATING EXHAUST GAS FORCES FOLLOWING AN *****************
C************************ EXPONENTIAL DECAY FUNCTION ***************************
C***** 24TH,JULY 1985 ********************************************************
C************************ CONSTANTS ********************************************
      DIMENSION RL(0:150),RL1(0:200),RLJ(0:200)
      A=2.
      B=9.
      C=12.
      D=30.
      P=5.
      Q=6.
      R=7.
      S=8.
      T=9.
      A1=1.2032E-4
      A2=3.76E-6
      B1=1.90984E-5
      B2=2.98413E-7
      C1=1.16929E-6
      C2=9.1351E-9
      D1=3.248035E-8
      D2=1.2687689E-10
      E1=3.43707E-10
      E2=6.7130368E-13
C*******************************************************************************
C***** FIRST & LAST 16 DEGREES OF THE MAIN CAM *********************************
      RL1(1)=0.0000270
      RL1(2)=0.0003300
      RL1(3)=0.0012580
      RL1(4)=0.0031390
      RL1(5)=0.0062660
      RL1(6)=0.0108660
      RL1(7)=0.0171950
      RL1(8)=0.0253250
      RL1(9)=0.0353440
      RL1(10)=0.0472510
      RL1(11)=0.0609780
      RL1(12)=0.0763890
      RL1(13)=0.0932900
      RL1(14)=0.1114310
      RL1(15)=0.1305190
      RL1(16)=0.1502250
      RL1(175)=RL1(1)
      RL1(174)=RL1(2)
      RL1(173)=RL1(3)
      RL1(172)=RL1(4)
      RL1(171)=RL1(5)
      RL1(170)=RL1(6)
      RL1(169)=RL1(7)
      RL1(168)=RL1(8)
      RL1(167)=RL1(9)
      RL1(166)=RL1(10)
      RL1(165)=RL1(11)
      RL1(164)=RL1(12)
      RL1(163)=RL1(13)
      RL1(162)=RL1(14)
      RL1(161)=RL1(15)
      RL1(160)=RL1(16)
C*******************************************************************************
C***** CONSTANT VELOCITY RAMP **************************************************
C*******************************************************************************
      DO 75 I=17,24
      RL1(I)=.1702+.02*(FLOAT(I)-17)
      RL3(I)=0.
   75 CONTINUE
C*******************************************************************************
C***** MAIN CAM OPENING POLYNOMIAL PORTION **************************************
C*******************************************************************************
      DO 80 J=63,0,-1
      X1=FLOAT(J)/63.
      IF(J.EQ.63) THEN
         X1=1.
      END IF
      RL(J)=7.874-10.79568*(X1)**A+5.693371*(X1)**B
     1             -2.351986*(X1)**C-0.08950479*(X1)**D
   80 CONTINUE
C*******************************************************************************
      J=64
      DO 81 I=25,87
      J=J-1
      RL1(I)=RL(J)
   81 CONTINUE
C*******************************************************************************
C***** MAIN CAM CLOSING POLYNOMIAL **********************************************
C*******************************************************************************
      DO 95 J=1,63
      X=FLOAT(J)/63.
      RL(J)=7.874-10.79568*(X)**A+5.693371*(X)**B
     1             -2.351986*(X)**C-0.08950479*(X)**D
```

```
   95   CONTINUE
C*************************************************************************
        J=64
        DO 96 I=151,88,-1
        J=J-1
        RL1(I)=RL(J)
   96   CONTINUE
C*************************************************************************
C***** CONSTANT VELOCITY RAMP ******************************************
C*************************************************************************
        DO 100 I=152,159
        RL1(I)=.3302-.02*(FLOAT(I)-151)
  100   CONTINUE
C*************************************************************************
C***** DWELL ************************************************************
C*************************************************************************
        DO 115 I=176,200,5
        RL1(I)=0.0
        RL3(I)=0.0
  115   CONTINUE
C*************************************************************************
C***** FORMATS **********************************************************
C*************************************************************************
  101   FORMAT(' ITER,2,1 $TIME,5.',F5.1,' $D,2,UY,',F12.10,
     1          ' $D,18,UX,',F12.10,' $LWRITE')
C*************************************************************************
C***** VG CAM OPENING POLYNOMIAL ****************************************
C*************************************************************************
        DO 85 I=25,45
        X3=FLOAT(I)-25.
        RL3(I)=A1*(X3)**P-B1*(X3)**Q+C1*(X3)**R-D1*(X3)**S
     1           +E1*(X3)**T
   85   CONTINUE
C*************************************************************************
C***** VG CAM CLOSING POLYNOMIAL ****************************************
C*************************************************************************
        DO 90 I=46,88
        X3=FLOAT(I)-46.
        WRITE(6,*)'I,X3',I,X3
        RL3(I)=3.9-(5.2640E-4*(X3)**3-1.88E-5*(X3)**4
        RL3(I)=3.9-(5.2640E-4*(X3)**3-1.88E-5*(X3)**4
     1           +4.2630469E-9*(X3)**5)
        WRITE(6,*)'RL3(I)',RL3(I)
   90   CONTINUE
C*************************************************************************
C*************************************************************************
        DO 120 I=1,200
  120   WRITE(10,101)FLOAT(I),RL1(I)/1000.,RL3(I)/1000.
C*************************************************************************
        STOP
        END
```

[EOB]

```
C*******************************************************************************
C***** MAJ5.FOR **** A PROGRAM TO DEDUCE A POLYNOMIAL VG CAM PROFILE **********
C*************** AS SEEN BY THE MIDDLE 'VGVA' PISTON ****************************
C***** 30TH,JULY 1985 ********************************************************
C************************ CONSTANTS ********************************************
        DIMENSION RL(0:100)
        REAL L3
        A=2.
        B=9.
        C=12.
        D=30.
        E=10.79568
        F=5.693371
        G=2.351989
        H=0.08950479
C*******************************************************************************
C********************* VG CAM PROFILE GENERATION ********************************
C***** FROM 26TH TO 53RD OF VG CAM DEGREES ************************************
C*******************************************************************************
        DO 100 I=63,35,-1
        X1=FLOAT(I)/63.
        X2=(FLOAT(I)-34.363636)/28.636363
        IF(I.EQ.63) THEN
           X1=1.
           X2=1.
        END IF
        IF(X2.LE.1.00.AND.X2.GT.0) THEN
        L3=E*((X1)**A-(X2)**A)+F*((X2)**B-(X1)**B)
     1    +G*((X1)**C-(X2)**C)+H*((X1)**D-(X2)**D)
        END IF
  100   WRITE(10,105)25+ABS(FLOAT(I)-63),L3/1000.
C*******************************************************************************
C***** FROM 54TH TO 88TH OF VG CAM DEGREES ************************************
C*******************************************************************************
        DO 101 J=0,34
        X1=FLOAT(J)/63.
        RL(J)=E*(X1)**A-F*(X1)**B+G*(X1)**C+H*(X1)**D
  101   CONTINUE
C*******************************************************************************
        J=35
        DO 102 I=54,88
        J=J-1
        RL(I)=RL(J)
  102   WRITE(10,105) FLOAT(I),RL(I)/1000.
  102   WRITE(10,105) FLOAT(I),RL(I)/1000.
C***** FORMAT ****************************************************************

  105   FORMAT(' ITER,2,1 $TIME,S.',F5.1,' $D,18,UX,',F12.10,' $LWRITE')

C*******************************************************************************
C*******************************************************************************
        STOP
        END
```

[EOB]

```
C*************************************************************************
C***** MINE.FOR ********************************************************
C****************** A PROGRAMME TO DETERMINE THE SECONDARY CAM PROFILE *********
C****************** USING A ROLLER FOLLOWER *********************************
C***** 28TH,OCT,1985 ***************************************************
C*************************************************************************
C********************************** CONSTANTS ********************************
      DIMENSION Y(180),R(180),U(180),V(180),BETA(180),dRdPHI(180)
      DIMENSION DER(14),EREST(14),SIGMA2(180),DX(180),DY(90),EREST2(14)
      DIMENSION PRT1(180),PRT2(180),PRT3(180),SIGMA1(180),PA(180)
      DIMENSION DXD(180),PSY(180),PSY1(180),d2RdPHI2(180),EREST1(14)
      DIMENSION CHY(180),S1(180),PHI(180),RHO(180),R1(180)
      DIMENSION dBETAdY(180),d2BETAdY2(180),dRdY(180),d2RdY2(180)
      DIMENSION dRdPHIDD(180),d2RdPHIDD2(180),DER1(14),DER2(14)
      DIMENSION dRdPHID(180  d2RdPHID2(180),UR(61),VR(61)
      INTEGER NDER,K,J,IFAIL,I
      REAL A,B,C,D,E,F,G,H,PI,OF,OS,S,S1,PHI,AM,DER1,DER2,EREST1
      REAL HBASE,EREST,FUN,DER,L,L1,PLIFT,PSI,HBASE1,HBASE2
      REAL PHID,RAD,DXDD,EREST2
      EXTERNAL FUN,PSI,PLIFT,PHID,RAD,DXDD
      COMMON/DATA/PI,L1,OS,RP,RF,L,RB,A,B,C,D,E,F,G,H,K,J,AM
C********************************** QUESTIONS ********************************
      WRITE(6,*) 'TELL ME VALUES OF RF,RB,RP,OS,L1,L,OF,AM '
      READ(5,*) RF,RB,RP,OS,L1,L,OF,AM
C*************************************************************************
      HBASE=0.001
      HBASE1=0.1
      HBASE2=0.1
      NDER=3
      IFAIL=0
C******************* INDICES & COEFFICIENTS **********************************
      A=2.
      B=9.
      C=12.
      D=30.
      E=10.79568
      F=5.693371
      G=2.351989
      H=0.08950479
      PI=3.1415926

C*************************************************************************
C********** VG CAM PROFILE GENERATION ************************************
C*************** FROM 1ST TO 28TH  DEGREE OF VG CAM ***********************
C*************************************************************************
      DO 100 K=62,35,-1
      J=63-K
      X1=FLOAT(K)/63.
      X2=(FLOAT(K)-34.363636)/28.636363
      IF(K.EQ.63) THEN
          X1=1.
          X2=1.
      END IF

      IF(X2.LE.1.00.AND.X2.GT.0) THEN
C***************** FOLLOWER MOTION ***************************************
       Y(J)=E*((X1)**A-(X2)**A)+F*((X2)**B-(X1)**B)
     1      +G*((X1)**C-(X2)**C)+H*((X1)**D-(X2)**D)
      END IF
       Y(J)=AM*Y(J)
C***************************** DXD & PSY *************************************
      DXD(J)=(-L1+SQRT(L1**2+4*(Y(J)+OF)*(OS+RP)))/2.0
      PSY(J)=ATAN(DXD(J)/(OS+RP))
C***************************** DX & DY ***************************************
      DX(J)=L*(1.0-COS(PSY(J)))
      DY(J)=L*SIN(PSY(J))-Y(J)
C********** ANGLE BETWEEN VERTICAL THROUGH CAMSHAFT CENTRE & D.O.M **************
      PSY1(J)=ATAN(DX(J)/DY(J))

C***************************** BETA ANGLE ************************************
      BETA(J)=ATAN(DX(J)/(DY(J)+RB+RF))

C****************** PHI=J+BETA (-BETA FOR CLOCKWISE ROTATION )*******************
      S1(J)=FLOAT(J)/57.29577951
      PHI(J)=S1(J)+BETA(J)
C****************** POLAR RADIUS OF THE PITCH PROFILE ***************************
      R(J)=(RB+RF+DY(J))/COS(BETA(J))

C************** NAG LIB ROUTINE FOR NUMERICAL DIFF.OF dR/dPHI ******************

      CALL D04AAF(S1(J),NDER,HBASE,DER,EREST,FUN,IFAIL)

C********************** dR/dPHI ******************************************
       dRdPHI(J)  DER(1)
C********************** d2R/dPHI2 ****************************************
       d2RdPHI2(J)  DER(2)
C************* NAG LIB ROUTINE FOR NUMERICAL DIFF. OF dBETA/dY ***************
      CALL D04AAF(Y(J),NDER,HBASE1,DER1,EREST1,PHID,IFAIL)
C********************** dBETA/dY *****************************************
       dBETAdY(J)=DER1(1)
C********************** d2BETA/dY2 ***************************************
       d2BETAdY2(J)=DER1(2)
```

```
C************ NAG LIB ROUTINE FOR NUMERICAL DIFF. OF dR/dY ********************
      CALL D04AAF(Y(J),NDER,HBASE2,DER2,EREST2,RAD,IFAIL)
C********************** dR/dY ***************************************************
      dRdY(J)=DER2(1)
C********************** d2R/dY2 *************************************************
      d2RdY2(J)=DER2(J)
C********************** dR/dPHID ************************************************
      dRdPHID(J)=dRdY(J)/dBETAdY(J)
C********************** dR/dPHIDD & d2R/dPHIDD2 *********************************
      dRdPHIDD(J)=1./((1./dRdPHI(J))+(1./dRdPHID(J)))
C     d2RdPHIDD2(J)=1./((1./d2RdPHI2(J))+(1./d2RdPHID2(J)))

C********************** SIGMA2 IS PITCH PROFILE CURVATURE ***********************

      PRT1(J)=(R(J)**2-(d2RdPHI2(J)**2)*R(J))
      PRT2(J)=(2.*(dRdPHI(J)**2))
      PRT3(J)=SQRT((R(J)**2+(dRdPHI(J)**2))**3)


      SIGMA2(J)=(PRT1(J)+PRT2(J))/PRT3(J)
C********************** SIGMA1 IS CAM PROFILE CURVATURE *************************
      SIGMA1(J)=SIGMA2(J)/(1.-RF*SIGMA2(J))
C************************ PRESSURE ANGLE ********************************************
      PA(J)=ATAN(dRdPHIDD(J)/R(J))
C************************ POLAR CO-ORDINATES OF CAM PROFILE *************************
      RHO(J)=SQRT(R(J)**2+RF**2-2*RF*R(J)*COS(PA(J)))

C     IF((R(J)**2+RHO(J)**2-RF**2)/(2*R(J)*RHO(J)).GE.1.0) THEN
C        CHY(J) = PHI(J)
C        WRITE(6,*) ' ACOS(*)  *>1 J = ',J
C     END IF


C     IF((R(J)**2+RHO(J)**2-RF**2)/(2*R(J)*RHO(J)).LT.1.0) THEN
       CHY(J)=PHI(J)+ACOS((R(J)**2+RHO(J)**2-RF**2)/(2*R(J)*RHO(J)))
C     END IF
C*************** TO DOUBLE CHECK VALUES OF R(J) **************************************
      R1(J)=RF*COS(PA(J))+RHO(J)*COS(CHY(J)-PHI(J))
C************** CARTISIAN CO-ORDINATES OF PITCH PROFILE *************************
      UR(J)=R(J)*COS(PHI(J))
      VR(J)=R(J)*SIN(PHI(J))
C************** CARTISIAN CO-ORDINATES OF CAM PROFILE ***************************
      U(J)=RHO(J)*COS(CHY(J))
      V(J)=RHO(J)*SIN(CHY(J))
C*******************************************************************************

      WRITE(10,*)J,1./SIGMA1(J),PA(J)*57.3,dRdPHIDD(J),d2RdPHI2(J)
      WRITE(24,*)J,1./SIGMA1(J)
      WRITE(13,*)J,R(J),FUN(S1(J)),PSY(J)*57.3,PSI(S1(J))*57.3,Y(J),
     1          PLIFT(S1(J))
      WRITE(11,*)J,PSY1(J)*57.3,BETA(J)*57.3,DY(J),DX(J),DXD(J)
       WRITE(12,*)J,PA(J)*57.3
       WRITE(8,*)Y(J),dBETAdY(J)
       WRITE(7,*)Y(J),d2BETAdY2(J)
       WRITE(16,*)Y(J),dRdY(J)
       WRITE(17,*)Y(J),d2RdY2(J)
       WRITE(18,*)J,dRdPHI(J)
       WRITE(19,*)J,dRdPHID(J)
       WRITE(21,*)J,dRdPHIDD(J)
       WRITE(4,*)CHY(J)*57.3,RHO(J)
       WRITE(3,*)PHI(J)*57.3,R(J)
       WRITE(2,*)J,R(J),R1(J)
       WRITE(1,*)J,BETA(J),PHID(Y(J)),R(J),RAD(Y(J))
      WRITE(9,*)U(J),V(J)
      WRITE(22,*)UR(J),VR(J)
  100 CONTINUE
C*******************************************************************************
C**** FROM 29TH TO 63 TH OF VG CAM DEGREES ************************************
C*******************************************************************************
      DO 104 I=34,2,-1
      J=63-I
      X1=FLOAT(I)/63.
      Y(J)=E*(X1)**A-F*(X1)**B+G*(X1)**C+H*(X1)**D
      Y(J)=AM*Y(J)

C***************************** DXD & PSY ****************************************
      DXD(J)=(-L1+SQRT(L1**2+4*(Y(J)+OF)*(OS+RP)))/2.0
      PSY(J)=ATAN(DXD(J)/(OS+RP))
C***************************** DX & DY ******************************************
      DX(J)=L*(1.0-COS(PSY(J)))
      DY(J)=L*SIN(PSY(J))-Y(J)
C********* ANGLE BETWEEN VERTICAL THROUGH CAMSHAFT CENTRE & D.O.M ***************
      PSY1(J)=ATAN(DX(J)/DY(J))


C***************************** BETA ANGLE ***************************************
      BETA(J)=ATAN(DX(J)/(DY(J)+RB+RF))

C****************** PHI=J+BETA (-BETA FOR CLOCKWISE ROTATION )*******************
      S1(J)=FLOAT(J)/57.29577951
      PHI(J)=S1(J)+BETA(J)
C****************** POLAR RADIUS OF THE PITCH PROFILE ***************************
      R(J)=(RB+RF+DY(J))/COS(BETA(J))

C************** NAG LIB ROUTINE FOR NUMERICAL DIFF.OF dR/dPHI *************
```

```
      CALL D04AAF(S1(J),NDER,HBASE,DER,EREST,FUN,IFAIL)
C********************* dR/dPHI ***************************************************
       dRdPHI(J) = DER(1)
C********************* d2R/dPHI2 *************************************************
       d2RdPHI2(J) = DER(3)
C************ NAG LIB ROUTINE FOR NUMERICAL DIFF. OF dBETA/dY *******************
      CALL D04AAF(Y(J),NDER,HBASE1,DER1,EREST1,PHID,IFAIL)
C********************* dBETA/dY **************************************************
       dBETAdY(J)=DER1(1)
C********************* d2BETA/dY2 ************************************************
       d2BETAdY2(J)=DER1(3)
C************ NAG LIB ROUTINE FOR NUMERICAL DIFF. OF dR/dY ***********************
      CALL D04AAF(Y(J),NDER,HBASE2,DER2,EREST2,RAD,IFAIL)
C********************* dR/dY *****************************************************
       dRdY(J)=DER2(1)
C********************* d2R/dY2 ***************************************************
       d2RdY2(J)=DER2(3)
C********************* dR/dPHID **************************************************
       dRdPHID(J)=dRdY(J)/dBETAdY(J)
C********************* dR/dPHIDD & d2R/dPHIDD2 ***********************************
.      dRdPHIDD(J)=1./((1./dRdPHI(J))+(1./dRdPHID(J)))
C      d2RdPHIDD2(J)=1./((1./d2RdPHI2(J))+(1./d2RdPHID2(J)))
.
C********************* SIGMA2 IS PITCH PROFILE CURVATURE *************************

       PRT1(J)=(R(J)**2-(d2RdPHI2(J)**2)*R(J))
       PRT2(J)=(2.*(dRdPHI(J)**2))
       PRT3(J)=SQRT((R(J)**2+(dRdPHI(J)**2))**3)

       SIGMA2(J)=(PRT1(J)+PRT2(J))/PRT3(J)
C********************* SIGMA1 IS CAM PROFILE CURVATURE ***************************
       SIGMA1(J)=SIGMA2(J)/(1.-RF*SIGMA2(J))
C********************* PRESSURE ANGLE ********************************************
       PA(J)=ATAN(dRdPHIDD(J)/R(J))
C********************* POLAR CO-ORDINATES OF CAM PROFILE *************************
      RHO(J)=SQRT(R(J)**2+RF**2-2*RF*R(J)*COS(PA(J)))
      CHY(J)=PHI(J)+ACOS((R(J)**2+RHO(J)**2-RF**2)/(2*R(J)*RHO(J)))
C***************** TO DOUBLE CHECK VALUES OF R(J) ********************************
       R1(J)=RF*COS(PA(J))+RHO(J)*COS(CHY(J)-PHI(J))
C************** CARTISIAN CO-ORDINATES OF PITCH PROFILE ***************************
       UR(J)=R(J)*COS(PHI(J))
       VR(J)=R(J)*SIN(PHI(J))
C************** CARTISIAN CO-ORDINATES OF CAM PROFILE *****************************
      U(J)=RHO(J)*COS(CHY(J))
      V(J)=RHO(J)*SIN(CHY(J))
C*******************************************************************************

      WRITE(10,*)J,1./SIGMA1(J),PA(J)*57.3,dRdPHIDD(J),d2RdPHI2(J)
      WRITE(24,*)J,1./SIGMA1(J)
      WRITE(13,*)J,R(J),FUN(S1(J)),PSY(J)*57.3,PSI(S1(J))*57.3,Y(J),
     1          PLIFT(S1(J))
      WRITE(11,*)J,PSY1(J)*57.3,BETA(J)*57.3,DY(J),DX(J),DXD(J)
       WRITE(12,*)J,PA(J)*57.3
       WRITE(8,*)Y(J),dBETAdY(J)
       WRITE(7,*)Y(J),d2BETAdY2(J)
       WRITE(16,*)Y(J),dRdY(J)
       WRITE(17,*)Y(J),d2RdY2(J)
       WRITE(18,*)J,dRdPHI(J)
       WRITE(19,*)J,dRdPHID(J)
       WRITE(21,*)J,dRdPHIDD(J)
       WRITE(4,*)CHY(J)*57.3,RHO(J)
       WRITE(3,*)PHI(J)*57.3,R(J)
       WRITE(2,*)J,R(J),R1(J)
       WRITE(1,*)J,BETA(J),PHID(Y(J)),R(J),RAD(Y(J))
      WRITE(9,*)U(J),V(J)
      WRITE(22,*)UR(J),VR(J)
  104 CONTINUE
C*******************************************************************************

      STOP
      END

C*******************************************************************************
C*******************************************************************************
      REAL FUNCTION FUN(S1)
      COMMON/DATA/PI,L1,OS,RP,RF,L,RB,A,B,C,D,E,F,G,H,K,J,AM
      REAL S1,L,RB,RF
       FUN=(RB+RF+L*SIN(PSI(S1))-PLIFT(S1))/
     1    (COS(ATAN(L*(1.-COS(PSI(S1))))/(L*SIN(PSI(S1))-
     2    PLIFT(S1)+RF+RB)))

C*******************************************************************************
      RETURN
      END
C*******************************************************************************
C*******************************************************************************
       REAL FUNCTION PSI(S1)
       COMMON/DATA/PI,L1,OS,RP,RF,L,RB,A,B,C,D,E,F,G,H,K,J,AM
       EXTERNAL PLIFT
       REAL S1,L1,RP,OS,OF

       DXD(J)=(-L1+SQRT(L1**2+4*(PLIFT(S1)+OF)*(OS+RP)))/2.
       PSI=ATAN(DXD(J)/(OS+RP))

C*******************************************************************************
       RETURN
```

```
      END
C*************************************************************************
C*************************************************************************
      REAL FUNCTION PLIFT(S1)
      COMMON/DATA/PI,L1,OS,RP,RF,L,RB,A,B,C,D,E,F,G,H,K,J,AM
      REAL S1,A,B,C,D,E,F,G,H,X1,X2,AM
      X1=1.-0.909456817*S1
      X2=1.-2.04627784*S1
      IF(S1.LE.0.48869219) THEN
      PLIFT=E*((X1)**A-(X2)**A)
     1       +F*((X2)**B-(X1)**B)
     2       +G*((X1)**C-(X2)**C)
     3       +H*((X1)**D-(X2)**D)
        PLIFT=AM*PLIFT
      END IF
      IF(S1.GT.0.48869219) THEN
      PLIFT=E*(X1)**A-F*(X1)**B+G*(X1)**C+H*(X1)**D
      PLIFT=AM*PLIFT
      END IF

C*************************************************************************
      RETURN
      END
C*************************************************************************
      REAL FUNCTION PHID(Y)
      COMMON/DATA/PI,L1,OS,RP,RF,L,RB,A,B,C,D,E,F,G,H,K,J,AM
      EXTERNAL DXDD
      REAL Y,L1,L,OS,RP,RB,OF,RF
      PHID=ATAN(L*(1.-COS(ATAN(DXDD(Y)/(OS+RP))))/
     1       (L*SIN(ATAN(DXDD(Y)/(OS+RP)))-Y+RB+RF))
C*************************************************************************
      RETURN
      END
C*************************************************************************
      REAL FUNCTION RAD(Y)
      COMMON/DATA/PI,L1,OS,RP,RF,L,RB,A,B,C,D,E,F,G,H,K,J,AM
      EXTERNAL DXDD
      REAL Y,L1,L,OS,RP,RB,OF,RF
      RAD=SQRT((RB+RF+L*SIN(ATAN(DXDD(Y)/(OS+RP)))-Y)**2.
     1      +(L**2)*(1.-COS(ATAN(DXDD(Y)/(OS+RP))))**2)
C*************************************************************************
      RETURN
      END
C*************************************************************************
      REAL FUNCTION DXDD(Y)
      COMMON/DATA/PI,L1,OS,RP,RF,L,RB,A,B,C,D,E,F,G,H,K,J,AM
      REAL Y,L1,L,OS,RP,RB,OF
      DXDD=(-L1+SQRT(L1**2+4*(Y+OF)*(OS+RP)))/2.
C*************************************************************************
      RETURN
      END
C*************************************************************************
```

[EOB]

```
C*************************************************************************
C***** PISHI.FOR ********************************************************
C****************** A PROGRAMME TO DETERMINE THE SECONDARY CAM PROFILE *********
C****************** USING A ROLLER FOLLOWER &ALSO DETERMINING*****************
C****************** HERTZ COMPRESSIVE CONTACT STRESSES ************************
C***** 28TH,OCT,1985 ***************************************************
C*************************************************************************S*******
C******************************** CONSTANTS ********************************
      DIMENSION Y(88),PHI(88),R(88),U(88),V(88),BETA(88),RHO(88)
      DIMENSION DER(14),EREST(14),SIGMA2(88),DX(88),DY(88),UR(88),VR(88)
      DIMENSION PRT1(88),PRT2(88),PRT3(88),SIGMA1(88),PA(88),CHY(88)
      DIMENSION DXD(88),PSY(88),CONSTRS(160),D1(160),PCONSTRS(160)
      DIMENSION Y2(180),DDY1(160),DDY2(180),PRES(160),FORCE(160),S1(88)
      DIMENSION PRES1(160),PRES2(180),FORCE1(160),FORCE2(180),Y1(160)
      DIMENSION PSY1(88),DER1(14),DER2(14),EREST1(14),EREST2(14),R1(88)
      DIMENSION dRdPHI(180),d2RdPHI2(180),dBETAdY(180),d2BETAdY2(180)
      DIMENSION dRdY(180),d2RdY2(180),dRdPHIDD(180),d2RdPHIDD2(180)
      DIMENSION dRdPHID(180),d2RdPHID2(180)
       INTEGER NDER,K,J,IFAIL,I,M
       REAL HBASE,DERIV,EREST,FUN,DER,L,L1,PHIPLIFT,PSI,HBASE1,HBASE2
       REAL A,B,C,D,E,F,G,H,PI,OF,OS,S,S1,D2,D1,DP,RV,AM,DER1,DER2,PHID
       REAL EREST1,EREST2,RAD,DXDD
       EXTERNAL FUN,PSI,PLIFT,PHID,RAD,DXDD
       COMMON/DATA/PI,L1,OS,RP,RF,L,RB,A,B,C,D,E,F,G,H,K,J,M,AM
C******************************** QUESTIONS ********************************
       WRITE(6,*) 'TELL ME VALUES OF RF,RB,RP,OS,L1,L,OF,AM '
       READ(5,*) RF,RB,RP,OS,L1,L,OF,AM
       WRITE(6,*) 'WHAT ENGINE SPEED?'
       READ(5,*) SPEED
C*************************************************************************
       HBASE=0.001
       HBASE1=0.1
       HBASE2=0.1
       NDER=3
       IFAIL=0
C****************** INDICES & COEFFICIENTS *********************************
       A=2.
       B=9.
       C=12.
       D=30.
       E=10.79568
       F=5.693371
       G=2.351989
       H=0.08950479
       PI=3.1415926
       EMAT=200E15
       RMEQ=0.7943
       RMF=0.11
       RIV=0.00012
       RKEQ=46907.0
       FPEQ=666.1
       A1=1.01787602E-3
       A2=1.01787602E-3
       A3=1.01787602E-3
C*************************************************************************
C********* MAIN CAM POLYNOMIAL FROM 25TH TO 88TH DEGREE OF CAM ANGLE **********
C*************************************************************************
       DO 150 M=1,61
C*************************************************************************
       DO 80 I=62,0,-1
       J=63-I
       X1=FLOAT(I)/63.
       IF(I.EQ.63) THEN
                   X1=1.0
       END IF
       Y1(J)=(7.874-E*(X1)**A+F*(X1)**B-G*(X1)**C-H*(X1)**D)/1000.
C**************** MAIN CAM ACCEL. ************************************
       DDY1(J)=(-2.*E+72.*F*(X1)**7-132.*G*(X1)**10
     1          -870.*H*(X1)**28)/3969E3
       DDY1(J)=(9.*(SPEED)**2)*DDY1(J)
C*************************************************************************
       RV=L1/(L-L1)
       PRES1(J)=(RMEQ*(A1/A3)*DDY1(J)+RKEQ*(A1/A3)*Y1(J)+FPEQ)/A3
       FORCE1(J)=PRES1(J)*A2*RV
C*************************************************************************
   80  CONTINUE
C*************************************************************************
C********* VG CAM PROFILE GENERATION ***************************************
C************** FROM 26TH TO 53RD DEGREE OF VG CAM ***************************
C*************************************************************************

       DO 100 K=62,35,-1
       J=63-K
       X1=FLOAT(K)/63.
       X2=(FLOAT(K)-34.063636)/28.636363
       IF(K.EQ.63) THEN
           X1=1.
           X2=1.
       END IF

       IF(X2.LE.1.00.AND.X2.GT.0) THEN
C**************** FOLLOWER MOTION ********************************************
```

```
        Y(J)=AM*(E*((X1)**A-(X2)**A)+F*((X2)**B-(X1)**B)
     1      +G*((X1)**C-(X2)**C)+H*((X1)**D-(X2)**D))
        Y2(J)=Y(J)/1000.
C*************** FOLLOWER ACCEL. ********************************************
        DDY2(J)=(2.*E+72.*F*((X2)**7-(X1)**7)+132.*G*((X1)**10
     1          -(X2)**10)+870.*H*((X1)**28-(X2)**28))/3969E3
        DDY2(J)=(9.*(SPEED)**2)*DDY2(J)*AM
       END IF
C*****************************************************************************

       RV=L1/(L-L1)
       PRES2(J)=(RV*RMEQ*(A2/A3)*DDY2(J)+RKEQ*(A2/A3)*Y2(J)*RV)/A3
       RM2=(RV**2)*RMF+RIV/(((L/1000.-L1/1000.)**2)
       FORCE2(J)=RM2*DDY2(J)+PRES2(J)*A2*RV
C*************************** DXD & PSY ***************************************
       DXD(J)=(-L1+SQRT(L1**2+4*Y(J)*(OS+RP)))/2.0
       PSY(J)=ATAN(DXD(J)/(OS+RP))
C*************************** DX & DY *****************************************
       DX(J)=L*(1.0-COS(PSY(J)))
       DY(J)=L*SIN(PSY(J))-Y(J)
C********** ANGLE BETWEEN VERTICAL THROUGH CAMSHAFT CENTRE & D.O.H ************
       PSY1(J)=ATAN(DX(J)/DY(J))
C*************************** BETA ANGLE **************************************
       BETA(J)=ATAN(DX(J)/(DY(J)+RB+RF))

C****************** PHI=J+BETA (-BETA FOR CLOCKWISE ROTATION )*******************
       S1(J)=FLOAT(J)/57.29577951
       PHI(J)=S1(J)+BETA(J)
C****************** POLAR RADIUS OF THE PITCH PROFILE ***************************

       R(J)=(RB+RF+DY(J))/COS(BETA(J))

*************** NAG LIB ROUTINE FOR NUMERICAL DIFF. ******************************

       CALL D04AAF(S1(J),NDER,HBASE,DER,EREST,FUN,IFAIL)

C*********************** dR/dPHI *****************************************
        dRdPHI(J) = DER(1)
C*********************** d2R/dPHI2 ***************************************
        d2RdPHI2(J) = DER(3)
C************ NAG LIB ROUTINE FOR NUMERICAL DIFF. OF dBETA/dY ***************

        CALL D04AAF(Y(J),NDER,HBASE1,DER1,EREST1,PHID,IFAIL)
C****************** dBETA/dY & d2BETA/dY2 ***********************************
        dBETAdY(J)=DER1(1)
        d2BETAdY2(J)=DER1(3)
C************ NAG LIB ROUTINE FOR NUMERICAL DIFF. OF dR/dY *******************

        CALL D04AAF(Y(J),NDER,HBASE2,DER2,EREST2,RAD,IFAIL)
C****************** dR/dY & d2R/dY2 **********************************************
        dRdY(J)=DER2(1)
        d2RdY2(J)=DER2(3)
C****************** dR/dPHID ****************************************************
        dRdPHID(J)=dRdY(J)/dBETAdY(J)
C****************** dR/dPHIDD &d2R/dPHIDD2 ***************************************
        dRdPHIDD(J)=1./((1./dRdPHI(J))+(1./dRdPHID(J)))
C       d2RdPHIDD2(J)=1./((1./d2RdPHI2(J))+(1./d2RdPHID2(J)))
C*********************** SIGMA2 IS PITCH PROFILE CURVATURE **********************

       PRT1(J)=(R(J)**2-(d2RdPHI2(J)**2)*R(J))
       PRT2(J)=(2*(dRdPHI(J)**2))
       PRT3(J)=SQRT((R(J)**2+(dRdPHI(J)**2))**3)

       SIGMA2(J)=(PRT1(J)+PRT2(J))/PRT3(J)
C*********************** SIGMA1 IS CAM PROFILE CURVATURE ************************
       SIGMA1(J)=SIGMA2(J)/(1.-RF*SIGMA2(J))
C*********************** PRESSUR ANGLE **********************************************
       PA(J)=ATAN(dRdPHIDD(J)/R(J))
C*********************** POLAR CO-ORDINATES OF CAM PROFILE **********************
       RHO(J)=SQRT(R(J)**2+RF**2-2*RF*R(J)*COS(PA(J)))
       CHY(J)=PHI(J)+ACOS((R(J)**2+RHO(J)**2-RF**2)/(2*R(J)*RHO(J)))
C************** TO DOUBLE CHECK VALUES OF PITCH PROFILE ************************
       R1(J)=RF*COS(PA(J))+RHO(J)*COS(CHY(J)-PHI(J))
C************** CARTISIAN CO-ORDINATES OF PITCH PROFILE ************************
       UR(J)=R(J)*COS(PHI(J))
       VR(J)=R(J)*SIN(PHI(J))
C************** CARTISIAN CO-ORDINATE OF CAM PROFILE ***************************
       U(J)=RHO(J)*COS(CHY(J))
       V(J)=RHO(J)*SIN(CHY(J))
C*****************************************************************************
  100  CONTINUE
C*****************************************************************************
C**** FROM 54TH TO 88 TH OF VG CAM DEGREES ***********************************
C*****************************************************************************
       DO 104 I=34,2,-1
       J=63-I
       X1=FLOAT(I)/63.
       Y(J)=E*(X1)**A-F*(X1)**B+G*(X1)**C+H*(X1)**D
       Y(J)=AM*Y(J)
       Y2(J)=Y(J)/1000.
       DDY2(J)=(2.*E-72.*F*(X1)**7+132.*G*(X1)**10
     1          +870.*H*(X1)**28)/3969E3
       DDY2(J)=(9.*(SPEED)**2)*DDY2(J)*AM

       RV=L1/(L-L1)
       PRES2(J)=(RV*RMEQ*(A2/A3)*DDY2(J)+RKEQ*(A2/A3)*Y2(J)*RV)/A3
```

```
      RM2=(RV**2)*RMF+RIV/((L/1000.-L1/1000.)**2)
      FORCE2(J)=RM2*DDY2(J)+PRES2(J)*A2*RV
C************************** DXD & PSY ****************************************
      DXD(J)=(-L1+SQRT(L1**2+4*Y(J)*(OS+RP)))/2.0
      PSY(J)=ATAN(DXD(J)/(OS+RP))
C************************** DX & DY ******************************************
      DX(J)=L*(1.0-COS(PSY(J)))
      DY(J)=L*SIN(PSY(J))-Y(J)
C********** ANGLE BETWEEN VERTICAL THROUGH CAMSHAFT CENTRE & D.O.M ************
      PSY1(J)=ATAN(DX(J)/DY(J))
C************************** BETA ANGLE ***************************************
      BETA(J)=ATAN(DX(J)/(DY(J)+RB+RF))

C***************** PHI=J+BETA (-BETA FOR CLOCKWISE ROTATION )*******************
      S1(J)=FLOAT(J)/57.29577951
      PHI(J)=S1(J)+BETA(J)
C***************** POLAR RADIUS OF THE PITCH PROFILE ****************************

      R(J)=(RB+RF+DY(J))/COS(BETA(J))

************** NAG LIB ROUTINE FOR NUMERICAL DIFF. ****************************

      CALL D04AAF(S1(J),NDER,HBASE,DER,EREST,FUN,IFAIL)

C********************** dR/dPHI ******************************************
       dRdPHI(J) = DER(1)
C********************** d2R/dPHI2 ****************************************
       d2RdPHI2(J) = DER(3)
C************ NAG LIB ROUTINE FOR NUMERICAL DIFF. OF dBETA/dY ***************

       CALL D04AAF(Y(J),NDER,HBASE1,DER1,EREST1,PHID,IFAIL)
C******************** dBETA/dY & d2BETA/dY2 ***********************************
       dBETAdY(J)=DER1(1)
       d2BETAdY2(J)=DER1(3)
C************ NAG LIB ROUTINE FOR NUMERICAL DIFF. OF dR/dY *******************

       CALL D04AAF(Y(J),NDER,HBASE2,DER2,EREST2,RAD,IFAIL)
C******************** dR/dY & d2R/dY2 *****************************************
       dRdY(J)=DER2(1)
       d2RdY2(J)=DER2(3)
C******************** dR/dPHID ************************************************
       dRdPHID(J)=dRdY(J)/dBETAdY(J)
C******************** dR/dPHIDD &d2R/dPHIDD2 **********************************
       dRdPHIDD(J)=1./((1./dRdPHI(J))+(1./dRdPHID(J)))
C      d2RdPHIDD2(J)=1./((1./d2RdPHI2(J))+(1./d2RdPHID2(J)))
C********************** SIGMA2 IS PITCH PROFILE CURVATURE ***********************

       PRT1(J)=(R(J)**2-(d2RdPHI2(J)**2)*R(J))
       PRT2(J)=(2*(dRdPHI(J)**2))
       PRT3(J)=SQRT((R(J)**2+(dRdPHI(J)**2))**3)

       SIGMA2(J)=(PRT1(J)+PRT2(J))/PRT3(J)
C********************** SIGMA1 IS CAM PROFILE CURVATURE *************************
       SIGMA1(J)=SIGMA2(J)/(1.-RF*SIGMA2(J))
C********************** PRESSUR ANGLE *******************************************
       PA(J)=ATAN(dRdPHIDD(J)/R(J))
C************************ POLAR CO-ORDINATES OF CAM PROFILE *********************
      RHO(J)=SQRT(R(J)**2+RF**2-2*RF*R(J)*COS(PA(J)))
      CHY(J)=PHI(J)+ACOS((R(J)**2+RHO(J)**2-RF**2)/(2*R(J)*RHO(J)))
C************** TO DOUBLE CHECK VALUES OF PITCH PROFILE **************************
       R1(J)=RF*COS(PA(J))+RHO(J)*COS(CHY(J)-PHI(J))
C************** CARTISIAN CO-ORDINATES OF PITCH PROFILE **************************
       UR(J)=R(J)*COS(PHI(J))
       VR(J)=R(J)*SIN(PHI(J))
C************** CARTISIAN CO-ORDINATE OF CAM PROFILE *****************************
      U(J)=RHO(J)*COS(CHY(J))
      V(J)=RHO(J)*SIN(CHY(J))
C*********************************************************************************
  104  CONTINUE
C*********************************************************************************
       IF(M.GE.1)THEN
       DI(M)=2.0/SIGMA1(M)
       END IF
       D2=2.*RF
C***************** PRESSURE INSIDE HYDRAULIC CHAMBER ****************************
      PRES(M)=PRES1(M)+PRES2(M)
C***************** CONTACT COMPRESSIVE FORCE ************************************
      FORCE(M)=FORCE1(M)+FORCE2(M)
C***************** RETAINING SPRING FORCE ***************************************
      FORCE(M)=FORCE(M)+140
C***************** FORCE PER UNIT LENGTH OF CAM WIDTH ***************************
      FORCE(M)=FORCE(M)/20.
C************** CAM CONTACT STRESS EXPRESSIONS **********************************
      CONSTRS(M)=0.591*SQRT(FORCE(M)*EMAT*((D1(M)+D2)/(D1(M)*D2)))
C********** MAX CONTACT STRESS BETWEEN ROCKER & PIVOT DISC **********************
      DP=2.0*RP
      PCONSTRS(M)=0.591*SQRT((3.0*FORCE(M)*EMAT)/DP)
C*********************************************************************************
      WRITE(21,*)M,FORCE(M),PRES(M),CONSTRS(M),PCONSTRS(M)
      WRITE(14,*)M,CONSTRS(M)
      WRITE(15,*)M,PCONSTRS(M)

  150  CONTINUE
C*****************************************************************************

      STOP
```

```
      END
C*****************************************************************************
C*****************************************************************************
      REAL FUNCTION FUN(S1)
      COMMON/DATA/PI,L1,OS,RP,RF,L,RB,A,B,C,D,E,F,G,H,K,J,M,AM
      EXTERNAL PSI,PLIFT
      REAL S1,PI,L,RB,RF
      FUN=(RB+RF+L*SIN(PSI(S1))-PLIFT(S1))/
     1     (COS(ATAN(L*(1.-COS(PSI(S1))))/(L*SIN(PSI(S1))-
     2     PLIFT(S1)+RF+RB)))
C*****************************************************************************
      RETURN
      END
C*****************************************************************************
      REAL FUNCTION PSI(S1)
      COMMON/DATA/PI,L1,OS,RP,RF,L,RB,A,B,C,D,E,F,G,H,K,J,M,AM
      EXTERNAL PLIFT
      REAL S1,L1,RP,OS,OF

      DXD(J)=(-L1+SQRT(L1**2+4*(PLIFT(S1)+OF)*(OS+RP)))/2.
      PSI=ATAN(DXD(J)/(OS+RP))
C*****************************************************************************
      RETURN
      END
C*****************************************************************************
      REAL FUNCTION PLIFT(S1)
      COMMON/DATA/PI,L1,OS,RP,RF,L,RB,A,B,C,D,E,F,G,H,K,J,M,AM
      REAL S1,A,B,C,D,E,F,G,H,X1,X2,AM
      X1=1.-0.909456817*S1
      X2=1.-2.04627784*S1
      IF(S1.LE.0.48869219) THEN
      PLIFT=E*((X1)**A-(X2)**A)
     1      +F*((X2)**B-(X1)**B)
     2      +G*((X1)**C-(X2)**C)
     3      +H*((X1)**D-(X1)**D)
      END IF
      PLIFT=AM*PLIFT
      IF(S1.GT.0.48869219) THEN
      PLIFT=E*(X1)**A-F*(X1)**B+G*(X1)**C+H*(X1)**D
      PLIFT=AM*PLIFT
      END IF

C*****************************************************************************
      RETURN
      END
C*****************************************************************************
       REAL FUNCTION PHID(Y)
       COMMON/DATA/PI,L1,OS,RP,RF,L,RB,A,B,C,D,E,F,G,H,K,J,M,AM
       EXTERNAL DXDD
       REAL Y,L1,L,OS,RP,RB,OF,RF
       PHID=ATAN(L*(1.-COS(ATAN(DXDD(Y)/(OS+RP))))/
     1       (L*SIN(ATAN(DXDD(Y)/(OS+RP)))-Y+RB+RF))
C*****************************************************************************
       RETURN
       END
C*****************************************************************************
       REAL FUNCTION RAD(Y)
       COMMON/DATA/PI,L1,OS,RP,RF,L,RB,A,B,C,D,E,F,G,H,K,J,M,AM
       EXTERNAL DXDD
       REAL Y,L1,L,OS,RP,RB,OF,RF
       RAD=SQRT((RB+RF+L*SIN(ATAN(DXDD(Y)/(OS+RP)))-Y)**2.
     1     +(L**2)*(1.-COS(ATAN(DXDD(Y)/(OS+RP))))**2)
C*****************************************************************************
       RETURN
       END
C*****************************************************************************
       REAL FUNCTION DXDD(Y)
       COMMON/DATA/PI,L1,OS,RP,RF,L,RB,A,B,C,D,E,F,G,H,K,J,M,AM
       REAL Y,L1,L,OS,RP,RB,OF
       DXDD=(-L1+SQRT(L1**2+4*(Y+OF)*(OS+RP)))/2.
C*****************************************************************************
       RETURN
       END
C*****************************************************************************
```

[EOB]

```
C       ----------------
C       program PULSE.FOR
C       program PULSE.FOR
C       ----------------

C       ------------------------------------------------------
C       TO CALCULATE THE TURBINE ENERGY IN AN EXHAUST PULSE
C       ------------------------------------------------------

        PROGRAM PULSE

C       ----------
C       PARAMETERS
C       ----------
        PARAMETER(NSMPS=10000)

C       ------------
C       COMMOM BLOCK
C       ------------
        COMMON/PSP/XMN,XMX,YMN,YMX
        COMMON/ICHAN/IIN,IOUT,IESC,ICOMP,ITURB,IACC,ILOAD,IAIMS,IJOU
        COMMON/PARAM/NSAMP,NCHAN1,NCHAN,ILENG,DTIME,NPOINTS
        COMMON/VAR/VARS(NSMPS,16)
        COMMON/TER/ITERM
        COMMON/AVO/AVO,EVO

C       ---------------
C       VARIABLE TYPING
C       ---------------
        INTEGER       ISTAT(16)
        INTEGER*2     DTHRESH(16),ITIME,IMODE,IPNT
        CHARACTER*1   ISTCH(16),IMDCH,LSBCH
        CHARACTER*80 TITLE
        CHARACTER*80 FNAM,FNAM1
        CHARACTER*15 CHNAM(16)

C       ------------------------------------------------
C       TERMINAL TYPE 3 (PERICOM) AND CHANNEL DEFINITIONS
C       ------------------------------------------------
        ITERM = 3
        IOUT  = 6
        IIN   = 5
        IESC  = 5
        IAIMS = 4

C       ------------
C       VALVE EVENTS *** EVO INCLUDES THE OPENING "RAMP" ***
C       ---   ------
        EVO   98.0
        AVO   345.0

C       ------------------------------
C       INITIALISE THE TERMINAL AND GHOST
C       ------------------------------
        CALL TINIT
        CALL PAPER(1)

C       ------------------------
C       DEFAULT SCREEN PLOT REGION
C       ------------------------
        CALL GRAFIX
        XMN   =  0.100
        XMX   =  1.280
        YMN   =  0.200
        YMX   =  0.980
        CALL PSPACE (XMN,XMX,YMN,YMX)
        CALL WSCREEN

C       ----------------------------------
C       ENTER SET NUMBER AND INPUT DATA FILE
C       ----------------------------------
5000    WRITE(IOUT,*) ' Enter name of PARAMETER and DATA file...'
        READ(IIN,101,ERR=5000,END=5555) FNAM

C       ------------------------------------------
C       SEARCH FOR FILE EXTENSION - REMOVE IF FOUND
C       ------------------------------------------
        DO 1010 INUM = 1,20
           IF(FNAM(INUM:INUM).EQ.'.') THEN
              DO 1020 JNUM = INUM,20
                 FNAM(JNUM:JNUM) = ' '
1020          CONTINUE
           END IF
1010    CONTINUE

C       ----------------------------
C       ADD THE FILE EXTENSION (.PRM)
C       ----------------------------
        CALL STR$TRIM(FNAM1,FNAM,LEN)
        FNAM1(LEN+1:LEN+4) = '.PRM'

        OPEN(UNIT=IAIMS,FILE=FNAM1,STATUS='OLD',
     1      FORM='UNFORMATTED',RECORDTYPE='VARIABLE',RECL=1,ERR=5000)

C       ------------------------------------------------------------
C       READ THE SINGLE (1024 BYTE) RECORD FROM THE PARAMETER FILE
C       ------------------------------------------------------------
        READ(IAIMS)  TITLE,
     1          (ISTCH(INUM),CHNAM(INUM),DTHRESH(INUM),INUM=1,16),
     1           ITIME,IMDCH,ISIZE,ILENG


C       CHANNEL STATUS ... ISTAT = 0,1,2,3  ... OFF DIG, OFF AN, ON DIG,
        NCHAN = 0
        DO 4000 INUM = 1,16
           ISTAT(INUM) = ICHAR(ISTCH(INUM))
C          NUMBER OF ENABLED CHANNELS
           IF(ISTAT(INUM).EQ.2.OR.ISTAT(INUM).EQ.3) NCHAN = NCHAN + 1
C          FILL CHNAM(*) WITH BLANKS
           DO 4010 JNUM = 1,15
              IF(ICHAR(CHNAM(INUM)(JNUM:JNUM)).EQ.0) THEN
                 CHNAM(INUM)(JNUM:JNUM) = ' '
              END IF
4010       CONTINUE

4000    CONTINUE


C       NUMBER OF 'ACTIVE' CHANNELS WILL BE THE NEXT HIGHEST POWER OF 2
C       ABOVE THE NUMBER OF 'ENABLED' CHANNELS
        IF(NCHAN.EQ.0)                  NCHAN1 = 1
```

```
      IF(NCHAN.EQ.2)                  NCHAN1 = 2
      IF(NCHAN.EQ.3)                  NCHAN1 = 4
      IF(NCHAN.EQ.4)                  NCHAN1 = 4
      IF(NCHAN.GE.5.AND.NCHAN.LE.8)   NCHAN1 = 8
      IF(NCHAN.GE.9.AND.NCHAN.LE.16) NCHAN1 = 16


C     NUMBER OF SAMPLES PER CHANNEL
      NSAMP = ILENG


C     TIME SCALE IN USE ... IMODE = 1,2,3   ... MICROSEC, MILLISEC, OR SECONDS
      IMODE = ICHAR(IMDCH)

C     TIME STEP
      IF(IMODE.EQ.1) DTIME = REAL(ITIME)/1000000.0
      IF(IMODE.EQ.2) DTIME = REAL(ITIME)/1000.0
      IF(IMODE.EQ.3) DTIME = REAL(ITIME)

C     ------------------------------------------------------
C     WRITE STATUS OF THE AQUISITION SYSTEM TO THE SCREEN
C     ------------------------------------------------------
C     TITLE AND HEADER
      WRITE(IOUT,6030)TITLE

C     SAMPLE PERIOD
      IF(IMODE.EQ.1) WRITE(IOUT,6040) ITIME,NCHAN,NSAMP
      IF(IMODE.EQ.2) WRITE(IOUT,6050) ITIME,NCHAN,NSAMP
      IF(IMODE.EQ.3) WRITE(IOUT,6060) ITIME,NCHAN,NSAMP

C     CHANNEL DEFINITIONS
      WRITE(IOUT,6070)
      DO 6000 INUM = 1,16
            IF(ISTAT(INUM).EQ.2) WRITE(IOUT,6010) INUM,CHNAM(INUM),
     1                           (REAL(DTHRESH(INUM))-2048)*10/2048
            IF(ISTAT(INUM).EQ.3) WRITE(IOUT,6020) INUM,CHNAM(INUM),
     1                           (REAL(DTHRESH(INUM))-2048)*10/2048
6000  CONTINUE


C     ----------------------------------------
C     READ IN THE DATA FROM THE ******.DAT FILE
C     ----------------------------------------
      CALL READ03(FNAM,IERR)

      IF(IERR.EQ.1) WRITE(IOUT,*)' ERROR DURING READ FROM ****.DAT'
      IF(IERR.EQ.1) GOTO 5000
      IF(IERR.EQ.2) WRITE(IOUT,*)' UNEXPECTED END OF FILE ON ****.DAT'
      IF(IERR.EQ.2) GOTO 5000

C     ------------------------------------------------
C     DATA READ SUCCESSFULLY ... NOW TO SCALE THE DATA
C     ------------------------------------------------
C     PRESSURE FIRST

      DO 108 IPNT = 5,NPOINTS+3
          VARS(IPNT,5) = VARS(IPNT,5) + 1.0
108   CONTINUE

C     ----------------------------
C     NEW MAXIMUM AND MINIMUM VALUES
C     ----------------------------
      VARS(2,5) = VARS(2,5) + 1.0
      VARS(3,5) = VARS(3,5) + 1.0

C     ------------------------------------------------------------
C     RESET SCREEN TO THE LOWER PORTION READY FOR THE GRAPHICS DISPLAY
C     ------------------------------------------------------------
      CALL LSCREEN

C     ------------------------------------------
C     NOW TO DISPLAY THE DATA ON THE GRAPHICS SCREEN
C     ------------------------------------------
      CALL GPLOT

C     ----------------------------------------
C     ALLOW USER TO ZOOM IN ON AREA OF INTEREST
C     ----------------------------------------
      WRITE(6,*)' Use cursor to select area of interest'
      CALL ZOOM

C     ----------------------------------------------
C     ALLOW USER TO IDENTIFY THE START OF THE PULSE
C     ----------------------------------------------
      CALL PSTART (T1,T2,AV0,EV0)

C     ------------------------------------------------------------
C     INTGRATE BETWEEN T1 AND T2 FOR MASS FLOW AND TURBINE ENERGY
C     ------------------------------------------------------------
      CALL PULSEN (T1,T2)


C     ------------
C     FORMAT BLOCK
C     ------------
6010  FORMAT(X,I4,9X,A15,3X,' DIGITAL',4X,F7.4)
6020  FORMAT(X,I4,9X,A15,3X,' ANALOG ',4X,F7.4)
6030  FORMAT(// ' AQUISITION SYSTEM STATUS'/
     1         ' ----------------------',//,
     1                          X,'TITLE:'1X,A80/)
6040  FORMAT(' SAMPLE PERIOD = ',I6,' [microsec]'
     1     2X,'NO.OF CHANS.=',I6,' NO.OF PTS.=',I8/)
6050  FORMAT(' SAMPLE PERIOD = ',I6,' [millisec]'
     1     2X,'NO.OF CHANS.=',I6,' NO.OF PTS.=',I8/)
6060  FORMAT(' SAMPLE PERIOD = ',I6,' [seconds] '
     1     2X,'NO.OF CHANS.=',I6,' NO.OF PTS.=',I8/)

6070  FORMAT(' CHANNEL      LABEL              TYPE'/
     1       ' -------      -----              ----')
100   FORMAT(A30)
161   FORMAT(/A80)
101   FORMAT(A80)
102   FORMAT(A20)


      CLOSE(IAIMS)  C       ---------------
      CLOSE(IPAR)   C       CLOSE READ FILE
                    C       ---------------
      STOP          5555    CLOSE(IIN)
                            STOP

                            END
```

```
C     ----------------------
C     subroutine PULSEN.FOR
C     ----------------------


      SUBROUTINE PULSEN (T1,T2)


C     ---------------
C     PARAMETER BLOCK
C     ---------------
      PARAMETER(NSMPS=10000,PI=3.1415926)

C     ------------
C     COMMON BLOCK
C     ------------
      COMMON/PARAM/NSAMP,NCH,NCHEN,ILENG,DTIME,NPOINTS
      COMMON/ICHAN/IIN,IOUT,IESC,ICOMP,ITURB,IACC,ILOAD,IAIMS,IJOU
      COMMON/MAP/XMIN,XMAX,YMIN,YMAX
      COMMON/PSP/XMN,XMX,YMN,YMX
      COMMON/VAR/VARS
      COMMON/AVO/AVO,EVO
      COMMON/SPE/SPEED

C     ---------------
C     VARIABLE TYPING
C     ---------------
      REAL VARS(NSMPS,16)

C     --------------------------
C     DEFINE RELEVANT PARAMETERS
C     --------------------------
      DORIF = .025
      DPIPE = .040
      AORIF = PI*DORIF*DORIF / 4.0
      APIPE = PI*DPIPE*DPIPE / 4.0
      CD    = 0.6
      PHI   = CD*AORIF/APIPE
      TREF  = 300.0
      PREF  = 100000.0
      P2    = 100000.0
C     INITIAL VALUE OF GAMMA - TO START THE CALCULATION
      GAMMA = 1.400
C     ---------------------------------
C     WRITE HEADER AND NO. OF POINTS TO FILE
C     ---------------------------------
      WRITE (1,*) ' PULSE POWER RELATED DATA '
      WRITE (1,10) INT((T2-T1)/DTIME) - 1
10    FORMAT(X,I5)
C     --------------------------------
C     INITIALISE VARIABLES AND COUNTERS
C     --------------------------------
      TOT1  = 0.0
      TOT2  = 0.0
      FLOW  = 0.0
      POWER = 0.0
      INUM  = 0
      NSUB  = 0
      NSON  = 0

C     ------------------------------------------------------------
C     LOOP THROUGH THE PRESSURE - TIME DATA TO CALCULATE THE ENERGY A
C     ------------------------------------------------------------
      DO 108 IPNT = 5,NPOINTS+3
          IF(VARS(IPNT,1).GE.T1.AND.VARS(IPNT,1).LE.T2) THEN
C            INTEGRATION WITHIN THIS RANGE
             INUM  = INUM + 1
             P1    = VARS(IPNT,5)*100000.0
             PR    = P2/P1

C            ---------------------------------------
C            PREVENT CALCULATION IF FLOW IS REVERSED
C            ---------------------------------------
             IF(PR.LT.1.000) THEN

C            ----------------------
C            IS THE NOZZLE CHOKED ?
C            ----------------------
C            THE CRITERION USED HERE FOR CRITICAL FLOW IS THAT GIVEN
C            BENSON & WOODS - Int J Mech Sci, 1961, pp231-250. IT IS
C            DERIVED FROM THE SFEE AND CONTINUITY FOR THE CASE WHEN T
C            UPSTREAM VELOCITY IS NOT ZERO - HENCE THE APPEARANCE OF
C            AREA RATIO SQUARED ( AR2 ) AND ( PHI*PHI ). FOR THE CASE
C            WHEN GAMMA = 1.4 THE CPR = 1.8674 - THIS IS ASSUMED HERE

             AR2 = (1/PR)**(2/GAMMA)*((GAMMA+1)/(GAMMA-1) -
     1             2/(GAMMA-1)*(1/PR)**((GAMMA-1)/GAMMA))

             ICHOK = 0
             IF(AR2.LE.PHI*PHI) ICHOK = 1


             IF(ICHOK.EQ.0) THEN
C               NOT CHOKED
                NSUB = NSUB + 1
                TEM1  = TREF*(P1/PREF)**((GAMMA-1.0)/GAMMA)
                CALL GASPO1(TEM1,0.0,CP,CV,GAMMA,RGAS)
                U2    = SQRT((2.0*CP*TEM1*(1.0-PR**
     1                    ((GAMMA-1.0)/GAMMA)))/
     1                    (1.0-PR**(2/GAMMA)*PHI*PHI))
C               INSTANTANEOUS MASS FLOW THROUGH THE ORIFICE PLATE
                DMDT  = (P2/(RGAS*TREF*(P2/PREF)**
     1                  ((GAMMA-1)/GAMMA)))*CD*AORIF*U2
C               PIPE VELOCITY
                DEN1  = P1 / (RGAS * TEM1)
                U1    = DMDT / (DEN1 * APIPE)

C               INSTANTANEOUS "TURBINE POWER" THROUGH THE ORIFICE PLA
                POWER = DMDT*U2*U2/2
             END IF

             IF(ICHOK.EQ.1) THEN
C               CHOKED - MASS FLOW DETERMINED BY SONIC VELOCITY AT TH
C                        TURBINE POWER DETERMINED BY ISENTROPIC EXPAN
C                        BETWEEN UPSTREAM AND AMBIENT PRESSURE - WITH
C                        ASSUMPTION OF ZERO EXIT VELOCITY :
C                        -W  = m * ( h3 - h1 - u1*u1 )
C                        THIS IS EQUIVALENT TO W = ho1 - ho3
```

```
                NSON   = NSON + 1
                CPR    = 1.8674
                TEM1   = TREF*(P1/PREF)**((GAMMA-1.0)/GAMMA)
                CALL GASP01(TEM1,0.0,CP,CV,GAMMA,RGAS)
C               THROAT CONDITIONS
                TEMT   = TEM1 /(1 + (GAMMA-1)/2)
                CALL GASP01(TEMT,0.0,CPT,CVT,GAMMAT,RGAST)
                DENT   = P1 / (RGAST*TEMT*CPR)
                U2     = SQRT(GAMMAT*RGAST*TEMT)
                DMDT   = DENT * AORIF * CD * U2
                DEN1   = P1 / (RGAS*TEM1)
C               PIPE VELOCITY
                U1     = DMDT / (DEN1 * APIPE)

C               INSTANTANEOUS "TURBINE POWER" THROUGH THE ORIFICE PLA
                POWER = DMDT*(CP*TEM1 + U1*U1/2.0 - CP*TREF)

              END IF

              END IF


C             INCREMENTAL MASS AND "TURBINE WORK"
              DM = DMDT*DTIME
              DW = POWER*DTIME

C             ACCUMULATE THE MASS FLOW AND "TURBINE WORK"
              TOT1 = TOT1 + DM
              TOT2 = TOT2 + DW

C       -------------------------------------
C       WRITE TO FILE 1 FOR FURTHER CHECKING
C       -------------------------------------
        WRITE(1,100) VARS(IPNT,1),TEM1,P1/100000.,U1,U2,
     1               DMDT,POWER/1000,PR,ICHOK
100     FORMAT(F8.4,X,F6.2,X,F4.2,X,F10.4,X,F10.4,X,F10.4,X,
     1         F10.4,X,F8.4,X,I5)


        END IF

108     CONTINUE

C       ------------------------------------------------
C       COMPUTE THE CONTINUOUS MASS FLOW AND TURBINE POWER
C       ------------------------------------------------
        FLOW  = TOT1/((T2-T1)*720/(AV0-EV0))
        POWER = TOT2/((T2-T1)*720/(AV0-EV0))

C       ----------------------------------------------------------------
C       COMPUTE THE THEORETICAL MAXIMUM POWER PRODUCED BY AN ISENTROPIC
C       TURBINE IN THE EXHAUST STREAM - BASED ON P&T AT EV0
C       ----------------------------------------------------------------
        CALL GASP01(T0,0.0,CP0,CV0,GAMMA0,RGAS0)
        TMASS = P0 * VOL / (RGAS0 * T0)
        POWID = TMASS * CP0 * T0 * SPEED *
     1           (1.0 - (PREF/P0)**((GAMMA0-1.0)/GAMMA0)) / 120.0


        CALL WSCREEN
```

```
        WRITE(IOUT,1) T1,T2,DTIME
1       FORMAT(' EV0 (s) = ',F8.4,' AV0 (s) = ',F8.4,' DT = ',F10.6)

        WRITE(IOUT,*)' Theoretical number of integration steps = ',
     1                                          INT((T2-T1)/DTIME)


        WRITE(IOUT,*)' '
        WRITE(IOUT,*)' Actual number of integration steps      = ',
     1                                          INUM

        WRITE(IOUT,*)' '
        WRITE(IOUT,*)' Number of subsonic integration steps    = ',
     1                                          NSUB

        WRITE(IOUT,*)' '
        WRITE(IOUT,*)' Number of supersonic integration steps  = ',
     1                                          NSON

        WRITE(IOUT,*)' '
        WRITE(IOUT,*)' '
        WRITE(IOUT,*)' '

        WRITE(IOUT,*)' PULSE POWER    = ',POWER/1000.,' [kW]'
        WRITE(IOUT,*)' '
        WRITE(IOUT,*)' MASS FLOW RATE = ',FLOW       ,' [kg/s]'
        WRITE(IOUT,*)' '
        WRITE(IOUT,*)' '
        WRITE(IOUT,*)' '
        WRITE(IOUT,*)' THEORETICAL MAX. POWER = ',POWID/1000.0,
     1               ' [kW]'


        RETURN
        END
```